Developments in Cardiovascular Medicine

Volume 117

The titles published in this series are listed at the end of this volume.

QUANTITATIVE CORONARY ARTERIOGRAPHY

Edited by

JOHAN H. C. REIBER
Laboratory for Clinical and Experimental Image Processing, Thoraxcenter, Erasmus University, Rotterdam, The Netherlands

and

PATRICK W. SERRUYS
Catheterization Laboratory, Thoraxcenter, Erasmus University, Rotterdam, The Netherlands

SPRINGER SCIENCE+BUSINESS MEDIA, B.V

Library of Congress Cataloging-in-Publication Data

Quantitative coronary arteriography / edited by Johan H.C. Reiber and Patrick W. Serruys.
p. cm. -- (Developments in cardiovascular medicine ; v. 117)
Includes index.
ISBN 978-94-010-5656-4 ISBN 978-94-011-3726-3 (eBook)
DOI 10.1007/978-94-011-3726-3
1. Angiocardiography. 2. Coronary heart diseases--Diagnosis. 3. Coronary arteries--Imaging. I. Reiber, J. H. C. (Johan H. G.) II. Serruys, P. W. III. Series.
[DNLM: 1. Angiography--methods. 2. Coronary Vessels--radiography. 3. Echocardiography--methods. 4. Vascular Surgery--methods. W1 DE997VME v. 117 / WG 300 Q104]
RC683.5.A5Q36 1991
616.1'230754--dc20
DNLM/DLC
for Library of Congress

ISBN 978-94-010-5656-4

Printed on acid-free paper

Contents

Foreword

In June 1989, a third conference concentrating on the progress in quantitative coronary angiography and related techniques was held in Rotterdam, again very successful as the two preceding events in 1985 and 1987. Technical as well as clinical aspects of digital and digitized coronarography, morphometry, parametric imaging and functional quantification of the human coronary circulation were presented and discussed by prominent exponents of those groups who have been active in this particular field for many years. This book contains the chapters representing the lectures held by leading experts during the symposium that update the knowledge currently available, including most recent aspects in angioscopy and intravascular ultrasound imaging. It also includes a historical review on the development of angiographic techniques from the very early days on to our times given by one of the pioneers in heart catheterization and angiography, Dr. Kurt Amplatz. Those who had the chance to listen to his talk, will surely remember his impressive, humorous lecture as one of the highlights of this meeting.

As in the previous conferences, Dr. Melvin Marcus was one of the most active participants. For many years, he had been deeply involved in the development and perfection of new techniques to study the coronary circulation. A considerable number of important basic contributions in this field has come from himself and his group in Iowa City in recent years. Discussing with him always meant enrichment. In his candid and informal way he could split tensions and create a relaxed, nonetheless highly scientific atmosphere. Dr. Marcus died prematurely in the middle of a very active life. Those who had the privilege to know him and learn from him, will surely keep him in their good memory as one of the gifted investigators and teachers in cardiovascular research.

Working Group Coronary Blood Flow and Angina pectoris, ESC

RÜDIGER W. R. SIMON, MD, FESC
Chairman

List of Contributors

Kurt Amplatz, University of Minnesota Hospital and Clinic, Department of Radiology, Box 292 UMHC, 420 Delaware Street S.E., Minneapolis, MN 55455, USA.

Bjoern A. J. Angelsen, Department of Biomedical Engineering and Division of Cardiology, University of Trondheim, N-7006 Trondheim, Norway.

Max Anliker, Institute of Biomedical Engineering and Medical Informatics, University of Zürich and Swiss Federal Institute of Technology, Moussonstr. 18, CH-8044 Zürich, Switzerland.

Gerhard Bauriedel, Medical Clinic I, Clinic Grosshadern, University of München, Marchioninistr. 15, D-8000 München 70, Germany.

Christophe Bauters, Service de Cardiologie B et Hémodynamique, Hôpital Cardiologique, F-59037 Lille Cedex, France.

Kevin J. Beatt, Academic Unit of Cardiovascular Medicine, Charing Cross and Westminster Medical School, 17 Horseferry Road, London SW1P 2AR, United Kingdom.

Michel E. Bertrand, Service de Cardiologie B et Hémodynamique, Hôpital Cardiologique, F-59037 Lille Cedex, France.

Ralf Bettinger, Department of Cardiology, Center of Internal Medicine, University Clinic, Theodor Stern Kai 7, D-6000 Frankfurt 70, Germany.

Edward L. Bolson, Division of Cardiology, Department of Medicine, University of Washington, School of Medicine, RG-22, Seattle, WA 98195, USA.

Nicolaas Bom, Thoraxcenter, Erasmus University and University Hospital Rotterdam-Dijkzigt, P.O. Box 1738, 3000 DR Rotterdam, The Netherlands.

J. G. Bosch, Thoraxcenter, Erasmus University, P.O. Box 1738, 3000 DR Rotterdam, The Netherlands.

Ron W. Brower, Medical Computing Consultants, P.O. Box 35010, 3005 DA Rotterdam, The Netherlands.

B. Greg Brown, University of Washington, Department of Medicine, Division of Cardiology, RG-22, Seattle, WA 98195, USA.

Martin Büchi, Department of Cardiology, Medical Policlinic, University Hospital, Raemistrasse 100, CH-8091 Zürich, Switzerland.
Graham J. Davies, Royal Postgraduate Medical School, Hammersmith Hospital, 150 Ducane Road, London W12 OHS, United Kingdom.
Harold T. Dodge, University of Washington, Department of Medicine, Division of Cardiology, RG-22, Seattle, WA 98195, USA.
James T. Dodge Jr., University of Washington, Department of Medicine, Division of Cardiology, RG-22, Seattle, WA 98195, USA.
Neal L. Eigler, Division of Cardiology, Cedars-Sinai Medical Center and UCLA School of Medicine, Box 48750, Los Angeles, CA 90048-0750, U.S.A.
Willem J. van der Giessen, Thoraxcenter, Erasmus University and University Hospital Rotterdam-Dijkzigt, P.O. Box 1738, 3000 DR Rotterdam, The Netherlands.
K. Lance Gould, Division of Cardiology, The University of Texas Health Science Center at Houston, P.O. Box 20708, Houston, TX 77225, USA.
John C. Gurley, Division of Cardiology, Department of Medicine, University of Kentucky, College of Medicine, MN-670, 800 Rose Street, Lexington, KY 40536-0084, USA.
Elma Gussenhoven, Thoraxcenter, Erasmus University and University Hospital Rotterdam-Dijkzigt, P.O. Box 1738, 3000 DR Rotterdam, The Netherlands.
Otto M. Hess, Cardiology, Medical Policlinic, Department of Internal Medicine, University Hospital, Raemistrasse 100, CH-8091 Zürich, Switzerland.
Berthold Höfling, Medical Clinic I, Clinic Grosshadern, University of München, Marchionini Str. 15, D-8000 München 70, Germany.
Richard L. Kirkheeide, Division of Cardiology, University of Texas Health Science Center at Houston, P.O. Box 20708, TX 77225, USA.
Gisbert Kober, Department of Cardiology, Center of Internal Medicine, University Clinic, Theodor Stern Kai 7, D-6000 Frankfurt 70, Germany.
Hans P. Krayenbühl, Cardiology, Medical Policlinic, Department of Internal Medicine, University Hospital, Baemistrasse 100, CH-8091 Zürich, Switzerland.
Jean M. Lablanche, Service de Cardiologie B et Hémodynamique, Hôpital Cardiologique, F-59037 Lille Cedex, France.
David T. Linker, Department of Biomedical Engineering and Division of Cardiology, University of Trondheim, N-7006 Trondheim, Norway.
G. B. John Mancini, Veterans Administration Medical Center, Cardiology Section (111A), 2215 Fuller Road, Ann Arbor, MI 48105, USA.
Lisa W. Martin, Division of Cardiology, Department of Medicine, University of Maryland Hospital, 22 S. Greene Str., Baltimore, MA 21201, USA.
Markus Muser, Institute of Biomedical Engineering and Medical Informatics, University of Zürich and Swiss Federal Institute of Technology, Moussonstr 18, CH-8044 Zürich, Switzerland.
Peter Niederer, Institute of Biomedical Engineering and Medical Informatics,

University of Zürich and Swiss Federal Institute of Technology, Moussonstr 18, CH-8044 Zürich, Switzerland.

Steven E. Nissen, Division of Cardiology, Department of Medicine, University of Kentucky, College of Medicine MN 670, 800 Rose Street, Lexington, KY 40536-0084, USA.

Hein Osenberg, Institute of Biomedical Engineering and Medical Informatics, University of Zürich and Swiss Federal Institute of Technology, Moussonstr 18, CH-8044 Zürich, Switzerland.

Dennis L. Parker, Department of Medical Informatics, LDS Hospital, University of Utah, 325 8th Avenue, Salt Lake City, UT 84143, USA.

J. Martin Pfaff, Division of Cardiology, Cedars-Sinai Medical Center and UCLA School of Medicine, Box 48750, Los Angeles, CA 90048-0750, USA.

Audrey von Pölnitz, Medical Clinic I, Clinic Grosshadern, University of München, Marchionini Str. 15, D-8000 München 70, Germany.

Johan H. C. Reiber, Thoraxcenter, Erasmus University and University Hospital Rotterdam Dijkzigt, P.O. Box 1738, 3000 DR Rotterdam, The Netherlands.

Richard A. Schatz, Department of Research and Education, Arizona Heart Institute Foundation, P.O. Box 10 000, Phoenix, AR 85016, USA.

Patrick W. Serruys, Thoraxcenter, Erasmus University and University Hospital Rotterdam-Dijkzigt, P.O. Box 1738, 3000 DR Rotterdam, The Netherlands.

Rüdiger W. R. Simon, Department of Cardiology, University Hospital, D-2300 Kiel, Germany.

Paul Simpson, Division of Cardiology, University of Washington, School of Medicine, RG-22, Seattle, WA 98195, USA.

C. J. Slager, Thoraxcenter, Erasmus University and University Hospital Rotterdam-Dijkzigt, P.O. Box 1738, 3000 DR Rotterdam, The Netherlands.

J. Richard Spears, Division of Cardiology, Department of Internal Medicine, Harper Hospital, 3990 John R., Detroit, MI 48201, USA.

Robert A. Vogel, Division of Cardiology, Department of Medicine, R.S2C22, University of Maryland Hospital, 22 South Green Str., Baltimore, MA 21201, USA.

Thomas Wendt, Department of Cardiology, Center of Internal Medicine, University Clinic, Theodor-Stern Kai 7, D-6000 Frankfurt 70, Germany.

James S. Whiting, Division of Cardiology, Cedars-Sinai Medical Center and UCLA School of Medicine, Box 48750, Los Angeles, CA 90048-0750, USA.

Jiang Wu, Department of Medical Informatics, LDS Hospital, University of Utah, 325 8th Avenue, Salt Lake City, UT 84143, USA.

Paul G. Yock, Cardiovascular Research Institute and Division of Cardiology, M-1186, University of California, San Francisco, CA 94143-0124, USA.

Part I

Quantitative coronary arteriography; methodologies

1. Quantitative and qualitative coronary arteriography*

B. GREG BROWN, PAUL SIMPSON, JAMES T. DODGE, JR., EDWARD L. BOLSON, and HAROLD T. DODGE

Summary

The clinical objectives of arteriography are to obtain information that contributes to an understanding of the mechanisms of the clinical syndrome, provides prognostic information, facilitates therapeutic decisions, and guides invasive therapy. Quantitative and improved qualitative assessments of arterial disease provide us with a common descriptive language which has the potential to accomplish these objectives more effectively and thus to improve clinical outcome. In certain situations, this potential has been demonstrated. Clinical investigation using quantitative techniques has definitely contributed to our understanding of disease mechanisms and of atherosclerosis progression/regression. Routine quantitation of clinical images should permit more accurate and repeatable estimates of disease severity and promises to provide useful estimates of coronary flow reserve. But routine clinical QCA awaits more cost- and time-efficient methods and clear proof of a clinical advantage.

Careful inspection of highly magnified, high-resolution arteriographic images reveals morphologic features related to the pathophysiology of the clinical syndrome and to the likelihood of future progression or regression of obstruction. Features that have been found useful include thrombus in its various forms, ulceration and irregularity, eccentricity, flexing and dissection. The description of such high-resolution features should be included among, rather than excluded from, the goals of image processing, since they contribute substantially to the understanding and treatment of the clinical syndrome.

* Supported in part by USPHS grants PO1 HL-30086, RO1 HL-19451, HL-18645, and HL-03174, in part by an Established Investigator Award from the American Heart Association (79—116), and in part by a grant from the John L. Locke, Jr. Charitable Trust, Seattle, Washington.

J. H. C. Reiber and P. W. Serruys (eds), Quantitative Coronary Arteriography, 3—21.

Clinical goals of arteriography; role of quantitation

> "The image intensifier offers a wealth of data which is, at present, only partially used and seldom measured in clinical practice."
>
> Geoffredo Gensini, M.D. (1), 1971

What was true in 1971 is still so today. The striking improvements in arteriographic image quality, the considerable increase in clinical caseload, and the newer options for invasive therapy have not often been paralleled by clinical application of newer methods for estimating disease severity and for assessing the effects of interventional therapy. Indeed, the visual assessment of disease remains the clinical standard despite its well-established flaws of inaccuracy and high variance [1—4] and, more recently, of vulnerability to the biases of the interventional cardiologist. Many reasons may be advanced for this. While most agree that stenosis measurement is necessary for *research* in arterial disease, these methods have usually been too slow and tedious to play a role in clinical practice. However, advances in digital image processing and quicker, more simple methods should eliminate this objection [5—12].

A more deeply ingrained problem is that, in the absence of an objectively based "language" for the description of arterial disease, a spectrum of individual "dialects" has evolved. Each experienced clinician has become comfortable with his/her own approach to arteriographic interpretation. When informed that lesions *visually* judged "90%" usually *measure* at 75—80% diameter reduction [12], the clinician replies (perhaps correctly) that while his visual estimate may be numerically incorrect, he understands the significance of such a lesion and can manage its clinical manifestations effectively. A consequence of this "artisian" approach to interpretation is that every clinician must "see" the arteriogram in order to gain his own impression of lesion severity and location. Indeed, if an accurate, speedy method to characterize disease were now available, it would seldom completely agree with any of these individual "dialects." Nearly every clinician would find it necessary to modify his description of disease in order to conform with the common language. This is a lot to expect from many experienced, proud practitioners. It is frivolous to expect such an adjustment among these artisans without a conclusive demonstration that the additional cost in equipment and technical staff is justified by improved patient outcomes, or practice efficiency, or both.

From a clinical viewpoint, the objectives of arteriography are *to obtain information* that: (1) contributes to an understanding of the mechanisms of our patient's clinical syndrome, (2) helps predict the likelihood of future cardiac events, (3) facilitates effective therapeutic decision-making, and (4) guides invasive therapy. How can *quantitative* assessment contribute to these

objectives? In a general sense, an accurate common description of disease is a necessary basis for effective communication and for clinical investigation, and thus for evolution of clinical understanding. Specific quantitative arteriographic contributions to improved understanding of pathophysiologic mechanisms [13—27], assessment of perfusion and flow reserve [28—33], pharmacologic effects [34—41], atherosclerosis progression [42—49] and assessment of thrombolysis [50—58] and angioplasty [59—65] may also be cited.

In addition to lumen dimensions, lesions have a variety of other morphologic features whose definition may contribute to the above clinical objectives. Thrombus is almost always present in the stenosis in the setting of myocardial infarction; it is commonly found with unstable angina, and is rarely seen in lesions causing stable angina. Defects in the luminal surface corresponding to ulceration, dissection, or hemorrhage into the plaque are common in unstable clinical syndromes; their presence may be associated with accelerated disease progression, or with thrombolytic success. Lesions may have characteristics of overall shape such as eccentricity, flexing during the cardiac cycle, post-stenotic dilatation, and marked ectasia of the "normal" arterial segment proximal or distal to the narrowing. These features, too, can provide useful information. These morphologic features are described in more detail below, together with observations regarding their clinical and prognostic value.

Quantitative assessment of lumen morphology

Limitations of the *visual* estimate of disease severity have been documented in detail elsewhere [2—4]. The accuracy and precision of more objective approaches to stenosis measurement are found to be superior to that of visual methods [12, 13]. There are two competing approaches to angiographic stenosis measurement. One is based on detection of lumen borders from perpendicular image-pairs to create a three-dimensional approximation of the diseased segment [1, 5, 6, 8, 9, 11—13]; a second approach uses photodensitometry or videodensitometry of the stenosis to extract three-dimensional information from a single angiographic view [61, 66—68]. Our laboratory has favored border detection because it is relatively insensitive to variation in conditions of image formation and film processing, and because absolute dimensions are directly obtained. In theory, the videodensitometric method has advantages, particularly with directly acquired digital images in which the Beer-Lambert approximation is more likely to apply [69].

The approach used in our laboratory has evolved since 1975 [13]. Simply stated, we measure cineagiographic images of arterial disease projected at high (5x) magnification onto a smooth white surface. Under these conditions, details of stenosis morphology are seen that are not commonly appreciated with conventional magnification and projection. The quality of the analysis

depends in large part on the quality of the basic cine images; image quality pertinent to QCA is thus given special attention in our cath labs. Cine frames are selected as clear and representative of the disease segment. Its borders and the borders of the catheter are traced on paper, with notation of their radial location in the image. Visual border detection and manual tracing can be replaced by automated techniques [6—11]. However, we believe that the human visual cortex, with its remarkable capacity to resolve subtle lumen boundaries among the wide variation in background gray scale, is the most sophisticated, reliable, and accurate edge-finder currently available. Also, it is relatively inexpensive to employ one!

Recent modifications have streamlined our measurement approach (Figures 1 and 2). Lesions are traced in vertical orientation on a standard form to increase their packing density. The form, which contains tracing orientation information, catheter borders, and mark-sense input information, is video-scanned and automatically digitized after line-thinning. Computer processing incorporates an automatic method of compensating for X-ray beam divergence, using new knowledge of the three-dimensional intrathoracic spatial location of the various coronary anatomic segments [70]. Pincushion distortion is corrected, using an analytic function [13]. For analysis, the traced

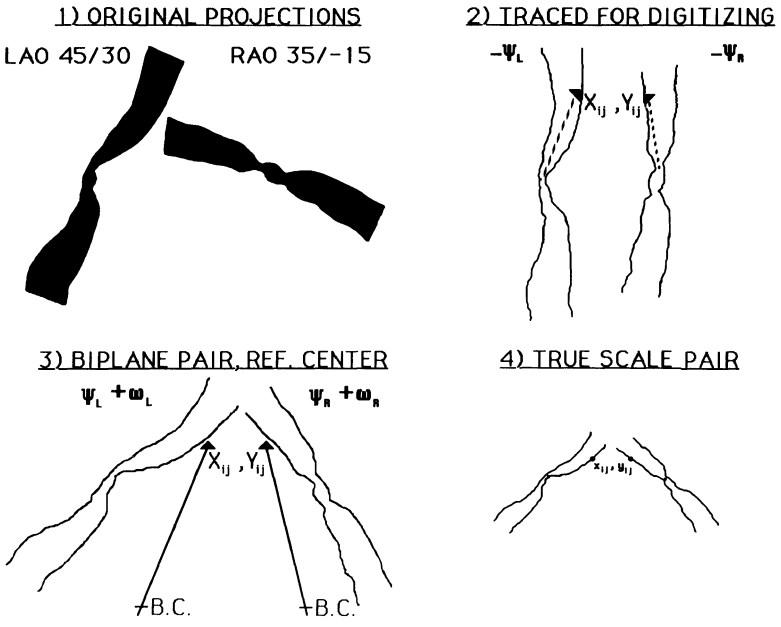

Fig. 1. Transformation from arteriographic lesion images in a perpendicular view pair to true-scale digital border representation after correction for magnification, pincushion distortion, X-ray beam divergence, tracing rotation, and rotation to achieve a proper match of common points in the biplane view-pair. See text for details.

lesion borders are rotated mathematically to compensate for tracing rotation (ψ_j) and also rotated by an amount (w_j) necessary to achieve a truly perpendicular biplane representation [70].

Since the mathematical description of this improved analysis has yet to be published, we take this opportunity to summarize the analytical steps we employ to transform a set of border points ($^*X_{ij}$, $^*Y_{ij}$) in the original

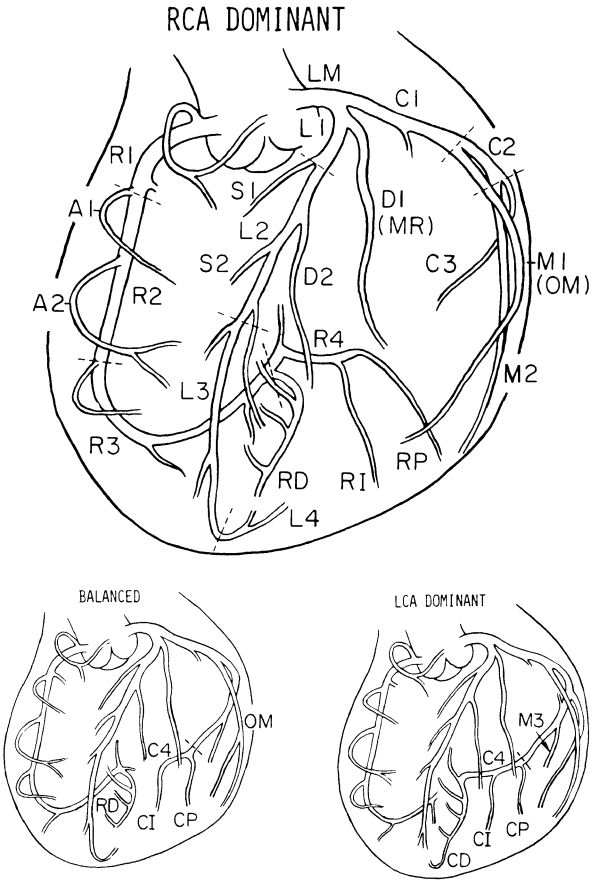

Fig. 2. A proposed coding system for identifying the coronary segmental anatomy that is clinically useful and easily remembered. Point locations in this segmental anatomy may be specified in polar coordinates to within a sphere of ± 1 cm diameter (± 1 s.d.) [70]. Lumen normal diameter at points in this anatomic display have been determined with coefficients of population variation ranging between 0.1 and 0.2 among 106 entirely normal coronary arteriograms. Segment and subsequent location (prox, mid, dist), coronary dominance, and branch length (short, med, long) must be specified to achieve such precision (Dodge JT, Brown BG, unpublished observations). (Reproduced from [70] with permission from the American Heart Association, Inc.).

projection-pair of stenosis images to a set of properly oriented, true-scale border points (x_{ij}, y_{ij}). This transformation is an iterative process for the ith border point in the jth angiographic view of the pair ($j = 1$ = LAO; $j = 2$ = RAO). Figure 1 illustrates the point-by-point transformation. The glossary of Table 1 defines the various terms. The comprehensive border-point transformation to adjust for tracing rotation, biplane rotation, X-ray beam divergence, pincushion distortion, and optical magnification is achieved in two steps, which are described conceptually and mathematically as follows:

Table 1. Glossary of parameters for quantitative arteriography.

1. *Coordinate systems*

($^*X_{ij}$, $^*Y_{ij}$) — A set of i digital border points approximating the two ($j = 1$ = LAO; $j = 2$ = RAO) traced, rotated views of the projected lesion image, centered on the lesion "reference point" (a local narrowing considered to represent the same point in the two views). This set is illustrated in Figures 1—2.

(X_{ij}, Y_{ij}) — A set of i border points approximating the two j views which have been rotated (Y_L, Y_R) to compensate for the tracing orientation and further rotated (w_L, w_R) to achieve a proper match of common points in the perpendicular view-pair. These points are referenced to the X-ray beam center to facilitate pincushion correction, and are illustrated in Figures 1—3. The transformation from ($^*Xij$, $^*Y_{ij}$) to (X_{ij}, Y_{ij}) is accomplished by Equations (1) and (2).

(x_{ij}, y_{ij}) — A set of i border points approximating the two j views which are now reduced to a true-scale, properly matched biplane view-pair centered on the lesion reference point. This set is illustrated in Figures 1—4. The transformation from (X_{ij}, Y_{ij}) to (x_{ij}, y_{ij}) is accomplished by Equations (3) and (4).

2. *System constants*

c — The so-called "pincushion constant" (13). $\Delta R' = (1 - cR^2)\Delta R$, where ΔR is a radial increment in the projected image plane and $\Delta R'$ is the "actual" increment in the pincushion-corrected image plane. c varies from lab to lab and for different angiographic field sizes and cine projection systems, and is determined by digitizing specified intersection points of a 1 cm grid image using a computer program designed for this purpose. For a 7 inch image field in our Philips laboratory and with our magnified projection system, c is 0.00004 cm^{-2}.

m — The so-called "beam divergence constant," [13] the rate of change of the dimensional correction factor with distance along the X-ray beam. m is determined by digitizing specified intersection points from a series of four grid images, using a computer program designed for this purpose. The grid images are filmed at four known distances from the input phosphor along the X-ray beam axis. For a 7 inch image field in our Philips laboratory, m is 0.0031 cm^{-1}.

(X_B, Y_B) — Location of the "center" of the X-ray beam, relative to the coordinate system fixed on the image surface of the projection table. It is that point in a grid image that does not shift when the image field size is electronically switched during the cine run. It is the center point of the radially symmetric "pincushion" correction.

3. *Projection constants*

A. *Coordinates*

(X_{pj}, Y_{pj}) — Location of the lesion "reference point" relative to the table coordinate system.

(X_{cj}, Y_{cj}) — Location of the traced catheter segment relative to the table coordinate system.

Table 1 (continued)

(X_{ij}, Y_{ij}) — Coordinate translation of the lesion reference point as the jth image is rotated (w_j) about the beam center to obtain a truly perpendicular view-pair.

$(r_a, \theta_a, \varnothing_a)$ — Polar coordinates specifying the average location of a given coronary segment relative to the coronary ostium (Figure 2). These have been determined from 37 normal-sized hearts and are available to the computer in tabular format [70].

$(r_c, \theta_c, \varnothing_c)$ — Polar coordinates specifying the average location of the traced catheter segment relative to the coronary ostium [70].

B. *Angles*

θ_L, θ_R — Angular rotation of the two biplane views about the patient long axis. These correspond to LAO and RAO angles with C-arm radiographic equipment (RAO negative).

$\varnothing_L$, $\varnothing_R$ — Angular azimuth of the two biplane views, corresponding to cranial (positive) and caudal (negative) angulation with C-arm radiographic equipment. Truly perpendicular view-pairs satisfy the equation: $\tan \varnothing_L \tan \varnothing_R = \cos(\theta_L - \theta_R)$.

w_L, w_R — Angular rotation of the LAO and RAO images about the X-ray beam center in order to achieve a truly perpendicular set of three-dimensional coordinate axes.

$$w_R = \sin^{-1}(\sin \varnothing_L / \cos \varnothing_R)$$
$$w_L = -\sin^{-1}(\sin \varnothing_R / \cos \varnothing_L)$$

Ψ_L, Ψ_R — Rotation back to their original orientation of the vertically traced lesion images from the LAO and RAO views. The vertical tracing is done for convenience.

C. *Derived constants*

CW_j — Pincushion-corrected catheter diameter, determined by multiplying the distance separating the two catheter borders traced from the projected image by $[1 - c(X_{cj}^2 + Y_{cj}^2)]$.

d_j — The true-scale distance separating the traced catheter segment from the diseased arterial segment, along the X-ray beam axis. This is used to compute the "beam divergence correction." It is obtained using the following formula, for $j = 2 =$ RAO.

$$d_R = r_c[\sin \varnothing_c \sin \varnothing_R + \cos \varnothing_c \cos \varnothing_R \cos(\theta_c - \theta_R)]$$
$$-r_a[\sin \varnothing_a \sin \varnothing_R + \cos \varnothing_a \cos \varnothing_R \cos(\theta_a - \theta_R)$$

with a similar expression for d_L in which L is substituted for R.

Steps to achieve true-scale biplane border representation

1. Assume foreknowledge of cw; c; m; X_p, Y_p; X_c, Y_c; and X_b, Y_b; θ_L, $\varnothing_L$; $\theta_R, \varnothing_R$.
2. Precalculate CW_j, d_j, w_j, Y_j, and X_{ij}, Y_{ij}, where: $j = 1 =$ LAO; $j = 2 =$ RAO.
3. Given $^*X_{ij}$, $^*Y_{ij}$, the coordinates (relative to the lesion center x_p, $Y_p = 0$, 0) of i traced border points in the j (LAO and RAO) views of the lesion, one can determine the coordinates X_{ij}, Y_{ij} of the border points rotated to compensate for Y (tracing rotation) and w (biplane rotation), and centered on the X-ray beam center, X_b, $Y_b = 0$, 0. Equations (1) and (2) below are used for this.
4. Having calculated these projected border points X_{ij}, Y_{ij}, the true-scale points, x_{ij}, y_{ij}, that are pincushion-corrected, beam-divergence-corrected,

and magnification-corrected, can be determined by Equations (3) and (4) below.

$$X_{ij} = ({}^*X_{ij}^2 + {}^*Y_{ij}^2)^{1/2} \cos\left[\tan^{-1}\left(\frac{{}^*Y_{ij}}{{}^*X_{ij}}\right) \pm w_j \pm Y_j\right] + \\ + X_{pj} - X_b + X_{tj} \tag{1}$$

$$Y_{ij} = ({}^*X_{ij}^2 + {}^*Y_{ij}^2)^{1/2} \sin\left[\tan^{-1}\left(\frac{{}^*Y_{ij}}{{}^*X_{ij}}\right) \pm w_j \pm Y_j\right] + \\ + Y_{pj} - Y_b + Y_{tj} \tag{2}$$

$$x_{ij} = [cw/CW_j + md_j]\left\{\left[1 - \left(\frac{c}{3}\right)(X_{ij}^2 + Y_{ij}^2)\right] X_{ij} - \right. \\ \left. - \left[1 - \frac{c}{3}(X_{pj}^2 + Y_{pj}^2)\right] X_{pj}\right\} \tag{3}$$

$$y_{ij} = [cw/CW_j + md_j]\left\{\left[1 - \left(\frac{c}{3}\right)(X_{ij}^2 + Y_{ij}^2)\right] Y_{ij} - \right. \\ \left. - \left[1 - \frac{c}{3}(X_{pj}^2 + Y_{pj}^2)\right] Y_{pj}\right\}. \tag{4}$$

Once the sets of true-scale border points describing the biplane images are obtained, centerlines between them are constructed and lumen diameters perpendicular to the centerlines are derived. The diseased segment is now described by a centerline in 3-D space with perpendicular diameters at multiple points along its course.

Primary computations include *lumen diameters* in each of the two views at the proximal and distal ends and at the point of greatest narrowing. *Lumen area* is $(\pi/4 \cdot D_{i1} \cdot D_{i2})$, an elliptical approximation. *Minimum area* is determined by computer search. Overall *segment length* and distance between the two 90% normal area points (*lesion length*) are computed as incremental sums along the centerline. The *Poiseuille resistance* is an integrated $1/A^2$ function described previously [16]. *Cone-angles of divergence and convergence*

and a *separation function* are computed; the latter is a function of flow rate and distal divergence, and relates to the probability of flow separation and distal turbulence, which is highly likely for divergence half-angles of 15° or more. *Atheroma volume* is obtained by integrating the *difference* between observed lumen area and "interpolated normal lumen area" along the length of the lesion. *Lumen volume* is an integration of lumen area over the length of the segment.

A number of measures may be *derived* from these primary measures, including *normal diameter* and *area* (proximal, distal, or both ends), as specified by the viewer; percent diameter and area reduction relative to the specified normals, maximum shear stress, entry and maximum Reynolds numbers, and total pressure loss are computed for three hypothetical levels of coronary flow.

Quantitative arteriography has been applied to study many clinical syndromes. Active investigational areas include the progression and regression of atherosclerosis [42—49], thrombolytic recanalization of acutely occluded arteries [50—58], percutaneous angioplasty [59—65], the relationship between the anatomic severity of atherosclerotic narrowing and its physiologic impact [16—33], coronary vasomotion [20, 27, 29, 34—41], and the mechanism of action of antianginal drugs [34—41]. A summary of these clinical findings is outside the scope of this manuscript. Suffice it to say that important advances in our understanding of coronary disease and its treatment have come, and will continue to come, from these studies.

Qualitative aspects of coronary assessment

Anatomic description

Identifying the *location* of a coronary lesion and judging its physiologic importance or clinical risk are among the "artisan's" skills in angiographic interpretation. Once again, lack of a precise common descriptive terminology impairs communication. Several systems for shorthand classification of coronary segmental anatomy have been proposed [71, 72]. A major problem with these numeric coding systems is that the numbers bear no relation to the commonly used names for the coronary branches; in addition, these systems differ among themselves. Figure 2 presents an easily remembered, concise, and clinically useful system for coding segmental anatomy [70]. Using this system, we have found that subsegmental location can be described effectively in polar coordinates relative to the coronary ostium. The variance ($\pm$ 1 SD) of such estimates approximates 1 cm [70]. Furthermore, we have recently found that the subsegmental lumen diameter of *normal* human coronary arteries can be specified with a coefficient of variation between 0.1 and 0.2 if we know the coronary anatomic dominance, subsegment location,

and qualitative branch length. This latter knowledge has important implications for characterizing diffuse atherosclerotic narrowing.

Lesion morphology

Certain characteristics of the lesion appear to defy quantitation and yet may have great value in explaining the dynamics of the clinical syndrome or predicting the future course of the obstructive process. Among these are thrombus, ulceration, lumen irregularity, eccentricity, ectasia, flexing, and dissection. Some of these morphologic features are illustrated in Figures 3—8. We have attempted to determine the incidence of certain features in lesions responsible for various clinical syndromes and their value in predicting subsequent lesion change [48]. Thrombus is uncommon in stable clinical syndromes; if an intraluminal thrombolucency partially obstructs a lumen, the prospect of "regression" of this obstruction over 5 years is increased more than 100-fold [48] (Figure 3). In our experience, thrombus is visible on close inspection of highly magnified arteriographic images in over 90% of acutely

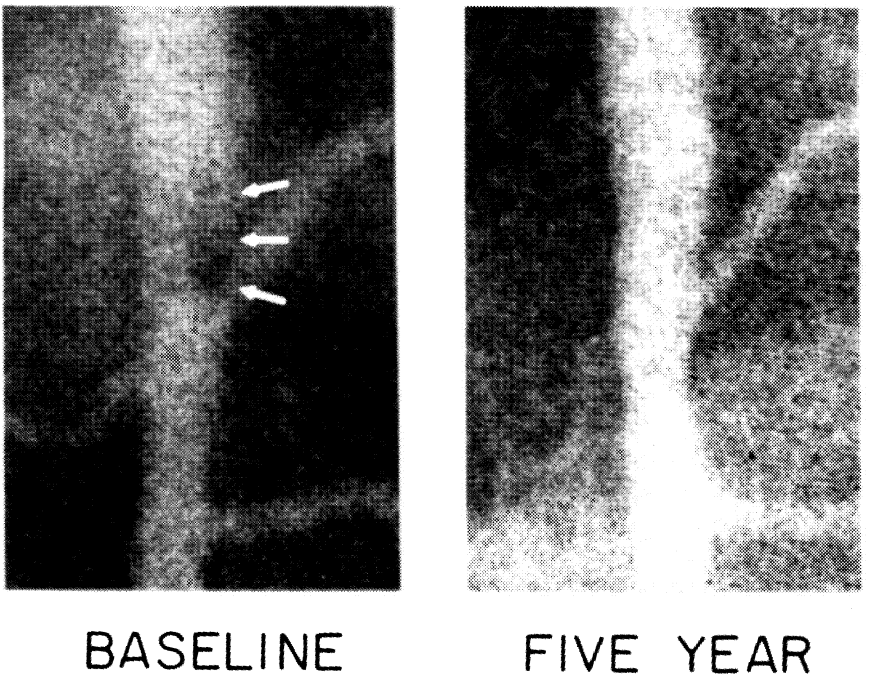

Fig. 3. Example of a mural thrombus (arrows) observed to narrow the RCA by 50% at baseline in a clinically stable patient. "Regression" of obstruction occurred over 5 years in 40% of vessels narrowed by such obstructive thrombus, significantly more often than the 0.3% regression frequency for lesions with a smooth intimal surface ($p < 0.001$). (Reproduced from [49] with permission from the American Heart Association, Inc.).

recanalized lesions responsible for acute myocardial infarction [54] (Figures 4—6). Thrombolucencies are also seen in the majority of active cases of unstable angina [73, 74]. Thrombus adherent to the plaque may be *mural* or *globular*, or may extend downstream from the point of attachment as a long intraluminal tail (Figures 4 and 6). In recanalized infarct lesions, mural thrombus signifies increased risk of reocclusion, while the globular form is likely to lyse further. Failure of *effective* recanalization, to a minimum lumen

Fig. 4. Example of "globular" thrombus in the right coronary artery of a patient treated for acute myocardial infarction. This injection was made just following PTCA to treat the totally occluded RCA. Such morphology is difficult to characterize in the standard fashion, and poses a considerable problem for automated border recognition techniques. Videodensitometry, an apparent solution to this problem, can also prove misleading [62]. Thrombus with this morphology is likely to lyse with time and thrombolytic agents.

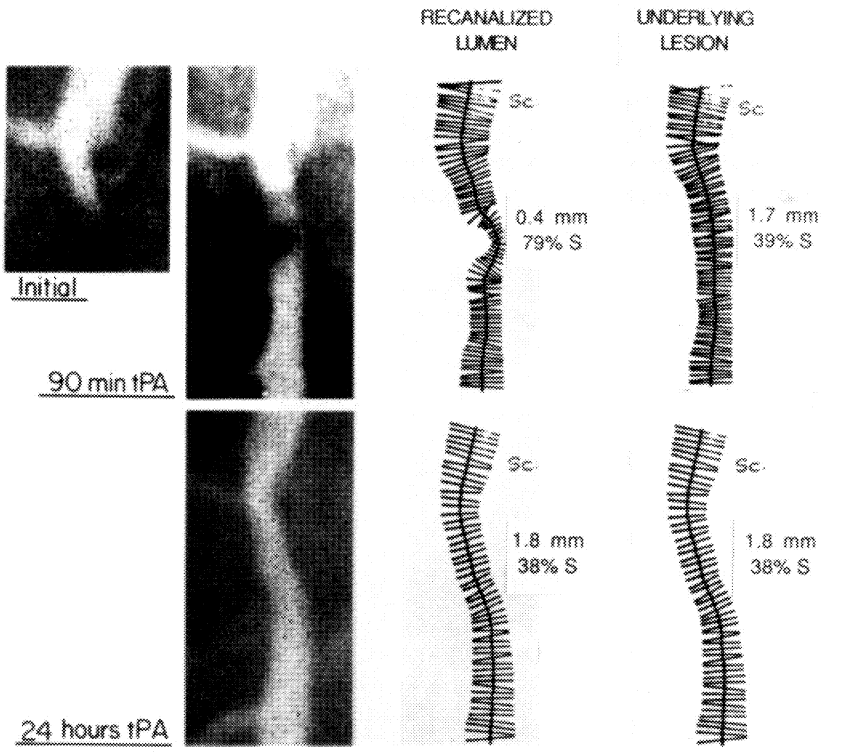

Fig. 5. A method for computer-assisted analysis of thrombolytic recanalization of an occluded RCA. Two lumens are traced; the *recanalized* lumen, as outlined by dense contrast, and the underlying atherosclerotic lumen, whose borders are faintly but clearly defined (on close inspection at high magnification) in the region of the thrombus. When the thrombus is lysed at 24 hours, the underlying lesion is revealed to be a mild, 38% stenosis.

diameter of $\geqslant$ 0.6 mm, predicts a 35—55% chance of acute reocclusion of an infarct artery initially pened by fibrinolytic therapy [51, 55, 57]. Thrombolysis has the potential to recanalize the average infarct lesion to a 50—55% stenosis, usually exposing the underlying plaque dissection or ulceration (Figure 6) that was the initial locus for thrombus formation [54, 73—78]. A plaque ulceration is uncommon except as above; however, if present, the risk of lesion progression is doubled [48] (Figure 7). Similarly, irregular lumen surfaces predict progression [76, 79—81]. Flexing of the artery at the site of the stenosis occurs in about 25% of lesions; surprisingly, flexing lesions are *less* likely to progress [48] (Figure 8).

Further investigation using high-resolution images and prospective study designs will be necessary to understand better the value of these morphologic features in clinical practice.

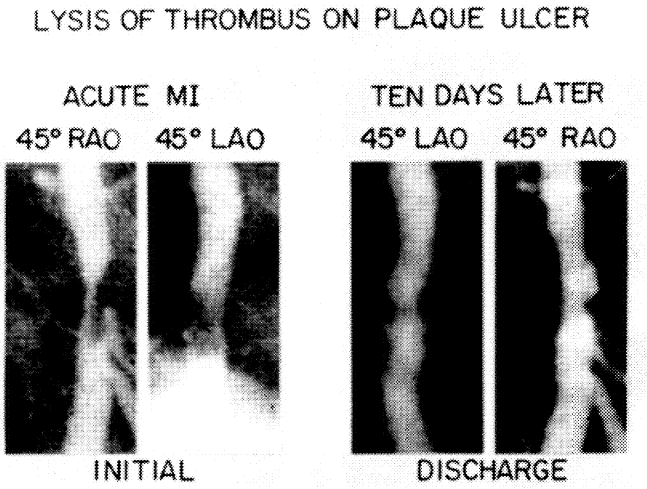

Fig. 6. Example of pharmacologic lysis of a long "tail" of thrombus adherent to a site eventually identified as a large plaque ulcer in a follow-up arteriogram obtained 10 days after treatment. This right coronary artery was initially subtotally occluded in the clinical setting of acute inferior myocaordial infarction. (Reproduced from [54] with permission of the American Heart Association, Inc.).

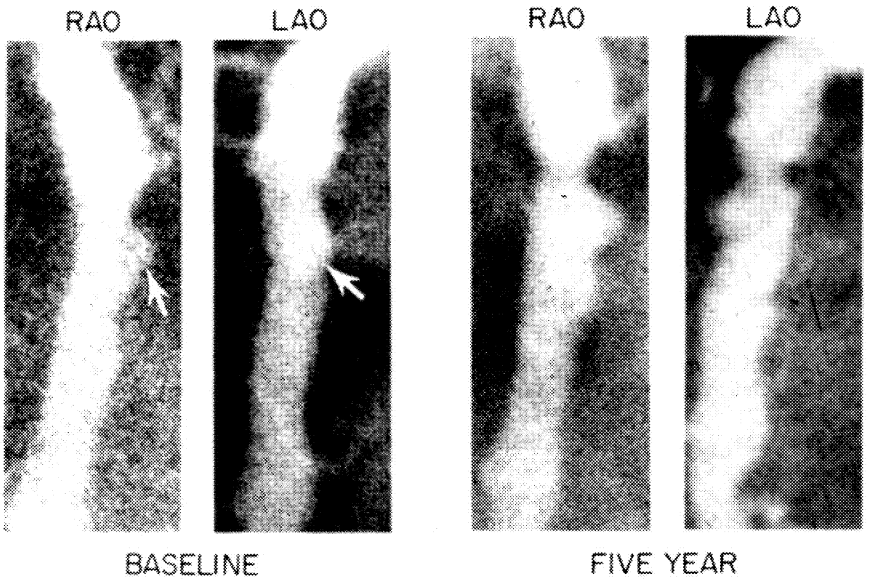

Fig. 7. Obvious ulceration (arrow) of the intimal surface was uncommon among clinically stable patients, occurring in 4 of 493 lesions. Progression of obstruction occurred in 50% of such ulcerated stenoses [49]. In this case, the ulcer persisted for 5 years. RAO = right anterior oblique view; LAO = left anterior oblique. (Reproduced from [49] with permission of the American Heart Association, Inc.).

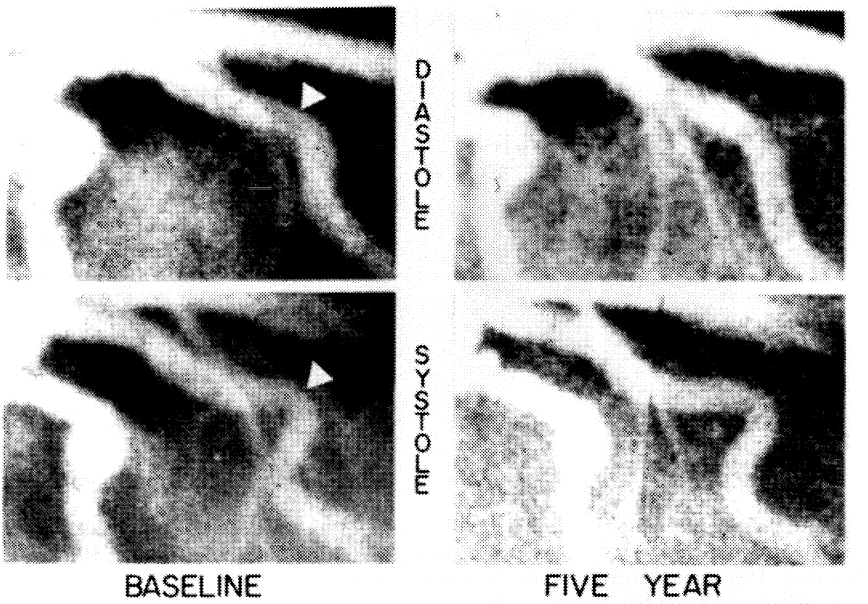

Fig. 8. A mild marginal branch lesion seen at a site of active arterial flexion (solid arrow) did not change during the 5-year angiographic interval. Surprisingly, only five percent of 110 flexing lesions progressed, as compared with 12% of 282 lesions without any distinctive morphologic features among 468 lesions studied. (Reproduced from [49] with permission of the American Heart Association, Inc.).

Acknowledgments

We thank Robert Braunwart for his excellent preparation of this manuscript.

References

1. Gensini GG, Kelly AE, Da Costa BCB, Huntington PP: Quantitative angiography: The measurement of coronary vasomobility in the intact animal and man. Chest 60: 522—530, 1971.
2. Detre KM, Wright E, Murphy ML, Takaro T: Observer agreement in evaluating coronary angiograms. Circulation 52: 979—986, 1975.
3. DeRouen TA, Murray JA, Owen W: Variability in the analysis of coronary arteriograms. Circulation 55: 324—328, 1977.
4. White CW, Wright CB, Doty DB, Hiratzka LF, Eastham CL, Harrison DG, Marcus ML: Does visual interpretation of the coronary arteriogram predict the physiologic importance of a coronary stenosis? N Engl J Med 310: 819—824, 1984.
5. Kirkeeide RL, Fung P, Smalling RW, Gould KL: Automated evaluation of vessel diameter from arteriograms. Comput Cardiol 1982: 215—218.
6. Tobis J, Nalcioglu O, Iseri L, Johnston WD, Roeck W, Castleman E, Bauer B, Montelli S, Henry WL: Detection and quantitation of coronary artery stenoses from digital subtrac-

tion angiograms compared with 35-millimeter film cineangiograms. Am J Cardiol 54: 489—496, 1984.
7. Spears JR, Sandor T, Als AV, Malagold M, Markis JE, Grossman W, Serur JR, Paulin S: Computerized image analysis for quantitative measurement of vessel diameter from cineangiograms. Circulation 68: 453—461, 1983.
8. Reiber JHC, Serruys PW, Slager CJ: Quantitative coronary and left ventricular cineangiography: Methodology and clinical applications. Martinus Nijhoff Publishers, Dordrecht, 1986.
9. Mancini GBJ, Simon SB, McGillem MJ, Le Free MT, Friedman HZ, Vogel RA: Automated quantitative coronary arteriography: Morphologic and physiologic validation in vivo of a rapid digital angiographic method. Circulation 75: 452—460, 1987.
10. Parker DL, Pope DL, van Bree R, Marshall HW: Three-dimensional reconstruction of moving arterial beds from digital subtraction angiography. Comput Biomed Res 20: 166—185, 1987.
11. Alderman EL, Berte LE, Harrison DC, Sanders W: Quantitation of coronary artery dimensions using digital image processing. Diagn. Radiol 314: 273—277, 1981.
12. Scoblionko DP, Brown BG, Mitten S, Calduell JH, Kennedy JW, Bolson EL, Dodge HT: A new digital electronic caliper for measurement of coronary arterial stenosis: Comparison with visual estimates and computer-assisted measurements. Am J Cardiol 53: 689—693, 1984.
13. Brown BG, Bolson EL, Frimer M, Dodge HT: Quantitative coronary arteriography: Estimation of dimensions, hemodynamic resistance, and atheroma mass of coronary artery lesions using the arteriogram and digital computation. Circulation 55: 329—337, 1977.
14. Blankenhorn DH, Brooks SH, Selzer RH, Crawford DW, Chin HP: Assessment of atherosclerosis from angiographic images. Proc Soc Exp Biol Med 145: 1298—1300, 1974.
15. Crawford DW, Brooks SH, Selzer RH, Brandt Jr. R, Beckenbach ES, Blankenhorn DH: Computer densitometry for angiographic assessment of arterial cholesterol content and gross pathology in human atherosoclerosis. J Lab Clin Med 89: 378—392, 1977.
16. McMahon MM, Brown BG, Cukingnan R, Rolett EL, Bolson E, Frimer M, Dodge HT: Quantitative coronary angiography: Measurement of the "critical" stenosis in patients with unstable angina and single-vessel disease without collaterals. Circulation 60: 106—113, 1979.
17. Rafflenbeul W, Urthaler F, Lichtlen P, James T: Quantitative difference in "critical" stenosis between right and left coronary artery in man. Circulation 62: 1188—1196, 1980.
18. Dodge HT, Sheehan FH, Kliman SH: Quantitative relationship of coronary stenosis and ventricular hypokinesia. Comput Cardiol 1981: 170—175.
19. Gould KL, Kelley KO, Bolson EL: Experimental validation of quantitative coronary arteriography for determining pressure-flow characteristics of coronary stenosis. Circulation 66: 930—937, 1982.
20. Brown BG, Lee AB, Bolson EL, Dodge HT: Reflex constriction of significant coronary stenosis as a mechanism contributing to ischemic left ventricular dysfunction during isometric exercise. Circulation 70: 18—24, 1984.
21. Harrison DG, White CW, Hiratzka LF, Doty DB, Barnes DH, Eastham CL, Marcus ML: The value of lesion cross-sectional area determined by quantitative coronary arteriography in assessing the physiologic significance of proximal left anterior descending coronary arterial stenoses. Circulation 69: 1111—1119, 1984.
22. Rafflenbuel W, Smith LR, Rogers WJ, Mantle JA, Rackley CE, Russell RO. Quantitative coronary arteriography: Coronary anatomy of patients with unstable angina pectoris reexamined 1 year after optimal medical therapy. Am J Cardiol 43: 699—707, 1979.
23. Wilson RF, Holida MD, White CW: Quantitative angiographic morphology of coronary

stenosis leading to myocardial infarction or unstable angina. Circulation 73: 286—296, 1986.
24. Goldstein RA, Kirkeeide R, Demer L, Merhige M, Nishikawa A, Smalling RW, Mullani NA, Gould KL: Relations between geometric dimensions of coronary artery stenoses and myocardial perfusion reserve in man. J Clin Invest 1473—1478, 1987.
25. Gage JE, Hess DM, Murakami T, Ritter M, Grimm J, Krayenbuehl HP: Vasoconstriction of stenotic coronary arteries during dynamic exercise in patients with classic angina pectoris. Reversibility by nitroglycerin. Circulation 73: 865—876, 1986.
26. Wilson RF, Marcus ML, White CW: Prediction of the physiological significance of coronary arterial lesions by quantitative lesion geometry in patients with limited coronary artery disease. Circulation 75: 723—732, 1987.
27. Ludmer PL, Selwyn AP, Shook TL, Wayne RR, Mudge GH, Alexander RW, Ganz P: Paradoxical vasoconstriction induced by acetylcholine in atherosclerotic coronary arteries. N Engl J Med 315: 1046—1051, 1986.
28. Zijlstra F, van Ommeren J, Reiber JHC, Serruys PW: Does quantitative assessment of coronary artery dimensions predict the physiological significance of a coronary stenosis? Circulation 75: 1154—1160, 1987.
29. Josephson MA, Brown BG, Hecht HS, Hopkins J, Pierce CD, Petersen RB: Noninvasive detection and localization of coronary stenoses in patients: Comparison of resting dipyridamole and exercise thallium-201 myocardial perfusion imaging. Am Heart J 103: 1008—1018, 1982.
30. Vogel R, LeFree M, Bates E, O'Neill W, Foster R, Kirlin P, Smith D, Pitt B: Application of digital techniques to selective coronary arteriography: Use of myocardial contrast appearance time to measure coronary flow reserve. Am Heart J 107: 153—164, 1984.
31. Wijns W, Serruys PW, Reiber HJC, van den Brand M, Simoons ML, Kooijman CJ, Balakumaran K, Hugenholtz PG: Quantitative angiography of the left anterior descending coronary artery: Correlations with pressure gradient and results of exercise thallium scintigraphy. Circulation 71: 273—279, 1985.
32. Demer LL, Gould KL, Goldstein RA, Kirkeeide RL, Mullani NA, Smalling RW, Nishikawa A, Merkige ME: Assessment of coronary artery disease severity by positron emission tomography: Comparison with quantitative arteriography in 193 patients. Circulation 79: 825—835, 1989.
33. Demer L, Gould KL, Kirkeeide R: Assessing stenosis severity: Coronary flow reserve, collateral function, quantitative coronary arteriography, position imaging, and digital subtraction angiography. A review and analysis. Prog in Cardiovaosc Dis 33: 307—322, 1988.
34. Feldman RL, Repine CJ, Curry RC, Conti CR: Coronary arterial responses to graded doses of nitroglycerin. Am J Cardiol 43: 91—97, 1979.
35. Rafflenbuel W, Urthaler F, Russell RO, Lichtlen P, James TM: Dilatation of coronary artery stenoses after isosorbide dinitrate in man. Br Heart J 43: 546—549, 1980.
36. Brown BG, Bolson EL, Petersen RB, Pierce CD, Dodoge HT: The mechanisms of nitroglycerin action: Stenosis vasodilatation as a major component of the drug response. Circulation 64: 1089—1097, 1981.
37. Brown BG, Josephson MA, Petersen RB, Pierce CD, Wong M, Hecht HS, Bolson E, Dodge HT: Intravenous dipyridamole combined with isometric handgrip for near maximal acute increase in coronary flow in patients with coronary disease. Am J. Cardiol 48: 1077—1085, 1981.
38. Mudge GH Jr, Goldberg S, Gunther S, Mann T, Grossman W: Comparison of metabolic and vasoconstrictor stimuli on coronary vascular resistance in man. Circulation 59: 544—550, 1979.
39. Feldman RL, Hill JA, Conti JB, Conti CR, Pepine CJ: Analysis of coronary responses to nifedipine alone and in combination with intracoronary nitroglycerin in patients with coronary artery disease. Am Heart J 105: 651—658, 1983.
40. Hossack KF, Brown BG, Stewart DK, Dodge HT: Diltiazem-induced blockade of sym-

pathetically mediated constriction of normal and diseased coronary arteries: lack of epicardial coronary dilatory effect in humans. Circulation 70: 465—471, 1984.
41. Brown BG, Bolson EL, Dodge HT: Dynamic mechanisms in human coronary stenosis. Circulation 70: 917—922, 1984.
42. Barndt Jr R, Blankenhorn DH, Crawford DW, Brooks SH: Regression and progression of early femoral atherosclerosis in treated hyperlipoproteinemic patients. Ann Intern Med 86: 139—146, 1977.
43. Blankenhorn DH, Brooks SH, Selzer RH, Barndt Jr R: The rate of atherosclerosis change during treatment of hyperlipoproteinemia. Circulation 57: 355—361, 1978.
44. Reiber JHC, Serruys PW, Kooijman CJ, Wijns W, Slager CJ, Gerbrands JJ, Schumbiers JCH, Boer A den, Hugenholtz PG: Assessment of short-, medium-, and long-term variations in arterial dimensions from computer-assisted quantitation of coronary cineangiograms. Circulation 71: 280—288, 1985.
45. Brown BG, Adams WA, Albers JJ, Lin J-T, Bolson EL, Dodge HT: Quantative arteriography in coronary intervention trials: Rationale, study design, and lipid response in the University of Washington Familial Atherosclerosis Treatment Study (FATS). In Evolution of the human atherosclerotic plaque. S Glagov, D Blankenhorn, R Wissler, W Newman (Eds.), Springer-Verlag, 1988: 000—000.
46. Arntzenius AC, Kromhout D, Barth JD, Reiber JHC, Bruschke AVG, Buis B, Gent CM van, Kempen-Voogd N, Strikwrede N, Velde EA van der: Diet, lipoproteins, and the progression of coronary atherosclerosis: The Leiden Interventional Trial. N Engl J Med 312: 805—811, 1985.
47. Blankenhorn DM, Nessim SA, Johnson RL, Sanmarco ME, Azen SP, Cashin-Hemphill L: Beneficial effects of combined colestipol-niacin therapy on coronary atherosclerosis and coronary venous bypass grafts. JAMA 257: 3233—3240, 1987.
48. Brown BG, Lin JT, Kelsey S, Passamani ER, Levy RI, Dodge HT, Detre KM: Progression of coronary atherosclerosis in patients with probable familial hypercholesterolemia. Arteriosclerosis 9 (suppl I): I-81 — I-90, 1989.
49. Feldman RL, Crick WF, Conti CR, Pepine CJ: Quantitative coronary angiography during intracoronary streptokinase in acute myocardial infarction: How long to continue thrombolytic therapy? Cathet Cardiovaosc Diagn 9: 9, 1983.
50. Serruys PW, Wijns W, Barnd M van den, Ribeiro V, Fioretti P, Simoons ML, Kooijman CJ, Reiber JHC, Hugenholtz PG: Is transluminal coronary angioplasty mandatory after successful thrombolysis? A quantitative coronary angiographic study. Br Heart J 50: 257—265, 1983.
51. Harrison DG, Ferguson DW, Collins SM, Skorton DJ, Ericksen EE, Kioschos JM, Marcus ML, White CW: Rethrombosis after reperfusion with streptokinase: Importance of geometry of residual lesions. Circulation 69: 991—999, 1984.
52. Sheehan FH, Mathey DG, Schofer J, Dodge HT, Bolson EL: Factors that determine recovery of left ventricular function after thrombolysis in patients with acute myocardial infarction. Circulation 71: 1121—1128, 1985.
53. Cribier A, Saoudi N, Berland J, Letec B: Regression of residual coronary stenosis after recanalization by fibrinolysis in myocardial infarction. Quantitative analysis of coronary angiography immediately after obstruction removal, at a 15-day and 3-month follow-up. Arch Mal Coeur 78: 353—360, 1985.
54. Brown BG, Gallery CA, Badger RS: Incomplete lysis of thrombus in the moderate underlying atherosclerotic lesion during intracoronary infusion of streptokinase for acute myocardial infarction: Quantitative angiographic observations. Circulation 73: 653—661, 1986.
55. Gold HK, Leinbach RC, Garabedian HD, Yasuda T, Johns JA, Grossbard EB, Palacios I, Collen D: Acute coronary reocclusion after thrombolysis with recombinant human tissue-type plasminogen activator: Prevention by a maintenance infusion. Circulation 73: 347—352, 1986.
56. Brown BG & Burroughs-Wellcome tPA Study Group: Low-dose infusion of tissue

plasminogen activator (tPA) for 12—24 hours after the initial dose. Quantitative arteriographic analysis. Circulation 76 (suppl IV): IV-305, 1987 (abstract).
57. Badger RS, Brown BG, Kennedy JW, Mathey D, Gallery C, Bolson EL, Dodge HT: Usefulness of recanalization to luminal diameter of 0.6 millimeter or more with intracoronary streptokinase during acute myocardial infarction in predicting "normal" perfusion status, continued arterial patency, and survival at one year. Am J Cardiol 59: 519—522, 1987.
58. Brown BG, Serruys PW: Qualitative and quantitative coronary arteriographic changes after thrombolysis: Early and late results. In: Thrombolysis in Cardiovascular Diseases. DG Julian, W Kübler, RM Norris, HJ Swan, D Collen, M Verstraete (Eds.), Marcel Dekker Publishers. New York, 1989: 103—127.
59. Serruys PW, Reiber JHC, Wijns W, van den Brand M, Kooijman H, ten Katen HJ, Hugenholtz PG: Assessment of percutaneous transluminal coronary angioplasty by quantitative coronary angiography: Diameter versus densitometric area measurements. 54: 482—488, 1984.
60. Johnsen MR, Brayben GP, Ericksen EE, Collins SM, Skorton DJ, Harrison DG, Marcus ML, White CW: Changes in cross-sectional area of the coronary lumen in the six months after angioplasty: A quantitative analysis of the variable response to percutaneous transluminal angioplasty. Circulation 73: 467—475, 1986.
61. Tobis J, Henry WL: Videodensitometric determination of minimum coronary luminal diameter before and after angioplasty. Am J Cardiol 59: 38—44.
62. Brown BG, Bolson EL, Dodge HT: Percutaneous transluminal coronary angioplasty and subsequent restenosis: Quantitative and qualitative methodology for their assessment. Am J Cardiol 60: 34B—38B, 1987.
63. Serruys PW, Luijten HE, Beatt KJ, Geuskens R, de Feyter PJ, van den Brand M, Rdiber JHC, ten Katen JH, van Es GA, Hugenholtz PG: Incidence of restenosis after successful coronary angioplasty: A time-related phenomenon. A quantitative angiographic study in 342 consecutive patients at 1, 2, 3, and 4 months. Circulation 77: 361—371, 1988.
64. Zijlstra F, den Boer A, Reiber JHC, van Es GA, Lubsen J, Serruys PW: Assessment of immediate and long-term functional results of percutaneous transluminal coronary angioplasty. Circulation 78: 15—24, 1988.
65. Fischell TA, Derby G, Tse TM, Stadius ML: Coronary artery vasoconstriction routinely occurs after percutaneous transluminal coronary angioplasty. A quantitative arteriographic analysis. Circulation 78: 1323—1334, 1988.
66. Sandor T, Als AV, Paulin S: Cine-densitometric measurement of coronary arterial stenoses. Cathet Cardiovasc Diag 5: 229—245, 1979.
67. Nichols AB, Gabrieli CFO, Fenoglio Jr JJ, Esser PD: Quantification of relative coronary arterial stenosis by cinevideodensitometric analysis of coronary arteriograms. Circulation 69: 512—522, 1984.
68. Collins SM, Skorton DJ, Harrison DG, White CW, Eastham CL, Hiratzka LF, Doty DB, Marcus ML: Quantitative computer-based videodensitometry and the physiological significance of a coronary stenosis. comput Cardiol 219—222, 1982.
69. Brown BG, Bolson EL, Dodge HT: Quantitative computer techniques for analyzing coronary arteriograms. Prog Cardiovasc Dis 28: 403—418, 1986.
70. Dodge Jr JT, Brown BG, Bolson EL, Dodge HT: Intrathoracic spatial location of specified coronary segments on the normal human heart: Applications in quantitative arteriography, assessment of regional risk and contraction, and anatomic display. Circulation 78: 1167—1180, 1988.
71. Austen WG, Edwards JE, Frye RL, Gensini GG, Gott VL, Griffith LSC, McGoon DC, Murphy ML, Roe BB: A reporting system on patients evaluated for coronary artery disease. Report of the Ad Hoc Committee for Grading of Coronary Artery Disease. Council on Cardiovascular Surgery, American Heart Association. Circulation 51: 7—40, 1975.

72. Principal Investigators of CASS and Associates: National Heart, Lung, and Blood Institute Coronary Artery Surgery Study. Circulation 63 (suppl I): I-1 — I-139, 1981.
73. Falk E: Unstable angina with fatal outcome: Dynamic coronary thrombus leading to infarction and/or sudden death. Circulation 71: 699—708, 1985.
74. Ambrose JA, Winters SL, Arora RR, Haft JI, Goldstein J, Rentrop KP, Gorlin R, Fuster V: Coronary angiographic morphology in myocardial infarction: A link between the pathogenesis of unstable angina and myocardial infarction. J. Am Coll Cardiol 6: 1223—1238, 1985.
75. Nakagawa S, Hanada Y, Koiwaya Y, Tanaka K: Angiographic features in the infarct-related artery after intracoronary urokinase followed by prolonged anticoagulation. Circulation 78: 1335—1344, 1988.
76. Levin DC, Gardiner Jr GA: Complex and simple coronary artery stenoses: A new way to interpret coronary angiograms based on morphologic features of lesions. Radiology 164: 675—680, 1987.
77. Mabin TA, Holmes Jr DR, Smith HC, Vlietstra RE, Bove AA, Reeder GS, Chesebro JH, Bresnahan JF, Orszulak TA: Intracoronary thrombus: Role in coronary occlusion complicating PTCA. J Am Coll Cardiol 5: 198—202, 1985.
78. Ellis SG, Roubin GS, King SB III, Douglas JS, Weintraub WS, Thomas RG, Cox WR: Angiographic and clinical predictors of acute closure after native-vessel coronary angioplasty. Circulation 77: 372—380, 1988.
79. Nash DT, Caldwell N, Ancona D: Accelerated coronary artery disease arteriographically proved. Analysis of risk factors. NY State J Med 74: 947—950, 1974.
80. Rösch J, Antonovic R, Trenouth RS, Rahimtoooola SH, Sim DN, Dotter CT: The natural history of coronary artery stenosis. Radiology 119: 513—520, 1976.
81. Kramer JR, Matsuda Y, Mulligan JC, Aronow M, Proudfit WL: Progression of coronary atherosclerosis. Circulation 63: 519—526, 1981.

2. Digital coronary angiography: advantages and limitations

G. B. JOHN MANCINI

Summary

Digital angiography has been available clinically for a decade. Initial enthusiasm stemming from the prospects of obtaining noninvasive images, reducing X-ray exposure, utilizing quantitative programs routinely, performing more sophisticated analyses and enhancing or manipulating images has been tempered by broad experience in the hands of both clinicians and investigators. Even though successes of differing degree have been achieved in all these stated areas, the most significant and unique contribution over film-based methods is that digital angiography provides live-time images available for immediate review, manipulation and analysis. It lets the angiographer, especially one involved in interventional techniques, use subjective or quantitative image data during the procedure to tailor the course of the study and document the results. Quantitation beyond simple measurements can be performed easily (roughness, flow reserve, etc). There are several unmet challenges, however, that stand in the way of greater utilization of this technology. Archival of digital images is slow, expensive, sometimes unreliable and generally incompatible from system to system. Issues about necessary matrix sizes, achievable resolution and image quality are not resolved. Available software is highly variable and often poorly documented or validated. Utilization of the new technology is often more cumbersome and less "user friendly" than using standard cineangiographic methods. This fosters resistance among technicians and clinicians to learn the methods of digital angiography. Finally, and perhaps most important, it must be recognized that an impaired ejection fraction and the presence of left main or triple vessel coronary disease are angiographic parameters of proven prognostic importance. Yet many clinicians are not compelled to do much more than only qualitatively "eyeball" these important parameters. The motivation to routinely quantitate even more sophisticated indexes is obviously proportionately less. Therefore, the rapid and accurate quantitation provided by digital angiography will continue to fail to justify more widespread clinical use of the technology until the need for such quantitation can be shown to be

J. H. C. Reiber and P. W. Serruys (eds), Quantitative Coronary Arteriography, 23–42.

not just of prognostic importance but perhaps also of medicolegal importance. It may well be that more stringent quality assurance requirements for documentation of the accuracy of interpretations of cardiac catheterization studies and the appropriateness of the clinical-decisions based upon these analyses (referral to surgery, angioplasty etc.) will be necessary to increase the utilization of digital cardiac angiography.

Introduction

This review is intended to summarize the existing and potential advantages and disadvantages of digital angiography as it relates specifically to coronary assessment. Even after 10 years of clinical usage, the facts in this chapter must be laced with a generous number of opinions and hopes held together by a good deal of optimism. A view is developed that suggests that technological and scientific developments are not the sole determinants of the fate of digital coronary angiography. Greater accountability for invasive procedures and quality control issues may well play an equally important and parallel role in promoting the transition to greater utilization of digital angiography.

Advantages of digital angiography

The biggest advantages of digital angiography are the following: (1) images are available immediately without the need to use film or wait for its development; (2) images can be subjected to contrast and edge enhancement or subtraction algorithms immediately; (3) selected frames can be used to create roadmaps; (4) stenoses can be analyzed with resident software so that results are available during the procedure or immediately thereafter and these analyses can be either simple or sophisticated in nature; (5) results available during the catheterization can, in an interactive fashion, help to modify or change the execution of the rest of the catheterization (eg. obtain better views, perform immediate angioplasty, select size of balloon, stent, burr, laser, angioscope or flow measuring devices, determine need for pacing or perfusion studies, etc.); (6) sophisticated perfusion studies can be performed with the resident software; (7) the study is not subject to vagaries of film development or problems that might ruin film; (8) quantitative programs can be applied in the absence of increased noise inherent in digitizing film images; (9) images and quantitative output can be specifically corrected for pincushion distortion that affects morphometrics, and scatter and veiling glare as well as other factors that affect videodensitometry; (10) computerization of X-rays allows novel applications that can decrease dose and redundant data or improve image quality at similar overall dosing levels; (11) an entire catheterization report can be generated as soon as the procedure is done; (12) this report can be accompanied by hardcopy images; (13) the report can

be accompanied by a video tape of the entire procedure or nondegraded digital copies of a few of the most important of the original images; and (14) the images may be transmitted remotely and integrated with other clinical image and nonimage information (Table 1).

One of the most important advantages of digital angiography is that it provides images of diagnostic quality that can be viewed immediately during the course of a cardiac catheterization study thereby providing information that might potentially alter the course of the examination itself or expedite the delivery of clinical care. For example, if insufficient or inadequate views are identified by review of the digital acquisitions during the procedure, more views in different projections may be obtained immediately thereby improving the comprehensiveness and adequacy of the catheterization. The study will not be subject to potential and unforeseen difficulties in film development that might ruin or compromise the diagnostic quality of the images. More importantly, it is becoming more common, due to logistical advantages and efforts to minimize patient admissions, to proceed immediately to angioplasty instead of waiting to develop and analyze film and then to schedule a second admission for the angioplasty itself. Since standard video chains and video-taped images are not always of diagnostic quality, expedited angioplasty at the time of the initial catheterization is best decided upon from the high quality digital image playback. Images can even be quantitated at that time and comparative calculations can be made immediately after the procedure. This provides an important documentation of the rationale for the angioplasty and hard evidence of the immediate anatomical (and sometimes functional) improvement provided by the intervention. In some cases, this ability may

Table 1. Existing and potential advantages of digital angiography.

1) images available immediately
2) contrast and edge enhancement or subtraction algorithms improve conspicuity
3) roadmaps aid interventional procedures
4) stenoses can be analyzed with resident software (both simple and sophisticated parameters)
5) immediate result helps to modify the catheterization
6) perfusion studies are possible
7) avoid cost and pitfalls of film and its processing
8) quantitative programs can be applied in the absence of increased noise inherent in digitizing film images
9) specific correction for pincushion distortion and scatter and veiling glare
10) novel applications that can decrease x-ray dose and redundant data or improve image quality at similar overall dosing levels
11) catheterization report can be generated as soon as the procedure is done
12) accompany report with hardcopy
13) provide video tape of the entire procedure or nondegraded digital copies of most important original images
14) remote transmission, review and integration with other clinical image and nonimage information

give an early clue to the presence of a suboptimal dilatation and this might lead to consideration of repeating the dilatation or using a larger balloon or a different device (burr, laser, stent etc).

Once developed, the quality of a standard cineangiogram cannot be changed. In contrast, digital angiograms can be subjected to powerful, even though simple, image processing techniques that may assist decision making in individual cases. For example, roam and zoom functions may allow more detailed analysis of lesions suspected of having complex features, thrombi or dissections after angioplasty. Filtration techniques may be used to either smooth out image noise or enhance edges thereby improving the subjective appreciation of the arteriographic information. Image contrast may be altered to allow better visualization of arteries and lesions. In studies devoid of patient motion, mask subtraction may aid in increasing conspicuity and contrast resolution.

For practitioners of angioplasty, roadmapping, either by provision of several optimal guiding shots on different monitors or by interlacing such images with live-time fluoroscopic images has proven extremely valuable as an aid to proper balloon placement. Quantification of images before and after the procedure is of value for documentation of results. In addition, quantitation may be important for initial sizing and selection of the devices to be used. This will be increasingly important as angioscopes, echocardiographic catheters, new flow measuring devices and stents become more commonly used during angiography.

Aside from the potential to alter or improve the immediately available image, another major advantage of digital coronary angiography is that the digital format expedites interrogation of the image data by either simple or sophisticated techniques. For example, simple percent diameter or percent area stenosis measurements can be made easily [1]. With simple calibration of the image by the use of a grid or the coronary catheter, absolute lumenal dimensions of the "normal" and stenotic segments may be obtained equally easily. The component analysis methodology of Kirkeeide et al. [2] can also be applied to provide a rapid indication of the theoretical flow reserve associated with any single lesion before and after an intervention. This measure, although theoretical, may be of greatest value in helping incorporate the effects of length of a single lesion into the overall potential effects that it may have on the functional adequacy of coronary blood flow. As evidence continues to accumulate about the prognostic importance of lesion complexity, methods other than subjective and categorical indexes of complexity may be more suited to defining this factor in a more precise, mathematical and sensitive way [3, 4]. This may also prove to be more useful for assessing subtle changes induced by either mechanical or pharmacologic means. Although all these methods can be performed after digitizing film images, the latter is extremely time-consuming and has remained suitable only for research purposes. Moreover, the process of digitization of film introduces another source of noise that contributes to the high noise frequency of

digitized film images and makes them more troublesome to quantitate than on-line digital images.

Although not yet totally refined, there are several methods now proposed for measuring actual coronary flow dynamics from digital arteriograms. These are outlined in other chapters in this book. These methods, coupled with the morphologic methods outlined above, will be extremely important since the role of the catheterization laboratory continues to change from documentation not just of morphological features but also of functional parameters of coronary artery disease [5—9]. The methods will be critical for assessing patients with moderate lesions, and confusing chest pain or exercise test results. In patients who cannot exercise these methods may compete with other non-exercise stress test methods such as dipyridamole thallium scanning.

Software programs currently available are extremely variable but by invoking good programming methods and with due regard to robustness and user-friendliness, technicians can be trained to use such programs easily and to perform nearly all of the simple and sophisticated quantitations. This would free up some of the angiographers' time.

Should sophisticated quantitation gain a foothold in clinical medicine then two further aspects of digital imaging make it the logical choice for routine utilization. First, pincushion distortion, albeit markedly reduced in newer radiographic systems, can be virtually eliminated by applying correction algorithms designed specifically for each imaging chain (10). These can correct the image by correcting the specific spatial distribution of the actual distortion without assuming strict radial symmetry of the pincushion effects. Secondly, accurate videodensitometry, a longstanding desire in clinical cardiology, will require meticulous corrections for scatter and veiling glare and other undesirable effects (see below) [11, 12]. Digital methods promise that such corrections will be made rapidly and with regard to the actual image intensity of the image being analyzed. Linearization of the radiographic input and output signals will be easier with digital images and will not be prone to the nonlinear sensitometric characteristics of film [13, 14].

Greater computerization of the radiographic imaging chain will lead to the wiser use of X-rays. For example, Weiss et al. [15] have shown that staggered imaging of the coronaries, i.e. 30 frames per second (fps) during the first 1/3 of systole and 6 fps thereafter will diminish radiation dose and redundant image data without compromising the diagnostic quality of the study. Alternatively higher doses per frame could improve image characteristics without increasing overall radiation exposure. Dual energy imaging may provide remarkable image quality that is not marred by misregistration typical of standard temporal subtraction methods [11].

With the advent of larger and more efficient networks, the ability to remotely transmit any digital image may be important for assisting in making a comprehensive patient assessment. Remote viewing of angiograms, exercise radionuclide images, echocardiographic test results and data from the history

or physical examination might be most conveniently collated in digital format. This would also, parenthetically, set the stage for utilization of programs designed to factor in all of the information in quantifiable ways and thereby assist in making diagnostic and therapeutic decisions. Implications for allowing greater ease and comprehensiveness when dictating and transferring final reports and summaries also should not be ignored. Such reports could be accompanied by identical, undergraded digital copies of the original diagnostic images. Several far-reaching implications of such capabilities have already been demonstrated in noncardiac imaging settings [16].

Limitations of digital angiography

Despite these attractive features, there are still substantial impediments to the full scale acceptance of digital coronary angiography. These include: (1) unresolved issues of spatial resolution; (2) unresolved issues of archival and data retrieval and transmission including the costs of such; (3) robustness of image processing methods and proneness to misregistration artifacts; (4) incompatibility of system; (5) lack of fully automated methods for edge extraction and rapid quantitation; (6) lack of a system optimized solely for digital angiography; (7) additional equipment must be purchased and is generally an "add-on" leading to potential difficulties with interfaces and compatibility; (8) additional training is required to make both physicians and operators comfortable with the existing operating systems and software packages; (9) depending on the manufacturer, acquisition of images may require execution of numerous computer commands and result in delays especially if the support personnel are unfamiliar with the routines; (10) software analyses and their validation are quite variable and often not comprehensive enough to perform all functions necessary for image manipulation and analysis (eg. EF, wall motion, end-systolic pressure-volume calculations, valve gradients, etc.); (11) the technology continues to evolve so that potentially costly upgrading of the system may be expected; (12) typical consoles are not suitable for catheterization conference; 13) video tape archival and display of digital images is not optimal; (14) new personnel (programmers, word processors, database managers, system analysts, vendor liaisons) may offset whatever savings might have accrued from a digital laboratory; (15) the cost of video display monitors and workstations and the ease of their use for comparing serial studies or retrieving old studies is of significant concern; and (16) videodensitometry may or may not be achievable in clinically practical ways and remains a large question mark (Table 2).

A few of these limitations are probably more theoretical than real. The first and most important relates to comparability of film and digital images and the perceived need for increased image resolution. Numerous studies are now available suggesting that even existing digital systems may be more comparable to film images than previously suspected on theoretical grounds. The key issues are twofold: first, the theoretical spatial resolution advantage

Table 2. Existing and potential disadvantages of digital coronary angiography.

1)	unresolved issues of spatial resolution
2)	unresolved issues of archival, retrieval, transmission and costs
3)	robustness of image processing methods and proneness to misregistration
4)	incompatibility of systems
5)	lack of fully automated methods for edge detection and quantitation
6)	lack of a system optimized solely for digital angiography ("add on")
7)	additional equipment expense
8)	additional training
9)	acquisition of images may require execution of numerous computer commands
10)	software analyses and their validation are quite variable and often not comprehensive
11)	costly upgrading
12)	typical consoles are not suitable for catheterization conferences
13)	video tape archival and display of digital images are not optimal
14)	new personnel (programmers, word processors, database managers, system analysts, vendor liaisons)
15)	the cost of video display monitors and workstations and the ease of their use
16)	videodensitometry may not be achievable

of film compared to digital images is based on high contrast test images that do not mimic actual in vivo performance, and second, several technical prerequisites are required in the acquisition and analysis of digital images before digital images can be expected to be comparable to film (use of standard radiographic doses, use of small focal spot size, use of 5 to 7 inch image intensifier, use of progressive scan video readout from a high quality camera, use of a high quality analog-to-digital converter, minimum matrix size of 512 × 512 pixels, automated analysis based on edge detection methods, appropriate magnification of digital images, and avoidance of temporal subtraction as a general rule). The following discussion summarizes the phantom and in-vivo experiments and clinical studies that support or challenge these views.

Comparative studies on digital and cinefilm approaches

Two important phantom studies merit review. LeFree et al. [17] used automatic quantitative arteriography to analyze cinefilm and digital radiographic images of an arterial phantom made of lucite and precision-drilled lumens ranging from 0.5 to 5.0 mm in diameter. Digitized and magnified film images were compared to digital images acquired using 512 × 512 and 1024 × 1024 matrixes and appropriately magnified. All three techniques were equivalent in measuring diameters with a high degree of overall accuracy ($r > 0.992$). All methods overestimated diameters below 1.0 mm, thereby confirming little improvement in spatial resolution of any of the methods. Videodensitometric analysis of the digital images outperformed film for measurement of relative areas ($r = 0.995$ vs $r = 0.940$, $p < 0.0032$).

A second phantom study was performed by Gurley et al. (18) who obtained

simultaneous film and 512 × 512 digital images of plastic arterial phantoms with lumens ranging from 0.9 to 4.7 mm and the stenoses ranged from 11 to 81% diameter stenosis. These were imaged after superimposing them on a phantom simulating the radiological characteristics of the human thorax. Images were not magnified and analyses were undertaken with hand-held calipers. Digital and cine analyses of percent diameter stenosis showed similar variabilities of 2.5 and 4.0%, respectively. Both methods showed mild underestimation of percent diameter stenosis with a mean difference of 3.9%. Both methods correlated equally well with the known percent diameter stenoses and the actual diameter narrowing ($r = 0.98$ for both techniques). The results of clinical studies, however, showed differences that are summarized below.

A unique, in-vivo validation study also directly compared digital and film images for coronary quantitation [1, 19]. This laboratory validated the algorithm used by LeFree et al. by inserting plastic cylinders with precision-drilled circular lumens ranging in diameter from 0.83 to 1.83 mm into the coronary arteries of anesthetized dogs. Images were obtained with the chest closed and during cessation of respiration. Film and 512 × 512 digital images were obtained consecutively in identical views. Analysis of absolute minimum diameters failed to demonstrate any superiority of film over digital imaging in quantitating these very small diameters. Moreover, film analyses showed a significantly greater standard error of the estimate for linear regression analyses of absolute dimensions than did digital analyses (0.24 vs 0.09 mm, $p < 0.03$).

Several clinical studies provide important insights into the differences between theoretical and actual deficiencies in existing digital imaging technology. Tobis et al. [20] reported a study in which different observers independently identified and measured focal coronary narrowings in using digital subtraction angiograms and standard 35 mm cineangiograms. The digital angiograms used 512 × 512 × 8 bit pixel matrix. Due to rapid evolution of digital hardware and software at that time, the study was undertaken in two parts. In Phase 1 of the study, 38 patients (35 with interpretable studies without misregistration artifacts) were studied with continuous fluoroscopic exposures and an interlaced camera readout of 30 frames per second. Images were subjected to subtraction using a blurred mask and then converted back to video tape. Two observers analyzed both these images and the corresponding 35 mm cineangiograms with manually operated calipers. Results within 10% were considered equivalent, otherwise results from the digital images were described as over- or underestimating the cineangiographic results which were used as the reference standard. The results demonstrated that agreement in quantitation within 10% occurred in 76% of cases. Underestimation by the digital technique occurred in 18% and overestimation in 6% of cases. While these results were quite favorable, the overall quality of film was better because the image acquisition parameters and processing methods resulted in substantial noise in the video images.

In Phase 2, 19 patients were studied with more advanced techniques. Pulsed radiographic mode and a progressive scan camera were utilized. In addition, only a single-frame mask was used and the observers were allowed to use an edge-enhancement algorithm and a 4x magnification algorithm. In this phase, 4 observers quantitated the paired cineangiograms and digital angiograms, again using hand-held calipers. The results showed no significant difference in the mean percent diameter narrowing for all the narrowings (53 ± 31% vs 52 ± 31%, digital vs film, respectively). No difference in variability of measurements between the 2 methods could be detected. In 2 patients, unsubtracted images were used due to excessive subtraction artifacts. It was apparent that even when the digital images were suboptimally processed by older methodologies, including using hand-held calipers, the digitally based quantitations compared quite favorably to the film-based results. This study suggested, however, that at least in some patients, misregistration continued to be a problem and that fluoroscopic exposure levels and interlaced camera readout were not optimal for digital applications in coronary quantitation.

Bray et al. [21] analyzed 32 lesions in 15 patients using the technique of high-pass temporal filtration digital subtraction with a real-time recursive processor and videotape storage and display. An interlaced camera readout, and radiographic exposure levels were utilized. A 480 × 792 × 8 bit image matrix and a framing rate of 30 Hz were used. Standard 35 mm cineangiograms were acquired simultaneously. Three observers using calipers analyzed the image sets and the overall results demonstrated a correlation coefficient of 0.73 with a standard error of the estimate of 9.1% diameter stenosis. The average severity (49% for film images and 47% for digital images) and the variability of the measurements (average standard deviation for film of 6.6% and for digital of 7.7%) were indistinguishable. Twenty-eight % of measurements were more than 10% different between methods and 5% were more than 20% different. This variability was substantially reduced when multiple observations were averaged and then compared.

The recursive filtration technique utilized by Bray and coworkers has several attractive characteristics. It is relatively economical with dedicated hardware because of minimal image memory requirements; the temporal filtration is automatic, requiring no operator input to select frames for masks, etc; results are seen in real-time without the need for post-processing; and the subtraction method is more tolerant of patient motion. This latter characteristic is due to the continually updated "moving mask" which is a weighted average of the old mask image and the new input image in a recursive loop. This has the effect of suppressing stationary image structures while the more rapidly moving contrast bolus and cardiac structures are selectively enhanced. The effect of slow respiratory motion, a common cause of misregistration artifact, is partially suppressed. Unfortunately, this methodology is not widely available and experience with it for coronary quantitation is limited. It is anticipated that problems with absolute videodensity measure-

ments may occur due to temporal differences in background subtraction across the image field. Nevertheless, for routine quantitation, this study was unable to demonstrate any striking loss of clinical information when digital imaging was compared to cineangiography. The study also confirms the merits of radiographic exposure levels and the authors suggest that progressive camera readout for such applications would improve results further.

Goldberg et al. [22] studied a total of 77 patients with mask-mode 512 × 512 × 8 bit, 30 frame per second digital angiography using boosted fluoroscopy (i.e. the tube current was between fluoroscopic levels and full radiographic levels and ranged between 10—30 mA). Single views were compared to standard cineangiography in 27 patients (95 arteries). Two angiograms agreed with visual assessment within one grade of severity in 84% of cases, including comparisons of normal segments. Multiple-view digital angiograms were compared in 50 patients (144 arteries) and visual agreement within one grade occurred in 90% including normal segments. It should be noted that the film images were acquired using magnification mode, whereas digital images were acquired in a 9 inch mode so that the entire coronary tree could be seen without panning to avoid misregistration artifact during subtraction. Use of the 9 inch mode has the effect of yielding a larger pixel size in the digital images, but despite this bias against the digital images, the comparisons outlined above were quite favorable. Moreover, the investigators reported that 95% of collateralized vessels noted on film images were also noted on the digital angiograms. The grade of the collateral vessels also agreed in 81% of instances with the cine assessment. As in the other studies, misregistration in several cases precluded analysis. Because only boosted fluorography was used, the authors stated that mask subtraction was mandatory to provide sufficient contrast resolution. One can conclude from this study that for practical purposes, the visual interpretation of coronary stenoses is quite comparable whether film or digital imaging is used.

Skelton et al. [23] examined the effects of digital image acquisition mode and subtraction techniques on the quantitation of cornary stenosis involving 100 discrete lesions in 45 patients. Each lesion was assessed from direct on-line digital, electrocardiogram-gated digital subtraction and digitized cine film images. Geometric measures of percent diameter stenosis and minimum lesion diameter showed correlations betwen 0.90 and 0.98 with slopes between 0.93 and 1.00. Thus, the measurements were not strongly affected by image acquisition mode or by electrocardiogram-gated digital subtraction. These geometrically drived results were superior to similar comparisons using videodensitometric techniques.

Gurley et al. [18] recently compared unprocessed digital angiograms and conventional cineangiograms for the diagnosis and quantification of coronary stenoses in both phantoms and clinical subjects. In contrast to the prior study, this group used unmagnified, 512 × 512 digital images and caliper quantification of the stenoses. The effects of image subtraction was not assessed and absolute minimum diameter measurements were not made.

Additionally, the two images were acquired simultaneously such that 85% of the image intensifier light intensity was used to expose film and only 15% of the light intensity was used to generate the digital image. While the differential sensitivity of the two may have made this splitting of the light signal adequate, definite confirmation of this was not provided. Even under these conditions, phantom studies showed no differences in performance between digital and film imaging (see above). In analysis of patient images, the overall interobserver variability was also equivalent. However, the authors noted that digital evaluation of percent stenosis in patients generally overestimated film results and that this overestimation was progressively more severe with milder lesions, lesions in vessels of less than 2 mm, and branch stenoses. This study underscores the need for each laboratory to ascertain the equivalence of the two imaging techniques under the specific or likely conditions of use. For the most part, the lack of automated quantitation, failure to use image magnification and potential diminution in light source for the generation of digital images leading to poorer signal to noise characteristics were potential biases against the digital imaging technique.

The reviewed studies suggest that analysis of digital and film based coronary angiograms is essentially equivalent when several factors are taken into account. In our experience, subtracted images yield results of equivalent precision but with slightly higher inter- and intraobserver variability even when gross misregistration is not evident. This increase is felt to be due to increased image noise and the potential presence of subtraction artifacts and, therefore, this laboratory does not recommend clinical use of subtraction techniques for coronary arteriography. Despite great advances in other aspects of digital imaging, misregistration artifact due to patient motion remains one of the commonest causes of image degradation and, therefore, the demonstrated accuracy of nonsubtracted quantitative digital angiography should enhance clinical implementation and acceptability. It is not yet clear whether the techniques outlined by Bray and coworkers or dual energy subtraction will overcome this problem.

Although film-based radiography has a very high theoretical resolution, numerous factors prevent attainment of this in clinical circumstances. The difference in attenuation coefficients between iodinated contrast medium and tissues is not great and may perturb edge-detection in areas with significant variations in background density. The usual measurement of the resolving power of a system by using tungsten wires or lead strips does not truly reflect the much poorer object contrast in coronary angiograms. Moreover, the usable spatial resolution of film, considering the physical properties of cesium iodide image intensifiers, the effects of the main objective lens in the image distributor and the cinecamera optics, is markedly deteriorated from the theoretical intrinsic resolution of cinefilm. Under some conditions, usable spatial resolution of film is approached by that of a high quality video pickup tube [24]. A second major factor is that the automated edge-detection scheme used in our investigation [1, 17] was optimized for the noise fre-

quency of digital images. It should also be recognized that the reported investigations used different imaging systems, film types and processing methods. Different processing systems and film types may alter the accuracy compared to digital images. Thus, the small differences shown in some studies may not apply under all circumstances and in all laboratories as evidenced by the work of Skelton and Gurley. Moreover, in spite of these differences, the relation between commonly measured parameters of coronary stenosis and reactive hyperemia have been shown to be equivalent amount modalities, suggesting that no major clinical differences are present [1].

It should be noted that all of the studies described above which compared the performance of quantitative arteriography from film to that from digital images have utilized digital images with a matrix density of no greater than 512 × 512. Metriculous studies using a matrix density of 1024 × 1024 have failed to demonstrate any substantive improvement in quantitative accurracy when used in currently available X-ray systems [17, 25—28].

Archival and retrieval of digital data

The issues of matrix size and usable resolution impact directly on another major unsettled issue in this field, that of archival and retrieval of digital data. A comprehensive discussion of this issue is provided by Cox and Dwyer [29]. Typically, a complete patient examination might entail a minimum of 5 to 6 coronary arteriograms, each lasting 5 to 10 seconds. Thus, at 30 frames per second and using a 512 × 512 bit matrix, this will yield about 500 megabytes of data. In a laboratory performing 1000 cases per year, the archival load would be in the 500 gigabyte range. Four times this amount would result by using 1024 × 1024 matrixes. These demands could be minimized by using lower frame rates, staggered acquisition frame rates [15], data compression [29], spatial multiplexing [30] or adaptive differential pulse code modulation [11]. Optical and/or digital tapes appear to be the most promising methods for digital archival demands of this magnitude. Long-term stability of these media has not been tested and the possible need for routine updating of images archived on these media has been raised [30]. Some existing laboratories use videotapes for long term storage at the expense of some short and long term degradation of image quality. Post-processing of videotaped digital images will be less than optimal. Some technologies (eg CT, MRI) record the digital images on film. Although this appears counterproductive to the goal of eliminating the costs of film, the advisability or costs of completely digital storage remain serious questions that are not nearly solved [31]. The attractiveness of simultaneous digital and cine imaging is therefore evident during this time of tremendous uncertainty [11, 18]. An alternative would be the provision of simultaneous digital and video recording. This would obviate the use of film and the time needed to develop it. This archival would be at a reasonable cost and widely compatible. Since post-processing of video

images might be less than optimal, the angiographer might need to make a decision about the likelihood of this need and use both digital and video tape archival in selected cases. Simultaneous digital recording on disc and digital tape might also be an attractive alternative.

Digital subtraction techniques

The availability of temporal subtraction methods such as mask mode and time interval difference methods provided an exciting and important contribution in cardiology primarily in the study of ventricular function using low doses of contrast material. Even in this application and especially in coronary applications, the susceptibility of temporal techniques to misregistration artifact has remained one of the most nettlesome problems in digital angiography. So much so that, in general, coronary arteriography using standard forms of temporal subtraction are not recommended. Continuing work in dual energy subtraction imaging, however, may eventually be incorporated clinically. The method promises to be more robust than standard temporal subtraction methods by being immune to spatial misregistration artifacts [11]. Dual-energy subtraction is not sensitive to either patient or cardiac motion because the two images to be subtracted are acquired in rapid succession. A weighted subtraction of a high energy image (approximately 120 kVp) and a low energy image (approximately 60 to 70 kVp) results in a subtraction image in which soft tissue contrast is absent. Image contrast due to bone is still present but appears to interfere minimally with visualization and can be mathematically corrected during quantitative analysis. It should be stressed that the signal-to-noise ratio of such images is inferior to that provided by temporal subtraction methods not marred by misregistration. Therefore, the method only outweighs temporal subtraction techniques when misregistration is present. Since this occurs commonly during coronary arteriography even with EKG-gated mask mode subtraction, the dual energy approach is extremely attractive. The method may also be used to advantage for ventriculography, especially exercise studies.

Coronary quantitation; edge definition and densitometry

Although digital angiography lends itself to both simple and complex quantitation, the lack of automation of this process is a major impediment to the routine and comprehensive use of quantitative methods. Advances in edge-detection are being made using sophisticated programming methods. The method of LeFree et al. [17], for example, is robust and easy to use and can be applied quite quickly for coronary quantitation. Similar strides must be made in ventriculographic edge detection methods to enhance utilization of the programs [32, 33].

Coronary videodensitometry using digital angiography can be considered one of the great advantages but also one of the existing disadvantages, or more properly, frustrations of digital angiography. The following clinical studies highlight some of these frustrations.

Wiesel et al. [34] evaluated a combined geometric and videodensitometric approach for measuring stenoses created in dogs. They used edge detection applied to the normal segment and videodensitometry applied to the stenosis to determine the absolute lumenal cross-sectional area by the following relationship: stenotic area = An × (1 − S/100), where An is the area of a normal segment determined geometrically and S is the relative stenosis severity based on the density profiles over the normal and stenotic segments. Relatively few stenoses were imaged and the minority were truly irregular. A moderately good correlation could be shown with known lesion area and the combined edge detection/videodensity approach ($r = 0.76$, standard error = 0.71 mm^2, absolute area deviation = 0.65 mm^2).

Tobis and coworkers [35] studied 19 patients before and after percutaneous transluminal coronary angioplasty (PTCA). They compared geometric and videodensitometric stenosis measurements obtained from digital angiograms. Although intimal tears and dissections are expected to make edge detection methods inaccurate after angioplasty, in fact, the mean stenosis measurements by either technique both before and after angioplasty were not significantly different. Interobserver variability was similar in each method. Since videodensitometry should, in theory, provide a rotationally invariant assessment of percent stenosis, they also compared results from orthogonal views of single lesions. Although the densitometry showed a good correlation of results, the performance of the edge detection methodology was no worse. There was, therefore, no apparent added value of densitometry in this clinical application.

Klein and coworkers [36] provided a pathoanatomic validation of videodensitometric analyses in 15 stenotic segments of excised human coronary arteries imaged by digital techniques. These investigators showed good results with videodensitometry when percentage area narrowing results were compared to analyses of pathologic sections ($r = 0.93$). This performance was somewhat better than a similar comparison using purely geometric methods. Measures of absolute area narrowing were not undertaken.

Sanz et al. [37] analyzed 13 consecutively acquired biplane digital subtraction angiograms before and after PTCA to determine intra- and interobserver variability of absolute lesion diameter, relative videodensitometric cross-sectional area, automated percent diameter stenosis and visual percent diameter stenosis. Both before and after angioplasty, measures of absolute diameter showed less interobserver variability than densitometry or percent automated diameter stenosis measurements. Importantly, in these routinely acquired clinical images, relative videodensitometric cross-sectional area correlated poorly with images from the orthogonal view.

Skelton and coworkers [23] undertook a large clinical study of 100 discrete lesions in 45 patients. Comparisons were made among direct on-line

digital, electrocardiogram-gated digital subtraction and digitized cinefilm images. Videodensitometric percent area stenosis data showed correlation coefficients among the different modalities between 0.80 to 0.89. These correlations were less and the apparent variability was greater than for similar comparisons of geometric measurements. No real gold standard was available to evaluate the significance of these results, but the investigators pointed out that many more factors contribute to nonlinearity of cineangiograms than on-line digital images. Other experience suggests that the inferior relation between film-derived and on-line digital-derived videodensitometric measurements is a result of larger errors in the film-derived data [17].

Katritsis et al. [38] studied 73 lesions in 63 patients who had undergone coronary anigoplasty. Digital subtraction coronary angiograms were analyzed with an automated border-detecting computer program capable of simultaneous geometric and densitometric cross-sectional area estimation. They showed good agreement between geometric and densitometric area percent stenoses calculated by the program on the pre-PTCA digital angiograms. After PTCA, however, important discrepancies between the two methods existed. Densitometric evaluation demonstrated a significantly greater mean coefficient of variation between different views after PTCA, but not before. This degree of variation was much larger than noted for geometric evaluations on the same views. The results are similar to those demonstrated by Sanz et al. [37] except for the finding that the deficiencies in densitometry from different views was limited only to the post-PTCA analyses. In general, although the distortion of the vessel lumen after angioplasty is assumed to render geometric methods potentially inaccurate, the altered geometry after angioplasty cannot fully explain the results of Katritsis and coworkers since a high degree of variability was not noted for geometric measurements either before or after angioplasty. The authors postulated that distortion of the vessel as a result of angioplasty may have interfered with the mixing of contrast medium and blood, hence invalidating any assumptions about uniform dye distribution, and thereby also invalidating densitometry measurements. Further studies will be required to more fully elucidate these practical problems.

The above studies were performed either in in-vivo models, in-vitro models of actual human coronary arteries, or patients undergoing routine catheterization. They represent extremely rigorous tests of the current applicability of densitometry in clinical practice. The results, although in general promising, are quite different from the excellent results noted almost routinely in phantom studies or in studies using highly selected images demonstrating optimal background conditions, meticulous density calibrations to ensure linearity, and absence of foreshortening of either normal or stenotic segments [17, 39—42]. In biplane images, one must be confident that the long axis of the lesion and normal segments are parallel to the image intensifier planes and perpendicular to the X-ray beams. This "triple orthogonality" can be achieved in new generation catheterization laboratories [43]

and the process can be automated substantially in digital catheterization laboratories [44].

At this point, it is felt that the role of videodensitometry should be in rapid calculation of relative cross-sectional areas in a single view, and if repeated studies are anticipated, then the same view must be utilized to avoid large errors due to potential differences in foreshortening, background, veiling glare, and scatter. The latter problems are spatially variable within isolated frames and temporally variable as contrast moves in and out of the field, and as brightness automatically changes in response to different background caused by panning. Accordingly, substantially increased efforts will be required before robust methods are devised that will allow for successful and rapid clinical application of videodensitometric techniques even with on-line digital images.

Nevertheless, digital angiography is the milieu within which these problems may be solved and allow more accurate implementation in the clinical setting. For example, Van Lysel et al. [11] have outlined potential, practical solutions to the influences of scatter, veiling glare, detector nonuniformity, heel effect, and beam hardening on videodensitometry. Scatter and veiling glare are modeled as convolutions of the primary transmission with point spread functions that are dependent on patient thickness. Empirical solutions to the problem using a spatially variable weighting of a scatter and glare image modeled by convolving the detected image were proposed. Corrections for nonuniformity (caused by curved image intensifier input surface) and anode heel effects were also proposed. Solutions involve dividing the detected image by a previously stored uniformity template. The uniformity template is formed by simply making an exposure with no scattering material in the beam at appropriate kVp and geometry. Beam hardening effects have been estimated to be small and bone residual is removed from dual energy images by subtracting the intensity integral of the bone signal over the region of interest [45].

Future of digital angiography

Another disadvantage is that digital angiography is an evolving technology making current systems vulnerable to obsolescence or costly upgrades. Importantly, most systems are "add on" and not necessarily optimized for digital imaging [30, 46—48]. Finally, it is currently questionable whether costs saved by not using film and by diminishing physician and technician time will be significant especially if new personnel such as database managers, system analysts, and wordprocessors are required to complement cardiac catheterization technicians [48]. The costs of setting up display monitors and/or work stations may be formidable. And there is currently some question about the ease of use of terminals for review and communication of study results.

Although much of the ultimate acceptance of the technology will be determined by engineering and scientific developments, it is worth emphasizing that these developments should ideally also be paralleled by an increased desire on the part of the clinician to perform quantitation during or immediately after a procedure. The desire to do this is currently not intense and this is not due solely to practical, technical issues. For example, despite the prognostic importance of relatively unsophisticated parameters such as the ejection fraction, many laboratories still "eyeball" this parameter even though it is incredibly simple to measure. Similarly, it is well known that visual interpretation of lesion severity is not reproducible or accurate and does not reliably predict the physiologic importance of a lesion. Yet subjective interpretations are still the norm and delivery of care is based on these decisions. Although clinicians have hidden behind the excuse of lack of a practical means of performing such analyses, digital methods are rapidly removing this excuse. In short, the current clinical practice of cardiac catheterization is characterized by an appalling lack of reproducibility and quality control of the data generated during the procedures. As a result, the adequacy of the interpretations and the quality of the decisions made from these interpretations is very difficult to judge. If professionals do not impose upon themselves an adequate degree of quality assurance and self-policing, it may not be long before licensing bodies and health insurance providers will begin to demand it. Ironically, these forces may do more to speed the integration of cardiac digital angiography into clinical practice than any of the scientific and technical advances already or soon to be achieved through this methodology.

References

1. Mancini GBJ, Simon SB, McGillem MJ, LeFree MT, Friedman HZ, Vogel RA; Automated quantitative coronary arteriography: morphologic and physiologic validation in vivo of a rapid digital angiographic method. Circulation 2: 452—460, 1978.
2. Kirkeeide, RL, Gould KL, Parsel L: Assessment of coronary stenoses by myocardial perfusion imaging during pharmacologic coronary vasodilation. VII. Validation of coronary flow reserve as a single integrated functional measure of stenosis severity reflecting all its geometric dimensions. J. Am Coll Cardiol 7: 103—113, 1986.
3. Ambrose JA, Hjemdahl-Monsen CE: Arteriographic anatomy and mechanisms of myocardial ischemia in unstable angina. J Am Coll Cardiol 9: 1397—1402, 1987.
4. Simon SB, LeFree MT, McGillem MJ, Kalfbleisch SJ, Anselmo EG, Sitomer J, DeBoe SF, Ellis S, Mancini GBJ: automated morphometric analysis of coronary artery lesions: an extension of quantitative coronary arteriography. Comput Cardiol, 1988: 347—350.
5. Bürsch JH, Heintzen PH: Evolving role of digital cardiac imaging: Historical perspectives. Am J Cardiac Imag 2: 16—25, 1988.
6. Ratib O, Rutishauser W: Recent developments of cardiac digital radiography. Int J Cardiac Imag 1: 29—40, 1985.
7. LeGrand V, Mancini GBJ, Bates ER, Hodgson JMcB, Gross MD, Vogel RA: Comparative study of coronary flow reserve, coronary anatomy and results of radionuclide exercise tests in patients with coronary artery disease. J Am Coll Cardiol 8: 1022—1032, 1986.

8. LeGrand V, Hodgson J McB, Bates ER, Aueron FM, Mancini GBJ, Smith JS, Gross MD, Vogel RA. Abnormal coronary flow reserve and abnormal radionuclide exercise test results in patients with normal coronary angiograms. J Am Coll cardiol 6: 1245—1253, 1985.
9. LeGrand V, Aueron FM, Bates ER, O'Neill WW, Hodgson JMcB, Mancini GBJ, Vogel RA: Value of exercise radionuclide ventriculography and thallium-201 scintigraphy in evaluating successful coronary angioplasty: Comparison with coronary flow reserve, translesional gradient and percent diameter stenosis. Europ Heart J 8: 329—333, 1987.
10. LeFree MT, Simon SB, Lewis RJ, Bates ER, Vogel RA: Digital radiographic coronary artery quantification. Comput Cardiol: 1985 99—102.
11. Van Lysel MS, Ergun DL, Miller WP, Toggart EJ, Cusma JT, Peppler WW, Molloi S, Mistretta CA: Cardiac digital angiography and dual-energy subtraction imaging: Current and future trends. Am J Cardiac Imag 1: 254—266, 1987.
12. Shaw C-G, Ergun DL, Myerowitz PD Van LySel MS, Mistretta CA, Zarnstorff WC, Crummy AB: A technique of scatter and glare correction for videodensitometric studies in digital subtraction videoangiography. Radiology 142: 209—213, 1982.
13. Corney GM; Sensitometric properties of radiographic films. In: The physics of medical imaging: recording system measurements and techniques. AG Haus (Ed.), American Institute of Physics, New York, 1979: 72—82.
14. Haus, AG: Sensitometric techniques in medical imaging. In: The physics of medical imaging: recording system measurements and techniques. AG Haus (Ed.), American Institute of Physics, New York, 1979: 83—104.
15. Weiss M, Bellotti J, Shiting J, Vas R, Nivatpumin T, Forrester J: Staggered acquisition: Improved coronary angiographic images at lower X-ray dose. Circulation 70 (Suppl II): IO-325, 1983. (Abstract)
16. De Simone DN, Kundel HL, Arenson RL, Seshadri SB, Brikman IS, Khalsa SS, Davey MJ, Brisbon NE: Effect of a digital imaging network on physician behavior in an intensive care unit. Radiology 169: 41—44, 1983.
17. LeFree MT, Simon SB, Mancini GBJ, Bates ER, Vogel RA: A comparison of 35 mm cine film and digital radiographic image recording: Implications for quantitative arteriography. Invest Radiol 23: 176—183, 1988.
18. Gurley JC, Nissen SE, Booth DC, Harrison M, Grayburn P, Elion JL, DeMaria AN: Comparison of simultaneously performed digital and film-based angiography in assessment of coronary artery disease. Circulation 78: 1411—1420, 1988.
19. Mancini GBJ: Morphologic and physiologic validation of quantitative coronary arteriography utilizing digital methods. In: New developments in quantitative coronary arteriography. JHC Reiber, PW Serruys (Eds.), Kluwer Academic Publishers, Dordrecht, 1988: 125—141.
20. Tobis J, Johnston, WD, Montelli S, Henderson E, Roeck W, Bauer B, Nalcioglu O, Henry, W: Digital coronary roadmapping as an aid for performing coronary angioplasty. Am J Cardiol 56: 237—241, 1985.
21. Bray BE, Anderson FL, Hardin CW Kruger RA, Sutton RB, Nelson JA: Digital subtraction coronary angiography using high-pass temporal filtration: a comparison with cineagiography. Cathet Cardiovasc Diagn 11: 17—24, 1985.
22. Goldberg HL, Moses JW, Fisher J, Tamari I, Borer JS: Diagnostic accuracy of coronary angiography utilizing computer-based digital subtraction methods; Comparison to conventional cineangiography. Chest 90: 793—797, 1986.
23. Skelton TN, Kisslo KB, Mikat EM, Bashore TM: Accuracy of digital angiography for quantitation of normal coronary luminal segments in excised, perfused hearts. Am J Cardiol 59: 1261—1265, 1987.
24. Mistretta CA; X-ray image intensifiers. In: The physics of medical imaging: recording system measurements and techniques. AG Haus (Ed.) American Institute of Physics, New York, 1979: 182—205.

25. Goldberg HL, Moses JW, Borer JS, Fisher J, Cohen B, Skelly NT, Carter J: The role of digital substraction angiography in coronary and bypass graft arteriography. Circulation 66 (suppl II): 11—229, 1982 (Abstract).
26. Ovitt TW, Newell JD: Digital subtraction angiography: Technology, equipment and techniques. Radiol Clinics of N Amer 23: 177—184, 1985.
27. Carmody RF, Yang PJ, Seeger JF, Capp MP: Digital subtraction angiography: Update, 1986, Invest Radiol 21: 899—905, 1986.
28. Mistretta CA, Peppler WW: Digital cardiac X-ray imaging: Fundamental principles. Am J Cardiac Imag 2: 26—39, 1988.
29. Cox GG, Dwyer SJ: Archiving digital formatted image data. In: Clinical applications of cardiac digital angiography. GBJ Mancini (Ed.), Raven Press, New York, 1988: 37—54.
30. Brennecke R: Digital imaging systems for coronary angiography. In: New developments in quantitative coronary arteriography. JHC Reiber, PW Serruys (Eds.), Kluwer Academic Publishers, Dordrecht, 1988: 1—12.
31. Don C: the future of radiography: Casetteless or filmless: J Can Assoc Radiol 39: 83—90, 1988.
32. Tehrani S, Weymouth TE, Mancini GBJ: Knowledge-guided left ventricular boundary detection. In: Proceedings of Applications of Artificial Intelligence VII, SPIE Technical Symposium on Aerospace Sensing, Orlando, 1989: 503—514.
33. Tehrani S, Weymouth TE, Mancini GBJ: An application of the blackboard architecture to left ventricular boundary detection. In: Proceedings of Computer Vision Pattern Recognition, San Diego, June 1989: 342—347.
34. Wiesel J, Grunwald AM, Tobiasz C, Robin B. Bodenheimer MM: Quantitation of absolute area of a coronary arterial stenosis; experimental validation with a preparation in vivo. Circulation 74: 1099—1106, 1986.
35. Tobis J, Nalcioglu O, Iseri L, Johnston WD, Roeck W, Castlemon E, Bauer B, Montelli S, Henry WL: Detection and quantitation of coronary artery stenoses from digital subtraction angiograms compared with 35-millimeter film cineangiograms. Am J Cardiol 54: 489—496, 1984.
36. Klein LW, Agarwal JB, Rosenberg MC, Stets G, Weintraub WS, Schneider RM, Hermann G, Helfant RH: Assessment of coronary artery stenoses by digital subtraction angiography: a pathoanatomic validation. Am Heart J 113: 1011—1017, 1987.
37. Sanz ML, Mancini GBJ, LeFree MT, Mickelson JK, Starling MR, Vogel RA, Topol EJ: Variability of quantitative digital subtraction coronary angiography before and after percutaneous transluminal coronary angioplasty. Am J Cardiol 60: 55—60, 1987.
38. Katritsis D, Lythall DA, Anderson MH, Cooper IC, Webb-Peploe MM: Assessment of coronary angioplasty by an automated digital angiographic method. Am Heart J 116: 1181—1187, 1988.
39. Kruger RA: Estimation of the diameter of an iodine concentration within blood vessels using digital radiography devices. Med Phys 8(5): 652—658, 1981.
40. Simons MA, Kruger RA: Vessel diameter measurement using digital subtraction radiography. Invest Radiol 20: 510—516, 1985.
41. Simons MA, Kruger RA, Power RL: Cross-sectional area measurements by digital subtraction videodensitometry. Invest Radiol 21: 637—644, 1986.
42. Simons MA, Bastion BV, Bray BE, Dedrickson DR: Comparison of observer and videodensitometric measurements of simulated coronary artery stenoses. Invest Radiol 22: 562—568, 1987.
43. Wollschläger H, Zeiher AM, Lee P, Solzbach U, Bonzel T, Just H: Optimal biplane imaging of coronary segments with computed triple orthogonal projections. In: New Developments in Quantitative Coronary Arteriography. JHC Reiber, PW Serruys (Eds.) Kluwer Academic Publishers, Dordrecht, 1988: 13—21.
44. Sitomer J. Anselmo EG, Feldt DA: On line mathematical model of bi-plane X-ray gantry. Comput Cardiol 1987: 659—662.

45. Naimuddin S, Hasegawa B, Mistretta CA: An improved convolution algorithm for scatter correction. Med Phys (in press).
46. Morris KG: A perspective: Designing the all digital cardiac catheterization laboratory. Am J Cardiac Imag 2: 251—258, 1988.
47. Alderman EL, Guthaner DF: Digital subtraction angiography in the evaluation of cardiac disease. Invasive Cardiology 317—335.
48. Smathers RL, Brody WR: Digital radiography: Current and future trends. Br J Radiol 58: 285—307, 1985.

3. Advantages and limitations of videodensitometry in quantitative coronary angiography

J. S. WHITING, J. M. PFAFF and N. L. EIGLER

Summary

Quantitative angiography of coronary arteries using densitometry is less sensitive than edge detection to variations in imaging system resolution, quantum noise, and stenosis cross-sectional shape. In theory, densitometry more directly measures stenosis cross-sectional area which is more closely related than vessel diameter to coronary flow of hemodynamics. However, densitometry is much more sensitive than edge detection to densitometric non-linearities, oblique projection of the artery, and overlap with other structures. The potential error from each of these sources is large, perhaps as much as 50%. Overlap and obliquity problems can often be identified by inspection of the angiogram and can be reduced by careful selection of radiographic views, although in many cases lesions are located such that it is impossible to obtain views which avoid both overlap and obliquity.

Important progress has been made recently on the correction of densitometric error due to scatter and veiling glare. The most promising approaches use a blurred and scaled version of each image to produce an estimate of scatter and veiling glare which is then subtracted from the raw images. Initial results with this type of algorithm appear able to reduce the densitometric error in coronary cross-sectional areas to less than 10%. Thus, at the present time it seems possible to perform quantitative densitometric angiography with a total error between 5 and 20%. Densitometric error depends on factors which differ from those influencing edge detection, and therefore the information from stenosis densitometry may be used to complement that from edge detection.

Introduction

The coronary angiogram contains X-ray intensity data which may be used to calculate the cross-sectional area of a coronary artery or stenosis from a single view, even if the cross-sectional shape is highly irregular. In this

J. H. C. Reiber and P. W. Serruys (eds), Quantitative Coronary Arteriography, 43—54.

review, we summarize the advantages and limitations of densitometry, discuss the magnitude of error due to each of the factors to which this method is sensitive, and review methods for minimization of these errors.

The basic advantage of densitometry is illustrated in Figure 1, which shows that, in principle, a single plane densitometric profile determines the cross-sectional area of even a highly eccentric lesion. The practical realization of this approach, however, is far from straightforward. Figure 2 shows a

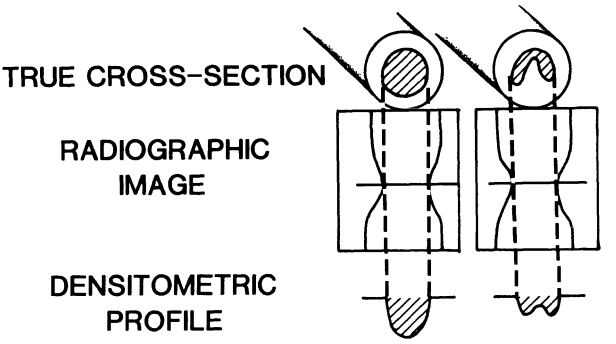

Fig. 1. This schematic illustrates the concept of densitometry for quantitative coronary angiography. The lumen on the left is circular, while that on the right is crescent-shaped, yet the projections of both lumens have the same edge outline. The densitometric profiles, however, clearly distinguish between them. The area of each densitometrically corrected profile is proportional to the cross-sectional area of the respective lumen. (Reproduced from ref. [8]).

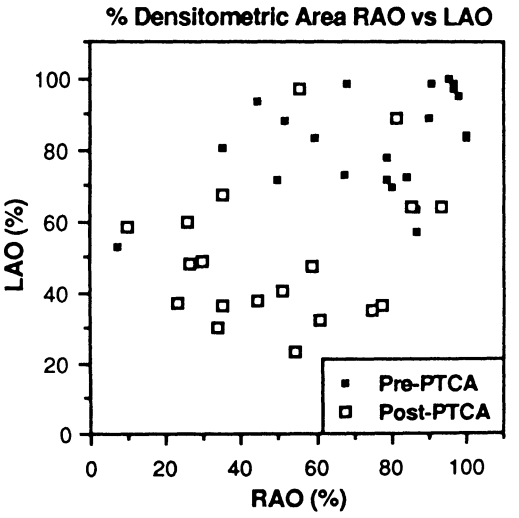

Fig. 2. These data show the comparison of densitometric percent area stenosis of the same coronary artery lesion from two views. Despite the theoretical independence of densitometric area measurements on radiographic projection, the correlation between views was very poor. (Reproduced from ref. [1]).

direct comparison of densitometric percent area stenosis of the same coronary artery stenosis from two views [1], demonstrating a very poor correlation between the measurements in one view versus the other. Although rare in the published literature, we believe such wide variability is typical for densitometric stenosis measurements unless extraordinary attention has been paid to correction of several important sources of error. In the next section, we shall review these sources of error and methods for their correction.

In principle, the transmitted X-ray intensity at each point along the vessel profile is related to the thickness of the coronary artery at that point. Videodensitometry is the determination of this relationship between coronary artery thickness and the X-ray image intensity. In the simplest case in which the X-ray beam is made up of a single X-ray energy with no scattered X-rays reaching the detector, the relationship between area and intensity is:

$$\text{Area} = (d/\mu C) \Sigma \ln(I_0/I)_i,$$

where d is the separation between pixels along the profile direction, μ is the attenuation coefficient for the contrast material in the artery, C is the concentration of iodine within the artery, I_0 is the intensity of the X-ray beam in the absence of attenuation by the artery, and I is the intensity of the X-ray beam after passing through the artery. For densitometry to be accurate, each of the factors within this formula must also be accurate. Table I lists the major sources of uncertainty or error in each of these factors.

Table 1. Sources of error in densitometric cross-sectional area.

Error source	Factor affected
Pincushion distortion	Pixel size: d
Scatter and veiling glare	Measured intensities: I, I_0
Beam hardening	Attenuation coefficient: μ
Structure noise	I, I_0
Contrast material streaming	Contrast concentration, C

Pincushion distortion

Densitometric measurement of a cross-sectional area requires that sources of spatial distortion and magnification be corrected, just as in the case of edge detection diameter measurements. The two major sources of magnification and distortion are radiographic magnification and pincushion distortion. Radiographic magnification is a simple geometric process as illustrated in Figure 3. Magnification of a given coronary artery segment can be determined either by knowing the distances between the arterial segment and the image intensifier and X-ray source, or by measuring the diameter of a known object

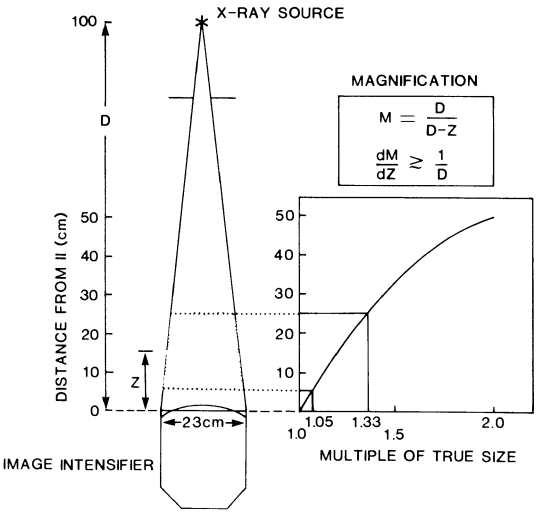

Fig. 3. This figure summarizes the geometry of radiographic magnification. For geometry typical of coronary angiography, radiographic magnification (defined as projected image size divided by true object size) is between 1.05 and 1.33. For the typical case of 100 cm between X-ray tube and image intensifier the magnification increases by about 1% for each centimeter an object moves away from the image intensifier. Thus, the error in densitometric area is about 1% for each centimeter separating a stenosis and its reference (e.g. a catheter) in the direction parallel to the X-ray beam. (Reproduced from Whiting et al. AJCI 2(3), 1988).

which is at the same distance from the image intensifier as the arterial segment to be measured. In either case, errors in the assumed position of the coronary segment to be measured result in approximately 1% error in diameter or in cross-sectional area for each 1 cm of uncertainty in position.

Pincushion distortion is also primarily a geometric phenomenon whose major source is the curvature of the input phosphor of the image intensifier [2]. The result of this distortion is that images are stretched in the radial direction by a factor which increases as the distance from the center of the image increases. Figure 4 shows data from a 1977 image intensifier [3] and a 1986 image intensifier [2]. It is clear from this figure that newer image intensifiers have much less pincushion distortion than those of a decade ago. With modern image intensifiers, the typical maximum pincushion distortion at the edge of a 7-inch image intensifier is about 2 or 3%. This distortion can be corrected by calibrating a given image intensifier tube using an image of a square grid to determine the distortion at each distance from the center of the tube. A second source of distortion in image intensifier tubes is a rotational distortion due to the earth's geomagnetic field [4]. The effect of this type of distortion on small object dimensions is usually quite small, although it does vary from place to place on the earth's surface and from projection to

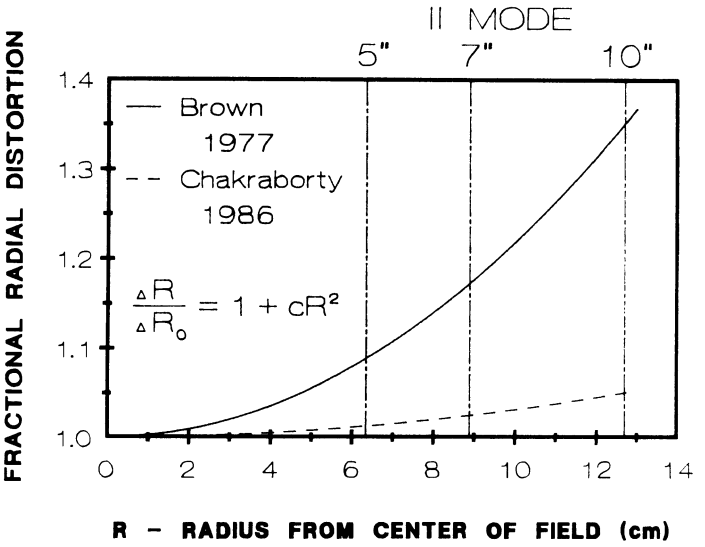

Fig. 4. Effect of pincushion distortion on radial dimensions. Older glass image intensifiers produced nearly 20% distortion near the image edge in the 7 inch image intensifier mode [3], while modern metal input tubes produce about 3% [2].

projection as the image intensifier is moved relative to the earth's field. It also depends on the design of the ferromagnetic shielding around the image intensifier tube.

Resolution

Unlike edge detection methods, densitometric methods of coronary stenosis quantification are relatively insensitive to image blur or unsharpness. This is because the increase in vessel width due to blurring is compensated by reduction of vessel contrast. Kruger [5] has shown that the densitometric cross-sectional area of a vessel is independent of the imaging system point spread function, and Parker, et al. [6] have shown the same result for unsharpness due to vessel motion. Thus, a potential advantage of densitometry is that it is independent of image resolution, unlike edge detection methods which overestimate vessel diameter when there is motion unsharpness and must be calibrated for the point spread function of the imaging system. However, densitometry is more sensitive than edge detection to other sources of error, namely: overlapping arterial brances, patient structure noise, vessel-beam orthogonality, and densitometric non-linearity of the image data.

Densitometry

There are two important sources of error in videodensitometric cross-sectional areas: uncertainty and non-linearity in the relationship between image intensity brightness and vessel thickness; and uncertainty in the thickness and composition of structures which are projected on top of the vessel. The main sources of densitometric non-linearity are X-ray scatter, image intensifier veiling glare, and beam hardening.

Scatter and veiling glare

The X-ray intensity of each point in a coronary angiogram is the sum of two components: a direct or "primary" component composed of X-rays transmitted straight through the patient; and an indirect, or "secondary" component composed of X-rays which have been deflected or scattered within the patient before reaching the imaging system. Light scattering in the image intensifier output phosphor and in the optical path to the video camera produces an additional secondary component, known as veiling glare. The useful imaging and densitometric information is contained in the primary X-ray intensity. However, X-ray scatter and veiling glare typically comprise 50 to 80% of the total intensity, as shown in Figure 5. As Figure 6 shows,

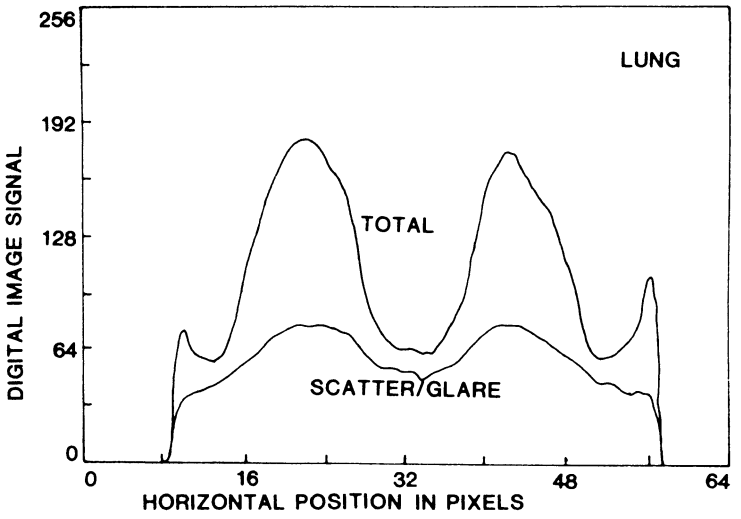

Fig. 5. Scatter and veiling glare contribution to total digital image signal varies with location across the thorax. The scatter and veiling glare fraction (of total intensity) ranges from about 0.4 over the lungs, where total intensity is highest, to about 0.8 over the center of the heart, changing rapidly from the edge to the center of the heart. Thus, it is likely that a calibration catheter and a coronary stenosis will require different corrections for scatter and veiling glare. (Reproduced from Naimuddin et al, Med Phys 14(3), 1987).

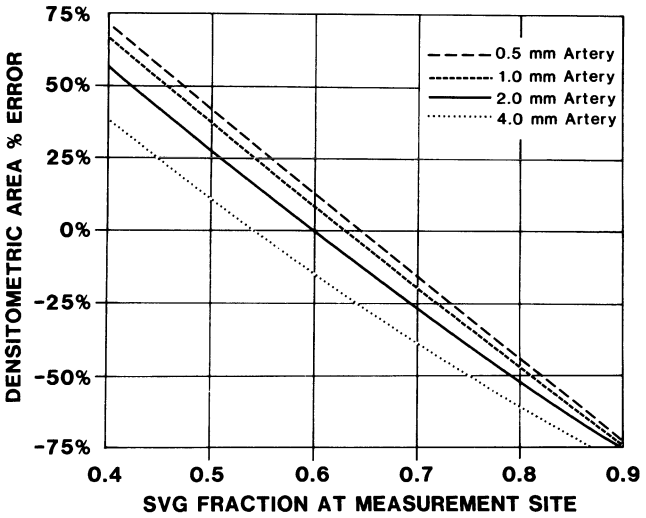

Fig. 6. This graph shows the calculated densitometric error when scatter and veiling glare is not subtracted. This simulation assumed a 2.0 mm reference catheter in a location with a scatter and veiling glare (SVG) fraction of 0.6. If the stenosis also has a diameter of 2.0 mm and the SVG fraction is the same, there is no error. However, up to 50% error occurs when the SVG at the site of the stenosis differs from that at the reference site.

error as high as 50% in relative cross-sectional area can result if scatter and veiling glare are not subtracted before logarithmic transformation of the image.

Scatter and veiling glare may be directly determined by blocking the primary beam with a lead square whose size is large relative to the width of the point spread function, but not large enough to significantly block scattered radiation from reaching the center of its shadow on the image receptor. The measured intensity at the center of the lead blocker image is the scatter and veiling glare contribution to that point in the image. Several investigators have used lead blocker measurements to estimate scatter and veiling glare at nearby unblocked points in the image, taking advantage of the fact that the scatter and veiling glare contribution varies slowly with location in uniform intensity regions of the image [7—9]. This approach has at least two disadvantages for coronary angiography. First, coronary arteries are often projected near the edge of the cardiac silhouette where background intensity is rapidly increasing toward the lung field. In these areas, the scatter and veiling glare is also changing rapidly, making the direct measurement inaccurate except directly adjacent to the lead blocker. Secondly, the lead blocker can obscure important angiographic features.

Another direct measurement of SVG has been described by Shaw [10], in which a nararow lead bar is moved across the field while a series of images is recorded. A "minimum pixel intensity" algorithm is then used to construct a single image corresponding to the intensities behind the bar, providing an

approximation of the SVG at each point throughout the image. The disadvantages of this method are that the lead bar may block the view of an important detail as it passes, the SVG is underestimated because the bar blocks a wider area of the primary beam than the small lead blockers described above, and cardiac motion during the scan may produce a rippling artifact.

A potentially more practical approach is to calculate an estimated correction from the image by assuming that scatter and veiling glare can be characterized by a point spread function (PSF). Shaw has estimated veiling glare by convolving a fixed PSF with the image and multiplying the result by a weighting factor [11]. Seibert convolved a calibrated inverse filter with the image to remove veiling glare [12].

Estimation of X-ray scatter using this same method is complicated by the fact that the scatter point spread function depends on patient thickness, X-ray beam energy, and imaging geometry [13], so that the inverse convolution filter must be calibrated for each patient and view.

Love and Kruger [14] approached this problem by making SVG measurements behind an array of 3 mm diameter lead balls to determine a weighting factor and bias for calibrating a correction based on convolution with a fixed SVG point spread function. They found that good estimates of SVG for opacified arteries could be obtained by convolution filtering even if the scaling parameters were derived from an image recorded prior to the arrival of contrast material. Thus, in clinical use, the lead beam-stops could be removed from the field before arterial opacification.

Malloi and Mistretta [15] have developed a similar method, except that they perform a gray scale transformation prior to convolution which converts the raw image intensities into approximate SVG intensities, based on measurements of SVG fraction versus gray level in an anthropomorphic chest phantom. Instead of using lead beam-stops, this method uses the X-ray factors, the distance from the focal spot to the image intensifier, and field size to calibrate the gray levels in the image so that in principle it can adjust to changes in SVG due to cardiac motion, respiration, or contrast material injection.

Beam hardening

The relationship between the thickness of an attenuating material and the transmitted X-ray intensity is an inverse exponential function, known as the Lamber-Beer law. The attenuation coefficient depends on the attenuating material composition and density and on the X-ray photon energy. Thus, for a mono-energetic X-ray beam passing through a uniform attenuating material, there is a linear relationship between the logarithm of intensity and attenuation thickness. The beam produced by X-ray tubes is poly-energetic, with a broad bremsstrahlung spectrum. When such a poly-energetic beam passes

through an attenuator, its spectrum is modified because the lower energy photons are attenuated more strongly. This phenomenon is called beam hardening because the modified spectrum has a larger proportion of more penetrating ("harder") high energy photons. Beam hardening affects angiographic densitometry by reducing the effective iodine attenuation coefficient as tissue thickness increases.

Figure 7 summarizes the influence of beam hardening on iodine densitometry. Each curve represents differential log intensity versus iodine thickness for a different tissue thickness. The range of tissue thicknesses (10—20 cm) is typical of the human thorax. The curvature of each curve is due to beam hardening by the iodine itself. Note that, for thicknesses typical of coronary arteries, iodine beam hardening is a much smaller absolute effect than hardening due to tissue. Thus, if the beams passing through a coronary artery segment and a calibrating catheter are both hardened by the same patient thickness, the maximum error due to iodine beam hardening is about 5%, occurring when the artery is about half the diameter of the catheter. However, as with scatter and veiling glare, larger errors are produced when the tissue beam hardening for the catheter and artery are different. This error is about 1.4% for each 1 cm difference in tissue beam hardening for a typically filtered beam. Correction for this error is possible using data such as that shown in Figure 7, by estimating the tissue thickness from the X-ray intensity following subtraction of scatter and veiling glare. However, we are

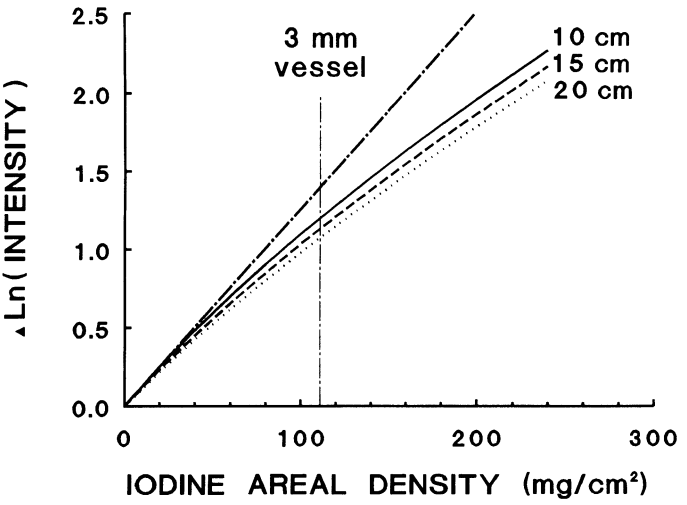

Fig. 7. Calculated effects of beam hardening for a 70 kVp X-ray beam with 3 mm aluminum filtration, assuming no scatter or veiling glare error. The graph shows the change in logarithmic intensity as a function of iodine areal density, which is proportional to vessel thickness. Beam hardening by water (patient soft tissue) changes the initial slope of lines, and beam hardening due to the iodine itself produces the observed curvature.

not aware of any validation thus far of combined corrections for scatter, veiling glare and beam hardening for quantitative coronary angiography.

Structure noise and contrast streaming

It is essential that all segments of the artery and any catheter used for calibration be uniformly filled with contrast material. Any streaming or dilution of contrast can produce large errors in vessel area, since densitometry measures the relative amounts of contrast material. Thus, densitometric accuracy depends on the ability to make contrast injections which completely replace blood within the arterial segments of interest.

Once the artery has been opacified, it is still necessary to determine for each pixel the amount of attenuation due to contrast material. This is complicated by the patients' anatomical structures, which produce intensity variations not related to contrast material. Two methods are available for separating these anatomical variations, known as patient structure noise, from contrast material attenuation. The first, mask subtraction, uses subtraction of the image from an identical image acquired prior to the arrival of contrast material. Mask subtraction is an excellent method for eliminating structure noise in densitometry provided that the only change between mask and image is opacification of the arteries. The primary limitation of this technique is that it is difficult to prevent changes between mask and image

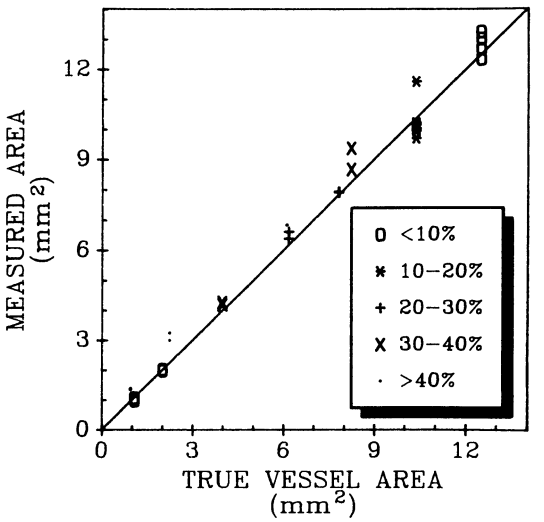

Fig. 8. X-ray phantom validation of densitometric cross-sectional areas measured in tubing with crescent-shaped lesions with a range of percent area reduction, demonstrating the insensitivity of denssitometry to lesion cross-sectional shape. (Reproduced from ref. [8]).

due to patient motion, particularly respiration. Any motion of patient structures between mask and contrast images results in random error due to patient structure noise. It is important to note that both the mask and the contrast image must be corrected for scatter, veiling glare and the Lambert-Beers law (i.e., logarithmically converted) prior to subtraction.

The second method for separating patient structure from arterial contrast is to use the (densitometrically corrected) intensity through patient structures adjacent to the artery as an estimate of the pre-injection arterial intensity. Accuracy can be improved by interpolating intensity measurements made on both sides of the artery. Structure noise is not entirely eliminated using this method, since not all structure-related variability can be fit by linear interpolation.

Because of the complex effect of the patient's anatomy, calibration using simple phantoms is insufficient to assure accurate densitometry. Excellent phantom results, such as those shown in Figure 8 should not be assumed to obtain in patients. The best check of the precision of relative densitometric areas is to compare measurements made in biplane views, in a range of patients and projection. This validation is essential before results using a given algorithm can be taken seriously.

References

1. Sanz ML, Mancini GB, LeFree MT, Nicholson JK, Starling MR, Vogel RA, Topol EJ: Variability of quantitative digital subtraction coronary angiography before and after percutaneous transluminal coronary angiography. Am J Cardiol 60: 55—60, 1987.
2. Chakraborty DP: Image intensifier distortion correction. Med Phys 14: 249—252, 1987.
3. Brown GB, Bolson E, Frimer M, Dodge HT; Quantitative coronary angiography: Estimation of dimensions, hemodynamic resistance, and atheroma mass of coronary artery lesions using the arteriogram and digital computation. Circulation 55: 329—337, 1977.
4. Solzbach U, Wollschläger H, Zeiher A, Just H: Optical distortion due to geomagnetism in quantitative angiography. Comput Cardiol 1988: 355—357.
5. Kruger RA: Estimation of the diameter of and iodine concentration within blood vessels using digital radiography devices. Med Phys 8: 652-658, 1981.
6. Parker DL, Clayton PD, Gustafson DE: The effects of motion on quantitative vessel measurements. Med Phys 12: 698—704, 1985.
7. Pfaff JM, Whiting JS, Eigler NE: Accurate densitometric quantification requires strict attention to the physical characteristics of x-ray imaging. In: New Developments in Quantitative Coronary Arteriography. JHC Reiber, PW Serruys (eds). Kluwer Academic Publishers, 1988: 22—33.
8. Pfaff JM: Quantitative Coronary Arteriography: Application of videodensitometric techniques for the evaluation of stenosis severity. PhD Thesis, University Microfilms International, Copyright 1988.
9. Maher KP, O'Connor MK, Malone JF: Experimental examination of videodensitometry of large opacifications in digital subtraction angiography. Phys Med Biol 32: 1273—1282, 1987.
10. Shaw CG, Plewes DB; Quantitative digital subtraction angiography: Two scanning techniques for correction of scattered radiation and veiling glare. Radiology 157: 247—253, 1985.

11. Shaw CG, Ergun DL, Myerowitz PD, Van Lysel MS, Mistretta CA, Zarnstorff WC, Crummy AB: A technique of scatter and glare correction for videodensitometric studies in digital subtraction videoangiography. Rad Phys 142: 209—213, 1982.
12. Seibert JA, Nalcioglu O, Roeck WW: Removal of image intensifier veiling glare by mathematical deconvolution techniques. Med Phys 12: 281—288, 1985.
13. Seibert JA, Boone JM: X-ray scatter removal by deconvolution. Med Phys 15: 567—575, 1988.
14. Love AL, Kruger RA: Scatter estimation for a digital radiographic system using convolution fitering. Med Phys 14: 178—185, 1987.
15. Malloi SY, Mistretta CA: Scatter-glare corrections in quantitative dual-energy fluoroscopy. Med Phys 15: 289—297, 1988.

4. An overview of coronary quantitation techniques as of 1989

JOHAN H.C. REIBER

Summary

In this chapter an extensive overview is presented on the state of the art in quantitative geometric and densitometric computer-aided analysis of coronary obstructions as of early 1989. All the data provided were obtained by requesting a total of 16 investigators known to the author to be actively involved in the development of quantitative coronary arteriography (QCA) techniques to complete a questionnaire including 29 questions on the different aspects of QCA. From this overview a number of conclusions can be drawn, particularly when comparing the results with those from early 1987: (1) there is an increased interest in the development of QCA-techniques for on-line use in the catheterization laboratory; (2) modern workstations and very powerful personal computers are increasingly being used; (3) software is mostly written in Pascal and C; (4) in the majority of the cases the edge definition is based on a combination of 1st- and 2nd-derivative functions; (5) correction for the limited resolution of the X-ray system is still insufficiently used; (6) in the majority of the cases image calibration is based on the measurement of the size of the coronary catheter segment; (7) there has been no signal of new developments in the definition of clinically relevant parameters except for the stenotic flow reserve; (8) densitometry remains a problematic technique; and (9) the use of more extensive and particularly standardized validation procedures should be encouraged.

Introduction

In the previous book in this series on Quantitative Coronary Arteriography [1] as well as in references [2, 3], overviews were presented on the quantitative geometric and densitometric computer-aided analysis of coronary obstructions as of early 1987. Since that time there has been a substantial amount of progress in this field, particularly in digital coronary arteriography [4]. Therefore, it is warranted to provide in this chapter an updated overview representing the state of the art in this field as of early 1989. All the data

J. H. C. Reiber and P. W. Serruys (eds), Quantitative Coronary Arteriography, 55–132.

presented in this chapter were obtained by requesting all investigators known to the author to be actively involved in the development of quantitative coronary arteriography (QCA-)techniques to complete a questionnaire including 29 questions on the different aspects of this topic. All 16 investigators returned the questionnaire; these are in alphabetical order:

Brown — Univ. of Washington, Seattle, WA, USA [5—7]
Brunt — Univ. of Manchester, Manchester, Great Britian [8]
Collins — Univ. of Iowa, Iowa City, IA, USA [9—13]
Doriot — Hôpital Cantonal Univ., Geneva, Switzerland [14—16]
Kirkeeide — Univ. of Texas, Houston, TX, USA [17—21]
LeFree — Quantitative Cardiac systems, Ann Arbor, MI, USA [22—25]
Lienard — Thomson CGR, Buc, France
Nichols — Presbyterian Hospital, New York, NY, USA [26, 27]
Oswald — Deutsches Herzzentrum, Berlin, Germany [28—30]
Parker — Univ. of Salt Lake City, Salt Lake City, UT, USA [31—34]
Reiber — Erasmus Univ., Rotterdam, The Netherlands [35—49]]
Sanders — Stanford Univ., Palo Alto, CA, USA [50—52]
Sandor — Harvard Medical School, Boston, USA [53]
Selzer — JPL, Los Angeles, CA, USA [54—60]
Vogel — Univ. of Maryland, Baltimore, ML, USA [22—25, 61, 62]
Wankling — Queen Elizabeth Hospital, Birmingham, Great Britain [63]

The numbers in brackets refer to the most relevant publications on QCA from these investigators.

The following subjects will be discussed in more detail in the subsequent sections: image acquisition/digitization of on-line digital imaging systems; image acquisition and digitization of 35 mm cinefilm; computer hardware and software; contour detection approaches for both the on-line and off-line systems; contour analysis approaches; densitometry; and validation procedures.

On-line digital cardiac imaging systems (Table 1)

Recent developments in digital cardiac imaging systems have been directed towards obtaining the quantitative measurements on-line during the catheterization procedure from video digitized images [64, 65]. By this approach the system will function as a tool providing the cardiologist with quantitative data useful for the selection of the appropriate sizes of intervention devices (e.g. intracoronary balloons, stents, atherectomy catheters, lasers, spark erosion catheters, etc.). In addition, the effect of an intervention (e.g. PTCA) can be assessed directly during the procedure; the angiographer can continue with the procedure until a quantitatively assessed acceptable result in terms of morphology and/or function has been obtained. Therefore, this approach is particularly of interest for diagnostic and/or therapeutic decision making during the catheterization procedure. The digital systems are characterized by a high density resolution (minimally 256 levels or 8 bits) and in principle

Table 1. Image acquisition/digitization on-line digital cardiac systems (1-1a).

	Doriot	LeFree	Lienard	Oswald
1. Name of Digital Cardiac System	Siemens Polytron 1000 VR	QCS-system interfaced to either Angiotec Cineloop, or to Philips DCI (via streamer tape)	General Electric CGR, DXC	Philips DCI
2. Limitations in matrix acquisition				
— Matrix size	512×256 512^2 1024^2	256^2 512^2 1024^2	— 512^2 1024^2	— 512^2 —
— Max. frame rate in frames/sec (f/s) (X-ray pulse width)	512×256: 50 f/s(> 10 ms) 512^2: 25 f/s(> 10 ms) 1024^2: 6 f/s(> 10 ms) for biplane acquisition divide max. frame rates by 2	256^2: 60 f/s 512^2: 30 f/s 1024^2: 6 f/s	— 512^2: 30 f/s(< 10 ms) 1024^2: 7.5 f/s	— 512^2: 50 f/s(3—8 ms) —
— Density resolution (bits)	10 bits	8 bits	8 or 10 bits	8 bits
3. Type video camera	Saticon	Plumbicon (Angiotec Cineloop)	Primicon	Plumbicon
Size video tube (inch)	1″	1.5″	1″	2″
Interlaced or progressive (noninterlaced) scanning mode	progressive	both interlaced and progressive	both interlaced and progressive	progressive

Table 1. Image acquisition/digitization on-line digital cardiac system (1-2a).

	Doriot	LeFree	Lienard	Oswald
4. How many images can be stored on the hard disk of the system?	21.500 (512 × 256) 8.550 (512^2) 2.100 (1024^2)	8.000 (256^2) 2.000 (512^2) 500 (1024^2)	— 15.000 (512^2) 2.800 (1024^2)	— 3600 (512^2) —
What kind of memory is used and what is its size?	690 × 2 MB Winchester disk; 95 MB Cartridge cassette; 2GB Optical disk	500 MB Winchester Disk	1400 MB Winchester disk (8″); 12 MB semiconductor memory (4 for CPU, 8 for image processor)	474 MB Winchester disk 3.3 MB of image memory
5. Is digital zoom available for coronary quantitation?	NO	YES	YES	
If YES, provide zoom factor	—	2, 4, 8, 16×	2×, ROI around coronary segment automatically selected	2×
Interpolation technique	—	bilinear interpolation	linear interpolation	replication
6. Horizontal pixel size for 512^2 matrix (without zoom) as measured at the input screen of the II	254 μm for 5.5″ II	293 μm for 6″ II	300 μm for 6″ II	247 μm for 6″ II
7. 35 mm Cinefilm acquisition possible simultaneously with digital acquisition?	YES: cinefilm: up to 50 f/s; Polytron: as in point 4; data applies to both mono and biplane	YES: dose/image quality trade-off	YES; no limitations	YES; no limitations
If YES, what are the limitations?				

Table 1. Image acquisition/digitization on-line digital cardiac system (1-1b).

	Parker	Reiber	Vogel
1. Name of Digital Cardiac System	Siemens Digitron III	Philips DCI	ADAC type S100C
2. Limitations in matrix acquisition			
— Matrix size	— 512^2 —	— 512^2 —	256^2 512^2 1024^2
— Max. frame rate in frames/sec (f/s) (X-ray pulse width)	— 512^2: 30 f/s(< 8 ms) —	— 512^2: 50 f/s(3—8 ms) —	256^2: 60 f/s(3—10 ms) 512^2: 30 f/s(3—10 ms) 1024^2: 4 f/s(3—10 ms)
— Density resolution (bits)	10 bits	8 bits	8 bits
3. Type video camera	Saticon	Plumbicon	Vidicon
Size video tube (inch)	1″	2″	1″
Interlaced or progressive (noninterlaced) scanning mode	progressive	progressive	progressive

Table 1. Image acquisition/digitization on-line digital cardiac system (1-2b).

	Parker	Reiber	Vogel
4. How many images can be stored on the hard disk of the system?	— — —	— 3.600 (512^2) —	10.000 (256^2) 2.500 (512^2) 625 (1024^2)
What kind of memory is used and what is its size?	—	474 MB Winchester disk 3.3 MB of image memory	40 MB Winchester disk 677 MB IBM disk
5. Is digital zoom available for coronary quantitation?	currently NO	YES;	YES;
If YES, provide zoom factor	—	2×	4×
Interpolation technique	—	replication	linear interpolation
6. Horizontal pixel size for 512^2 matrix (without zoom) as measured at the input screen of the II	390 µm for 7″ II	247 µm for 6″ II	300 µm for 6″ II
7. 35 mm Cinefilm acquisition possible simultaneously with digital acquisition?	YES; lower X-ray dose	YES; no limitations	currently NO; will be added soon
If YES, what are the limitations?			

a linear transfer function of the imaging chain from the output of the image intensifier to the brightness levels in the digitized images, making these more suitable for densitometric analysis than the conventional cinefilm approach. In some systems (e.g. Philips DCI) the linear transfer function has been modified according to a well-defined nonlinear function to achieve a better image display quality (white compression on the DCI).

As the terms on-line, off-line, etc. in general have been used rather loosely, it is appropriate here to define these more accurately. The ultimate requirements of the hardware and software are met in the *on-line* situation, where quantitative results must become available immediately after the corresponding arteriographic investigation, i.e. after coronary arteriography in a particular angiographic view with the patient still on the table. *Post-processing* refers to the situation that analysis of the image data takes place after the complete cardiac catheterization has been finished, usually after the patient has left the catheterization laboratory; however, at that time the image data are still available in the memory (e.g. on the harddisk) of the system. Of course, processing times are not so critical anymore in this situation. We would define *reviewing* as the processing of a previously performed patient study which is not available anymore in the memory of the system, and therefore has to be recovered from mass storage into the imaging system. Finally, *off-line* is applicable in situations where the image data are processed on another workstation, which has no direct link to the digital imaging system; this may be a PC-based workstation for quantitative coronary and left ventricular angiography which can read in digital tapes or selected cineframes via a cine-projection system.

At the present time there are seven groups (in alphabetical order Doriot, LeFree, Lienard, Oswald, Parker, Reiber and Vogel) actively involved in the development and use of state-of-the-art quantitative software packages for on-line coronary arteriography. Doriot and Parker use the Siemens Polytron 1000VR and the Siemens Digitron III, respectively, LeFree uses his QCS PC-based workstation which can be interfaced either to the Angiotec Progressive Video System FMX-1220 with Cineloop, or via streamer tape to the Philips DCI, Lienard the General Electric CGR DXC system, Oswald and Reiber the Philips DCI and Vogel the ADAC type S100C (Table 1, item 1).

To quantitate the coronary morphology, the minimal requirement for image acquisition must be 512^2 matrices at a rate of 25 frames/s (Europe) or 30 frames/s (USA) with a density resolution of 8 bits. In addition, pulsed X-ray radiation should be used to minimize motion blur in the images. From Table 1, item 2 it appears that all systems satisfy these minimal requirements with the Philips DCI in monoplane version even allowing 50 or 60 frames/s. The Angiotec Cineloop system and the ADAC system also provide 256^2 (at 60 frames/s monoplane) and 1024^2 matrix sizes (at 6 and 4 frames/s, respectively); the Siemens Polytron facilitates 512×256 (at 50 f/s) and 1024^2 matrices (at 6 f/s), and the GE system the 1024^2 size matrix (at 7.5 f/s) in addition to the standard 512^2 matrices. The X-ray pulse width varies

from short 3—8 ms values (Philips), < 8 ms (Siemens Digitron), 3—10 ms (ADAC), < 10 ms (GE CGR) and > 10 ms (Siemens Polytron), respectively; a short pulse width is necessary to minimize motion blur in the images.

The type and size of the video cameras used in the digital systems vary from a 1″ vidicon tube on the ADAC system with progressive readout, a 1″ primicon with both standard interlaced and progressive scanning on the GE CGR system, a 1.5″ plumbicon with both interlaced and progressive scanning on the Angiotec system, a 2″ plumbicon with progressive scanning on the Philips DCI, to a 1″ saticon (progressive readout) on the Siemens system (Table 1, item 3). For more detailed information on these different readout techniques, the reader is referred to ref. [66].

Of great concern in the practical application of these systems is the kind and size of image memory available, since that determines how many images can be stored on the system before the image data must be transferred to medium or long-term storage media. All systems use Winchester disks varying in size from a 474 MB disk for the Philips system to a 1400 MB disk for the GE CGR system (Table 1, item 4). The number of images that can be stored vary accordingly, and is also dependent on the fact whether one uses recoverable image compression techniques. If we limit ourselves to the 512^2 images, the range in images that can be stored on-line vary from 2000 on the Angiotec Cineloop to 15.000 on the GE system. Only Doriot mentioned that a 2GB optical disk is connected to the Siemens Polytron.

At this point in time none of the companies has a satisfactory solution for long-term storage of the vast amount of data. Although various companies now offer the Honeywell high speed streamer tape, this can only be seen as an intermediate solution, because of its high price ($100.000.—), significant read and write times and nonstandard (preformatted), relatively expensive VHS-tapes.

The question was also posed whether regions of interest (ROI's) in the image can be magnified for coronary quantitation, and if so, to what degree and by which interpolation technique (Table 1, item 5). ADAC has a 4-fold digital zoom based on linear interpolation, the QCS/Angiotec system features 4 different magnification modes (2, 4, 8 and 16-fold) with bilinear interpolation, the GE system 2-fold magnification with linear interpolation, and the Philips DCI 2-fold with replication.

Question 6 was concerned with the horizontal pixel size for a 512^2 matrix (no zoom) as measured at the input screen of the image intensifier (II). If we normalize all the values to a 6″ II field-of-view, it becomes apparent that the Siemens Digitron III has the largest pixel size (334 μm) and Philips the smallest value (247 μm); other values included 277 μm for the Siemens Polytron, 293 μm for the QCS/Angiotec system, and 300 μm for the ADAC and GE/CGR systems. These different pixel sizes are related to the definition of the digitizing matrix with respect to the size of the image intensifier output screen. In some systems the entire circular shape of the II output screen is included in the digitizing matrix, which means that a certain portion

of the 512^2 pixels does not contain useful information; at the other extreme, the digitizing matrix fits within the circular shape of the II output screen, which means that significant portions of the area of the II output screen are lost, while in other systems (e.g. Philips DCI) one has attempted to optimize the superimposition of the matrix on the II output screen, such that a minimal amount of image information is lost resulting in a small pixel size. It is of course true, that the smaller the pixel size, the more pixels are available for contour detection. In general, however, one cannot state that a smaller pixel size results in a more accurate edge detection performance; the accuracy is also to a large degree dependent on the actual edge detection algorithm implemented. It should be noted that some systems (Siemens Polytron, GE CGR DXC, and ADAC) allow acquisitions at a matrix size of 1024^2 with resulting decrease in the pixel size by 50%. However, the number of frames per sec at this size is low (max. 7.5 f/s), making this mode not useful for cardiac applications.

Finally, it was investigated whether 35 mm cinefilm can be acquired simultaneously with the digital acquisition. The ADAC system does not have this feature, although it will be added soon, while all other systems have this facility available (Table 1, item 7).

Image acquisition and digitization of 35 mm cinefilm (Table 2)

For the digitization of a complete cineframe or regions of interest in a cineframe, three basic approaches have been adopted: (1) optical magnification by means of a cine-video projector with one or more lens systems and a standard video or modern CCD-camera; (2) high resolution digitization of the entire cineframe by means of a cine-digitizer equipped with either a high resolution linear or area array CCD-camera, and subsequent selection of region of interest for further processing; and (3) digitizing with standard, high quality video or CCD camera and subsequent digital or electronic magnification of regions of interest in the 512^2 matrix in the host processor.

The systems with optical magnification vary from a Phototek cinedigitizer with 512^2 area-type CCD-camera (Brunt), a customized cinefilm digitizing system with 1″ vidicon (Collins), a self-modified Tagarno projector with 1″ plumbicon (Doriot), a Vanguard XR-35C cineprojector with 1.5″ plumbicon (LeFree), a Vanguard XR-70 cineprojector with vidicon tube (Nichols), a recently developed Arripro 35 projector with 512^2 area-type CCD-camera (Oswald), a 3rd generation cine-video converter (CIVICO IV) with 512^2 area-type CCD camera (Reiber), a customized system from Imaging Technology, Inc with 1″ vidicon tube (Sandor), a GE CAP35 with vidicon (1024^2 image matrix) or Vanguard M35C with 1″ vidicon (Selzer), an ADAC S100C with 1″ vidicon (Vogel), to a customized system with 2/3″ vidicon (Wankling). In two of these systems a single magnification factor (2-fold) is available; in five systems three discrete magnification factors (range 0.7 to 7-fold) can be selected, while a continuous setting is available on the remain-

ing five systems. In practice, a 2-fold magnification factor will be used most frequently. Brown et al. use a magnification factor of 5.5-fold with their analog projection system (5). In all these cine-digitizers, except for the Arripro 35 and the CIVICO IV developed at the Erasmus University in Rotterdam, the lens selection and camera positioning is done manually.

In the CIVICO IV the CCD camera is mounted on an x-y table controlled by stepping motors (Figure 1). Since the head of the camera containing the CCD-chip can be separated from the body of the camera, the x-y table needs to transport only approximately 100 grams and therefore can be a light weight construction resulting in fast responses. Three different lenses (0.7, 1 and 2.2-fold magnifications) can be inserted in the imaging path. The light source is a light emitting diode (LED) with a narrow light spectrum; the emitted amount of light can be linearly adjusted. A user-controlled, motor-driven diaphragm and automated light control system further provide for optimal image quality in the selected region of interest.

The systems with high resolution digitization of the entire cineframe use either a high resolution linear CCD-array that allows the digitization of a cineframe at a matrix size of 2048 × 3000 pixels with subsequent selection of regions of interest with magnifications of 2- and 4-fold (Kirkeeide), or a high resolution Videk Megaplus CCD camera on a standard Siemens Cipro projector resulting in a 1300 × 1030 pixels matrix (Sanders).

Following the third approach, the entire cinefilm is digitized via a standard,

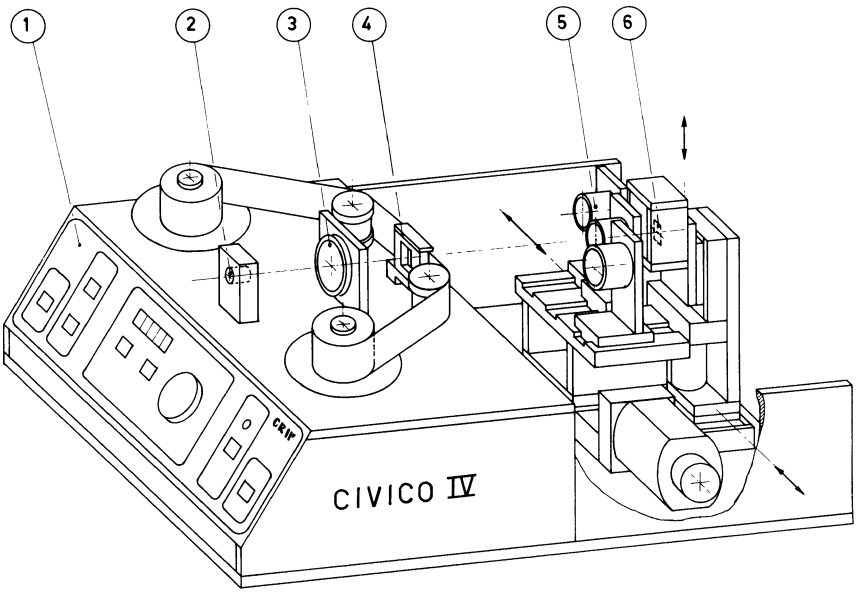

Fig. 1. Schematic drawing of the 3rd-generation cine-video converter (CIVICO IV) developed at the Central Research Workshop of the Erasmus University Rotterdam.

high-quality video camera into a 512^2-matrix and regions of interest can be magnified digitally in the host processor to a full 512^2 or smaller matrix. Examples of these approaches are the standard Tagarno 35AX cineprojector with 1″ newvicon (LeFree) and the facility of magnifying ROI's of sizes 32^2, 64^2, 128^2, or 256^2 back to 512^2-matrix size using bilinear interpolation on the QCS-host processor (LeFree), the same projector with subsequent digital magnification of regions of interest or 64^2, 128^2 or 256^2 pixels to full scale 512^2 using either replication, linear of cubic interpolation on the 80386 host processor (Reiber). It should be clear that by this last approach, any other cineprojector with standard video output could also be used.

The last point of Table 2, item 8 concerns the horizontal pixel size (μm) for a 512^2 matrix without zoom as measured at the input screen of the image intensifier. This item may give rise to some confusion, as two of the film based systems (Kirkeeide, Sanders) digitize the film images at a higher resolution than 512^2 using high resolution CCD cameras. Therefore, we must distinguish the three earlier discussed possibilities:

A. Film-based systems with optical magnification using standard or high resolution video or CCD cameras; for these systems the pixel size is given in Table 3 at a frequently used optical magnification factor.
B. Film-based systems without optical magnification but digitization with a high resolution CCD camera; for these systems only one value can be given for the pixel size.
C. Film-based systems which use a standard high quality video camera and digitize the image at 512^2 matrix size; for subsequent analysis regions of interest may be magnified digitally. For these systems the pixel size in the original 512^2 matrices is given in Table 3.

From this item the pixel density (number of pixels per mm as measured at the input screen of the image intensifier) can be calculated. Unlike the data of 1987 presented in references [1, 2], I have chosen not to provide these data referred to the isocenter with the average focus-to-image intensifier distance, since these last parameters were not always provided, making comparisons more difficult. In Table 3 all the pixel sizes are related to the input screen of the image intensifier, thereby normalizing to a 6″ input screen. In this manner the resulting pixel sizes can be compared much easier. For completeness the earlier provided data on the digital systems (Table 1, item 6) have been included as well in Table 3.

From this table it can be appreciated that most investigators using a film-based system with optical zooming or with a high resolution camera have chosen for a pixel size ranging from 50—88 μm, which is a factor of 2.8—4.9 smaller than that provided by the best digital systems.

Computer hardware and software (Table 4)

A great variety of host computer systems has been used for the development and clinical application of the quantitative software (Table 4, item 9). These

Table 2. Cinefilm digitization (2-1a).

	Brown	Brunt	Collins	Doriot	Kirkeeide
8. Type cinefilm digitizing system	Human Hand-Brain-Eye-System	Phototek	Customized	Tagarno projector + self constructed imaging chain	collaboration between Univ. of Zürich and Univ. of Texas
Type camera used	NA	Pulnix TM700 CCD camera (512^2); will be replaced by Kodak Megaplus (1024^2); both cameras of area-type	Vidicon (1″), 559 lines; Cohu, model 8000	Plumbicon (1″)	CCD camera (2048 × 3000); linear type
Kind of image magnification available	analog magnification	optical	optical	optical	digital
Magnification factors achievable	5.5×	2×	1, 3.7, 7×; uses 3.7× for most purposes	1—7×, continuous	2, 4×
For cine-digitizer with different optical lenses, is the lens selection manual or computer controlled?	NA	manual	manual	single lens system; manual positioning of lens and video camera	NA
Horizontal pixel size for 512^2 matrix (no zoom) measured at input screen of the II (only for cinefilm-based systems)	NA	280 μm for 7″ II	60 μm at 3.7× magnification and 7″ II	312 μm for 6.6″ II	100 μm for 7″ II

Table 2. Cinefilm digitization (2-1b).

	LeFree	Lienard	Nichols	Oswald	Parker	Reiber
8. Type cinefilm digitizing system	a. Tagarno 35AX b. Vanguard XR-35C and XRTV3	NA	Vanguard XR-70 Coronary Analyzer	Arripro 35	—	two versions: a. Tagarno 35AX with standard built-in video camera b. CIVICO IV (3rd generation Cine-Video-Converter presently under development at Erasmus University)
Type camera used	a. Newvicon (1″); 525 lines b. Plumbicon (1.5″); 525 lines	—	Vidicon (Panasonic WV-1500)	Sony CCD (512^2)	—	a. 1″ newvicon b. CCD (512^2) area-type camera
Kind of image magnification available	a. none b. optical	—	optical	optical	—	a. digital b. optical
Magnification factors achievable	a. 1, 2, 4, 8, 16× b. 1, $2\sqrt{2}$, 4×	—	2×	1—2.6×, continuous	—	a. 1, 2, 3, 4× b. 0.7, 1, 2.2×
For cine-digitizer with different optical lenses, is the lens selection manual or computer controlled?	a. NA b. manual	—	manual	manual/computer controlled	—	a. NA b. computer controlled
Horizontal pixel size for 512^2 matrix (no zoom) measured at input screen of the II (only for cinefilm-based systems)	298 μm for 6″ II	—	286 μm for 6″ II	204 μm for 7″ II	—	a. 188 μm for 6″ II b. 185 μm for 6″ II

Table 2. Cinefilm digitization (2-1c).

	Sanders	Sandor	Selzer	Vogel	Wankling
8. Type cinefilm digitizing system	Siemens Cipro projector with CCD camera	Imaging Technology, Inc.	a) GE CAP35 b) Vanguard M35C	ADAC S100C	—
Type camera used	Videk Megaplus CCD camera (1300 × 1030 pixels)	Vidicon (1″) 525 lines	a) Vidicon (1024 × 1024) from MegaVision Inc. b) Vidicon (1″) (512 × 512) from Spatial Data Systems	Vidicon (1″) 525 lines	Vidicon (2/3″) 625 lines
Kind of image magnification available	electronic; bilinear interpolation	optical	a) optical (zoom) b) optical (turret lens)	optical	optical
Magnification factors achievable	0.5, 1, 2×	continuous	a) up to 1.6: 1 b) 1, 2.5, 3.7×	1, 2.5, 4×	variable
For cine-digitizer with different optical lenses, is the lens selection manual or computer controlled?	NA	manual	a) manual b) manual	manual	manual
Horizontal pixel size for 512^2 matrix (no zoom) measured at input screen of the II (only for cinefilm-based systems)	50 μm for 6″ II	≃ 60 μm (estimated value) for 6″ II	190 μm for 7″ II (95 μm for 1024 system)	300 μm for 6″ II	?

Table 3. Horizontal Pixel size in digitized image normalized to 512^2 matrix and referred to the input screen of a 6″ image intensifier.

Investigator	Digital systems	Film-based systems			
		with optical magnification		with high resolution CCD/video camera	with standard video camera
		size	zoom		
Brunt	—	120	2×	—	—
Collins	—	51	3.7×	—	—
Doriot	277	142	2×	—	—
Kirkeeide	—	—	—	86	—
LeFree	293	122	2.4×	—	293
Lienard	300	—	—	—	—
Nichols	—	143	2×	—	—
Oswald	247	88	2×	—	—
Parker	334	—	—	—	—
Reiber	247	84	2.2×	—	188
Sanders	—	—	—	50	—
Sandor	—	60	?	—	—
Selzer	—	65	2.5	51 (1.6 zoom)	—
Vogel	300	230	2.5	—	—
Wankling	—	?	?	—	—

included VAX-11/750 (Brown, Doriot, Parker), DEC/VAX — WS3200 workstation (Oswald), MicroVax II (Collins, Sandor, Selzer), PDP 11/45 (Selzer), PDP 11/73 (Vogel), Motorola 68008 (Nichols) and 68030 microprocessors (Lienard), HP Vectra RS-20 personal computer (Sanders), Sun 3/160C (Brunt), Sun 3/260 (Sandor) and Sun 4/260 (Parker), Apollo 3000 (Kirkeeide), PC 80386 (LeFree and Reiber), to an Olivetti M24SP (Wankling). If we compare this list with the one from 1987, it becomes clear that there has been a definite shift from the more traditional PDP and Vax computers to workstations and very powerful personal computers characterized by decreased cost and increased performance for the workstations and high-end PC's.

The image data digitized either by means of a video or a CCD camera must be stored in an image processing system before any image processing functions can be applied. Here again the variety in complexity and thus cost is large: from truly image processing systems such as DeAnza Gould IP8500 (Collins), IP6400 (Doriot), IP5500 (Selzer), IP8432L (Oswald), Vicom VDP (Lienard), Sun 4/260 + TAAC1 (Parker), to an ADAC Array Processor (Vogel) and Virtual Imaging View 2000 workstation (LeFree) and finally to image processing cards which can be inserted in the hostprocessors, such as Imaging Technologies FG100 (Reiber, Sandor), MegaVision 1024XM (Selzer), Matrox PIP 1024 frame grabber (Wankling), AVS model IPB-3000 (Brunt). In the system developed by Brown, selected cineframes are pro-

Table 4. Hostprocessor (4-1a).

	Brown	Brunt	Collins	Doriot	Kirkeeide	LeFree
9. Hostcomputer	Vax-11/750	Sun 3/160C	MicroVax II	Vax-11/750	Apollo 3000	PC/AT compatible 80386
Image Processor	NA	AVS, model IPB-3000	DeAnza-Gould IP8500	DeAnza-Gould IP6400	none	Virtual Imaging View 2000
Operating System	VMS	Unix	VMS	VMS	Domain	MS-DOS
Application software written in:	Flex	Pascal	Fortran-77	Fortran	Fortran/Pascal	C

Table 4. Hostprocessor (4-1b).

	Lienard	Nichols	Oswald	Parker	Reiber
9. Hostcomputer	68030 Motorola	68008 Motorola	DEC/VAX-WS3200	two versions, a. VAX-11/750; being converted to b. b. Sun 4/260 + TAAC1	Compaq 80386 (20 MHz)
Image Processor	VICOM VDP	only graphics overlay	Gould IP8432L	a. Digitron I b. Sun 4/260 + TAAC1	Imaging Technologies FG 100
Operating System	Versados	Motorola VME/10 Development System	VMS	a. VMS b. Unix	MS-DOS (V3.1)
Application software written in:	Pascal + Assembler	C	Fortran	a. Fortran b. C	Microsoft C(V4.0)

Table 4. Hostprocessor (4-1c).

	Sanders	Sandor	Selzer	Vogel	Wankling
9. Hostcomputer	HP Vectra RS-20 (80386, 20 MHz)	MicroVax II Sun 3/260, 3/60, 386i	1) MicroVax II 2) PDP 11/45	DEC 11/73	Olivetti M24 SP
Image Processor	Epix 4 MB Video	ITI frame grabber + (type?) Warrior array processor	1) Megavision 1024 XC 2) DeAnza IP 5500	ADAC array processor	Matrox PIP 1024 frame grabber
Operating System	MS-DOS/Microsoft Windows	VMS, SunOS	1) VMS and JPL Mini-Vicar 2) RSX-11M	RT11	MS-DOS
Application software written in:	C	Fortran, C	Fortran	Fortran	C

jected with a standard cinefilm projector onto a large writing tablet, allowing manual tracing of the boundaries of the arterial segment of interest; the coordinates of these boundary points are sent to the host computer for subsequent analysis. As a result, Brown does not need an image processor. In the Apollo 3000 (Kirkeeide) an image store and display is part of the workstation. Nichols only displays the analog video image and uses a graphics overlay for the display of alphanumeric characters, contours and lines on the screen.

With so many different host computer systems employed, the variety of Operating Systems is also large: VMS (Brown, Collins, Doriot, Parker, Oswald, Sandor, Selzer), Unix (Brunt, Parker), SunOS (Sandor), Domain (Kirkeeide), RSX-11M (Selzer), RT11 (Vogel), Motorola VME/10 (Nichols), MS-DOS (LeFree, Reiber, Sanders, Wankling) and Versados (Lienard). Again comparing the present situation with that of 1987, there has been a definite shift towards the modern operating systems UNIX and MS-DOS; the last one is used predominantly on the PC's.

The choice in the high level computer language in which the application software packages have been written is much smaller: the more conventional language Fortran is still used by eight investigators (Collins, Doriot, Kirkeeide, Oswald, Parker, Sandor, Selzer and Vogel), while the majority now uses one of the more modern languages Pascal (Brunt, Kirkeeide, Lienard) and C (LeFree, Nichols, Parker, Reiber, Sanders, Sandor, Wankling); Brown uses Flex.

Contour detection approaches (Table 5)

An overview of the specifications related to the contour detection approaches of the various systems are presented in Table 5. For the computer-assisted definition of the boundaries of a selected coronary segment, in general, the followings steps need to be distinguished:

1) definition of coronary segment to be analyzed;
2) edge definition.

The different implementations of these steps will be discussed in some more detail in the following paragraphs.

Definition of coronary segment to be analyzed (Table 5, item 10)

In general, the following four different approaches can be distinguished in order of increasing automation and algorithmic complexity:

1. User positions a cursor over stenotic and normal segments (Nichols).
2. User indicates number of arterial segment points, subsequently connected by interpolation (Brunt, Collins, Kirkeeide, Sanders, Sandor, Selzer).
3. User indicates number of arterial segment points followed by automated path line tracing (Doriot).

Table 5. Contour detection (5-1a).

	Brown	Brunt	Collins	Doriot	Kirkeeide	LeFree
10. Definition of coronary segment to be analysed	user manually traces boundaries of coronary segment on projected image; computer creates centerline	user indicates number of center points within coronary segment, which are subsequently connected by interpolation	user indicates number of center points within coronary segment, which are subsequently connected by interpolation	user indicates number of center points within coronary segment, followed by automated centerline tracking	user input/automated refinement	automated centerline tracking
11. Edge definition based on:	manual tracing and visual inspection	1st-derivative function (dynamic programming)	graph searching derived from weighted combination of 1st and 2nd derivatives calculated in two dimensions	zero-crossing of 2nd-derivative function	1st-derivative function	**threshold between 1st- and 2nd- derivative extrema**
Edges corrected for line-spread function of X-ray system?	NO	YES	NO; image filtering carefully tuned to produce accurate measurements for small vessels	YES; addition of a correction term depending on the vessel diameter	YES; on the basis of calibration curves assessed from phantom studies	NO; indirectly compensated for by edge detector combined with catheter scaling
12. Do you apply corrections for pincushion distortion?	YES, by correcting only the contour positions of the detected catheter and arterial segments for geometric distortion; it is assumed that the distortion is radially symmetric about the center of the II; analytical function provides the relative magnification as a function of the distance of a pixel to the center of the II	YES, by correcting the entire image, i.e. pixel position and intensity values (image warping) based on detected intersection points of cm-grid	NO	YES, by correcting only the contour positions of the detected catheter and arterial segments for geometric distortion; it is assumed that the distortion is radially symmetric about the center of the II; analytical function provides the relative magnification of the distance of a pixel to the center of the II	YES, by correcting only the contour positions of the detected catheter and arterial segments for geometric distortion; it is assumed that the distortion is radially symmetric about the center of the II; analytical function $A + Br^2$ is derived from the intersection points of the cm-grid held against the II-input screen	NO

Table 5. Contour detection (5-1b).

	Lienard	Nichols	Oswald	Parker	Reiber
10. Definition of coronary segment to be analyzed	automated centerline tracking	user positions cursor over stenotic and normal segments	automated centerline tracking	automated centerline tracking	automated pathline tracking
11. Edge definition based on:	1st semi-derivative	full-width at half maximum (FWHM) of density profile	max. response of weighted sum of 1st- and 2nd-derivatives	matched filter	contour path determined in cost matrix based on weighted sum of modified 1st- and 2nd-derivative functions; 2 iterations
Edges corrected for line-spread function of X-ray system?	NO	NO	NO	NO (small distortion)	YES; by applying deconvolution techniques
12. Do you apply correction for pincushion distortion?	NO	NO	YES, 2 options: a. by correcting the entire image, i.e. pixel positions and intensity values ("warping") for the distortion b. by correcting only the contour positions of the detected catheter and arterial segments for the geometric distortion. Correction vectors defined from intersection points of cm-grid held against the II-input screen	at present, usually NOT. If required, the entire image is corrected, i.e. both pixel positions and intensity values ("image warping")	YES, by correcting only the contour positions of the detected catheter and arterial segments for the geometric distortion; correction vectors defined from intersection points of cm-grid held against the II-input screen

Table 5. Contour detection (5-1c).

	Sanders	Sandor	Selzer	Vogel	Wankling
10. Definition of coronary segment to be analyzed	user indicates number of center points within coronary segment, which are subsequently connected by interpolation	two passes: 1) user marks tentative centerlines; 2) final centerline is computed from edges	user indicates number of center points within coronary segment, which are subsequently connected by interpolation	automated centerline tracking	automated centerline tracking
11. Edge definition based on:	max. response of weighted sum of 1st- and 2nd-derivative functions	inflection point of 5-degree polynomial fitted through vessel profile (= max. response of 1st derivative)	max. response of 1st-derivative	weighted sum of 1st- and 2nd-derivative function	2nd-derivative function
Edges corrected for line-spread function of X-ray system?	NO	NO	NO	NO	NO
12. Do you apply correction for pincushion distortion?	NO; believes this is not required for modern systems	YES; by correcting only the contour positions of the detected catheter and arterial segments for the geometric distortion; correction vectors defined from intersection points of cm-grid held against the II-input screen	YES: by correcting only the contour positions of the detected catheter and arterial segments for the geometric distortion; correction vectors defined from intersection points of cm-grid held against the II-input screen	optional; by correcting the entire image, i.e. pixel position and intensity values (image warping) based on detected intersection points of cm-grid	YES, warping region of interest

Table 5. Contour detection (5-2a).

	Brown	Brunt	Collins	Doriot	Kirkeeide	LeFree
13. Method of calibration to convert pixel measurements to absolute sizes (mm)	manual tracing of the boundaries of the catheter segment	automated edge definition of catheter segment	automated or manual edge definition of catheter segment	calibration is inherent to the 3D-reconstruction process of the left and right coronary arterial tree ("Calibration" cube with 15 steel markers)	preferred: — analytically from X-ray system settings (if in isocenter) in biplane views — automated edge definition of catheter segment — distance between cardiomaker rings on catheter as assessed in biplane views	automated edge definition of catheter segment
14. Correction procedure for differential magnification between catheter and arterial segment from biplane views available on your system? ('out-of-plane' magnification)	YES, now use the intrathoracic spatial relations of normal-sized human hearts to estimate the out-of-plane magnification correction	NO (routinely); however, software is available	NO	not necessary; see point 13	YES	NO

Table 5. Contour detection (5-2b).

	Lienard	Nichols	Oswald	Parker	Reiber
13. Method of calibration to convert pixel measurements to absolute sizes (mm)	automated edge definition of catheter segment	determine FWHM of catheter segment	3 options: a. analytically from geometric X-ray system settings in single/ biplane views b. automated edge definition of catheter segment c. distance between cardiomarker rings on catheter as assessed in biplane views	analytically from geometric X-ray system settings in biplane views	automated edge definition of catheter segment
14. Correction procedure for differential magnification between catheter and arterial segment from biplane views available on your system? ('out-of-plane' magnification)	NO	NO	YES	YES, inherent in 3D-reconstruction	under development; will use method proposed by Brown

TABLE 5. Contour detection (5-2c).

	Sanders	Sandor	Salzer	Vogel	Wankling
13. Method of calibration to convert pixel measurements to absolute sizes (mm)	— automated edge definition of catheter segment — determine diameter of metallic marker on catheter	automated edge definition of catheter segment	automated edge definition of catheter segment; when catheter not usable, based on distance between cardiomaker rings on catheter as assessed in biplane views	automated edge definition of catheter segment	manual or automated edge definition of catheter segment
14. Correction procedure for differential magnification between catheter and arterial segment from biplane views available on your system? ('out-of-plane' magnification)	NO	NO	NO	NO	NO

4. User indicates only starting and end points of arterial path line, or position of obstruction and definition of search window, followed by automated path line tracing (LeFree, Lienard, Oswald, Parker, Reiber, Vogel, Wankling).

By the first approach, Nichols only places windows over the stenotic and normal segments, and the width of the arterial segment within each of these windows is computed with edge detection techniques.

If the edge positions of an entire coronary segment must be computed, the best approach is to detect these points along scanlines perpendicular to a local path line of the segment. The next three approaches have been directed towards the definition of such a connected path line. The term path line is frequently used in this chapter instead of the commonly used word centerline, since the path line usually does not follow the true center of the vessel; a precisely detected centerline is not required, since the path line only functions as an initial model for the subsequent contour detection. The only requirement to this path line is that it remains within the arterial boundaries to be detected.

The second user-interactive approach, therefore, requires that the operator defines with a sonic pen, writing tablet or mouse a number of path line points which are subsequently connected by interpolation. This path line is usually smoothed; from these data the scanlines perpendicular to the local path line directions can be determined for the subsequent computation of the edge positions. A clear disadvantage of this technique is that the amount of user-interaction may become significant, particularly in curved segments, in which the distance between subsequent points must be chosen small to make sure that the connecting lines will not be drawn outside of the arterial segments.

Reiber et al. in an earlier version (CAAS) of their quantitative coronary analysis system and Selzer et al. have advocated to update this path line by a new one computed from the contour positions once these have been detected and possibly corrected manually, and to repeat the contour detection procedure. By means of this iterative approach the influence of the user definition of the path line points on the detected contour positions can be minimized.

In a slightly more complicated approach, these path line points are connected by automated path line tracing techniques (Doriot).

Finally, automated path line tracers have been developed requiring an absolute minimum amount of user-interaction. This is a must for on-line QCA-systems; other requirements for on-line use include: (1) very short processing time (preferably less than a few seconds); (2) robustness (success score preferably higher than 90%); and (3) if additional manual interventions are necessary in the remaining 10% of the cases, these should also be very simple and effective. LeFree's and Vogel's method requires the operator assignment of the approximate center of the lesion and the diameter of a circle defining the region of interest within which the path line is to be found. This technique is fast and relatively robust, but lacks the possibility of a simple manual correction; if it fails, the procedure must either be redone or

individual path line points must be repositioned one by one. The other implementations require only the manual definition of a starting point and an end point, and the path line tracer then automatically searches for the connecting path line. There is only one constraint on this manual procedure, namely that these two points are to be placed *inside* the arterial segment; there is no need for these points to be close to the actual center of the vessel, any place within the vessel is acceptable. Also, since the arterial path to be detected only functions as a rough model for subsequent contour detection, it does not need to follow the actual centerline of the vessel. Unfortunately, data on success scores, processing times and correction procedures are not available for the different implementations.

For completeness, the work by Hoffman et al. using an innovative double-square-box algorithm for the automated tracing of the arterial path lines in subtracted digital angiograms [67] should be mentioned, as well as the approach by Smets et al. [68], who uses a path line tracer developed by Fischler [69], again applied to subtraction images. Barth et al. have developed a technique for the automated three-dimensional recognition of the coronary tree on subtracted digital (Siemens Digitron II) image pairs [70, 71]. The tracing is started by marking the root of the tree with two points to select the vessel and the flow direction. The algorithm proceeds by looking for continuations in any direction similar to a radar scanner. It requires manual interaction only for corrections in critical regions of the images, where vessels are superimposed in both views, or where the vessel dimensions are below detectability.

Figure 2 shows an example of the automated path line tracer technique developed by Van der Zwet et al. at the Erasmus University [49, 72]. In this particular implementation a combination of two algorithms have been used for the automated detection of the path line of the selected segment. The first one, a tracing algorithm, is used to find all curves (traces) in the image that are candidates for being (a part of) the path line. The second algorithm (a box algorithm) is used to provide seed points that may belong to the path line being searched for, but have not been included in the traces found so far. From these seed points the tracing algorithm may find new traces which may be part of the desired path line. The algorithm stops as soon as a connective path has been found between the beginning and end points, or when the box algorithm cannot find additional seed points, while the path line has not been found yet. In situations that the detected path line does not follow the path that the user had in mind, the user may provide one additional point in the missing portion of the segment. The program will then search for a new path line, from the beginning point via the correction point to the end point. If necessary, this correction procedure can be repeated. On the basis of an evaluation study including a total of 103 short and long arterial segments, it was concluded that the algorithm found an acceptable path line in the first iteration in 89.3% of the cases; in 99.0% of the cases an acceptable path line was found in two iterations. Implemented on a Compaq 80386 (20 MHz) the

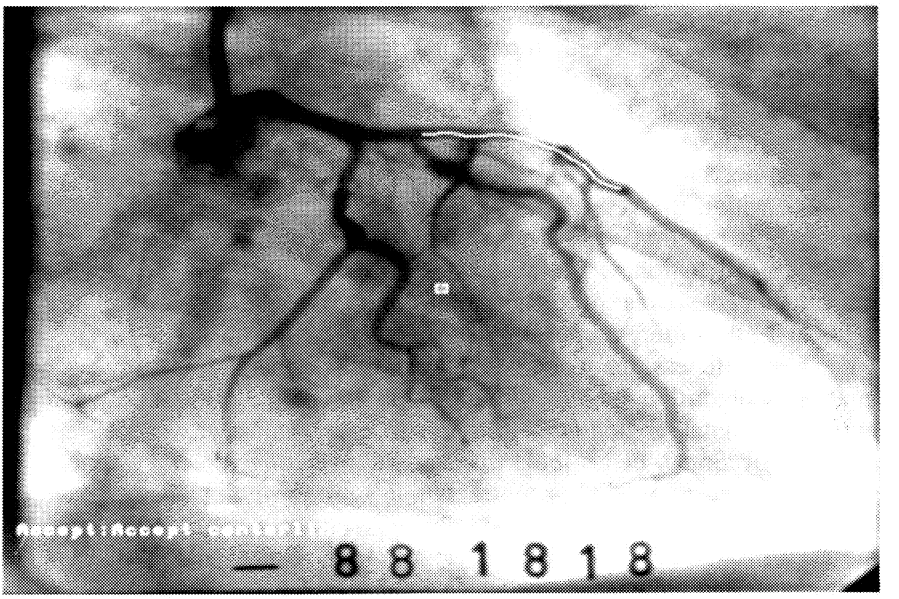

Fig. 2. Following the manual definition of the beginning and end points of the mid portion of the LAD, the path line is detected automatically [105].

average and maximum processing times were very low (first iteration: 265 ms and 1.89 s, second iteration: 211 ms and 0.52 s, respectively).

Edge definition (Table 5, item 11)

Still always there does not seem to be one generally accepted contour detection technique, although there is a trend towards the use of a combination of 1st- and 2nd derivative functions (1—3). The following six approaches are in use:

1. Manual tracing (Brown)
2. 1st-derivative function (Brunt, Kirkeeide, Selzer)
3. 1st semi-derivative function (Lienard)
4. 2nd-derivative function (Doriot, Wankling)
5. 1st- and 2nd-derivative functions (Collins, LeFree, Oswald, Reiber, Sanders, Vogel)
6. matched filter (Nichols, Parker, Sandor)

The first approach based on manual tracing of the arterial boundaries is quite obvious and does not require computer-supported edge detection techniques.

The following four approaches are based on the use of 1st-derivative, 1st semi-derivative, 2nd-derivative or a combination of 1st- and 2nd-derivative functions. Of importance to know is also whether the edge positions are

defined by the maximal values of these derivative functions or by the zero-crossing; unfortunately, these data are not available from all investigators. The typical shapes of these functions for a model of a scanline perpendicular to the local direction of a path line of an arterial segment is shown in Figure 3. It has been our experience that using the maximal values of only the 1st- or 2nd-derivative functions fit the arterial segments too tightly or too widely, respectively; in these cases certain correction values should be included to shift the detected edge positions towards the true arterial boundary positions. On the other hand, it is not clear that such approach will work under all kinds of imaging conditions and for all vessel sizes. These implementations should certainly be validated using perspex phantom studies with the models

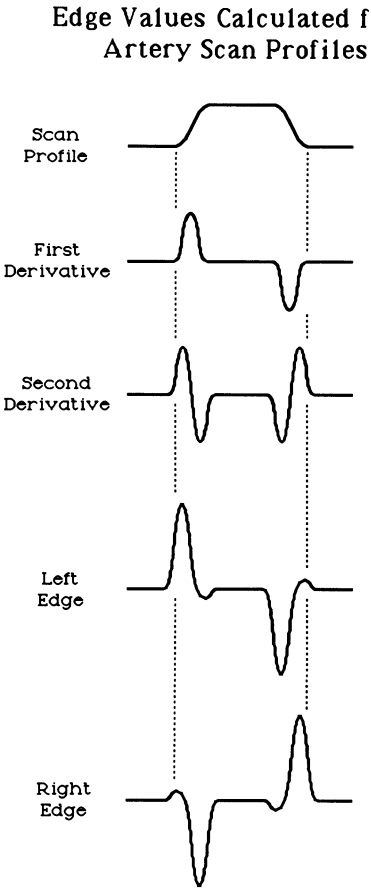

Fig. 3. Schematic presentation of the brightness profile of an arterial vessel assessed along a scanline perpendicular to the local path line direction, and the computed 1st-derivative, 2nd-derivative and the combinations of these 1st- and 2nd-derivative functions; the maximal values of the last functions determine the edge positions.

filled with different concentrations of the contrast agent and acquired at different kV-levels.

We as well as others have found that the maximal response of the weighted sum of the first- and second-derivative functions define very accurately the actual boundary positions [41].

Another important aspect in the contour detection procedure is the question whether the contour positions are detected on a scanline by scanline basis or using techniques which take all the edge information along the arterial segment into account. Following the first approach, expectation windows are usually defined for each scanline predicted by the positions detected on the previous scanline to limit the search window. Under practical circumstances, the edge positions may easily wander off into sidebranches or follow other intervening structures. Linear programming techniques have been found to be very attractive because of the property that the entire contours are traced in corresponding cost matrices, i.e. the edge positions are not determined per individual scanline, but all information gathered from all the other scanlines is taken into account in finding an optimal path in the sense of minimal costs, or maximal edge strengths. As a result, this approach is less sensitive to intervening structures such as branches and overlying structures than the local approach. Usually, this approach is performed iteratively.

In our new ACA-package for the on-line arterial contour detection on the Philips DCI system the minimum cost approach is performed twice to obtain accurate results [49]. These same contour detection techniques are also applied in the off-line film-based PC-system of Reiber; in this case additional accuracy and precision can be obtained by making use of the optical zooming features. First, using the initial path line as a model, a global approximation of the contours is found in the original nonmagnified image (matrix size 512^2). Next, a ROI of size 256^2 encompassing the segment being analyzed is magnified two-fold using a linear interpolation technique. In the second iteration the first rough approximations of the contours are used as new models, and accurate contours of the arterial segment are found, again using the minimum cost algorithm. These contours are displayed and the user may correct, if necessary, (a part of) these contours by erasing and redrawing this portion. When the user applies an extensive correction to one of the contours, the minimum cost algorithm is again applied using the corrected portion as a model, and allowing only a limited scan width. It must be clear that corrections should be kept to a minimum as the goal of all these QCA-developments is to achieve automated contour detection approaches. However, in the limited number of cases that the user really does not agree with the automatically detected contours, (s)he should be able to apply corrections as the human observer has the final responsibility for the accuracy of the detected contours. Figure 4 shows the contours detected in the first iteration in the nonmagnified image and Figure 5 the finally detected contours in the second pass in the two-fold magnified image [49]. These same

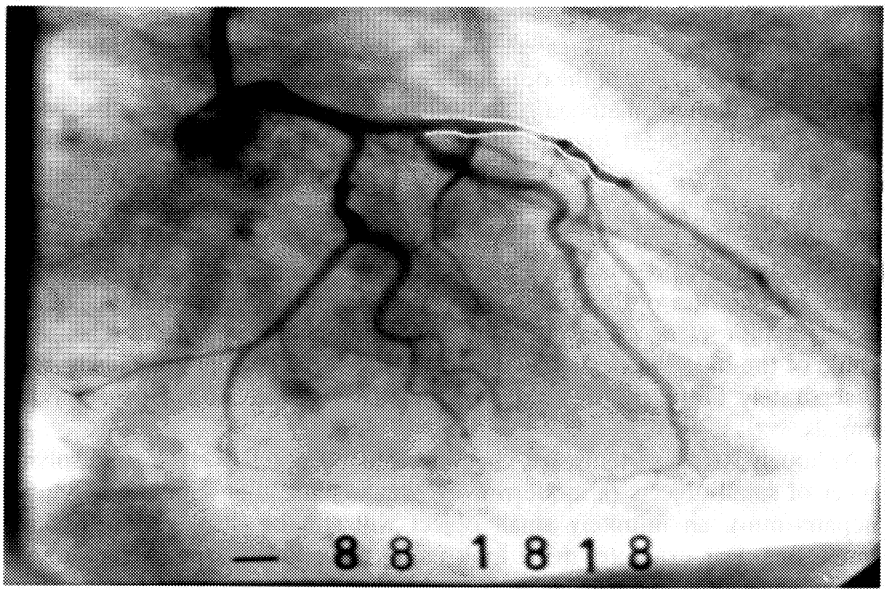

Fig. 4. Using the automatically detected path line of Fig. 2, the arterial boundaries are detected in the first iteration in the nonmagnified image using minimal cost criteria.

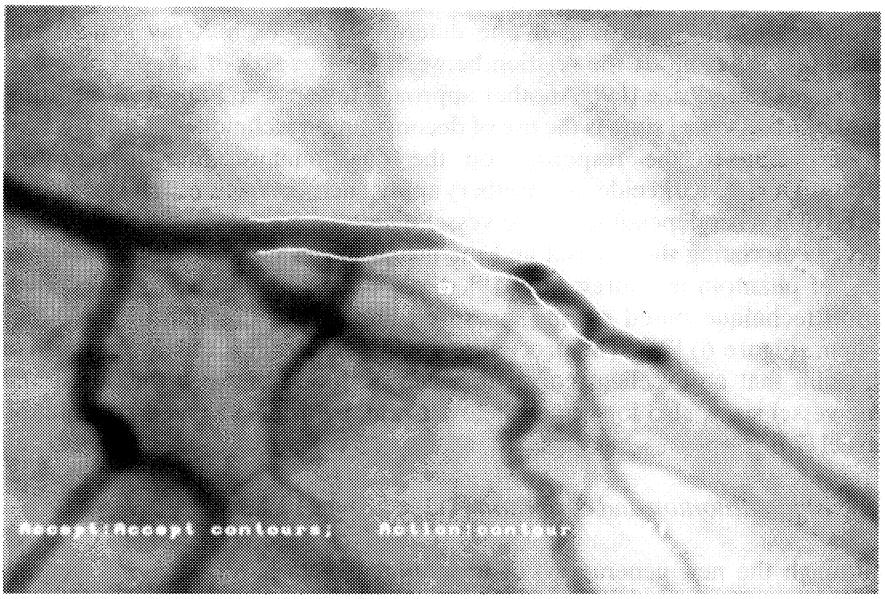

Fig. 5. In the second iteration, a ROI encompassing the arterial segment of Figure 4 is magnified two-fold and linearly interpolated, and the final contours are detected with the same edge detection technique and using the contours of Figure 4 as models.

contour detection techniques are also applied in the off-line film-based PC-system of Reiber; in this case additional accuracy and precision can be obtained by making use of the optical zooming features.

Following the last, matched filter approach, Nichols et al. define the width of the arterial segment by the full-width-at-half-maximum (FWHM) of the video densitometric profile measured along a scanline. Parker et al. apply a matched filter kernel to the density profiles defined perpendicular to the automatically detected centerline of the vessel to obtain a likelihood matrix [31, 31]. Dynamic programming techniques are then applied to the likelihood matrix to find the optimal paths and thus the optimal boundaries of the vessel. Sandor et al. have used the inflection point on a transverse scan profile of the blood vessel's image as its border or "edge" point. This is done by separately fitting the two sides of the vessel profile with 5-degree polynomials.

Although X-ray systems are characterized by a relatively high resolving power of small objects (a modern 6—7″ image intensifier should resolve 3.8 linepairs/mm), an infinitely small object will still be displayed with finite dimensions. For example, if we look along a scanline perpendicular to the copper wires of a cm-grid, an approximately Gaussian-shaped function will be measured. As a result, most quantitative coronary arteriographic systems with automated edge detection techniques cannot measure arterial sizes accurately below 0.7—0.8 mm. However, it is just the vessel sizes below 1 mm which are of most interest for QCA-studies [2]. This limitation in resolution can be improved if one determines for each X-ray system and image intensifier mode the relation between the true size of a vessel phantom and its measured size [19]. Another approach towards an improved measurement of small vessel sizes is the use of deconvolution techniques [73].

According to the responses on the questionnaire, four investigators (Brunt, Doriot, Kirkeeide and Reiber) apply such corrections. Doriot adds a correction term depending on the vessel diameter, Kirkeeide uses calibration curves correlating the derived and the actual vessel sizes developed with the help of phantom measurements [19], while Reiber applies a novel deconvolution technique based on the measured line-spread function of the X-ray system (Figure 6) [73]. The procedure applied by Brunt is unknown. Barth et al. claim that an excellent correlation can be found between measured and true vessel sizes, also for vessels below 1 mm, by using a shaped convolution kernel [74].

Pincushion distortion and correction (Table 5, item 12)

Although the new generations of image intensifiers hardly demonstrate any pincushion distortion, particularly with multi-mode intensifiers used in the smallest modes (4—6″), it is still useful to have a correction procedure available for the older types. Pincushion distortion results in a selective magnification of an object near the edges of the image as compared to its size in the center of the field. These differences need to be corrected for, if

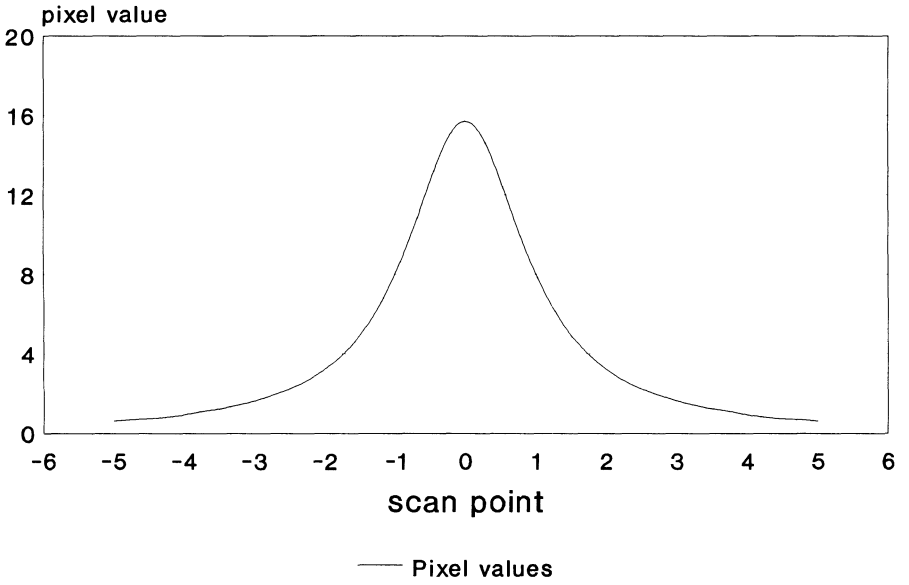

Fig. 6. Typical example of the line-spread function measured for a particular X-ray system.

absolute diameter measurements are to be derived from coronary arteriograms. The standard procedure to assess the degree of distortion present is to film a cm-grid, which is positioned against the input screen of the image intensifier. Theoretically, this needs to be done only once for a given image intensifier tube at each of the available magnification modes. However, in practice, it may be advisable to redo this at three month intervals and certainly after a service procedure on the X-ray system; quality control services on the X-ray systems including such repeated measurements for QCA-studies are now commercially available [75].

From the questionnaire it becomes clear that the following two major approaches can be distinguished:

A. *Only contour positions corrected*
   1. Radially symmetric parabolic correction function:
      Brown, Doriot, Kirkeeide
   2. Correction vectors computed from cm-grid for the individual intersection points of the wires:
      Oswald, Reiber, Sandor, Selzer

B. *Entire image (position + intensity) corrected*
   1. Based on detected intersection points of cm-grid:
      Brunt, Oswald, Wankling (only ROI)
   2. Image warping:
      Optional: Parker, Vogel

Collins, LeFree, Lienard, Nichols and Sanders do not correct for the pincushion distortion.

In approach A1, the investigators base their correction procedure on the theory that pincushion distortion is radially symmetric about the central X-ray beam, because of the rotational symmetry of the curved image intensifier's input screen and its internal fields [76]. An empirically determined analytical function of the radius is then used to correct for the distortion. However, in practice S-shaped distortion can be noticed on the cm-grid image among others due to the earth magnetic field, which makes that the radial symmetry is not valid anymore under those circumstances.

Approach A2 makes no assumption about the geometrical distribution of the distortion, but stores the relative magnifications of all the intersection points of the cm-grid. For a given point in the image which does not concur with one of the display intersection positions, the correction vector can be determined by bilinear interpolation between the correction vectors of the four neighboring intersection points.

These implementations have an important computational advantage in common, in that only contour positions are corrected for the distortion.

In the second approach (B) the entire image is corrected, usually both for the geometric position of the individual pixels as well as their intensity. This can be done again on the basis of the detected intersection points of the cm-grid (B1) or by using a 1 cm spaced orthogonal array of bronze ball bearings (B2) (Vogel). For these purposes image warping techniques are applied. An important advantage of this approach is that densitometric measurements can also be corrected for the pincushion distortion. A disadvantage, of course, is the computational expense.

There exists one possibly major problem with the pincushion correction procedures presently applied and that is that the cm-grids are always acquired in one particular setting of the X-ray system (e.g. AP view), while the correction vectors are also applied to other angiographic views. Onnasch et al. and Solzbach et al. have demonstrated that the distortion is rotation dependent due to the earth magnetic field [77, 78]. If the additional errors are small, one does not need to worry about this rotational dependency; otherwise, the correction vector data have to be established for individual angiographic views which would make it rather cumbersome. More research is necessary for this particular problem. So far none of the investigators has worried about this potential problem.

Calibration (Table 5, item 13)

To compute absolute sizes of an arterial segment analyzed requires the determination of a calibration factor. This is a very important step in the entire analysis procedure, since any error made here will be carried over to the vessel diameter measurements.

From the responses of the questionnaire it can be derived that six major approaches have been developed:

A. *Manual definition of the boundaries of a catheter segment*
   Brown
B. *Automated edge definition of a catheter segment*
   Brunt, Collins, LeFree, Lienard, Kirkeeide, Nichols, Oswald, Reiber, Sanders, Sandor, Selzer, Vogel, Wankling
C. *Analytically from geometric X-ray system setting*
   Kirkeeide (if isocentrically acquired from biplane views), Oswald, Parker
D. *Biplane assessment of the distance of cardio-marker rings on the catheter (1 cm spacing)*
   Kirkeeide, Oswald, Selzer
E. *Assessment diameter of metallic marker on the catheter*
   Sanders
F. *Use of a calibration cube with 15 steel markers for 3D reconstruction*
   Doriot

If the diameter of the catheter is used as a scaling device, the contours of a short segment of the tip or shaft may be either manually defined (A) with a writing tablet (Brown from biplane images), or contour detection techniques similar to those used for the coronary segments may be applied (B). A priori information may be included in the iterative edge detection procedure, based on the fact that the selected part of the catheter is the projection of a cylindrical structure. In this way parallel contours can be obtained, also for curved segments [72]; however, tapering segments should always be avoided. It should also be realized that the size of the catheter as given by the manufacturer, in general, deviates from its true size, especially for disposable catheters. Therefore, for intervention studies it is advisable to measure the size of the catheter following the catheterization procedure with a micrometer [40, 44, 48]. This approach is usually applied to single plane analyses. The change in magnification for two objects located at different points along the X-ray beam axis is about 1.5% for each centimeter that separates the objects axially with the commonly used focus-image intensifier distances. If biplane data is available, one may correct for this out-of-plane magnification; this is done by Brown (A). The biplane images should, of course, always be selected in the same phase of the cardiac cycle.

Following the third approach (C), the size of an object in the single plane through the center of rotation of the X-ray system (isocenter) and parallel to the image intensifier input screen can be determined from simple geometric principles from the height levels of X-ray tube and image intensifier. This computed calibration factor is only applicable to objects in the plane of the catheter parallel to the image intensifier input screen. Therefore, for objects above or below the center of rotation a slightly more complicated analysis must be carried out, requiring a second, preferably orthogonal view of the object. Wollschlaeger et al. have developed a method to calculate the exact radiological magnification factors for each point in the fields of view of

biplane multidirectional isocentric X-ray equipment [79, 80]. By this approach they avoid two potential error sources: contour detection of the catheter segment, and the differential magnification of the scaling device and the arterial segment. Parker also determines the calibration factors from the geometric X-ray system settings in biplane images; one of the options of Kirkeeide's and Oswald's method is also based on this approach.

From the above, it is clear that for the measurement of truly absolute sizes of coronary segments, two views, preferably but not necessarily orthogonal to each other, are required. However, if one is only interested in the changes in sizes of coronary segments as a result of short- or long-term interventions, excellent results can be achieved from single plane views. For these situations one must make sure that for the repeat angiogram the X-ray system is positioned in exactly the same geometry as during the first angiogram. This requires registration of the angles and height levels of the X-ray system, preferably on line with a microprocessor-based geometry read-out system [44]. Although the calibration factor used for a particular coronary arterial segment is then only an approximation of the true calibration factor, the same systematic error will be present for the first and repeat angiograms.

Some time ago, several new types of catheters with cardiomarker rings have been designed on the request of a number of investigators. Kirkeeide determines the distance between the cardiomarker rings (1 cm spacing) in biplane angiograms (D), while Sanders measures the diameter of a metallic marker on the catheter (E). In Kirkeeide's approach biplane views are a must because of foreshortening problems in the different views. The approach by Sanders does not require biplane images since the size of the cylindrical structure does not change in the different views; however, for single plane acquisitions the out-of-plane magnification error remains present. In this last case, the catheter manufacturer must assure that the outside shape of the rings is not convex or concave; they must be perfectly cylindrical. Because of the high contrast of the marker in the X-ray images, the edges can be defined relatively reliably.

Finally, Doriot uses a calibration cube with 15 steel markers for calibration purposes for his 3D reconstruction techniques (F). The acquisition of such a calibration device can only be done once the patient has left the table, which is a disadvantage.

At this point in time, three investigators correct for out-of-plane magnification. Brown uses the intrathoracic spatial relations assessed from normal sized human hearts [7], while Kirkeeide and Oswald determine the out-of-plane distances from biplane views. The majority of the investigators (Brunt, Collins, LeFree, Lienard, Nichols, Reiber, Sanders, Sandor, Selzer, Vogel and Wankling) do not apply such corrections. As mentioned earlier, Doriot and Parker apply these corrections as part of their 3D reconstruction processes.

Contour analysis approaches (Table 6)

From the contours of the analyzed arterial segment, following smoothing, pincushion correction and calibration, a diameter function can be determined by computing the distances between the left and right edges. From these data various clinically relevant parameters (Table 6, item 20) can be calculated, which have been summarized in Table 7 indicating how many of the total of sixteen investigators use a particular parameter. From Table 7 it can be concluded that the majority of the investigators use the "simple" parameters obstruction diameter, reference diameter, %-D stenosis, obstruction area and %-A stenosis assessed by different techniques. Less frequently used are the length of the obstruction, the area of the atherosclerotic plaque, the symmetry of the stenosis, and finally the transstenotic pressure gradient at a given flow. All parameters mentioned above will be discussed briefly below.

Obstruction diameter

Thirteen of the total of sixteen investigators responded that they use the obstruction diameter. Obviously, this is one of the most important parameters to be measured in QCA. To determine the effects of interventions on the severity of coronary obstructions, one should compute the changes in minimal obstruction diameter and not those in percentage diameter narrowing, as the reference position in general will also be affected by the intervention [81, 82]. The minimal obstruction diameter is also present to the inverse fourth power in the formules describing the pressure loss over a coronary obstruction. Of relevance, although not included in Table 6, is also to know how the minimal obstruction diameter is computed precisely, e.g. as the single smallest diameter value, as the average value of this smallest diameter value and its two or three neighbors; also how heavily were the originally detected contours smoothed, etc. Some answers to these questions could be obtained if data were provided on the variations in the diameter measurements of perspex models of smooth tubes.

Obstruction area

For the assessment of the obstruction area three possibilities have been developed and implemented: (1) by assuming circular cross sections; (2) by assuming elliptical cross sections; and (3) by densitometry. If only a single view is available, or if one wants to determine the cross-sectional area per individual view, the only assumption that one can make is that of a circular cross section of the artery. If more views are available, then a reasonable approximation of the true cross-sectional area can also be obtained by averaging the results from the individual views.

For a pair of orthogonal views, an elliptical cross section can be assumed. However, a number of limitations are present which are usually overseen: (1)

Table 6. Contour analysis (6-1a).

	Brown	Brunt	Collins	Doriot	Kirkeeide	LeFree
17. Reference for %-D stenosis measurement	user-defined	computer estimation of pre-disease reference dimensions at obstruction; tapering of vessel allowed	user-defined	user-defined	user-defined	user-defined
18. Do you calculate roughness measure of arterial segment as an indication for diffuse atherosclerosis?	NO	NO (in coronary studies); previously done for femoral studies	NO	NO	NO	NO
20. Derived parameters coronary arterial segment	— obstruction diam. — obstruction area (elliptical cross sections)	— obstruction diam. — obstruction area (circular cross sections)	— obstruction diam. — obstruction area (circular cross sections; by densitometry)	— obstruction diam. — obstruction area (circular cross sections; elliptical cross section when possible; by densitometry)	— obstruction diam. — obstruction area (circular cross sections for single plane images; elliptical cross sections for biplane image pairs)	— obstruction diam. — obstruction area (circular cross sections for single plane images; elliptical cross sections for biplane image pairs)
	— reference diam. — %-D stenosis — %-Area stenosis (elliptical cross sections)	— reference diam. — %-D stenosis — %-Area stenosis (circular cross sections)	— reference diam. — %-D stenosis — %-Area stenosis (circular cross sections; by densitometry)	— reference diam. — %-D stenosis — %-Area stenosis (circular cross sections; elliptical cross sections when possible; by densitometry, under development)	— reference diam. — %-D stenosis — %-Area stenosis (assuming elliptical cross sections)	— reference diam. — %-D stenosis — %-Area stenosis (circular cross sections for single plane images; elliptical cross sections for biplane image pairs)
	— length of obstruction — area atherosclerotic plaque — transstenotic pressure gradient (mmHg) at given flow	— — area atherosclerotic plaque —	— — —	— length of obstruction — —	— length of obstruction — — transstenotic pressure gradient (mmHg) at given flow	— length of obstruction — —

Table 6. Contour analysis (6-1b).

	Lienard	Nichols	Oswald	Parker	Reiber
17. Reference for %-D stenosis measurement	user-defined	user-defined	2 options: a. user-defined b. computer estimation of pre-disease reference dimensions at obstruction; tapering of vessel allowed	—	— user-defined — interpolated technique for estimation of 'normal' vessel dimensions (tapering of vessel allowed)
18. Do you calculate roughness measure of arterial segment as an indication for diffuse atherosclerosis?	NO	NO	NO	NO	under development
20. Derived parameters coronary arterial segment	—	— obstruction diam.	— obstruction diam.	—	— obstruction diam.
	—	— obstruction area (densitometric)	— obstruction area (circular or elliptical cross sections, or by densitometry)	— obstruction area (by densitometry)	— obstruction area (circular cross sections)
	—	— reference diam.	— reference diam.	—	— reference diam.
	— %-D stenosis	— %-D stenosis	— %-D stenosis	—	— %-D stenosis
	— %-Area stenosis (by densitometry)	— %-Area stenosis (by densitometry)	— %-Area stenosis (circular or elliptical cross sections, or by densitometry)	—	— %-Area stenosis (circular cross sections)
	—	—	—	—	— length of obstruction
	—	—	—	—	— symmetry of stenosis
	—	—	—	—	— area atherosclerotic plaque
	—	—	— transstenotic pressure gradient (mmHg) at given flow	—	— transstenotic pressure gradient (mmHg) at given flow

Table 6. Contour analysis (6-1c).

	Sanders	Sandor	Selzer	Vogel	Wankling
17. Reference for %-D stenosis measurement	user-defined (1 or 2 reference segments)	user-defined	computer estimation of pre-disease reference dimensions at obstruction; tapering of vessel not taken care of	user-defined	user-defined
18. Do you calculate roughness measure of arterial segment as an indication for diffuse atherosclerosis?	YES, measure variation σ of vessel diameters	YES, variance of subsegments (being implemented in new version)	YES; standard deviation of differences between diameter profile and least squares straight line	NO	NO
20. Derived parameters coronary arterial segment	— obstruction diam.	— obstruction diam.	— obstruction diam.	— obstruction diam.	—
	—	— obstruction area (by densitometry)	— obstruction area (circular cross sections; optional: elliptical cross sections; or densitometry)	— obstruction area (circular cross sections for single plane images; elliptical cross sections for biplane image pairs)	
	— reference diam.	— reference diam.	— reference diam.	— reference diam.	—
	— %-D stenosis	— %-D stenosis	— %-D stenosis	— %-D stenosis	— %-D stenosis
	—	— %-Area stenosis (by densitometry)	— %-Area stenosis (circular cross sections; optional: elliptical cross sections; by densitometry)	— %-Area stenosis (circular cross sections; elliptical cross sections; or by densitometry)	— %-Area stenosis (either circular cross section, or by densitometry)
	— length of obstruction	— length of obstruction	— length of obstruction	—	— length of obstruction
	—	—	— area atherosclerotic plaque	—	—
	—	—	— optional; transstenotic pressure gradient (mmHg) at given flow	—	—

Table 6. Contour analysis (6-2a).

	Brown	Brunt	Collins	Doriot	Kirkeeide	LeFree
21. How do you choose your angiographic views?	calculate 'optimal' views; permit small variations from calculated views to provide best visual image of lesion	visual determination of best views	visual determination of best views	select standard views (e.g. RA030, LA060) with (near future on Bicor) or without (at present Kardoskop U) cranial/caudal angulations	start with standard views, then optimize for patient anatomy	start with standard views, then possibly visual customization to particular anatomy
22. What do you do with the results from two corresponding (preferably orthogonal) views?	combine the results in a 3D-presentation using elliptical cross sections	use as separate items	use as separate items	average the diameters from the two views	combine the results in a 3D-presentation using elliptical cross sections	combine the results in a 3D-presentation using elliptical cross sections
23. For a 3D-presentation of the data from the two views, how are the detected arterial segments registered?	on the basis of the positions of the minimal diameter values in the two views	—	—	concordance is established by the 3D-reconstruction process	user defines "common" points, computer refines for best correlation	program defaults to minimal diameter positions, but provides the ability to override with anatomical landmarks

Table 6. Contour analysis (6-2b).

	Lienard	Nichols	Oswald	Parker	Reiber
21. How do you choose your angiographic views?	—	select optimal view: no foreshortening of vessel segment of interest	2 options: a. calculate "optimal" views b. visually determine which views best suit your purpose	visual determination of best views	start with standard views, then optimize for patient anatomy
22. What do you do with the results from two corresponding (preferably orthogonal) views?	—	only use single plane analyses with densitometry	2 options: a. average the results from the 2 views; b. combine the results in a 3D-presentation using elliptical cross sections	average the results from the two views	use as separate items
23. For a 3D-presentation of the data from the two views, how are the detected arterial segments registered?	—	NA	3 options: a. on the basis of the minimal diameter values in the 2 views; b. on the basis of the positions of the minimal densitometric cross-sectional values in the two views; c. on the basis of the positions of sidebranches	—	NA

Table 6. Contour analysis (6-2c).

	Sanders	Sandor	Selzer	Vogel	Wankling
21. How do you choose your angiographic views?	select standard views	for follow-up study use enlarged photo of first study	select standard views	visual determination of best views	—
22. What do you do with the results from two corresponding (preferably orthogonal) views?	use as separate items	—	average the results from the two views; optional: combine the results in a 3D-presentation using elliptical cross sections	combine the results in a 3D-presentation using elliptical cross sections.	—
23. For a 3D-presentation of the data from the two views, how are the detected arterial segments registered?	NA	—	on the basis of the positions of side-branches or other landmarks	on the basis of the positions of the minimal diameter values in the two views	—

Table 7. Derived parameters coronary arterial segment.

— Obstruction diameter (mm)	13×
— Obstruction area (mm^2)	
* circular	9×
* elliptical	7×
* densitometric	7×
— Reference diameter (mm)	13×
— %-D stenosis (%)	15×
— %-A stenosis (%)	
* circular	9×
* elliptical	7×
* densitometric	8×
— length of obstruction (mm)	9×
— symmetry of stenosis	1×
— area atherosclerotic plaque (mm^2)	4×
— transstenotic pressure gradient (mmHg) at given flow	5×

the point of minimal diameter in one view does not need to coincide with the point of minimal diameter in the other view; (2) calculating an elliptical cross section requires that the minimal diameters in the two views are used as the short and long axes of the ellipse, which does not need to be a correct assumption, since the orientation of the assumed elliptical cross section is unknown [83].

The third approach by densitometry would theoretically provide the best approximation of the cross-sectional area, since the value is not directly dependent on the measured diameter, but on the integrated densities within the boundaries of the vessel. However, as will be discussed under the Section Densitometry, this approach also has severe limitations and has not been shown to be very reliable in clinical practice.

Based on the pros and cons of the different approaches, I am in favor of the simplest technique, i.e. assuming a circular cross section per view and averaging the results from possibly other available angiographic views.

Reference diameter

Although the absolute minimal obstruction diameter is one of the parameters of choice to describe the changes in the severity of an obstruction as a result of an intervention, percentage diameter narrowing in an individual case is intuitively a very convenient parameter to work with.

The conventional way to determine the percentage diameter stenosis of a coronary obstruction, requires the user to indicate a reference position. A reference diameter is then usually computed as the average value of a number of diameter values in a symmetric region centered around the user-defined reference position. This or a similar approach, which is denoted the user-defined reference technique, has been taken by Brown, Collins, Doriot,

Kirkeeide, LeFree, Lienard, Nichols, Oswald, Reiber, Sanders, Sandor, Vogel and Wankling.

However, it is clear that this computed %-D narrowing of an obstruction depends heavily on the selected reference position. In arteries with a focal obstructive lesion and clearly normal proximal arterial segment, the choice of the reference region is straightforward and simple. However, in cases where the proximal part of the arterial segment shows combinations of stenotic and ectatic areas, or in cases where a 'normal' portion is just clearly not available, the choice may be very difficult. This selection procedure for the normal reference is not at all standardized and, in practice, is difficult to reproduce reliably during sequential analyses. To minimize these variations, alternative methods have been developed which are not dependent on a user-defined reference region. By these methods an estimation of the normal or pre-disease arterial size and luminal wall location is obtained on the basis of the computer centerline and the 90th percentile of the diameter values (Selzer [54, 56, 59], on the basis of a first-degree polynomial computed through the diameter values of the proximal and distal portions of the arterial segment followed by a translation to the 80th percentile level (reference diameter function) (Reiber, [35, 42]) or by the so-called iterative linear regression technique (Van der Zwet [49, 72]); tapering of the vessel to account for a decrease in arterial caliber associated with branches is taken care of in the last two approaches. The reference diameter is now taken as the value of the reference diameter function at the location of the minimal obstruction diameter. This approach is denoted the interpolated or computer-defined reference technique. An important practical advantage of this technique is, that knowledge about the exact location of a reference, either proximal or distal to the stenosis, is not required for the analysis of repeated angiograms. On the other hand, this technique requires that coronary arterial segments are analyzed in a standardized manner, i.e. from branch point to branch point, so that the lengths of the segments are approximately equal in repeated or sequential analyses; in other words, the diameter functions should be based on roughly the same number of measurement points. This kind of standardization is not difficult to realize, but requires discipline on the part of the analyst.

An example of our technique is shown in Figure 7 for the obstruction in the mid portion of the LAD in the RAO-projection of Figure 5. The actual contours as well as the estimated pre-disease reference contours of the arterial segment are superimposed in the image. Figure 8 shows the presentation of the final results for the obstruction of Figure 7 as displayed on the video screen. In the left upper quadrant the magnified ROI and the contour data are displayed in a minified mode. The difference in area between the reference and the detected luminal contours is marked over the obstructive lesion; this area is a measure for the atherosclerotic plaque in this particular angiographic view (see Section Area atherosclerotic plaque). In the lower left quadrant the diameter function and derived parameters are displayed. The

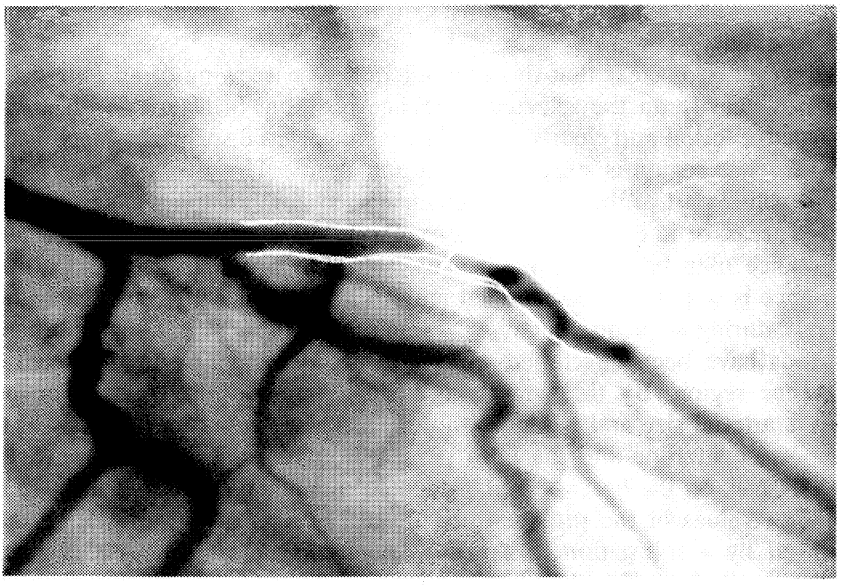

Fig 7. For the example of Figure 5, the reference contours have been determined and displayed in the image. The straight line connecting the reference contours at the obstruction is denoted the computer-defined reference diameter. The area between the reference and the detected luminal contours over the obstructive region defines the area of the atherosclerotic plaque in this particular angiographic view.

straight line in the diameter function is the reference diameter function. In the upper right quadrant of the image the characteristic function for the assessment of the stenotic flow reserve as proposed by Kirkeeide [18] is presented; in this case a value of 2.61 was found.

The precise implementations of the computer estimation of the pre-disease reference dimensions by Brunt and Oswald are unknown; apparently, their approaches also allow tapering of the vessel.

Percent diameter — and area-stenosis

From the obstruction D_0 and reference D_r diameters, either assessed by the user- or computer-defined approach, the percent diameter stenosis (%-D stenosis) can simply be caculated as follows:

$$\%\text{-D stenosis} = (1 - D_0/D_r) \times 100\%$$

and the percent area stenosis (%-A stenosis) from the obstruction area (A_0) as computed by one of the three methods described earlier and the reference area (A_r) computed by the same method as follows:

$$\%\text{-A stenosis} = (1 - A_0/A_r) \times 100\%.$$

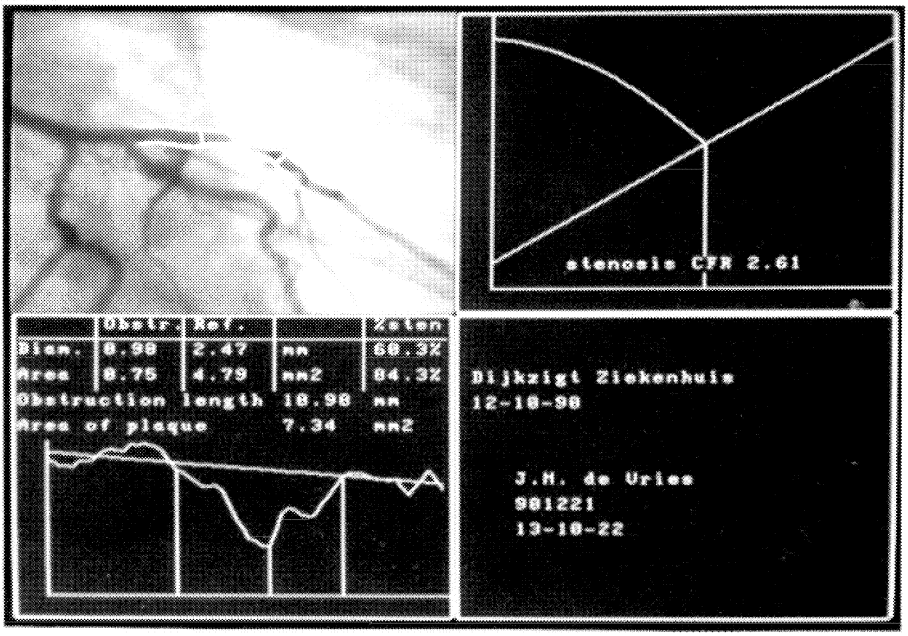

Fig. 8. Presentation of the final results for the obstruction of Figure 7 on the video screen of the PC-based coronary analysis system. In the left upper quadrant the magnified ROI encompassing the obstructed segment and the contour data are displayed in a minified mode. In the lower left quadrant the diameter function and derived parameters are presented. The straight line in the diameter function is the reference diameter function. The characteristic function for the assessment of the stenotic flow reserve as proposed by Kirkeeide [18] is presented in the upper right quadrant. Finally, hospital and patient demographic data are given in the lower right quadrant.

For a single view measurement assuming circular cross sections, this last formula simplifies to:

$$\%\text{-A stenosis} = (1 - D_0^2/D_r^2) \times 100\%.$$

Length of stenosis

According to the responses on the questionnaire nine investigators compute the length of the stenosis from the diameter function; details on the definition of this length parameter are not available. Although this seems a rather trivial parameter to compute, in practice, this is not the case particularly not in vessels with irregular dimensions. It has been our experience that this may lead to significant variations in the outcomes of the analyses, particularly if the user is allowed to change the boundaries of the stenotic length. The computer-defined reference technique allows an automated assessment of the length, which may be somewhat dependent on the length of the entire arterial

segment analyzed. In our latest implementation the beginning and end points of the obstruction are defined on the basis of local maxima criteria or by the crossing points of the actual arterial diameter function with the reference diameter function [49].

Area atherosclerotic plaque (mm^2)

The area of the projection of the obstructive plaque in a coronary arteriogram is denoted area of the atherosclerotic plaque in that particular angiographic view. This parameter can be computed if the following data can be determined reliably: extent of the obstructive region and the original size of the vessel at the stenosis before disease occurred (e.g. by the computer-defined reference technique). Basically, the area of the atherosclerotic plaque is then simply the integral of the distances between the luminal and the reference contours over the obstructive region, although other implementations are feasible as well, such as the sum of the pixels between the luminal and reference contours, and so forth. Four investigators (Brown, Brunt, Reiber, Selzer) provide this particular parameter.

Symmetry of stenosis

According to the questionnaire this parameter [84, 85] is only determined by Reiber et al. Their approach is based on the interpolated or computer-defined reference diameter technique and the reconstruction of a centerline over the obstructive region. Vessel midpoints for the proximal and distal "normal" portions are calculated by averaging the coordinates of the left and right contour points. For the obstructive region the vessel midpoints are obtained by interpolation between the proximal and distal vessel midpoints with a second-degree polynomial. The symmetry measure is given as a value between 0 and 1, and defined as follows: denote the area of the atherosclerotic plaque at the left-hand side of the vessel A_1 and at the right-hand side A_r. The symmetry measure is then calculated as:

$$\text{symmetry measure} = 1 - |A_1 - A_r| \div (A_1 + A_r).$$

A symmetry measure of 1 denotes a concentric obstruction with the number decreasing with increasing asymmetry or eccentricity of the obstruction. Zero represents the most severe case of asymmetry or eccentricity.

For completeness of this overview, the work by Vassanelli et al. should be mentioned, who have used the following definition of the eccentricity EI of a stenosis: $EI = B - 1/3A$, where A is the radius of the "normal" vessel and B the distance between the center of the "normal" vessel and the centerline in the stenotic segment; EI is greater than zero for eccentric segments and less than zero in concentric ones [86]. A stenosis is considered irregular if more than 25% of the nonadjacent segments are eccentric. Comparison with

histologic data showed that 88/93 (94.6%) sections were correctly predicted as eccentric and 8/11 (72.7%) as irregular.

Transstenotic pressure gradient (mmHg) at given flow

From the available morphologic data of the obstruction, the Poiseuille and turbulent resistances at different flows and thus the resulting transstenotic pressure gradients can be computed on the basis of the well-known fluid-dynamic equations [18, 21, 42, 58]. These hemodynamic data are provided by Brown, Kirkeeide, Oswald, Reiber and Selzer.

Roughness measure of arterial segment

Focal obstructions are of course easy to recognize. In most cases a focal obstruction will be superimposed on diffuse coronary artery disease, which may be manifest by a below normal size of the vessel, or by irregular changes in the size of the vessel. A number of investigators have tried to quantitate this roughness of the arterial wall as an indication of the degree of diffuse atherosclerosis.

Information about the "roughness" of the arterial segment and thus about diffuse coronary artery disease may be obtained by subdividing the coronary segment into any integer number of subsegments with a length of about 5 mm and calculating for each subsegment the minimal, maximal, mean diameter and the standard deviation of the diameter values [42]. On the basis of the ratio of the standard deviation value and the difference between minimal and maximal diameter, it can be determined whether a subsegment is focally or diffusely diseased, or normal. However, clinical validation procedures need to be carried out to determine the true value of this parameter.

Sanders uses the variation σ of the vessel diameters as a measure for diffuse atherosclerosis, while Selzer et al. fit a least-squares straight line through the vessel width profile and use the residual variance as a roughness measure. Sandor et al. also compute a variance related to subsegments. The other investigators do not calculate a roughness index for diffuse atherosclerosis. Crawford et al. have developed various edge roughness measures for femoral arteries [55]; two edge roughness measures were defined by the root-mean-square differences between two sets of edge coordinates obtained by the use of filters of different lengths.

How do you choose your angiographic views? (Table 6, item 21)

Quantitative coronary arteriographic (QCA) studies require that coronary segments are analyzed in at least two, preferably orthogonal, views because

of the possibly asymmetric shape of the coronary obstructions. In addition, each segment should preferably be filmed in planes parallel to the input screen of the image intensifier in the various views to avoid problems with foreshortening. This is the concept of triple-orthogonality which may be difficult to achieve in routine practice [79]. However, every attempt should be made to achieve such a goal.

The original idea behind this question was to obtain information about the selection of the angiographic views at the time of the catheterization procedure, i.e. it belongs to the angiographic acquisition phase, not to the analysis part of QCA. However, it may have given rise to some confusion; the investigators may have understood that this question referred to the angiographic view and frame selection process for QCA on the basis of already available angiographic data. As such, the outcomes should be read with the above in mind.

The investigators responded as follows to this question:

— *Visual determination of best views*
Brunt, Collins, Nichols, Oswald, Parker, Vogel
— *Select standard views with/without cranial/caudal angulations*
Doriot, Sanders, Selzer
— *Start with standard views, then optimize for patient anatomy*
Kirkeeide, LeFree, Reiber
— *Calculate "optimal" views*
Brown, Oswald

Three investigators (Lienard, Sandor and Wankling) did not respond to this question.

Thus calculation of "optimal" views is only done by Brown and Oswald. Brown starts out by calculating the optimal views on the basis of the average known directions of the individual arterial segments as assessed from 37 normal individuals [7], and then permits small variations from these calculations to provide the best visual image of a lesion.

What do you do with the results from two corresponding (preferably orthogonal) views? (Table 6, item 22)

This point was already discussed under the section about the determination of the obstruction area. According to the responses, six of the investigators (Brown, Kirkeeide, LeFree, Oswald, Selzer, Vogel) compute elliptical cross sections from the biplane data, requiring that the two views be matched such that the positions of the stenosis in both views coincide [5]. It is generally assumed, that the points of minimum diameter in both views correspond to the same site in the artery. However, it was discussed earlier that such an assumption can be a potential source of error. Doriot, Oswald, Parker and Selzer average the results (assuming circular cross sections) from the two views, while Brunt, Collins, Reiber and Sanders use the data as separate

items. Finally, Nichols only performs single plane analyses with densitometry. Lienard, Sandor and Wankling did not respond to this question.

For a (pseudo) 3D-presentation of the data from the two views, how are the detected arterial segments registered? (Table 6, item 23)

This part can also be of relevance for the determination of the elliptical cross sections mentioned in the previous paragraph. The matching procedure implemented by Brown, LeFree, Oswald and Vogel is indeed based on the assumption that the positions of the minimal diameter values in the two views correspond to the same 3D arterial position. Kirkeeide requires that the user defines "common" points in the two views followed by a computer refinement for best correlation, which represents an improvement in the matching procedures as compared to the simple approach mentioned above. Oswald registers the two views on the basis of the positions of the minimal densitometric cross-sectional values in the two views, which is theoretically a sound approach. A third possibility is by means of registration of the arterial segments on the basis of the positions of sidebranches as advocated by Oswald and Selzer, although this will not provide a solution for foreshortened segments. Finally, Doriot establishes the concordance by the 3D reconstruction process itself. All the other investigators do not provide (pseudo) 3D-presentations.

Densitometry (Table 8)

Theoretically, densitometry seems the ultimate solution for the computation of the vessel's cross-sectional area from a single angiographic view. It has been shown to work well in perspex phantoms; however, the application on routine coronary angiograms has been less successful. This is due to various error sources, among others: (1) the polychromatic X-ray source; (2) veiling glare and scatter; (3) beam hardening; (4) the orientation of the vessel of interest with respect to the X-ray beam; (5) sidebranches or branches lying very close to the arterial segment of interest will cause errors in the background correction technique; (6) if cinefilm is used the nonlinearity of the cinefilm; etc. For more details the reader is referred to the chapter in this book by James S. Whiting and references [1, 2, 3, 16, 36] which provide overviews on this technique.

Based on the questionnaire it was found that seven investigators (Collins, Lienard, Nichols, Oswald, Parker, Vogel and Wankling) perform at present densitometric analyses (Table 8, item 24), while two investigators (LeFree and Selzer) have the software available but do not use it for different reasons; finally, Doriot and Reiber are in the process of redevelopment of the technique. Seven of them use the Lambert-Beer Law to describe mathematically the X-ray absorption process from the X-ray source to the image intensifier; Wankling determined the corresponding transfer function empiri-

Table 8. Densitometry (8-1a).

	Brown	Brunt	Collins	Doriot	Kirkeeide	LeFree
24. Do you perform densitometric analysis of cross-sectional data from one angiographic view? Your technique is based on the following transfer functions:	NO	NO	YES	under development	NO	can but choose not to use it at present because of unsatisfactory results
— X-ray absorption from X-ray source to image intensifier (II)	—	—	Lambert-Beer Law	—	—	—
— from output II to brightness level in digitized image	—	—	assessed from digitized sensitometric strip on cinefilm with 11 steps	—	—	—
25. Do you correct for:						
— X-ray scatter?	—	—	NO	YES, planned to do so	—	—
— Veiling glare?	—	—	NO	YES, planned to do so	—	—
— Angulation of the vessel with respect to the input screen of the II?	—	—	NO	YES	—	—
— Background contribution?	—	—	by linear interpolation of background measurements from both sides or single side of vessel contours	YES	—	—
— Pincushion distortion?	—	—	NO	NO	—	—

Table 8. Densitometry (8-1b).

	Lienard	Nichols	Oswald	Parker	Reiber
24. Do you perform densitometric analysis of cross-sectional data from one angiographic view? Your technique is based on the following transfer functions:	YES	YES	YES	YES	under development
— X-ray absorption from X-ray source to image intensifier (II)	Lambert-Beer Law	Lambert-Beer Law	transfer function for entire chain empirically defined based on diameter-area relation	Lambert-Beer Law	Lambert-Beer Law
— from output II to brightness level in digitized image	linear transfer function	logarithmic transformation and use of characteristic curve of cinefilm		logarithmic transfer function	linear, logarithmic transfer function or sensitometric measurement per cinefilm
25. Do you correct for:					
— X-ray scatter?	NO	NO	NO	NO; active research	NO
— Veiling glare?	NO	NO	NO	NO: active research	NO
— Angulation of the vessel with respect to the input screen of the II?	NO	NO	NO	YES	NO
— Background contribution?	YES; by linear interpolation of background measurements left and right of vessel contours	YES; by linear interpolation of background measurements left and right of vessel contours	YES; by linear interpolation of background measurements left and right of vessel region	YES; by linear interpolation of background measurements left and right of vessel contours; mask subtraction if artefact free (ideally, an average mask)	YES; by linear interpolation of background measurements left and right of vessel contours
— Pincushion distortion?	NO	NO	YES; by warping the region of interest	NO	NO

Table 8. Densitometry (8-1c).

	Sanders	Sandor	Selzer	Vogel	Wankling
24. Do you perform densitometric analysis of cross-sectional data from one angiographic view? Your technique is based on the following transfer functions:	NO	NO	available, but not used in current studies	YES	YES
— X-ray absorption from X-ray source to image intensifier (II)	—	—	Lambert-Beer Law	Lambert-Beer Law	empirically determined
— from output II to brightness level in digitized image	—	—	transfer function assessed by calibrated density strip with 21 steps	logarithmic transfer function	empirically determined
25. Do you correct for:					
— X-ray scatter?	—	—	NO	NO	NO
— Veiling glare?	—	—	NO	NO	NO
— Angulation of the vessel with respect to the input screen of the II?	—	—	NO	NO	NO
— Background contribution?	—	—	YES, by linear interpolation of background measurements left and right of vessel contours	NO	YES, by linear interpolation of background measurements left and right of vessel contours
— Pincushion distortion?	—	—	NO	YES, optional (see 12)	NO

cally, while Oswald determined an overall transfer function from X-ray source to the brightness levels in the digitized image.

For the transfer function from the output of the image intensifier up to the brightness levels in the digitized image various approaches have been implemented: (1) for digital systems a linear transfer function is usually assumed (Lienard, Reiber), although logarithmic functions have also been used if internally a nonlinear function is applied, e.g. for white compression (Parker, Vogel); (2) for cinefilm approaches usually a logarithmic transfer function is used (Nichols, Reiber); (3) this approximation can be improved by a densitometric measurement per cinefilm (Collins, Reiber, Selzer); and (4) Wankling determined an empirical transfer function.

Finally, the question was posed whether one corrects for X-ray scatter, veiling glare, the angulation of the vessel, for the background contribution and for pincushion distortion. The individual data can be found in Table 8. From these data it can be concluded that the majority of these investigators do not apply such corrections with some of them actively involved in research in these directions, while all except for Vogel correct for the background contribution; this is usually done by measuring the background levels at both sides of the vessel, performing a linear interpolation for the pixels within the vessel's contours and subtracting these data from the brightness levels in the vessel.

Measurement variabilities and validation procedures

Although different approaches on the morphologic and densitometric analysis of coronary obstructions have been published in the literature as described above, it is very difficult if not impossible at this point in time to compare these systems quantitatively. The question how well all these systems work with routinely obtained coronary arteriograms cannot be answered. The absence of data about the accuracy and precision of the edge detection and analysis procedures, the success scores under different image qualities, computation time, etc. and the use of different parameters to describe the validation results make comparisons very difficult [87].

Validation procedures can be proposed to determine the accuracy and precision of the edge detection and densitometric technique, as well as the reproducibility of the image analysis procedures (see paragraphs below). Of major concern is also the interlaboratory variability. Different investigators will most likely use different criteria to select the angiographic views and within a particular view the frames(s) optimally suitable for quantitative analysis. For example, the following frame selection criteria are known to the author:

1) select a frame near end diastole with maximal sharpness and tightest (or largest) minimal diameter;

2) select a frame in the diastasis period with maximal sharpness and tightest obstruction diameter;
3) select three frames, one near end diastole, one near end systole and one in the diastasis period, each with maximal sharpness and tightest obstruction diameter and average the results.

Other selection criteria can also be defined; of concern is also in which cardiac cycle following the contrast injection the frames are selected. In a recent extensive study on the precision and reproducibility of quantitative coronary angiography, Selzer et al. concluded that sampling sequentially end diastole yielded the most precise estimates (i.e, exhibiting minimum variability within a cycle) of the vessel measures. With regard to reproducibility (i.e. similar values across cycles) sampling randomly within the cycle was best [88].

The overall interlaboratory variabilities can be assessed by sending sets of routinely obtained coronary angiograms in a blinded fashion with intervals of e.g. half a year to the laboratories and comparing the outcomes. Such variability studies should be carried out under the auspices of a body with sufficient authority to determine whether a QCA-laboratory satisfies certain stringent criteria.

Based on these observations the following validation procedures should be carried out in my opinion to validate a coronary quantitation system, as well as a quantitative coronary analysis laboratory.

Proposed validation procedures

A. *Assessment accuracy and precision of edge detection and densitometric techniques*

— Phantom studies of coronary obstructions with dimensions from 0.5 to 5.0 mm performed under different imaging conditions (various concentrations of the contrast agent, different kV-levels covering the routinely used range) and under static and dynamic flow conditions [89].
— In vivo animal studies with hollow plastic cylinders of various luminal shapes and sizes inserted in the coronary arteries [25, 90, 91].
— In addition, for densitometric studies the hypothesis that the results are independent of the angiographic views in which these studies were acquired, must be tested.

B. *Reproducibility of the image analysis procedure*

— Repeated analysis of a set of clinical coronary arteriograms obtained under various imaging conditions to assess inter- and intra-observer variabilities, as well as short- and long-term variabilities in the arteriographic data acquisition and image analysis procedures. In these reproducibility studies corresponding frames and segments to be analyzed may be selected on a consensus basis by the observers.

C. *Interlaboratory variability*

— Repeated blinded analyses of a set of routine coronary angiograms with a sufficient time interval (e.g. $\frac{1}{2}$ year) between analyses such that a priori information is absent. Variabilities will occur in: (1) view selection; (2) cardiac cycle selection; (3) frame selection; (4) segment selection; and (5) quantitative analyses. These parameters should all be carefully monitored.

Parameters describing the validation results

It is suggested to describe the results from the validation studies in terms of the mean signed differences (accuracy) and the standard deviations (precision) of these signed differences (measurement 1 — measurement 2; not absolute differences) between the true and measured values or between the values from repeated measurements.

Approaches towards standardization in arteriographic data acquisition and analysis

It has been shown that the variabilities in the arterial measurements can be decreased by standardizing on the arteriographic data acquisition and analysis procedures [41, 44]. In summary, the following measures have been proposed:

— Precise registration of the angulations and height levels of the X-ray system components for the different arteriographic views, so that the repeat arteriographies can be performed in the same views.
— Administration of vasodilative drug immediately prior to the angiographic investigations. The optimal vasodilative drug should give a quick response (within 30 s. to 1 min.), a maximal response and should have no influence on the hemodynamic state of the patient. Jost et al. have proposed to administer 10 mg of isosorbide dinitrate sublingually (capsule when available) 10 min. prior to arteriography [92].
— Use of modern isoviscous and iso-osmolar contrast agents [93—95]. Jost et al. have shown that the vasodilatory changes in vessels due to the contrast medium administration are significantly smaller with a nonionic contrast medium ($< 5.8\%$) as compared to an ionic contrast medium ($< 18.9\%$) [93].
— Administration of contrast medium preferably by ECG-triggered injector.
— Selection of contrast catheter constructed of such material that high quality images result (high angiographic image contrast and edge gradient) [40].
— Measurement of actual size of the catheter with micrometer following the catheterization procedure.

Details regarding the validation procedures performed by the various investigators can be found in Table 9. Summaries of these results will be discussed in the following paragraphs.

Table 9. Validation procedures (9-1a).

	Brown	Brunt	Collins	Doriot	Kirkeeide	LeFree
26. *Accuracy diameter measurements based on edge detection technique*						
Model used for assessment accuracy edge detection technique	brass artery of known diameter	perspex model with circular obstructions; diameters ranging from 0.5 to 3.2 mm	perspex model with circular obstructions; diameters ranging from 0.7 to 4.1 mm	perspex model with circular obstructions; diameters ranging from 0.5 to 4 mm	in progress	perspex model with circular obstructions; diameters ranging from 0.5 to 5.0 mm
Accuracy diameter measurement (mean signed difference between true and measured values)	0.030 mm	0.03 mm (after correction for LSF)	0.0 mm (mean absolute error = 0.06 ± 0.04 mm)	results not yet available	—	—
Precision diameter measurement (standard deviation of the differences)	0.080 mm	0.02 mm	0.07 mm	—	—	SEE = 0.17 mm
Correlation coeff. with true values	—	—	0.99	—	—	$r = 0.992$ (slope = 1.021)
These values were assessed at the following kV-levels:	80 kV	66kV	various	—	—	79—90kV
and concentrations of the contrast agent:	100%	100%	100%	—	—	100%
27. *In vivo validations*						
Have you done any in vivo validations?	YES, postmortem arteries pressure injected with barium gelatin; histologic planimetry of lumen at site of cineanalysis	NO	YES; videodensitometry compared with high frequency epicardial echo measurement of lesion area in humans ($r = 0.86$)	NO	NO	YES; in vivo canine model stenoses 0.84 — 1.83 mm in size
Mean differences	—	—	—	—	—	−0.069 mm
S.d. of differences	$r = 0.94$	—	—	—	—	0.24 mm, $r = 0.79$.

Table 9. Validation procedures (9-1b).

	Lienard	Nichols	Oswald	Parker	Reiber
26. *Accuracy diameter measurements based on edge detection technique*					
Model used for assessment accuracy edge detection technique	4 perspex models with circular obstructions; diameters ranging from 0.375 to 2.0 mm	perspex model with obstruction diameters ranging from 0.50 to 2.51 mm	perspex model with circular obstructions; diameters ranging from 0.5 to 5.0 mm	—	perspex model with circular obstructions; diameters ranging from 1.0 to 5.95 mm
Accuracy diameter measurement (mean signed difference between true and measured values)	2.5% for %-D stenosis (digital)	—	—	—	−0.007 mm (512^2 digital)
Precision diameter measurement (standard deviation of the differences)	2% for %-D stenosis (digital)	0.12 mm (SEE); measurements are performed 5—10 times and averaged	—	—	0.146 mm (512^2 digital)
Correlation coeff. with true values	—	$r = 0.99$	$r = 0.9998$ D measured = 0.91 + 1.0 Dtrue	— —	—
These values were assessed at the following kV-levels:	65 kV	—	80 kV	—	60, 93 kV
and concentrations of the contrast agent:	80 mg/ml	75%	100,75%	—	100,50%
27. *In Vivo validations*					
Have you done any in vivo validations?	NO	YES, comparison of densitometrically determined severity of stenosis from coronary cineangiogram with areas of acrylic resin casts	NO	NO	NO
Mean differences	—	—	—	—	—
S.d. of differences	—	area stenosis 0.71 mm^2 (SEE); $r = 0.99$	—	—	—

Table 9. Validation procedures (9-1c).

	Sanders	Sandor	Selzer	Vogel	Wankling
26. *Accuracy diameter measurements based on edge detection technique*					
Model used for assessment accuracy edge detection technique	perspex model with circular obstructions; diameters ranging from 1 mm to 4.5 mm	female cast of metal cylinders using rapidly polymerizing monomer base; diameters ranging from 0.50 to 6.26 mm	perspex model with circular obstructions; diameters ranging from 1 mm to 5.0 mm	perspex model with circular obstructions; diameters ranging from 0.5 to 5 mm	perspex model with circular obstructions; diameters ranging from 2 to 4 mm
Accuracy diameter measurement (mean signed difference between true and measured values)	0.069 mm		— 0.025 mm	—	—
	0.066 mm	—	0.155 mm	0.189 mm (film) 0.168 mm (512^2 digital) 0.135 mm (1024^2 digital)	—
Precision diameter measurement (standard deviation of the differences)					
Corr. coeff. with true values	$r = 0.998$	$r = 0.998$; excl. 0.5—0.8 mm model sizes	$r = 0.9982$	$r = 0.99$	—
These values were assessed at the following kV-levels:	70, 80, 90kV	75kV	75 — 80kV	70kV	
and concentrations of the contrast agent:	25, 50, 60, 80, 100%,	100%	100%	100%	—
Note:	using small and large focal spot; 3 different X-ray rooms	focal spot size 1.0 mm; images scanned 30× at resolution of 10 μm/pixel and averaged	—	—	—
27. *In vivo validations* Have you done any in vivo validations?	NO	NO	NO	YES, in vivo canine model stenoses 0.84 — 183 mm in size	NO
Mean differences	—	—	—	—	—
S.d. of differences	—	—	—	0.09 mm; $r = 0.98$	—

Table 9. Validation procedures (9-2a).

	Brown	Brunt	Collins	Doriot	Kirkeeide	LeFree
28. *Variability repeated analyses* (*non-densitometric*)						
Variability in repeated analysis of the same angiographic studies						
Mean differences:						
Obstruction diam. (mm)	0.10 mm	0.07	—	—	—	—
%-D stenosis	3.0%	4% (for range 1—3 mm)	—	—	—	—
%-A stenosis	4.0%	—	—	—	—	—
S.d. of differences						
Obstruction diam. (mm)	0.10	0.05	—	—	—	SEE (corr. coeff.) 0.16 mm (0.95)
%-D stenosis	2.5%	3%	—	—	—	8.5% (0.92)
%-A stenosis	5.5%	—	—	—	—	9.8% (0.83)
29. *Validation DENSITOMETRIC technique*						
Model used:	NA	NA	perspex model with circular cross sections ranging in size from 0.78 mm^2 to 12.6 mm^2	—	—	NA
Accuracy and precision densitometric technique:						
Mean differences:						
%-A stenosis:	—	—	—	—	—	—
Area-stenosis (mm^2):	—	—	$r = 0.87$	—	—	—

Table 9. Validation procedures (9-2b).

	Lienard	Nichols	Oswald	Parker	Reiber
28. *Variability repeated analyses* (*non-densitometric*)					
Variability in repeated analysis of the same angiographic studies					
Mean differences:					
Obstruction diam. (mm)	—	—	0.08 mm	—	−0.04
%-D stenosis	—	—	—	—	0.43
%-A stenosis	—	—	—	—	0.71
					(512^2 digital)
S.d. of differences					
Obstruction diam. (mm)	—	—	0.09 mm	—	0.07
%-D stenosis	—	—	—	—	2.50
%-A stenosis	—	5.34% (SEE); $r = 0.96$	—	—	2.61
					(512^2 digital)
29. *Validation DENSITOMETRIC technique*					
Model used:	perspex model (see 26)	perspex model (see 26)	—		
Accuracy and precision densitometric technique:					
Mean differences:					
%-A stenosis:	2.1%	—	—	—	—
Area-stenosis (mm^2)	—	—	—	—	—

Table 9. Validation procedures (9-2c).

	Sanders	Sandor	Selzer	Vogel	Wankling
28. *Variability repeated analyses (non-densitometric)*					
Variability in repeated analysis of the same angiographic studies					
Mean differences:					
Obstruction diam. (mm)	—	—	0.047	—	—
%-D stenosis	—	—	−0.69%	—	—
%-A stenosis	—	—	—	—	—
S.d. of differences					
Obstruction diam. (mm)	—	—	0.041 ($r = 0.992$)	—	—
%-D stenosis	—	—	0.88% ($r = 0.976$)	—	—
%-A stenosis	—	—	—	—	—
29. *Validation DENSITOMETRIC technique*:					
Model used:	—	—	—	see 26	see 26; and asymmetric obstructions
Accuracy and precision densitometric technique:					
Mean differences:					
%-A stenosis:	—	—	—	—	—
Area-stenosis (mm^2)	—	—	—	—	—

Table 9. Validation procedures (9-3a).

	Brown	Brunt	Collins	Doriot	Kirkeeide	LeFree
29. (*continued*)						
S.d. of differences:						
%-A stenosis:	—	—	—	—	—	—
Area stenosis (mm^2)	—	—	—	—	—	—
Repeated analyses:			intraobs. var.:			
Mean differences:			$r = 0.87$			
%-A stenosis:	—	—	interobs. var.:	—	—	—
			$r = 0.98$			
Area-stenosis (mm^2):	—	—	—	—	—	—
S.d. of differences:						
%-A stenosis:	—	—	—	—	—	—
Area stenosis (mm^2):	—	—	—	—	—	—
Variability densitometric analysis of obstructions assessed from different angiographic views:						
Mean differences:						
%-A stenosis:	—	—	RAO vs LAO	—	—	20.5 ($r = 0.46$)
Area stenosis (mm^2)	—	—	minimal lumen area:	—	—	—
			$r = 0.94$			
S.d. of differences:						
%-A stenosis:	—	—	—	—	—	—
Area stenosis (mm^2)	—	—	—	—	—	—

Table 9. Validation procedures (9-3b).

	Lienard	Nichols	Oswald	Parker	Reiber
29. (*continued*)					
S.d. of differences:					
%-A stenosis:	1%	4.1% (SEE); $r = 0.98$	—	—	—
Area stenosis (mm^2)	—	0.32 mm^2 (SEE); $r = 0.99$	—	—	—
Repeated analyses:					
Mean differences:					
%-A stenosis:	—	—	—	—	—
Area-stenosis (mm^2):	—	—	—	—	—
S.d. of differences:	—	*Interobserver var.*	—	—	—
%-A stenosis:		5.3% (SEE); $r = 0.96$			
Area stenosis (mm^2)	—	*Intraobserver var.*	—	—	—
		2.6% (SEE); $r = 0.99$			
		0.26 mm^2 (SEE); $r = 0.99$			
Variability densitometric analysis of obstructions assessed from different angiographic views:					
Mean differences:					
%-A stenosis:	—	—	—	—	—
Area stenosis (mm^2):	—	—	—	—	—
S.d. of differences:					
%-A stenosis:	—	—	—	—	—
Area stenosis (mm^2):	—	0.11 mm^2 (SEE); $r = 0.98$	—	—	—

Table 9. Validation procedures (9-3c).

	Sanders	Sandor	Selzer	Vogel	Wankling
29. (*continued*)					
S.d. of differences:					
%-A stenosis:	—	—	—	2.16%; $r = 0.99$	—
Area stenosis (mm^2)	—	—	—	—	—
Repeated analyses:					
Mean differences:					
%-A stenosis:	—	—	—	—	—
Area-stenosis (mm^2):	—	—	—	—	—
S.d. of differences:					
%-A stenosis:	—	—	—	—	—
Area stenosis (mm^2):	—	—	—	—	—
Variability densitometric analysis of obstructions assessed from different angiographic views:					
Mean differences:					
%-A stenosis:	—	—	—	$r = 0.46$	—
Area stenosis (mm^2):	—	—	—	—	—
S.d. of differences:					
%-A stenosis:	—	—	—	—	—
Area stenosis (mm^2)	—	—	—	—	—

Validation studies on arterial dimensions (nondensitometric)

A. *Phantom studies* (Table 9, item 26)

As described in the previous section on Proposed Validation Procedures the first validation study to test a particular design and implementation of a quantitative coronary arteriographic system should be concerned with the accuracy and precision of the actual edge detection technique based on phantom studies of coronary obstructions. Brass models or models made of any other material with a very high X-ray absorption coefficient should not be used, since these do not mimic the clinical situation; instead, perspex models that can be filled by various concentrations of contrast medium are much more appropriate.

Fourteen investigators have presented results on the accuracy and precision of these techniques. The models used have indeed been perspex models of various sizes (range 0.3—6.26 mm) (Brunt, Collins, Doriot, LeFree, Lienard, Nichols, Oswald, Reiber, Sanders, Sandor, Selzer, Vogel and Wankling) and brass arteries (Brown). Some of the data are based on cinefilm measurements, others on digital acquisitions, depending on the facilities available for the different investigators; where appropriate 'digital' has been specified. The results on the accuracy of the different techniques are all very good, ranging from 0.00 mm to 0.03 mm. For the precision data, values ranged from 0.02 to 0.189 mm; most of the data have now been specified in terms of the standard deviation of the mean signed differences between the true and measured values. Of course, data specified according to other definitions (absolute differences, standard error of the estimate) cannot simply be compared with these values. These problems have also been recognized by D. Herrington [88]. A number of correlation coefficients with the true values are all above 0.99. In general, the studies mentioned above were performed at different kV-levels ranging from 60—93 kV, and at different concentrations varying from 22 to 100%. Apparently, nobody has performed a dynamic phantom study with contrast agent pumped through the model with a roller pump. It would be of tremendous interest to see the results under those dynamic conditions.

B. *In vivo validations* (Table 9, item 27)

Five investigators (Brown, Collins, LeFree, Nichols and Vogel) have performed in vivo validations of their technique. Brown and Nichols compared their results with planimetric data of postmortem material and found correlation coefficients of 0.94 and 0.99, respectively; in Nichols' study the SEE (area stenosis) was 0.71 mm^2. Collins et al. compared the lesion cross-sectional area data by densitometry (which is in their case proportional to the absolute area; not calibrated in mm^2) with the data by high-frequency epicardial echo measurement, ($r = 0.86$) [12]. Collins and Johnson et al. have

performed additional in vivo validation studies comparing the luminal areas from densitometry with coronary vasodilator reserve defined by peak-to-resting velocity ratio's with intraoperative and intracoronary Doppler measurements [11]. They found correlation coefficient values of $r = 0.71$ for the LAD, $r = 0.92$ for the Cx and $r = 0.74$ for the RCA. LeFree, Mancini and Vogel performed a truly in vivo study with dogs instrumented with precision-drilled, plastic cylinders to create intraluminal stenoses; the stenosis diameters ranged from 0.83 to 1.83 mm [25, 91]. LeFree reported an accuracy of −0.069 mm and a precision of 0.24 mm ($r = 0.79$) with his QCS system. Vogel on his on-line digital system, found a precision of 0.09 mm ($r = 0.98$) for the obstruction diameter.

Finally, Kirkeeide et al. have compared in vivo pressure drop and coronary flow reserve measurements with predicated values; unfortunately, no results were presented.

C. *Variability repeated analyses* (*nondensitometric data*) (Table 9, item 28)

Limited data is only available from seven investigators (Brown, Brunt, LeFree, Nichols, Oswald, Reiber, and Selzer) on the variability in repeated analyses of the same angiographic studies. The mean differences (accuracy) in the obstruction diameter ranged from −0.04 to 0.10 mm, in the %-D stenosis from 0.43 to 4%, and in the %-A stenosis from 0.71 to 4%. The values for the standard deviation of the differences (precision) in the obstruction diameters ranged from 0.041 mm to 0.10 mm, with correlation coefficients ranging from 0.95 to 0.992, in the %-D stenosis from 0.88% to 8.5%, (correlation coefficients between 0.92 and 0.976), and in the %-A stenosis from 2.6 to 9.8% (r-values between 0.83 and 0.96). Again, we must be very careful in comparing these numbers, since different definitions may have been used. Collins et al. compared their minimal lumen diameters by automated edge detection techniques with those obtained by the Brown/Dodge method (manual tracing on optically magnified images) and found an $r = 0.90$ and SEE = 0.33 mm.

D. *Validation data densitometric techniques* (Table 9, item 29)

Accuracy and precision densitometric technique

Only Collins and Lienard reponded with some limited data on the accuracy and precision of the technique, i.e. data describing how large the differences with truly known values are. Collins used a perspex model with circular cross sections ranging in size from 0.78 mm^2 to 12.6 mm^2 and found a correlation coefficient of $r = 0.87$. In addition, he compared their luminal areas defined by videodensitometry with the minimal cross-sectional areas assessed by the Brown-Dodge technique (average value from three sequential end-diastolic cineframes) and found correlation coefficients of $r = 0.89$ for the LAD, $r = 0.94$ for the Cx, and $r = 0.78$ for the RCA; overall for all vessels an $r = 0.82$

was found [11]. Lienard used four perspex models with circular obstructions with the diameters ranging from 0.375 to 2.0 mm. He found a mean difference in %-Area stenosis of only 2.1% and a standard deviation of the differences of 1%.

Nichols also determined the precision in the area stenosis measurements by densitometry and found values of 4.1% (SEE) and $r = 0.98$ for percent area-stenosis and 0.32 mm^2 (SEE), and $r = 0.99$ for the absolute area stenosis. Finally, Vogel et al. reported a precision in the %-area stenosis measurement of 2.16% ($r = 0.99$) using a perspex model with circular obstructions and diameters ranging from 0.5 to 5.0 mm.

From these phantom studies acquired under ideal circumstances one may be inclined to believe that densitometry is a very attractive technique to be used for the assessment of the severity of coronary obstructions from only a single angiographic view. However, the reality in routine practice is different, as has been mentioned earlier in the section on Densitometry.

Variability in repeated analyses of densitometric studies

Only Collins and Nichols have studied the variability in repeated analyses of densitometric studies. Collins found correlation coefficients in the cross-sectional area measurements for interobserver variations on the same frames of $r = 0.98$, and for intraobserver variations of $r = 0.87$. Nichols found inter- and intra-observer variabilities in %-A stenosis of 5.3% (SEE) and 2.6% (SEE) with correlation coefficients of 0.96 and 0.99, respectively. The intra-observer variability in absolute area stenosis was found to be 0.26 mm^2 (SEE) with $r = 0.99$.

Variability of densitometric analysis of obstructions assessed from different angiographic views

Finally, we have looked at the variability of densitometric measurements of the same obstructions, but assessed from different angiographic views. It was discussed earlier that the results should be independent of the angiographic view if the technique works well. Four investigators, Collins, LeFree, Nichols and Vogel responded. Collins found a correlation coefficient of 0.94 between the cross-sectional area data from RAO and LA0 views; the relation between the data could be described by $y = 1.04x + 0.002$. LeFree found a mean difference in the %-area stenosis of 20.5% and $r = 0.46$, and therefore prefers not to use densitometry. Nichols found a precision of 0.11 mm^2 (SEE) with $r = 0.98$ in the absolute area measure. Finally, Vogel responded with the $r = 0.46$ value as described above for LeFree [61].

Discussion

In this chapter an extensive overview of the major developments in off- and

on-line quantitative coronary arteriography has been presented. It is clear from the text and from the details given, that these developments are rather heterogeneous. However, this should not only be seen as a negative sign. As long as optimal results have not been achieved in certain areas, there is a need for competition and new ideas to come up with better approaches.

It is very difficult if not impossible at this point in time to compare these systems quantitatively, i.e. the question how qualified a particular design is for the objective and reproducible analysis of routinely obtained coronary angiograms cannot be answered. Data about the accuracy and precision of the edge detection and analysis procedures, the success scores under different image qualities, the computation time, etc. are usually not provided in the publications; if they are provided, different parameters to describe the validation results have been used making comparisons very difficult [87]. In film-based systems the quality of the cine-to-video converter is also of major concern; there is a wide variety of projectors around that have not been tested and compared according to standardized procedures.

These computer-based systems also have definite inter- and intra-observer variabilities, although these are usually not given. There are always a number of phases in the analysis procedures, such as the definition of the centerline of the coronary segment, the possibility to make manual corrections to the otherwise automatically detected contours, etc. that will result in observer variations.

Taken together, it is evident that there is a clear need for standardized procedures to determine the inter- and intra-laboratory variabilities. A QCA-center should only be qualified to perform such work if it satisfies certain criteria. It is to be expected that such qualifying procedures will be defined and implemented in the very near future.

In the coronary angiograms the lumen of the artery is usually reasonably well visualized due to the administration of iodine-containing contrast medium. This means that one only sees the boundaries of the channel that is left open. One can never tell for sure whether a vessel is diffusely diseased or not, and thus whether the reference diameter that one is measuring is a true representation of the original size of the vessel. Indications for the presence of diffuse disease may be a deviation in caliber of the vessel relative to normal values, although normal values for all the coronary segments are hardly available, or the presence of irregularities in the contour as assessed by roughness measures of the segment [96—98]. The normal cross-sectional area of a specific vascular segment has also been found to be substantially influenced by the coronary branching pattern [99], left ventricular mass [100] and possibly by other independent factors, such as gender, age and ethnic origin. In patients with single vessel disease with normal caliber coronary vessels, one may assume that diffuse disease plays a very minor role. Under such circumstances the use of the interpolated or computer-defined reference technique is certainly indicated; however, if there is any doubt about the presence of diffuse disease, this interpolated technique will also under-

estimate the original sizes of the vessel. Until to date it has not been possible to image the intima of the coronary vessels by X-ray techniques, nor is it likely to be possible in the future. However, here exist excellent opportunities for high-frequency intravascular echocardiographic approaches [12, 101].

Systems with facilities for densitometry, usually also provide geometric data on the arterial dimensions (diameter values), since the densitometric data is derived from the brightness data within the arterial boundaries; these systems may be defined as hybrid systems. However, as was discussed before, the accuracy of the edge detection approaches in densitometric applications is of less importance, provided that the boundaries are defined at or slightly outside of the true boundaries and the background correction technique works well. The question then becomes whether in those systems that do have accurate contour detection facilities, the densitometric data have completely made the geometric data obsolete. Gould and Kirkeeide automatically compare the cross-sectional area measures by automated edge detection techniques on biplane angiograms with the densitometric data [18]. They have also found that disagreements between the two methods may occur, especially for eccentric lesions in which their border recognition technique using the orthogonal biplane views is not as accurate as the densitometric technique [102, 103], or in cases where other optically dense structures (catheters, other vessels, etc.) are superimposed on the arterial segment of interest. In the latter circumstance, the diameter was best determined by the automated border recognition approach.

With the present limitations in the accuracy and precision in densitometry, using only densitometric data may be useful in selected studies in which a great number of conditions have been fulfilled, such as coronary segments imaged en face, no intervening sidebranches, relatively homogeneous background, etc. In all other applications especially in intervention studies, where the results pre- and post-intervention must be compared (from at least two angiographic views), the first choice at present must be the vessel diameter data and the second choice the densitometrically assessed cross-sectional area data. In other words, densitometric data may be used complementarily, but should not replace the diameter data. As soon as the densitometric techniques have been improved to the extent, that the cross-sectional data can be measured under most clinical circumstances with an accuracy and precision comparable to the present results of the best contour detection approaches, the situation changes and one may decide to rely only on the densitometric data.

Finally, it will be of great interest to follow the studies in which the on-line and off-line systems will be compared. The question is whether one will be able to achieve the same accuracy and precision with on-line acquired 512^2 images as with the off-line cine-approaches. Appropriate interpolation schemes may prove to be extremely important in obtaining the required number of pixels with valuable information for automated edge detection techniques. It is the author's opinion that due to the continuous improve-

ments in the various components of the X-ray imaging chain and in the contour detection and analysis procedures, the 512^2 digital approach will be able to demonstrate an accuracy and precision approaching those of the cinefilm-based generations of a few years ago, while the most recent implementations of cinefilm-based systems will continue to show a slight but definite advantage in the accuracy and precision of the quantitative data.

Acknowledgements

The author wishes to acknowledge the critical reading of this chapter by G. Loois, M.Sc. of the Application Department, Philips Medical Systems, Best, the Netherlands and by Craig D. von Land, M.Sc, and the secretarial work by Bertie Smit-van der Deure, both of the Laboratory of Clinical and Experimental Image Processing, Erasmus University Rotterdam.

References

1. Reiber JHC, Serruys PW: New developments in quantitative coronary arteriography. Kluwer Academic Publishers, Dordrecht/Boston/London, 1988.
2. Reiber JHC: An overview of morphologic and densitometric approaches for the quantitation of coronary stenoses. Automedica 10: 171—200, 1989.
3. Reiber JHC, Serruys PW: Quantitative Coronary Angiography. In: Cardiac Imaging — Principles and Practice. ML Marcus, HR Schelbert, DJ Skorton, GL Wolf (eds). W.B. Saunders Company, Philadelphia, 1990.
4. Mancini GBJ: Digital coronary angiography; advantages and limitations. Chapter 2 (this book).
5. Brown BG, Bolson E, Frimer M, Dodge HT: Quantitative coronary arteriography. Estimation of dimensions, hemodynamic resistance, and atheroma mass of coronary artery lesions using the arteriograms and digital computation. Circulation 55: 329—337, 1977.
6. Brown, BG, Gallery CA, Badger RS, Kennedy JW, Mathey D, Bolson EL, Dodge HT: Incomplete lysis of thrombus in the moderate underlying atherosclerotic lesion during intracoronary infusion of streptokinase for acute myocardial infarction: quantitative angiographic observations. Circulation 73: 653—661, 1986.
7. Dodge Jr. JT, Brown BG, Bolson EL, Dodge HT: Intrathoracic spatial location of specified coronary segments on the normal human heart. Applications in quantitative arteriography, assessment of regional risk and contraction, and anatomic display. Circulation 78, 1988: 1167—1180
8. Astley SM, Brunt JNH: Exploitation of computer vision technology in coronary cineangiographic analysis. Comp Card: 579—582, 1987.
9. Fleagle SR, Johnson MR, Skorton DJ, Marcus ML, Collins SM: Geometric validation of a robust method of automated edge detection in clinical coronary arteriography. Comp Cardiol: 197—200, 1987.
10. Johnson MR, McPherson DD, Hunt MM, Hiratzka LF, Marcus ML, Kerber RE, Collins SM, Skorton DJ: Videodensitometry is independent of angiographic projection and lumen shape. J Am Coll Cardiol 9: 183A, 1987 (Abstract).

11. Johnson MR, Skorton DJ, Ericksen EE, Fleagle SR, Wilson RF, Hiratzka LF, White CW, Marcus ML, Collins SM: Videodensitometric analysis of coronary stenoses; in vivo geometric and physiologic validation in humans. Invest Radiol 23: 891—898, 1988.
12. Johnson MR, McPherson DD, Fleagle SR, Hunt MM, Hiratzka LF, Kerber RE, Marcus ML, Collins SM, Skorton DJ: Videodensitometric analysis of human coronary stenoses: validation in vivo by intraoperative high-frequency epicardial echocardiography. Circulation 77: 328—336, 1988.
13. Fleagle SR, Johnson MR, Wilbricht CJ, Skorton DJ, Wilson RF, White CW, Marcus ML, Collins SM: Automated analysis of coronary arterial morphology in cineangiograms: geometric and physiologic validation in humans. IEEE Trans Med Imaging 8: 387—400, 1988.
14. Doriot P-A, Pochon Y, Rasoamanambelo L, Chatelain P, Welz R, Rutishauser W: Densitometry of coronary arteries — an improved physical model. Comput Cardiol: 91—94, 1985.
15. Doriot PA, Rutishauser W: On the accuracy of densitometric measurements of coronary artery stenosis based on Lambert-Beer's absorption law. In: New developments in quantitative coronary arteriography. JHC Reiber, PW Serruys (eds). Kluwer Academic Publishers, Dordrecht/Boston/London, 1988: 115—124.
16. Doriot P-A, Guggenheim N, Dorsaz P-A, Rutishauser W: Morphometric versus densitometric assessment of coronary vasomotor tone — an overview. Eur Heart J 10 (Supp F): 49—53, 1989.
17. Kirkeeide RL, Fung P, Smalling RW, Gould KL: Automated evaluation of vessel diameter from arteriograms. Comput Cardiol: 215—218, 1982.
18. Gould KL, Kirkeeide RL: Assessment of stenosis severity. In: State of the art in quantitative coronary arteriography. JHC Reiber, PW Serruys (eds). Martinus Nijhoff Publishers, Dordrecht/Boston/Lancaster, 1986: 209—228.
19. Wong W-H, Kirkeeide RL, Gould KL: Computer applications in angiography. In: Cardiac Imaging and Image Processing. SM Collins, DJ Skorton (eds). McGraw-Hill Book Company, New york, 1986, pp 206—238.
20. Kirkeeide RL, Gould KL, Parsel L: Assessement of coronary stenoses by myocardial perfusion imaging during pharmacologic coronary vasodilation. VII. Validation of coronary flow reserve as a single integrated functional measure of stenosis severity reflecting all its geometric dimensions. J Am Coll Cardiol 7: 103—113, 1986.
21. Kirkeeide RL: Coronary obstructions, morphology and physiologic significance. Chapter 11 (this book).
22. LeFree M, Simon SB, Lewis RJ, Bates ER, Vogel RA: Digital radiographic coronary artery quantification. Comput Cardiol: 99—102, 1985.
23. LeFree MT, Simon SB, Mancini GBJ, Vogel RA: Digital radiographic assessment of coronary arterial geometric diameter and videodensitometric cross-sectional area. SPIE 626: 334—341, 1986.
24. Sanz ML, Mancini GBJ, LeFree MT, Mickelson JK, Starling MR, Vogel RA, Topol EJ: Variability of quantitative digital subtraction coronary angiography before and after percutaneous transluminal coronary angioplasty. Am J Cardiol 60: 55—60, 1987.
25. Mancini GBJ, Simon SB, McGillem MJ, LeFree MT, Friedman HZ, Vogel RA: Automated quantitative coronary arteriography: morphologic and physiologic validation in vivo of a rapid digital angiographic method. Circulation 75: 452—460, 1987.
26. Nichols AB, Gabrieli CFO, Fenoglio Jr JJ, Esser PD: Quantification of relative coronary arterial stenosis by cinevideodensitometric analysis of coronary arteriograms. Circulation 69: 512—522, 1984.
27. Nichols AB, Brown C, Han J, Nickoloff EL, Esser PD: Effect of coronary stenotic lesions on regional myocardial blood flow at rest. Circulation 74: 746—757, 1986.
28. Oswald H, Beier J, Fleck E: Densitometrisch Korrigierte Gefässdurchmesser in der digitalen Koronarangiographie. In: Koronare Herzerkrankung und dilatative Kardio-

myopathie: Diagnostik und Therapie. E. Fleck (ed.). MMW Taschenbuch, München, 1988: 25—27.
29. Beier J, Oswald H, Fleck E: Erkennung und Quantifizierung von Koronarstenosen aus angiografischen Röntgenbildern. In: Mustererkennung 1988. H Bunke, O Kübler, P Stucki (eds). Informatik Fachberichte 180. Springer Verlag, 1988: 24—30.
30. Oswald H, Fleck E, Beier J: Densitometric correction of vessel diameter from digital arteriograms. In: Digitale Bildgebende Verfahren, Interventionelle Verfahren, Integrierte Digitale Radiologie. GH Schneider, E Vogler (eds), Springer Verlag, 1988: 774—778.
31. Parker DL, Pope DL, Peterson JC, Clayton PD, Gustafson DE: Quantitation in cardiac video-densitometry. Comput Cardiol: 119—122, 1984.
32. Pope DL, Parker DL, Clayton PD, Gustafson DE: Left ventricular border recognition using a dynamic search algorithm. Radiology 155: 513—518, 1985.
33. Parker DL, Pope DL, Van Bree RE, Marshall H: Three-dimensional reconstruction and cross-section measurements of coronary arteries using ECG-correlated digital coronary arteriography. In: Progress in Digital Angiocardiography. PH Heintzen, JH Bürsch (eds). Kluwer Academic Publishers, Dordrecht/Boston/London, 1988: 181—192.
34. Parker DL, Wu J, Pope DL, Van Bree R, Caputo GR, Marshall HW: Three-dimensional reconstruction and flow measurements of coronary arteries using multi-view digital angiography. In: New Developments in Quantitative Coronary Arteriography. JHC Reiber, PW Serruys (eds). Kluwer Academic Publishers, Dordrecht/Boston/London, 1988: 225—247.
35. Kooijman CJ, Reiber JHC, Gerbrands JJ, Schuurbiers JCH, Slager CJ, Boer A den, Serruys PW: Computer-aided quantitation of the severity of coronary obstructions from single view cineangiograms. First IEEE Comp Soc Int Symp on Medical Imaging and Image Interpretation, IEEE Cat No 82 CH1804-4: 59—64, 1982.
36. Reiber JHC, Slager CJ, Schuurbiers JCH, Boer A den, Gerbrands JJ, Troost GJ, Scholts B, Kooijman CJ, Serruys PW: Transfer functions of the X-ray-cine-video chain applied to digital processing of coronary cineangiograms. In: Digital Imaging in Cardiovascular Radiology. PH Heintzen, R Brennecke (ed). Georg Thieme Verlag, Stuttgart, 1983: 89—104.
37. Serruys PW, Reiber JHC, Wijns W, Brand M van den, Kooijman CJ, Katen HJ ten, Hugenholtz PG: Assessment of percutaneous transluminal coronary angioplasty by quantitative coronary angiography: diameter versus densitometric area measurements. Am J Cardiol 54: 482—488, 1984.
38. Reiber JHC, Kooijman CJ, Slager CJ, Gerbrands JJ, Schuurbiers JCH, Boer A den, Wijns W, Serruys PW: Computer assisted analysis of the severity of obstructions from coronary cineangiograms: a methodological review. Automedica 5: 219—238, 1984.
39. Reiber JHC, Kooijman CJ, Slager CJ, Ree EJB van, Kalberg RJN, Tijdens, FO, Plas J van der, Frankenhuyzen J van, Claessen WCH: Taking a quantitative approach to cineangiogram analysis. Diagn Imag 7: 87—89, 1985.
40. Reiber JHC, Kooijman CJ, Boer A den, Serruys PW: Assessment of dimensions and image quality of coronary contrast catheters from cineangiograms. Cathet Cardiovasc Diagn 11: 521—531, 1985.
41. Reiber JHC, Serruys PW, Kooijman CJ, Wijns W, Slager CJ, Gerbrands JJ, Schuurbiers JCH, Boer A den, Hugenholtz PG: Assessment of short-, medium- and long-term variations in arterial dimensions from computer-assisted quantitation of coronary cineangiograms. Circulation 71: 280—288, 1985.
42. Reiber JHC, Serruys PW, Slager CJ: Quantitative coronary and left ventricular cineangiography; methodology and clinical applications. Martinus Nijhoff Publishers, Boston/Dordrecht/Lancaster, 1986.
43. Kooijman CJ, Kalberg R, Slager CJ, Tijdens FO, Plas J van der, Reiber JHC: Densitometric analysis of coronary arteries. In: Signal Processing III: Theories and Applications. IT Young, J Biemond, RPW Duin, JJ Gerbrands (eds). North-Holland, Amsterdam/New York/Oxford/Tokyo 1986: 1405—1408.

44. Reiber JHC, Serruys PW, Kooijman CJ, Slager CJ, Schuurbiers JCH, Boer A den: Approaches towards standardization in acquisition and quantitation of arterial dimensions from cineangiograms. In: State of the Art in Quantitative Coronary Arteriography. JHC Reiber, PW Serruys (eds). Martinus Nijhoff Publishers, Dordrecht/Boston/Lancaster, 1986: 145—172.
45. Reiber JHC, Koojiman CJ, Slager CJ, Boer A den, Serruys PW: Improved densitometric assessment % area-stenosis from coronary cineangiograms. X World Congress of Cardiology, Washington: 39, 1986 (Abstract).
46. Reiber JHC: Morphologic and densitometric analysis of coronary arteries. In: Progress in Cardiovascular Angiocardiography. PH Heintzen, JH Bürsch (eds). Kluwer Academic Publishers, Dordrecht, 1988: 137—158.
47. Reiber JHC: Morphologic and densitometric quantitation of coronary stenoses; and overview of existing quantitation techniques. In: New Developments in Quantitative Coronary Arteriography. JHC Reiber, PW Serruys (eds.). Kluwer Academic Publishers, Dordrecht 1988: 34—88.
48. Reiber JHC, Boer A den, Serruys PW: Quality control in performing quantitative coronary arteriography. Am J Cardiac Imaging 3: 172—179, 1989.
49. Zwet PMJ van der, von Land CD, Loois G, Gerbrands JJ, Reiber JHC: An on-line system for the quantitative analysis of coronary arterial segments. Comp Cardiol 1990 (in press).
50. Sanders WJ, Alderman EL, Harrison DC. Coronary artery quantitation using digital image processing. Comput Cardiol: 15—20, 1979.
51. Alderman EL, Berte LE, Harrison DC, Sanders W: Quantitation of coronary artery dimensions using digital imaging processing. In: Digital Radiography. WR Brody (ed). SPIE 314: 273—278, 1982.
52. Ellis S, Sanders W, Goulet C, Miller R, Cain KV, Lespérance J, Bourassa MG, Alderman EL: Optimal detection of the progression of coronary artery disease: comparison of methods suitable for risk factor intervention trials. Circulation 74: 1235—1242, 1986.
53. Sandor T, D'Adamo A, Hanlon WB, Spears JR: High precision quantitative angiography. IEEE Trans Med Imag MI-6: 258—265, 1987.
54. Selzer RH, Blankenhorn DH, Crawford DW, Brooks SH, Barndt R. Computer analysis of cardiovascular imagery. Proc Caltech/JPL Conf on Image Processing Techn, Data Sources and Software for Comm and Scient Appl, Pasadena 1976: 1—20.
55. Crawford DW, Brooks SH, Selzer RH, Barndt Jr. R. Beckenbach ES, Blankenhorn DH: Computer densitometry for angiographic assessment of arterial cholesterol content and gross pathology in human atherosclerosis. J Lab Clin Med 89: 378—392, 1977.
56. Ledbetter DC, Selzer RH, Gordon RM, Blankenhorn DH, Sanmarco ME: Computer quantitation of coronary angiograms. In: Noninvasive Cardiovascular Measurements, HA Miller, EV Schmidt, DC Harrison (eds). SPIE 167: 17—20, 1978.
57. Blankenhorn DH, Brooks, SH. Angiographic trials of lipid-lowering therapy. Arteriosclerosis 1: 242—249, 1981.
58. Siebes M, D'Argenio DZ, Selzer RH: Computer assessment of hemodynamic severity of coronary artery stenosis from angiograms. Comput Methods and Programs in Biomedicine 21: 143—152, 1985.
59. Selzer RH, Shircore A, Lee PL, Hemphill L, Blankenhorn DH: A second look at quantitative coronary angiography: some unexpected problems. In: State of the art in quantitative coronary arteriography. JHC Reiber, PW Serruys (eds). Martinus Nijhoff Publishers, Dordrecht/Boston/Lancaster, 1986: 125—143.
60. Selzer RH, Hagerty C, Azen SP, Siebes M, Lee P, Shircore A, Blankenhorn DH: Precision and reproducibility of quantitative coronary angiography with applications to controlled clinical trials. J Clin Invest 83: 520—526, 1989.
61. Vogel RA: Comparison of automated edge detection and videodensitometric quantitative coronary arteriography. In: New Developments in Quantitative Coronary Arterio-

graphy. JHC Reiber, PW Serruys (eds). Kluwer Academic Publishers. Dordrecht/Boston/London, 1988: 143—152.
62. Hodgson JMcB, LeGrand V, Bates ER, Mancini GBJ, Aueron FM, O'Neill WW, Simon SB, Beauman GJ, LeFree MT, Vogel RA: Validation in dogs of a rapid digital angiographic technique to measure relative coronary blood flow during routine cardiac catheterization. Am J Cardiol 55: 188—193, 1985.
63. Wankling PF, Perry RA, Seth A, Hunt AC, Escaned J, Newell JA, Shiu MF: An objective computer system for the quantification of artery stenoses. Int J Cardiac Imaging 5: 85—92, 1990.
64. Verhoeven LAJ: Digital cardiac imaging. Medicamundi 32: 111—116, 1987.
65. Fleck E, Oswald H: Digital cardiac imaging: an effective aid in complex coronary angioplasties. Medicamundi 33: 69—73, 1988.
66. Kruger RA, Riederer SJ: Basic Concepts of Digital Subtraction Angiography. GK Hall Medical Publishers, Boston, 1984.
67. Hoffman KR, Doi K, Chan H-P, Fencil P, Fujita H, Muraki A. Automated tracking of the vascular tree in DSA images using a double-square-box region-of-search algorithm. Proc SPIE 626: 326—333, 1986.
68. Smets C, Verbeeck G, Suetens P, Oosterlinck A: A knowledge-based system for the three-dimensional reconstruction of the cerebral blood vessels from a pair of stereoscopic angiograms. In: Pattern Recognition in Practice III. ES Gelsema, LN Kanal (eds). Elsevier Science Publishers BV (North-Holland), Amsterdam, 1988: 425—436.
69. Fischler MA, Wolf HC: A general approach to machine perception of linear structure in imaged data. Technical Note 276, SRI Intern, 1983.
70. Barth K, Eicker B, Koch R, Marhoff P: Automated three-dimensional recognition of the coronary tree with clinical DSA image pairs. Comp cardiol: 187—190, 1988.
71. Barth K, Koch R, Marhoff P: Fast automatic recognition and 3D reconstruction of the coronary tree from DSA-projection pairs. In: Progress in Digital Angiocardiography. PH Heintzen, JH Bürsch (eds). Kluwer Academic Publishers, Dordrecht/Boston/London, 1988: 193—200.
72. Reiber JHC, Zwet PMJ van der, Land CD von, Koning G, Loois G, Zorn I, Brand M van den, Gerbrands JJ: On-line quantification of coronary angiograms with the DCI system. Medica Mundi 34: 89—98, 1989.
73. Zwet P van der: On-line quantitation of coronary arterial dimensions (Personal Communication).
74. Barth K, Eicker B, Bittner U, Marhoff P: The improvement of vessel quantification with image processing equipment for high resolution digital angiography. In: Computer Assisted Radiology. HU Lemke, ML Rhodes, CC Jaffe, R Felix (eds). Springer-Verlag, Berlin, 1989: 220—225.
75. Reiber JHC, Koning G, Land CD von: Quality control in quantitative coronary arteriography for long-term intervention studies (submitted for publication).
76. Lavayssière B, Liénard J, Marchand JL: RII geometrical distortion modelling and calibration. In: Computer Assisted Radiology. HU Lemke, ML Rhodes, CC Jaffee, R Felix (eds). Springer-Verlag, Berlin, 1987: 225—229.
77. Buschmeyer L, Onnasch DGW, Heintzen PH: Korrektur magnetfeldbedingter Bildverzeichnungen in bewegten Röntgen- Bildverstärker- Fernseh-Systemen. Biomedizinische Technik, Band 34: 209—210, 1989.
78. Solzbach U, Wollschäger H, Zeiher A, Just H: Optical distortion due to geomagnetism in quantitative angiography. Comp cardiol: 355—357, 1989.
79. Wollschläger H. Optimal biplane imaging of coronary segments with computer exact triple orthogonal projections. In: New developments in quantitative coronary arteriography. JHC Reiber, PW Serruys (eds). Martinus Nijhoff Publishers, Dordrecht, 1988: 13—21.
80. Wollschläger H, Lee P, Zeiher A, Solzbach U, Bonzel T, Just H: Improvement of

quantitative angiography by exact calculation of radiological magnification factors. Comput cardiol: 483—486, 1985.
81. Beatt KJ, Luijten HE, Reiber JHC, Serruys PW: Early regression and late progression in coronary artery lesions in the first 3 months following coronary angioplasty. In: New developments in quantitative coronary arteriography. JHC Reiber, PW Serruys (eds). Martinus Nijhoff Publishers, Dordrecht, 1988: 167—180.
82. Beatt KJ, Luijten HE, Feyter PJ de, Brand M van den, Reiber JHC, Serruys PW: Change in diameter of coronary artery segments adjacent to stenosis after percutaneous transluminal coronary angioplasty: failure of percent diameter stenosis measurement to reflect morphologic changes induced by balloon dilation. J Am Coll cardiol 12: 315—323, 1988.
83. Spears JR, Sandor T, Baim DS, Paulin S: The minimum error in estimating coronary luminal cross-sectional area from cineangiographic diameter measurements. Cath Cardiovasc Diagn 9: 119—128, 1983.
84. Ambrose JA, Winters SL, Stern A, Eng A, Teichholtz LE, Gorlin R, Fuster V: Angiographic morphology and the pathogenesis of unstable angina pectoris. J Am Col Cardiol 5: 609—616, 1985.
85. Levin DC, Gardiner GA: Complex and simple coronary artery stenoses: a new way to interpret coronary angiograms based on morphologic features of lesions. Radiology 164: 675—680, 1987.
86. Vassanelli C, Menegatti G, Morando G, Girardi P, Zardini P: The eccentricity and irregularity of coronary artery stenosis: two additional computerized parameters of quantitative coronary angiography. Comp Cardiol: 631—634, 1988.
87. Herrington DM, Walford GA, Pearson TA: Issues of validation in quantitative coronary angiography. In: New Developments in Quantitative Coronary Arteriography. JHC Reiber, PW Serruys (eds). Kluwer Academic Publishers, Dordrecht, 1988: 153—166.
88. Zelzer RH, Hagerty C, Azen SP, Siebes M, Lee P, Shircore A, Blankenhorn DH: Precision and reproducibility of quantitative coronary angiography with applications to controlled clinical trials. J Clin Invest 83: 520—526, 1989.
89. Simons MA, Kruger RA, Power RLB: Cross-sectional area measurements by digital subtraction videodensitometry. Invest Radiol 21: 637—644, 1986.
90. Block M, Bove AA, Ritman EL: Coronary angiographic examination with the dynamic spatial reconstructor. Circulation 70: 209—216, 1984.
91. Mancini GBJ. Morphologic and physiologic validation of quantitative coronary arteriography utilizing digital methods. In: New developments in quantitative coronary arteriography. JHC Reiber, PW Serruys (eds). Kuwer Academic Publishers, Dordrecht/Boston/London, 1988: 125—141.
92. Jost S, Rafflenbeul W, Knop I, Bossaller C, Gulba D, Hecker H, Lippolt P, Lichtlen PR: Drug plasma levels and coronary vasodilation after isosorbide dinitrate chewing capsules. Eur Heart J 10 (Suppl F): 137—141, 1989.
93. Fischer HW: Catalog of intravascular contrast media. Radiology 159: 561—563, 1986.
94. Jost S, Rafflenbeul W, Gerhardt U, Nellessen U, Reil G-H, Hecker H, Lichtlen P. Vergleich von hoch- und niederosmolaren Röntgenkontrastmitteln in der quantitativen Koronarangiographie. Z Kardiol 77: 755—766, 1988.
95. Jost S, Rafflenbuel W, Gerhardt U, Hecker H, Nellessen U, Reil G-H, Lichtlen PR: Influence of ionic and non-ionic radiographic contrast media on the vasomotor tone of epicardial coronary arteries. Eur Heart J 10 (Supp F): 60—65, 1989.
96. Lichtlen PR: Koronar-angiographie. Verlag Dr med D Straube, Erlangen, 1979.
97. MacAlpin RN, Abbasi AS, Grollman JH, Eber L: Human coronary artery size during life. A cinearteriographic study. Radiology 108: 567—576, 1973.
98. Rafflenbeul W, Heim R, Dzuiba M, Henkel B, Lichtlen P: Morphometric analysis of coronary arteries. In: Coronary Angiography and Angina Pectoris. PR Lichtlen (ed). Georg Thieme Publisher, Stuttgart 1976: 255—265.

99. Hutchins GM, Miner MM, Boitnott JK: Vessel caliber and branch-angle of human coronary artery branch-points. Circ Res 38: 572—576, 1976.
100. Hort W. Lichti H, Kalbfleisch H, Köhler F, Frenzel H, Milzner-Schwartz U: The size of human coronary arteries depending on the physiological and pathological growth of the heart, the age, the size of the supplying areas and the degree of coronary sclerosis. A postmortem study. Virchows Arch (Pathol Anat) 397: 37—59, 1982.
101. Bom N, Slager CJ, Egmond FC van, Lanceé CT, Serruys PW: Intra-arterial ultrasonic imaging for recanalization by spark erosion. Ultrasound in Med and Biol 14: 257—261, 1988.
102. Kirkeeide RL, Smalling RW, Gould KL: Automated measurements of artery diameter from arteriograms. Circulation 66: II—325, 1982 (Abstract).
103. Kirkeeide RL, Parsel L, Gould KL: Prediction of coronary flow reserve of stenotic coronary arteries by quantitative arteriography. Circulation 70: II-250, 1984 (Abstract).

Part II

Quantitative coronary arteriography; physiological aspects

5. Peptides and the circulation

GRAHAM J. DAVIES

Summary

In health coronary blood flow is automatically regulated at the level of small vessels to adjust flow to changes in perfusion pressure and myocardial oxygen demand. Coronary disease is associated with the occurrence of flow limiting resistance in the epicardial (large) arteries which is partly fixed and dynamic depending on the relative contributions of atherona, thrombosis and constriction and which causes the myocardial ischaemia seen in the various clinical presentations. There are many mediators of normal control mechanisms and pathological coronary responses; some are recently discovered such as the vasoactive peptides and some have been known for many years but their relevance has been clarified by recent research.

Neuropeptide Y is a sympathetic neurotransmitter which constricts small coronary vessels and, in the experimental situation, causes a flow reduction sufficient to induce myocardial ischaemia without any effect on the larger coronary arteries. Its effect is mainly direct through post junctional NPY receptors, Endothelin is the most potent vasoconstrictor peptide yet discovered, released from endothelial cells with a very long duration of action; its role remains to be elucidated. Vasopressin, a circulating vasoconstrictor peptide released from the pituitary gland, is important in the maintenance of blood pressure following acute haemorrhage and is used to reduce bleeding from eosophageal varices. Occasional reports of vasopressin induced myocardial ischaemia exist. The circulating renin angiotensin system provides a rapid homeostatic response to acute changes in blood pressure and fluid and electrolyte status and may operate on a local tissue level. The kallikrein kinin system is activated in septicaemic and endotoxic shock producing marked vasodilatation and hypotension which can be attenuated by a bradykinin antagonist. Somatostation is widespread in the body; it inhibits the release of growth hormone and insulin and selectively reduces portal venous pressure during intravenous infusion, possibly by inhibition of gut vasodilator peptides. Calcitonin gene related peptide and substance P are both dilator neurotransmitter peptides found in human heart, the former long acting and the

J. H. C. Reiber and P. W. Serruys (eds), Quantitative Coronary Arteriography, 135—143.

latter short acting. Atrial natriuretic factor is a peptide produced locally in the atria of human hearts and regulates blood volume by responding to atrial distension.

It is clear that the control of the circulation is complex and involves peptide hormones and neurotransmitters. This realisation has served to stimulate much research in cardiovascular control mechanisms.

Introduction

In health coronary blood flow is automatically regulated to adjust flow to varying coronary perfusion (aortic diastolic) pressures and to the varying demands of the myocardium for oxygen. It is unclear, in normal individuals, whether the integrity of these control mechanisms is preserved at the extreme ends of the physiological range and in the presence of extreme stimuli. The smooth muscle cells of the tunica media form a structure which has inherent tone but in coronary arteries in vivo this tone is modulated by autonomic innervation [1] and by vasoactive substances produced by endothelial cells [2].

Diseases affecting the coronary arteries usually involve the epicardial (large) segments, atheroclerosis being the most common of these. When significant epicardial coronary artery luminal stenosis occurs due to the presence of an atheromatous plaque, the various physiological constrictor mechanisms may induce transient reductions of blood flow sufficient to cause myocardial ischaemia and angina pectoris instead of regulating blood flow according to requirement. Furthermore, the physiological mechanisms may be altered by disease, for example the coronary smooth muscle hyperreactivity of Prinzmetal's variant angina and the impairment of endothelium dependent coronary vascular smooth muscle relaxation seen in atherosclerosis.

An atheromatous plaque may, by fissuring, induce localised coronary thrombosis, which suddenly becomes the limiting resistance in that regional circulation, causing a reduction in flow sufficient to case myocardial infarction. The same process will cause unstable angina if the thrombus is not completely occlusive, as the physiological mechanisms of coronary constriction or enhanced constriction due to thrombus related constrictor substancers may cause intermittent coronary occlusion with consequent transient myocardial ischaemia.

The extent to which the coronary microcirculation is involved in these disease processes is unknown but evidence is accumulating that micro embolism and microvascular constriction may, at least, be a secondary event in some of these ischaemic syndromes [3].

In recent years a number of vasoactive peptides have been found in human tissues and have been shown to exert certain cardiovascular effects when administered into the circulation. The physiological and possible patho-

physiological role of these peptides is unknown at present but the available information in relation to the human circulation will be presented below.

Neuropeptide Y

Neuropeptide Y is found in sympathetic nerves supplying the human heart. These nerves run in the advantitia of the spicardial coronary arteries but can also be seen traversing the media of these arteries and coursing through the myocardium. Neuropeptide Y containing fibres are particularly abundant in the vicinity of arteries which are less than 100 microns in diameter. In the nerve terminal it is found in large storage granules co — localised with noradrenalin which is stored in smalol granulas. The two neurotransmitters are co — released in response to nerve stimulation but the patterns of stimulation causing their release differ somewhat. Binding sites for neuropeptide Y have been found in human heart and are particularly abundant in coronary arterial smooth muscle.

When admininistered in nanomolar concentrations directly into the human epicardial coronary arteries in vivo blood flow falls dramatically leading rapidly to transmural myocardial ischaemia and angina pectoris [4]. The arteriographic pattern obtained is very suggestive of obstruction at the level of the small vessels and is completely unlike that found during epicardial coronary artery spasm. That the obstruction is caused by constriction of these small vessels is indicated by the fact that flow can be restored and myocardial ischaemia relieved by the intra coronary administration of isosorbide dinitrate. When flow begins to return it can be seen on the cine coronary arteriogram that the epicardial coronary arteries are widely patent during the period when the flow has not returned to the basal level. This small vessal constriction has also been demonstrated in the open chested dog by simultaneously measuring flow, coronary calibre and pressure gradient across the epicardial segment of the coronary artery [5].

Recent studies of forearm blood flow show that the potent constrictor effect of infused neuropeptide Y is not diminished by alpha receptor blockade using phentolamine [6] and therefore neuropeptide Y appears to exert its effect predominantly through activation of a specific receptor.

Endothelin

This 21 amino-acid peptide, recently identified as the constricting factor produced by porcine endothelial cells, is the most potent vasoconstrictor peptide known [7]. Like neuropeptide Y it has been shown to reduce regional blood flow in the human by intense constriction of the small arteries and the arterioles [8]. However, its biological half life is very long, in the region of 30

minutes, so that the recovery of blood flow may be measured in hours rather than minutes. Its relevance to physiological control mechanisms and to pathogenetic mechanisms remains unclear.

Vasopressin

Vasopressin, through its antidiuretic action, plays an important role in osmoregulation and its release from the anterior pituitary is mediated through osmoreceptors. However, it is also a vasoconstrictor and its release can be induced by hypotension and hypovolaemia mediated through the high pressure (casrotid sinus) and the low pressure (left atrium) receptors [9]. It is localised mainly in the hypothalamus and anterior pituitary and the pressure responsive releasing mechanisms are influenced by circulating catecholamines through alpha and beta adrenergic pathways. Release of vasopressin may be inhibited by atrial natriuretic peptide and stimulated by somatostatin, both acting through the hypothalamus.

The normal circulating levels in plasma are well below those necessary to have significant effects on blood presssure. However, in hypovolaemic hypotension high plasma levels may be found and represent an important mechanism for recovery from haemorrhage [10]; indeed, blocking the action of vasopressin significantly delays blood pressure recovery following haemorrhage. Increasing the plasma concentration from 5 to 18 and to 36 pg/ml by intravenous infusion of 0.15 and 0.40 ng/kg/min vasopressin in man increases forearm vascular resistance, total systemic vascular resistance and arterial blood pressure and decreases heart rate and cardiac output [11]. By intravenous infusion at higher doses it is used to treat bleeding oesophageal varices [12]; the therapeutic effect is achieved by lowering portal venous pressure by splanchnic arterial vasoconstriction.

There is very little information on the effects of vasopressin on the human coronary circulation. A recent study in patients with coronary atherosclerotic disease reports no change in coronary or systemic vascular resistance following inhibition of vasopressin using a synthetic analogue [13]. However there is good clinical evidence that it constricts the coronary circulation (at least at high plasma levels) as myocardial ischaemia and infarction have been reported in patients receiving an intravenous infusion of vasopressin to treat bleeding oesophageal varices [14].

Angiotensin

Angiotensin II is a circulating vasoconstrictor peptide derived from angiotensin I by the activity of angiotensin converting enzyme in the lung. Angiotensin I is the product of the action of renin, released by the kidney, on circulating angiotensinogen, generated by the liver. In conditions associated

with elevated plasma renin levels systemic vascular resistance is increased by small vessel vasoconstriction causing hypertension and this action can be reversed by angiotensin converting enzyme inhibitors. The circulating renin angiotensin system, in particular renin secretion by the kidney, provides an extremely rapid and efficient homeostatic response to acute changes in blood pressure and fluid and electrolyte status [15].

Renin and angiotensinogen are also produced by arterial tissue and it is therefore possible that the renin angiotensin system operates at a local level, participating in the control of arterial tone [16].

Somatostatin

This peptide is present in the hypothalamus, anterior pituitary, pancreas, stomach, intestine, gall bladder, kidney and parathyroid gland. It inhibits the release of growth hormone, insulin and various gut hormones. Intravenous infusion in patients with hepatic cirrhosis decreases portal venous pressure without changing systemic haemodynamics [17]. This effect is possibly mediated by inhibition of gut vasodilator peptides.

Calcitonin gene related peptide

Calcitonin gene related peptide (CGRP) is found in unmyelinated sensory, substance P containing, perivascular, nerves. Alpha (GRP) is a potent vasodilator which is active in the human, predominantly on the arterial circulation with very little demonstrable venous effect [18]. Although it has been shown to increase blood flow in the forearm, when administered directly into the human coronary circulation it dilates the epicardial cornary arteries but has little effect on the arterioles and consequently increases coronary blood flow very little above the basal value. The dose response curve lies between concentrations of 10—11 M and 10—9 M and the maximum epicardial coronary arterial dilatation is similar to the maximum response to intracoronary nitrate administration [9]. Although, under basal conditions, there is little increase in coronary flow in response to CGRP, when coronary flow is reduced by a focal active process in the epicardial arteries it may be restored by CGRP administration; thus CGRP can relieve attacks of myocardial ischaemia and angina pectoris which are caused by such mechanisms.

When administered intravenously in humans CGRP causes a marked reduction in systemic vascular resistance, an increase in left ventricular stroke volume and cardiac output and a small increase in heart rate. These changes are consistent with the effect of an arterial dilator and could be of therapeutic value in clinical situations requiring left ventricular afterload reduction, such as heart failure.

Substance P

This 11 amino acid peptide was one of the first vaspactive peptides to be discovered although its role and its mechanism of action are still not fully elucidated [20]. It is present in humans in the central and peripheral nervous systems and in the latter is found mainly in the unmyuelinated sensory nerve fibers, which are known to be capable of sustaining antidromic conduction. Substance P is widely distributed throughout the body, including the skin and gut, as well as being localized to nerve fibers supplying blood vessels including the coronary arteries. Although it is mainly localized within vascular nerves its action appears to be dependent on the integrity of the endothelium [21]. It is the most potent vasodilator substance known and, when administered into the human coronary circulation, it causes a dose dependent increase in coronary epicarial artery calibre and in coronary blood flow with its dose response curve ranging between 10—12 M and 10—10 M [22]. The magnitude of the coronary flow increase is intermediate between that of CGRP and that of adenosine suggesting a moderate dilating effect on small vessels. Its effect is very short lived, having a biological half life of approximately 15 seconds. Its response exhibits marked tachyphylaxis and would make it unsuitable as a possible therapeutic agent. Within the human skin substance P is the neurotransmitter released by antidromic stimulation which causes the triple response to injury; it could be a mediator of short term readjustments in coronary vasomotor tone.

Atrial natriuretic peptide

Atrial natriuretic factor was discovered in 1981 [23] and the peptide sequenced in 1984 [24]. It is present in the atria of the human heart in health but also in the ventricles in patients with heart failure [25].

In patients it is released during supraventricular tachycardia and is responsible for the associated polyuria with natriuresis. In the laboratory it can be released by atrial pacing [26] and by stimulation of supraventricular trachycardia [27]; the peak plasma level occurs after approximately 30 minutes of tachycardia and there is a positive correlation with atrial pressure and dimensions. In patients with heart failure the plasma level is elevated; intravenous infusion reduces atrial pressure and systemic vascular resistance and increases the cardiac index.

The role of atrial natriuretic peptide in man appears to be primarily to control blood volume, responding to atrial distension by causing arterial vasodilatation and increased glomerular filtration, increasing excretion of sodium and water.

Bradykinin

Bradykinin, a nine amino acid peptide, is one of a number of kinins which

are generated from kininogens by the action of kallikrein in plasma and rapidly inactivated by kininases [28]. They act as local hormones and plasma levels are low. Kallikrein is derived from prekallikrein which is produced by the liver. Ninety percent of kinin present in blood is inactivated during the first passage through the lung vasculature.

The kallikrein kinin system is activated and bradykinin produced in septicaemia and endotoxic shock [29]. Minute amounts in plasma are sufficient to reduce blood pressure and increase protein permeability. The hypotension in endotoxic shock can be attenuated by administration of a bradykinin antagonist [30].

Forearm blood flow is increased by 20 to 25 mg/min infused into the brachial artery [31] and such small concentrations will dilate coronary arteries when directly infused [32]. Bradykinin is a potent stimulator of prostacyclin biosynthesis in the heart [33]. It relaxes bovine intrapulmonary arteries by endothelium dependent mechanisms involving the actions of cGMP and cAMP the formation of which can be stimulated by endothelium derived relaxing factor and prostacyclin, respectively [34]. It relaxes pulmonary veins by a mechanism involving only cGMP.

All tissues, through their proteolytic enzymes, are capable of releasing bradykinin from plasma [33]. Regional myocardial ischaemia may lead to local kallikrein activation which may have a local vasodilatory action and relieve myocardial ischaemia.

Conclusion

The recent discovery of new vasoactive peptide and the re-evaluation of previously known neurotransmitters and hormones has led to greater awareness of the complexity of cardiovascular control mechanisms which has greatly stimulated research in this field.

References

1. Vatner SF, Franklin DK, Van Citters RL, Braunwald E: Effects of carotid sinus nerve stimulation on the coronary circulation of the conscious dog. Circ Res 27: 11—21, 1970.
2. Furchgott RF and Zawadzki JV: The obligatory role of endothelial cells in the relaxation of arterial smooth muscle by acetyl choline. Nature Lond 268: 373-376, 1980.
3. Davies MJ, Thomas A: Thrombosis and acute coronary artery lesions in sudden cardiac ischemic death. N Engl J Med 310: 1137—1140, 1984.
4. Clarke JG, Davies GJ, Kerwin R, Hackett D, Larkin S, Lee Y, Dawbarn D, Bloom SR, Yacoub M, Maseri A: Coronary artery infusion of neuropeptide Y in patients with angina pectoris. Lancet 1: 1057—1059, 1987.
5. Clarke J, Larkin S, Osinawa O, Davies GJ, Taylor K, Maseri A: Neuropeptide Y reduces dog coronary blood flow by increased small vessel resistance. Clin Sci 73: 6, 1987.
6. Clarke J, Larkin S, Benjamin N, Davies G, Maseri A: The effect of neuropeptide Y on sympathetic vasoconstriction in human forearm resistance vessels. Eur Heart J 9: 12p, 1988.

7. Yanigasawa M, Kurihara H, Kimura S, Tomobe Y, Kobayashi M, Mitsui Y, Yazaki Y, Goto K, Masaki T: A novel potent vasoconstrictor peptide produced by vascular endotheha cells. Nature 332: 411—415, 1988.
8. Clarke JG, Benjamin N, Larkin SW, Webb DJ, Keogh BE, Davies GJ, Maseri A: Endothelin is a potent long-lasting vasoconstrictor in man. Am J Physiol (Heart Circ Physiol 26) 257: H2033—2035, 1989.
9. Bayliss PH: Osmoregulation and control of vasopressin secretion in healthy humans. Am J Physiol 253: R671-R678, 1987.
10. Sachs H, Share L, Osinchak J, Carpi A: Capacity of the neurohypophysim to release vasopressin. Endocrinology 81: 755—770, 1967.
11. Ebert TJ, Cowley Jr JW, Skelton M: Vasopressin reduces cardiac function and augments cardiopulmonary baroreflex resistance increases in man. J Clin Invest 77: 1136—1142, 1986.
12. Sirinek KR et al: High dose vasopressin for acute variceal haemorrhage. Clinical advantages without adverse effects. Arch Surg 1232: 876—880, 1988.
13. Glazier JJ, Gavias H, Mills RM, Ruocco NA, Bresnahan M, Ryan TJ: Effect of inhibition or arginine vasopressin on systemic and coronary haemodynamics. JACC 13: 172A, 1989.
14. Conn HO: A plethora of therapies. In: Westaby D, Macdougall B, Williams R, eds. Variceal bleeding. Pitman Medical, London, 1982: 221—52.
15. Campbell DJ: Tissue renin-angiotensin system: sites of angiotensin formation. J Cardiovasc Pharmacol 10 (suppl 7): 81—8, 1987.
16. Swales JD: Arterial wall or plasma renin in hypertension? Clin Sci 565: 293—298, 1979.
17. Bosch J, Kravetz DK, Rodes J: Effects of somatostatin on hepatic and systemic haemodynamics in patients with cirrhosis. Gastroenterology 80: 518—525, 1981.
18. McEwan JR, Benjamin N, Larkin S, Fuller RW, Dollery CT, MacIntyre I, Maseri A: Vasodilatation by calcitonin gene-related peptide and substance P: a comparison of their effects on resistance and capacitance vessels of human forearms. Circulation 77: 1072—1080, 1988.
19. McEwan J, Larkin S, Davies G, Chierchia S, Brown M, Stevenson J, MacIntyre I, Maseri A; Calcitonin gene-related peptide: a potent dilator of human epicardial coronary arteries. Circulation 74: 1243—1247, 1986.
20. von Euler US, Gaddum JH: An unidentified depresssor substance in certain tissue extracts. J Physiol (LOnd) 72: 74—87, 1931.
21. Bolton TB, Clapp LH: Endothelial dependent relaxant actions of carbachol and substance P in arterial smooth muscle. Br J Pharmacol 87: 713—723, 1986.
22. Crossman DC, Larkin SW, Fuller RW, Davies GJ, Maseri A: Substance P dilates epicardial coronary arteries and increases coronary blood flow in humans, Circulation. In Press. 1989.
23. de Bold AJ, Borenstlen HB, Veress AT, Sonnenberg H: A rapid and potent natriuretic response to intravenous injection of atrial myocardial extract in rat. Life Sci 28: 89—94, 1981.
24. Currie MG, Geller DM, Cole BR: Purification and sequence analysis of bioactive atrial peptides (atriopeptins). Science 223: 67—69, 1984.
25. Edwards BS, Ackerman DM, Lee ME, Reeder GS, Wold LE, Burn JC: Identification of atrial natriuretic factor within ventricular tissue in hamsters and humans with congestive cardiac failure. J Clin Invest 81: 82—86, 1988.
26 Ellenbogen KA, Mohanty PK, Sowers JR, Walsh M, Thamas MD: Atrial natriuretic factor release is enhanced by incremental atrial pacing. Am Heart J 226: 489—496, 1988.
27. Tsai R-C, Yamaji T, Ishibashi M, Takaku F, Pang S-C, Yeh S-J, Lee Y-S, Hung J-S, Delon W: Atrial natriuretic peptide during supraventricular tachycardia and relation to haemodynamic changes and renal function. Am J Cardiol 61: 1260-1264, 1988.

28. Mullins RJ, Hudgens RW: Increased skin lymph protein clearance after a 6 hr arterial bradykinin infusion. Am J Physiol 253: H1462—H1469, 1987.
29. Aasen AO, Smith-Erichsen N, Amundsen E: Plasma kallikrein-kinin system in septicaemia. Arch Surg 118: 343—345, 1983.
30. Weipert J, Hoffman H, Siebeck M, Whalley ET: Attenuation of arterial blood pressure fall in endotoxin shock in the rat using the competitive bradykinin antagonist Lys-Lys-[Hyp2, Thi5, 8, dPhe7] — BkB4148). Br J Pharmacol 94: 282—284, 1988.
31. De Pasquale NP, Burch GE: Digital vascular responses to intra-arterial injections of bradykinin, kallidin and eledoisin in man. Circulation 34: 211—217, 1966.
32. Nakano J: Effects of synthetic bradykinin on the cardiovascular system. Arch Int Pharmacodyn Ther 157: 1—13, 1965.
33. Needleman P, Key SL, Denny SE, Isakson PC, Marshall GR: The mechanism and modification of bradykinin-induced coronary vasodilatation. Proo Nat Acad Sci USA 72: 2060—2063, 1975.
34. Muller-Esterl W, Fritz H: Human kininogens and their function in the kallilrein-kinin system. In Proteases: Potential role in health and disease. ed. WH Horl, Heildland A, New York: Plenum Publishing Corp. 1, 1984: 284—290.

6. Quantitative coronary arteriography at rest and during exercise

OTTO M. HESS, MARTIN BÜCHI, RICHARD L. KIRKEEIDE, MARKUS MUSER, HEIN OSENBERG, PETER NIEDERER, MAX ANLIKER, K. LANCE GOULD, and HANS P. KRAYENBÜHL

Summary

Coronary vasomotion plays an important role in the regulation of coronary perfusion at rest and during exercise. Normal coronary arteries show vasodilation of the proximal (+ 20%) and distal (+ 40%) segments during supine bicycle exercise.

Patients with normal coronary arteries and reduced coronary flow reserve (= *microvascular angina*) show exercise-induced vasoconstriction of the distal epicardial arteries (− 24%), whereas the proximal vessels show vasodilation (+ 25%). This abnormal reaction of the distal epicardial vessels to exercise is probably due to an abnormal neurohumoral tone which may cause or contribute to the paradoxical vascular response of the distal vessels during exercise.

Patients with *coronary artery disease* show exercise-induced vasoconstriction of the stenotic vessel segments. The exact mechanism of this exercise-induced stenosis narrowing is not clear, but might be related either to a passive collapse of the disease-free vessel wall, active vasoconstriction arising from alpha-adrenergic stimulation by circulating catecholamines, an insufficient production of the endothelium-derived relaxing factor due to atherosclerotic alterations of the stenotic vessel segment or to increased platelet aggregation with release of thromboxane A2 and serotonin.

Introduction

Quantitative assessment of coronary vasomotion during exercise has been performed for several years [1—5]. Not only normal, but also stenotic coronary arteries show coronary vasomotion at the site of the stenosis due to the fact that approximately 70% of all stenoses have a normal musculoelastic wall segment within the stenosis [6, 7]. Brown and coworkers [7] have suggested that active vasoconstriction or a passive collapse of the free vessel

J. H. C. Reiber and P. W. Serruys (eds), Quantitative Coronary Arteriography, 145—153.

wall contribute to the decrease in cross-sectional area of stenotic vessel segments. Coronary vasoconstriction with a decrease in coronary blood flow would be particularly important at times of high flow rates such as during dynamic exercise. The purpose of the present study is to discuss the effect of dynamic exercise on coronary vasomotion in patients with normal coronary arteries with reduced pharmacological coronary flow reserve and in patients with coronary artery disease with stable, exercise-induced angina pectoris.

Exercise protocol

Simultaneous biplane coronary arteriography was used for quantitative evaluation of normal and stenotic coronary vessel segments at rest and during supine bicycle exercise. Moderate to severe coronary artery stenoses and normal vessel segments were chosen for analysis. Biplane analysis was performed in most patients in the right and left anterior oblique projection; in some patients cranio-caudal angulation was necessary for proper visualization of the stenotic segment. Cinefilm was used as the data carrier (filming rate 50 frames/s) and 5 to 8 ml of a nonionic contrast material (Iopamiro® 370) were used for coronary arteriography. Control biplane arteriography was performed with the patient's feet in elevated position attached to the bicycle ergometer. Aortic and pulmonary artery pressures were recorded immediately before coronary arteriography. Exercise was usually begun at a level of 50 to 75 Watts, which was increased every 2 minutes in increments of 25 to 50 Watts. Biplane coronary arteriograms with concurrent aortic and pulmonary artery pressure recordings were obtained every 2 minutes and at the end of exercise. Sublingual nitroglycerin (1.6 mg) was administered immediately after termination of the exercise test and repeat coronary arteriography was carried out 5 minutes thereafter.

Quantitative coronary arteriography

Quantitative evaluation of biplane coronary arteriograms was performed with two different systems: Before November, 1988 [1, 2, 4, 5] the outlines of coronary arteries were traced manually (4- to 6-times) in a blinded fashion during mid- to late-diastole and were digitized with an electronic digitizer (Numonics Corp,) interfaced to a PDP 11/34 computer. A portion of the catheter of known dimension, near its tip, was traced for each cineframe and was used as a scaling factor. Interobserver variability of this manual system was found to be small with a standard-error-of-the-estimate (SEE) for monoplane data of 0.39 mm^2 (= 9.3% of the mean vessel area) and for biplane data of 0.30 mm^2 (= 7.9% of the mean vessel area).

After Nov. 1988 an automatic system was used for quantitative coronary arteriography [8]. This system is based on a 35 mm filmprojector, a slow-scan

CCD-camera (image digitization) and a computer workstation (apollo DN 3000, image storage and processing). Calibration was performed by the isocenter technique which is based on two fixed reference points in the center of the two image intensifiers. Contour detection was carried out in biplane projection using a geometric-densitometric edge-detection algorithm (Figure 1). Interobserved variability was found to be small with a standard-error-of-the-estimate for biplane data of 0.14 mm^2 (= 4.1% of the mean vessel area).

The methodology for computerized analysis of coronary arteriograms has been described elsewhere [9]. Briefly, a three-dimensional model of the vessel was constructed by matching centerlines of the individual biplane tracings, assuming the vessel cross section to be ellopsoidal. The proximal and distal, as well as the minimal cross sectional areas of the vessel segment were calculated by the computer.

Normal coronary vasomotion

Coronary vasomotion in 7 normal patients (Group A; Figure 2) with no evidence of coronary artery disease and normal pharmacological coronary flow reserve as assessed by coronary sinus thermodilution was studied at rest and during exercise [4]. Coronary luminal areas of the proximal and distal left anterior descending and left circumflex coronary arteries were analyzed and were found to increase with exercise, which was even further accentuated after sublingual administration of 1.6 mg sublingual nitroglycerin. Coronary luminal area of the *proximal vessels* (Figure 2) increased by 20% during exercise and by 45% after sublingual nitroglycerin administered at the end of the exercise test. Luminal area of the *distal vessels* (Group A; Figure 2) increased by 40% during exercise and by nearly 100% after administration of sublingual nitroglycerin [4]. Thus, in normal patients considerable coronary vasodilation occurs during dynamic exercise, which is, however, not maximal; following the administration of nitroglycerin, coronary luminal area increased more than during exercise.

Microvascular angina

Myocardial ischemia in patients with normal coronary arteries and normal left ventricular function has been reported by several investigators [4, 10, 11]. This condition with lactate production during atrial pacing has been called syndrome X [10, 11]. Several mechanisms have been considered to be responsible for this syndrome, such as coronary arterial spasms, small vessel disease, biochemical disorders or abnormal coronary vasomotor tone [4, 10, 11]. Vasomotion of the proximal and distal coronary vessels was studied in 6 patients (Group B; Figure 2) with normal coronary arteries, ischemia-like

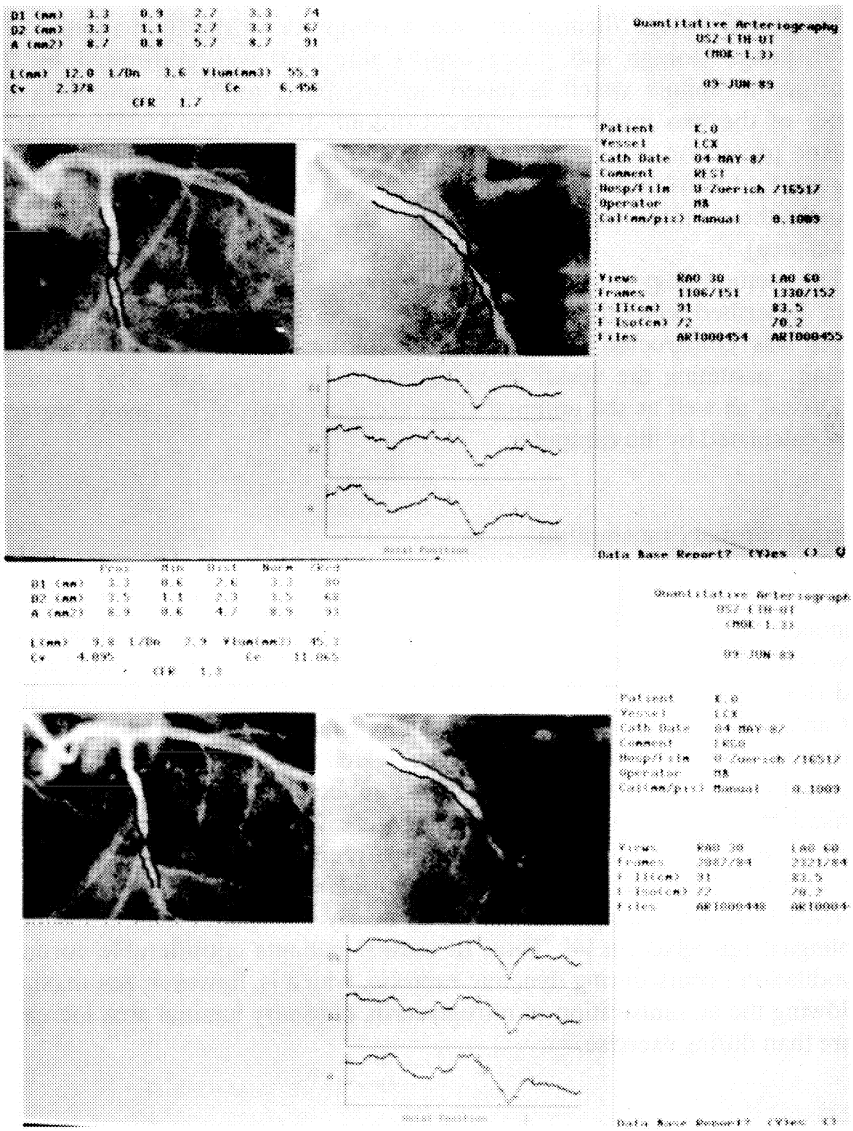

Fig. 1. Quantitative coronary arteriography was carried out by an automatic system, which is based on a 35 mm filmprojector, a slow scan CCD-camera (image digitization) and a computer workstation (image storage and processing). Contour detection was performed in biplane projection using a geometric-densitometric edge-detection algorithm. Luminal areas of a normal and a stenotic vessel segment were analyzed at rest (upper panel) and during submaximal bicycle exercise (lower panel). Patient's data (right) and coronary luminal areas (top left of each panel) are given for each individual sequence.

symptoms and a reduced coronary flow reserve after intravenous dipyridamole as determined by coronary sinus thermodilution. Quantitative coronary arteriography was carried out at rest and during symptom-limited exercise, as

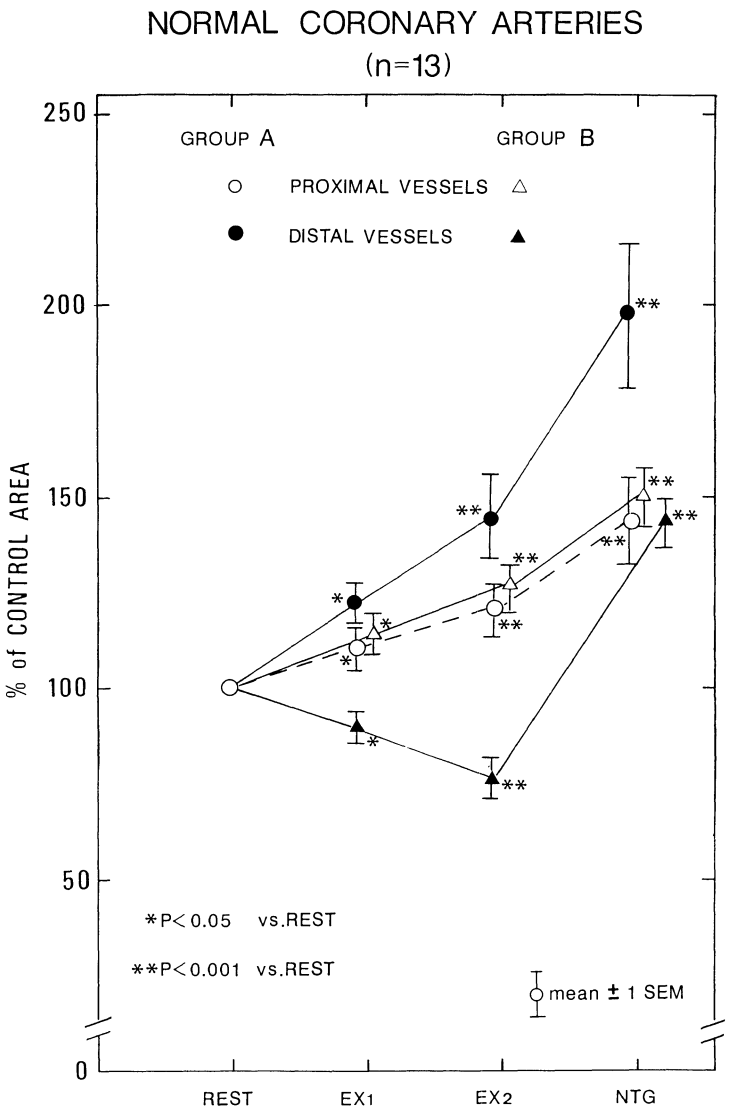

Fig. 2. Coronary luminal areas of the proximal (open symbols) and distal (closed symbols) coronary arteries were determined at rest, during a first (EX1) and a second (= submaximal; EX2) level of supine bicycle exercise, as well as 5 minutes after 1.6 mg sublingual nitroglycerin (NTG). Patients with normal coronary arteries were subdivided into 2 groups: Group A consisted of 7 control patients with normal coronary flow reserve (mean 2.5 ± 1.0, as determined by coronary sinus thermodilution) and Group B of 6 patients with reduced coronary flow reserve (mean 1.2 ± 0.3, $p < 0.05$). Coronary vasodilation of the proximal and distal coronary arteries was observed during exercise and after nitroglycerin in the control group. However, in Group B, there was coronary vasoconstriction of the distal coronary arteries during exercise, whereas the proximal vessels showed exercise-induced vasodilation. Thus, patients with normal coronary arteries but reduced coronary flow reserve show an abnormal dilator response during supine bicycle exercise. SEM: standard error of the mean.

well as after sublingual administration of 1.6 mg nitroglycerin (Group B; Figure 2). *Proximal vessels* showed exercise-induced coronary vasodilation (+ 25%) as in the control group, whereas *distal vessels* showed coronary vasoconstriction (− 24%) during exercise, which was reversible after administration of nitroglycerin (+ 44%). Thus, abnormal vasomotion of the distal coronary arteries appears to be responsible for a decrease in coronary blood flow during exercise in these patients, which could explain the occurrence of myocardial ischemia with lactate production during exercise or pacing-induced tachycardia. This abnormal reaction of the distal coronary vessels to exercise could be explained by an abnormal vasomotor tone [12]. These changes could be effective through reflexes enhancing alpha-adrenergic tone, which can cause vasoconstriction of the arterioles, but also of the adjacent smaller epicardial arteries. [12].

Coronary artery disease

Coronary vasomotion of stenotic coronary arteries represents a significant element in the pathogenesis of myocardial ischemia [7]. Brown and coworkers [13] have reported a decrease in coronary luminal areas of normal and stenotic vessel segments by 14 and 35%, respectively, during isometric handgrip exercise. After intracoronary infusion of nitroglycerin, a second handgrip test showed an increase instead of a decrease in coronary luminal area of the stenosis and the normal vessel. These authors concluded, that active vasoconstriction during handgrip test is probably caused by reflex activation of the sympathetic nervous system, which can be prevented by nitroglycerin. Dynamic bicycle exercise is associated [1] with coronary stenosis narrowing, but in contrast to handgrip exercise, normal coronary arteries show vasodilation (Figure 3). This exercise-induced vasoconstriction is dependent on the severity of coronary stenosis, since mild to moderate lesions ($<$ 50% diameter reduction, mean 45%) showed only minimal vasoconstriction (− 10%, n.s. versus rest) during bicycle exercise, whereas severe lesions ($>$ 50% diameter reduction, mean 64%) showed significant stenosis narrowing (− 32%, $p < 0.001$ versus rest). The mechanism of exercise-induced stenosis narrowing is unclear, but represents an important observation in the pathophysiology of acute myocardial ischemia in patients with classic angina pectoris.

The following mechanism could explain this phenomenon:

1. passive collapse of the disease-free vessel wall due to an increase in coronary blood flow during exercise (Venturi mechanism) [7];
2. active vasoconstriction arising from alpha-adrenergic stimulation by circulating catecholamines and activation of the sympathetic nervous system during exercise [1];
3. insufficient production of the endothelium-derived relaxing factor during

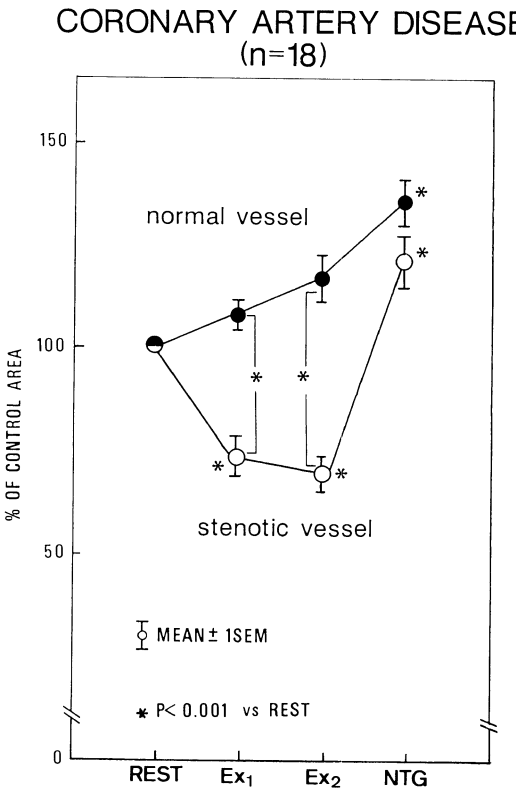

Fig. 3. Coronary luminal area of a normal (closed symbols) and a stenotic (open symbols) vessel segment in 18 patients with coronary artery disease at rest, during a first (EX1) and a second (EX2) level of supine bicycle exercise, as well as 5 minutes after 1.6 mg of sublingual nitroglycerin (NTG). The normal vessel segment showed coronary vasodilation during exercise and after sublingual nitroglycerin, whereas the stenotic segment showed exercise-induced coronary vasoconstriction, which was reversible after sublingual administration of nitroglycerin. Thus, exercise-induced stenosis narrowing is an important mechanism in the pathophysiology of myocardial ischemia during dynamic exercise in patients with classic angina pectoris.

exercise due to atherosclerotic alterations of the stenotic vessel segment [14];

4. increased platelet aggregation during exercise due to turbulent blood flow with release of thromboxane A2 and serotonin [15].

It is likely that more than one of these mechanisms are responsible for the observed exercise-induced vasoconstriction. As blood flows through a coronary stenosis, its flow velocity increases, while its pressure decreases at the point of its greatest narrowing. Most of the pressure loss persists also distal to the stenosis due to turbulence. During exercise, blood flow increases up to four times, which increases the pressure gradient across the stenosis 16-fold. Since exercise-induced vasoconstriction can be prevented by intra-

coronary nitroglycerin [1] or diltiazem [16]. the concept of a passive collapse might be valid only in patients with severe coronary artery stenoses in whom flow velocity may be high in the resting state. The occurrence of turbulence distal to the stenosis suggests platelet aggregation with release of thromboxane A2 and serotonin as a complementary mechanism responsible for active vasoconstriction. Thus, a decrease in turbulence during exercise with a decrease in blood flow velocity after coronary vasodilation (e.g. nitroglycerin or calcium antagonists) could explain a reduction or elimination of exercise-induced vasoconstriction. Increased levels of circulating catecholamines suggest a vasoconstrictory element via alpha-adrenergic stimulation. Since only stenotic but not normal vessel segments show exercise-induced vasoconstriction, it has to be assumed that other factors than increased catecholamine levels are responsible for this phenomenon, such as endocardial dysfunction with an insufficient production of the endothelium-dependent relaxing factor [14]. It has been shown experimentally, that atherosclerotic vessel segments respond differently to stimulation of the endothelium by acetylcholine: normal vessels show vasodilation, whereas stenotic vessels show vasoconstriction [17]. Recently, Hodgson and coworkers [18] reported opposite effects of intracoronary acetylcholine on coronary vasomotion of the proximal and distal coronary arteries: proximal vessel segments showed coronary vasoconstriction in patients with mild coronary artery disease, whereas distal vessel segments showed vasodilation. Thus, epicardial coronary arteries might show differing rersponses of the proximal and distal coronary arteries to pharmacological [18] or physiologic stimuli, such as in patients with microvascular angina.

References

1. Gage JE, Hess OM, Murakami T, Ritter M, Grimm J, Krayenbuehl HP: Vasoconstriction of stenotic coronary arteries during dynamic exercise in patients with classic angina pectoris: reversibility by nitroglycerin. Circulation 73: 865—876, 1986.
2. Gaglione A, Hess OM, Corin WJ, Ritter M, Grimm J, Krayenbuehl HP: Is there coronary vasoconstriction after intracoronary beta-adrenergic blockade in patients with coronary artery disease. J Am Coll Cardiol 10: 299—310, 1987.
3. Gordon JB, Zebede J, Wayne RR, Mudge GH, Ganz P, Selwyn AP: Coronary constriction with exercise: possible role for endothelial dysfunction and alpha tone. Circulation 74 (Suppl.II): II—481, 1986 (Abstract)
4. Bortone AS, Hess OM, Eberli FR, Nonogi H, Marolf AP, Grimm J, Krayenbuehl HP: Abnormal coronary vasomotion during exercise in patients with normal coronary arteries and reduced coronary flow reserve. Circulation 79: 516—527, 1989.
5. Hess OM, Bortone AS, Eid K, Gage JE, Nonogi H, Grimm J, Krayenbuehl HP: Coronary vasomotor tone during static and dynamic exercise. Europ Heart J.
6. Freudenberg H, Lichtlen PR: The normal wall segment in coronary stenosis — a postmortem study. Z Kardiol 70: 863—869, 1981.
7. Brown BG, Bolson EL, Dodge HT: Dynamic mechanisms in human coronary stenosis. Circulation 42: 917—922, 1984.
8. Buchi M, Hess OM, Suter TH, Kirkeeide RL, Muser M, Osenberg H, Niederer P,

Anliker M, Gould KL, Krayenbuehl HP: Validation of a new automatic system for biplane quantitative coronary arteriography. Int J Cardiovasc Imaging.
9. Kirkeeide RL, Gould KL: Cardiovascular imaging: Coronary artery stenosis. Hosp Pract 19: 160—163, 1984.
10. Arbogast R, Bourassa MG: Myocardial function during atrial pacing in patients with angina pectoris and normal coronary arteriograms. Am J Cardiol 32: 257—263, 1973.
11. Opherk D, Zebe H, Weihe E, Mall G, Dürr C, Gravert B, Mehmel HC, Schwarz F, Kübler W: Reduced coronary dilatory capacity and ultrastructural changes of the myocardium in patients with angina pectoris but normal coronary arteriograms. Circulation 63: 817—825, 1981.
12. Cannon RO, Watson RM, Rosing DR, Epstein SE: Angina caused by reduced vasodilator reserve of the small coronary arteries. J Am Coll Cardiol 1: 1359—1373, 1983.
13. Brown BG, Lee AB, Bolson EL, Dodge HT: Reflex constriction of significant coronary stenosis as a mechanism contributing to ischemic left ventricular dysfunction during isometric exercise. Circulation 70: 18—24, 1984.
14. Bassenge E, Stewart DJ: Interdependence of pharmacologically-induced and endothelium-mediated coronary vasodilation in antianginal therapy. Cardiovasc Drugs and Ther 1: 47—55, 1988.
15. Folts JD, Gallagher K, Rowe GG: Blood flow reductions in stenosed canine coronary arteries: vasospasm or platelet aggregation? Circulation 65: 248—255, 1982.
16. Nonogi H, Hess OM, Ritter M, Bortone A, Corin WJ, Grimm J, Krayenbuehl HP: Prevention of coronary vasoconstriction by diltiazem during dynamic exercise in patients with coronary artery disease. J Am Coll Cardiol 12: 892—899, 1988.
17. Ludmer PL,Selwyn AP, Shook TL, Wayne RR, Mudge GH, Alexander RW, Ganz P: Paradoxical vasoconstriction induced by acetylcholine in atherosclerotic coronary arteries. N Engl J Med 315: 1046—1051, 1986.
18. Hodgson JMcB, Marshall JJ: Direct vasoconstriction and endothelium-dependent vasodilation; mechanisms of acetylcholine effects on coronary flow and arterial diameter in patients with nonstenotic coronary arteries. Circulation 79: 1043—1051, 1989.

Part III

Coronary angioscope; epicardial and intravascular echocardiography

7. Coronary angioscopy

THOMAS WENDT, RALF BETTINGER, and GISBERT KOBER

Summary

Direct visual examination of the interior surfaces of intact human coronary arteries is now a reality, both via intraoperative and transluminal approaches.

As an additional investigation to angiography it improves the knowledge about the corresponding morphology of angiographically visible changes.

Since the first report about percutaneous and intraoperative coronary angioscopy using the new generation of ultrathin, flexible endoscopes by Spears et al. in 1982, more than 2000 coronary angioscopies have been reported until now by approximately 20 study groups worldwide.

Due to yet unsolved technical problems and a much more sophisticated examination technique, percutaneous coronary angioscopy, today, cannot be performed routinely but must be reserved to specific scientific trials.

However, concerning the intraoperative approach, important indications were defined such as the visual control of coronary atherectomy, intraoperative balloon dilatation and laserangioplasty, the inspection of the grafts prior to implantation and finally the qualitative assessment of the distal anastomosis after graft insertion.

The most important clinical result brought about by angioscopy involves the postulation of a concept of the different clinical forms of coronary artery disease based on the morphological stages of atherosclerosis, which were defined by angioscopy and consequently related to clinical symptoms.

Scientific studies today are concerned with determinants for the patency rate of bypasses, the restenosis rate of PTCA, the acute and chronic effects of drugs, and the mechanisms of all kinds of catheter-supported angioplasties.

The next important progress in coronary angioscopy will undoubtedly be the simultaneous visual control of coronary laser angioplasty.

Introduction

Towne's provocatively imposed question in 1977: "vascular endoscopy:

J. H. C. Reiber and P. W. Serruys (eds), Quantitative Coronary Arteriography, 157–180.

useful tool or interesting toy?" [82] can now be answered clearly in favour of angioscopy. With its help, morphological information can be obtained in-vivo, which is not possible by any other method. As a result, substantial consequences for therapy often ensue from these data.

In this chapter an overview is given on the development, the various techniques, the indications and the current status of percutaneous and intraoperative coronary angioscopy.

Historical review

As with many supposedly new ideas, it has to be realized that angioscopy is actually quite old.

Cardioscopy was first attempted in 1913 by Rhea and Walker, who used a rigid, cylindrical tube similar to today's rectoscopes in an intraoperative trial. Because the lens was recessed in a sheath, direct contact between the lens and the endocardium was impossible and circulating blood interfered with vision. Therefore this pioneer's deed was deemed unsatisfactory and thus never published. It was, however, referred to by Cutler et al. in 1924 [14].

The following years, smaller instruments, the improvement of illumination, the refinement of the technical accessories [1, 2, 4, 6, 55, 62, 63] and the problem of temporary elimination of the nontransparent blood by flushing [64] or displacement [27, 61] were worked upon for the intraoperative use.

In 1961, Carlens and Silander [7] made the first step towards the transluminal application by advancing a rigid, 7 mm scope with right-angle view through the jugular vein for inspection of the right heart. With a thin rubber balloon, which was attached superior to the distal lens of the scope and inflated with 5 ml of saline, it was possible to press the instrument against the endocardium for sharp images of the right atrium and ventricle. Although the illumination was adequate for inspection, photography required an exposure time of approximately 60 seconds and, therefore, could only be obtained while the heart was arrested.

However, these efforts and subsequent studies [8, 74] had only modest success, as the rigid instruments did not allow a protective inspection of the tortuous vessels.

It took until 1958 for the technology of flexible glassfibers [26] to find its first practical application in medicine [29]. With that, it was possible to transport light as well as an image of the object through the winding vessels, which were at first of large caliber [12, 13, 18, 22, 57, 70, 71, 81, 89, 90, 91].

However, angioscopy of the small vessels such as e.g. the coronary arteries was only possible after the development of ultrathin fiberglass endoscopes at the beginning of the eighties.

The first prototypes of these flexible endoscopes with an orthograde view were less than 2 mm in diameter at a length of 100 to 120 cm, but had neither a steering mechanism nor a working channel.

Using these simple instruments, several groups in the United States, Europe and Japan started coronary angioscopy at the same time. Soon there after, in 1982, Spears et al. were the first to describe the intraoperative as well as the percutaneous technique [77].

In the group of W. Grundfest and coworkers at the Cedars Sinai Medical Center, intraoperative coronary angioscopy flourished rapidly [9, 16, 17, 23, 24, 25, 46, 47, 48, 72, 73]. Very early this center could look back upon 172 coronary angioscopies in the first 100 explored patients [28].

Together with the experience of other groups numerous useful applications were proposed for the intraoperative approach [11, 15, 30, 32, 35, 41, 52, 65, 66, 67, 80, 92, 93, 95, 96, 97, 98], which will be referred to below.

The most important clinical result brought about by angioscopy involved the postulation of a concept of the different clinical forms of coronary artery disease by Forrester et al. in 1987 [17] based on the morphological stages of atherosclerosis, which were defined by angioscopy and consequently related to clinical symptoms.

These intraoperative results incited interest in the percutaneous application which was lagging behind because of the more sophisticated examination technique [3, 5, 30, 31, 33, 35, 38, 40, 58, 68, 69, 75, 76, 88], with which a lower success rate was achieved. Initially, a success rate of approximately 50% was achieved [35, 75, 92], as opposed to a success rate of 90% with the intraoperative approach [25, 30, 95].

Nevertheless, with increasing experience in the percutaneous method, important clinical questions could be successfully investigated with this technique: Forrester's concept could be supported in acute coronary syndromes [37, 51, 84], the course of coronary thrombosis [50, 53, 78, 79] and thrombolysis [36, 95] could be observed, and the effect of balloon dilatation be judged by looking at the inner surface before and after the procedure [34, 54, 86, 87, 93, 96].

Important in-vitro studies were concerned with the development of coronary thrombosis and thrombolysis [83], with rheological mechanisms within stenoses in relation to their cross-sectional area [85], as well as with the reliability of angioscopic data in comparison to angiography and macroscopy [94].

By miniaturization and improvements in the steerability of the scopes [58, 86], it has recently been possible to increase the success rate of percutaneous coronary angioscopy significantly and to enlarge the number of coronary segments within reach. Mizuno and coworkers [50], for instance, report about first experiences with a 1.1 mm angioscope, that contains 4 channels, an angulation system and a distal occlusion cuff.

Basic principles of operation: irrigation (I) and angulation (II)

I: Aside from the steering mechanism, which is important for the selective probing of the coronary tree and for centering the tip inside the vessel to

obtain images of diagnostic quality, flushing is the second decisive aspect in coronary angioscopy.

During percutaneous angioscopy a sufficient flushing of the target lesion is much more difficult to achieve than with the intraoperative approach.

If angioscopes without an integrated channel are used, flushing is performed through the 8 to 9.5 French guiding catheter in the percutaneous approach, and through a 5 French sheathing catheter enclosing the scope when applied intraoperatively.

The flushing solution, preferably lactated Ringer's solution at room temperature, is supplied by a Y connector and exits next to the distal lens. Intraoperatively, the cold cardioplegic solution can be used for irrigation.

The total amount of flushing volume depends on the local situation. Intraoperative flushing can be done with larger volumes, as a substantial part is immediately eliminated by suction. An approximate estimation of the fluid loading, however, must be done keeping in mind an upper limit of 500 ml, even though other authors [19] detected no fluid overload at 1000 ml.

During cardiac catheterization, a 50 ml syringe is used and flushing is done per volume of 10 ml with a flow of 2 to 4 ml/sec., in such a way that there is sufficient visualization for a few seconds. Intraoperative continuous flushing can be done while the heart is arrested. Especially intraoperatively the flushing dilates the collapsed vessel and excellent visualization can be accomplished.

To diminish the necessary flushing volume and to obtain better images, a reduction of disturbing orthograde, retrograde or collateral blood flow can be achieved by auxiliary blocking maneuvers: transluminally by additional blocking balloons (Fogarty type) that may be expanded proximally and/or distally of the angioscope's tip, and intraoperatively by clamping. As described above, recent angioscopes have an integrated flushing channel as well as a distal occlusion cuff.

II: Different techniques have been developed for steering the angioscope, especially during cardiac catheterization: One possibility for steering the angioscope's tip is the double guiding catheter technique [95]. As a first step, a common 0.12 inch guide wire is placed before the target lesion; next, a 5 French inner catheter is pushed completely over it. Finally, the guide wire is removed and exchanged for the angioscope.

With this approach, almost every region of interest can be reached as long as the 5 French catheter fits the coronary lumen. The advantage of this procedure lies in the fact that the tip is not allowed to touch and possibly injure the endothelium. Its disadvantage lies in the fact that the irrigation capacity is reduced, although flushing is possible via both catheters.

Another possibility of steering is achieved in the over-the-wire technique [95]. In this case, a loop is fixed at the distal end of the scope, by which the instrument can be moved to the region of interest along a guide wire using it as a rail.

However, pushing the angioscope along the guide wire through curves, the wire itself is straightened, as today's angioscopes are stiffer than guide wires. Moreover, in such situations the sharp edged tip of the angioscope may scratch along the endothelium with the possibility of injuring it.

With its loop, it can also get hooked during withdrawal into the guiding catheter. Therefore, a distal channel of about 10 cm length, the proximal orifice of which must not leave the guiding catheter, is better than the loop.

On the other hand, this technique has the advantage that the tip is brought into a center position within the vessel by the wire; however, only in straight segments.

An improvement of the over-the-wire-principle is the integrated flushing channel of newer angioscopes, which can additionally carry a guide wire.

Intraoperatively, active angulation of the tip does not play such an important role, because of the short distance between insertion and inspection site and the possibility of manipulating the tip and the vessel manually from the outside.

Special technical equipment

Today, various angioscopes are offered by several commercial companies such as Advanced Cardiovascular Systems, American Edwards, Fukada, Fuji, Olympus, Storz, Trimedyne, and others.

The older, simpler instruments are 0.8 to 1.8 mm in diameter, have a working length of 100 to 120 cm and contain 2000 to 3000 arranged optical fibers of 5 micron each for transmission of the endoscopic picture. Their angle of view field is 55 degrees in air and 42 degrees in saline solution, their depth of view field is 1 to 15 mm with an optimum visual distance of 4 mm.

Recent instruments contain the transmission fibers for illumination and imaging within a diameter of 0.5 mm. They are offered either without any extras or with additional flushing channels, balloons or steering mechanisms, however, at the expense of enlarging the overall diameter.

In addition, a colour video camera, a high resolution monitor, a halogen light source and a videorecorder are necessary. Freeze frame printers (Polaroid) and colour video printers (e.g. by Bauer, Mitsubishi) have proven convenient for a quick documentation of the findings. Other parts like sheaths, pressure lines, three way ports, syringes and sterile bags to wrap the camera are at hand in any cath-lab.

Sterilization of the angioscope can be achieved either by ethylen oxide or by immersing the flexible part of the scope for 30 minutes in a plexiglas tube which is filled with a 10% Gigasept (R) solution.

Review of angioscopic findings

Angioscopy provides numerous morphological details, that cannot be ob-

tained with any other in vivo method. After Grundfest et al. [17, 25] had described various stages of atherosclerosis by their morphological appearance, our group defined the different morphological criteria of these stages (Table 1) and compared them with postmortem angiographic findings and the genuine findings after the vessels were cut open and could be inspected with the naked eye [94].

Table 1. Frankfurt — Angioscopic — Classification [94].

Morphologic definition	Surface	Colour	Shape	Mobility
normal	smooth reflecting	pink	0	no
lipogenic plaque	smooth, intact non-reflecting elevated	yellow	round	no
ulcerous plaque	rough crater-like	yellow and white	edged	no
ulcerous plaque with thrombosis	rough crater-like hilly	yellow and red	edged	no
fibrous plaque	smooth + bulging rough + fringed flaps + cones	white	round or edged	possible
walladherent thrombosis	non-reflecting prickly and/or rippled	dark red and/or white	plain	tightly attached
thrombus	smooth reflecting	red	spherical	possible
dissection	smooth	white	lamella	yes

The results were as follows: Comparing angioscopy with angiography, we found that angiography was unable to tell anything about the morphology of lesions, which was, however, easily possible with angioscopy. On the other hand, only with angiography, we were able to define the extent of narrowing of a stenosis.

This part of the comparison of the three evaluation methods was a good confirmation of what could be expected. However, surprising results were obtained from the comparison angioscopy versus macroscopy (Table 2).

All 28 segments, that had been described as normal, were truly normal. Lipogenic plaques were presumed 15 times, however, confirmed in only 11 cases. In 4 cases, light reflections were misinterpreted as lipogenic plaques, 5 additional subintimal plaques were ignored. All ulcerous plaques with or without thrombosis, as well as all fibrous plaques were found and interpreted correctly without any exception. Occlusions were presumed by angioscopy 4 times, which was found to be true only twice. Curves imitated cleft occlusions

Table 2. Post mortem comparison between angioscopy and macroscopy in 16 intact human cadaveric hearts.

	normal	lipogenic plaque	ulcerous plaque	ulc./thr. plaque	fibrous plaque	occl.	diss.
angioscopy vs macroscopy	28	15	5	1	21	4	4
	28	11	5	1	21	2	2
ignored	0	5	0	0	0	0	0
misinterpreted	0	4	0	0	0	2	0
correct							2

in two cases. With dissections, angioscopy was even superior to macroscopy. Only 2 out of 4 angioscopically obvious dissections or movable flaps could be found after the vessel was cut open.

These results indicate that angioscopic judgements are reliable in case of normal intima, ulcerous and fibrous plaques, whereas light reflections and curves are possible pitfalls in the interpretation of lipogenic plaques and occlusions, which have to be considered.

Transluminal techniques

During fluoroscopy, the angioscope is carefully pushed through an 8.0 French guiding catheter, which was placed via the brachial or femoral artery in the coronary ostium. As the scope is still relatively stiff, it is important to pay attention that the guiding catheter is not luxated out of the coronary ostium as the scope is being moved forwards.

If a simple angioscope without steering mechanism is used, good pictures are merely exceptional and a selective probing is impossible as well. In this case, the double guiding catheter technique, which has been described above, can be of great value.

If the angioscope has a distal loop or an integrated channel, it can be pushed along a guide wire to the region of interest.

Another possibility is offered by the recent angioscopes with an integrated distal balloon. The tip can be lifted off the wall by inflation of the cuff and is then centered inside the lumen, a requirement for good images. In addition, the orthograde blood flow is diminished, further improving the visualization.

A lactated Ringer's solution at room temperature is recommended for irrigation. Following injection of saline into the right coronary artery, one female patient in our series presented ventricular fibrillation, which could be converted to sinusrhythm immediately; others complained of angina. With lactated Ringer's solution we noted no side-effects.

Concerning the likelihood of recording good pictures from potential inspection sites, the right coronary artery is the most suitable vessel, as all of the flushing performed through the guiding catheter hits its lumen, whereas a

large part of the irrigation reaches the circumflex during inspection of the left anterior descending and vice versa.

On the other hand, the LAD is easier to probe than the RCA. In general, the Cx is unsuitable, because of its rectangular outlet. Vein grafts to the left coronary artery are generally not as suitable for transluminal angioscopy as those to the right coronary artery, because they exit at an angle and move around the heart, while the vein grafts to the RCA run straight downward at first.

A further difficulty of the percutaneous approach lies in the fact that the heart moves from systole to diastole, striking the angioscope from wall to wall. This can only be remedied by additional or integrated balloons; guiding wires are insufficient in this case.

Intraoperative techniques

In comparison to the percutaneous approach the intraoperative technique is far easier: the distances are shorter, the tip and the vessel can be manipulated from the outside, the heart is arrested while the patient is supported on a bypass pump, the duration of flushing does not play a similarly decisive role, the coronaries are emptied of blood, and the danger of volume overloading is small as much of the flushing solution is absorbed by the suction.

A disadvantage is the fact, that pushing the angioscope intraoperatively is usually done without fluoroscopic control; however, the tip can be seen through the vessel wall by the light shining through it.

The angioscope or the angioscope holding catheter is inserted through the arteriotomy or the bypass vein and moved in gentle rotating motion up- and downwards. Under favourable conditions the angioscope can also be driven retrograde out of the left main stem and be pushed transaortically orthograde into the RCA by the so called "crisscross-maneuver" [59].

Besides the inspection of the coronary tree, the visual control of intraoperative angioplasties and the inspection of the veins and internal mammary arteries before implantation, the intraoperative examination is useful for checking the suture lines of the distal anastomosis.

The transluminal approach: results

During cardiac catheterization we have performed percutaneous coronary angioscopy in 24 selected patients via the brachial or the femoral approach. Eight patients underwent coronary angioscopy before and after PTCA, two before and after intracoronary lysis.

Three simple angioscopes with diameters between 0.8 and 1.0 mm (American Edwards) were used, the tips of which we left unaltered in the 1st, equipped with a distal loop in the 2nd and equipped with a short, distal channel in the 3rd.

The following example describes the examination of a 54-year old male patient.

Eleven years after aortocoronary bypass grafting the patient complained of increasing exertional angina. Coronary angiography revealed a long, cloudy and irregular stenosis in the mid portion of the venous graft to the right coronary artery (Figure 1).

Six weeks later the patient came for angioplasty of this stenosis. Angiography then performed showed a total occlusion which had formed meanwhile (Figure 2a). Angioscopically, a fresh, red thrombus could be identified as the cause of the occlusion (Figure 2b). For technical reasons (NTSC video system) the thrombotic material appears green instead of red, as could be seen with the naked eye.

After intracoronary lysis with urokinase over a period of 30 minutes the well filled periphery of the right coronary artery was visible angiographically, as well as the remaining cloudy areas in the formerly occluded segment (Figure 3a).

In the early stage of lysis, red thrombi could be noted angioscopically; shortly after small, in some areas, bigger, white fibrin flaps, fringed out like fern leaves (Figure 3b). At the end of the lysis, only minor white fibrin threads attached to a smooth vessel endothelium and sticking to the guide wire were found (Figure 3d).

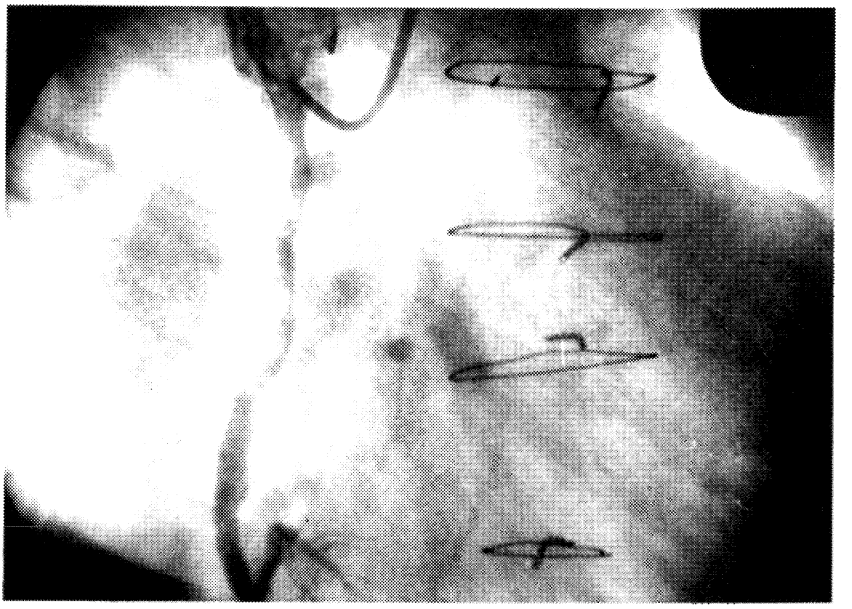

Fig. 1. Angiography of a vein graft to the right coronary artery: cloudy, irregular stenosis, suspected thrombus.

Summarizing our results, which have been published in detail elsewhere [92, 93, 95, 96, 99], we found that percutaneous coronary angioscopy offers additional information on the morphology of stenoses, their longitudinal and circumferential order, the presence of occluding or wall-adherent thrombi as well as intimal dissections. Furthermore, stenoses could be examined before

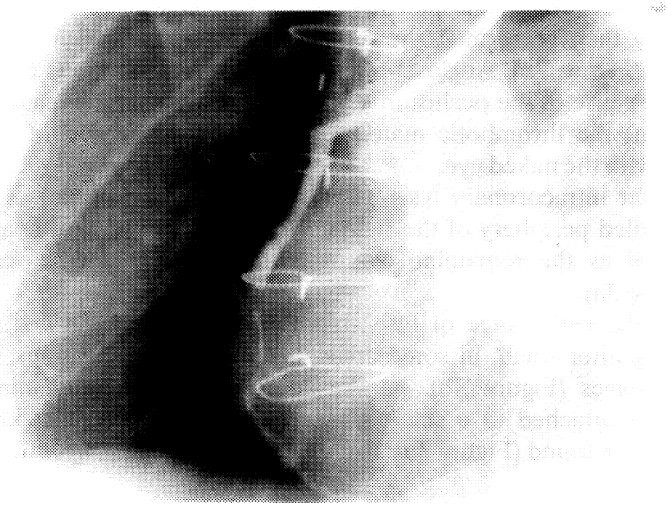

(a)

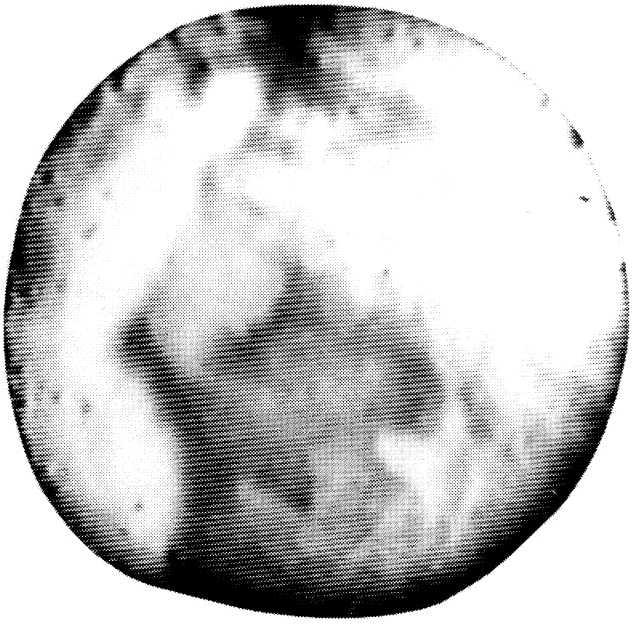

(b)

(c)

Fig. 2. (a) Angiography directly preceding planned angioplasty: novel occlusion in the segment of the former high grade stenosis. (b) Angioscopic finding: Laterally on the left and right side of the picture, white fibrin networks can be identified; in the center, the occluding thrombus is visible (oblique shading); above that a further red clot (narrow shading). (c) Schematic illustration.

and after PTCA, thereby helping to understand more about the mechanism of balloon angioplasty.

The initial 45% success rate on images of sufficient quality could not be improved in the course of the study using these angioscopes. Failure was mainly due to the lack of steerability. In some cases, the improved blood flow after successful angioplasty impeded visualization after PTCA in patients in whom coronary angioscopy had been successful prior to angioplasty. Stenoses or occluded vessels and bypasses allowed a good view even with little flushing.

In contrast to the swiftness of intraoperative angioscopy, the percutaneous technique lasted on average 10 to 15 minutes.

Besides the above mentioned single occurrence of ventricular fibrillation due to injection of saline solution, no major complication was noted.

The intraoperative approach: results

During aortocoronary artery bypass graft surgery, we performed 73 coronary

angioscopies in 41 patients. Thirty-three patients were examined in Frankfurt, 8 in cooperation with the colleagues in Gießen, who have had their own experience with intraoperative coronary angioscopy before [52].

Fifteen coronary arteries were inspected without further interventions, 6 before and after atherectomy, 22 before and after intraoperative balloon dilatation and 7 before and after intraoperative argon-laser angioplasty. The suture lines of the distal anastomoses were inspected through the implanted vein 23 times.

Again, one example shall illustrate the intraoperatively obtained images. It describes the findings of a patient, who was treated with laser angioplasty (Trimedyne Optilase 900) according to the protocol shown in Figure 4.

The aim of this study [97, 98] was to describe the immediate angioscopic results of human coronary argon-laser angioplasty. While the heart was arrested, a first angioscopy of the region of interest was performed by inserting the scope retrograde through the arteriotomy. Then, the angioscope was pulled out and the first laser procedure was performed using a 2.0 mm spectraprobe. After that, the laser probe was pulled out and exchanged for the angioscope to inspect the lasered site. After that, a second laser angioplasty was done with a 2.0 mm hot tip probe followed by control angioscopy in the same manner. In order to improve the result, an additional balloon dilatation was finally performed, again controlled by angioscopy. A follow-up angiography took place on day 6 postoperatively.

The 51-year-old male patient came to surgery because of restenosis following 3 primarily successful PTCAs. The preoperative angiogram of the left coronary artery is shown in Figure 5a, the intraoperative image of the distal end of this stenosis in Figure 5b.

After withdrawal of the scope, the spectraprobe was advanced and laser

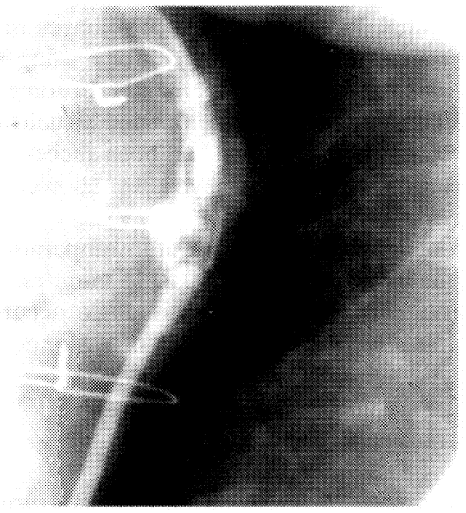

(a)

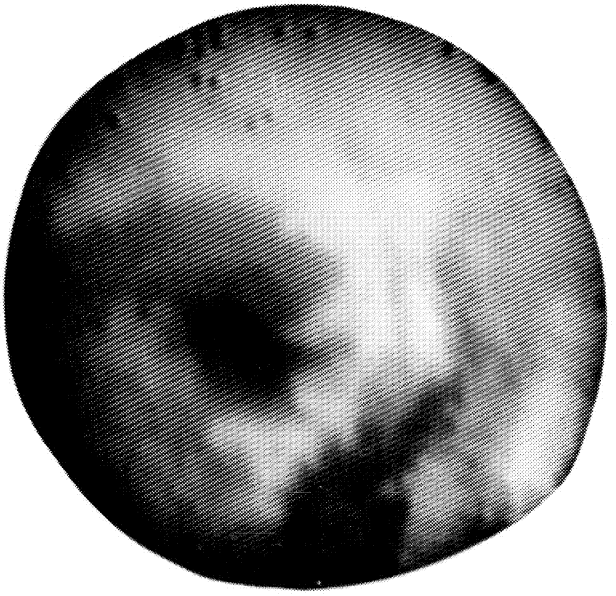

(b)

(c)

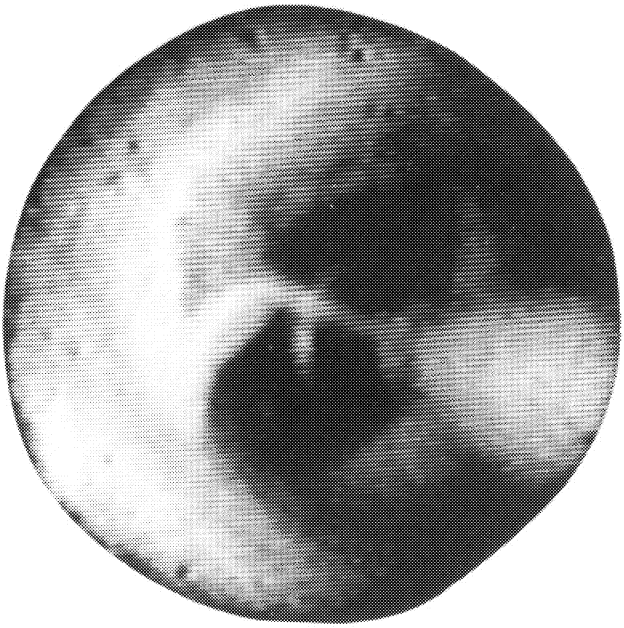

(d)

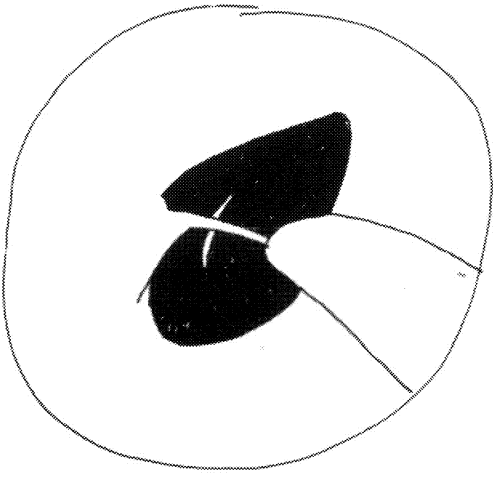

(e)

Fig. 3. (a) Angiography after intracoronary lysis: reopened graft. Remnants of thrombi are visible in the formerly occluded, now tortuoured segment near the middle sternal cerclage. (b) Angioscopic finding after 10 minutes of lysis: fern leaf-like white fibrin flap. (d) Angioscopic finding after 30 minutes of lysis: thin fibrin thread being attached to the smooth vessel wall and sticking to the guide wire, which enters the picture at the 4 o'clock position. The symmetric formation on both sides of the thread is a light reflection of the metal tip of the wire lying below. (c, e) Schematic illustrations.

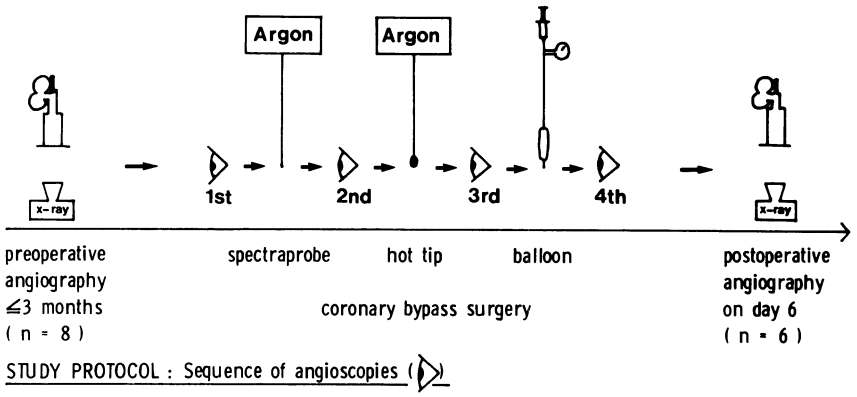

Fig. 4. Study protocol of the angioscopic control of intraoperative coronary argon-laser angioplasty.

angioplasty performed with an energy of 5 W. Doing so, the probe could easily pass the stenosis, which had not been possible before. Control angioscopy showed an increased, round shaped lumen, no carbonisation, no perforation, but a sharp edged fissure (Figure 5d), probably due to the free beam of the spectraprobe.

After that, the hot tip probe was advanced and a second laser procedure performed with 4 W. Angioscopically (Figure 5f), some large, yellow-white, fluttering masses, which prolapsed into the lumen and had not been there before, could be detected.

To improve this result, a balloon angioplasty was carried out in order to press and attach the flaps to the wall. However, this attempt had only little success; the masses were flattened, but were still fluttering in the irrigation stream (Figure 6b).

The control angiography six days later showed an open mammary artery graft to the LAD (not illustrated) and an open diagonal branch. The laser treated segment of the LAD, however, was occluded (Figure 6a).

Summarizing these as well as the other intraoperative results achieved by our group [99], we may state in accordance with other authors [24, 43, 44, 56, 60], that intraoperative coronary angioscopy is a quick and safe procedure, and therefore a useful tool with respect to the intraoperative indications described below.

However, we do not agree with the opinion of Lee et al. [45], that intraoperative coronary angioscopy is suitable for the quantification of the degree of coronary stenoses. In our mind, this is not realistic, as the distance between the distal lens of the scope and the object is unknown, flushing dilates the lumen and gauging is still impossible intraluminally. The quantification of stenoses, therefore, should be reserved to angiography.

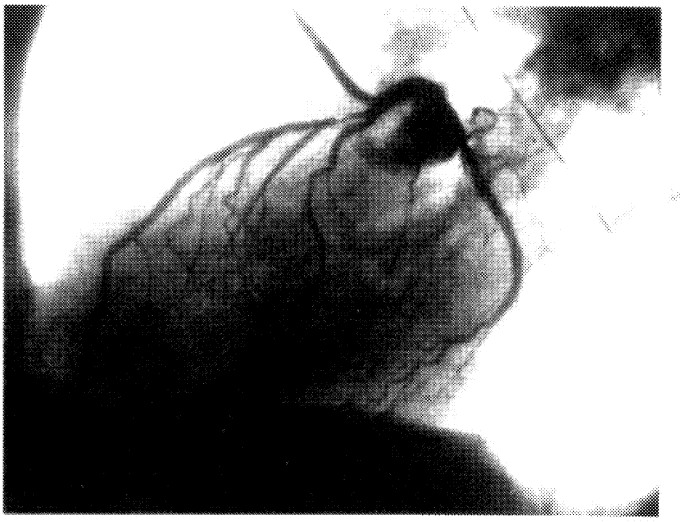

(a)

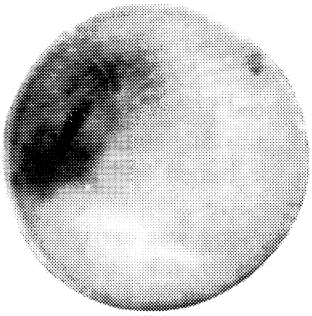

(b)

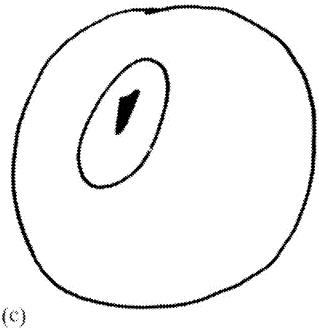

(c)

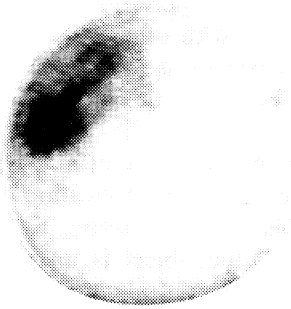

(d)

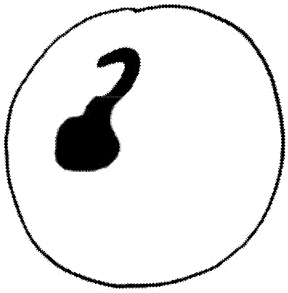

(e)

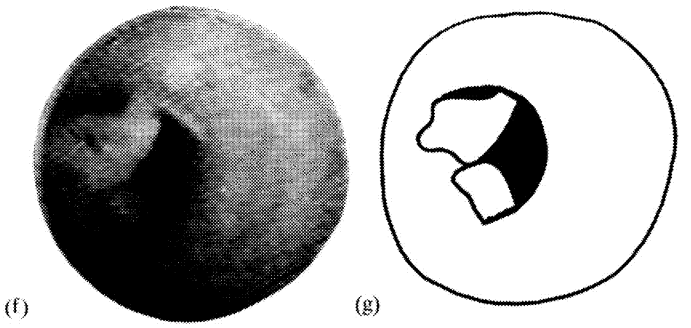

Fig. 5. (a) High grade, proximal LAD stenosis immediately distal to the origin of the first diagonal branch as relapse after three primarily successful PTCAs. (b) Angioscopic finding: severe, fibrous narrowing without ulceration, thrombus or dissection. (d) Angioscopic finding after spectraprobe lasering: increased, round shaped lumen with a hook-like, sharp edged fissure in the one o'clock position. (f) Angioscopic finding after hot tip lasering: yellow-white, fluttering masses. (c, e, g) Schematic illustrations.

Complications

As possible complications and side effects of angioscopy, the literature cites overloading of liquid due to an excessive quantity of flushing, embolisation of plaque particles, injury of the vessel wall in the form of dissection, perforation or subsequent thrombosis, coronary artery spasm, infection, and finally exceeding the ischemic tolerance of the myocardium.

The latter could not be improved even by using perfluorocarbon [10, 20, 21, 39, 49], a liquid which became known as artificial blood, having a high affinity to oxygen; it is much too viscous to inject as a flushing solution through the flushing catheter or the thin irrigation channel of today's scopes in sufficient quantity.

Severe complications have not been observed by our team nor by others.

However, just recently [42], the danger of damaging the intimal surface has been described; the chances of such complications increase with the stiffness of the angioscopes.

Limitations

Besides the fact that the quality of the images improves with the operator's skill and experience, two major limitations to coronary angioscopy continue to exist:

First, blood interference with the visual field remains a potential problem. Even the smallest amount of intraluminal blood can produce a hazy red image which can only be cleared with sufficient irrigation.

Secondly, despite some newer guide wire steering mechanisms, the lack of

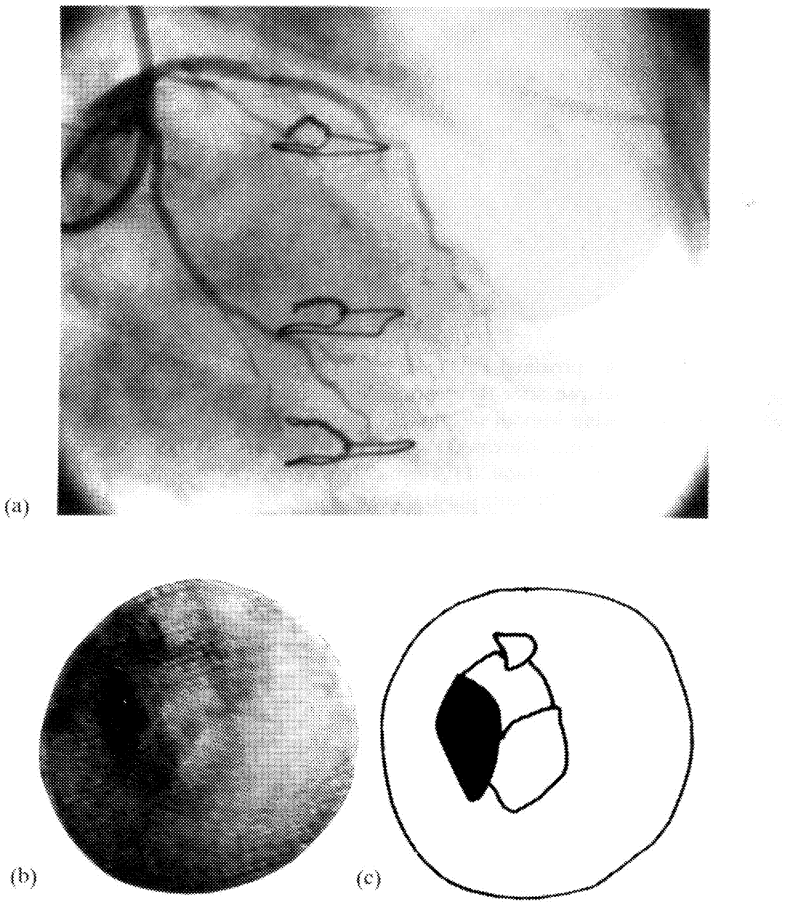

Fig. 6. (a) Postoperative angiography: occlusion of the laser treated LAD segment; the large, first diagonal branch is open. (b) Intraoperative angioscopic finding following all laser procedures and additional balloon angioplasty: flattened, but still fluttering flaps. (c) Schematic illustration.

a true angulation system impedes probing of the distal segments of the coronary tree and it impedes coaxial advancement, which is necessary for good pictures.

Necessary technical improvements

Therefore, the following technical improvements are desirable:

The tip must be more flexible and made steerable from the outside. The body should have a distal occlusion cuff to block the blood stream and to center the tip in the vessel lumen. The scope should have an irrigation

channel which is made wide enough to additionally carry a guide wire or laser fiber. The whole angioscope should also be radiopaque. A useful accessory would be a calibration device.

Indications and applications

Because of the fact that at present the intraoperative examination technique is still the easiest to perform and that the greatest experience exists with this method, the accepted indications for coronary angioscopy lie in the field of intraoperative use and are as follows:

The immediate control of coronary atherectomy, intraoperative balloon dilatation and laserangioplasty, the inspection of the grafts prior to implantation and the qualitative assessment of the distal anastomosis after graft insertion.

In these cases, angioscopy is superior to other control techniques such as intraoperative angiography, electromagnetic flow measurements or cardiogreen injections, and allows immediate revision before the vessel is closed.

Indeed, Grundfest et al. reported 3 cases of misplaced sutures documented by angioscopy that led to a revision of the anastomosis [26].

Furthermore, vessels which have not been angiogrammed preoperatively such as an internal mammary artery, or those which had only an obscure angiographic visualization due to occlusion, can be inspected for further significant stenoses and plaques. Moreover, the transplanted vein can be examined for intimal lesion, injured valves or poorly ligated side branches.

As percutaneous coronary angioscopy cannot be performed routinely at present, useful applications are scientific trials during cardiac catheterization such as the investigation of the determinants for the patency rates of bypasses, the restenosis rate of PTCA, the acute and chronic effects of drugs, the correlation of stenosis morphology and clinical complaints, and, finally, the mechanisms of all kinds of catheter supported angioplasties.

Future aspects

Translating and integrating research findings into clinically useful diagnostic or therapeutic maneuvers will require several years. If technical problems continue to be solved and image quality continues to improve, percutaneous coronary angioscopy may become another important tool in the armamentarium of the invasive cardiologist.

Acknowledgements

The authors would like to express their appreciation to the Vascular Sur-

geons: L. Eckel MD, E. Krause MD, K. Sarai MD and P. Satter MD of the University Clinic Frankfurt and F. Hehrlein MD, R. Moosdorf MD and H. Scheld MD of the University Clinic Giessen, who helped to collect much of the angioscopic data.

The studies concerning the authors' own data were supported in part by the Riese-Foundation, the Dr. Carl Wilder-Foundation and the German Heart Foundation.

Special thanks are due to Mrs. P. Bettinger, Mrs. B. Hallerbach, Storz and American Edwards.

References

1. Allen D, Graham E: Intracardiac surgery — a new method. J Am Med Ass 79: 1028—1030, 1922.
2. Allen D: Intracardiac surgery. AMA Arch Surg 8: 317—319, 1924.
3. Beck A, Reinbold W, Blum U, Nanko N, Milic St: Papacharalampos X: Clinical application of percutaneous transluminal angioscopy. Herz 13: 392—399, 1988.
4. Bolton H, Bailey C, Costas-Durieux, J: Cardioscopy — Simple and practical. J Thorac Surg 27: 323—329, 1954.
5. Bonan R, Parisella M, Fournier J, Crepeau J, Cote G, De Guise P, Waters D: Percutaneous coronary angioscopy: technique and results. Europ Heart J, 8 (Suppl.II): 222, 1987 (Abstract).
6. Butterworth R: A new operating cardioscope. J Thorac Surg 22: 319—322, 1951.
7. Carlens E, Silander T: Method for direct inspection of the right atrium: Experimental observation in the dog. Surgery 49: 622—624, 1961.
8. Carlens E, Silander T: Cardioscopy. J Cardiovasc Surg 4: 512—515, 1963.
9. Chaux A, Lee M, Blanche C, Kass R, Sherman T, Hickey A, Litvack F, Grundfest W, Forrester J, Matloff F: Intraoperative coronary angioscopy: technique and results in the initial 58 patients. J Thorac Cardiovasc Surg 92: 972—976, 1986.
10. Clark L, Kaplan S, Becattini F: The physiology of synthetic blood. J Thorac Cardiovasc Surg 60: 757—773, 1970.
11. Cortis B, Hussein H, Khandekar C, Pricipe J, Tkaczuk R: Angioscopy in vivo. Cath Cardiovasc Diagn 10: 493—500, 1984.
12. Crispin H, van Baarle A: Intravascular observation and surgery using the flexible fibrescope. Lancet 1: 750—751, 1973.
13. Crispin H: Experience with the vascular brush. J Cardiovasc Surg 28: 45—49, 1987.
14. Cutler E, Levine S, Beck C: The surgical treatment of mitral stenosis: Experimental and clinical studies. Arch Surg 9: 689—821, 1924.
15. Ferris E, Ledor K, Ben-Avi D, Baker M, Robbins K, McCowan T, Sharma B: Percutaneous angioscopy. Radiology 157: 319—322, 1985.
16. Forrester J, Grundfest W, Litvack F, Lee M, Chaux A, Matloff J, Carroll R, Foran R, Berci G, Morgenstern L: Intraoperative vascular endoscopy using flexible fibreoptics. Circulation 70 (Suppl II): 297, 1984 (Abstract).
17. Forrester J, Litvack F, Grundfest W, Hickey A: A perspective of coronary disease seen through the arteries of living man. Circulation 75: 505—513, 1987.
18 Gamble W, Ennis R: Experimental intracardiac visulization. N Engl J Med 276: 1397—1403, 1967.
19. Gehani A, Ashley S, Brooks S, Kester R, Ball SG, Rees MR: Percutaneous angioscopy and sapphire tip lasing of intimal flaps following angioplasty. Heart and Vessels 4, 1: 52, 1988 (Abstract).

20. Geyer R: Fluorocarbon-polyol artificial blood substitutes. N Engl J Med 289: 1077—1082, 1973.
21. Glogar D, Kloner R, Muller J, DeBoer I, Braunwald E: Fluorocarbons reduce myocardial ischemic damage after coronary occlusion. Science 211: 1439—1441, 1980.
22. Greenstone S, Shore J, Heringman E: Arterial endoscopy (arterioscopy). Arch Surg 93: 811—812, 1966.
23. Grundfest W, Litvack F, Lee M, Matloff J, Carroll R, Foran R, Berci G, Morgenstern L, Forrester J: High resolution intraoperative angioscopy of peripheral and coronary arteries in man. Personal communication.
24. Grundfest W, Litvack F, Hickey A: The current status of angioscopy and laser angioplasty. J Vasc Surg 5: 667—673, 1987.
25. Grundfest W, Litvack F, Sherman T, Carroll R, Lee M, Chaux A, Kass R, Matloff J, Berci G, Swan H, Morgenstern L, Forrester J: Delineation of peripheral and coronary detail by intraoperative angioscopy. Ann Surg 202: 394—400, 1985.
26. Hansell C: Improvements in or relating to means for transmitting radiant energy such as light, and to apparatus for therewith. British Patent No. 295601, Feb. 21st, 1929.
27. Harken D, Glidden E: Experiments in intracardiac surgery. J Thorac Surg 12: 566—572, 1932.
28. Hickey A, Litvack F, Grundfest W, Lee M, Chaux A, Blanche C, Kass R, Sherman T, Glick D, Swan HC, Matloff J, Forrester J: Coronary angioscopy: the spectrum of disease in the first 100 patients. J Am Coll Cardiol 9: 197A, 1987 (Abstract).
29. Hirschowitz B, Curtiss L, Peters C, Pollard H: Demonstration of a new gastroscope, the "fibrescope". Gastroenterology 35/1: 50—52, 1958.
30. Höher M, Hombach V, Hannekum A, Eggeling Th, Hopp HW, Hilger HH: Perkutane und intraoperative Koronarendoskopie. Z Kardiol 76 (Suppl. 2): 21, 1987 (Abstract).
31. Höher, M, Hombach V, Höpp H, Hilger H: Percutaneous coronary angioscopy during cardiac catheterization. J Am Coll Cardiol 11 (Suppl. II): 65A, 1988 (Abstract).
32. Höher M, Hombach V, Höpp, H, Eggeling Th, Kochs M, Arnold G, Hannekum A, Hügel W: Diagnostische Bedeutung der Angioskopie bei Patienten mit koronarer Herzkrankheit. Z Kardiol 77: 152—159, 1988.
33. Höher M, Behrenbeck D, Winter U, Hombach V, Hilger H: Perkutane Gefäßendoskopie mittels ultradünner Fiberendoskope: erste Erfahrungen. Z Kardiol 74 (Suppl III): 99, 1985 (Abstract).
34. Höher M, Hombach V, Höpp HW, Hannekum A, Hilger HH, Hirche H: Percutaneous and intraoperative coronary angioscopy. Circulation (Suppl. IV): IV—185, 1987 (Abstract).
35. Hombach V, Höher M, Hannekum A, Hügel W, Buran B, Höpp HW, Hirche HJ: Erste klinische Erfahrungen mit der Koronarendoskopie. Deutsche Medizinische Wochenschrift 111: 1135—1140, 1986.
36. Inoue K, Kuwaki K, Ueda K: Angioscopy guided coronary thrombolysis. J Am Coll Cardiol 9: 62A, 1987 (Abstract).
37. Inoue K, Kuwaki K, Ueda K, Takano E: Angioscopic macropathology of coronary atherosclerosis in unstable angina and acute myocardial infarction. J Am Coll Cardiol 11: 65A, 1988 (Abstract).
38. Inoue K, Kuwaki K, Takahashi M: In vivo transluminal angioscopy. Circulation 70 (Suppl II): II—322, 1984 (Abstract).
39. Kanter K, Jaffin J, Ehrlichman R, Flaherty J, Golt V, Gardner T: Superiority of perfluorocarbon cardioplegia over blood or crystalloid cardioplegia. Circulation 64 (Suppl. II): II—75—83, 1981 (Abstract).
40. Kuwaki K, Inoue K, Ueda K: Percutaneous transluminal coronary angioscopy during cardiac catheterization: the results of experiences in the first 30 patients. Circulation 76 (Suppl. IV): 186, 1987 (Abstract).
41. Lee M, Reis R, Lee G, Chan M, Theis J, Ikeda R, Rink J, Petersen L, Solomon B,

Siegal R, Hannah H, Hanna E, Bommer W, Mason D: Intraoperative cardiovascular endoscopy in patients with heart disease. Clin Res 33: 12A, 1986 (Abstract).
42. Lee G, Beerline D, Lee M: Hazards of angioscopic examination: Documentation of damage to the arterial intima. Clin Res 36: 110A, 1988 (Abstract).
43. Lee G, Ikeda R, Stobbe D, Ogata C, Embi A, Chan C, Reis R, Mason D: Intraoperative use of dual fiber optic catheter for simultaneous in vivo visualization and laser vaporization of peripheral atherosclerotic obstructive disease. Cath Cardiovasc Diagn 10: 11—16, 1984.
44. Lee G, Ikeda R, Stobbe D, Ogata C, Theis J, Hussein H, Mason D: Laser irradiation of human atherosclerotic obstructive disease: simultaneous visualization and vaporizastion achieved by a dual fiberoptic catheter. Am Heart J 105: 163—164, 1983.
45. Lee G, Garcia HJ, Corso P, Chan M, Ring J, Pichard A, Lee K, Reis R, Mason D: Correlation of coronary angioscopic to angiographic findings in coronary artery disease. Am J Cardiol 58: 238-241, 1986.
46. Litvack F, Grundfest W, Hickey A, Lee M, Chaux A, Forrester J: Coronary angioscopy: correlation of morphology with clinical syndrome. Europ Heart J 8 (Suppl. II): 222, 1987 (Abstract).
47. Litvack F, Grundfest W, Lee M, Carroll R, Foran R, Chaux A, Berci G, Rose H, Matloff J, Forrester J: Angioscopic visualization of blood vessel interior in animals and humans. Clin Cardiol 8: 65—70, 1985.
48. Litvack F, Hickey A, Grundfest W, Lee M, Sherman T, Doyle L, Chaux A, Blanche C, Kass R, Matloff J, Swan H, Foerrester J: Angioscopy is superior to angiography for detecting complex atheroma. Circulation 74 (Suppl. II): II—362, 1986 (Abstract).
49. Mitsuno T, Ohyanagi H, Naito R: Clinical studies of a perfluoro-chemical whole blood substitute. Ann Surg 195: 60—69, 1982.
50. Mizuno, Arakawa K, Shibuya T, Horiuchi K, Okamoto Y, Miyamoto A, Isojima K, Kurita A, Satomura K, Nakamura H, Arai T, Kikuchi M: A serial observation of coronary thrombosis in vivo by a new angioscope. J Am Coll Cardiol 11 (Suppl II): 30A, 1988 (Abstract).
51. Mizuno K, Miyamoto A, Satomura K, Shibuya T, Okamoto Y, Seguchi H, Isojima K, Kurita A, Arai T, Nakamura H: Angioscopic endothelial macropathology in patients with acute coronary syndromes. J Am Coll Cardiol 13, No. 2: 14A, 1989 (Abstract).
52. Moosdorf R, Scheld H, Stertmann W, Hehrlein W: Koronare Endoskopie — Eine neue intraoperative Kontrollmethode nach Endarteriektomie der rechten Kranzarterie. Thorac Cardiovasc Surg 35 (Suppl. I): 14—15, 1987.
53. Morice MC, Marco J, Castillo-Fenoy A, Fajadet J, Glatt B, Royer T: A new technique for investigation and treatment of acute myocardial infarction: percutaneous coronary angioscopy. Europ. Heart J 9 (Suppl. A): 211, 1988 (Abstract).
54. Morice M-C, Marco J, Fajadet J: Percutaneous coronary angioscopy before and after angioplasty in acute myocardial infarction. Preliminary results. Circulation 76 (Suppl. IV): IV—282, 1987 (Abstract).
55. Murray G: A cardioscope. Angiology 1: 334—336, 1950.
56. Olcott C: Clinical applications of video angioscopy. J Vasc Surg 5: 664—666, 1987.
57. Olinger C: Carotid artery endoscopy (autopsy). Surg Neurol 7: 7—13, 1977.
58. Ramee S, White C, Banks A, Aita M, Doyle T, Michaels M, Graeber G, Price H: Percutaneous coronary angioscopy using a steerable microangioscope. J Am Coll Cardiol 11, (Suppl. II): 173A, 1988 (Abstract).
59. Richens D: Intraoperative coronary angioscopy: experimental and clinical experience. In: Angioscopy: vascular anf coronary applications. G White, R White (Eds.) Year Book Medical Publishers, Chicago, 1989: 149—156.
60. Richens D, Rees M, Watson D: Laser coronary angioplasty under direct vision. Lancet 2: 683—690, 1987.
61. Sakakibara S, Iikawa T, Hattori J, Inomata K: Direct visual operation for aortic stenosis: Cardioscopic studies. J Int Coll Surgeons 29: 548—562, 1958.

62. Sakakibara T, Aiki T, Tsuda J, Inoue A: The cardioscope. Nippon Geka Gakkai Zasski 40: 905—911, 1939.
63. Sakakibara S, Iikawa T, Hattori J: An operative method for cardiac septal defect with use of a cardioscope. Shujutsu 10: 285—289, 1956.
64. Sakakibara T: Cardioscope. Rinsho Igaku 29: 703—707, 1941.
65. Sanborn T, Rygaard J, Westbrook B, Lazar H, McCormick J, Roberts A: Intraoperative angioscopy of saphenous vein and coronary arteries. J Thorac Cardiovasc Surg 91: 339—343, 1986.
66. Sanborn T: Vascular endoscopy: current state of the art. Brit Med Bull 42: 270—275, 1986.
67. Sanborn TA, Rygaard JA, Westbrook BM, Lazar HL, McCormick JR, Roberts AJ, Madoff I: Intraoperative angioscopy of saphenous vein and coronary arteries. J Thorac Cardiovasc Surg 91: 339—343, 1986.
68. Schwartz A, Aulich A, Lahrkamp H: Percutaneous transluminal angioscopy: a new approach to intravasal interventional techniques. Laser 1: 5—9, 1986.
69. Schwartz A, Aulich A, Lahrkamp H: Percutaneous transluminal angioscopy: a new approach to intravascular interventional techniques Laser 3: 30—32, 1987.
70. Seeliger, K.: Direkte intravasculäre fibroskopische Lymphoskopie und ductus thoracicus Kanülierung. Folia angiologica 21: 287—292, 1973.
71. Seeliger K, Witte M, Kintner K, Bracamonte R, Cardenas A: Endoscopy of the thoracic duct (lymphoscopy) via the external jugular vein in dogs. Lymphology 7: 109—116, 1974.
72. Sherman C, Litvack F, Grundfest W, Lee M, Chaux A, Kass R, Swan H, Matloff J, Forrester J: Fiberoptic coronary angioscopy identifies thrombus in all patients with unstable angina. Circulation 72 (Suppl. II): 446, 1985 (Abstract).
73. Sherman C, Litvack F, Grundfest W, Lee M, Hickey A, Chaux A, Kass R, Blanche C, Matloff J, Morgenstern L, Ganz W, Swan H, Forrester J: Demonstration of thrombus and complex atheroma by in-vivo coronary angioscopy in patients with unstable angina pectoris. New Engl J Med 315: 913—919, 1986.
74. Silander T: Cardioscopy without thoracotomy. Acta Chir Scand 127: 67—84, 1964.
75. Spears J, Spokojny A, Marais H, Grossman W: Coronary angioscopy during cardiac catheterization. J Am Coll Cardiol 6: 93—97, 1985.
76. Spears J, Marais H, Serur J: In vivo coronary angioscopy.J Am Coll Cardiol 1: 1311—1314, 1983.
77. Spears J, Marais H, Serur J, Paulin S, Grossman W: In vivo coronary angioscopy. Circulation 66 (Suppl. II): 366, 1982 (Abstract).
78. Susawa T, Yui Y, Hattori R: Direct observation of coronary thrombus using a newly developed ultrathin (1.2 mm) flexible angioscope. J Am Coll Cardiol 9: 197A, 1987 (Abstract).
79. Takahashi M, Yui Y, Susawa T: Evaluation of coronary thrombus by a newly developed ultrathin (0.75 mm) flexible quartz microfiber angioscope. Circulation 76 (Suppl. IV): 282, 1987 (Abstract).
80. Tanabe T, Yokota A, Sugie S: Cardiovascular fibreoptic endoscopy: development and clinical application. Surgery 87: 375—378, 1980.
81. Towne J, Bernhard V: Vascular endoscopy — an adjunct to carotid surgery. Stroke 8: 569—571, 1977.
82. Towne JB, Bernhard VM: Vascular endoscopy: useful tool or interesting toy? Surgery 82: 415—419, 1977.
83. Uchida Y, Masuo M, Tomaru T, Kato A, Sugimoto T: Fiberoptic observation of thrombosis and thrombolysis in isolated human coronary arteries. Am. Heart J 112: 691—696, 1986.
84. Uchida Y, Tomaru T, Nakamura F, Furuse A, Fujimori Y: Percutaneous coronary angioscopy in patients with ischemic heart diseases. Am Heart J 114: 1216—1222, 1987.
85. Uchida Y, Tomaru T, Kato A: Angioscopy of blood flow through stenotic arteries: rheologic mechanisms of thrombosis. Am Heart J 114: 63—69, 1987.

86. Uchida Y, Furuse A, Hasegawa K: Percutaneous coronary angioscopy using a novel balloon guiding catheter in patients with ischemic heart diseases. Circulation 76 (Suppl. IV): IV—185, 1987 (Abstract).
87. Uchida Y, Masuo M, Tomaru T, Kato S: Fiberoptic observation of coronary luminal changes caused by transluminal coronary angioplasty. Circulation 72, (Suppl. III): III—218, 1985 (Abstract).
88. Vincent G, Fox J: Cardiovascular endoscopy, Cardiovasc. Rev Rep 6: 1227—1234, 1985.
89. Vollmar J, Junghanns K: Die Arterioskopie. Langenbecks Arch Klin Chir 325: 1201—1212, 1969.
90. Vollmar J, Storz L: Vascular endoscopy: Possibilities and limits of its clinical application. Surg Clin North Am 54: 111—122, 1974.
91. Vollmar J: Die Gefäßendoskopie. Ein neuer Weg der intraoperativen Gefäßdiagnostik. Endoscopy 1: 141—151, 1969.
92. Wendt Th, Müller Th, Eckel L, Krause E, Rauber K, Riemann H, Sarai C, Satter P, Sievert H, Stauder M, Vallbracht Ch, Kober G, Kaltenbach M: In vivo Angioskopie: Technik, Indikationen und Ergebnisse beim Menschen. Z Kardiol 76 (Suppl I): 51, 1987 (Abstract).
93. Wendt Th, Eckel L, Krause E, Müller Th, Radünz N, Sarai C, Sievert H, Vallbracht C, Satter P, Kaltenbach M, Kober G: Coronary balloon dilatation — angioscopic findings. Europ Heart J 8 (Suppl II): 222, 1987 (Abstract).
94. Wendt Th, Reinemer H, Müller Th, Panitz HG, Friedel M, Schneider M, Hübner K, Kaltenbach M, Kober G: Angioskopie, Angiographie und pathologische Anatomie des Kranzgefässsystems. Z Kardiol 77 (Suppl I): 149, 1988 (Abstract).
95. Wendt Th, Eckel L, Kaltenbach M, Krause E, Müller T, Radünz N, Sarai K, Satter P, Schräder R, Sievert H, Vallbracht C, Kober G: Coronary angioscopy during cardiac catheterization and surgery. In: New developments in quantitative arteriography. JHC Reiber, PW Serruys (Eds.), Kluwer Academic Publishers, Dordrecht/Boston/London, 1988: 248—260.
96. Wendt Th, Eckel L, Krause E, Müller Th, Radünz N, Sarai C, Sievert H, Vallbracht Ch, Satter P, Kaltenbach M, Kober G: Coronary balloon dilatation-angioscopic findings. In: Advances in Laser Medicine I. Müller, G Biamino, FGJ (Eds.) Ecomed verlagsgesellschaft mbh, Landsberg Lech, 1988: 275—281.
97. Wendt Th, Moosdorf R, Bettinger R, Kamlot A, Reinemer H, Scheld HH, Hehrlein FW, Kober G: Immediate angioscopic results following human coronary argon laser angioplasty. Heart and Vessels 4: 63, 1988 (Abstract).
98. Wendt Th, Moosdorf R, Bettinger R, Kamlot A, Hehrlein WF, Kober G: Intraoperative koronare Argon Laser Angioplastie: angioskopische und angiographische Ergebnisse. Z Kardiol 78 (Suppl. I): 21, 1989 (Abstract).
99. Wendt, Th: Neue Einblicke. Angioskopie und Mikroendoskopie. E. Theo Hofmann Verlag, Frankfurt am Main, 1990.

8. Intravascular ultrasound: direct visualization of atheroma within the arterial wall

PAUL G. YOCK, DAVID T. LINKER and BJOERN A. J. ANGELSEN

Cardiovascular Research Institute and Division of Cardiology, University of California, San Francisco, California, USA

* *Department of Biomedical Engineering and Division of Cardiology, University of Trondheim, Trondheim, Norway.*

Summary

Catheter-based, two-dimensional intravascular ultrasound imaging has emerged in the past two years as a promising new technology for the assessment of atherosclerosis. Several university-based and commercial groups have developed prototype systems which have two basic designs. In one type of system (solid state) a radial array of transducer element is activated by a sequencing circuit to provide a two-dimensional beam perpendicular to the tip of the catheter. In the second type of system (mechanical) the transducer or reflector is rotated by a cable running the length of the catheter, again resulting in a 360 degree beam perpendicular to the catheter tip. Current prototype catheters are in the 5 to 9 French size range and have center frequencies between 20 and 40 MHz.

Initial clinical studies have been performed in the peripheral arteries of patients. These studies show that the plaque burden is substantially greater than would be anticipated from angiography and that the distribution of atheroma within the vessel wall is often unpredictable based on the angiographic images. Ultrasound imaging is already being used clinically at some centers to guide the process of mechanical plaque extraction (atherectomy).

Trials of coronary artery imaging have begun recently. Other areas which appear promising for further development include combined imaging and therapeutic catheters (balloons, atherectomy, lasers), tissue characterization, three-dimensional image reconstruction and combined imaging and Doppler ultrasound.

Introduction and basic catheter design features

Brief history of development

Although intravascular ultrasound imaging is now receiving attention as a "new" imaging modality, developmental work on catheter ultrasound dates

J. H. C. Reiber and P. W. Serruys (eds), Quantitative Coronary Arteriography, 181–197.

back nearly three decades. In 1960 Cieszynski recorded intracardiac echoes by inserting a catheter-mounted transducer through the jugular vein in animals [1]. Real-time recording of a catheter ultrasound signal was first reported by Carleton and Clark in 1968, using an A-mode format to track the dynamics of left ventricular contraction in dogs [2]. The first two-dimensional catheter imaging system was designed by Bom and colleagues in 1972, based on a radial array of 32 transducer elements activated in sequence by wires running the length of the catheter [3]. The system was successfully used in animals to obtain intracardiac images, but work on the catheter project was suspended in light of the rapid advances in noninvasive, transcutaneous cardiac imaging with ultrasound.

Fundamentals of current catheter designs

Interest in catheter-based ultrasound imaging resurfaced in the early 1980s with the explosive development of balloon angioplasty and other catheter interventions. Several groups began development efforts aimed at producing high-resolution prototype systems operating at 20 MHz or higher frequencies. One commercially-based group adapted the multi-element, solid state approach (Figure 1) with an innovative modification [4]. Instead of assigning wires to each transducer element, a miniature integrated circuit was incorporated into the tip of the catheter to provide the appropriate sequencing of signals. This design offered the promise of greater catheter flexibility and simplified manufacture of the catheter shaft.

A number of other groups, including Bom's team in Rotterdam, began work on mechanical catheter systems based on the expectation that superior image quality could be achieved by this approach compared with the solid-state technology [5—8]. Two principal factors contributed to this analysis:

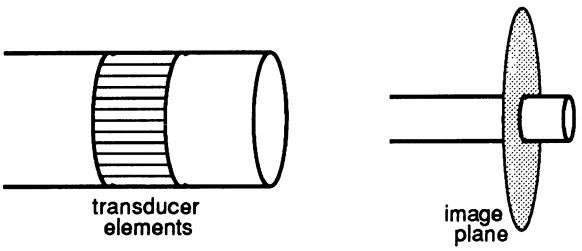

Fig. 1. Schematic of solid-state, multiple element transducer. Individual elements are activated in sequence or in groups, sweeping out an image plane perpendicular to the catheter tip (right). Reproduced with permission from Yock PG, Linker DT, Angelsen BAJ, Two-dimensional, intravascular ultrasound: technical development and initial clinical experience. J Am Soc Echocard, 1989 (in press).

first, the mechanical approach allowed use of high-quality ceramic piezoelectric transducers that are difficult to use in a tiny, multi-element format. Second, the mechanical approach provided a relatively large aperture (effective beam-forming area of the transducer) within the constraints of the size of the catheters.

Two basic approaches have been taken in the design of the mechanical catheters. In one, the transducer is directly attached to the end of the cable and is rotated at the tip of the catheter (Figure 2A). This approach shares a disadvantage with solid-state system caused by the fact that there is a zone of "ring-down" artifact for a short distance in front of the transducer which is unavailable for imaging. This problem results in an annulus of bright artifact appearing immediately around the catheter, so that any tissue structure within this region cannot be imaged accurately (Figure 3). Since catheters tend to be pushed to the side of vessels by blood flow, this is a potentially significant problem for these systems. A second mechanical design overcomes

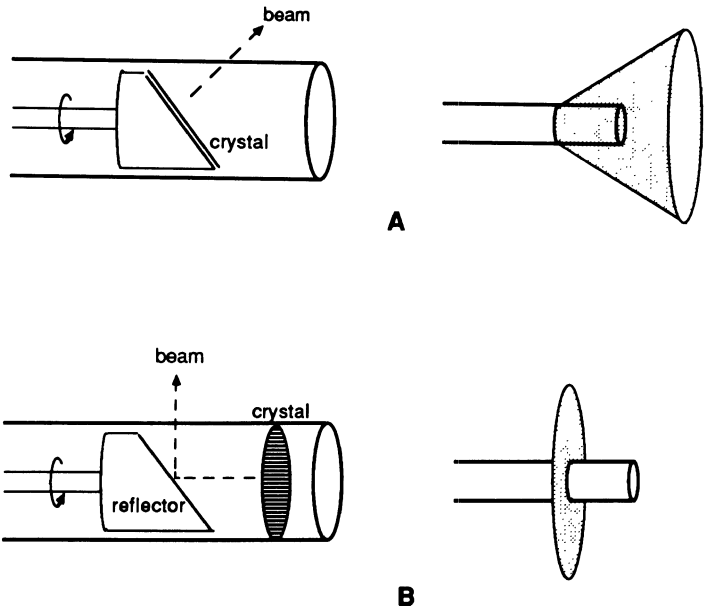

Fig. 2. (A) Mechanical catheter design in which the transducer is rotated by means of a cable. In this case the transducer is tipped slightly forward, producing a cone-shaped image. (B) Reflector system. The crystal is mounted in the tip of the catheter facing rearward; the signal reflects off a rotating surface, creating a scan plan perpendicular to the catheter tip. Reproduced with permission from Yock PG, Linker DT, Angelsen BAJ, Two-dimensional, intravascular ultrasound: technical development and intitial clinical experience. J Am Soc Echocard, 1989.

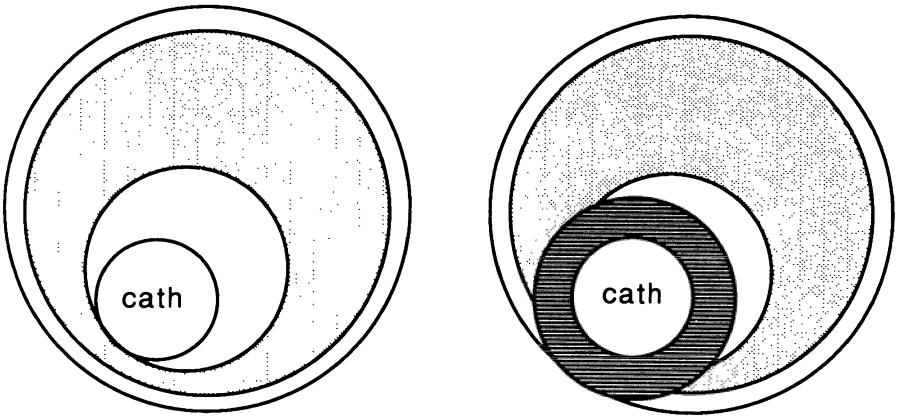

Fig. 3. Schematic showing effect of "ring-down" artifact on a catheter image. An annular zone of bright artifact (hashed area in right panel) is created around the catheter, obscuring visualization in this region. This is a significant difficulty in the case of catheter imaging, since the catheter frequently is pushed against the side of the lumen (left panel).

this specific difficulty by using a rotating reflector (Figure 2B). The extra beam path within the catheter allows the region of ring-down artifact to be consumed within the catheter, so that as the beam exits the catheter skin it is fully available for imaging.

Basic system specifications

Current prototype catheters from the different groups are available in sizes ranging between 5 and 9 French (diameters of 1.6 to 2.9 mm). At present, the only catheter being used clinically in an over-the-guidewire configuration is the solid state system [4]. This feature, combined with the catheter flexibility, constitute important advantages for this approach to catheter imaging. The mechanical systems which are presently approved for peripheral vessel applications in the United States are fixed-wire systems (a short length of guidewire is attached to the tip of the catheter). Over-the-wire systems for the mechanical catheters are currently undergoing testing. Another relative disadvantage of the mechanical catheter systems is the necessity for connecting to a motor drive unit. These have been designed by the different engineering groups either as sterile, hand-held units or as part of an arm that is suspended over the catheterization table.

Center frequencies for the peripheral imaging catheters are in the 20—25 MHz range for the currently available systems. This frequency range represents a compromise between the competing requirements of resolution

(better at higher frequencies) and penetration (better at lower frequencies). In the coronary arteries, where an effective radial penetration less than 1 cm will suffice, higher frequencies may be appropriate. Bom and colleagues have demonstrated excellent image quality at 40 MHz in in-vitro studies [8]. At this frequency, however, blood reflections may considerably reduce effective penetration of the beam. Even at 20 MHz blood is frequently imaged with a cloudy, swirling appearance. Fortunately, this effect does not significantly impair visualization of the arterial wall structures at this frequency.

Rate of image acquisition and display is another important parameter of system function which varies between the solid state and mechanical systems. In the current implementation of the solid state technology, frame rates are 10/second or lower. Low acquisition rates are potentially problematic if the catheter moves quickly relative to the vessel wall, since the image may not be fully defined before the catheter moves. This appears not to be a significant problem in the peripheral circulation, but is an issue in the coronary arteries, particularly in the atrioventricular groove vessels. The current mechanical systems have generally higher frame rates than the solid state technology, ranging from 15—30/second, depending on the depth of image.

In-vitro studies on image interpretation and morphometry

Differentiation of media: the three-layer appearance

One of the main factors that has made intravascular ultrasound a potentially viable imaging technology for assessment of atherosclerosis is a fortuitous property of arterial wall acoustics: the arterial media is generally a weak reflector of ultrasound relative to the adventitia, most forms of atheroma, and the internal and external elastic laminae. As a result, the media is generally well defined in the intravascular images as a dark stripe defining the contour of the normal vessel wall. This finding was first appreciated in in-vitro studies of human pathologic arterial specimens, where the three-layer appearance of both diseased and normal vascular segments was described (Figure 4) [9]. The studies of Meyer and colleagues showed an excellent correlation between the appearance of the layers on ultrasound and on high-resolution magnetic resonance scanning [10]. Gussenhoven and co-workers studied the appearance of normal and diseased arterial specimens at 40 MHz, and found that the media of elastic arteries was significantly more echo-dense than in muscular arteries, frequently obscuring the three-layered appearance [11]. These authors also evaluated the appearance of different plaque types, demonstrating that fibromuscular lesions generally imaged as weakly echo-reflective regions, fibrous areas appeared brighter (more strongly reflective), and calcified regions were intensely echogenic, often

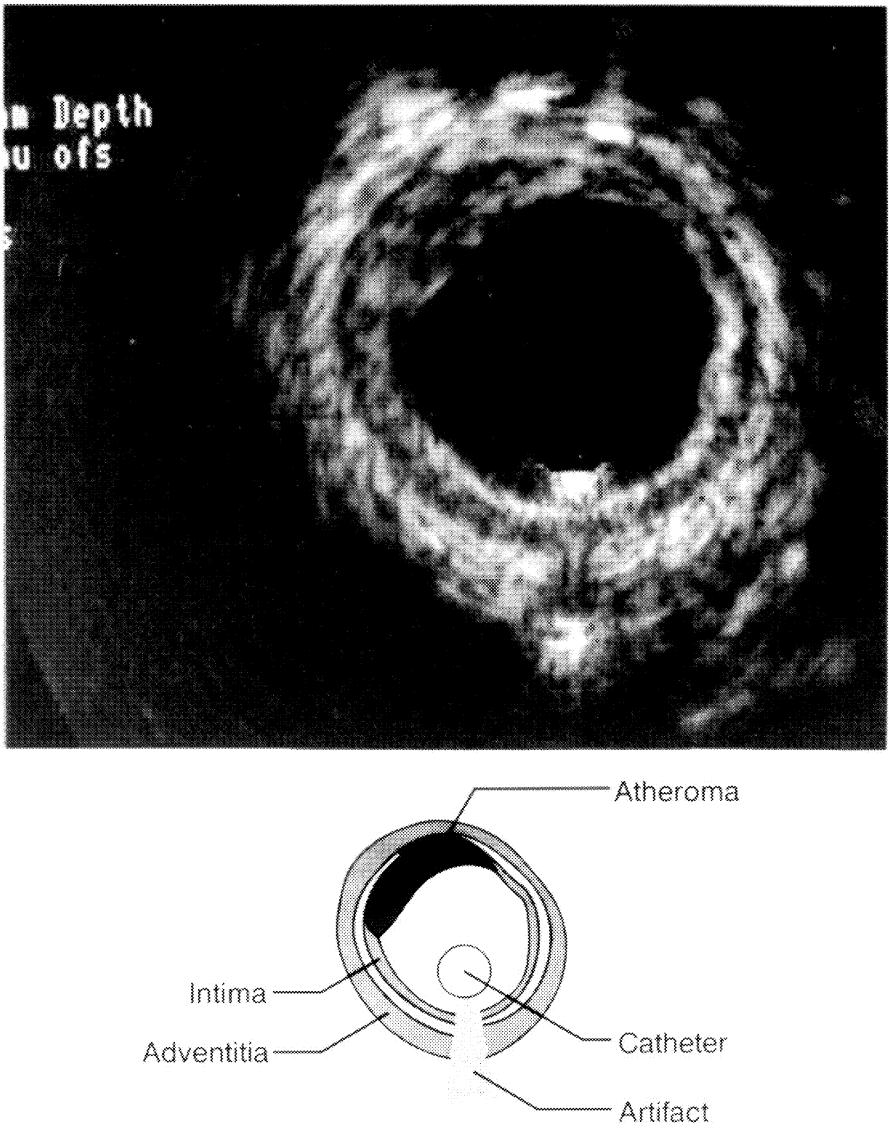

Fig. 4. Ultrasound image of pathologic specimen showing three-layered appearance. The media (not labeled) is echo-poor relative to the inner layer and adventitia. A positioning artifact is seen at 6 o'clock. Reproduced with permission from Yock PG, Johnson EL, Linker DT, Intravascular Ultrasound: development and clinical potential. Am J Card Imaging 2: 185—193, 1988.

shadowing structures beyond. In a pilot study of coronary atheromata Mallery and colleagues identified the appearance of "lipid lakes" as regions of relative echolucency within areas of atheroma [12]. Potkin et al. have

demonstrated that fibrous and calcific lesions can be correctly identified from ultrasound scans in the large majority of cases [13]. Lipid-filled regions may be more difficult to characterize if closely associated with fibrous or calcific tissue, due to the bright echogenicity of these latter regions.

Early morphometric studies

Several early morphometric studies have assessed the accuracy of intravascular ultrasound in measuring lumen size and wall thickness [7, 11, 13, 14, 15]. In general, lumen measurements have been shown to be highly accurate when compared to histologic sections. Measurements of wall thickness have correlated slightly less well, potentially due to the effects of variable attenuation of the ultrasound signal moving through wall layers of different composition. The early studies have also suffered from a methodologic problem due to inhomogeneous shrinkage artifacts of the histologic sections during fixation, leading to a distortion in the reference measurements to which the ultrasound image measurements are compared [13].

Significance of the bright inner layer

There is continued discussion concerning the origin of the bright, inner layer frequently visualized immediately internal (on the luminal side) of the media on both in-vitro and clinical studies. Meyer et al. speculated that although this layer was seen in sections which were normal histologically, it might represent an artificat resulting from corrugation of the intimal surface resulting from fixation [10]. This interpretation has been supported by the intermittent appearance of the internal layer in clinical studies of peripheral vessels. Unpublished observations from our group suggest that the major cause of the inner layer echo is not the intima but the internal elastic lamina, a structure which images brightly on transmission acoustic microscopy. This layer also corrugates with fixation, so that the appearance of the inner layer may indeed be exaggerated in imaging non-pressure fixed pathologic specimens.

Clinical utility of intravascular imaging

Initial clinical studies in the periphery

Pilot clinical studies in the peripheral circulation have been reported by several groups using the different systems [4—8]. Overall, these studies have documented the safety of the catheters and the ability to obtain images which show the actual shape and size of the lumen, identify intraluminal processes such as thrombus and dissection, and shown the extent and distribution of atheroma within the vessel wall (Figure 5—7). Although specific comparisons with quantitative angiography have not been published,

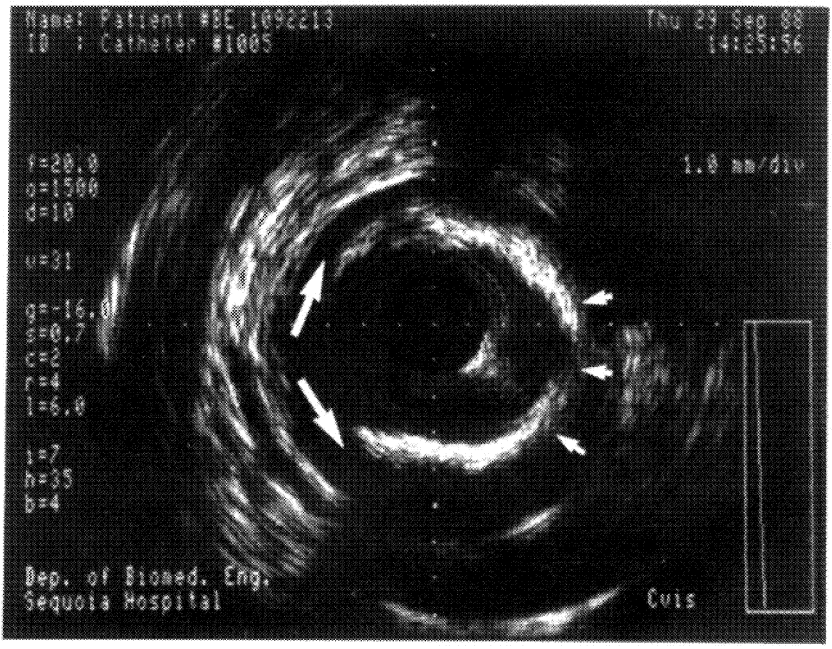

Fig. 5. Dissection in an iliac artery following mechanical atherectomy. A horseshoe-shaped, calcified plaque is attached to the vessel wall to the right in the image (small arrows). The dissection plane (large arrows) has lifted the arms of the plaque away from the vessel wall.

the general impression from the pilot studies is that the extent of atherosclerotic disease is significantly underestimated by angiography. In addition, although frankly eccentric deposits of atheroma or plaque are correctly identified by angiography, the distribution of atheroma within the vessel wall generally cannot be predicted from the angiogram.

Imaging in conjunction with catheter-based therapies

The major initial clinical application for intravascular ultrasound imaging will be as a visualization technology to assist in the performance of the various catheter therapeutic procedures. In general, there are two areas in which ultrasound may prove useful as an enabling technology: (1) in providing guidance for "debulking" of atheroma, allowing the maximal amount of atheroma to be extracted without perforating the vessel; and (2) in providing guidance for "tunneling" through a completely obstructed segment of artery in order to establish a lumen for further operations.

Atherectomy. Perhaps the most straightforward application of imaging is in the context of catheter atherectomy, in which plaque is either shaved and extracted [16] or abraded [17, 18] by means of a rotating mechanical device.

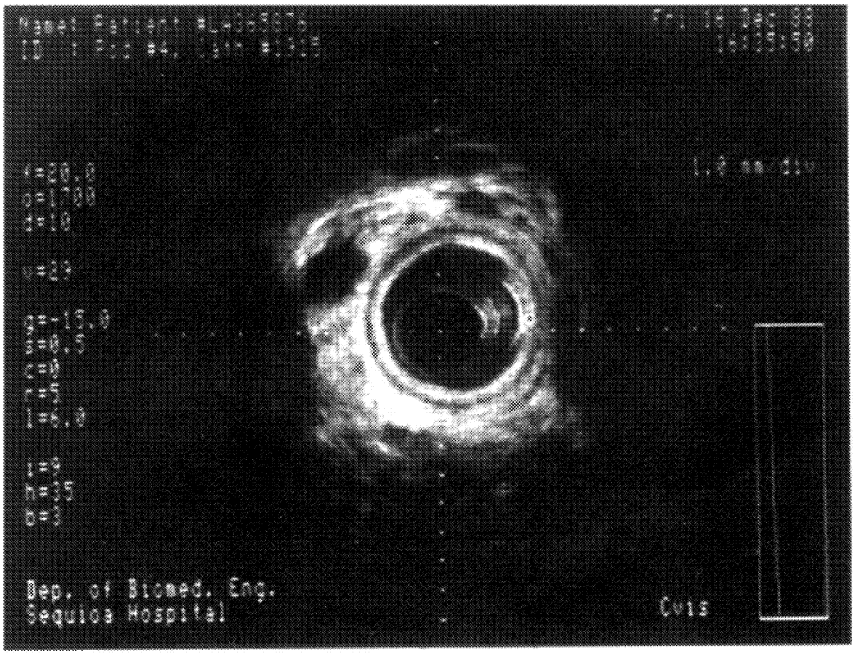

Fig. 6. Scan from a minimally diseased femoral artery showing slight intimal thickening (inner bright layer). The dark medial stripe is clearly visualized.

Currently the most extensive clinical experience has been accumulated with the Simpson Atherocath (TM), which is a shaving device with a side-cutting mechanism at its tip which is positioned along the side of the vessel in a region judged to contain a significant accumulation of atheroma [16]. This is a "directional" atherectomy device that must be oriented both axially (by advancing the catheter) and radially (by rotating the catheter) to the appropriate region of the vessel wall for excision of atheroma.

Preliminary experience by our group has shown that ultrasound imaging can be of considerable practical benefit in use of the Simpson atherectomy device [5]. In general, positioning of the device and the initial cuts can be accomplished without use of the catheter, since the load of atheroma is large compared to the amount taken with the early cuts. An exception to this rule is the case of a complete occlusion, where the path taken by the guidewire in the initial passage may be subintimal and not through the center of the plaque material. In this case the usual "quadrant cutting" strategy (rotating the device to make cuts in all four quadrants) will inevitably result in some cuts being made in normal vessel wall. We have found that by placing the imaging catheter along the track created by the guidewire in these cases, a subintimal passage can be identified and the orientation for appropriate atherectomy defined.

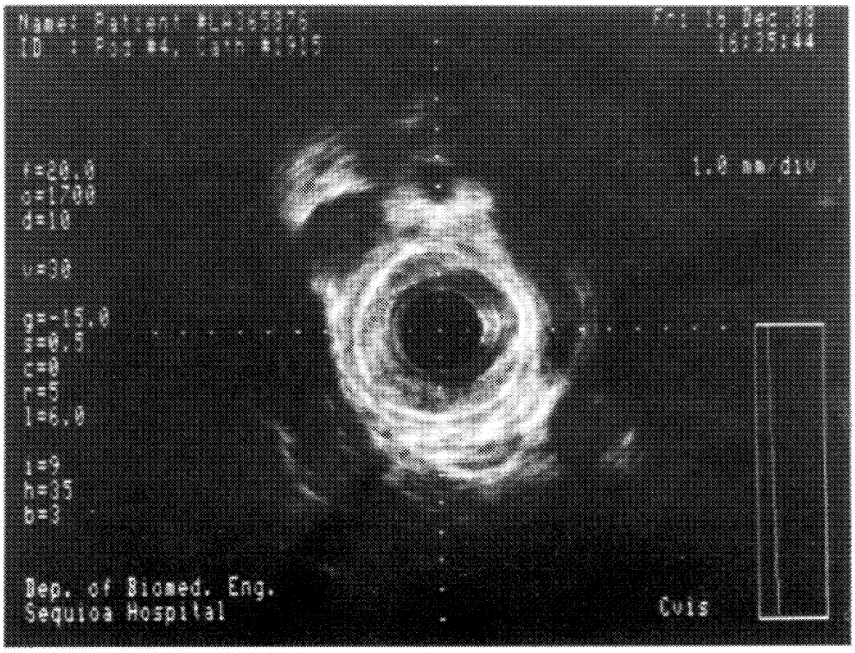

Fig. 7. Image from the same vessel as in Figure 6, in a section with significant atherosclerotic disease. The media appears thinned in comparison to the more normal segment, and is covered by a narrow layer of bright atheroma, probably consisting mainly of fibrous tissue. Overlying of this bright brand (on the luminal side) is a thicker layer of soft, less echogenic atheroma.

Once the initial passes with the atherectomy device have been made, it is highly useful to image with the ultrasound catheter to determine the regions of the vessel wall that require further attention. The logistics of interrupting the atherectomy procedure for imaging are not difficult in practice, since the atherectomy device must periodically be emptied of atheroma. This provides a natural pause in the procedure during which time the imaging can be performed. It is a very common situation, in our experience, to find that the neolumen created by the atherectomy device is eccentric, having media on one boundary and a relatively thick accumulation of residual atheroma elsewhere. Imaging provides definitive guidance for directing the device to the areas of residual plaque and for determining when the lumen is approaching the perimeter of media.

In our early experience we have also found that angiography substantially underestimated the plaque load remaining after the initial passes of the atherectomy device. Residual deposits of atheroma occupying 50 or 60 percent of the true lumen may appear nearly normal on angiography. There are several potential reasons for this occurrence: (1) The regions adjacent to the area of maximal stenosis also have significant accumulations of atheroma,

although they appear "normal" on angiography by virtue of their larger lumen caliber; (2) The media and adventitia are expanded in the region of severe disease relative to the neighboring segments as a part of the atherosclerotic process, so that the "true" lumen in the diseased segment is actually larger than elsewhere in the vessel; (3) The atherectomy device may stretch the vessel during the procedure, transiently dilating both the lumen and the media/adventitia perimeter. In combination, these factors appear to be substantial enough to seriously compromise the ability of angiography to provide definitive guidance for debulking by atherectomy.

Several of the other atherectomy devices undergoing clinical testing are coaxial and not directional in their basic operation, so that the cutting or abrading action occurs in a symmetric fashion around the guidewire [17, 18]. Since radial orientation of the device is not an issue with these catheters, intravascular imaging will not be necessary in positioning in this respect. Ultrasound imaging may still be helpful, however, in deciding the dimensions of the neolumen to be created. Currently, the size of lumen created is a function of the fixed diameter of the cutting/abrading device selected. Future iterations of the catheters may have an adjustable cutting radius that can be varied during the procedure. In either case, it may be useful to be able to identify the dimensions of the medial border in order to select a definitive channel size. In addition, the appearance of the vessel on ultrasound scanning may influence the type of atherectomy device initially selected. It may be the case, for example, that regions of predominantly eccentric atheroma are best addressed by a directional device, whereas long regions of concentric atheroma can be most efficiently treated with a coaxial cutter.

Balloon angioplasty. The positioning of balloon catheters for angioplasty is determined by angiography, which allows reasonably accurate centering of the balloon in the region of maximal stenosis. For this reason, and because inflation of the balloon is an intrinsically symmetric process, there seems at this point to be little need for ultrasound imaging as a guiding therapy for placement of the balloon. Perhaps there are details of plaque substructure — for example, the extent and distribution of hard accumulations of calcium — that might dictate some particular strategies in balloon, sizing, placement or inflation technique. For the present such considerations are highly speculative.

An application for catheter ultrasound of more immediate practical interest is in the assessment of dissections created by balloon angioplasty [19]. Although dissection is part of the mechanism of successful angioplasty, severe dissections are a major contributor to the phenomenon of abrupt reclosure, in which a dilated vessel occludes during the first hours following the procedure. It is possible that dissections created by balloon angioplasty can be characterized at the time of the procedure in terms of the risk of progression to abrupt reclosure. Those dissections which appear to be unstable could be treated with an additional therapy such as laser balloon "welding" or stenting. The extent of dissection may also influence the rates of

restenosis, the aggressive myointimal proliferative response that causes a narrowing of the dilated segment in the several months following angioplasty. Data from an animal model of angioplasty suggest that when significant media is exposed by a dissection, rates of restenosis increase substantially [20]. Other morphologic features of the post-angioplasty segment, such as the overall size and regularity of the lumen, the degree of stretching of media and adventitia, or the extent of early thrombus formation, may be predictive of restenosis.

There is indirect evidence to suggest that the choice of balloon angioplasty as the appropriate therapy for a particular lesion may be influenced by features of the atheroma that can be characterized from the ultrasound image. Based on pathologic studies, Waller and colleagues have suggested that there may be an optimal, middle range of calcium substructure in a lesion that is predictive of a favorable angioplasty result [21]. Lesions which have too little calcium may not have a sustained angioplasty effect, whereas severely calcified lesions may undergo such extensive disruption with angioplasty that there is an increased incidence of abrupt reclosure and, potentially, restenosis.

Laser angioplasty. Although laser angioplasty systems have been developed and are undergoing clinical testing in both peripheral and coronary arteries, perforation continues to be a significant concern. One promising new technology for guidance of laser therapy is laser-induced fluorescence, in which fluorometric analysis of the material adjacent to the catheter tip is performed by means of the same fiber bundle that is used for ablation [22]. Even if this method proves to be clinically reliable in discriminating normal vessel wall from atheroma, however, there are at least two potential limitations in practice. First, the current prototype systems rely primarily on the detection of media as the signal to stop penetration with the catheter. Unfortunately, the media tends to be thinned (or absent altogether) precisely in those areas in which the accumulation of atheroma is the greatest. A second theoretical problem with the system is that detection of media serves as a boundary condition for the laser catheter, but does not provide an indication of which direction is the most favorable to proceed in the first place. This is an intrinsic limitation of the fluorescence method, since it only provides information about tissue to a depth of approximately 100 microns. By contrast, ultrasound effectively penetrates a distance of 1 cm or more in the frequency range of the catheter transducers, offering the prospect of aiming a laser device along an axis which is the safest and most direct route through the lesion. This remains only a theoretical prospect at present, however, since the catheter technology combining the ultrasound sensing and laser ablating capabilities would be relatively complex. One group has reported initial developmental efforts on a system for simultaneous ultrasound imaging and laser ablation in a side-cutting mode [23].

Intravascular stents. Stenting, like balloon angioplasty, is a radially symmetric procedure for which angiography appears to provide relatively satisfactory guidance. There are several areas in which intravascular imaging could provide useful information in addition to the angiogram, but these applications are theoretical at present. These include the ability of ultrasound imaging to: (1) identify regions where the deployed stent is not closely apposed to the vessel wall, potentially creating an area of flow disturbance at risk for thrombosis; (2) specify the appropriate final size of the expanded stent, based on a knowledge of the perimeter of media and the distribution of atheroma; (3) predict lesions at high risk for acute thrombotic occlusion, based on the amount of thrombus or exposed media present at the time of stent implantation; (4) aid in the assessment of stent restenosis (the location of the stent within the restenosis lesion can be easily determined because of the echogenicity of the metal stent components).

Demonstration of clinical utility

High-resolution intravascular imaging has potential application across the entire range of catheter-based or operative vascular procedures. It is clearly too early in the evolution of the technology to determine what the extent of practical clinical value of imaging will be in these contexts. With the increasingly severe cost constraints in the interventional vascular arena, the utility of imaging will have to be convincingly documented in clinical trials before reimbursement is available. Given that the technology is currently in a prototype stage, and that understanding of the features of the images is currently at a very rudimentary level, it seems likely that it will require at least several years to complete significant clinical trials.

Comparison with fiberoptic angioscopy

In attempting to predict the eventual clinical utility of intravascular ultrasound, it is useful to contrast this technology with fiberoptic angioscopy, the other major high-resolution, intravascular imaging technique. Although angioscopy has had a somewhat longer period of concerted technical development than intravascular ultrasound, it has been only recently advocated as a practical clinical modality. Part of the reason for this delay involves the requirement for an effective flushing and/or occlusion system in order to clear the visual field of blood. Methods are presently evolving which allow intermittent visualization without the need for high volumes of flushing solution. The lack of a flushing requirement remains a relative practical advantage for intravascular ultrasound, however. The ability to image in a blood-filled environment means that the logistics of imaging with ultrasound are relatively simple, and that prolonged periods of imaging can be performed without any risk of ischemia.

A more fundamental difference between the two technologies is in the basic image format. Fiberoptic angioscopy provides a detailed view of the inner surface of the vessel wall and any intraluminal processes such as thrombus or intimal flaps. The image is three-dimensional, oriented in a forward-looking direction, and is substantially enhanced by the color of the tissues being examined. The ultrasound image is a two-dimensional "slice" at the level of the catheter tip. The main advantage of this format is that details of arterial wall structure below the surface are clearly defined. The current catheters provide an image plane which is perpendicular to the catheter tip. Differentiation of tissue structures depends on varying acoustic properties of the tissue, and may not provide as fine a distinction as the color/texture information from angioscopy.

Catheter performance characteristics are also significantly different between the two modalities. The imaging fibers of the angioscopes have undergone substantial miniaturization; high resolution catheters with diameters of less than 1 mm are being manufactured. The ultrasound catheters are currently 5 French (1.6 mm) or larger in caliber, and it appears that it will be difficult to achieve reduction in size below 3 French with existing technology. Shaft flexibility will probably be relatively comparable between the ultrasound catheters and the angioscopes. Because the ultrasound catheters image radially, a soft tip can be incorporated to facilitate tracking. This feature is not possible with the angioscopes, because of the end-imaging format.

Future development

Combined imaging/therapeutic devices

The ability to image while simultaneously treating an atherosclerotic segment with a single catheter has obvious clinical appeal. The concept of a combined device seems most readily applicable in the case of a directional therapy such as atherectomy or laser, where the cutting/ablating action can be oriented to a specific region of the vessel wall. Addition of imaging to balloon angioplasty might be useful in precise positioning of the balloon or perhaps in gauging the appropriate inflation pressure and time parameters. Developing combined imaging and therapeutic catheters represents a considerable technical challenge, particularly given the restrictions in miniaturizing the ultrasound catheter alone.

Tissue characterization

Computer-assisted analysis of the backscattered radiofrequency signal offers the potential of obtaining more precise information about tissue composition than is available in the image proper. Pilot studies from our group have suggested that the degree of calcification in an atherosclerotic lesion can be

quantitated by straightforward analysis of the amplitude of backscatter [24]. More sophisticated analysis of the signals may provide detailed information about plaque characteristics such as the extent of fatty versus fibrous tissue. The potential clinical significance of this information is unclear at present, although it is conceivable that precise information about tissue composition could influence choice of a specific therapy. Tissue characterization in the context of catheter ultrasound has two distinct advantages over noninvasive, transcutaneous ultrasound: (1) in the case of catheter ultrasound, the transducer is immediately adjacent to the tissue of interest, so the effects of variable attenuation of the signal as it travels through intervening tissue are minimized; (2) the high frequencies of the catheter transducers in general increase the diagnostic sensitivity of the tissue characterization technique.

Three-dimensional image reconstruction

Catheter images are well suited for three-dimensional reconstruction, since the spatial information can be accumulated as a series of two-dimensional "slices" which are indexed according to axial position in the vessel. Early efforts at three-dimensional presentation of ultrasound scans of arteries by Kitney and colleagues have demonstrated the feasibility of the approach and the power of the three-dimensional format in conveying an accurate impression of vessel pathology.

Combined Doppler and imaging ultrasound

Although velocities measured by a Doppler catheter can be used to estimate coronary flow reserve, direct measurements of flow have not been possible. Cross-section area determinations by imaging, combined with mean velocity determination by Doppler, offer the prospect for real-time measurement of flow in vessels. Conceivably, flow patterns could be displayed in a two-dimensional, color-flow format, although the clinical value of this form of display would need to be validated.

Conclusions

Intravascular ultrasound is in the early stages of validation as a potentially useful new imaging modality. Initial feasibility has been demonstrated: it appears relatively certain that high quality images can be obtained from catheters with sufficiently good performance characteristics to be safely inserted into the peripheral and coronary vessels. The clinical applications for these imaging catheters are potentially broad, particularly in the context of providing guidance for second-generation catheter therapies. Extensive clinical testing will be required before the range of practical applications for catheter ultrasound can be determined.

Acknowledgements

Images presented here were obtained using the UltraScan (TM) system from Cardiovascular Imaging Systems (CVIS) of Sunnyvale, CA. We appreciate the skilled assistance in manuscript preparation by Barbara Herz.

References

1. Cieszynski T: Intracardiac method of ultrasound heart-structure investigation. Polsk Przeglad Chirug 33: 1071—1961
2. Carleton RA, Clark JG: Measurement of left ventricular diameter in the dog by cardiac catheterization. Validation and physiologic meaningfulness of an ultrasonic technique. Circ Res 22: 545—548, 1968.
3. Bom N, Hoff H ten, Lancée CT, Gussenhoven WJ, Serruys PW, Slager CJ, Roelandt J: Early and present examples of intraluminal echography. SPIE 1068: 146—150, 1989.
4. Hodgson JMcB, Eberle MJ, Savakus AD: Validation of a new real time percutaneous intravascular ultrasound imaging catheter. Circulation 78: II-21, 1988 (Abstract).
5. Yock P, Linker D, Saether O, Thapligal H, Arenson J, White N, Ports T, Angelsen B: Intravascular two-dimensional catheter ultrasound: initial clinical studies. Circulation 78: II-21, 1988 (Abstract).
6. Pandian N, Kreis A, Desnoyers M, Isner J, Salem D, Sacharoff A, Bolesza E, Wilson R, Caro R: In vivo ultrasound angioscopy in humans and animals: intraluminal imaging of blood vessels using a new catheter-based high resolution ultrasound probe. Circulation 78: II-22, 1988 (Abstract).
7. Mallery JA, Tobis JM, Gessert J, Griffith J, Georgeson S, Morcos NC, Henry WL: Evaluation of an intravascular ultrasound imaging catheter in porcine peripheral and coronary arteries in vivo. Circulation 78: II-21, 1988 (Abstract).
8. Roelandt JR, Serruys PW, Bom N, Gussenhoven EJ, Egmond FC von, Lancée CT, Hoff H ten, Alphen WJ von: Intravascular real-time, high resolution two-dimensional echocardiography. J Am Coll Cardiol 13: 4A, 1989 (Abstract).
9. Yock PG, Linker DT, Thapliyal HV, Arenson JW, Samstad S, Saether O, Angelsen BAJ: Real-time, two-dimensional catheter ultrasound: a new technique for high resolution intravascular imaging. J Am Coll Caridol 11: 130A, 1988 (Abstract)
10. Meyer CR, Chiang EH, Fechner KP, Fitting DW, Williams DM, Buda AJ: Feasibility of high-resolution, intravascular ultrasonic imaging catheters. Radiology 168: 113—116, 1988.
11. Gussenhoven EJ, Essed CE, Lancée CT, Mastik F, Frietman P, Egmond FC von, Reiber J, Bosch H, Urk H von, Roelandt J, Bom N: Arterial wall characteristics determined by intravascular ultrasound imaging: an in vitro study. J Am Coll Cardiol 14: 947—952, 1989.
12. Mallery JA, Tobis JM, Gessert J, Griffith J, Bessen M, MacLeay L, Henry WL: Identification of tissue components in human atheroma by an intravascular ultrasound imaging catheter. Circulation 78: II-22, 1988 (Abstract).
13. Potkin BN, Bartorelli AL, Gessert JM: Coronary artery imaging with intravascular high-frequency ultrasound. Circulation, 1989 (in press).
14. Pandian NG, Kreis A, Brockway B, Isner JM, Sacharoff A, Boleza E, Caro R, Muller D: Ultrasound angioscopy: real-time, two-dimensional, intraluminal ultrasound imaging of blood vessels. Am J Cardiol 62: 493—494, 1988.
15. McKay C, Waller B, Gessert J, Collins S, Catellier M, Fleagle S, Marcus ML: Quantitative analysis of coronary artery morphology using intracoronary high frequency ultrasound:

validation by histology and quantitative coronary arteriography. J Am Coll Cardiol 13: 228A, 1989 (Abstract).
16. Simpson JB, Selmon MR, Robertson GC, Cipriano PR, Hayden WG, Johnson DE, Fogarty TJ: Transluminal atherectomy for occlusive peripheral vascular disease. Am J Cardiol 61: 96G—101G, 1988.
17. Fourrier JL, Auth D, Lablanche JM, Brunetaud JM, Gommeaux A, Bertrand ME: Human percutaneous coronary rotational atherectomy: preliminary results. Circulation 78: II-82, 1988 (Abstract).
18. Stack RS, Perez JA, Newman GE, McCann RL, Wholey MH, Cummins FE, Galichia JT, Hoffman PU, Tcheng JE, Sketch Jr. MH, Lee MM, Phillips HR: Treatment of peripheral vascular disease with the transluminal extraction catheter: results of a multicenter study. J Am Coll Cardiol 13: 227A, 1989 (Abstract).
19. Tobis JM, Mallery JA, Gessert J, Griffith J, Bessen M, MacLeay L, Morcos NC, Henry WL: Intravascular ultrasound visualization before and after balloon angioplasty. Circulation 78: II-84, 1988 (Abstract).
20. Steel PM, Chesebro JH, Stanson AW, Holmes Jr. DR, Dewanjee MK, Badimon L, Fuster V: Balloon angioplasty. Natural history of the pathophysiological response to injury in a pig model. Circ Res 57: 105—112, 1985.
21. Waller BF, Miller J, Morgan R, Tejada E. Atherosclerotic plaque calcific deposits: an important factor in success or failure of transluminal coronary angioplasty (TCA). Circulation 78: II-376, 1988 (Abstract).
22. Leon MB, Lu DY, Prevosti LG, Macy WW, Smith PD, Granovsky M, Bonner RF, Balaban RS: Human arterial surface fluorescence: atherosclerotic plaque identification and effects of laser atheroma ablation. J Am Coll Cardiol 12: 94—102 1988.
23. Martinelli MA, von Thuna PC, Hatch F: Ultrasonic imaging of coronary arterial thickness and internal abnormalities. SPIE proceedings, 1989 (in press).
24. Linker DT, Yock PG, Thapliyal HV, Arenson JW, Johansen E, Grønningsaeter A, Lønstad HK, Angelsen BAJ: In vitro analysis of backscattered amplitude from normal and diseased arteries using a new intraluminal ultrasonic catheter. J Am Coll Cardiol 11: 4A, 1988 (Abstract).

9. Current intra-arterial ultrasound imaging systems and automatic contour detection

NICOLAAS BOM, J.G. BOSCH, J.H.C. REIBER,
E. GUSSENHOVEN, C.J. SLAGER and R.W. BROWER

Summary

Three techniques for the intra-arterial ultrasonic visualization of the lumen cross section are described. These are based on: 1) single rotating transducer; 2) single fixed transducer with rotating mirror; and 3) fixed transducers in a multiple phased array. In vivo tests have shown that the single transducer currently produces the clearest images at the cost of a complex mechanical rotational design. The multiple phased array requires further development to realize its full potential. These catheter tip transducers are finding application in desobstruction techniques such as laser ablation and spark erosion, where it is important to precisely guide the catheter and avoid arterial perforation. Finally, a method for quantifying the extent of tissue desobstruction is described based on a minimum cost algorithm for automatically detecting the contours of complex structures produced by intra-arterial visualization techniques.

Introduction

Relatively little work has been reported on the use of catheter tip transducers capable of internally imaging the lumen and vascular wall of coronary arteries. This is so despite the fact that there is a major clinical problem that might be resolved if a high-quality intra-arterial ultrasonic imaging device were available.

The use of percutaneous transluminal coronary angioplasty (PTCA), introduced by Gruentzig [1] in 1979, has had a major impact on the treatment of symptoms of myocardial ischaemia, resulting in a significant reduction in surgical referrals of patients with single or double vessel coronary artery disease. During PTCA a specially constructed catheter with a balloon at the tip is positioned inside the obstructed lumen. The balloon is inflated and the stenosis is dilated, but not removed. The initial success rate has been encouraging, notwithstanding the fact that approximately one third

J. H. C. Reiber and P. W. Serruys (eds), Quantitative Coronary Arteriography, 199–210.

of the treated lesions show signs of restenosis within 6 months of treatment. In another 5 to 10% of the cases the dilatation procedure itself is unsuccessful, for example, when the balloon cannot pass the obstruction or when a clinically significant dilatation is not achieved.

It is hoped that the removal of the obstruction would diminish the risk of restenosis. Furthermore, such techniques would allow for the treatment of both total and partial obstructions not accessible by the current balloon dilatation techniques.

Much work is being directed toward the development of new techniques for the complete removal of the obstruction during cardiac catheterisation. Current desobstruction methods represent a variety of approaches and technologies: for example, a rotating abrasive tip [2]; an atherectomy catheter tip method [3], and the "hot tip" method [4]. The application of an intense laser beam transmitted by fiber optics [5, 6, 7] and the use of 'spark erosion' [8, 9] have been explored in our laboratory.

During the removal of tissue by these techniques, however, perforating the arterial wall must be avoided. The curvature of the artery itself and the eccentric location of the obstruction demand appropriate steering of the catheter tip. The information needed for such a procedure can be provided by intra-arterial echo imaging. Furthermore, such an imaging technology should also be able to yield information on the extent to which the desobstruction technique has been successful.

The principal technical problem in developing such intra-arterial imaging techniques has been one of miniaturization. This has required the use of very small transducers, necessitating high frequency transmission and detection techniques. The well understood technology of present day echocardiography, as well as aspects of electro-mechanical design, have thus been severely strained. Three echo based methods are described below. This chapter concludes with a discussion of a technique to quantify the lumen size and the extent of desobstruction.

Intra-arterial imaging techniques

Single rotating transducer

One tested design for a mechanically rotating ultrasonic transducer mounted in a catheter is shown in Figure 1. The outer diameter of the tip is 1.6 mm and the transducer frequency is 30—40 MHz. Real-time images can be produced at a rotational speed of 1000—3000 rpm (Figure 2). So far the device has been tested in short segments of arteries obtained from the anatomy laboratory.

As can be seen in the cross-sectional image of Figure 2, the stenotic areas can be easily recognized. This particular example was taken from a femoral artery. The image shows the typical acoustic characteristics of a muscular

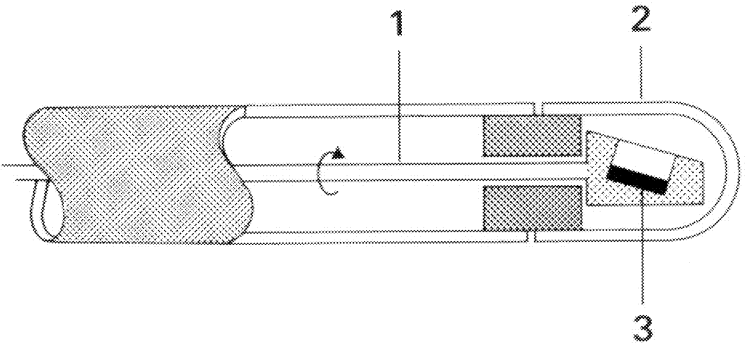

Fig. 1. Illustration of the catheter tip echo principle showing the shaft (1), acoustically transparent dome (2) and transducer element (3).

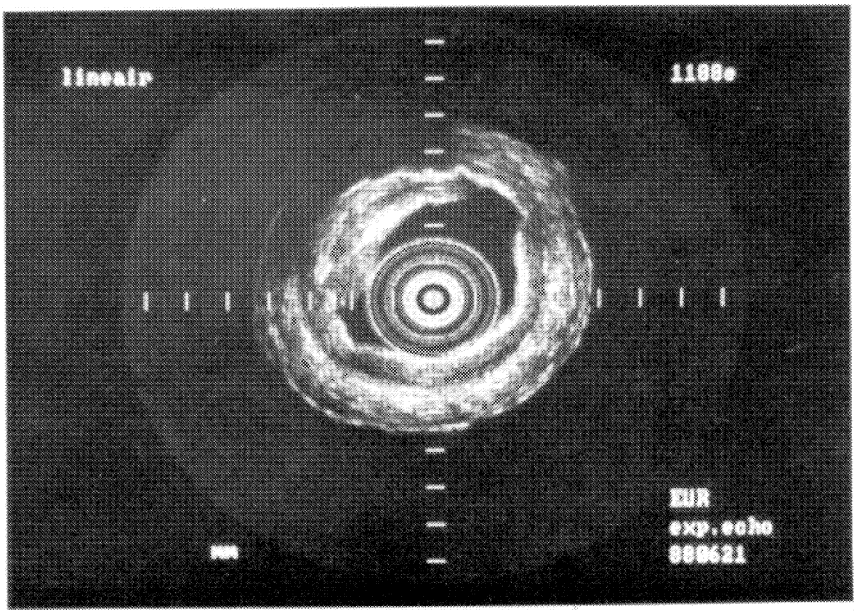

Fig. 2. Cross-sectional echo image obtained in an in-vitro study from a femoral artery (see text) using the transducer illustrated in Figure 1.

artery with an echo-free media. The eccentrically located obstruction (clockwise between 09 and 01 o'clock) is clearly visible and varies in echo intensity. Collagen appears to be highly reflective, while the fatty parts correspond to a lower echo brightness level. The lamina elastica interna can also be identified as a highly reflecting thin layer. Initial in vivo experiments in a pig resulted in well delineated realtime cross-sectional images of carotid arteries.

Single fixed transducer, rotating mirror

A schematic drawing of an improved catheter tip design is illustrated in Figure 3. It consists of a flexible shaft (1), transparent dome (2), echo element (3) and rotating mirror (4). The mirror is mounted at the end of the shaft and is the only part of the structure which rotates. The piezoelectric element is positioned over an air-backing for optimal sensitivity and emits backwards towards the rotating mirror.

Fixed transducer elements, phased array configuration

As early as 1969 we initiated a program to develop a miniature phased array imaging technique using state-of-the-art technology [10]. A 32-element circular array with an outer diameter of 3.2 mm mounted at the tip of a No. 9 French catheter was constructed (Figure 4). The array configuration was a compromise between the optimal design from the point of view of acoustics and the limitations imposed by technological constraints. The final design was chosen to operate at 5.6 MHz with a narrow main beam at the expense of a pronounced grating lobe at +/− 56 degrees. As a consequence, the resulting scan was made up of three components: an image based on echoes generated within the main beam and two superimposed images of reduced intensity from grating lobe echoes, rotated over +/− 56 degrees. Due to the technical difficulties and the limited resources available at the time, the effort was shifted to noninvasive work. Nevertheless, real-time intraluminal images were recorded.

It was clear, however, that this was the most attractive mechanical design in the sense that it required no moving parts. Today, at 20 MHz this phased array principle has been reactivated and has become available as an "over the guide wire" echo catheter system. A slight disadvantage of this design might be the somewhat extended dead zone area due to the circumferential mounting of the echo elements.

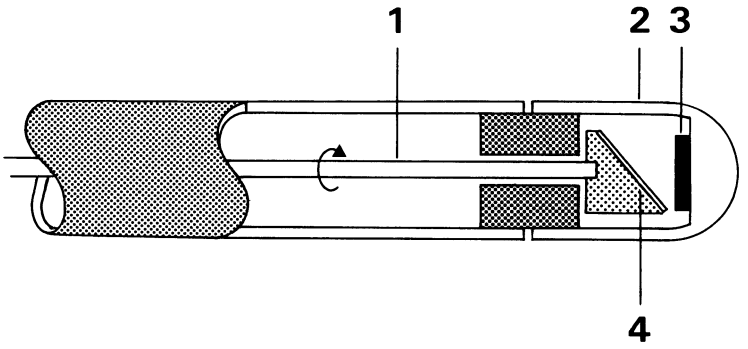

Fig. 3. Catheter tip with a rotating mirror (by permission of the author).

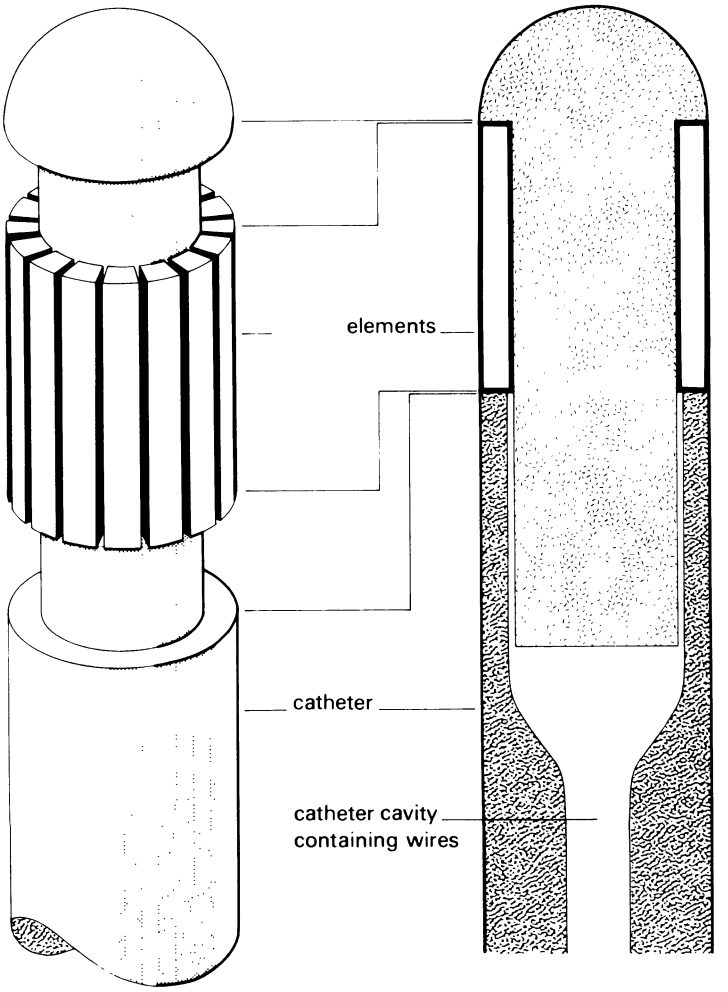

Fig. 4. Schematic diagram of phased array construction at a catheter tip. (see Bom, 1972).

Image processing

Regardless of the source of the images, a method to define the contours of the observed structures would be a valuable adjunct and thus provide a basis for quantifying the changes associated with therapeutic techniques such as PTCA, laser desobstruction, or 'spark erosion'. Because of the well known inter- & intraobserver variability in manual edge definition and its labor intensive nature, this process should be automated as much as possible.

For the automatic detection of the intraluminal contour, we adapted an automated contour detection technique developed for endocardial contours

in short-axis echocardiographic cross-sections of the left ventricle [11]. This contour detection scheme is based on minimum-cost criteria using a novel iterative approach. Minimum-cost contour detection has been used earlier with success in our laboratory on coronary and left ventricular angiograms and on technetium-99 m and thallium-201 scintigrams [12, 13]. This technique is not very sensitive to image noise and small disturbances, and can be optimized with respect to specific characteristics of the image.

The principle of 'minimum cost' contour detection is the following. Each picture element in the two-dimensional echo image is assigned a cost value according to the intensity gradient (high gradient = low cost). A path is then determined through the cost image so that the total cost is minimum. This path must obey a number of constraints including the requirement that it must end at the same point where it began; the resulting path is then a closed curve.

The practical implementation of this principle for the echo image can be described as follows:

1. A circle with a fixed radius is defined around the center of the transducer. This circle is used as a first model for the contour to be detected (Figure 5A). The total area to be processed is defined by a fixed radial distance on either side of this circle (shown in Figure 5A by the inner and outer circles). The image is then resampled along scan lines perpendicular to

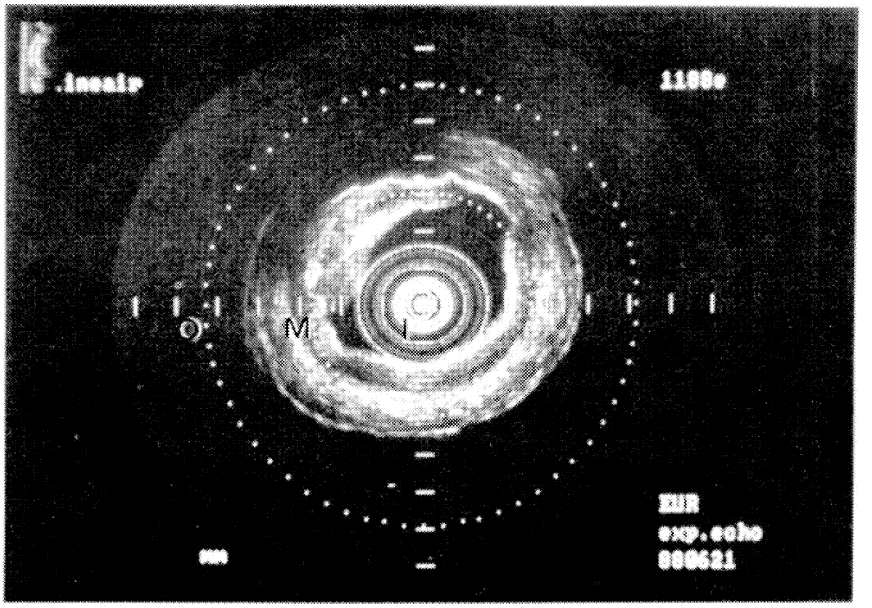

Fig. 5A. The middle circle (M) represents the first luminal 'model' used in the detection of the wall position. The inner & outer circles (I, 0, respectively) denote the boundaries of the region of interest.

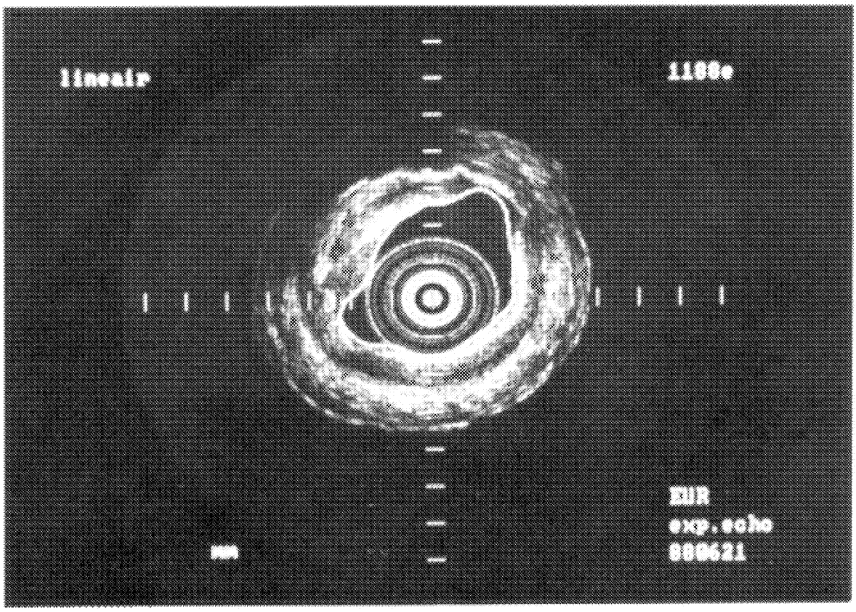

Fig. 5B. The automatically detected contour after the first pass iteration.

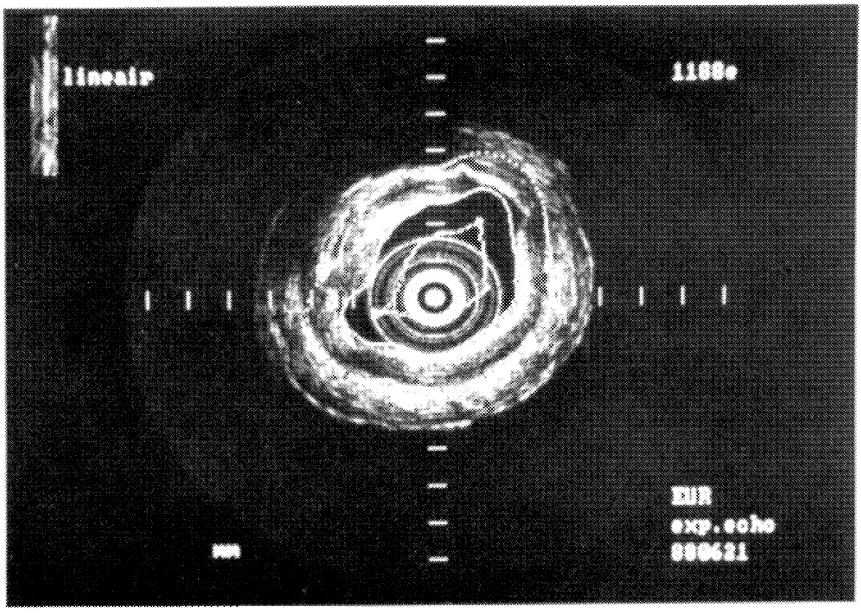

Fig. 5C. The detected contour of figure 5B is used as an improved model, generating a new region of interest based on its own shape. In the second iteration the scanlines are taken perpendicular to this model contour.

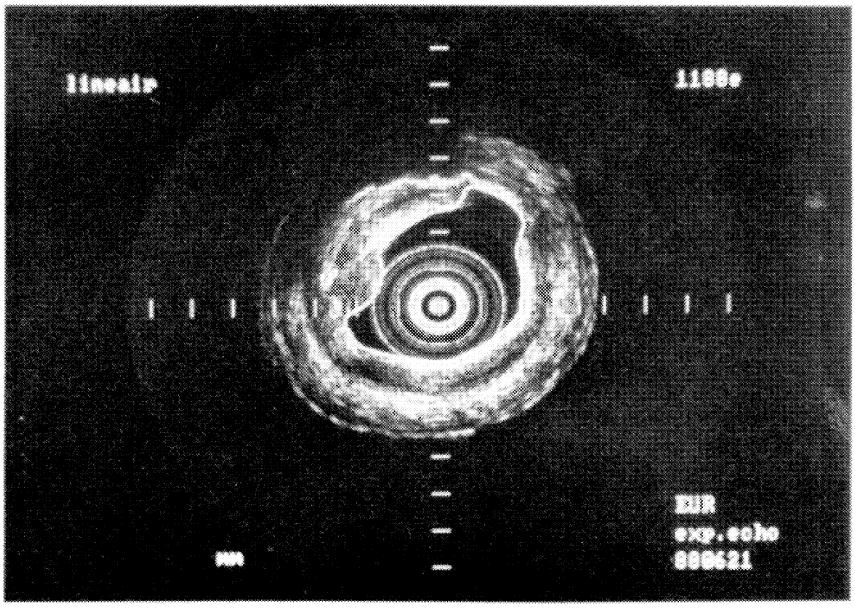

Fig. 5D. The resulting final contour (2nd iteration).

the local direction of this model. This results in a rectangular array of resampled image data resembling a polar transformation of the image.

2. A spatial first-derivative value is computed for each point in this transformed image and a cost matrix generated. The cost value for each point is defined by the spatial first-derivative value and the mean grey value to the left of this point. Low cost values will be associated with points with a high probability of being part of the luminal contour, and vice versa.
3. An optimal path (i.e. a path with minimal overall cost) through this cost matrix is computed. The algorithm for determining the optimal path has been described previously [12, 14]. This path is subject to constraints on connectivity and smoothness. As the luminal contour is a closed curve, the beginning and endpoints of the path should be connected.
4. The points of the path are transformed back into the original image, interpolated and smoothed. This results in a closed curve that is a first approximation of the actual luminal contour (Figure 5B).
5. As described above the contour resulting from this first iteration will be used as an improved model in the second iteration. In this second iteration, the image is resampled along the new model, i.e. scan lines are defined perpendicular to the local direction of the first contour (Figure 5C). The minimum cost contour detection is again applied and in most cases an accurate luminal contour is found (Figure 5D). If necessary, manual corrections can be made to this otherwise automatically detected luminal contour.

Practical example, spark erosion & lumen detection

Slager [8, 9] has introduced the combination of echo and electrode spark erosion at the catheter tip, although many design-related problems still need to be resolved. Firstly, there is the direct blood-echo tip contact. For diagnostic purposes only, the probe should be redesigned in such a way that the echo tip is covered. Unfortunately, this prevents easy integration with ablation methods. Secondly, the rotational motion must be designed in such a way that the actual orientation of the catheter tip corresponds well with the echo display orientation on the monitor.

As a concluding example of the potential utility of this technology, a cross-sectional intra-luminal echocardiogram was obtained from a specimen of carotid artery both before and after application of the 'spark erosion' desobstruction technique. This is illustrated in Figures 6A and 6B. In Figure 6C the resulting minimum cost contour is shown. The 'spark erosion' technique has taken a clear and quantifiable bite out of the plaque.

At this stage one can only speculate about the relative merits of intra-luminal echocardiography with respect to competing technologies such as angiography. However, it is an open question whether angiography has the precision to detect, much less quantify, complex cross-sectional structures. The repeated measurement of such cross-sections could provide a powerful tool for the investigation of progression/regression of disease and the evaluation of desobstruction techniques.

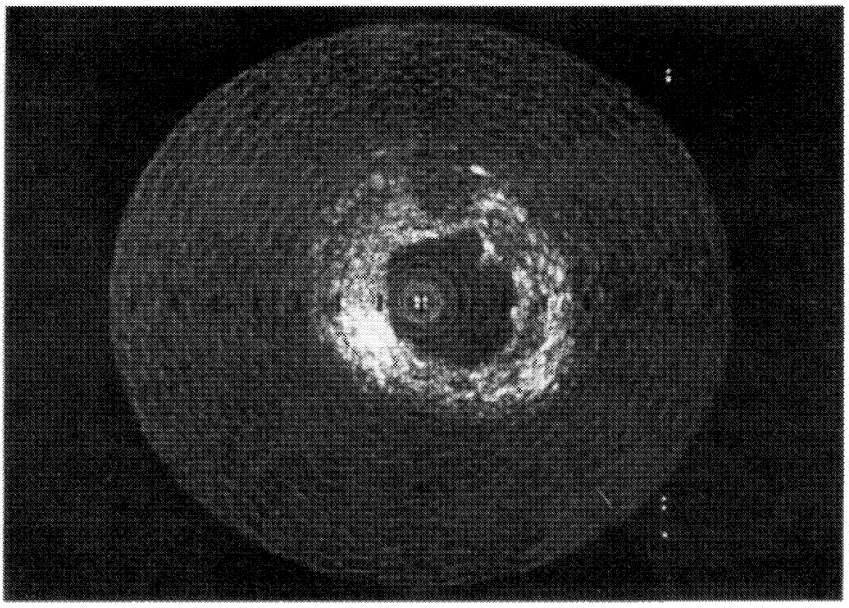

Fig. 6A. Specimen of carotid artery before spark erosion, unprocessed cross-sectional echo image.

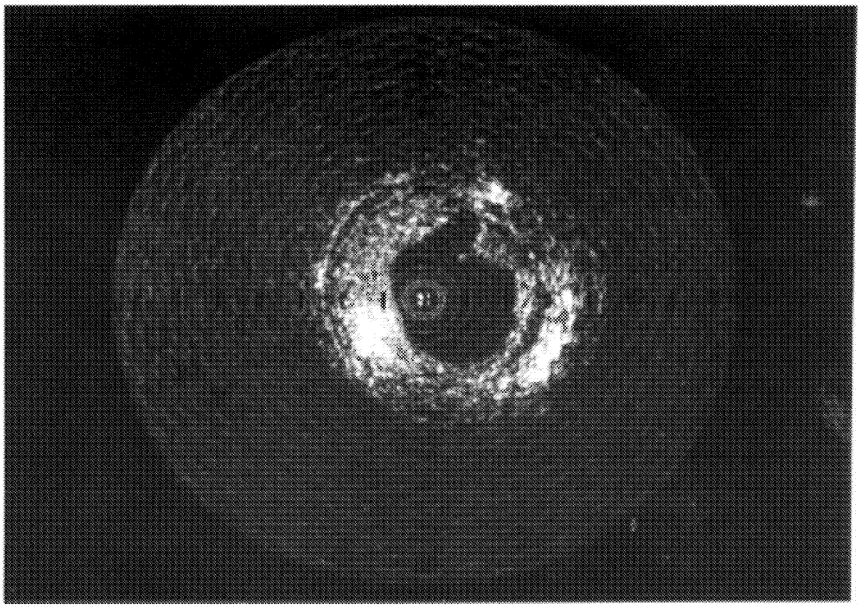

Fig. 6B. Echo image of same section of Figure 6A of carotid artery after spark erosion.

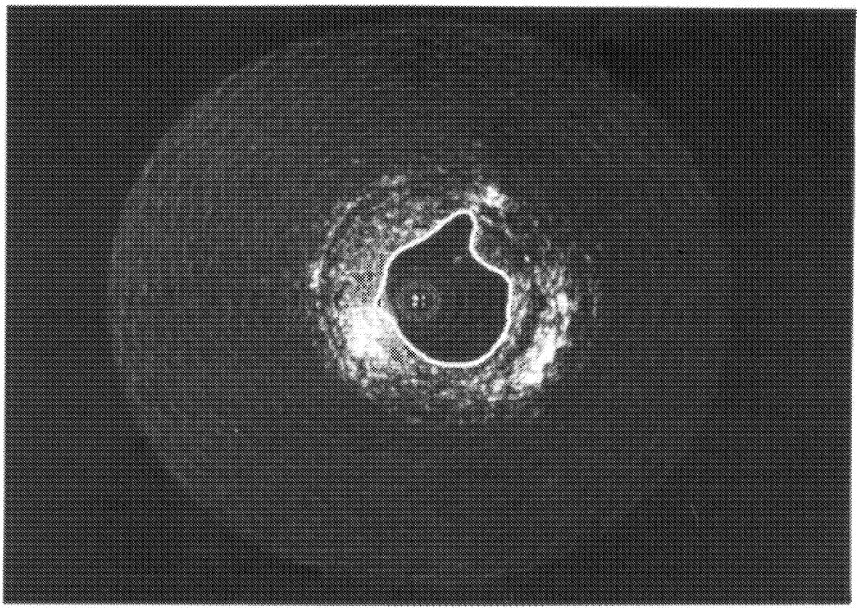

Fig. 6C. The same section of Figure 6B processed with the minimal cost contour detection algorithm.

Conclusion

The need for intra-luminal techniques to visualize the cross-section of arteries is clear. Such techniques will have a direct impact on both the actual performance of desobstruction techniques and on the determination of their efficacy. This is particularly so when follow-up studies must be performed to determine the presence of progression/regression of disease. Three techniques for the intra-arterial ultrasonic visualisation of the lumen cross-section have been described. At this moment the best results are obtained with a single rotating transducer. However, flexible shaft design problems will most likely limit the ultimate utility of this method. The phased-array method requires more work to fully develop its potential. At the same time the image processing tools for quantifying the intraluminal echos are being developed.

References

1. Gruentzig AR, Senning A, Siegenthaler WE: Nonoperative dilatation of coronary-artery stenosis: percutaneous transluminal coronary angioplasty. N Engl J Med 301: 61—68, 1979.
2. Hansen DD, Hall M, Intlekofer MJ, Auth D, Ritchie JL: In vivo rotational angioplasty in atherosclerotic rabbits; comparision of angioscopy and angiography. Circulation 74 (Supp. II: II-362, 1986 (Abstract).
3. Simpson JB, Johnson DE, Brader LJ, Gifford HS, Thapliyal HV, Selmon MR. Transluminal coronary atherectomy (TCA): results in 21 human cadaver vascular segments. Circulation 74 (Supp. II): II-202, 1986 (Abstract).
4. Sanborn TA, Faxon DP, Haudenschild CC, Ryan TJ: Laser radiation of atherosclerotic lesions: decreased incidence of vessel perforation with a fiberoptic laser heated metallic tip. J Am Coll Cardiol 3: 490, 1984 (Abstract)
5. Choy DSJ, Stertzer SH, Rotterdam HZ, Bruno MS: Laser coronary angioplasty: experience with 9 cadaver hearts. Am J Cardiol 50: 1209—1211, 1982.
6. Cross FW, Bowker TJ, Bown SG: Contact sapphire-tip angioplasty with a pulsed Nd-YAG laser. Lasers Med Sci 1: 311, 1986 (Abstract).
7. Borst C: Percutaneous recanalization of arteries: status and prospects of laser angioplasty with modified fibre tips. Lasers Med Sci 2: 137—151, 1987.
8. Slager CJ, Essed CE, Schuurbiers JCH, Bom N, Serruys PW, Meester GT: Vaporization of atherosclerotic plaques by spark erosion. J Am Coll Cardiol 5: 1382—1386, 1985.
9. Slager CJ: Echo-vonkerosie rekanalisatie inrichting. Dutch Patent Application No 8700632, 1987, March 17.
10. Bom N, Lancée CT, Egmond FC van: An ultrasonic intracardiac scanner. Ultrasonics 10: 72—76, 1972.
11. Bosch JG, Reiber JHC, Burken G van, Gerbrands JJ, Gussenhoven WJ, Bom N, Roelandt JRTC: Automated endocardial contour detection in short-axis 2-D echocardiograms: methodology and assessment of variability. Comput Cardiol: 137—140, 1989.
12. Gerbrands JJ, Hoek C, Reiber JHC, Lie SP, Simoons ML: Automated left ventricular boundary detection from Technetium-99 m gated blood pool scintigrams with fixed or moving regions of interest. In: Proceedings 2nd Intern. Conf. on Visual Psychophysics and Medical Imaging, CC Jaffee (ed), IEEE Cat. No 81 CH1676—6, 1982: 155—159.
13. Reiber JHC: Quantitative analysis of left ventricular function from equilibrium gated

blood pool scintigrams: an overview of computer methods. Eur J Nucl Med 10: 97—110, 1985.

14. Leeuwen PJ van, Reiber JHC: Automated detection of left ventricular boundaries from 35 mm contrast cineangiograms. In: Signal processing III: Theories and Applications. IT Young, J Biemond, RPW Duin, JJ Gerbrands (eds), North-Holland, Amsterdam, 1986: 1409—1412.

Part IV

Coronary blood flow and flow reserve

10. Assessment of coronary blood flow and velocity in the catheterization laboratory

ROBERT A. VOGEL and LISA W. MARTIN

Summary

Over the past two decades, radiographic, inert gas washout and catheter techniques have been developed which allow measurement of relative and absolute coronary blood flow. Although contrast medium is not an ideal indicator substance for application of the Stuart-Hamilton, Kety-Schmidt, or Sapirstein principles, transit-time methodology has been successfully employed through combination with digital radiographic techniques. Parameter images have been utilized to display coronary flow reserve data. Scintigraphic assessment of Xenon-133 and catheter measurement of hydrogen washout allow determination of regional myocardial perfusion using the Kety-Schmidt principle, although inaccuracies at low and high flow states have been reported. The most widely used approaches use coronary sinus thermodilution and intracoronary Doppler catheters. Impedance catheter and guidewire techniques have recently been introduced. The latter two are regionally specific, and promise to provide assessment of coronary blood flow simply and inexpensively in the catheterization laboratory.

Introduction

Despite its clinical importance for patients with coronary ischemia and myocardial infarction, the measurement of regional coronary blood flow remains difficult. Over the past two decades, radiographic, inert gas washout, and catheter means for assessing coronary blood flow have been introduced and are listed in Table 1. This chapter discusses the applications and limitations of these techniques, and focuses on a new methodology for measuring absolute coronary blood flow using impedance catheters and guidewires.

J. H. C. Reiber and P. W. Serruys (eds), Quantitative Coronary Arteriography, 213—227.

Table 1. Techniques for measuring coronary blood flow in the catheterization laboratory.

Transit-time
Videodensitometry
Contrast Medium Appearance Time
Inert Gas Washout
Xenon-133
Hydrogen Electrode Catheter
Catheter
Coronary Sinus Thermodilution
Doppler
Impedance Catheter/Guidewire

Radiographic techniques

Most clinical methods for measuring regional blood flow or perfusion are based on one of the following principles: indicator dilution (Stuart-Hamilton), inert substance washout (Kety-Schnidt), or first pass distribution (Sapirstein) [1, 2]. Coronary sinus thermodilution, Xenon-133 myocardial washout, and thallium-201 scintigraphy are representative examples of applications of these three methods. However, none of these general principles can be used directly for the radiographic measurement of coronary blood flow largely because of the effects of the contrast media on the coronary circulation and the method by which it is injected. Primarily, all of these methods require that the indicator substance does not alter the regional flow being measured.

Unlike the substances used in the traditional clinical methods, all contrast media have substantial vascular effects, although non-ionic media may disturb blood flow less than ionic agents. Injection of contrast media into the coronary circulation results in a three phase response [3]. Initially, over the first 1—2 seconds, a minor increase of approximately 10% in coronary blood flow results from the increased perfusion pressure. From 2—4 seconds following contrast administration, coronary flow drops to approximately 50% of its initial level. Thereafter, the widely recognized hyperemic response follows raising baseline flow approximately 3-fold. Injection of contrast media during hyperemic flow results in similar phase 1 and phase 2 changes, although the hyperemic response is minimally higher than initial levels. Despite changes in the absolute magnitude of coronary blood flow, the relative ratio of hyperemic and baseline flow following contrast media administration remains approximately proportional during the first 5 seconds. These phenomenon limit the radiographic measurement of absolute coronary blood flow and the relative measurement of coronary flow reserve to the first 1.5 and 5 seconds following contrast injection, respectively.

Other problems exist with the use of contrast media as blood flow

indicators. The Stuart-Hamilton principle requires administration of a fixed or known amount of an indicator, which must remain intravascular and detectable quantitatively downstream. Contrast media cannot be administered easily in fixed or known amounts without subselective injection to prevent reflux. Moreover, contrast media increases peripheral coronary intravascular volume as part of their vasodilator effect. This effects downstream contrast media quantification by effectively increasing the vascular volume under study. Whereas this is not a major problem for methods limited to intracoronary artery contrast media detection, those techniques for measuring regional myocardial perfusion must take this effect into consideration. Because of the complexities of contrast media diffusion, surface adherence, capillary sludging, and vasoreactivity, the requirement of tracer inertness necessary for application of the Kety-Schmidt principle is not fulfilled. Lastly, the factors of minimal first-pass uptake and regional variability of image intensifier veiling glare and radiation scatter and absorption make the use of the Sapirstein principle problematic.

Using alternative geometric approaches, Rutishauser et al. and Smith et al. developed the first successful radiographic techniques for assessing regional coronary blood flow [4—7]. These similar approaches measure the density of contrast medium at 2 sequential locations in a proximal coronary artery to determine the transit-time of the contrast bolus between the two points. The volume of the arterial segment between the chosen points is then determined geometrically from the segment's mean diameter and length. The flow transversing the arterial segment is calculated from the segment's volume and the bolus' transit-time with the following equation:

$$\text{regional flow} = \text{vascular volume}/\text{transit time} \quad (1)$$

This approach cannot be applied to branching, distal, or circuitous arterial segments. For segments that cannot be positioned parallel to the plane of the image intensifier, multiple radiographic projections and three-dimensional analysis must be used. Although it requires precise determinations of transit-time and arterial diameter, this technique does measure absolute blood flow (ml/minute). Using current technology, Spiller et al. have found excellent correlations between data obtained by electromagnetic flow meter and mean and phasic blood flow measurements obtained by a similar approach (8). The reported technique uses determinations of wave-front transit-time in opposition to the measurements of mean transit-time used by the previous investigators. Use of measurements obtained during this earliest phase of contrast transit, before blood flow is perturbed by the contrast itself, gives this approach a theoretical advantage.

An indicator-dilution videodensitometric method, which measures relative coronary flow ratios rather than absolute blood flow, was first reported by Foerster et al. [9]. A fixed amount of contrast media is injected and indicator-dilution analysis is performed on videodensitometric data obtained over an arterial region of interest. This approach eliminates the need for precise

measurements of arterial diameter and length and can be applied to more distal arterial segments. It is complicated, however, by streaming and reflux of contrast media. Using subselective contrast injection and linearized contrast density detection, Elion et al. (10) have found this method to be valid, and have displayed regional arterial coronary flow reserve measurements using parametric images.

In an attempt to increase the detection of very low concentrations of contrast medium, digital radiography was introduced during the past decade [11, 12]. The simplest enhancement operation employed is mask-mode subtraction, which is accomplished by subtracting a radiographic image obtained just before injection of contrast media (mask) from each of the subsequent contrast containing images. This eliminates densities common to the mask and subsequent frames, ideally leaving visualization of only the contrast containing structures. The quality of mask-mode subtraction images is very sensitive to subject motion, which alters the superposition of the mask and contrast containing frames and produces registration artifacts. Because of the cyclical cardiac motion, registration artifact can be minimized by use of electrocardiographic-synchronized mask selection.

The use of ECG-synchronized mask mode subtraction for the purpose of measuring regional blood flow was first proposed by Robb et al. [13]. These investigators demonstrated that digital subtraction results in a significant increase in the ability to visualize contrast medium transit in its myocardial phase after selective coronary injection. Our laboratory combined this approach with a modification of the vascular volume/transit-time analysis of Rutishauser and Smith. We developed color and intensity coded parametric images to depict the timing and density of selectively injected boluses of contrast medium as they transit the coronary circulation [14, 15]. Relative coronary flow ratios are assessed in myocardial regions-of-interest by quantitatively comparing parametric images obtained at baseline and hyperemic conditions.

Measurement of relative regional coronary blood flow is achieved using independent assessment of transit-time and vascular volume. Relative contrast media transit-time to myocardial region-of-interest are analyzed within the initial 5 second period by application of a threshold criteria, equal to approximately one-third peak. As a first-order approximation, relative vascular volume is assessed proportional to peak regional contrast medium density by the following equation:

$$\text{vascular volume} = k\ (\text{integrated contrast medium density})/\ (\text{contrast medium concentration}) \tag{2}$$

where k represents the primary radiographic imaging system transfer function. Assuming that the vascular space has been filled with contrast medium but that additional vasodilatation or substantial diffusion has not yet occurred, vascular volume is then proportional to mask-mode subtracted density. Relative flow ratios can then be calculated by substitution of density

data for vascular volume in equation 1, which determines regional flow as vascular volume/transit time. Despite the difficulties associated with the use of contrast media and the densitometric rather than geometric assessment of relative vascular volume employed, good correlations between electromagnetic flowmeter and digital radiographic determinations of relative regional coronary blood flow have been found using this approach. Independent validation of this technique has been provided by Mistretta et al. and Serruys et al. [16, 17].

This approach can be implemented on a pixel by pixel basis with parametric images in which individual pixel color and intensity are modulated according to the transit time and density values calculated for that pixel. Region-of-interest density/transit-time values are then calculated as the mean of the individual pixel ratios, thus increasing precision by averaging several thousand ratios. Parametric images have the advantages of providing simultaneous visualization of the entire arterial bed undergoing analysis and recognition of problems in injection of contrast medium, such as streaming. This parametric method has been utilized to determine the physiological significance of individual coronary stenoses, especially pertinent for the consideration of coronary angioplasty [18]. The technique is helpful in situations of multi-vessel disease for determination of the significance of lesser grade stenoses. In this circumstance, stress testing, even with thallium-201 scintigraphy, often fails to adequately assess these additional distributions, as patients cease exercising when they develop ischemia of their primary distribution. This approach has also been found helpful for the assessment of myocardial ischemia in patients with chest pain and radiographically normal coronary arteries [19]. A close correlation between radiographically measured coronary flow reserve and stress scintigraphic data have been found, which confirms the independence of anatomical and physiological assessments of coronary anatomy and physiology.

There are several technical and clinical limitations of the parametric imaging technique for measuring coronary flow reserve. Whereas digital radiographic equipment is expensive, the great advantages of immediate review, image enhancement and quantitation has led to its widespread use in catheterization laboratories, especially those performing angioplasty. Patient motion, and the need for atrial pacing and electrocardiographic-synchronized power injection of contrast medium required for the parametric imaging approach complicates the performance of this technique. Overlap of coronary artery distributions has also been found to be problematic. Moreover, coronary flow reserve can be reduced by many factors other than epicardial coronary stenosis, including: myocardial hypertrophy, hypertension, prior myocardial infarction, collateralization, coronary spasm and intrinsic vascoreactivity, syndrome X, prolonged ischemia, angioplasty, and vasoactive drugs [1]. Arterial, ventricular end-disatolic, and intrathoracic pressures, which can vary during arteriographic procedures, also affect flow reserve. Changes in coronary flow in one artery may affect flow in other arteries. Lastly, as a

relative parameter, flow reserve ratios are altered by changes in resting blood flow. This latter problem is especially problematic immediately following angioplasty which has been found often to be associated with determinations of low flow reserve despite adequate dilatation [20, 21]. This is thought likely due to increases in resting blood flow occurring during this period. These factors need to be considered in using flow reserve to clinically determine physiological severity of lesions and may explain, in part, conflicting anatomic and physiological data.

Several alternative digital radiographic methods for measuring absolute and relative coronary blood flow have been proposed. Parker et al. have performed three-dimensional reconstruction of coronary artery distributions enabling application of the transit-time approach to circuitous vessels [22]. Rutishauser et al. have compared the results of parametric images generated by several appearance-time indices, as well as using Fourier analysis, and have found them clinically helpful [23]. Eigler, Pfaff, Whiting et al. have analyzed the radiographic assessment of contrast medium transit using linear systems which analyze contrast transit by transfer function analysis [24]. Regions-of-interest for densitometric analysis are employed over the proximal coronary artery and distal myocardial perfusion bed. This approach obviates the need for ECG-synchronized power contrast injection. Initial data have suggested that physiologically significant stenoses can be detected without need for hyperemic flow assessment by analysis of the system transfer function under baseline conditions. This is thought to result from the alterations in resistance vessels which dilate to compensate for the upstream stenosis.

Contrast medium washout analysis of regional coronary blood flow has also been studied using the Kety-Schmidt principle. Resultant washout ratios vary with severity of coronary stenosis, but their correlation with actual flow ratios have been reported to be of variable accuracy. Detailed comparison of washin and washout parameters have been reported by Nissen et al. [25]. As mentioned above, this group has developed an approach for measuring relative and absolute coronary blood flow using subselective contrast media injection and indicator-dilution analysis [10]. Color coded parametric images of regional arterial coronary flow reserve result from the first aspect of this approach. Using comparison of coronary artery and aortic densitometry combined with assessment of cardiac output, absolute coronary blood flow analysis can be accomplished secondarily. Unfortunately, although promising, each of the digital radiographic methods are technically complex and have been largely performed only for investigative studies to date.

Diffusable indicators

Following infusion of a diffusable indicator into the coronary circulation, the

regional concentration of the indicator will depend upon its integrated arterial concentration, myocardial extraction ratio and myocardial perfusion. This Kety-Schmidt principle has been used to measure the blood flow to many tissues including the coronary circulation using several inert substances, notably Xenon-133 [2, 26]. Time-concentration curves of myocardial transit of these substances have been followed using both planar and tomographic scintigraphic imaging. Measurements are generally made during the desaturation or washout phase during which absolute regional myocardial perfusion can be calculated from the time course of desaturation, alone. In order to obtain regional information, Xenon is infused selectively into the coronary circulation. Unfortunately, this approach requires long-term steady state hemodynamics and the addition of scintigraphic equipment. Under conditions of regional, especially subendorcardial, ischemia, the indicator is preferentially distributed to those areas with higher myocardial perfusion, resulting in over-estimations of flow [27]. Nonlinearity of perfusion estimates have also been found under high flow conditions.

In order to make the inert gas washout approach more compatible with cardiac catheterization methods, our laboratory has introduced a hydrogen washout, platinum catheter detection method which can be employed during standard coronary angioplasty [28]. Hydrogen-saturated saline is infused through the angioplasty catheter at a rate of 10 ml/minute for 30 seconds subselectively. High impedance electrical potential measurements are obtained from a platinum tipped pacing catheter positioned in the pulmonary artery to monitor the effluent concentration of hydrogen during its washout phase. In contrast to previously used washout techniques, this approach uses subselective administration of the inert gas tracer and nonselective detection. As with all washout techniques, it assumes that coronary blood flow remains constant during the approximate 5 minutes required for the measurement. This approach additionally requires that cardiac output remains constant during the same period. Validation of this approach was performed in a canine model using radio-labelled microspheres as the standard. Although good correlations were obtained, as with other reported washout techniques, some overestimation of low flow conditions and underestimations of high flow conditions were found. As is true of the other washout methodologies, this approach cannot assess transmyocardial perfusion abnormalities. Due to alterations in the platinum electrode surface, some degree of baseline wander was often observed. The ability to measure regional myocardial perfusion is of, at least, theoretic interest as it allows assessment of region-of-risk when combined with measurements of regional coronary blood flow. The theoretic validity of assessing region-of-risk by simultaneous assessment of segmental coronary blood flow and myocardial perfusion was demonstrated in our laboratory [28]. Region-of-risk was calculated from the ratio of blood flow (ml/minute) to perfusion (ml/minute/gm), simultaneously determined using electromagnetic flowmeter and platinum catheter hydrogen washout tech-

niques, respectively, in a canine model. A good correlation was found between the two determinations over a wide range of risk areas.

Catheter techniques

In 1971, Ganz et al. introduced a thermodilution method for measuring coronary sinus flow in humans which uses the indicator-dilution principle [29]. A catheter is introduced retrograde to the coronary sinus through which is infused room temperature saline at a constant rate. Adequate mixing is achieved through infusion of the reference solution perpendicular to the flow of blood in the coronary sinus. Although this technique is simple and inexpensive, it has two major problems. Firstly, the position of the catheter in the coronary sinus is ofter unstable making repeated determinations inaccurate [2]. Regional specificity, even with the catheter positioned in the great cardiac vein, is often problematic, leading measurements to be only estimates of overall coronary blood flow. Secondly, coronary flow reserve measurements using maximal hyperemic stimuli often give values of approximately 2, in comparison with determinations greater than 3—4 using other methodologies.

In an attempt to increase the regional specificity of flow measurements, subselective and balloon catheters have recently been developed which allow measurement of coronary blood flow velocity using Doppler techniques [30, 31]. Although absolute coronary blood flow cannot be measured by this approach, coronary flow reserve can be determined by comparing blood velocities under pharmacologically induced hyperemic and baseline conditions. Papaverine, injected intracoronary, has proven especially useful for this purpose as it provides both near maximal vasodilation and short duration of action [32]. Major advantages of this approach are that both phasic and mean blood flow data are provided continuously and that injection of an indicator substance is not required. This technique is, however, sensitive to catheter position and velocity measurements are significantly reduced when the catheter is located translesionally [33].

Our laboratory has recently developed a method for measuring absolute coronary blood flow using either a standard angioplasty catheter or guidewire and the indicator-dilution principle [34, 35]. The initial intraluminal device employed was a standard angioplasty catheter modified with the addition of a third lumen which terminates in a small side hole located just proximal to the balloon (Figure 1). Impedance measurements are made at the catheter's tip by two pairs of microelectrodes. Impedance is measured at a frequency of 50 kHz and a constant current of 10 μA between the two proximal and distal microelectrodes spaced 2 mm apart. One-half ml of 5% glucose solution (D5W) is injected over a 3—6 second period through the proximal port. The solution is hypotonic relative to blood, thereby causing an increase in impedance measurable at the microelectrodes. Absolute coronary

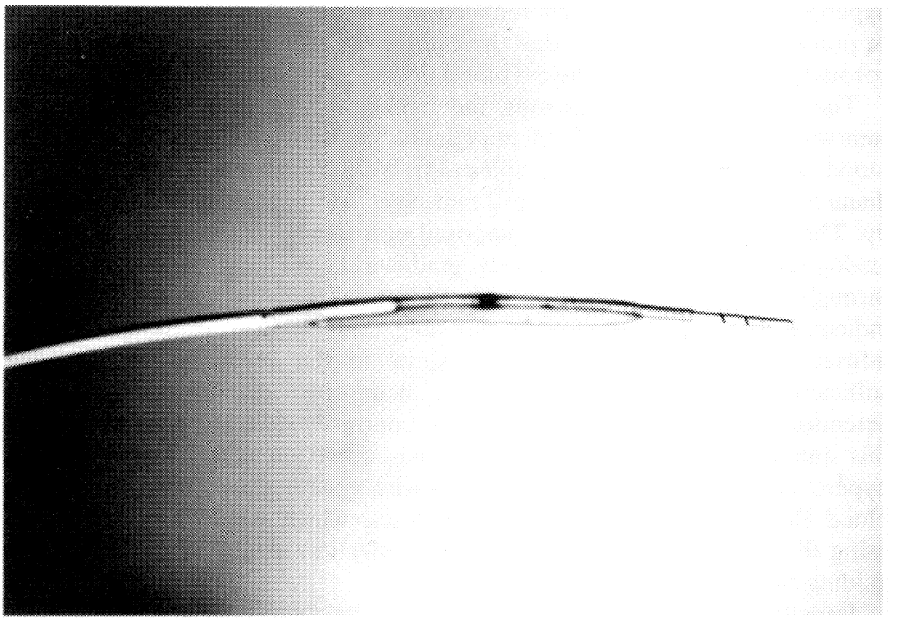

Fig. 1. Absolute coronary blood flow measuring impedance angioplasty catheter.

blood flow is determined by inverse proportionality to the area under the impedance curve, in a manner analogous to the determination of cardiac output using thermodilution catheters. Absolute flow is calculated by the following equation:

$$\text{flow} = K_s I/A \tag{3}$$

where K_s = sensitivity constant, which is the slope of the impedance-D5W concentration relationship, I = amount of D5W indicator, and A = area under the first-pass transit curve. By the indicator-dilution principle, blood flow is determined at the site of introduction of the indicator substance. Subsequent arterial branching does not affect this determination, as long as adequate mixing is achieved. The impedance catheter utilizes two factors to ensure adequate indicator mixing. Firstly, the D5W indicator is sprayed out the side hole in a direction perpendicular to blood flow, similar to the technique employed in the coronary sinus thermodilution catheter. Secondly, the presence of the dilatation balloon causes turbulence, further increasing mixing. Experimental studies have shown that mixing is essentially complete within 1—2 cm distance from the point of ejection. While coronary artery irregularities may further increase mixing, it is unlikely that the impedance catheter could accurately measure absolute coronary blood flow while positioned across the stenosis due to partial occlusion of the lumen. Whereas this does not appear to be a problem for resting blood flow, maximal

hyperemic flow is substantially reduced with a catheter placed translesionally. In practice, this necessitates that the catheter be withdrawn proximally in the coronary vessel in order to assess blood flow.

The necessity of withdrawing the impedance catheter proximal to the stenosis led us to develop an impedance guidewire capable of measuring blood flow using the same principles [35]. We are currently studying a 0.014″ diameter guidewire which has a 2 mm electrode gap located 5 cm from its tip. The tip of the electrode is composed of a spring wire with characteristics analogous to standard angioplasty guidewires. We employ the guidewire through any standard over-the-wire dilatation catheter, ejecting the D5W indicator through the catheter's end hole. This allows the indicator to be infused at a point immediately proximal to the coronary stenosis, with sufficient distance to achieve mixing being provided by the guidewire extended distally across the stenosis. In contrast to the impedance catheter, this much smaller diameter guidewire has not been found to reduce even hyperemic flow substantially. The guidewire system allows determination of blood flow through very proximal stenoses, which would not be possible using the catheter system, as the point of ejection would be in the aorta or guiding catheter.

Impedance measurements are affected by blood conductivity, vessel volume, and parallel conduction. The unwanted contribution to impedance measurements of parallel conduction is reduced by minimizing the electrode gap. Preliminary studies suggest that vessel cross-sectional area varies inversely with baseline impedance. Whereas this may enable the catheter and guidewire systems to assess vessel dimensions [36], this is a complicating feature for the measurement of blood flow. This effect is partially negated by the larger component of parallel conduction contributing to measured impedance which occurs in smaller vessels, which have decreased intrinsic conductivity. Additionally, partial correction of the effect of vessel diameter is achieved in practice by normalizing the sensitivity constant, k_s, to baseline impedance values.

Validation of these approaches to measuring absolute coronary blood flow was performed in four phases [37]. In-vitro studies in arterial phantoms, experimental studies in canine femoral arteries, experimental studies in canine coronary arteries, and clinical studies during coronary angioplasty have been performed. The catheter and guidewire systems were found to accurately measure saline flow in plastic tube phantoms ranging from 2—4 mm diameter, employing baseline impedance corrected sensitivity constants. These data support that the two basic requirements for application of the indicator-dilution principle, namely adequacy of mixing and linearity of indicator detection are met by this technique. The latter was additionally validated by direct measurement of the linearity of the area under first pass curves resulting from injection of from 0.1 to 2.0 ml indicator boluses.

Due to intrinsic limitations of measuring absolute coronary blood flow, validation of the catheter and guidewire systems was performed in canine

femoral arteries used timed arterial collection as the standard. Blood flow was varied over a wide range from 5—300 ml/minute using vessel constriction and vasodilating drugs. Close correlations between catheter and guidewire calculated and timed arterial collection data were found ($r = 0.96$).

Blood flow measurements were also studied in canine coronary vessels ranging in diameter from 2.3—3.3 mm using stenosis and pharmacologically varied blood flow. Again, close correlations were found between impedance catheter and electromagnetic flow-meter determinations over a wide range of flow. A slightly lower correlation coefficient (0.94) was found, likely due to intrinsic inaccuracies in electromagnetic flowmeter determination (Figure 2). Of importance, the injection of the 0.5 ml indicator bolus was found to affect intrinsic blood flow minimally. Several examples of measurements of absolute coronary blood flow first pass impedance curves are shown in Figure 3. Injection of the D5W bolus is seen to cause little change in intrinsic coronary blood flow (top panels). The inverse relationship between blood flow and area under the first-pass curves is seen in the lower panels.

Following successful validation of the impedance catheter in experimental situations, we have started to employ it during clinical angioplasty. Repeated first-pass curves obtained during angioplasty of a mid left anterior descending coronary stenosis are shown in Figure 4. Coronary blood flow was calculated to be approximately 30 ml/min. These findings suggest that it will

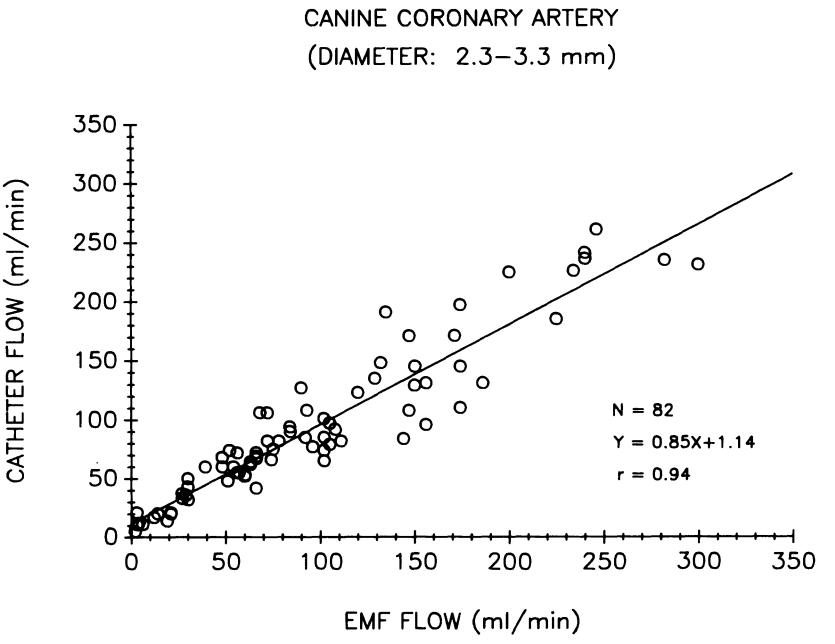

Fig. 2. Correlation between impedance cathether and electromagnetic flowmeter determinations of absolute coronary blood flow in canine model.

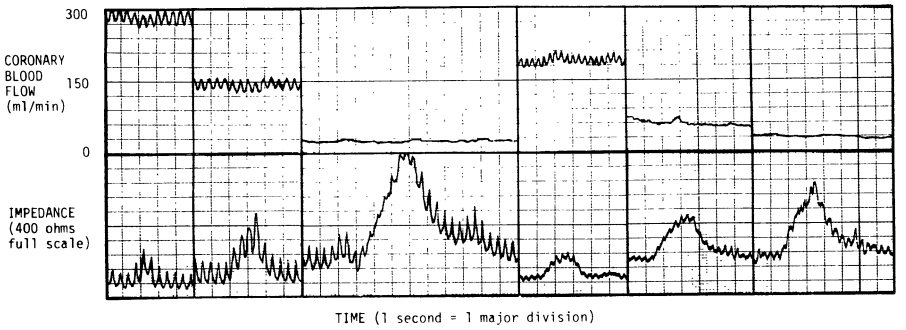

Fig. 3. Examples of coronary blood flow and first-pass impedance curves from which absolute coronary blood flow is calculated, obtained in a canine coronary artery model.

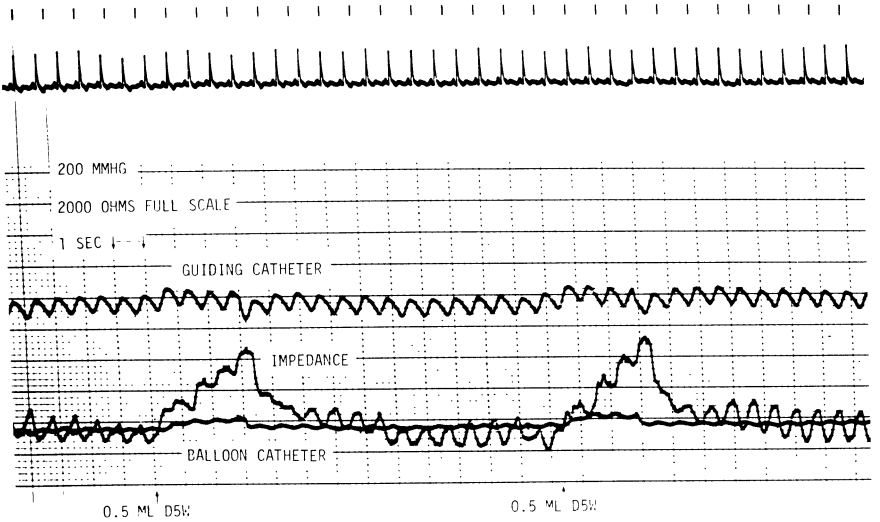

Fig. 4. Examples of first-pass impedance catheter tracings obtained during clinical angioplasty of left anterior descending coronary artery.

be clinically possible to measure absolute coronary blood flow in interventional situations using standard catheter and guidewire systems. It is likely that the impedance guidewire will have the greatest clinical application because it can be used with any over-the-wire system and produces the least compromise of the vessel lumen. We are also currently investigating the impedance guidewire as a means for assessing coronary cross-sectional area [36]. We have observed that passage of the guidewire electrode gap across experimental stenoses results in an abrupt and reproducible increase in baseline impedance. This may allow assessment of interventional success,

although it is not likely that it would provide information on most interventional complications such as dissection.

Technological advances in digital radiographic and catheter systems now allow measurement of relative and absolute coronary blood flow in the catheterization laboratory. It remains to be proven that these measurements affect interventional and clinical patient management. This is likely to occur as techniques become simpler and more refined.

References

1. Vogel RA: The radiographic assessment of coronary blood flow parameters. Circulation 72: 460—465, 1985.
2. Marcus ML: Methods of measuring coronary blood flow. In: The Coronary Circulation in Health and Disease. ML Marcus (Ed). McGraw-Hill Book Company, New York, 1983: 25—64.
3. Hodgson JMcB, Mancini GBJ, LeGrand V, Vogel RA: Characterization of changes in coronary blood flow during the first six seconds after intracoronary contrast injection. Invest Radiol 20: 246—252, 1985.
4. Rutishauser W, Bussmann W-D, Noseda G, Meier W, Wellauer J: Blood flow measurement through single coronary arteries by Roentgen densitometry. Part I. A comparison of flow measured by a radiographic technique applicable in the intact organism and by electromagnetic flowmeter. Am J Roentgenol 109: 12—20, 1970.
5. Rutishauser W, Noseda G, Bussmann W-D, Preter B: Blood flow measurement through single coronary arteries by Roentgen densitometry. Part II. Right coronary artery flow in conscious man. Am J Roentgenol 109: 21—24, 1970.
6. Smith HC, Frye RL, Donald DE, Davis GD, Pluth JR, Sturm RE, Wood EH: Roentgen videodensitometric measure of coronary blood flow. Determination from simultaneous indicator-dilution curves at selected sites in the coronary circulation and in coronary artery-saphenous vein grafts. Mayo Clin Proc 46: 800—806, 1971.
7. Smith HC, Sturm RE, Wood EH: Videodensitometric system for measurement of vessel blood flow, particularly in the coronary arteries, in man. Am J Cardiol 32: 144—150, 1973.
8. Spiller P, Schmiel FK, Pölitz B, Block M, Fermor U, Hackbarth W, Jehle J, Körfer R, Pannek H: Measurement of systolic and diastolic flow rates in the coronary artery system by X-ray densitometry. Circulation 68: 337—347, 1983.
9. Foerster JM, Link DP, Lantz BMT, Lee G, Holcroft JW, Mason DT: Measurement of coronary reactive hyperemia during clinical angiography by video dilution technique. Acta Radiol 22: 209—216, 1981.
10. Elion JL, Nissen SE, DeMaria AN: Functional imaging of coronary flow reserve. Am J Card Imag 1: 103—110, 1987.
11. Crummy AB, Struther CM, Sackett JF, Ergun DL, Shawl CG, Kruger RA, Mistretta CA, Turnipseed WD, Lieberman RP, Myerowitz PD, Ruzicka FF: Computerized fluoroscopy: Digital subtraction for intravenous angiocardiography and arteriography. Am J Radiol 135: 1131—1140, 1980.
12. Myerowitz PD, Turnipseed WD, Shawl C-G, Mistretta CA, Swanson DK, Chopra PS, Berkoff HA, Kronke GM, Dhanani SP, Rowe GG, Van Lysel M, Crummy AB: Computerized fluoroscopy: New techniques for the noninvasive evaluation of the aorta coronary artery bypass grafts, and left ventricular function. J Thorac Cardiovasc Surg 83: 65—73, 1982.
13. Robb RA, Wood EH, Ritman EL, Johnson SA, Sturm RE, Greenleaf JF, Gilbert BK,

Chevalier PA: Three-dimensional reconstruction and display of the working canine heart and lungs by multiplanar X-ray scanning videodensitometry. Comp Cardiol: 151—163, 1974.
14. Vogel R, LeFree M, Bates E, O'Neill W, Foster R, Kirlin P, Smith D, Pitt B. Application of digital techniques to selective coronary arteriography: use of myocardial contrast appearance time to measure coronary flow reserve. Am Heart J 107: 153—164, 1984.
15. Hodgson JMCB, LeGrand V, Bates ER, Mancini GBJ, Aureon FM, O'Neill WW, Simon SB, Beauman GJ, LeFree JT, Vogel RA: Validation in dogs of a rapid digital angiographic technique to measure relative coronary blood flow during routine cardiac catheterization. Am J Cardiol 55: 188—193, 1985.
16. Cusma JT, Toggart EJ, Folts JD, Peppler WW, Hangiandreou NJ, Lee C-S, Mistretta CA. Digital subtraction angiographic imaging of coronary flow reserve. Circulation 75: 461—472, 1987.
17. Zijlstra A, Boer A den, Reiber JHC, Es GA van, Lubsen J, Serruys PW. Assessment of intermediate and long-term functional results of percutaneous transluminal coronary angioplasty. Circulation 78: 15—24, 1988.
18. LeGrand V, Mancini GBJ, Bates ER, Hodgson JMcB, Gross MD, Vogel RA: A comparative study of coronary flow reserve, coronary anatomy and the results of radionuclide exercise tests in patients with coronary heart disease. JACC 8: 1022—1032, 1986.
19. LeGrand V, Hodgson JMcB, Bates ER, Aueron FM, Mancini GBJ, Smith JS, Gross MD, Vogel RA. Abnormal coronary flow reserve and abnormal radionuclide exercise test results in patients with normal coronary angiograms. JACC 6: 1245—1253, 1985.
20. Bates ER, Aueron FM, LeGrand V, LeFree MT, Mancini GBJ, Hodgson JM Vogel RA: Comparative long-term effects of coronary artery bypass graft surgery and percutaneous transluminal coronary angioplasty on regional coronary flow reserve. Circulation 72: 833—839, 1985.
21. Kern MJ, Deligonal U, Vandormael M, Labovitz A, Gudipati CV, Gabliani Gk, Bodet J, Shawl Y, Kenny HL. Impaired coronary vasodilator reserve in the immediate post-coronary angioplasty period: Analysis of coronary flow velocity indexes and regional cardiac venous efflux. JACC 13: 860—872, 1989.
22. Parker DL, Pope DL, Van Bree RE, Marshall H. Blood flow measurements in digital cardiac angiography using 3-D coronary artery reconstructions. In: Progress In Digital Angiography, PH Heintzen, JH Bürsch (Eds.), Kluwer Academic Publishers, Dordrecht, 1988: 215—220.
23. Rutishauser W, Rastib O, Chappuis F, Doriot P-A, Meier B. Coronary blood flow and myocardial perfusion studied by digital coronary arteriograms. In: Progress In Digital Angiography, PH Heintzen, HJ Bürsch (Eds.), Kluwer Academic Publishers, Dordrecht, 1988: 211—226.
24. Eigler NL, Pfaff JM, Whiting JS, Zeiher A, Forrester JS, Swan HJC. Digital angiographic transfer-function analysis of regional myocardial perfusion: Measurement system and coronary transit linearity. In: Progress In Digital Angiography, PH Heintzen, HJ Bürsch (eds.): Kluwer Academic Publishers, Dordrecht, 1988: 265—274.
25. Nissen SE, Elion JL, Booth DC, Evans J, DeMaria AN: Value and limitations of computer analysis digital subtraction angiography in the assessment of coronary flow reserve. Circulation 73: 562—571, 1986.
26. Canon PJ, Dell RB, Dwyer Jr EM: Measurement of regional myocardial perfusion in man with Xenon-133 and a scintillation camera. J Clin Invest 51: 964—977, 1972.
27. Klocke FJ, Koberstein RC, Pittman DE, Bunell IL, Greene DG, Rosing DR: Effects of heterogeneous myocardial perfusion on coronary venous H2 desaturation curves and calculations of coronary flow. J Clin Invest 47: 2711—2724, 1968.
28. Grines CL, Mancini GBJ, McGillem MJ, Gallagher KP, Vogel RA: Measurement of regional myocardial perfusion in mass using subselective hydrogen infusion and washout techniques: A validation study. Circulation 86: 1373—1379, 1987.

29. Ganz W, Tamura K, Marcus HS, Donoso SR, Yoshida S, Swan HJC. Measurement of coronary sinus blood flow by continuous thermodilution in man. Circulation 44: 181—195, 1971.
30. Wilson RF, Laughlin DE, Ackell PH, Chilian WM, Holida MD, Hartley CJ, Armstrong ML, Marcus ML, White CW: Transluminal, subselective measurement of coronary artery blood flow velocity and vasodilator reserve in man. Circulation 72: 82—92, 1985.
31. Sibley DH, Millar HD, Hartley CJ, Whitlow PL: Subselective measurement of coronary blood flow velocity using a steerable Doppler catheter. JACC 8: 1331—1340, 1986.
32. Wilson RF, White CW: Intracoronary papaverine: an ideal coronary vasodilator for studies of the coronary circulation in conscious humans. Circulation 73: 444—451, 1986.
33. Serruys PW, Jullier EY, Zijlstra F, Beatt KJ, Feyter PJ de, Suryapranata H, Brand Mvcn den, Roelandt J: Coronary blood flow velocity during percutaneous coronary angioplasty as a guide for assessment of the functional results. Am J Cardiol 61: 253—259, 1988.
34. Vogel RA, Martin LW, Johnson RA. Impedance measurement of absolute coronary blood flow using a standard angioplasty catheter. Circulation 78: II-413, 1988 (Abstract).
35. Martin LW, Vogel RA, Johnson RA, Englehardt JM, Scott H: Impedance measurement of absolute blood flow using an angioplasty guidewire. JACC 13: 194A, 1989 (Abstract).
36. Vogel RA, Martin LW, Johnson RA: Impedance measurement of absolute arterial diameter using a standard angioplasty catheter. JACC 11: 130A, 1988 (Abstract).
37. Vogel RA, Martin LW: Intraluminal coronary artery devices: impedance catheter and guidewire measurement of absolute coronary blood flow. Texas Heart Inst J (in press).

11. Coronary obstructions, morphology and physiologic significance

RICHARD L. KIRKEEIDE

Summary

The problem of interpreting the physiologic significance of coronary stenoses, i.e. their flow-limiting behavior, from their morphology is reviewed in this paper. This problem is approached from a fluid dynamic viewpoint starting with the observed effects of stenoses on the pressure-flow relations in coronary arteries. Recognizing that stenosis morphology is important physiologically only to extent that it effects the pressure drop-flow relation of stenoses, a theoretic analysis and in vitro stenosis model experiments are described. From these experiments, the pressure drop-flow relations for stenoses of various geometries could be accurately predicted. It is then shown how these predictive relations can be used with standardized hemodynamic test conditions to assess the flow-limiting behavior of stenoses through derivation of the stenosis flow reserve. Finally, the appropriate uses of stenosis flow reserve, its sensitivity to diffuse coronary disease, and the need for measuring the size of the stenosis bed at risk is discussed.

Introduction

Assessing the clinical significance of coronary stenoses remains one of the most common and important exercises in the practice of cardiology. Patients demonstrating symptoms suggestive of significant coronary artery disease are referred by the cardiologist for coronary arteriography. In the subdued light of the viewing room and with the patient's history and symptoms in mind, the cardiologist scans the coronary images looking for, among other things, evidence of coronary disease. Are the coronary vessels smooth and of normal size? Does the dye flow evenly and with normal velocity through the coronary tree? Are all the major coronary vessels apparent? Is there any collaterization between normally distinct perfusion fields? These questions arise because the cardiologist is trying to understand why the patient's symptoms, usually related to poor myocardial perfusion, are occurring. Only

J. H. C. Reiber and P. W. Serruys (eds), Quantitative Coronary Arteriography, 229–244.

after a probable cause of the patient's myocardial problems has been inferred, can the cardiologist consider his therapeutic strategy for the patient.

This admittedly verbose review of the reasons for analyzing a coronary arteriogram was included, prior to discussions of pixels and pressure drops, to underscore that when analyzing the image of a partially blocked coronary artery, it is the possible effect that this stenosis has on myocardial blood flow that is clinically relevant. Assigning clinical significance to any geometric characteristic of the stenosis i.e., its apparent relative diameter reduction, shape or length, can rightfully be done only when the influence of that characteristic on blood flow is understood.

This chapter then describes a brief conceptual tour of how myocardial blood flow is influenced by stenoses by the pressure losses incurred by blood flow thru stenoses, how certain geometric characteristics of stenosis influence pressure losses, and how this understanding of stenosis hydraulics can be merged with quantitative coronary arteriography to rationally describe the flow limiting potential of an angiographically demonstrated coronary stenosis. Included in this tour will be stops to admire the pitfalls and strengths of assessing the physiological significance of coronary stenoses as well as some possible routes for the future.

Effect of coronary stenoses on coronary flow

The effect of stenoses on coronary blood flow is demonstrated in Figure 1, derived from an experiment in which a series of discrete stenoses were produced in the circumflex artery of a dog. The figure plots mean coronary pressure (distal to the stenoses) against the simultaneously recorded mean coronary flow (electromagnetic flowmeter). Without a stenosis (topmost curve with triangles) progressive vasodilation of the distal bed (i.e. adenosine) caused flow to increase from its resting level near 0.3 ml/s to an observed maximum of nearly 3 ml/s, while pressure decreased only slightly (95—90 mmHg) from the aortic pressure level. With a 60% area reduction stenosis, coronary pressure and flow were normal at rest, but moved downwards along the curving pressure-flow relation as the distal bed was progressively dilated. The maximal attainable flow for this stenosis was about 2.5 ml/s with an associated 25 mmHg drop in coronary pressure to 70 mmHg. The 85% stenosis showed the same type of hemodynamic behavior, falling pressure with increased flow, but to a greater degree. Flow in this case could be increased to just over 1 ml/s at the cost of a 50 mmHg pressure drop.

Several important points regarding the influence of stenoses on coronary flow can also be illustrated through Figure 1. Flow changes in a stenosed coronary artery are determined by a host of factors other than the stenosis. Resting conditions for example, were near normal despite the presence of the 60 and 85% stenoses. Only with more severe stenoses did resting coronary pressure significantly drop and then without a concomitant drop in coronary

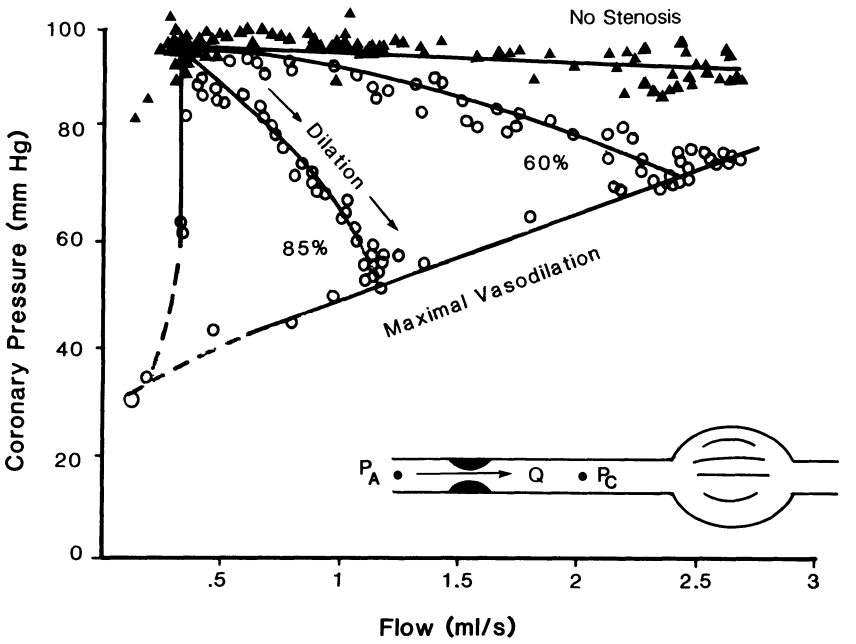

Fig. 1. Effect of stenoses on coronary pressure-flow relations.

flow. Coronary autoregulation was clearly at work in this case. The baroreceptors and resting myocardial oxygen demand also play a determining role in fixing the pressure-flow coordinates of resting conditions (95 mmHg, 0.3 ml/s). The distal coronary bed is also seen to present a flow barrier, in the form of the maximal vasodilation pressure-flow relation, which is independent of stenosis severity. Hemodynamically then, stenoses can be viewed simply as abnormal pressure-flow pathways which must be followed when going from one flow demand state to another. How far along such a path the coronary circulation can travel is largely fixed by nonstenotic factors.

Influence of stenosis geometry on stenosis pressure losses

It should be apparent from the preceding discussion that the ability to assign physiologic significance to a given stenosis morphology must hinge on the ability to derive the pressure drop-flow relation for a stenosis when given its geometric characteristics. Various engineers and physicians have recognized this principle and pursued such understanding. The interested reader would be well advised to review their writings [1—9] since the following can offer only a brief overview of the subject.

The total pressure drop (dP) across moderate to severe stenoses derives largely from two sources: frictional losses along the entrance and throat

regions of the stenosis and inertial losses stemming from the sudden expansion of the flow as it emerges from the stenosis throat. As frictional losses are linearly related to flow and sudden expansion losses scale with the square of the flow, pressure drop can be expressed by the relation

$$dP = C_v Q + C_e Q^2, \tag{1}$$

where C_v and C_e are the viscous and expansion loss coefficients of the stenosis. The curvilinear nature of the drop in coronary pressure with increasing flow seen in Figure 1, graphically reflects this equation with the curvilinear nature of the data demonstrating the presence of the nonlinear inertial losses. An important implication of Equation (1) is that stenosis flow resistance (dP/Q) besides being dependent on stenosis geometry (C_v and C_e) is directly related to flow. In a strict sense therefore, a stenosis physiologic significance cannot be judged solely on the basis of its appearance but rather, only in association with a given flow. Depending on the application, this flow could be either the measured flow through the stenosis or a hypothetical desired flow.

Before addressing this flow problem the dependencies of C_v and C_e on specific stenosis geometries can be suggested by considering the stenosis flowfield shown in Figure 2. As the flow enters the stenosis it accelerates i.e., its velocity profile is axially stretched in direct proportion to the reduction in lumen area. Because of this convective acceleration, pressure falls in the direction of flow due to both conversion of pressure energy to kinetic energy (which can be later converted back to pressure energy) and viscous wall friction (which is permanently lost). This flow field continues through the stenosis with viscous losses accumulating until the flowfield dramatically changes as the flow enters the sudden lumen expansion region at the distal end of its throat. Although the vessel lumen can change abruptly, the flowfield may not be able to follow due to its now large axially directed momentum. If this is the case the flow exits the stenosis as a high velocity jet bounded radially by a recirculation zone or eddy. Due to the large velocity differences across these two flows, shear stresses develop which diffuse the jet and irreversibly deplete the flow's energy. Since the flow separation point marks the boundary between the viscous and expansion flow fields, it also marks the sections along which their accompanying pressure losses must be computed.

By analogy to the viscous pressure losses along pipes, we can expect these losses (dP_v) to be describable by a relation suggested by Young et al. [1—3]

$$dP_v = K_v \frac{\mu}{D_0} V_0 \tag{2}$$

from which C_v is then written

$$C_v = K_v \frac{\mu}{D_0 A_0} \tag{3}$$

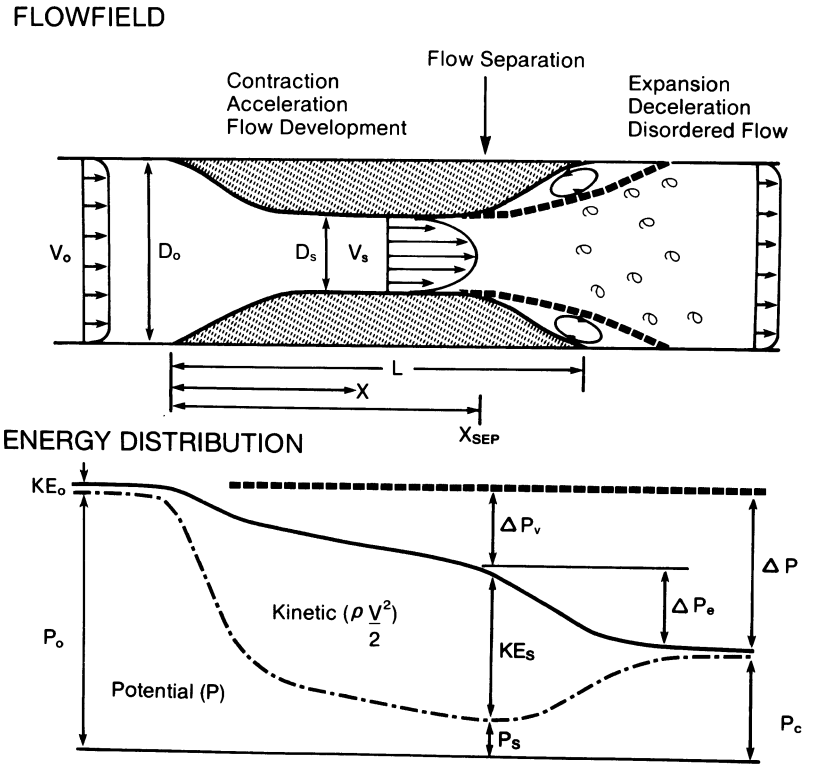

Fig. 2. Generalized flowfield and energy distribution for a stenosis.

where D_0 and A_0 are the proximal normal lumen diameter and area, μ is the blood's absolute viscosity and K_v is a dimensionless coefficient. As cross-sectional area and shape will in general vary along stenoses, K_v needs to be computed by an integral relation. Deriving K_v from the pressure loss equation suggested for use with quantitative arteriography by Brown et al. [9], K_v can be written as

$$K_v = 32 \int \frac{A_0}{A} \left(\frac{D_0}{D'} \right)^2 \frac{\mathrm{d}x}{D_0} \tag{4}$$

where, A and D' are the cross-sectional area and hydraulic diameter at a given position along the stenosis and $\mathrm{d}x$ is the axial spacing between consecutive cross-sectional geometries defined by quantitative arteriography. Integration of Equation (4) then proceeds from the defined proximal normal section to the assumed point of flow separation.

Expansion pressure losses are usually described by equations of the form

$$\mathrm{d}P_e = K_e \left(\frac{A_0}{A_s} - 1 \right)^2 \frac{\rho V_0^2}{2} \tag{5}$$

where A_s and A_0 are the cross-sectional areas along the stenosis at which the flow separates and distally reattaches to the vessel wall respectively, ρ is the blood density (1.0 gm/cm^3) and K_e a dimensionless coefficient whose value is approximately 1. Comparison of Equations (1) and (5) shows C_e to be describable as

$$C_e = \frac{\rho K_e}{2A_0^2}\left(\frac{A_0}{A_s} - 1\right)^2. \tag{6}$$

To compute the pressure drop across a stenosis, Equations (1), (3), (4), and (6) can then be used along with an assumed or measured flowrate Q. Using this technique, Young [1] found that pressure drops across hollowed plugs of known dimension, inserted into the femoral, carotid and aortic arteries of dogs could be predicted within 2.2 mmHg of their measured values. Gould [8] created stenoses in canine coronary arteries by the external balloon technique. Using the Brown method of quantitative arteriography [9], tracing the vessel borders by hand, predicted pressure drops were within +/− 18 mmHg at the 95% confidence level.

While the reported experimental data certainly validate the form of Equations (3), (4), and (6), questions remain regarding their application to the types of stenosis geometries seen in arteriograms. For example, how does the exit geometry of a stenosis influence its pressure drop? The equations for K_v and C_e take no account of exit geometry. Where should the flow separation point be located along a stenosis? Its position is required in Equation (4) as the upper limit for integrating viscous losses along stenoses. When post-stenotic dilatation exists, what is the hemodynamically relevant cross section(s)? Although at present only a couple of these questions can be answered, the use of in vitro model experiment to be discussed offers an efficient and general method of solving these problems.

In vitro studies of predicting stenosis pressure drop from its geometry

Modelling theory has been long used to understand and predict the behavior of structures which are not available for testing themselves e.g., airfoils, racing yachts, skyscrapers, and heart valves. For the purpose of understanding stenosis pressure losses, modelling theory permits us to work with a dimensionless and simplified form of the pressure drop equation i.e.,

$$\frac{\mathrm{d}P}{\rho V_0^2} = \frac{K_v}{\rho D_0 V_0/\mu} + C_e \tag{7}$$

where the equations left-side is the so-called Euler number and describes pressure drop in relation to the flows kinetic energy, and the Reynolds number is recognized in the denominator term on the right-side of the equation. To ensure the clinical applicability of the model experiments, the

Reynolds number of the modelled flow conditions must be within the range for coronary arteries i.e., below 2000.

In the experiments to be discussed, we were curious about the influence of stenosis entrance and exit geometries and lumen cross-sectional shape on the pressure drop. Thus a series of stenosis models were constructed of the general form shown in Figure 3 and placed into a flow apparatus. Flow conditions were then varied and pressure drops measured over the 0-2000 Reynolds number range. Figure 4 demonstrates the results for a 90% stenosis tested in this manner. Values of K_v and C_e where found by fitting the data to the equation form $y = K_v/x + C_e$ where y and x were the measured dimensionless pressure drops and flows respectively.

We first examined the ability of Equation (4) to account for the effects of stenosis length on pressure drop by testing two families of models (90 and 94% area reductions) within which stenosis length (L) was widely varied. As seen in Figure 5, Equation (4) closely accounted for the observed behavior. However a minor "entrance effect" was observed (for short stenoses, the measured viscous losses were higher than predicted) which could be accounted for by modifying Equation (4) slightly i.e.,

$$K_v = 32\left[0.45\,\frac{A_0}{Am}\left(\frac{D_0}{D'm}\right)^2 + 0.86\int\frac{A_0}{A}\left(\frac{D_0}{D'}\right)^2\frac{dx}{D_0}\right] \qquad (8)$$

where Am and $D'm$ are the minimum area and hydraulic diameter along the segment, respectively.

With this correction, the major effects of differing entrance and exit

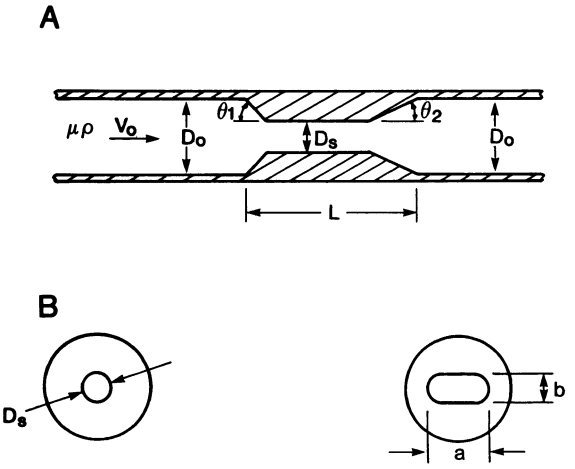

Fig. 3. Geometry for modeled coronary stenoses. (A) Axial geometries; (B) Cross-section geometries.

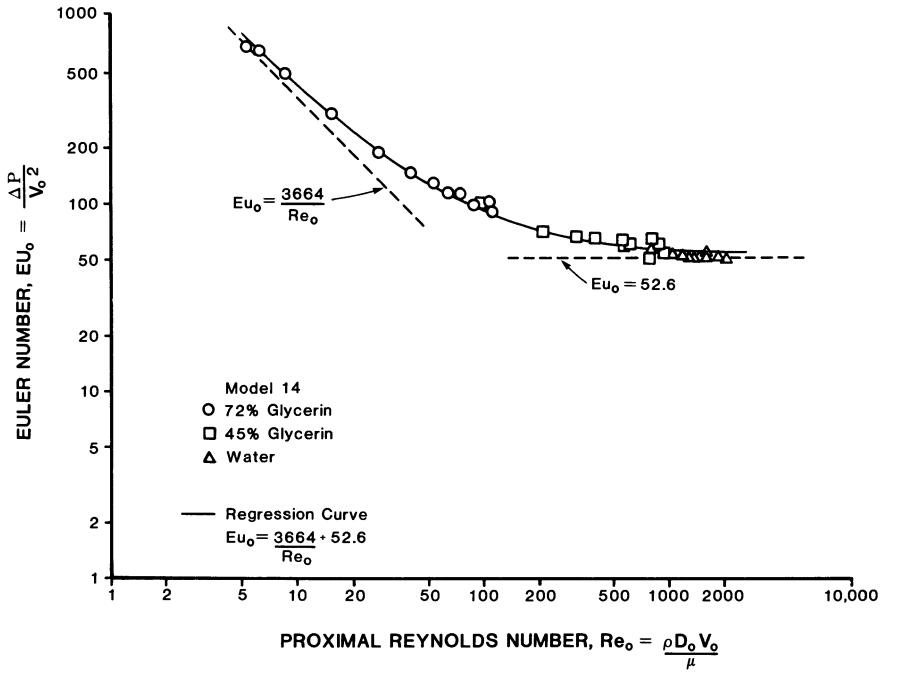

Fig. 4. Pressure drop-flow relation for a 90% stenosis in dimensionless terms. Regression analysis according to form of Equation (7).

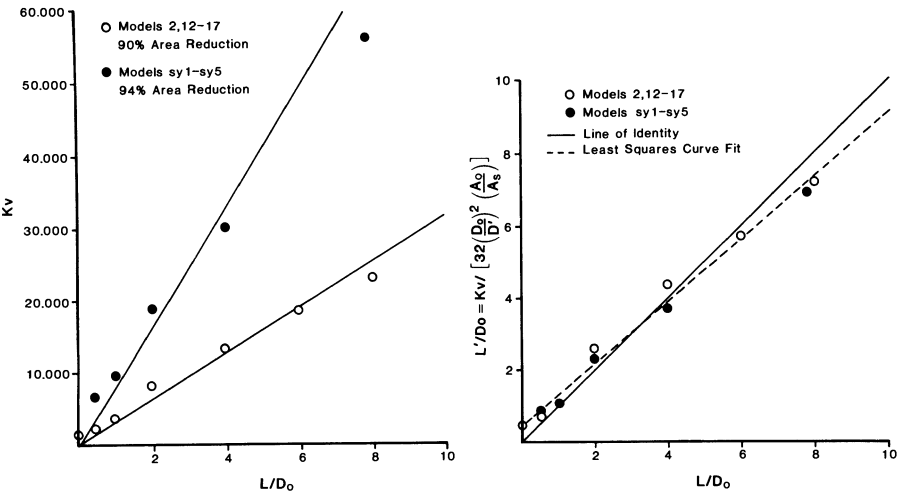

Fig. 5. Effect of area reduction and stenosis length on viscous pressure losses across stenoses. Left panel, correlation of measured values with Equation 4. Right panel, same data following "entrance effect" correction, Equation (8).

geometries could be predicted as shown in Figure 6. As the entrance or exit angle of the stenoses increased (making the stenosis a more abrupt contraction) viscous losses increased. Predicting these effects by Equation (8) required only that the flow separation point be located at that point along the stenosis where the stenosis started to expand. As stenosis exit angles down to 18 degrees behaved in a similar manner, we now locate the flow separation point along a coronary stenosis at that point where the lumen expansion angle first exceeds 18 degrees.

Stenosis length, measured to the point of flow separation, was found to have a significant effect on the expansion pressure losses as demonstrated in Figure 7. The expansion loss coefficient, K_e, was seen to increase linearly with stenosis length as described by the regression formula

$$K_e = 1.21 + 0.08\,(L/D) \tag{9}$$

where L is the length of the stenosis to the flow separation point.

The reason for the length's influence on expansion pressure losses is not completely understood. However, it can be shown theoretically that depending on the shape of the velocity profiles at the points of flow separation and distal reattachment, K_e could vary from 1 to 2. The lower value being found when the velocity profiles are flat at both locations, while the higher K_e value results when the velocity profile at separation is fully-developed but flat at reattachment.

Finally we examined the influence of lumen cross-sectional shape on stenosis pressure drop. As demonstrated in Figure 8, measured viscous losses could be closely predicted by Equation 8, regardless of whether the cross-section was circular or oval (major-to-minor diameter ratios between 1

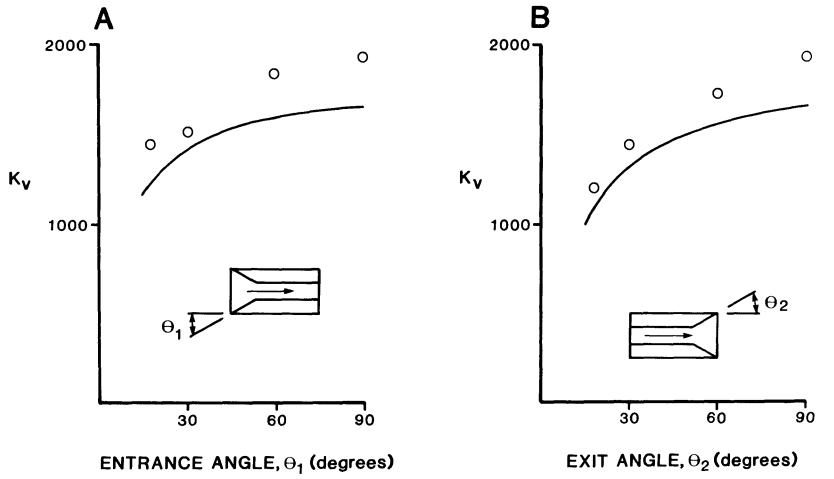

Fig. 6. Influence of entrance and exit geometries (Panels A and B) on viscous pressure losses. Solid lines indicate values predicted by Equation (8).

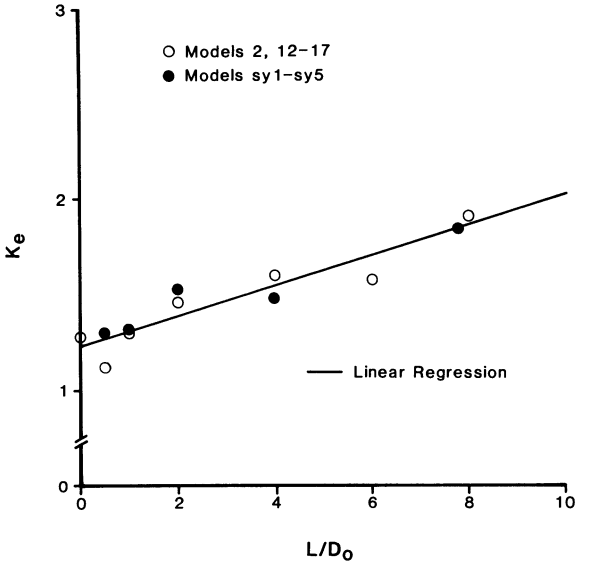

Fig. 7. Expansion losses increase linearly with stenosis length. Linear regression results shown in Equation (9).

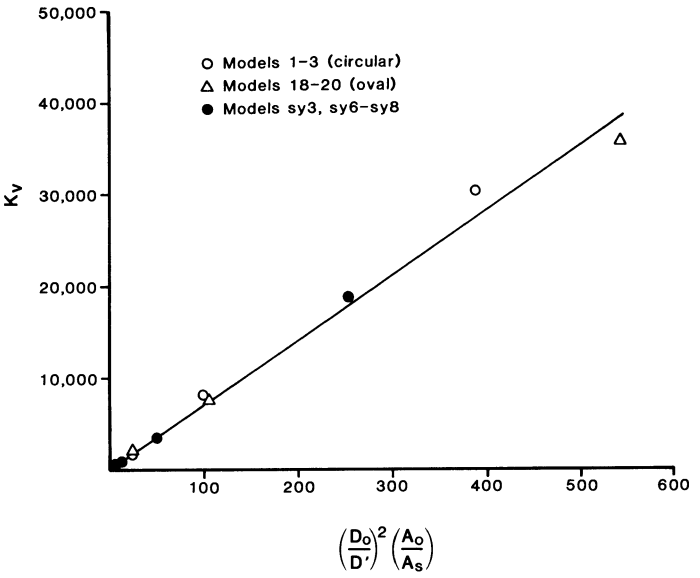

Fig. 8. Influence of cross-sectional shape and area reduction on viscous pressure loss coefficient K_v.

and 3). This result provides a positive check on the use of the hydraulic diameter (D') to account for non circular cross sections. Cross-sectional shape had no apparent effect on expansion pressure losses.

Figures 9 and 10 show the predicted-to-measured correlations for the coefficients K_v and C_e. Considering the data from all model experiments these modified equations predict within 5% the experimentally measured values of any stenosis geometry, as demonstrated in these figures.

We now have the means for translating the geometric characteristics of a coronary stenosis to its pressure drop-flow relation. Figure 9 shows that for the broad range of stenosis geometries considered, the K_v value of the stenosis can be accurately predicted by use of Equation (8). Only in the case of mild stenoses does the uncertainty in predicting K_v reach a significant level but only as a percent error of small absolute pressure drops. The viscous coefficient (C_v) in the stenosis pressure drop relation, Equation (1), is found via Equation (3) when given the assumed blood viscosity (4 centipoise) and the normal diameter and area of the vessel. The expansion loss coefficient was similarly found to be predictable by use of Equations (6) and (9) as shown in Figure 11. Implementing these equations for use in the analysis of coronary arteriograms then requires the extraction of the vessel diameters and areas along the stenotic segment in absolute (cm) terms. For this purpose quantitative arteriographic methods, similar to those originally proposed by

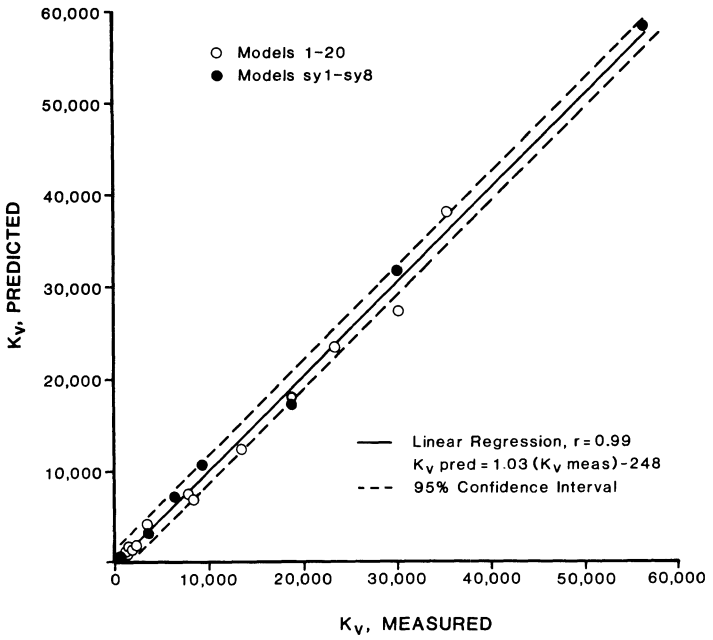

Fig. 9. Correlation of predicted to measured K_v values. K_v predicted by Equation (8).

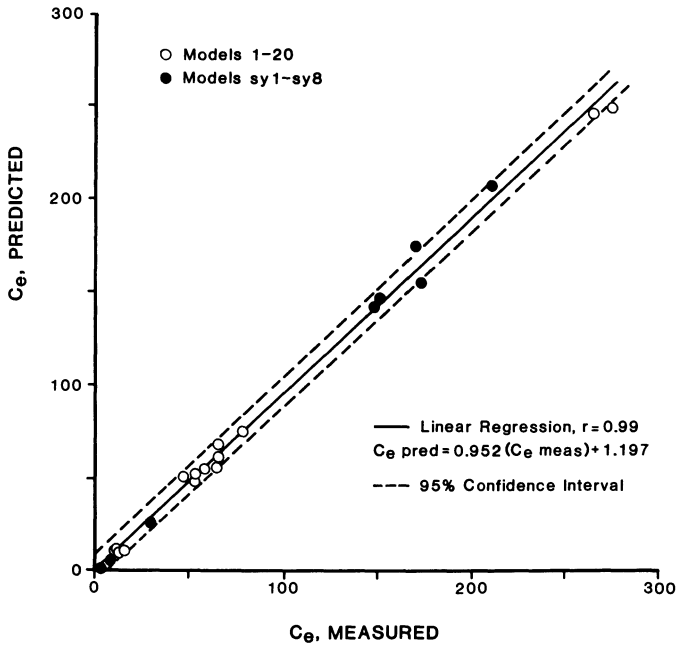

Fig. 10. Correlation of predicted to measured C_e values. C_e predicted by Equations (6) and (9).

Brown et al. [9] with the exception of the use of automatic vessel border recognition, have been implemented. A detailed description of these methods has been presented by Buchi et al. [10] From the extracted major and minor diameters ($d1$ and $d2$) found from the border recognition of biplane views of the stenosis, the cross-sectional area and hydraulic diameter at each increment along the vessel is computed by the relations

$$A = 0.7854\,(d1)\,(d2)$$

and

$$D' = \frac{2\,(d1)\,(d2)}{d1 + d2}.$$

Stenosis flow reserve

Having traveled along coronary pressure-flow curves, within stenosis flowfields, and seen how formulas have been developed to express the pressure drop-flow relation of a stenosis from its geometry, the problem is now how to express such information in a clinically meaningful way. Stating the viscous and expansion loss coefficient values for a stenosis would be likely greeted by

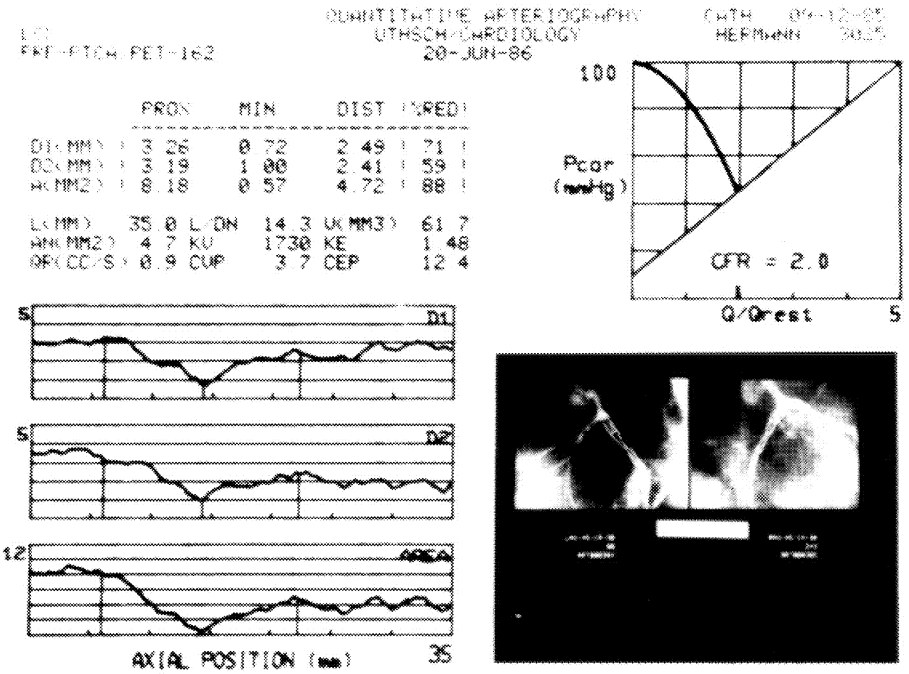

Fig. 11. Quantitative analysis of biplane views of a stenosis, prior to angioplasty, in the left circumflex coronary artery.

blank stares from most physicians. More importantly, such data would not clearly suggest the physiologic significance of the stenosis i.e., its potential flow-limiting effects. To overcome this problem, we developed the idea of stenosis flow reserve as a standardized test of the flow-carrying capacity of coronary stenoses.

Stenosis flow reserve derives from the concepts discussed with Figure 1. However, in place of measured values for resting pressure and flow, and the maximally vasodilated pressure-flow relation assumed values (ml/s) we chose to use resting relative flow so that the results would be akin to the coronary flow reserve which is generally understood by cardiologists. The specific hemodynamic assumption made in deriving stenosis flow reserve is: aortic pressure equals 100 mmHg, the maximally vasodilated pressure-flow relation for the distal bed goes from 0 relative flow at 10 mmHg to 5 times resting flow at 100 mmHg. The final and most important assumption is that of the resting coronary flow level. Realizing that volumetric flow rates vary widely depending on the size of the dependent myocardial bed but that resting flow velocity is roughly independent of normal vessel size, ranging from 10—20 cm/s for coronaries of the aorta, we derive resting flow as the product of

resting flow velocity times the normal cross-sectional area of the arterial segment under study.

Figure 11 shows the stenosis flow reserve concept applied to a moderately severe stenosis in a left circumflex coronary artery. Included in the report are the geometric characteristics of the analyzed arterial segment and stenosis e.g., the stenosis caused an 88% area reduction with a minimal area of 0.57 mm^2. Integrating the geometry between the indicated proximal and distal limits by Equation (10) and (9), K_v and K_e were found to be 1730 and 1.48 respectively. Shown in the upper right corner of the report is the derivation of the stenosis flow reserve for this stenosis, 2.0. Thus, for these conditions, this stenosis reduces arterial flow capacity to 40% of normal. In this analysis Vo was assumed to be 20 cm/s and the resting flowrate then equals Vo times the designated normal area. For the example shown in Figure 11, the distal end of the stenosis was taken to be normal (0.047 cm^2) and the normal resting flowrate of 0.94 cc/s is derived.

Stenosis flow reserve . . . strengths and weaknesses

The strengths and weaknesses of stenosis flow reserve stem from the same facts: it views only one small piece of the coronary circulation, and only under a fixed set of standardized hemodynamic conditions. Given these facts, one would expect good correlations between the derived stenosis flow reserve and in vivo measurements of coronary flow reserve only when the assumed conditions are close to those in vivo. In animal experiments constrained to provide such similarities, stenosis flow reserve was closely correlated to flowmeter measured coronary flow reserve [11]. In any more complicated situation, e.g., serial stenoses along an artery, CAD with hypertension, or CAD with reduced distal vasodilatory capacity, correlations between stenosis flow reserve and any in vivo measured flow reserve index should not be expected. Since in vivo flows are responsive to so many hemodynamic factors, their values are representative of the coronary system as-a-whole rather than any one factor. Obviously such system measures have great value in diagnosing whether or not a problem exists in the delivery of flow through an artery or to a defined region of myocardium. They cannot however be logically considered as specific to the cause of the flow delivery problem. Stenosis flow reserve in viewing only a 2—3 cm section of coronary artery is fundamentally constrained to stating whether or not that section of artery can be a cause of the flow delivery problem.

A true potential weakness of stenosis flow reserve stems from its dependency on normal resting flowrate and our present methods by which it is inferred. Next to the relative area reduction caused by a stenosis, resting flowrate is the most important factor determining the stenosis flow reserve value. This sensitivity results from the fact that stenosis pressure drop is dependent on the square of the flowrate as seen in Equation (1). We presently depend on being able to identify in the arteriogram a normal

section of segment under analysis, and thereby the vessel's normal cross-sectional area and resting flowrate. Marcus has however repeatedly warned that what appears to be a normal coronary artery is often in fact diffusely diseased [12]. In such cases, the assumed normal area and resting flowrate would both be lower than true normal values and stenosis flow reserve would then be artificially high, underestimating the physiologic significance of the stenosis.

The potential problem associated with diffuse coronary disease points to the need for an alternate means for assigning an appropriate resting flow rate for the segment understudy. In vivo measurement of flow would certainly be useful in this regard so long as the resting conditions were "normal". Such a flow measurement could possibly be made from a coupling of quantitative arteriography techniques with an intracoronary Doppler measurement of flow velocity. Quantifying the angle of the doppler catheter with respect to the flow axis would permit conversion of the perceived Doppler frequency to units of velocity. Measurement of the vessel area at the point of the Doppler cathether could then permit calculation of the volumetric flowrate in absolute terms. Another approach to deciding on the appropriate resting flowrate for an artery would look to the size of the dependent myocardial bed. If the mass of the distal bed would be known, and a resting myocardial flow value is assumed (e.g. 100 ml/min/100 gm) or measured, the resting flowrate which the bed "demands" from the artery could be found.

Conclusion

I have attempted in this review to outline my ideas and working strategy in dealing with the assessment of coronary stenoses. Although a fluid dynamics approach to the problem may seem complicated and inappropriate to some, blood is after all an incompressible fluid and thus subject to the physical principles and laws governing the flow of all such fluids. These principles in fact simplify matters by providing an analysis framework by which the various anatomic characteristics of stenoses can be logically combined into a single physiologic measure of stenoses. Certainly much can be done to improve such fluid dynamics views of stenoses. For example, we need to understand how bifurcations, edge roughness and post-stenotic dilation influence the stenosis flowfield and thus its pressure-flow characteristics. The availability of moderately-priced flow visualization software may be of value for understanding these effects. More pressing, however, is the need to know the size of the myocardial bed downstream of stenosis. Such information would more easily permit us to decide whether the structure of a coronary stenosis seen in an arteriogram is consistent with its functional imperative, the delivery of blood to the downstream bed. Finally, although not much has been explicitly said concerning quantitative arteriography in this review, the hemodynamic interpretations of stenosis geometry outlined here could

clearly not have been performed without QCA. For both acquiring the detailed description of stenosis geometry in absolute dimensions and for interpreting these data, QCA is required.

References

1. Young DF, Cholvin NR, Roth AC: Pressure drop across artifically induced stenoses in the femoral arteries of dogs. Circ Res 36: 734—785, 1975.
2. Seeley BD, Young DF: Effect of geometry on pressure losses across models of arterial stenoses. J. Biomechanics 9: 439—448, 1976.
3. Young DF, Cholvin Nr, Kirkeeide RL, Roth AC: Hemodynamics of arterial stenoses at elevated flow rates. Circ Res 41: 99—107, 1977.
4. Gould KL: Pressure-flow characteristics of coronary stenoses in unsedated dogs at rest and during coronary vasodilation. Circ Res 43: 242—253, 1978.
5. Mates RE, Gupta RL, Bell AC, Klocke FJ: Fluid dynamics of coronary artery stenosis. Circ Res 42: 152—162, 1978.
6. Lipscomb K, Hooten S: Effect of stenotic dimensions and blood flow on the hemodynamic significance of model coronary arterial stenoses. Amer J Cardiol 42: 781—792, 1978.
7. Young DF: Fluid mechanics of arterial stenoses. J Biomedical Eng 101: 157—175, 1979.
8. Gould KL, Kelly KO, Bolson EL: Experimental validation of quantitative coronary arteriography for determining pressure-flow characteristics of coronary stenosis. Circulation 66: 930—936, 1982.
9. Brown BG, Bolson E, Frimere M, Doge HT: Quantitative coronary arteriography: estimation of dimensions, hemodynamic resistance, and atheroma mass of coronary artery lesions using the arteriogram and digital computation. Circulation 55: 329—337, 1977.
10. Büchi M, Hess OM, Kirkeeide RL, Suter T, Muser M, Osenberg HP, Niederer P, Anliker M, Gould KL, Krayenbühl HP: Validation of a new automatic system for biplane quantitative coronary arteriography. Int J Cardiac Imaging, 1990 (in press).
11. Kirkeeide RL, Gould KL, Parsel L: Assessment of coronary stenoses by myocardial perfusion imaging during pharmacologic coronary vasodilation. VII. Validation of coronary flow reserve as a single integrated functional measure of stenosis severity reflecting all its geometric dimensions. J Am Coll Cardiol 7: 103—113, 1986.
12. Marcus ML, Harrison DG, White CW, McPherson DD, Wilson RF, Kerber RE: Assessing the physiologic significance of coronary obstructions in patients: importance of diffuse undetected atherosclerosis. Prog CV Dis 31: 39—56, 1988.

12. Application of indicator dilution principles to regional assessment of coronary flow reserve from digital angiography

STEVEN E. NISSEN and JOHN C. GURLEY

Summary

Although cineangiography is widely utilized to assess the severity of coronary artery disease, conventional arteriography exhibits intra- and interobserver variability and provides no information regarding flow characteristics. We have investigated application of indicator-dilution principles to computer analysis of digital subtraction angiography (DSA) as a means to calculate coronary flow reserve (CFR). Using a background-corrected epicardial coronary region of interest, CFR is directly proportional to the ratio of the quantity of contrast administered under hyperemic and basal conditions, and inversely proportional to the area under the contrast time curve. Utilizing this indicator-dilution algorithm, normal canine coronaries exhibit a CFR ratio exceeding 4:1. In the presence of artificially induced stenoses, we compared the indicator-dilution method to surgically implanted electromagnetic flow (EMF) probes and found a good correlation between DSA and EMF, CFR, $r = 0.86$.

Initial studies utilized a single frame per cardiac cycle which provided inadequate temporal resolution for slow heart rates. The method was subsequently modified to utilize 30 frames per second ECG-gated DSA and hand injection of contrast. A separate validation study showed close correlation in the animal model between CFR measured by DSA and EMF probe, $r = 0.86$. We subsequently investigated this method in 21 patients (35 vessels). Normal CFR in seven patients without stenoses was 4.8:1 $\pm$ 0.65. Patients with unstable angina had much lower flow reserve averaging 1.7 $\pm$ 0.3. Angioplasty generally improved CFR. We have recently applied the indicator-dilution method to calculation of absolute coronary blood flow (CBF), in an animal model. In this application, we used paired injections of contrast, one in the left ventricle (30 to 40 ml) and a second subselectively in the coronary. By comparing the area under these two epicardial contrast intensity curves, the proportion of cardiac output perfusing the coronary could be calculated. CBF was calculated by measuring total cardiac output

J. H. C. Reiber and P. W. Serruys (eds), Quantitative Coronary Arteriography, 245–263.

using a thermodilution catheter. A close correlation between EMF and DSA was confirmed, $r = 0.89$.

These data indicate that an indicator-dilution model can be applied to contrast injection in the coronary arteries and CFR or CBF can be calculated accurately in both an animal model and in a patient population. Further investigations will be required to determine the clinical utility of these findings.

Introduction

Cineangiography is universally utilized to assess the severity of coronary artery disease (CAD) and to guide therapy in patients with coronary obstructions. However, the accuracy of conventional arteriography in accurately depicting the severity of CAD has been seriously questioned. There is significant intra- and interobserver variability in the interpretation of coronary angiograms and pathological studies have demonstrated that angiographic estimates of coronary obstruction do not necessarily correspond to subsequent pathologic examination [1—3].

Traditionally, the severity of a stenosis is reported as percent reduction in luminal area. However, this measurement is significantly influenced by overlapping vessels, collateral blood flow, and angle-of view [4,5]. Furthermore, many patients with coronary artery disease have diffuse vessel involvement with focal stenoses superimposed upon a generalized narrowing. In this setting, percent luminal area reduction cannot accurately reflect the severity of the disease.

Even when conventional coronary arteriography is accurate in classifying the severity of stenoses, arteriography provides no data regarding functional consequences of obstructive lesions. There is a nonlinear relationship between percent luminal reduction and functional impairment which further complicates accurate visual interpretation of films [6]. Thus, percent stenosis alone, measured by quantitative angiography or assessed by visual inspection of coronary angiograms, is an unreliable means to determine the physiology of coronary obstruction and a limited standard upon which to base therapeutic decisions.

Perhaps of even greater significance, the angiographic luminal reduction associated with coronary stenotic lesions does not predict the decrease in either resting coronary blood flow or coronary reserve capacity produced by the lesion [7]. A major reduction in coronary hyperemic flow reserve does not occur until approximately 75% cross-sectional reduction is reached. Between 75 and 90% luminal area reduction, coronary flow reserve declines from near normal to very low levels in a curvilinear fashion. Thus, a very small change in luminal diameter can have enormous physiological consequences.

Accordingly, considerable effort has been undertaken to utilize the coronary angiogram to extract physiological information. Using either cine-angiography or digital subtraction angiography, a variety of algorithms have been proposed for the assessment of coronary flow reserve from coronary images. Each method has inherent value and nearly all techniques have significant limitations. We have extensively evalutated methods based upon indicator dilution theory to determine the value and limitations of this approach.

Coronary flow reserve

In comparison to anatomic assessment of coronary stenoses, measurement of coronary hyperemic flow reserve (CFR) has many potential advantages. Coronary flow reserve is defined as the ratio of maximal coronary flow produced by ischemic or pharmacologic stimuli compared to resting flow measured under basal conditions. In the absence of epicardial coronary stenoses, normal dogs or man exhibit flow reserve ratios generally exceeding 4:1 and can range as high as 7 or 8:1. The introduction of epicardial coronary stenoses has been shown to blunt the hyperemic response and thus a reduction in coronary reactive hyperemia represents an excellent physiological descripter of significant coronary lesions [8].

A major consideration in the development of digital angiographic methods for the assessment of coronary flow reserve was the development of an adequate means by which to induce maximal arteriolar vasodilation within the coronary resistance vessels. Initial studies in many laboratories utilized temporary coronary occlusion in the dog to induce reactive hyperemia. Since coronary occlusion was not suitable for use in man, other methods have evolved. These have included the use of radiographic contrast and more recently, the intracoronary administration of papaverine hydrochloride to produce maximal reactive hyperemia [9]. Intracoronary papaverine is a superior method for induction of hyperemia, since it produces a prompt near-maximal increase in coronary flow with a duration that persists only a few minutes.

Although coronary flow reserve is an excellent predictor of the physiological consequences of epicardial stenoses, flow reserve has its own inherent limitations. Since flow reserve is a ratio of maximal hyperemic-to-basal flow, the method is sensitive to any condition which increases basal flow. It is well established that tachycardia, ventricular hypertrophy, and factors affecting the metabolic state of the myocardium can alter basal flow. Under conditions of increased basal flow, the ratio of maximal hyperemic-to-basal flow will be decreased even in the absence of an epicardial lesion. The presence of confounding variables which elevate basal flow must be considered in any clinical setting in which coronary flow reserve is utilized as an indicator of the severity of coronary disease.

Indicator-dilution method

Theoretical principles

One approach to determine the coronary flow reserve from digital angiography is based upon the mathematical principles of indicator-dilution theory. The equations describing the behavior of tracer substances were originally published in the 1920's and are also known as the Stewart-Hamilton method. The principles have been extensively studied for indicators such as indocyanine green or iced saline. In digital angiography the indicator is radiographic contrast media. However, instead of sampling the indicator directly, the brightness of contrast for a region of interest (ROI) in the coronary image is utilized to determine the relative concentration of iodine present in the vessel. Indicator-dilution theory predicts that the area under a density-time curve derived from a coronary ROI will be directly proportional to the quantity of contrast injected and inversely proportional to the flow (Figure 1).

Unlike other indicators, absolute volumetric flow cannot be calculated from a density-time curve using radiographic contrast because the density of the region of interest is affected by other parameters, specifically, radiographic factors such as kVp and patient thickness. However, if a known quantity of contrast is administered under two different flow states and if both the radiographic technique and the ROI analyzed are unchanged, then the ratio of the area under these two time intensity curves will reflect relative flow.

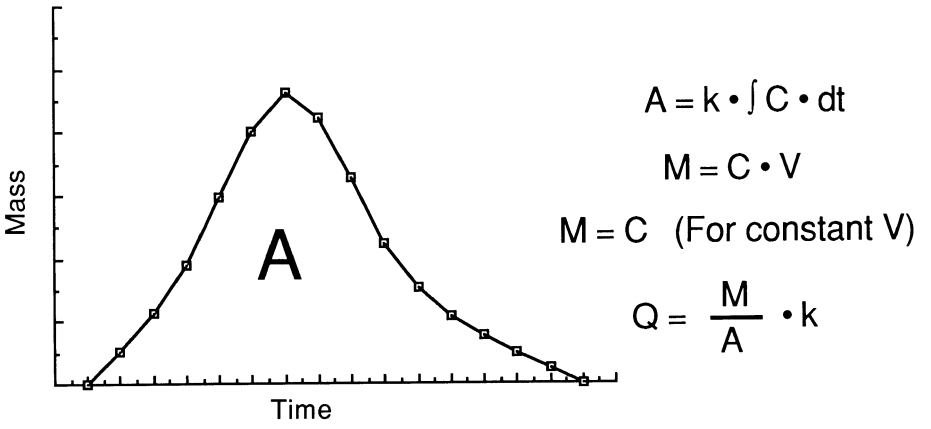

Fig. 1. Mathematics of the indicator-dilution method as applied to radiographic images. The area (A) of a concentration (C) — time (t) curve is utilized to calculate flow. When radiographic images are analyzed, a region of interest is placed over a coronary segment of constant volume (V) and the mass of contrast (M) measured from the brightness of the image. In radiographic imaging, the absolute flow cannot be measured using a concentration — time curve, since the radiographic factors (K) cannot be measured.

This principle is applicable to measurement of coronary flow reserve. Time-density curves are obtained during basal and hyperemic conditions using a constant region-of-interest. Since the area under the curve is inversely related to flow, the ratio basal area divided by hyperemic area represents coronary flow reserve. The factors related to radiographic technique cancel as long as X-ray parameters are kept constant. This method is schematically illustrated in Figure 2. This indicator-dilution method was first applied in the calculation of coronary flow reserve by Forrester et al. [10] and has been subsequently evaluated in our laboratory both in an animal model of coronary artery disease and in man.

Indicator-dilution assumptions

There are several theoretical aspects of the Stewart-Hamilton method which must be considered in its application to radiographic contrast. The classic indicator-dilution equations assume that there is a linear relationship between the concentration of the indicator and its measured quantity. This

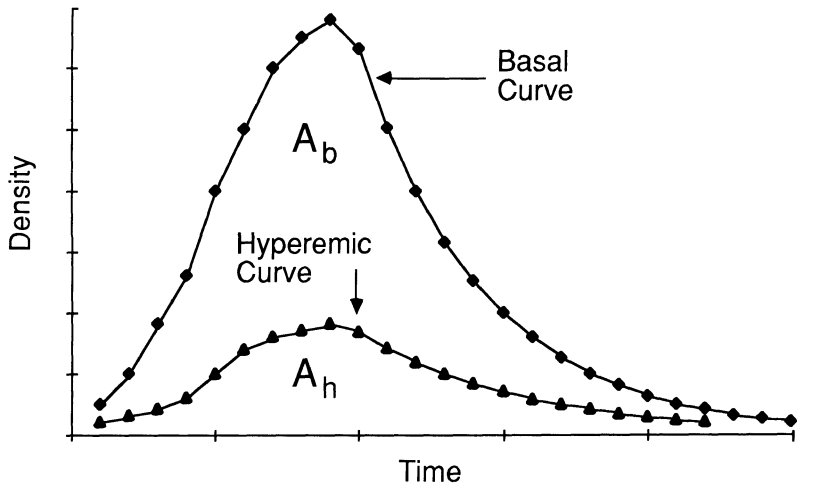

$$CFR = \frac{A_b}{A_h} \times \frac{M_h}{M_b}$$

Fig. 2. Method for calculating coronary flow reserve from a pair of density-time curves. Coronary flow reserve (CFR) is directly proportional to the area under the basal density time curve (A_b) and the volume or mass of contrast injected (M_h) under hyperemic conditions. CFR is inversely proportional to the area under the density-time curve obtained under hyperemic conditions (A_h) and volume or mass of contrast injected under basal conditions (M_b).

assumption is not correct for iodinated contrast since radiographic absorption varies logarithmically with the density or thickness of any absorbing material. This principle is known as the Beer-Lambert law. Thus, a logarithmic transformation is required for digital subtraction angiography prior to application of indicator-dilution analysis. In some settings, a simple logarithmic transformation may not prove adequate since distortions of the density-absorption relationship may result from factors such as scatter and veiling glare. These nonlinearities must be corrected for some critical applications. In the studies described in this review, scatter and veiling glare were minimal factors because the subtraction process attenuates such nonlinearities because they are present both in the mask and contrast frames.

The use of radiographic contrast as an indicator for calculation of coronary flow reserve makes several important assumptions. It is assumed that the quantity of indicator delivered is small compared to the volumetric flow in the coronary. An additional assumption is that mixing in the coronary is complete prior to contrast arrival at the site where densitometry will be performed. In each case, these assumptions can be satisfied with close attention to experimental methodology.

Validation of indicator-dilution methods

Experimental design

We have validated the application of indicator-dilution methods to calculate coronary flow reserve from digital angiography in an animal model of coronary artery disease [11]. Nine dogs were instrumented with an electromagnetic flow probe (EMF) and two pneumatic occluders on the left circumflex coronary artery. The circumflex was subselectively cannulated with a 5 French catheter. Digital angiography was performed under basal conditions and repeated following the induction of reactive hyperemia produced by a 15 second coronary occlusion. Stenoses were produced by partial inflation of one of the pneumatic occluders. For each level of stenosis, digital subtraction angiography was performed under both basal conditions and following induction of hyperemia. For each level of stenosis, simultaneous electromagnetic flow (EMF) was recorded during the digital imaging acquisition.

Data analysis

The ratio of hyperemic-to-basal coronary blood flow by EMF was measured by planimetry of the continuous flow tracings. The digital coronary angiograms were subjected to ECG-gated mask-mode subtraction using only end-diastolic frames. Thus, digital subtraction was performed in a phasic manner in which an end-diastolic mask was subtracted from each end-diastolic image to obtain a series of apparently stationary frames. Density-time curves for

two ROI's were analyzed, one placed over the proximal epicardial coronary artery and a second ROI placed over the adjacent myocardium (Figure 3). For each end-diastolic image, summated intensity value for the myocardial background ROI were subtracted from the coronary ROI values to obtain a difference curve. This correction was necessary because myocardial density begins to appear during the later phases of coronary epicardial opacification. Thus, the coronary ROI contains density attributable both to contrast in the coronary artery and to the opacification of underlying myocardium.

Coronary flow reserve was computed from digital angiography by measuring the area under the curve obtained under basal conditions and dividing this value by the area under the curve obtained under hyperemic conditions. Representative pairs of background corrected density-time curves are illustrated in Figure 4. In the absence of stenosis, the area under the density-time curve obtained during basal conditions was much larger than a similar curve obtained during post-occlusion hyperemia. In the presence of a critical stenosis, there is no increase in blood flow following temporary occlusion and the difference in curve area is completely blunted.

In this study, the hyperemic-to-basal flow ratios obtained by electromagnetic probe were compared to similar measurements performed by digital angiography. The comparison was performed for a wide range of pneumatic coronary stenoses varying from approximately 25 to 90% stenosis.

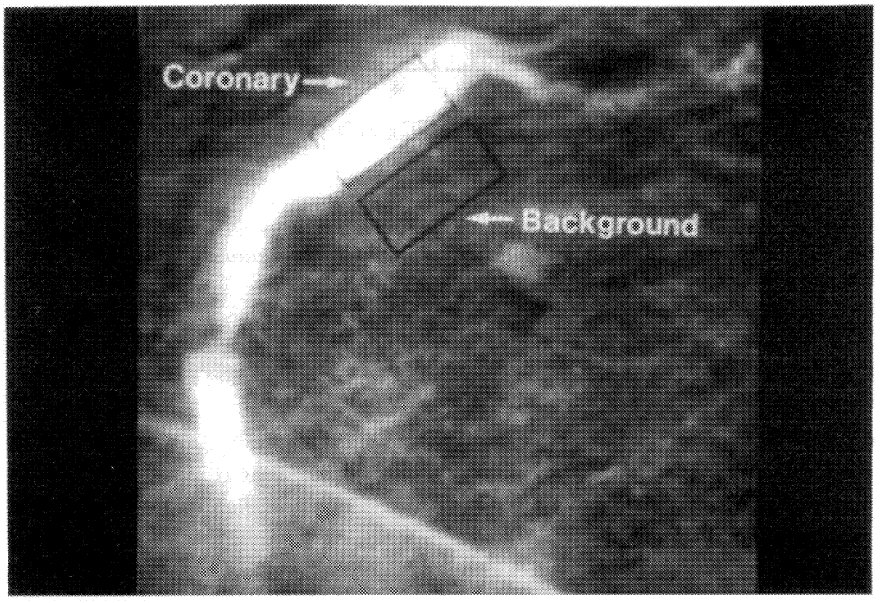

Fig. 3. Location of coronary and background regions of interest for indicator-dilution analysis of coronary flow reserve.

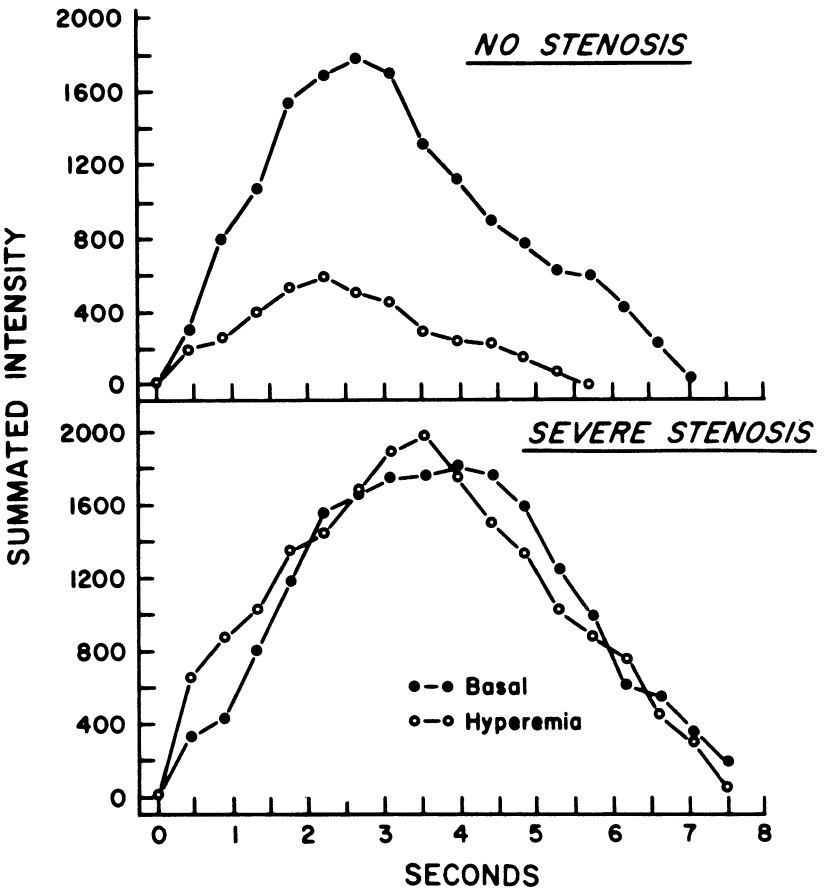

Fig. 4. Coronary density-time curves under basal and hyperemic conditions in the presence of no stenosis (top panel) and in the presence of a severe stenosis (bottom panel). The presence of a severe stenosis blunts the development of hyperemia in response to temporary coronary occlusion. As a result, the area under the basal and hyperemic curves is similar under both basal and hyperemic conditions when a severe stenosis is present.

Results

A total of 38 stenoses were evaluated in which the range of values for the ratio of hyperemic-to-basal coronary flow by EMF was 0.8:1 to 4.2:1. Thus, coronary stenoses with a broad spectrum of physiological significance were evaluated. CFR computed by indicator-dilution analysis using the ratio of areas of background corrected density-time curves varied from 0.9:1 to 4.5:1. Comparing coronary flow reserve measured from the EMF probe with CFR calculated from digital angiography, there was a close correlation between these two methods (Figure 5). The correlation coefficient was $r = 0.86$ and

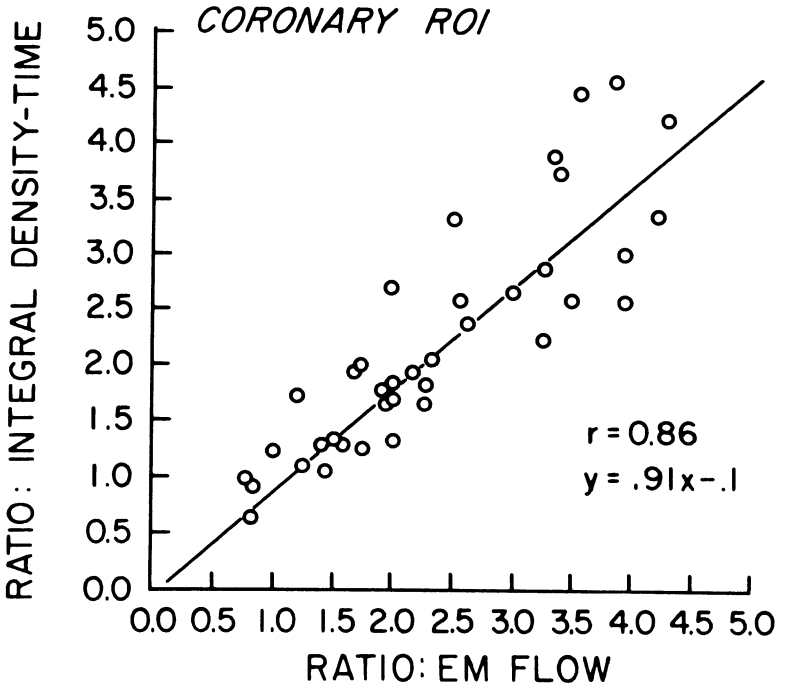

Fig. 5. Linear regression analysis comparing coronary flow reserve ratio measured by electromagnetic flow (horizontal axis) with flow reserve measured as the integral from digital angiography of background corrected density-time curves obtained under basal and hyperemic conditions from a coronary region of interest (vertical axis).

the regression equation was close to the line of identity $y = 0.91x - 0.1$. These data demonstrate that in an animal model of coronary artery disease, indicator-dilution analysis of digital subtraction angiography can yield highly accurate measurements of CFR.

Limitations

Several limitations were apparent from these initial studies. Subselective cannulation of the coronary artery was required since indicator dilution theory requires injection of precise quantities of contrast to be injected in the analyzed vessel. Any spillage of contrast media into adjacent vessels or the aorta renders the indicator-dilution method inaccurate, because the area under the density-time curve is directly proportional to the volume of contrast administered. An additional limitation is the requirement of the digital subtraction process for close registration of mask and contrast end-diastolic images. Thus, body movement or respiratory motion can significantly degrade the quality of the subtraction process and subsequent density values in ROI's.

Furthermore, temporal resolution was limited because the method utilized only end-diastolic gated images for analysis. As a result, some of the indicator-dilution curves were constructed from analysis of less than 10 end-diastolic frames. At slow heart rates, the accuracy of the technique could be potentially compromised by the relatively few number of data points utilized to produce the time-intensity curve. Indeed, preliminary studies of the indicator-dilution method in man demonstrated that this latter limitation was significant. Compared to anesthetized dogs, humans generally had slower heart rates and thus provided fewer cardiac cycles from which to obtain end-diastolic density values to construct a time-intensity curve.

An additional limitation was the necessity to use ECG-gated pressure injections to deliver intracoronary contrast media in this study. Many clinicians are hesitant to power inject contrast medium in the coronary artery using any mechanical device which might be subject to failure. For safety reasons, power injection is an undesirable requirement and has limited acceptance of this and other methods for computation of CFR from digital angiography.

Coronary reserve using hand injections

Because of the difficulties inherent in end-diastolic ECG-gated power injection of contrast, we subsequently modified the indicator-dilution approach using hand injection of contrast. Instead of end-diastolic gating, we utilized 30-frame per second ECG-gated digital subtraction angiography in this subsequent study. By increasing the framing rate, the necessity for end-diastolic ECG-gated power injection was effectively eliminated. With 150 to 200 frames in each study, the potential impact of beginning a coronary injection during the cardiac cycle is markedly reduced. The revised methodology using higher framing rates also permits curves to have distinctive systolic and diastolic oscillations (Figure 6). Thus, the relative contributions of systolic and diastolic coronary blood flow are represented in the area under the curve.

Validation of hand injection method

Coronary flow reserve determination using indicator-dilution analysis and hand injection of contrast medium was validated using an animal model similar to the one previously described [12]. However, in this study intracoronary papaverine (8—10 mg) was used to induce coronary reactive hyperemia rather than temporary occlusion. Digital angiography was performed with a more advanced pulse mode progressive scan imaging system at 30-frames per second, a pixel matrix of 512 × 512 and a radiographic dose of 20 microroentgens per frame. Logarithmic transformation of the digital images was utilized to linearize the exponential relationship between

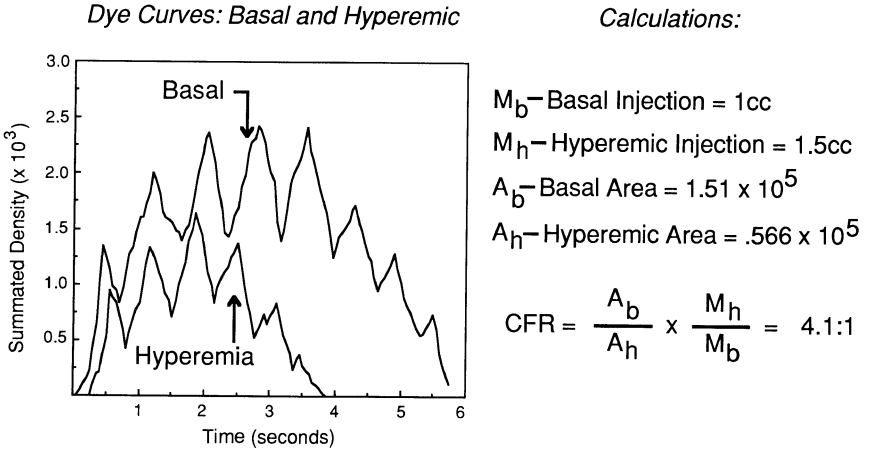

Fig. 6. Representative density-time curve obtained from 30 frames per second digital angiography performed under basal conditions and following induction of reactive hyperemia. An example of calculation of coronary flow reserve (CFR) is shown on the right.

radiographic attenuation and contrast concentration. Phasic subtraction was performed such that each contrast containing frame was subtracted by a mask-frame obtained from the same-phase of the cardiac cycle.

Since 30-frames per second digital angiography was utilized, background corrected coronary time-intensity curves required analysis of as many as 200 consecutive frames. This required manual placement of the region of interest for each frame — a tedious and time-consuming process. Software is currently under development in our laboratory which will perform this function automatically. The 30-frames per second digital angiograms yielded very high-quality curves which eliminated reliance upon a few data points to construct an indicator curve.

Results

Validation studies using hand injection and 30-frames per second acquisition were performed for a total of 20 different stenoses in five animals. Coronary flow reserve was simultaneously measured using EMF and compared to flow reserve ratios calculated by analysis of the indicator-dilution curves. Linear regression analysis demonstrated a close correlation between flow reserve determined by EMF and the hand injection method (Figure 7). The correlation coefficient was close, $r = 0.86$. These studies demonstrated that CFR could be measured from digital angiography without the need for ECG-gated power injection. Although the method required analysis of many frames, it has the advantage of adequate temporal resolution to ensure an accurate curve even at relatively slow heart rates.

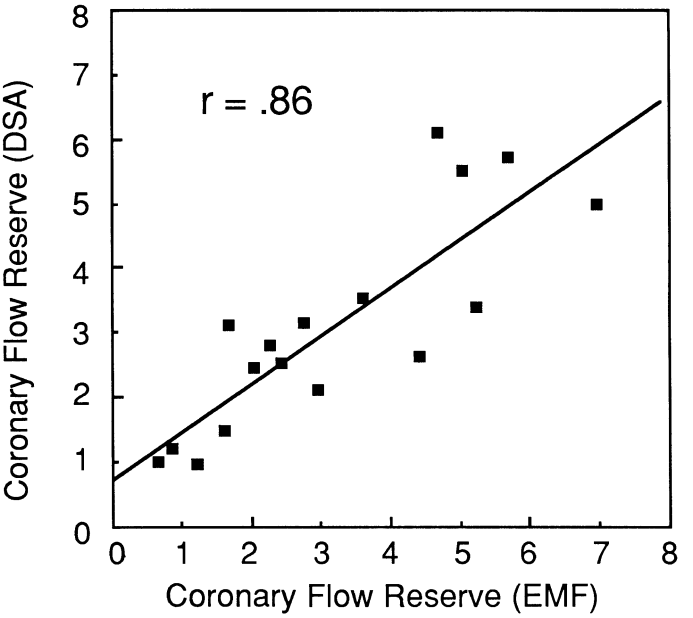

Fig. 7. Linear regression analysis comparing coronary flow reserve measured by electromagnetic flow probe (EMF) with flow reserve calculated from digital angiography (DSA). In this study, hand-injection of contrast utilized along with 30 frames per second digital angiography.

Coronary flow reserve in man

We have applied the indicator-dilution method to analyze coronary flow reserve in a small patient population using 30 frames per second angiography and hand injection of contrast. A total of 35 vessels were analyzed in twenty-one patients including seven with normal coronary arteries, eight patients with unstable angina, and eleven arteries before and after angioplasty.

Since the indicator-dilution method requires subselective injection of contrast in the coronary artery, evaluation of the left anterior descending or circumflex vessels required a specialized adaptation of the technique. For these left coronary vessels, contrast was injected through a balloon angioplasty catheter thus permitting administration of a small quantity of contrast medium subselectively into the vessel. For the right coronary artery, a standard angiography cathether was utilized. In human studies, digital subtraction angiography was performed under basal conditions and again following induction of reactive hyperemia using intracoronary papaverine. As previously described, images were logarithmically converted, gated subtraction was performed, and two regions of interest were analyzed, one for the epicardial vessel and the other for the adjacent myocardium. For each frame,

both regions of interest were manually placed by an operator and summated intensity from the coronary curve was corrected for the background ROI. CFR was computed as previously described:

$$\frac{Q_H}{Q_B} = \frac{A_B}{A_H} \times \frac{M_H}{M_B}$$

Q_B and Q_H represent basal and hyperemic coronary flow, while A_B and A_H represent the integral of the basal and hyperemic dye curves, respectively, M_B and M_H represent the quantities of dye injected for the basal and hyperemic imaging sequences, respectively.

In addition, both quantitative angiography and visual assessment of stenoses were performed for each lesion evaluated by indicator-dilution analysis.

Results of human studies

Employing the indicator-dilution method, statistically significant differences among patient subgroups were noted for CFR (Figure 8). Coronary flow reserve for normal vessels was 4.8:1 ± 0.65. Patients with stable angina had a mean coronary flow reserve of 3.2:1 with a standard deviation considerably higher than demonstrated for normals (± 1.3). Thus, as might be expected,

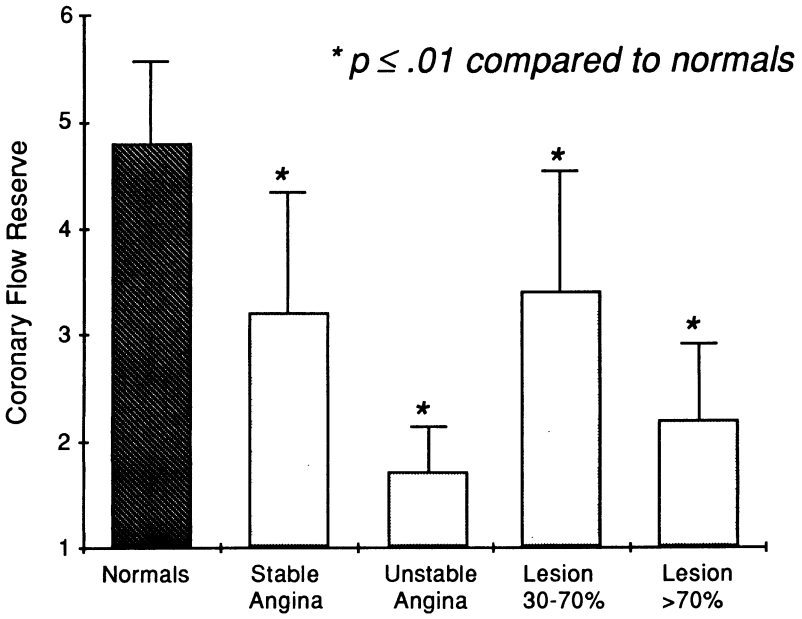

Fig. 8. Coronary flow reserve in normal subjects and in patients with stable angina, unstable angina, coronary lesions of intermediate severity (30—70%) and coronary lesions of greater severity (> 70%).

considerable heterogeneity for CFR was apparent in the stable angina population. However, patients with unstable angina were more homogeneous with a coronary flow reserve averaging 1.7 ± 0.3.

There was a general correlation between lesion severity by quantitative angiography and CFR as measured by digital angiography. For patients with a lesion severity of greater than 70%, coronary flow reserve averaged 2.3 ± 0.8, while patients with lesions in the 30—70% range exhibited a coronary flow reserve of 3.3 ± 1.2. Despite this general correlation, there was considerable disparity between CFR determinations from digital angiography and percent stenosis as measured either by visual grading or quantitative arteriography. Thus, overall correlation between percent stenosis and coronary flow reserve for lesions in the 30—90% range was $r = 0.62$ for visual grading and $r = 0.67$ for quantitative arteriography (Figure 9). Thus, either measure of percent stenosis was a relatively poor prediccor of CFR as measured by the indicator dilution method.

For the eleven patients studied before and after PTCA, coronary flow reserve averaged 2.0:1 prior to angioplasty and increased to 3.7:1 approximately 30 minutes following angioplasty (Figure 10). In this setting, the percent change in stenosis as determined by quantitative arteriography correlated only moderately with the change in CFR as measured by indicator-dilution analysis of digital angiography. This finding should not be surprising since it is well recognized that PTCA distorts vessel anatomy and thus impairs conventional anatomic analysis of stenoses.

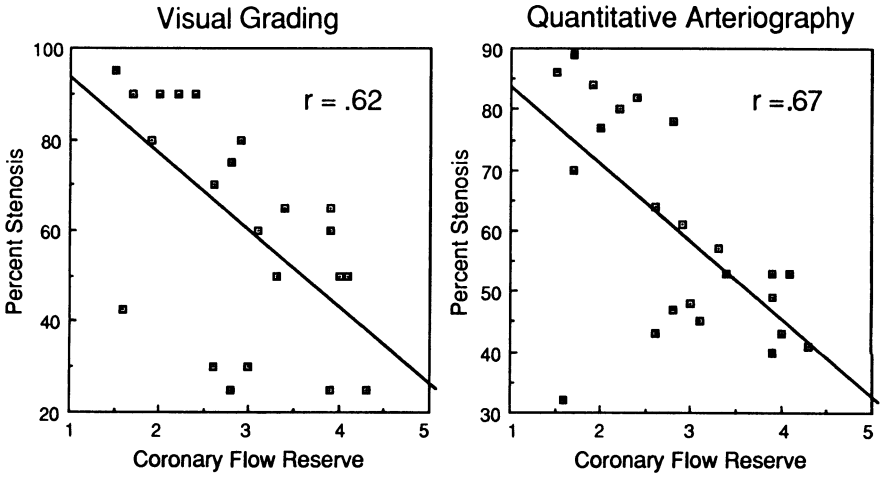

Fig. 9. Linear regression analysis comparing coronary flow reserve measured by the indicator-dilution technique with percent stenosis derived either by visual grading (left panel) or quantitative arteriography (right panel). In both cases, there was only a moderate correlation between flow reserve values and percent stenosis.

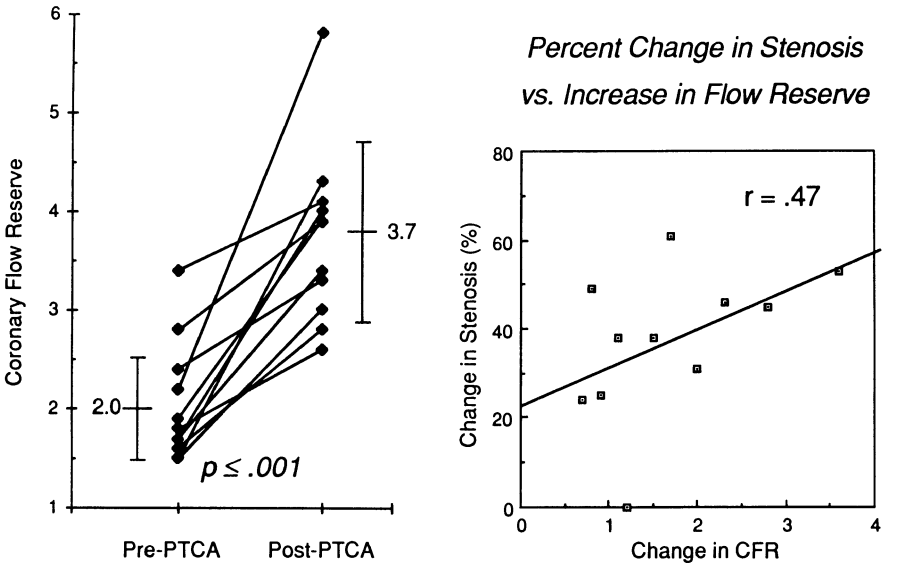

Fig. 10. Improvement in flow reserve following percutaneously transluminal coronary angiography (PTCA). Although coronary flow reserve (CFR) increased in all patients, there was only a moderate correlation between the change in DFR and the change in percent stenosis as measured by quantitative arteriography.

Absolute coronary flow

Further studies in our laboratory have sought to apply indidator dilution principles to the measurement of absolute coronary blood flow from digital angiography [13]. We investigated a potential approach to this problem in an animal model in which two contrast injections were performed, one subselectively in the coronary as previously described. A second injection was performed through a pigtail catheter placed into the left ventricle using a large volume of contrast (30—40 ml) and digital subtraction. A background corrected time-intensity curve for an epicardial coronary ROI is obtained for each of the two injections. Since the quantity of dye injected subselectively is known and the quantity injected in the left ventricle is known, it is possible to calculate the percent of cardiac output perfusing the circumflex coronary artery by comparing the areas of the coronary density-time curves (Figure 11). Since cardiac output could be determined by the thermodilution method, volumetric coronary blood flow could be indirectly calculated using this method. We validated the approach in an animal model similar to the one described for previous experiments. However, in this case, the animal was instrumented with a pigtail catheter in the left ventricle to permit administration of a large enough volume of contrast to opacify the coronary

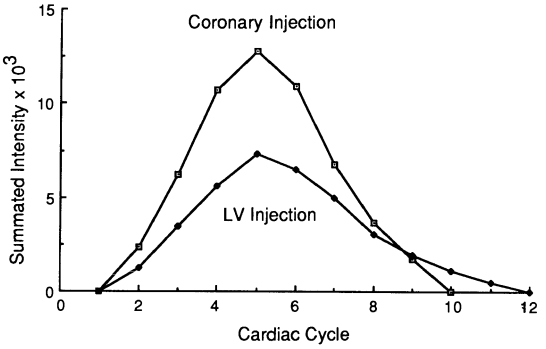

$$\frac{Q_{LCx}}{Q_{LV}} = \frac{M_{LCx}}{M_{LV}} \times \frac{A_{LV}}{A_{LCx}}$$

$$.0323 = \frac{2}{40} \times \frac{35.62 \times 10^3}{55.07 \times 10^3}$$

$$.0323 \times 3300 = 106.6 \text{ ml/min}$$

Fig. 11. Mathematics of calculation of absolute blood flow from a pair of contrast injections, one intracoronary and the other in the left ventricle. The ratio of circumflex blood flow (Q_{LCx}) to total cardiac output (Q_{LV}) is equal to the mass of contrast injected in the circumflex (M_{LCx}) divided by the mass of contrast injected in the left ventricle (M_{LV}) multiplied by the area under the contrast time-intensity curve for the left ventricular injection (A_{LV}) divided by the area under the intensity-time curve for the circumflex region of interest (A_{LCx}). In this case, 2 ml of contrast was injected in the circumflex and 40 ml in the left ventricle. Using the areas shown in this figure, left circumflex blood flow was equal to 0.0323 expressed as a fraction of cardiac output. Thermodilution cardiac output was 3300 ml/minute which resulted in a calculated coronary blood flow of 106.6 ml/minute.

arteries. Further, a thermodilution catheter was placed in the pulmonary artery to measure cardiac output.

Results

Coronary blood flow was measured by EMF and digital angiography at 21 flow levels in five animals (Figure 12). This wide range of flows was achieved by either increasing flow using injection of intracoronary papaverine and/or limiting flow by the introduction of epicardial stenoses. There was a close correlation between flow values obtained by the electromagnetic method and that calculated by digital angiography. These data demonstrate the potential for digital angiography to be employed in the calculation of absolute coronary blood flow. If flow is expressed as percent of cardiac output, these calculations do not require any other assumptions beyond the indicator-dilution method.

Summary and conclusions

These studies illustrate the value and limitations of the indicator-dilution methods for analysis of coronary flow reserve and absolute coronary blood flow. The indicator-dilution method is an adaptation of well-established physiological principles which have been applied to the problem of radiogra-

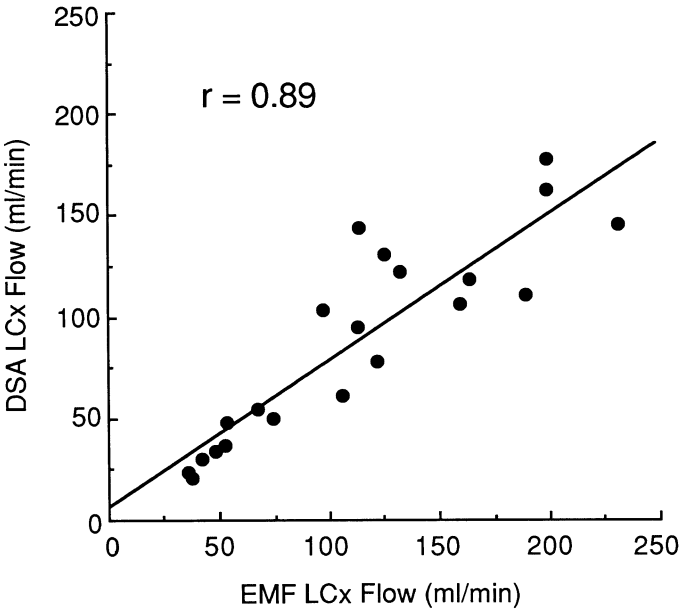

Fig. 12. Linear regression analysis comparing left circumflex (LCx) blood flow as measured by electromagnetic probe (EMF) to flow calculated from indicator-dilution analysis of digital subtraction angiography (DSA).

phic imaging. Initial studies demonstrate a good correlation for calculation for CFR using end-diastolic gated image acquisition and ECG-gated power injection of contrast in the coronaries (Figure 5). At the relatively high heart rates present in the animal model, a sufficient number of data points were produced to accurately construct an indicator-dilution curve. Because slower heart rates prevalent in human subjects provided a fewer number of data points for each curve, this method was subsequently modified to utilize hand injection of contrast with 30-frames per second image acquisition. This latter method also demonstrated a close correlation for calculation of CFR in an animal model of CAD (Figure 7). However, the hand-injection method requires manual placement of regions of interest for as many as 200 consecutive angiographic frames and is therefore very time-consuming.

In further studies, we have applied the indicator-dilution method in a clinical setting to determine flow reserve in a variety of disease states (Figure 8). Major differences for coronary flow reserve as measured by the indicator-dilution method were demonstrated for patients with stable or unstable angina in comparison to a normal population. As anticipated, only moderate correlation was observed between lesion severity by quantitative arteriography or visual assessment and coronary flow reserve. In another subgroup, the indicator-dilution method was applied to the measurement of CFR before

and after balloon angioplasty (Figure 10). Statistically significant changes in flow reserve were observed although the correlation between the improvement in stenosis appearance and flow reserve was only moderate. Presumably this disparity reflects the limitations in assessment of the severity of stenoses following distortion of vessel anatomy by PTCA.

Lastly, we have adapted this method to the measurement of absolute coronary blood flow in an animal model. Under controlled conditions, a close correlation was obtained for absolute coronary flow calculated by analysis of a pair of coronary angiograms, one performed indirectly via a catheter placed in the left ventricle and a second injection subselectively in the circumflex.

The data obtained in these studies demonstrate that indicator-dilution analysis is a flexible and potentially useful tool in the evaluation of coronary flow and coronary flow reserve. Further investigations are underway to compare the indicator-dilution method with other reported techniques for the assessment of the physiological consequences of coronary stenoses. A large database of patients with a wide variety of coronary lesions will be required to determine the relative value of the various methods for analysis of angiography. Given the inherent limitations in the visual assessment of coronary obstructions, it is anticipated that insights generated from computer analysis in digital angiography will ultimately find application in routine clinical care.

References

1. Arnett EN, Isner JM, Redwood DR, Kent KM, Baker WP, Ackerstein H, Roberts WD: Coronary artery narrowing in coronary heart disease: comparison of cineangiographic and necropsy findings. Ann Intern Med 91: 350—356, 1979.
2. Gray CR, Hoffman HA, Hammond WS, Miller KL, Oseasohn RO: Correlation of arteriographic and pathologic findings in the coronary arteries in man. Circulation 26: 494—499, 1962.
3. Grondin CM, Dyrda I, Pasternac A, Campeau L, Bourassa MG, Lesperance J: Discrepancies between cineangiographic and post-mortem findings in patients with coronary artery disease and recent myocardial revascularization. Circulation 49: 703—708, 1974.
4. Levin DC, Baltaxe HA, Sos TA: Potential sources of error in coronary arteriography. II. In interpretation of the study. Am J Roentgenol 124: 386—393, 1975.
5. Zir LM, Miller SW, Dinsmore RE, Gilbert JP, Hawthorne JW: Interobserver variability in coronary angiography. Circulation 53: 627—632, 1976.
6. Gould KL, Lipscome K: Effects of coronary stenoses on coronary flow reserve and resistance. Am J Cardiol 34: 48—55, 1974.
7. White CW, Wright CB, Doty DB, Hiratza LF, Eastham CL, Harrison DG, Marcus ML: Does visual interpretation of the coronary arteriogram predict the physiologic importance of a coronary stenosis? N Engl J Med 310: 819—824, 1984.
8. Gould KL, Lipscomb K, Hamilton GW: Physiologic basis for assessing critical coronary stenosis, instantaneous flow response and regional distribution during coronary hyperemia as measures of coronary flow reserve. Am J Cardiol 33: 87—94, 1974.

9. Wilson RF, White CW: Intracoronary papaverine: an ideal coronary vasodilator for studies of the coronary circulation in conscious humans. Circulation 73: 444—451, 1986.
10. Foerster JM, Link DP, Lantz BM, Lee G, Holcroft JW, Mason DT: Measurement of coronary reactive hyperemia during clinical angiography by video dilution technique. Acta Radiol 22: 209—216, 1981.
11. Nissen SE, Elion JL, Booth DC, Evans J, DeMaria AN: Value and limitations of computer analysis of digital subtraction angiography in the assessment of coronary flow reserve. Circulation 73: 562—571, 1986.
12. Gurley, JC, Nissen SE, Elion JL, Evans J, McMinn M, DeMaria AN: Determination of coronary flow reserve by digital angiography: Validation of a practical method not requiring power injection or ECG gating. JACC 16(1): 190—197.
13. Nissen SE, Grayburn P, Evans J, Elion JL, Gurley JC, DeMaria AN: Calculation of absolute coronary blood flow from digital angiography: Correlation with electromagnetic flow. Circulation 74 (Suppl II): 485, 1986 (Abstract).

13. 3D reconstruction of the coronary arterial tree from multiview digital angiography: A study of reconstruction accuracy

DENNIS L. PARKER and JIANG WU

Summary

In this paper we discuss the current state of 3D reconstruction of the coronary artery vascular bed from multiview ECG correlated digital cardiac angiography and provide details on progress toward applications in geometric assessment of lesion severity, absolute blood flow determinations and the correlation of lesion morphology with calcium deposition determined by quantitative computed tomography. Each of these applications requires accurate determinations of the three-dimensional position, orientation and cross-sectional area on a significant fraction of the major branches of the vascular bed. We therefore review some studies of reconstruction accuracy and precision using: a) contrast embedded latex arterial casts; and b) computer simulation where care is taken to account for the physics of the imaging system (scatter, beam hardening, etc.).

3D reconstruction is a multistep process that requires specification of the vascular bed structure and approximate location in each image, a dynamic programming algorithm to determine accurate vessel centerline and edge locations and compute the 3D vessel structure, and orientation corrected densitometry to determine vessel lumen areas (independently for each image).

The computer simulations and vessel cast studies have demonstrated that sub-pixel accuracy and precision are possible using densitometric techniques and that scatter and beam hardening cause a systematic (although small) error in measurement that depends on vessel size. Reconstruction accuracy of any specific vessel segment depends on the number of views in which the segment is clearly visible. The fraction of the arterial bed that cannot be analyzed decreases approximately exponentially with the number of views.

Introduction

The development of techniques for 3D reconstruction of the coronary artery

J. H. C. Reiber and P. W. Serruys (eds), Quantitative Coronary Arteriography, 265–294.

vascular bed from angiographic projections may ultimately facilitate various applications that require accurate measurements of global vessel morphology. Such applications include the quantification of the morphology in diffuse disease, the correlation of morphology with information from other modalities such as computed tomography, and the determination of absolute blood flow. For example, transit time or "time of flight" measurements of blood flow can be obtained by tracking the leading edge (or some other characteristic) of a contrast media bolus as it passes through the known dimensions of an arterial segment. Flow is then defined as the volume traversed divided by the time of transit. The absolute accuracy of such flow determinations will obviously depend directly on the accuracy of the determination of vessel dimensions.

Projection X-ray imaging currently offers the best spatial and temporal resolution of vascular details. From these images it is possible to visualize the passage of iodinated contrast media and it is also possible to make measurements of vessel dimensions. However, it is not possible to determine the lumen area, the relative orientation and the related absolute length of vessel segments from the images of a single imaging plane. By combining detail from two or more imaging planes the complete three-dimensional structure (cross-sectional area, length and orientation) can be determined. Knowledge of the projection orientation allows the bolus location to be mapped from its position on the projection image back to the location in the 3D vessel structure.

Measurements of vessel dimensions and flow in the coronary arteries are significantly complicated by the branching nature of the vascular bed and the fact that the arteries themselves are in continuous motion throughout the cardiac cycle. The branching requires that bolus position determinations be made more often than once per cardiac cycle and the motion requires that the relative motion of the vessel segment itself must be known. It is thus necessary to know the continuous 3D positions of the arterial segments at all time points of interest in the cardiac cycle. The accuracy of blood flow measurements will be directly related to how accurately the coronary anatomy is known.

In this paper we address details related to the accurate determination of vascular structure and dimensions. We begin with a review of the reconstruction process itself and discuss the potential sources of error, including physical degradation such as scatter and beam hardening. We review simulation studies and some results from studies on coronary artery casts. We also present some details of geometric coordination (registration) of vascular data from 3D reconstruction with cardiac images from ultrafast computed tomography. The principal application of these latter studies is in the correlation of calcium determined from ultrafast CT with coronary anatomy (lesion severity) determined from coronary angiography.

Reconstruction theory and simulation studies

Three-dimensional vessel reconstruction as used in this paper consists of the determination of the three-dimensional vascular bed structure from 2 or more digital angiographic projection images. The technique we have developed takes advantage of several apparently intrinsic properties of the imaged coronary arteries. For example, 1) vessels of interest for measurement are typically between 1 and 10 mm in diameter and are visualized in routine X-ray imaging by injection of a radio-opaque (iodinated) contrast media; 2) segments of interest typically appear sparse in a projection image, with significant lengths of vessel segments being observed without the clutter of overlapping vessels; 3) reasonably good subtraction images can be obtained where only contrast enhanced vessels are visible (where such subtraction cannot be performed, it is often true that the background overlapping the vessel is sufficiently uniform to be predicted and subtracted based on neighboring measurements); 4) the density of contrast media is constant interior to the vessel lumen and usually zero outside. (This latter assumption breaks down when contrast has had time to pass into the capillaries of the tissues.); and 5) vessels are connected.

The final result in our reconstruction process is a linked set of elements where each element has position coordinates (x, y, z) and dimensions (radius). Our technique for 3D vessel reconstruction has been presented in detail previously [1, 2] and is similar in some respects to other techniques [3—6]. For the purposes of this paper, some aspects of the process are reviewed.

Images to be used in the reconstruction process are obtained from ECG correlated digital angiographic views of the arteries to be reconstructed. In the case of the simulation studies, images of an original 3D structure are obtained by a forward projection algorithm, which is described below. The images are processed with the previously published algorithm for detecting vessel edges and centerlines [1, 2, 7]. Using these determined vessel centerlines, the 3D vessel centerline reconstruction is obtained. Densitometric measurements of the vessel cross-sectional area are then made and corrected for vessel orientation. The radius of the vessel is determined from the area. The theory and algorithm of the densitometric measurement is briefly reviewed later. After the reconstruction process a new 3D structure is created. The original and reconstructed structures are then directly compared on a point by point basis. For the simulation studies, the vessels are assumed to be circular.

Vascular densitometry

Densitometric measurements of vessel dimensions are founded on the basic interactions between X-rays and matter. For a typical digital angiographic imaging system, it would appear [8, 9] that the relationship between signal

voltage, $S(u, v)$, received as input to the analog-to-digital (A/D) converter from a specific location u, v in the image, and the X-ray path length through the anatomy can be approximated by an expression of the form:

$$S(u, v) \approx \mathrm{G} \ln \left[h(u, v) * \int_0^{E_{\max}} \left(I_0(u, v, E) e^{-\int \mu(x, y, z, E)\, \mathrm{d}l} + \right. \right.$$

$$\left. \left. + I_s(u, v, E) \right) \mathrm{d}E \right], \tag{1}$$

where, $\mu(x, y, z, E)$ is the linear attenuation coefficient, which is a function of position in the anatomy and the X-ray energy, E; $I_0(u, v, E)$ is the incident X-ray intensity as a function of energy; I_s is the X-ray scatter; $h(u, v)$ is the effective point spread transfer function of the imaging system accounting for system blurring (the symbol * represents a 2D convolution); and G represents the post-logarithmic gain of the imaging electronics. Note that the integral in the exponential is along the X-ray path.

To the extent that the incident intensity is mostly mono-energetic, that scatter is negligible and that the image system transfer function is well localized (i.e. a delta function), Equation (1) can be simplified to:

$$S(u, v) = G \ln I_0(u, v) - G \int \mu(x, y, z)\, \mathrm{d}l. \tag{2}$$

If contrast medium is added to and is uniform throughout the arteries of interest, the measured signal will be:

$$S_c(u, v) = G \ln I_0(u, v) - G \int \mu(x, y, z)\, \mathrm{d}l - G\mu_I \rho_I t_I, \tag{3}$$

where μ_I and ρ_I are respectively the mass attenuation coefficient and density of the iodine, and t_I is the X-ray path length through the vessels. The digital number in the DSA image is the following difference:

$$d(u, v) = S(u, v) - S_c(u, v) = G\mu_I \rho_I t_I = k' t_I, \tag{4}$$

In this case, the value at u, v in a projection image is directly proportional to the incident X-ray path length (t_I) through the vessels.

For a circular vessel at an angle θ_i with respect to the imaging plane, the central vessel diameter (D) at position (i) is proportional to the maximum density value, $d_{i\max}$:

$$D_i = k\, \mathrm{d}_{i\max} \cos \theta_i \tag{5}$$

Similarly, the integral vessel area (A) at position (i) is related to the integral

density:

$$A_i = k \sum_j d_{ij}\, \Delta x \cos \theta_i = \frac{\pi}{4} D_i^2. \tag{6}$$

Here, j is the index orthogonal to the vessel, Σd_{ij} is the summation of the projected vessel density profile and Δx is the sample space of the profile. By eliminating D_i in the above, an estimate of the conversion factor, k, is obtained:

$$k_i = \frac{4}{\pi} \frac{\sum_j d_{ij}\, \Delta x}{d_{i\,\max}^2 \cos \theta_i}. \tag{7}$$

The angle, θ_i, can be obtained from an accurate 3D reconstruction of the vessel centerline. Detailed discussion of the above equations are found in references [1, 2, 11].

Thus, in the absence of image degradation and to the extent that Equation (2) is valid, densitometric measurements of the vascular bed are obtained by first obtaining the 3D reconstruction of the vessel centerlines, then using Equation (7) to obtain the densitometric conversion factor, k, and Equations (5) and (6) to determine the vessel dimensions. Because the vessels deviate somewhat from circular cross sections and to reduce the error in k due to random errors, an estimate of k is usually obtained from some average of many local measurements.

Reconstruction accuracy: densitometric errors

The accuracy obtained in the densitometric measurements of the vascular bed will depend on many factors including the accuracy of the parameters included in Equations (5), (6) and (7), as well as the validity of Equation (2). To begin to understand the effects of the various errors we first consider beam hardening and scatter.

If the imaging system is degraded by beam hardening and scatter, an error in A_i is expected, which is dependent on the errors in measuring $d_{i\,\max}$ and $\Sigma d_{ij}\, \Delta x$. If we assume the relative errors in $d_{i\,\max}$ and $\Sigma d_{ij}\, \Delta x$ to be δ_i and ε_i, respectively, we have:

$$d'_{i\,\max} = (1 - \delta_i)\, d_{i\,\max}; \qquad \sum_j d'_{ij} = (1 - \varepsilon_i) \sum_j d_{ij}. \tag{8}$$

The conversion factor, k, obtained from a single vessel profile measurement is then:

$$k_{mi} = k_{\text{true}} \frac{(1 - \varepsilon_i)}{(1 - \delta_i)^2}. \tag{9}$$

The area for the profile obtained using the single conversion factor becomes:

$$A_{mi} = A_{\text{true } i} \frac{(1 - \varepsilon_i)^2}{(1 - \delta_i)^2} \tag{10}$$

And the measured radius becomes:

$$r_{mi} = \sqrt{\frac{A_{mi}}{\pi}} = \sqrt{\frac{A_{\text{true } i}}{\pi} \frac{(1 - \varepsilon_i)^2}{(1 - \delta_i)^2}} = r_{\text{true } i} \frac{1 - \varepsilon_i}{1 - \delta_i}. \tag{11}$$

In practice, we use an average k over a range of radii and angles in the image:

$$\bar{k} = \frac{1}{n} \sum_{i=1}^{n} k_i. \tag{12}$$

The measured area can then be expressed:

$$A_{mi} = \bar{k} \sum_j d_{ij} \, \Delta x = \frac{\bar{k}}{k_{\text{true}}} A_{\text{true } i} (1 - \varepsilon_i). \tag{13}$$

The corresponding radius becomes:

$$r_{mi} = \sqrt{\frac{A_{mi}}{\pi}} = r_{\text{true } i} \sqrt{\frac{\bar{k}}{k_{\text{true}}} (1 - \varepsilon_i)} \approx r_{\text{true } i} \sqrt{\frac{\bar{k}}{k_{\text{true}}}} \left(1 - \frac{\varepsilon_i}{2}\right). \tag{14}$$

Estimates of the magnitude of these errors were determined by computer simulation and are presented later.

Reconstruction accuracy: image registration with computed tomography

The accuracy of the densitometric measurements depends, among other things, on the accuracy in the determination of the vessel orientation relative to the imaging plane which in turn depends on the accuracy of the vessel centerline determination as well as the accuracy in the knowledge of the view orientation. In order to improve the accuracy in the determination of the view orientation as well as facilitate intercomparison of the 3D vessel centerline location with the vessel visualized with computed tomography, we have implemented a view calibration procedure based upon marks external to the patient.

The general relationship between the 3D coordinates (x, y, z) of a point and the projected coordinates (u, v) are typically related by the transforma-

tion [13]:

$$T \begin{bmatrix} x \\ y \\ z \\ 1 \end{bmatrix} = \begin{bmatrix} t_{11} & t_{12} & t_{13} & t_{14} \\ t_{21} & t_{22} & t_{23} & t_{24} \\ t_{31} & t_{32} & t_{33} & t_{34} \end{bmatrix} \begin{Bmatrix} x \\ y \\ z \\ 1 \end{Bmatrix} = s \begin{Bmatrix} u \\ v \\ 1 \end{Bmatrix}. \tag{15}$$

The corresponding transformation for the digital angiography system used in this study (a Siemens Angioskop) with arbitrary view angles is:

$$\mathbf{x}' = R \begin{bmatrix} x \\ y \\ z \end{bmatrix} = \begin{bmatrix} r_{11} & r_{12} & r_{13} \\ r_{21} & r_{22} & r_{23} \\ r_{31} & r_{32} & r_{33} \end{bmatrix} \begin{Bmatrix} x \\ y \\ z \end{Bmatrix} = s' \begin{Bmatrix} u - u_0 \\ v - v_0 \\ w \end{Bmatrix}$$

$$= \frac{D - z'}{L} \begin{Bmatrix} u - u_0 \\ v - v_0 \\ w \end{Bmatrix} \tag{16}$$

where

$$R = \begin{bmatrix} -\cos\alpha\cos\phi & \cos\alpha\sin\phi\sin\theta - \sin\alpha\cos\theta & -\cos\alpha\sin\phi\cos\theta - \sin\alpha\sin\theta \\ \sin\alpha\cos\phi & -\sin\alpha\sin\phi\sin\theta - \cos\alpha\cos\theta & \sin\alpha\sin\phi\cos\theta - \cos\alpha\sin\theta \\ -\sin\phi & -\cos\phi\sin\theta & \cos\phi\cos\theta \end{bmatrix}$$

and:

α, ϕ, and θ, are the angle within the view, (rotation of the image), the LAO/RAO angle and the Cranial/Caudal angle respectively. We define the position, $\mathbf{u}'$, as the image vector relative to the projected origin (i.e. $\mathbf{x} = \mathbf{0}$ implies $\mathbf{u}' = \mathbf{0}$).

Comparing Equation (15) with Equation (16) we can relate the scaling factors between both systems. Using a notation where repeated indices imply summation over the values 1, 2 and 3 we can write:

$$s = t_{3k}\, x_k + t_{34} \qquad \text{and} \qquad s' = \frac{D}{L} - \frac{r_{3k}\, x_k}{L}. \tag{17}$$

By using a set of points for which the coordinates are known both in the 3D coordinate system and the projection space, it is possible to write a single matrix equation with the projection geometry as the unknown vector:

$$\begin{bmatrix} x_1 & y_1 & z_1 & 1 & 0 & 0 & 0 & 0 & x_1u_1 & y_1u_1 & z_1u_1 \\ 0 & 0 & 0 & 0 & x_1 & y_1 & z_1 & 1 & x_1v_1 & y_1v_1 & z_1v_1 \\ \cdot & \cdot & \cdot & \cdot & \cdot & \cdot & \cdot & \cdot & & & \\ \cdot & \cdot & \cdot & \cdot & \cdot & \cdot & \cdot & \cdot & & & \\ x_n & y_n & z_n & 1 & 0 & 0 & 0 & 0 & x_nu_n & y_nu_n & z_nu_n \\ 0 & 0 & 0 & 0 & x_n & y_n & z_n & 1 & x_nv_n & y_nv_n & z_nv_n \end{bmatrix} \begin{bmatrix} t''_{11} \\ t''_{12} \\ t''_{13} \\ t''_{14} \\ t''_{21} \\ t''_{22} \\ t''_{23} \\ t''_{24} \\ t''_{31} \\ t''_{32} \\ t''_{33} \end{bmatrix} = \begin{bmatrix} u_1 \\ v_1 \\ u_2 \\ v_2 \\ \cdot \\ \cdot \\ u_n \\ v_n \end{bmatrix} \tag{18}$$

or

$$\mathbf{At} = \mathbf{u}. \tag{19}$$

The above equation can be solved in a least squares sense:

$$\mathbf{t}'' = [\mathbf{A}^t\mathbf{A}]^{-1}\,\mathbf{A}^t\mathbf{u}. \tag{20}$$

From these relations we can determine the transformation coefficients between both systems:

$$t_{jk} = r_{jk} \quad (j = 1, 2) \quad t_{3k} = -r_{3k}/L \quad t_{34} = D/L$$

$$t''_{jk} = \frac{t_{jk} + t_{3k}u_{jo}}{t_{34}} \quad (j = 1, 2) \quad t''_{3k} = \frac{-t_{3k}}{t_{34}}. \tag{21}$$

It is thus possible to relate the coefficients from both systems and, in principle, determine the relative view orientation for the Angioskop. Unfortunately, given the Angioskop transformation, a singularity occurs at the angle $\phi = \pm 90°$, at which point the other two angles are equivalent. This simply means that at that angle it is impossible to distinguish a cranial/caudal rotation from a within view rotation. This property has little, if any, effect on the accuracy of the 3D reconstruction. It is also known that the within view rotation is very small ($< 5°$) and this fact can, in principle, be used to obtain a better estimate of the cranial/caudal angle.

Methods

The accuracy of the reconstruction process was assessed by computer simulations and by comparisons with reconstructions from computed tomography.

Computer simulation

The validity of the simulation study presented directly depends on how well the physics of the forward projection process is emulated. A projection image of the 3D data structure is obtained by a discrete simulation of Equation (1). The incident X-ray intensity is simulated as a filtered Bremsstrahlung distribution with discrete intensity values at energy increments of 5 keV up to a selected kVp. The X-rays pass through a few millimeters of pre-filtering aluminum, 20 cm of water simulating soft tissue, and the vessel structure to be imaged. To maximize beam hardening, an iodine concentration in the vessels of 0.37 g/cc is assumed. Published attention coefficients for the elemental constituents are used [10]. Scatter is assumed to be uniformly distributed across the vessel, and is specified as a fraction, f, of the detected primary X-ray intensity before adding the contrast media. This uniform approximation is valid because the vessel sizes in an image are small and the

changes in scatter across the vessel dimensions should also be small. Veiling glare is neglected.

The complex problem of computing path lengths through the vessel structure is addressed numerically by dividing vessel surfaces into small patches and projecting each patch to the image plane. A pixel, receiving X-rays which penetrate one or more vessels, will receive one or more pairs of patches. Each pair is from the front and back surface of one vessel where the X-ray penetrates. The distance between each pair of patches is the X-ray path length through the vessel. The total path length for the pixel is the summation of the distances for all the patch pairs projected to the pixel.

Computed tomography

In order to compare images obtained from digital angiography with those from computed tomography, small radio-paque marks were placed on the external surface of a plastic cylinder containing a barium impregnated latex coronary artery cast. This phantom was imaged using the Ultrafast Computed Tomography scanner with 3 mm slice thickness and 2 mm spacing between slices. The absolute locations of the marks were determined on each of the images. The phantom was also imaged with various orientations using the digital angiography system. Using an estimate of the view orientation obtained from the Siemens Angioskop, the points representing the marks were projected onto the DSA images and the corresponding marks were determined. The locations of the marks in the DSA images were then used in conjunction with Equations (15) to (21) above to obtain the actual view geometry relative to the CT geometry. Using these corrected geometries, a pair of the vessel images were then used to obtain a 3D reconstruction using the two view algorithm.

Results

Simulation experiments

To test the accuracy of the reconstruction process outlined in Equations (1) through (7) two sets of simulations were performed. For the first set, projection images of circular vessels of various radii, parallel to the imaging plane, were computed in the presence of beam hardening and with various amounts of scatter (f = 0.0, 0.2 and 0.6). The densitometric conversion factor was computed first from vessels of the same size as the one measured (analogous to Equation (11)) and second as an average of k over all vessel sizes (analogous to Equation (14)). The results are plotted in Figure 1 for vessel sizes ranging from 0.5 to 2.5 mm and from 0.5 to 4.0 mm.

In terms of the equations presented earlier, scatter and beam hardening will always cause the measured $d'_{i\,\max}$ and d'_{ij} to be smaller than the corre-

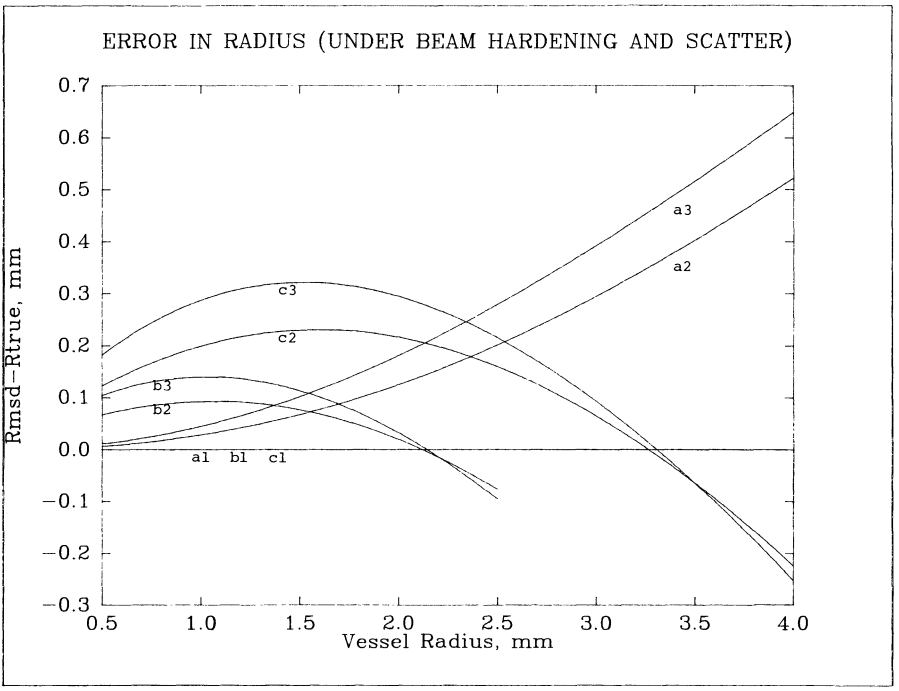

Fig. 1. Computer determined vs. true vessel radii from a simulation of the effects of scatter and beam hardening (60 kVp, 2 mm aluminum, 20 cm water, 0.37 g/cc Iodine) for vessels parallel to the imaging plane. The three cases simulated are: 1) $f = 0.0$ and no beam hardening; 2) $f = 0.2$ and beam hardening; and 3) $f = 0.6$ and beam hardening. For k the following situations were distinguished: a) k is determined for each size from vessels of the same size; b) k is determined from an average over all vessel sizes of interest (0.5 to 2.5 mm); and c) same as (b) for size range of 0.5 to 4.0 mm.

sponding true values. Thus, the error terms, δ and ε, defined in Equation (8), will be positive. Curves a2 and a3 in Figure 1 represent a plot of Equation (11) and illustrate that δ_i is larger than ε_i and the relative magnitude increases with vessel size. Curves b2, b3, c2 and c3 are obtained from Equation (14) and show that the value of k determined by averaging over a range of vessel sizes is slightly larger than the "true" value that would be obtained in the absence of beam hardening and scatter. This increase in k provides some slight compensation for the measurement error due to ε_i. Thus, because the error, ε_i increases as a function of vessel radius, the error in measurement for these curves is seen to decrease as the radius increases. It is evident that the range of error increases when the range of vessel sizes increases. Finally, although these results were obtained assuming the vessels were parallel with the imaging plane, the effect of vessel angulation would be to effectively stretch the range of vessel sizes.

For the second set of simulations, a realistic vessel data structure was

obtained by modification of a human coronary artery reconstruction reported previously [12]. The results of the forward projection used to create 2D images of the arterial structure are shown in Figure 2. These two view projections are separated by 90 degrees. The image matrix size is 256 × 256 with 0.5 mm/pixel on the surface of the simulated image receptor. One pixel corresponds to approximately 0.4 mm referred back to the 3D position of the vessels. For constructing a 3D lumen area, a weighted combination of the two lumen area measurements determined from the two views is used to discriminate against measurements from overlapping vessels and from vessels highly angulated relative to the image plane.

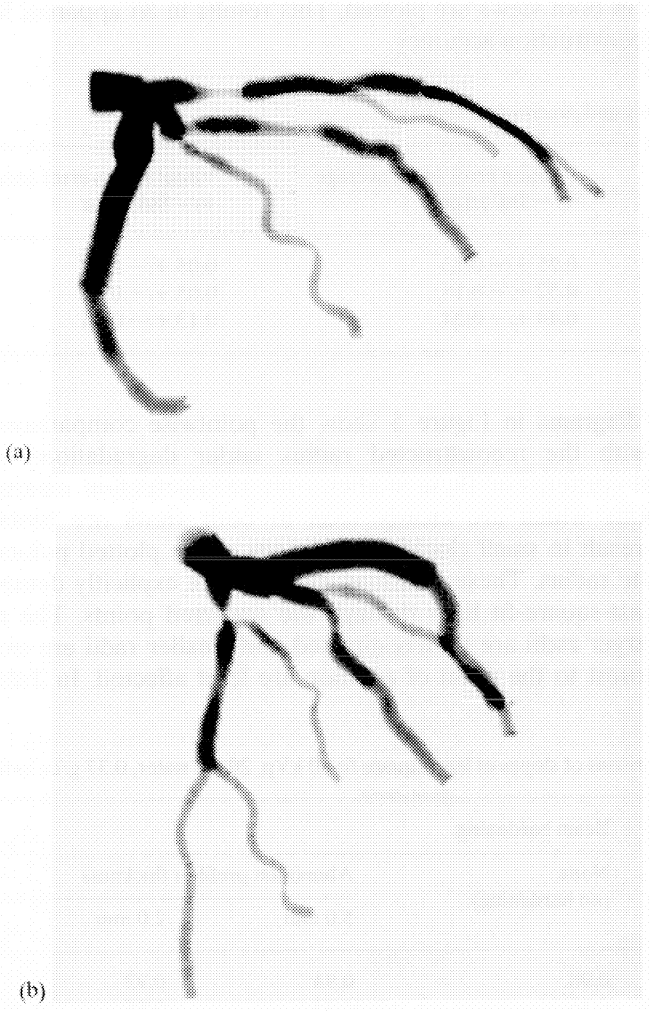

Fig. 2. Densitometric projection of a 3D artery representation onto two views (view separation angle is 90°).

The results of the simulation study are shown in Table 1 and 2 and Figures 3 through 6. Shaded surface displays of the original and reconstructed 3D structures are shown at three different viewing angles in Figure 3. The initial and reconstructed lumen area values of the two structures are compared on a point by point basis. The pointwise matching is accomplished by selecting the reconstructed point in the closest 3D proximity to the original point. Figure 4 shows comparisons of the true radii with the reconstructed radii. In Figure 4a, measurements from all vessel points are plotted. It is expected that the accuracy of densitometric measurements will be affected in regions of the projected images when vessels overlap. The effect of vessel overlap is examined in Figure 4b, where only those points which are clearly visible in both views are plotted. This results in an apparent improvement in the reconstruction accuracy.

Table 1. Accuracy and precision vs visibility.

Visibility	Position error (mm) average +/− Std. error	Vessel radius error (mm) +/− Std. error
Both Views	0.25 +/− 0.13	0.05 +/− 0.07
One View	0.32 +/− 0.18	0.05 +/− 0.16
Neither View	0.44 +/− 0.24	0.13 +/− 0.46

The three diagrams in Figure 5 show the pointwise comparisons of the true radius with the reconstructed radius under degradations of beam hardening and scatter. For these studies, only reconstruction measurements for those points which are clearly seen in both views are plotted. The degradations result in small clockwise rotations of the plotted points around an intermediate radius. These rotations can be more explicitly demonstrated by plotting least-square-fit lines through the scattered points. The rotations suggest that larger radii are underestimated and smaller radii are overestimated. Radii closest to the point of rotation are least affected. In Table 2, we

Table 2. Comparisons of slopes of least square fit 60 kVp, 20 cm water, 0.37 g/cc iodine.

Scatter fraction	Beam hardening			
	None (no hardening)	Aluminum prefilter thickness		
		5.0 mm	2.0 mm	0.0 mm
0.0	0.98	0.94	0.93	0.93
0.2	0.88	0.85	0.85	0.84
0.6	0.81	0.79	0.79	0.79

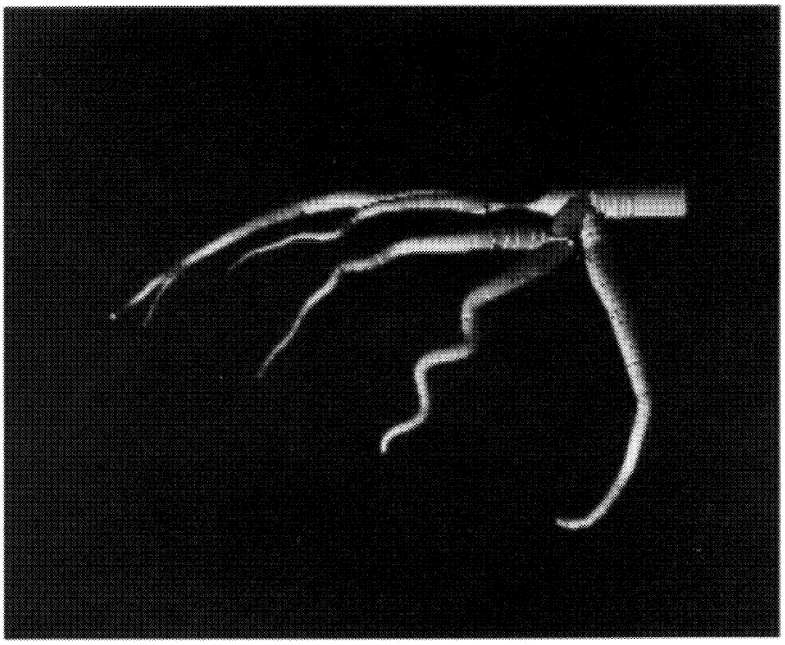

(a)

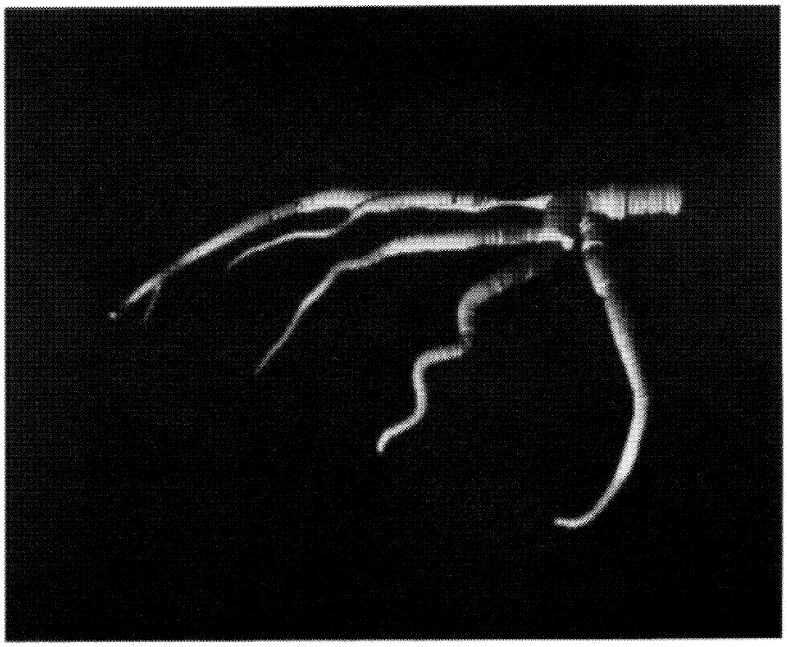

(b)

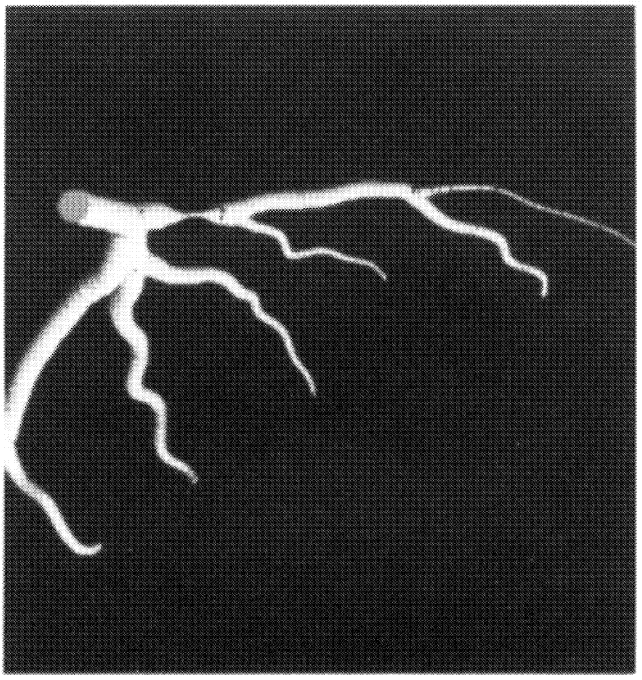

(c)

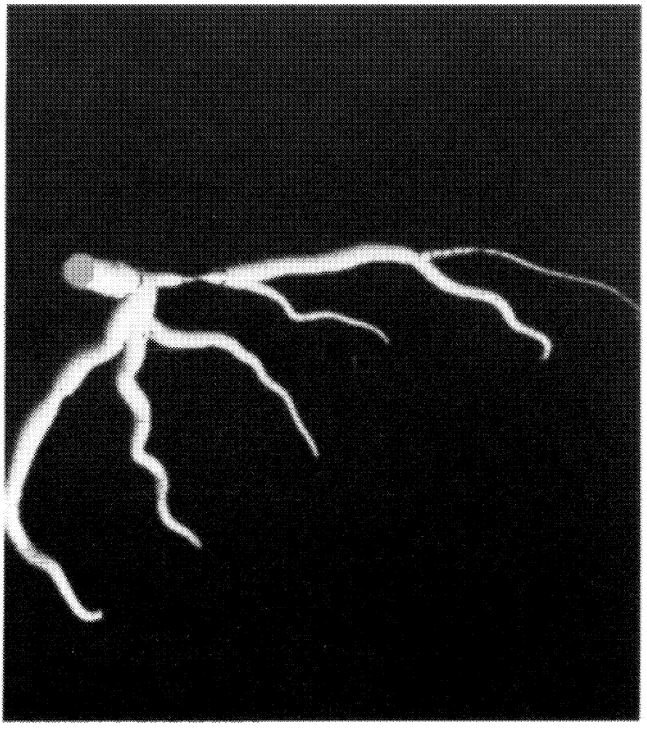

(d)

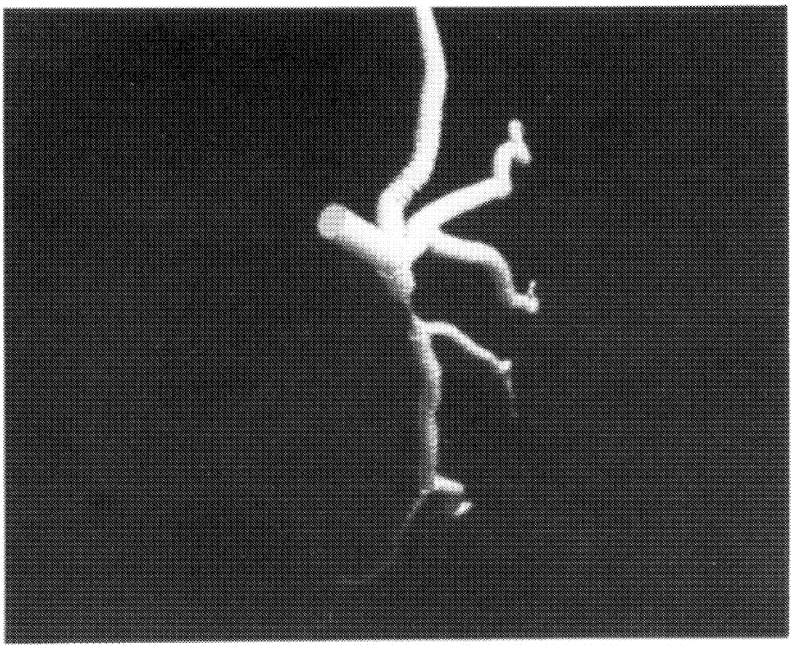

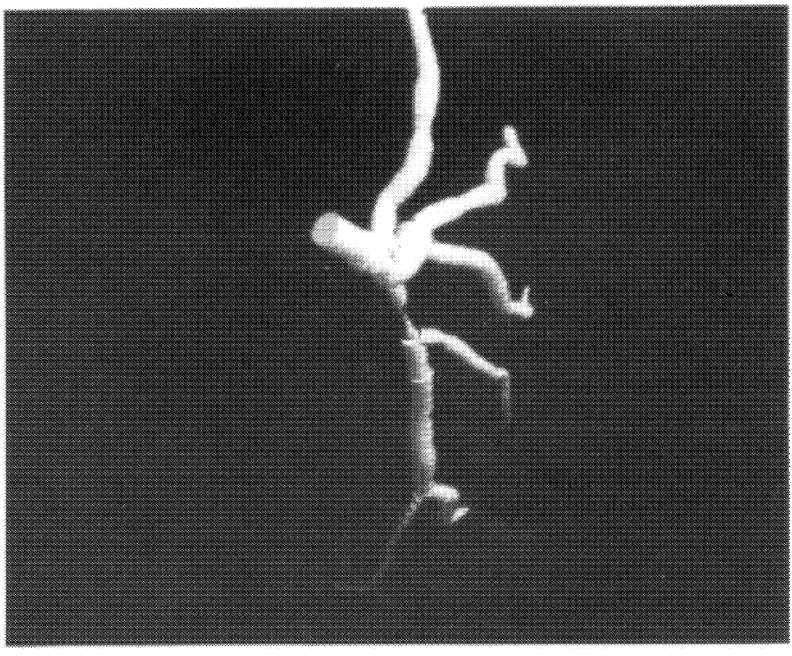

Fig. 3. Shaded surface displays of the original (a, c, e) and reconstructed (b, d, f) arterial representation from three different views.

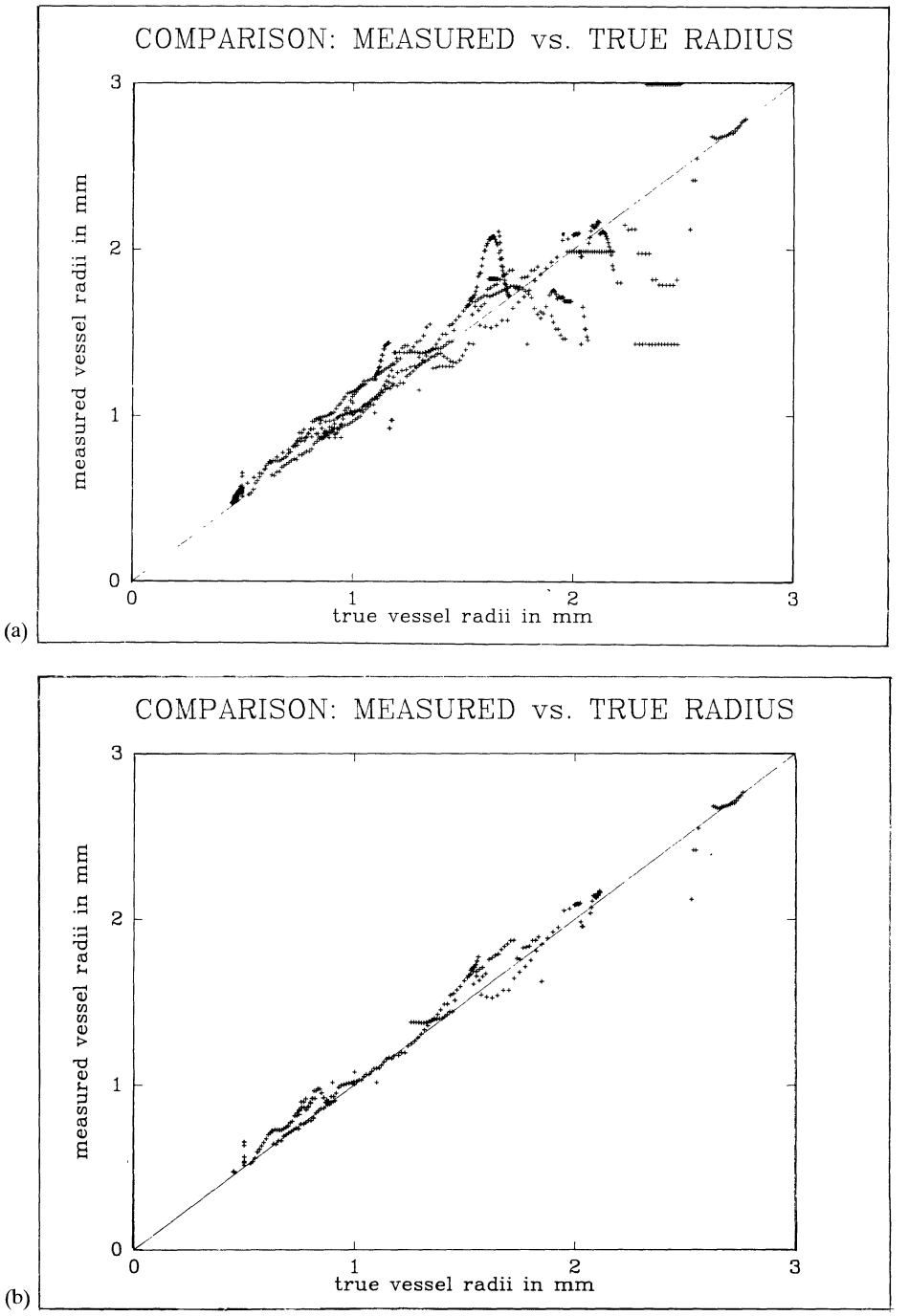

Fig. 4. Comparisons of the radius measurements in the 3D representation with the original ("true") on a pointwise basis; (a) all measurements are compared; (b) only measurements for those points that are clearly seen in both views are compared.

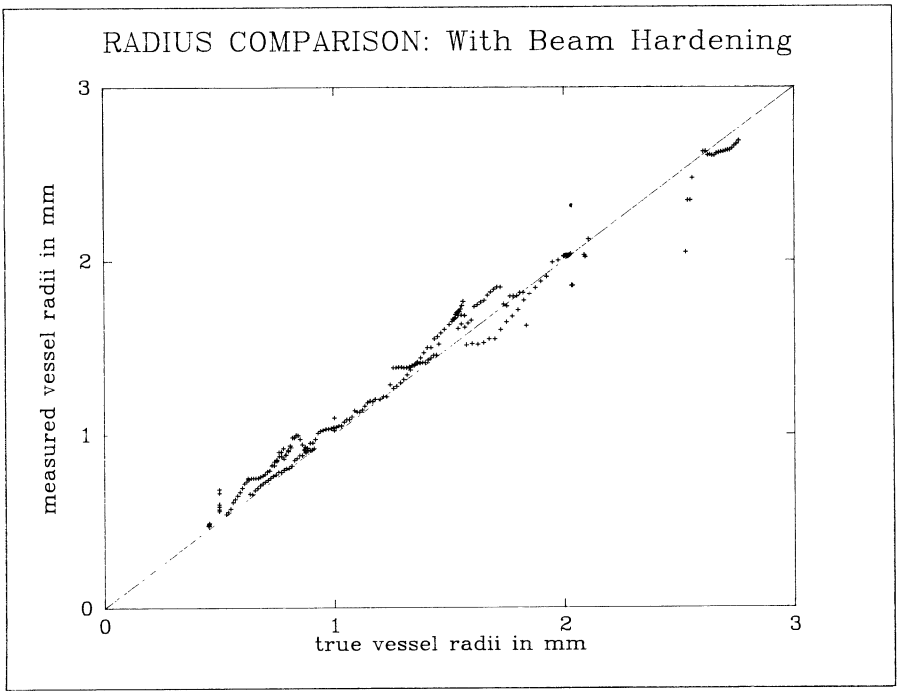
RADIUS COMPARISON: With Beam Hardening
measured vessel radii in mm
true vessel radii in mm
0
1
2
3

(a)

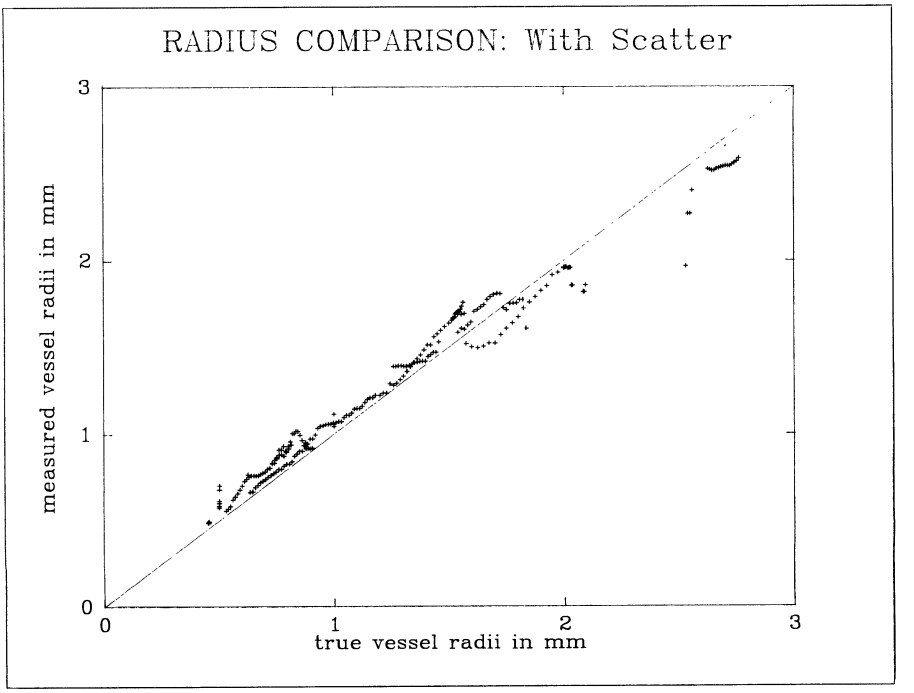
RADIUS COMPARISON: With Scatter
measured vessel radii in mm
true vessel radii in mm
0
1
2
3

(b)

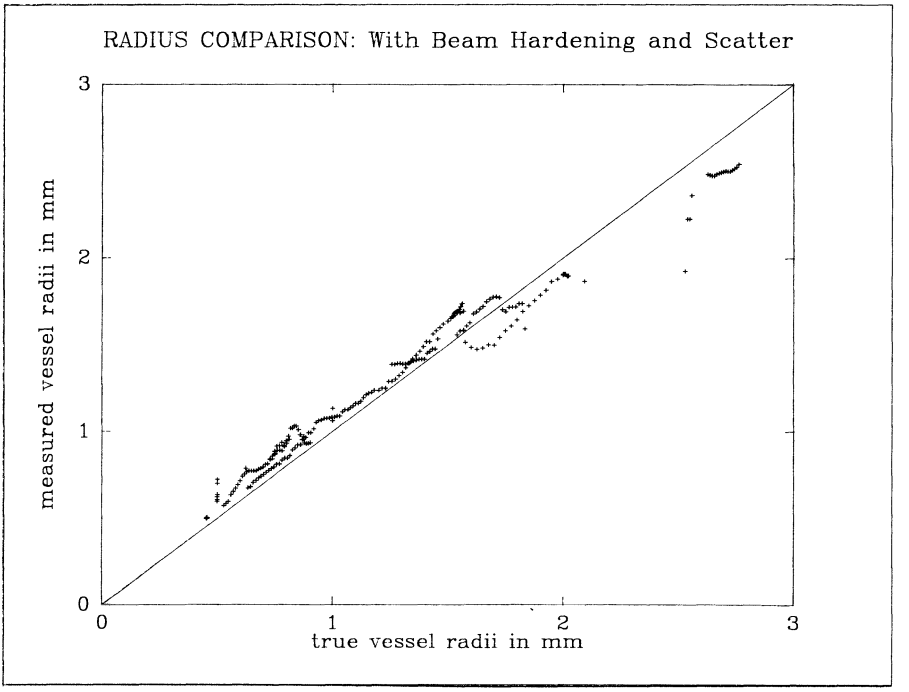

Fig. 5. Pointwise comparison of the true radius with the reconstructed radius in the presence of beam hardening (60 kVp, 2 mm aluminum and 20 cm soft tissue, iodine concentration of 0.37 g/cc) and scatter $f = 0.2$; (a) beam hardening only; (b) scatter only; and (c) beam hardening and scatter.

list the slopes of the least-square-fit lines under various amounts of scatter and beam hardening. Beam hardening is changed by varying the aluminum prefilter thicknesses. Data in the Table show that an increase in scatter causes an increase in the rotation, while aluminum prefiltration causes virtually no change. Figure 6 combines errors measured in Figure 5c with Figure 1 (curve c2). The solid curve represents the error caused by beam hardening and scatter ($f = 0.2$). The scattered points show the reconstruction errors of the clinical phantom under the same degradations. The scattered points follow the trend of the curve well within the range of one pixel (0.4 mm). The differences are caused by the randomness in determining vessel centerlines as well as the vessel orientation angles to the image plane. The vessels of Figure 5c have variable orientations, and thus variable path lengths which, for any given size, are greater than or equal to the basic paths of the vessels in Figure 1. Thus, the nonlinearity due to scatter and beam hardening will be variable, but systematically shifted to smaller "true" vessel dimensions. The curve of Figure 1 represents a limiting value for the data of Figure 5c.

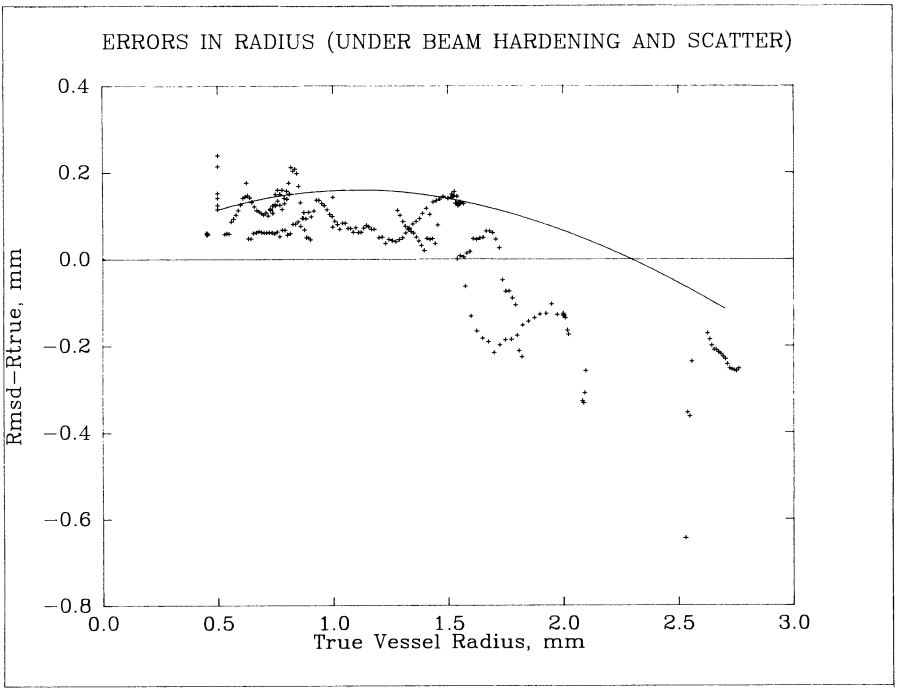

Fig. 6. Predicted errors in radius (curve) and reconstruction errors (points) of the coronary artery phantom. The curve represents a limiting value for the scattered errors.

Comparison with computed tomography

X-ray projection images of the coronary artery cast are shown in Figure 7. These images show the marks which have been placed on the external surface of the phantom and which are used to determine the relative view orientations. Computed tomography images of the cast with external marks were obtained using the previously described protocol (e.g. Figure 8a, c, e, g). The approximate angiographic view orientation is used to project the mark locations determined by CT back onto the angiographic images (Figure 7c and 7d). Finally, the relative accuracy of the 3D coronary reconstruction was evaluated by combining the 3D vessel reconstruction with the original CT images. Some example images are shown in Figure 8 (b, d, f, h) and Figure 9.

Discussion

The studies presented in this paper provide an indication of the accuracy that can be obtained in the reconstruction of the coronary artery vascular bed from two or more digital angiographic views. From the simulation study it is

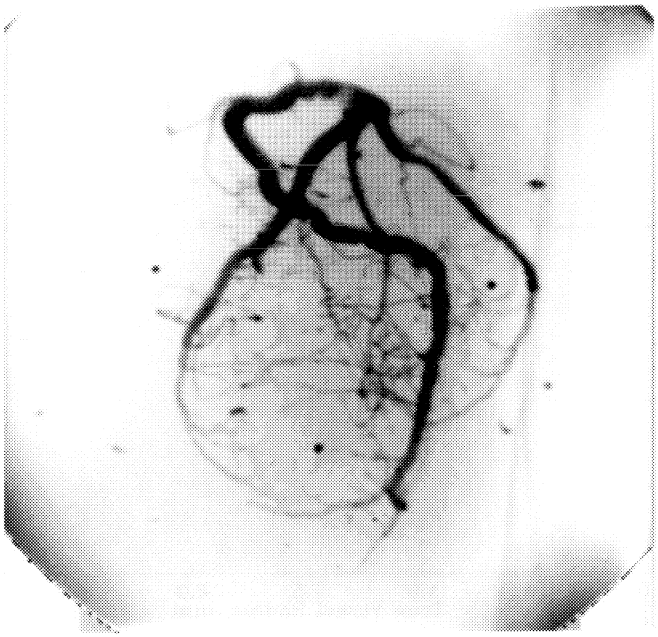

(a)

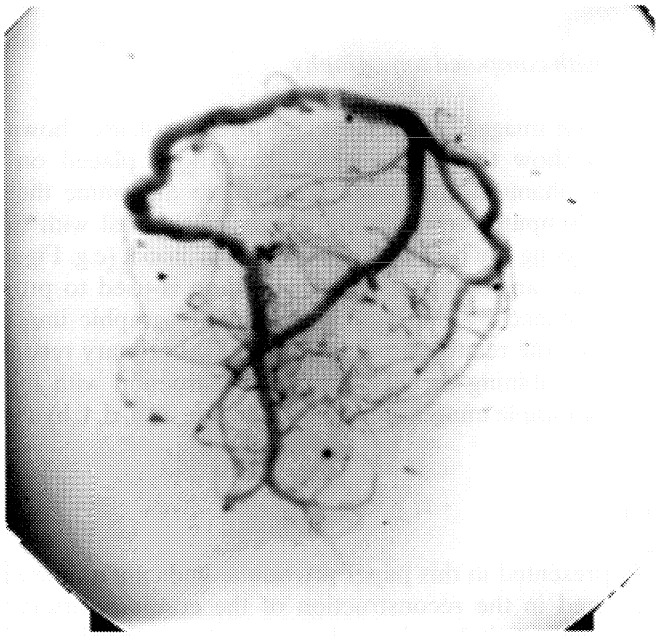

(b)

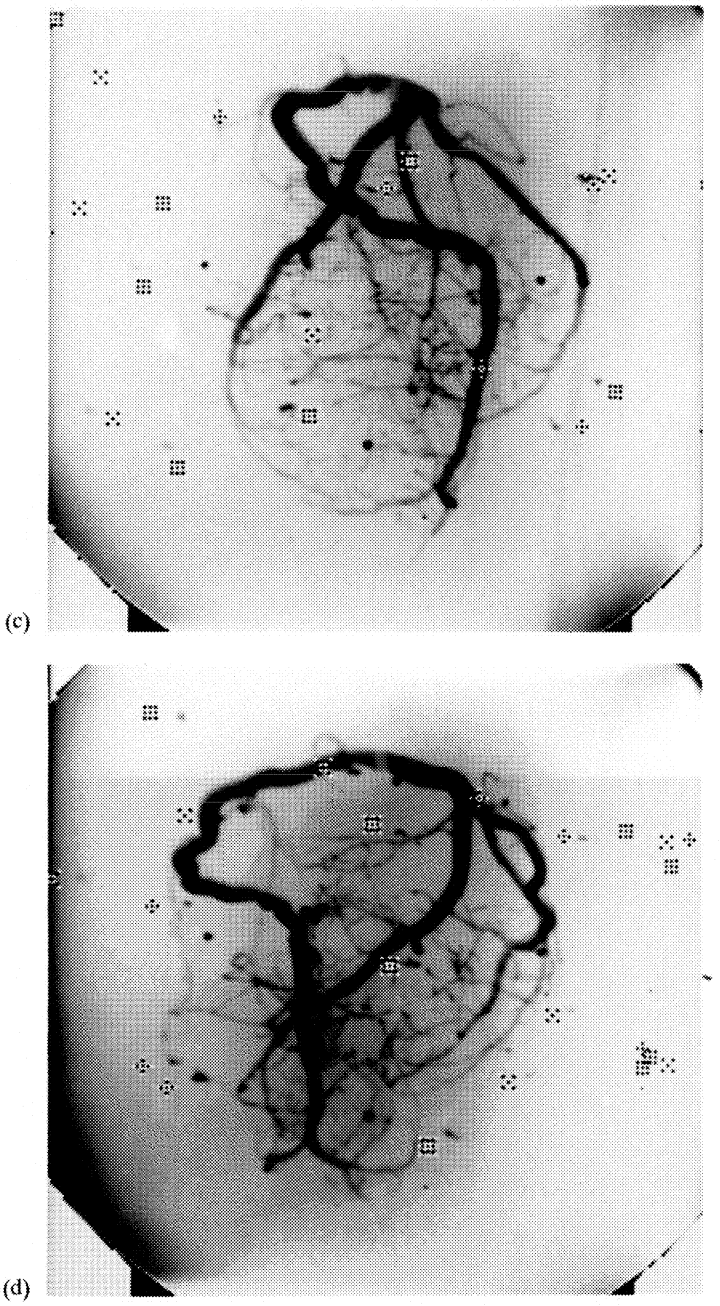

Fig. 7. (a) and (b): X-ray projection images of the pig coronary artery cast showing small radio-opaque marks used for view orientation determination: (c) and (d) Mark locations determined from CT are reprojected onto images from (a) and (b) using the approximate view orientation.

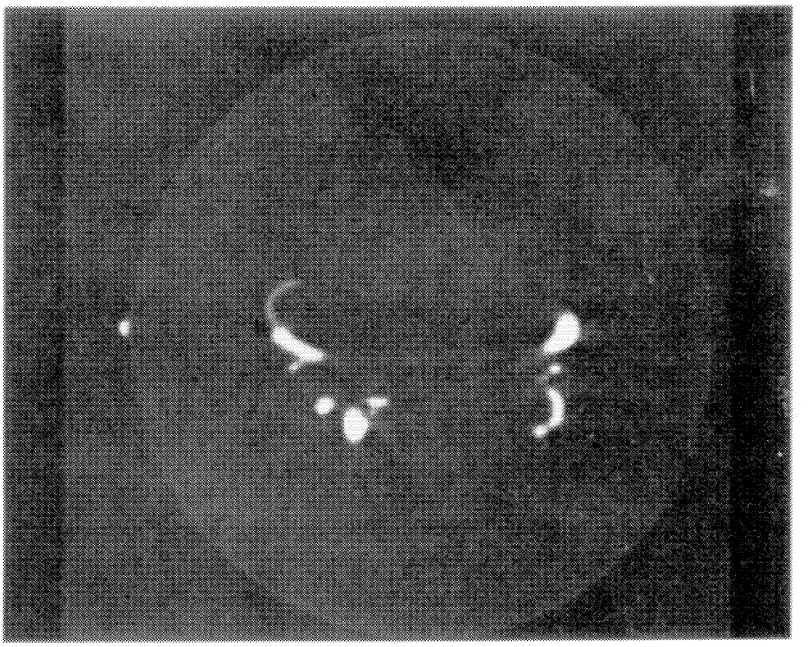

(a)

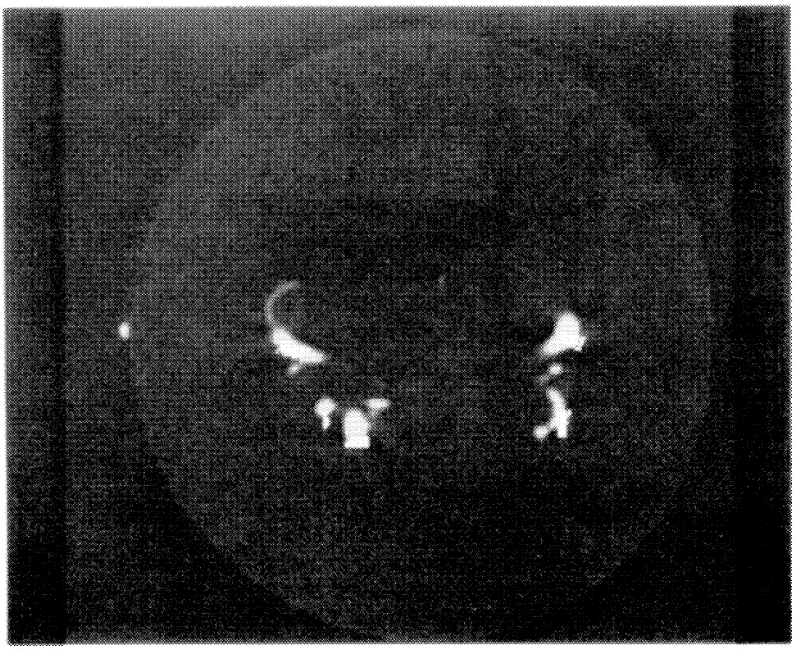

(b)

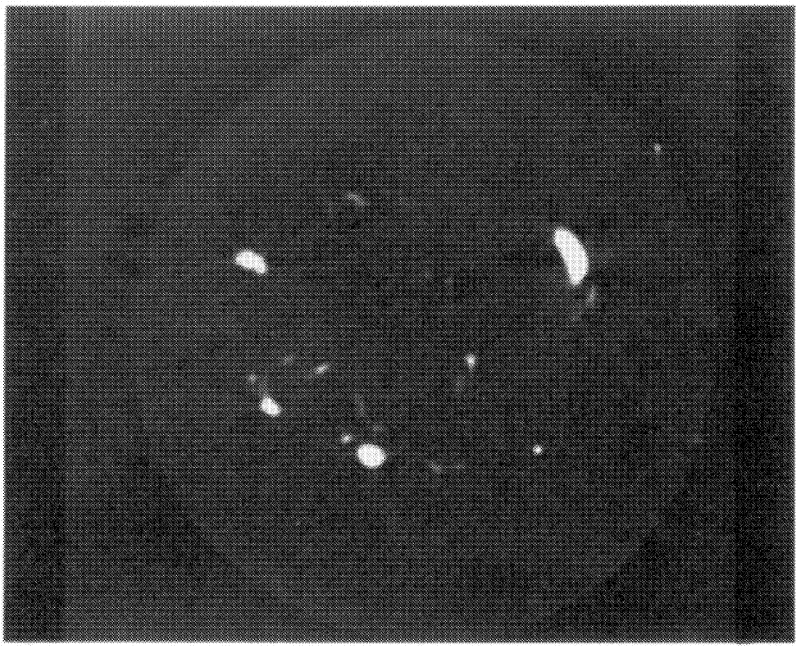

(c)

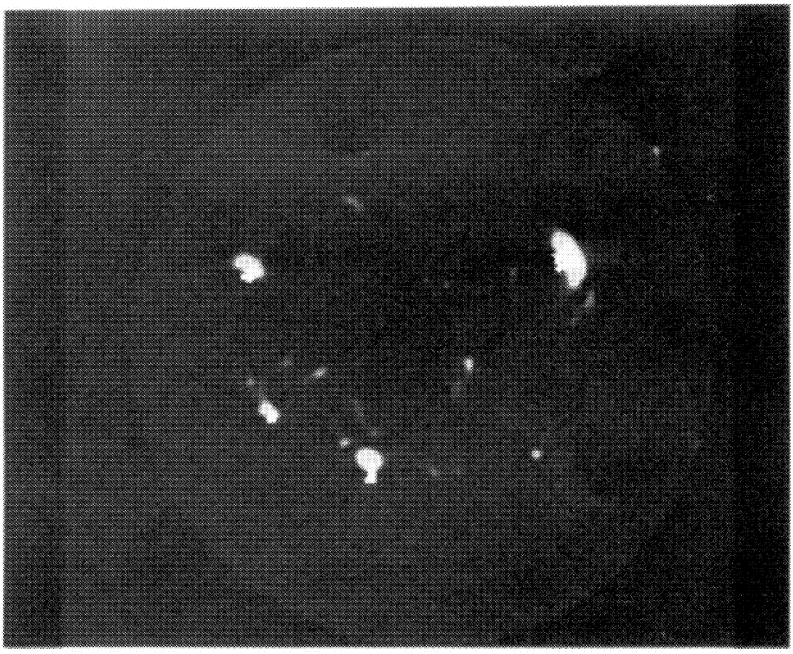

(d)

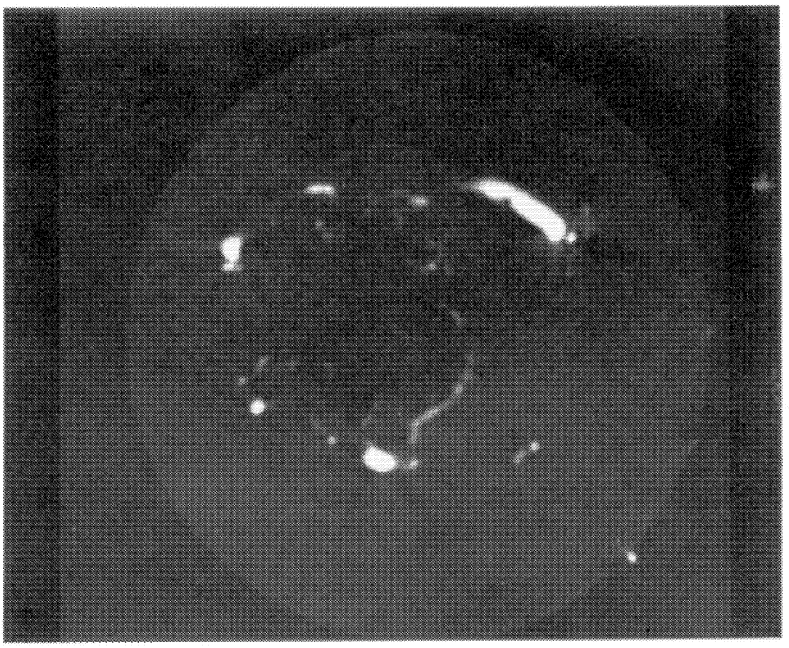

(e)

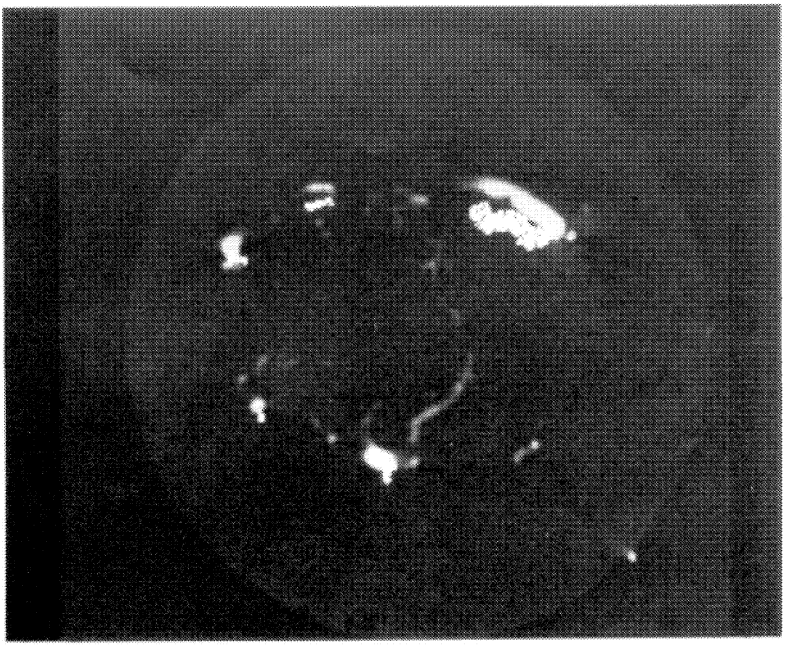

(f)

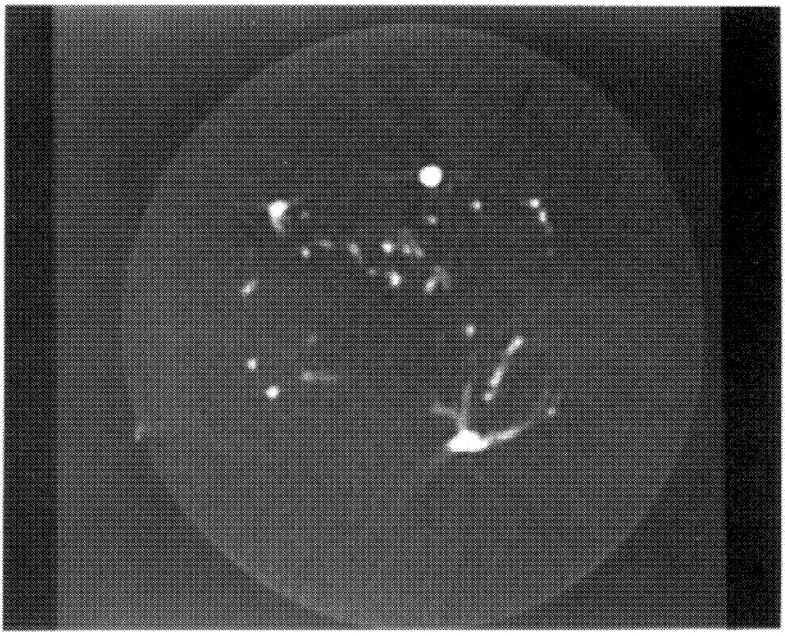

(g)

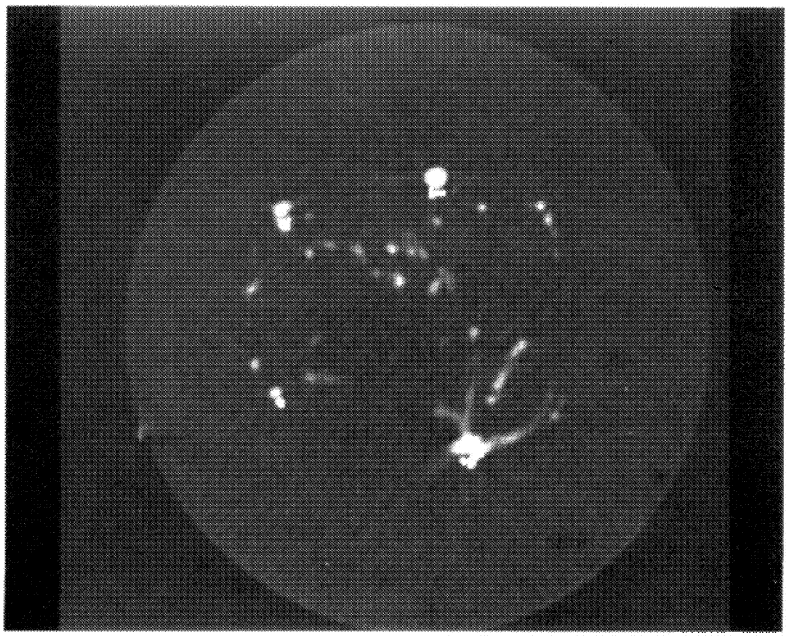

(h)

Fig. 8. Computed tomography images of pig coronary artery phantom. External marks are visible on the surface of the cylinder. (a, c, e, and g) are the original CT images; (b, d, f, and h) show points from the 3D reconstruction superimposed back on the CT images.

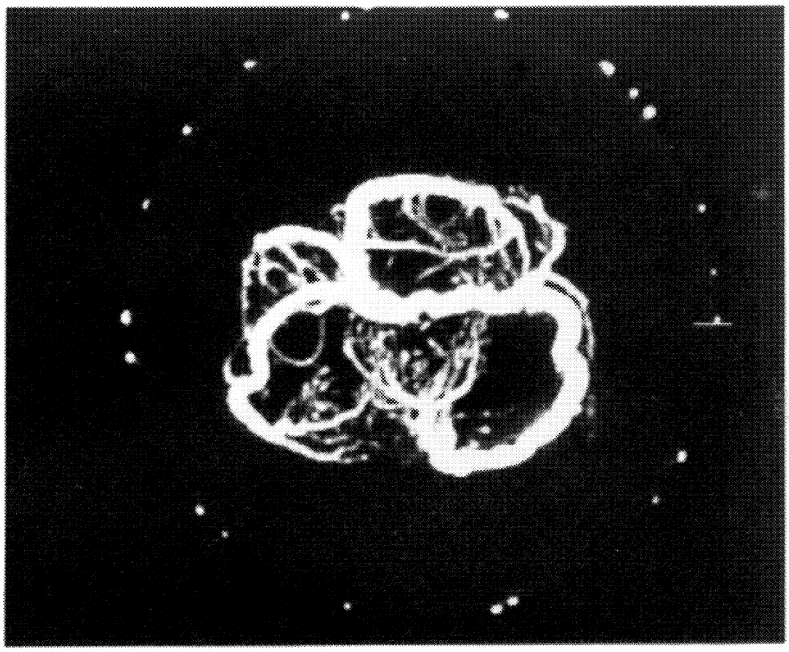

(a)

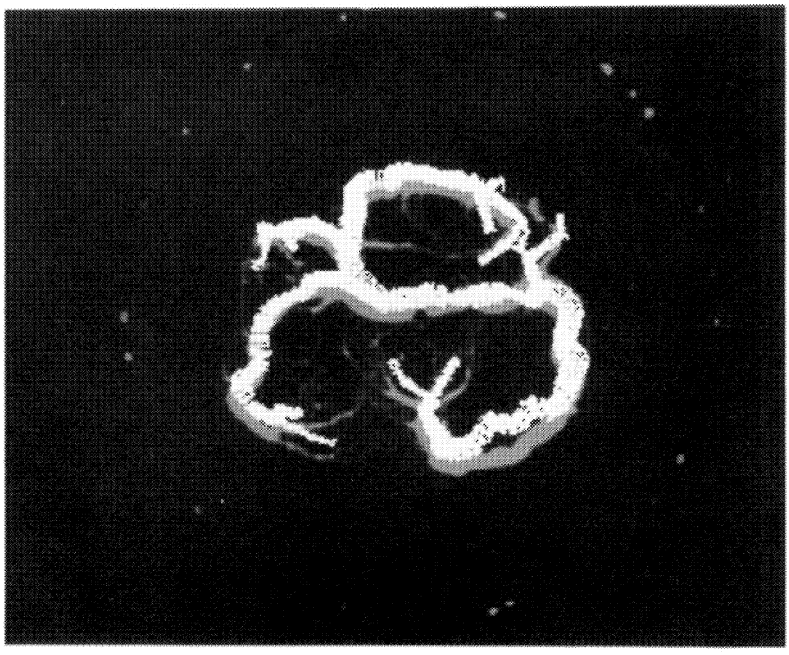

(b)

Fig. 9. (a) A projection image through the set of axial CT images. (b) same as (a) with points representing the 3D reconstruction added.

evident that uncorrected X-ray scatter can cause a small, but significant systematic error in the measured vessel dimensions. It is seen from the Figure 4 and 5 that the error is smallest for the small vessels and increases rapidly with vessel size. The overall error is reduced when an averaging process over a range of vessel sizes is used to determine k. For coronary arteries, vessels involved in reconstructions normally range between 0.5 and 3.0 mm. In this case, the averaging method is well behaved.

The simulation results presented in Table 1 indicate that the accuracy of centerline determination is on the order of the linear dimensions of one pixel. These results also indicate that the precision in this measurement is a strong function of the number of views in which the vessel is clearly visible. Note that the simulation study is clearly under ideal conditions. A qualitative assessment of the results from the CT registration experiments indicate that the vessel centerlines are very close to the vessel positions found in CT while a systematic shift has appeared to occur. The cause of this shift, which is on the order of the vessel dimensions, remains to be determined.

Data presented in Figure 4 and Table 1 show that significantly better lumen measurement accuracy is obtained when the vessel segment is clearly visualized in two views. In Table 1 it is evident that the measurement precision is a strong function of visibility. This observation suggests that the inclusion of information from one or more additional views will increase the reconstruction accuracy because additional views can be expected to increase the fraction of the arterial bed that is clearly imaged in at least two views. Problems due to vessels which are highly angled with respect to the image plane are not directly addressed in the study. However, it is obvious that X-rays forming images of these vessels undergo longer distances than the vessel diameters and suffer more severe degradations from beam hardening and scatter. The probability that a vessel segment is nearly parallel to the imaging plane in at least one view will increase with the number of views available. Measurements from the view with smaller vessel angle are expected to give more accurate reconstructions.

For a vessel segment to be unambiguously visualized in any projection image, it is sufficient for the projected vessel segment to be separated from other projected vessels by a small distance determined by the imaging resolution and the distance required for background measurement. This is illustrated in Figure 10. It is also necessary that vessel segments inclined greater than some maximum angle be eliminated from analysis. Thus, independent of the type of statistical distribution the vessel visibility may follow, the probability that a vessel segment can be measured will be the product of the probability that the vessel segment is visible and the probability that it is inclined less than the given angle:

$$f_m = f_v \sin \theta_{\max}. \tag{22}$$

To the extent that there is independence of the vessel distribution between views, the fraction of vessel segments measurable in at least one out of N

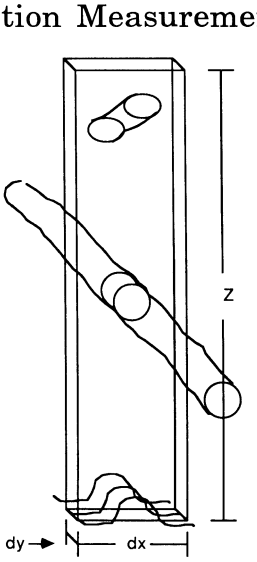

Fig. 10. Imaging region required for visualization of central vessel segment. The presence of another vessel segment in the volume segment will reduce the accuracy of measurements made from the region.

views is:

$$\alpha = 1 - (1 - f_m)^N = 1 - (1 - f_v \, sin \, \theta_{max})^N. \tag{23}$$

This function is plotted in Figure 11 for various visibility fractions.

The effects of beam hardening and scatter are not linear with respect to vessel sizes. Although beam hardening has little effect in conjunction with the 20 cm of water equivalent tissue simulated, it will likely be more significant through thinner body parts. Scatter, on the other hand, results in a significant systematic error. Because the error is systematic, it is likely that the magnitude of the error can be predicted and corrected. Ideally, such correction would be performed in the presence of some measurements of the scatter distribution in the image.

Conclusions

This study provides some indication of the accuracy that may be currently obtainable from 3D reconstruction of the coronary artery bed from 2 view digital angiography images. Because of the effects which are not considered in this study, including motion artifacts due to the heart and respiration, it is likely that measurement accuracy will be lower than that obtained in the simulation study. It is shown that the accuracy in morphology measurements

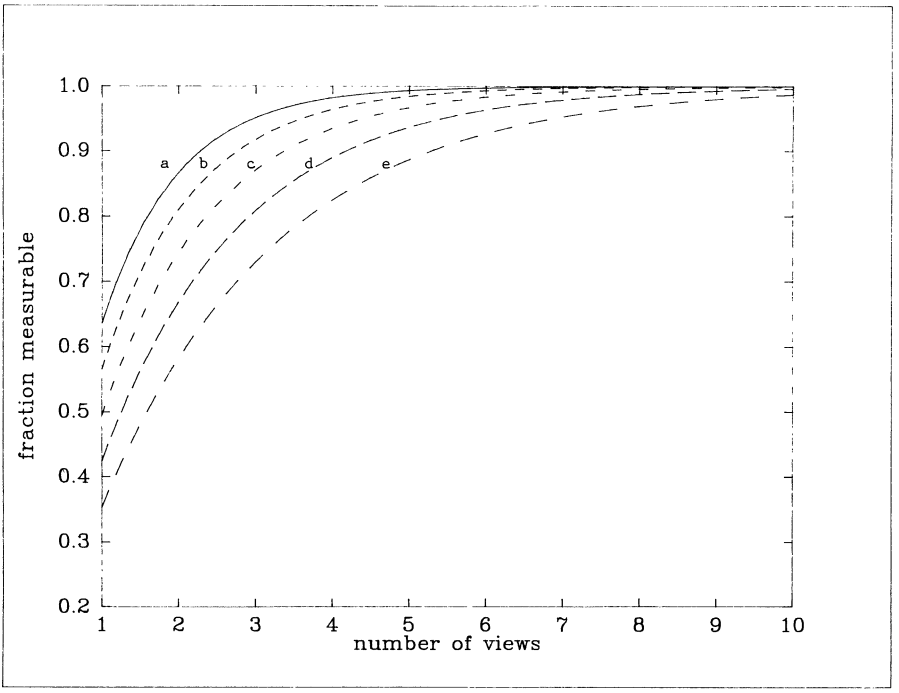

Fig. 11. Fraction of vascular bed that can be measured as a function of the number of views and the fraction of the vascular bed visible in each view. The visible fraction is (a) 0.9, (b) 0.8, (c) 0.7, (d) 0.6, and (e) 0.5.

(vessel position and lumen area) are strong functions of the number of views in which the vessel is clearly visible and is imaged nearly parallel to the imaging plane.

Measurements which are derived from vessel morphology (such as flow and calcium lesion positions) will be affected by the accuracy in the morphology determinations.

Acknowledgements

This work is supported by grants from Siemens Gammasonics, the Richards Memorial Medical Foundation and NIH grant HL36910.

References

1. Parker DL, Pope DL, Van Bree RE, Marshall HW: Three dimensional reconstruction of moving arterial beds from digital subtraction angiography. Comp Biomed Res 20: 166–185, 1987.

2. Parker DL, Wu J, Pope DL, Van Bree RE, Caputo GR, Marshall HW: Three-dimensional reconstruction and flow measurements of coronary arteries using multi-view digital angiography, In: New developments in quantitative coronary arteriography. JHC Reiber, PW Serruys (eds). Kluwer Academic Publishers, Dordrecht, 1988: 225—247.
3. Garrison JB, Ebert WL, Jenkins RE, Yionoulis SM, Malcom H, Heyler GA: Measurement of three-dimensional positions and motions of large numbers of spherical radiopaque markers from biplane cineradiograms. Comp Biomed Res 15: 78—97, 1982.
4. Kim HC, Min BG, Lee TS, Lee SJ, Lee CW, Park JH, Han MC: Three-Dimensional Digital Subtraction Angiography. IEEE Trans on Med Imaging Vol MI-1(2): 152—158, 1982.
5. Reiber JHC, Gerbrands JJ, Troost GJ, Kooijman CJ, Slump ch: 3-D reconstruction of coronary arterial segments from two projections. In: Digital Imaging and Cardiovascular Radiology. PH Heintzen, R Brennecke (eds). Georg Thieme Verlag, Stuttgart, 1983, pp. 151—63.
6. Guggenheim N, Dorsaz PA, Doriot PA, Descouts P, Rutishauser W: Determination of Intra-arterial volumes from biplane coronary angiography. Comp Cardiol, 1988: 71—74.
7. Pope DL, Parker DL, Gustafson DE, Clayton PD: Dynamic search algorithms in left ventricular border recognition and analysis of coronary arteries. Comp Cardiol, 1984: 71—75.
8. Nalcioglu O, Roeck WW, Seibert JA, Lando AV, Tobis JM, Henry WL: Quantitative aspects of image intensifier-television-based digital X-ray imaging. In: Digital Radiography. JG Kereiakes, SR Thomas, CG Orton (eds) Plenum Publishing Corporation, 1986.
9. Curry TS III, Dowdey JE, Murry RC Jr: Christensen's Introduction to the Physics of Diagnostic Radiology, 3rd Ed. Lea & Febiger Publishers, Philadelphia, 1984.
10. Hubbell JH: Photon Cross Sections, Attenuation Coefficients and Energy Absorption Coefficients from 10 keV to 100 GeV. NSRDS-NBS 29 (U.S. GPO, Washington, DC, 1969).
11. Kruger RA: Estimation of the diameter of the iodine concentration within blood vessels using digital radiography devices. Med Phys 8(5): 652—658, 1981.
12. Wu J, Parker DL, Caputo GR, Marshall HW: A clinical study of 3D reconstruction and measurement of coronary arteries. Dynamic Cardiovascular Imaging 1(4): 273—278, 1988.
13. MacKay SA, Sayre RE, Potel MJ: 3D Galatea: Entry of three-dimensional moving points from multiple perspective views. Computer Graphics, 16(3): 213—222, 1982.

Part V

Intracoronary prostheses

14. Stenting of coronary arteries: Are we the sorcerer's apprentice?

PATRICK W. SERRUYS, KEVIN J. BEATT and
WILLEM J. VAN DER GIESSEN

Summary

Stenting of coronary arteries following coronary angioplasty may have a role in relieving procedure-related abrupt occlusion and in the reduction of late intimal hyperplasia responsible for "restenosis". In the period from March 1986 to January 1988, the initial 117 Wallstent endovascular devices were implanted in the native coronary arteries or saphenous vein bypass grafts in 105 patients. Follow-up angiograms (mean 5.3 ± 4.3 months) were obtained in 86 patients with 96 stents and analyzed quantitatively by a computer assisted cardiovascular angiographic analysis system. Complete occlusion occurred in 25 stents in 25 patients (26%), with 22 of these occlusions documented within the first 14 days. In the 71 remaining patent stents, there was a significant improvement in minimal luminal diameter (MLD) and percentage diameter stenosis (DS) immediately following stenting (1.9 ± 0.4 mm to 2.6 ± 0.5; 36 ± 11% to 19 ± 7%, respectively, $p < 0.001$). However, there was significant late reduction in MLD and increase in mean DS in the stented segment to 2.3 ± 0.8 mm and 31 ± 16% at follow up ($p < 0.002$). Despite this late angiographic narrowing, MLD and DS remained superior to the immediate post-angioplasty result ($p < 0.002$). Significant hyperplasia, defined as a change in minimal luminal diameter $\geqslant 0.72$ mm or increase in diameter stenosis to $\geqslant 50\%$, occurred in 30% and 14% of stents, respectively. We conclude that early occlusion remains a significant limitation with this particular coronary stent. Although hyperplasia occurs in a significant number of stented lesions, the early intrinsic dilating function of the stent appears to attenuate the effects of this process.

Introduction

The original work of Andreas Gruentzig in 1977 [1] provided the stimulus for the rapid technological growth that has been seen in the field of interventional cardiology. More recently, there has been an explosion of new devices

J. H. C. Reiber and P. W. Serruys (eds), Quantitative Coronary Arteriography, 297–311.

designed to ablate coronary artery narrowings, recanalise occluded vessels, and to prevent restenosis; this growth has been so overwhelming, that it is currently difficult to evaluate the relative merits of each and to define their places in clinical practice. In many of these areas the cardiologist has been acting solely as a technician limiting his concern to the technical and procedural aspects, and sometimes overlooking the complex biological and physiological mechanisms of atherosclerosis in general, and more particularly of the restenosis process.

In achieving the perceived benefit of the therapeutic intervention with these devices, the vessel wall is subjected to thermal and mechanical insults, which may have hidden long-term consequences, such as the restenosis process [2, 3], which has now been iatrogenically induced in tens of thousands of patients.

One of the most recent developments has been the use of the intravascular stent [4] although the original concept of intravascular stenting precedes the introduction of coronary artery interventional cardiology by many years. In 1969 Dotter developed a coilspring endovascular prothesis in an attempt to improve the longterm patency of peripheral atherosclerotic vessel submitted to recanalisation and dilatation. Even at the time he envisaged that "prompt fibroblastic development and a rapid formation of a new, firmly anchored autogenous lining surface" would be a critical factor in the longterm patency of the device [5].

Since the original description of Dotter's tubular coil spring [5], many variants of the original concept have been deployed experimentally, including: thermal shaped memory alloy stents [6—8], self expanding steel spirals [9—12], self expandable stainless steel mesh stents [13—15], balloon expandable stainless steel mesh stents [16—19], balloon expandable interdigitating coils [20, 21], synthetic polymeric stents and biodegradable stents [22]. These various devices differ greatly in their fundamental geometry (mesh, single wire), composition (metal, plastic) and mechanical behavior (active or passive expansion). Besides these fundamental difference, there are a variety of subtle dissimilarities which may be important in themselves such as thickness of filaments, alloy composition, electrostatic behavior, biocompatible or therapeutic coatings [23]. The prolonged presence of these materials residing in the arterial wall may generate late unknown and unexpected consequences.

What is the rationale for stenting an atherosclerotic vessel during or after dilatation?

In the first place the stent may optimize the dilatation process, by containing the irregular surface of the atherosclerotic plaque created by the disruptive action of the balloon. Two potential adverse effects, distal embolisation of maroscopic debris originating from the plaque and a protruding obstructive flap may be contained by the stent acting as a scaffolding device. The balloon expandable stent in particular may be advantageous in the situation when the

operator electively uses the device to dilate the lesion and implant the stent in a single manoeuver. The self expanding stent on the other hand, by exerting a continuous radial force has the effect of increasing the diameter of the lumen until a balance is reached between the expanding force of the stent and the circumferential compliance of the vessel [4, 24]. The physiopathological consequence of this is unknown, but recently this interaction has been documented to continue for at least 24 hours and possibly longer, resulting in continued improvement in the vessel lumen over and above that obtained at implantation [25]. The recoil phenomenon which is poorly documented and probably underestimated as a cause of "restenosis", will be equally prevented by both types of stent [26]. In addition, both types of stent have a smoothing effect which reduces the turbulent and laminar resistances and may be beneficial in preventing restenosis [14, 15]. Much has been made of the ability of the stent to prevent restenosis, with various theoretical proposals as to how this can be achieved and why one particular design might be more effective than another [4, 20]. An attractive concept which favors the rigid stent is that the limitation of vessel wall stress seems to be protective against atherogenesis [27]. The self expanding stent by stretching the wall might have the effect of accelerating the restenosis process. However, whether the accelerated process is mostly related to pulsatile stress rather than stress per se remains to be demonstrated. Although there may be some experimental work in animals to support these claims, there is as yet no evidence to support them in the clinical situation and must therefore be regarded as speculative. There may be ultimately little difference between compliant and uncompliant devices (considering the amount of radial forces at the site of the wires exerted on the vessel wall). The initial intuitive and simplistic concept, not supported by experimental evidence that the stent may act as a barrier preventing the migration of cellular structures (monocytes, marcophages, smooth muscle cells) into the intima during the healing process, has not been realised and the other potential mechanisms of prevention of restenosis by stenting the internal wall of the vessel have not yet been fully elucidated or unequivocally demonstrated. An alternative mechanism is that chronic compression by the stent of vasa vasorum underlying an atherosclerotic plaque may result in ischaemia of this microscopic vascular network and thereby limit the subsequent progression of the atherosclerotic plaque [28].

The mechanism of restenosis prevention put forward by Palmaz et al. [18] is open to criticism on the basis that it is a too dynamic interpretation of what is in essence a series of post mortem "snap shots" which are difficult to reconstruct in time (Figure 1).This evidence recently reiterated by Schatz is extremely appealing and attractive, but remains an unsubstantiated interpretation [29]. The struts of the mesh prevent the protrusion of sizeable atherosclerotic plaques inside the lumen of the vessel and act as a "macroscopic sieve", containing and pushing the atherosclerotic plaque away from the neo-intimal lining into the adventitia. In addition, a sclerotic thinning of the media is apparently induced converting the muscular and dynamic medial

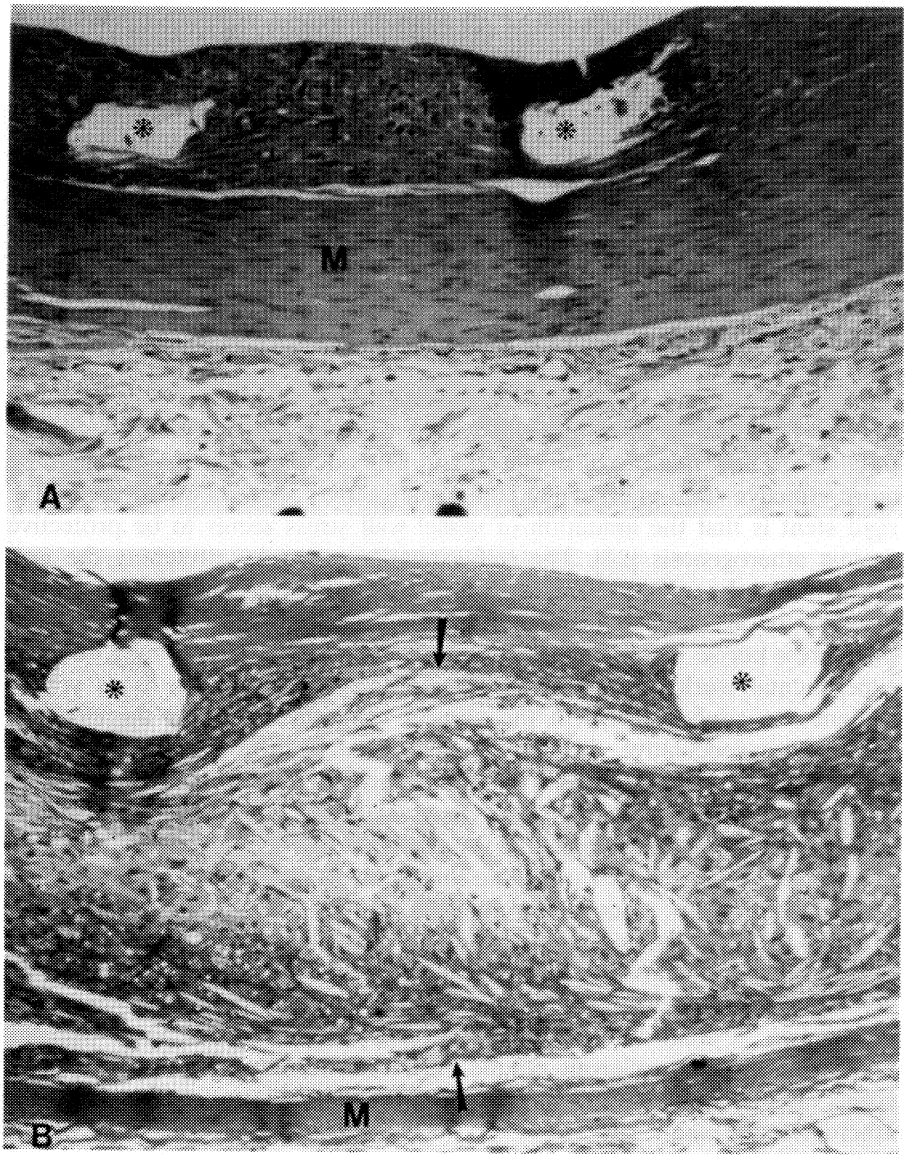

Fig. 1. Microphotography of cross section of an atherosclerotic rabbit aorta 1 week (Panel A) and 6 months (Panel B) after stenting. Note the thin layer of thrombus (T) covering the stent struts(*) and the thick media (M) at 1 week. By 6 months, thrombus is replaced with acellular ground substance and endothelium. A large plaque is evident (arrows) but does not encroach the lumen (from Schatz [29], reprinted with the permission of Circulation).

layers of the vessel into a practically nonvasoactive and noncompliant "pipe". Whether this is true and applicable to the human clinical situation remains to be demonstrated.

There is a consensus among investigators in the field that stent implantation improves the immediate post dilatation result, producing a smooth straight line appearance of the dilated segment. This visual impression has been confirmed by quantitative analysis using both edge detection and videodensitometric techniques [24]. Favorable results have also been reported in the "bail-out" situation,when the stent has been implanted following dilatation where presence of intimal dissection has led to a poor and even critical hemodynamic result [30, 31].

The thrombogenic nature of the stent remains a concern, although there may be important differences between the different devices [29, 32, 33]. This concern is reflected in the anticoagulant regimens used in patients in whom the Medinvent stent was implanted (Table 1). This complex and aggressive protocol reflects the insecurity of the clinician and the knowledge that none of the anticoagulant agents on their own will reliably prevent thrombus formation. It is a paradox that similar devices but with different metallic compositions have been used for just the opposite effect: to create thrombotic occlusion in experimental animals [34—36].

At the Xth Congress of the European Society of Cardiology, Richard Schatz reported the immediate results in fifteen patients who had received a Palmaz stent. According to a FDA-approved protocol, the stents were implanted in vessels (mostly right coronary arteries) supplied by a collateral circulation. At that time he was convinced that all the patients could be treated with heparin and dextran during the procedure and aspirin and dipyridamole alone after discharge. There were no instances of abrupt closure and no patient required warfarin. These initial results suggested that this balloon expandable stent was relatively nonthrombogenic, which eliminated the need for both routine administration of lytic agents during the procedure and warfarin thereafter. Unfortunately, the angiographic follow-up at 6 months of these first 15 patients has disclosed 4 total occlusions and one restenosis. Since then, patients have been given coumadin.

Concern has also been expressed as to whether the composition of the stent is able to trigger an allergic response, particularly in individuals who may be hypersensitive to the individual metals that make up the composition of the device. Although there have been reports of transient inflammatory infiltrates in the adventitia following stent implantation, it is reassuring that there are no reports of foreign body cells in the immediate vicinity of the implanted device in the experimental animal model [13, 18, 37]. Human data to support this assumption is, however, still lacking.

Stent induced restenosis

Do we know what happens at PTCA and understand the process of restenosis?

Data from normal and atherosclerotic arteries of experimental animals and

Table 1. Intracoronary stent: multicenter European trial drug regimen.

Day before implant procedure	— Salicylic acid 2 × 500 mg — Dipyridamole 4 × 75 mg — Sulphinpyrazone % × 200 mg — Ca-antagonist: Nifedipine 3 × 20 mg/day
Day of implant procedure	— Salicylic acid 1 × 100 mg — Dipyridamole 4 × 75 mg (patients above 90 kg: 3 × 150 mg) — Sulphinpyrazone 4 × 200 mg
Before PTCA	— Diltiazem 5 mg — Heparin 10.000 I.U. — Dextran 500 mg/4 hr
At implantation	— 100,000 I.U. Urokinase in 250 ml NaCl given intra coronary (i.c.) up to the end of the procedure. Start drip at guide-wire insertion given over 30—60 min and another 250 ml (100,000 I.U.) for each extra hour. — Heparin 5000 IU. I.V.
(Post implantation)	At start of transfer, patient to receive *heparin* at the rate of 24,000 I.U. per 24 hr. to control PTT at minimum 70 sec. (This corresponds to about 400 I.U./kg/24 hr). For large patients the maximum rate is 30,000 I.U. per 24 hr. If PTT > 200 sec (5 × control value) the infusion is slowed. If PTT < 70 seconds infusion flow is increased. *No less than 24,000 I.U. heparin per 24 hr is to be given.*
Post implantation (day)	Start the oral anticoagulation with Acenocoumarol to be started from the first day (i.e.: 6 tablets of 4 mg each the first day, then 4 the day after and 2 the third day and then according to "QUICK".
Continuing anticoagulation	— Oral anticoagulation: Acenocoumarol: Quick to be maintained in the range of: 17%—25% (T.P. Thromborel S, Behring). *N.B.* Heparin will be stopped when the therapeutic level of oral anticoagulants is reached. — Salicylic acid 1 × 100 mg/day — Dipyridamole 4 × 75 mg/day (patients above 90 kg: 3 × 150 mg/day) — Sulphinpyrazone 4 × 200 mg/day — Ca-antagonist Nifedipine 3 × 20 mg/day
Longterm	This anticoagulation regimen is stopped after the 6 month coronary angiography control. Aspirin (100 mg 1 × day) should be given ad eternam.

human autopsied hearts have shown that following balloon dilatation the arterial intima or atherosclerotic plaque may split down to the internal elastic membrane [2, 3, 38]. Frequently, also damage of the arterial media with overdistension and splitting occurs. Next to or partially as a result of locally turbulent blood flow, a complex interaction between the exposed subendothelial surfact and blood elements occurs. This results in platelet deposition

locally in the region of the internal elastic membrane, which may be massive in case of tearing of the media, and the release of a variety of mitogens which may contribute to neointimal cell invasion and proliferation [39]. The most well recognised of these factors is platelet derived growth factor (PDGF), which may be released predominantly by platelets, endothelial cells as well as intimal smooth muscle cells [40]. Recently,the dimeric structure of this protein has been identified [41], while the three isoforms of PDGF may stimulate effects unique to each isoform through interaction with different classes of PDGF recptor [42]. There is now evidence that intimal mesenchymal cells or modified smooth muscle cells (but not medial smooth muscle cells) may by themselves release PDGF [40]. This may initiate the vicious circle responsible for the sustained proliferative process as it occurs in restenosis. However, the conditions under which this takes place, or the triggers responsible for this event are far from understood. In animal experiments, for example, two types of experimental arterial injury have been described: the first induced by passive trauma such as a catheter in situ or balloon denudation of the endothelial lining, and the second induced by a more disruptive stimulus, causing not only endothelial denudation, but also tearing of the media, which is the typical sequel of balloon dilatation [39, 43, 44]. Both are associated with the deposition of platelets on the vessel wall, with subsequent migration of smooth muscle cells from the media and their proliferation to form a neointima, and both can be prevented or inhibited by reducing the circulating platelets to very low levels. The first type associated with repeated trauma and presumably repeated thrombus formation, regress following removal of the traumatising stimulus. The second more disruptive type, however, results frequently in a lesion that is progressive in terms of smooth muscle cell proliferation and lipid accumulation. The reasons why one type of lesion regresses, while the other progresses are not clear. A possible explanation may come from studies on failure of synthetic arterial grafts. Once endothelial covering of synthetic grafts has progressed, smooth muscle cell proliferation appears to slow down, except in the region of anastomosis [45]. Thus a continued release of growth factors may occur even after complete endothelial covering either in areas of turbulent flow, resulting in continuous endothelial damage and repair, or at sites where the barrier between neointima and media is minimal. Evidence for continued mediator release by endothelial cells under specified conditions has very recently been published [46]. The presence of a nondegradable stent in the arterial wall may form such a trigger for continued mediator release. Immediately after stent implantation its luminal surface becomes covered with a combined platelet-fibrin deposition [13]. Within one week of implantation into previously dilated normal porcine arteries (Figure 2), there is complete endothelial covering of the stenting device [37] varying between 60 and 125 micorns, which acts to isolate the thrombogenic stimulus from the vessel lumen. Contained within this layer are abundant myofibrillar cells and macrophages: the harbingers of the restenosis process. These cells can be

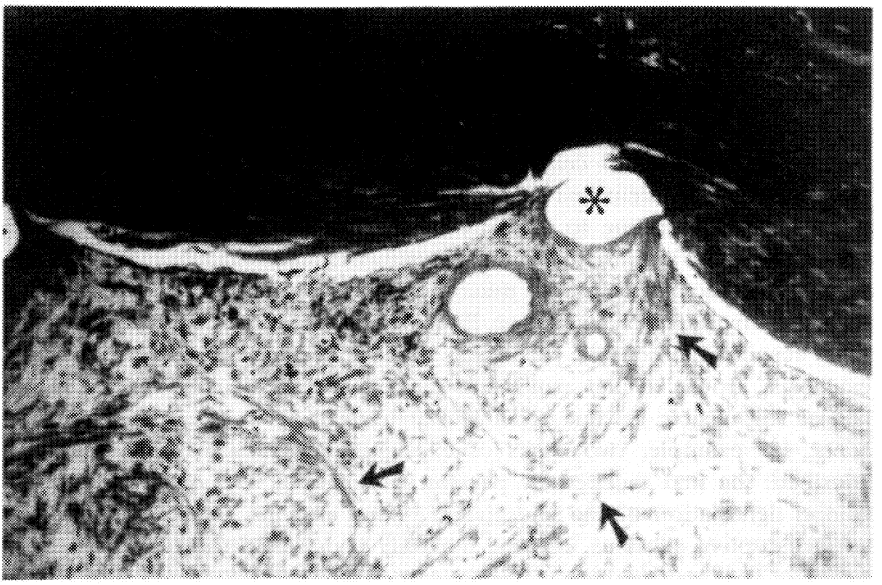

Fig. 2. Histologic cross section of a porine left descending anterior coronary artery 1 month after stent placement (magnification 200 x). The voids marked (*)originally contained the stent wires. In the neointima strands of elongated cells (arrows) are present in abundance.

seen to originate in the immediate vicinity of the individual stent filament adjacent to the internal elastic lamina, forming "geysers" of elongated cells fanning out to fill the neointimal tissue in an evenly distributed fashion. In some animals this process results in complete obstruction of the stented coronary artery as early as one month after implantation. Electronmicroscopic examination (Figure 3) of these fusiform elongated cells reveal oval nuclei with marginated chromatin, and abundant rough endoplasmatic reticulum. Bundles of contractile proteins can be demonstrated (small arrows) in a subplasmalemmal situation. These myofibroblasts or synthetic type smooth muscle cells are identical to those observed in the neointima after one week. It is therefore attractive to speculate that the same modified smooth muscle cells that imigrate through the internal elastic membrance (IEM) and which are implanted in the restenosis process after PTCA, [46, 47] can be operative in *an accelerated fashion* once a stenting device damages this natural barrier (IEM), making it more permeable to the migrating cells or providing a direct stimulus for cell migration. Recently, it has been suggested that the restenosis following primary balloon angioplasty is an unfavorable lesion for interventions such as atherectomy and stenting [48, 49, 50]. From preliminary data presented by Simpson et al. at the 38th session of the American College of Cardiology, it appears that restenosis rate following atherectomy as a primary intervention is 23.5%, while the restenosis rates are 36.8, 42.1 and 53.8%, when atherectomy was performed as the

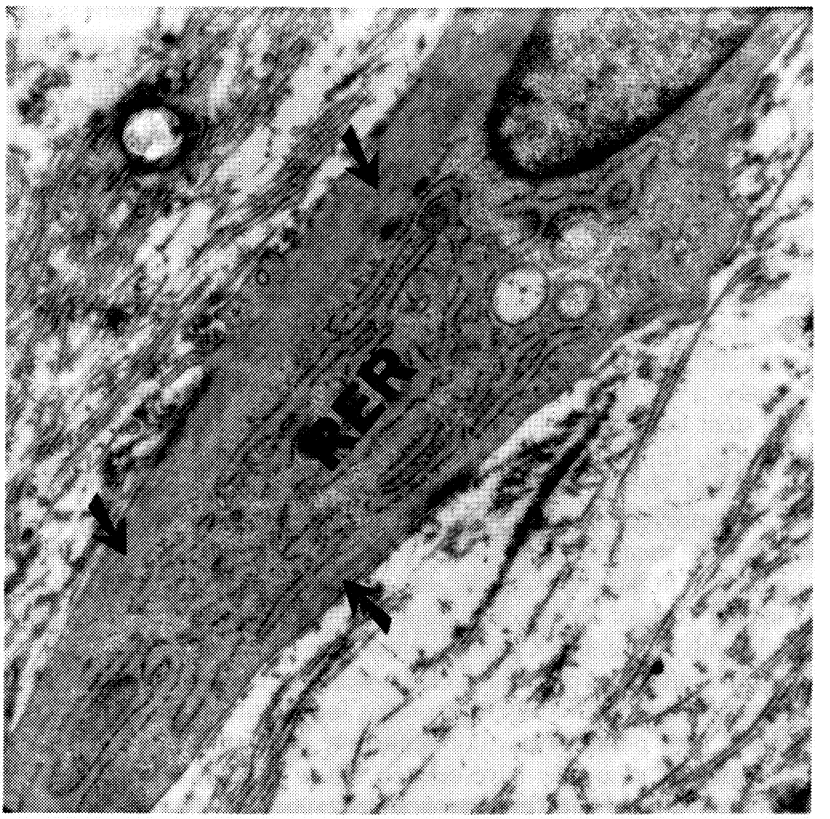

Fig.3. Transmission electron microscopy of the elongated cell-type of figure 2 (Magnification 25,000 x). Abundant rough endoplasmatic reticulum (RER) is present within these cells. Along the cell membrane bundles of myofilaments (arrows) are also prominent.

secondary treatment following a first, second and third recurrence of stenosis [51]. A similar opinion has been expressed by the group of Sigwart et al. [48]. Their preliminary data would seem to suggest that elective stenting for restenosis early after previous angioplasty carries an increased risk (41%) of restenosis within the stent. It could be that the active fibrocellular proliferation associated with the early phase of restenosis after balloon angioplasty is further stimulated by stent implantation.

In this respect, one of the questions posed by Spencer King III in his editorial is judicious and pertinent: whether the treatment is worse than the disease? [33]. Perhaps a more appropriate question is whether we have to apply these more costly interventions, as the initial procedure, in order to achieve a reduction of the restenosis rate? Such is the dilemma we have to face. Certain authors have already drawn the conclusion that atherectomy, for example is a *favorable* primary approach for the treatment of selected *unfavorable* lesions [50].

The intracoronary stent like many other novel forms of treatment seems to be following the well worn path of initially elated euphoria where enthusiasm holds sway of over scientific evidence followed by critical scepticism with little optimism for the future. A period of critical scientific evaluation is now needed, in which the lessons learned from the past are implemented. The initial experience has revealed three factors associated with complications: small vessels < 3 mm, low blood flow with poor run off, and evidence of hypercoaguability or local thrombus formation. This has led most investigators to restrict the use of this stent to saphenous bypass grafts with large diamenters and to the native circulation as "bail-out" device. In Europe, according to the data from the Working group on endoluminal prostheses,* Medinvent stents have been implanted in 187 patients between March 1986 and January 1988 in both native coronary arteries and bypass grafts. Although stent implantation is capable of producing a superior haemodynamis result [19, 25], the preliminary data suggest that the restenosis rate is between 14 and 30% according to the applied criteria (diameter stenosis $\geqslant$ 50% $\geqslant$ 0.72 mm reduction in the minimal luminal diameter [54, 53] (Figure 4). The Palmaz stent, currently being used in three centers in Europe has been implanted in situations which are considered low risk of acute problems, but high risk of reocclusion (total occlusions, protected myocardium from collaterals). The intracoronary stent represents a two edged sword although the scaffolding properties of the device are attactive and of shown benefit, it may provide a iatrogenic stimulus for erratic and uncontrolled cell proliferation. This potential has not been fully appreciated by the interventional cardiologist, who may have opened a new Pandora's box of complex biological interactions, but who may well be rescued by the cellular biologist in the future. The device is a logical vehicle for the topical release of agents that will ideally enhance endothelialization, but suppress the keloid type reaction of the traumatized vessel wall. The solution of this problem is not helped by the lack of joint effort on the part of the pharmaceutical industry and the industry producing the mechanical device, which is a source of frustration to investigators in the field, but hopefully will be overcome in the future. The initial hopes that stent implantation may prevent or diminish restenosis has not been fulfilled. In addition, early thrombotic occlusion in the native coronary circulations has led many to abandon temporarily this as an indication except for emergency "bail-out" indications.

Are we the sorcerer's apprentice?

A case report will illustrate our concern better than a long series of arguments. A male patient from Los Angeles with two major risk factors for CAD: diabetes and hypercholesteremia, sustained in 1977 an inferior myocardial infarction. Post-infarction angina was treated by 2 saphenous vein

* Participating Centers and Collaborators: See appendix.

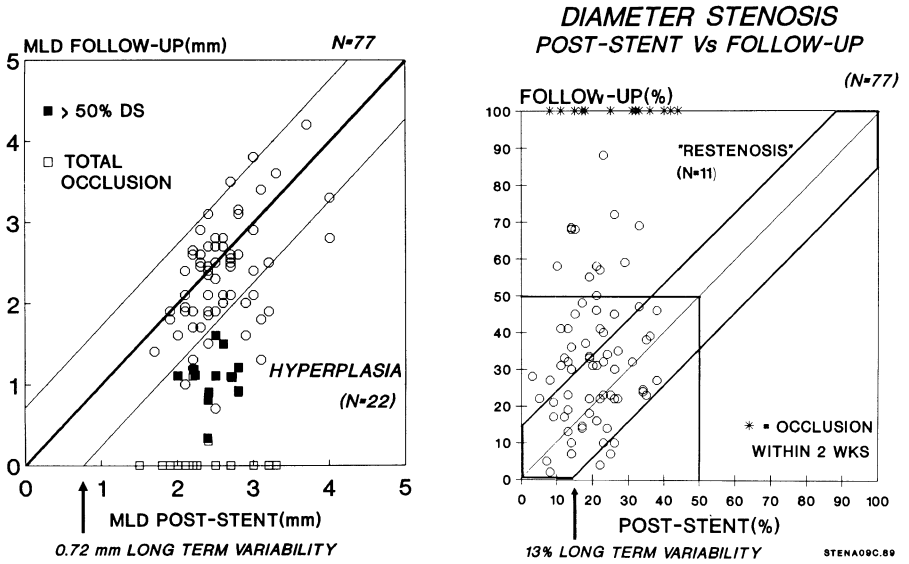

Fig.4. Diagram demonstrating the change in the minimal luminal diameter following stent implantation. The individual minimal lumen diameter (MLD) immediately following stent implantation (horizontal axis) are compared to that at angiographic follow-up (vertical axis). The two lines to either side of the identity Line represent the long-term variability for repeat measurement. All points (n = 21)that fall below the lower line are therefore considered to have undergone a significant deterioration (intimal hyperplasia > 0.72 mm) and in addition the closed blocks also fullfil the criterion of ⩾ 50% diameter stenosis.

grafts on an obtuse marginal and on a diagonal branch. Following recurrent angina he was reoperated and both internal mammary arteries were used to bypass the LAD and the RCA. Between 1984—1987 the vein graft on the left marginal artery was dilated on 4 occasions. In April 1987 his cardiologist referred the patient to Ulrich Sigwart in Lausanne for a stent implantation in both SVG. Seven months later in November 1987 repeated dilatation was necessary within both stents. Five months later the patient has restenosis again; this time, a hot balloon angioplasty was considered but rejected by Richard Spears in Detroit (would the absorbed laser energy convert the stent into a "hot roster"), and the first atherectomy inside the stent was performed by John Simpson in Palo Alto. In July 1988, the patient underwent a second atherectomy, which did not prevent restenosis. Disappointed by these results, lasing with excimer laser (wavelength 308 nm) was successfully attempted in Los Angeles by Jim Forrester and his group [54]. Unfortunately for the patient, the stenotic lesion seems to be more stubborn than the treating physicians and has recurred once more. Tired of these multiple and varied interventions, the patient has decided for the time being to stay away from the sorcerer's apprentice and this long and thorny path has certainly brought

down to earth the interventional cardiologist who has to face the unavoidable reality: in addition to a mechanical device a pharmacological approach will be necessary to achieve victory over restenosis.

References

1. Gruentzig AR, Senning A, Siegenthaler WE: Nonoperative dilatation of coronary-artery stenosis: percutaneous transluminal coronary angioplasty. N Engl J Med 301: 61—68, 1979.
2. Block PC, Myler RK, Stertzer S, Fallon JT: Morphology after transluminal angioplasty in human beings. N Engl J Med 305: 382—384, 1981.
3. Essed CE, van den Brand M, Becker AE: Transluminal coronary angioplasty and early restenosis: Fibrocellular occlusion after wall laceration. Br Heart J 49: 393—396, 1983.
4. Sigwart U, Puel J, Mirkovitch V, Joffre F, Kappenberger L: Intravascular stents to prevent occlusion and restenosis after transluminal angioplasty. N Engl J Med 316: 701—706, 1987.
5. Dotter CT: Transluminally placed coil-spring endarterial tube grafts: long-term patency in canine popliteal artery. Invest Radiol 4: 329—332, 1969.
6. Cragg A, Lung G, Rysavy J, Castaneda-Zuniga W, Amplatz K: Nonsurgical placement of arterial endoprostheses: a new technique using nitinol wire. Radiology 147: 261—263, 1983.
7. Dotter CT, Bushmann RW, McKinney MK, Rösch J: Transluminal expandable nitinol coil stent grafting: preliminary report. Radiology 147: 259—260, 1983.
8. Sugita Y, Shimomitsu T, Oku T, Murabayashi S, Kambic He, Harasaki H, Shirey E, Golding L, Nose Y: Nonsurgical implantation of vascular ring prosthesis using thermal shape memory Ti/Ni alloy (nitinol wire). Trans Am Soc Artif Litern Organs 32: 30—34, 1986.
9. Maass D, Zollikofer CL, Largiader F, Senning A: Radiological follow-up of transluminally inserted vascular endoprostheses: an experiment study using expanding spirals. Radiology 152: 659—663, 1984.
10. Lawrence DD, Charnsangavej C, Wright KC, Gianturco C, Wallace S: Percutaneous endovascular graft: experimental evaluation. Radiology 163: 357—360, 1987.
11. Duprat G, Wright KC, Charnsangavej C, Wallace S, Gianturco C: Self-expanding metallic stents for small vessels: an experimental evaluation. Radiology 162: 467—472, 1987.
12. Rollins N, Wright KC, Charnsangavej C, Wallace S, Gianturco C: Self-expanding metallic stents: preliminary evaluation in an atherosclerotic model. Radiology 163: 739—742, 1987.
13. Rousseau H, Puel J, Joffre F, Sigwart U, Duboucher C, Imbert C, Knight C, Kropf L, Wallsten H: Self-expanding endovascular prosthesis: an experimental study. Radiology 164: 709—714, 1987.
14. Puel J, Juilliere Y, Bertrand ME, Rickards AF, Sigwart U, Serruys PW: Early and late assessment in stenosis geometry after coronary arterial stenting. Am J Cardiol 61: 546—553, 1988.
15. Serruys PW, Juilliere Y, Bertrand ME, Puel J, Rickards AF, Sigwart U: Additional improvement of stenosis geometry in human coronary arteries by stenting after balloon dilatation: a quantitative angiographic study. Am J Cardiol 16: 71G—76G, 1988.
16. Palmaz JC, Sibbitt RR, Reuter SR, Tio FO, Rice WJ: Expandable intraluminal graft: a preliminary study. Radiology 156: 73—77, 1985.
17. Palmaz JC, Sibbitt RR, Tio FO, Reuter SR, Peters JE, Garcia F: Expandable intraluminal vascular graft: a feasibility study. Surgery 99: 199—205, 1986.

18. Palmaz JC, Windeler SA, Garcia F, Tio FO, Sibbitt RR, Reuter SR: Atherosclerotic rabbit aortas: expandable intraluminal grafting. Radiology 160: 723—726, 1986.
19. Schatz RA, Palmaz JC, Tio FO, Garcia F, Garcia O, Reuter SR: Balloon-expandable intracoronary stents in the adult dog. Circulation 76: 450—457, 1987.
20. Roubin GS, Robinson KA, King III SB, Gianturco C, Block AJ, Brown JE, Siegel RJ, Douglas JS: Early and late results of intracoronary arterial stenting after coronary angioplasty in dogs. Circulation 76: 891—897, 1987.
21. Duprat G, Wright KC, Charnsangavej C, Wallace S, Gianturco C: Flexible balloon-expanded stents for small vessels, Radiology 162: 276—278, 1987.
22. Slepian MJ, Schmidler A: Polymeric Endoluminal Paving/Sealing: A bio-degradable alternative to intracoronary stenting. Circulation 11—409 A, 1988.
23. Williams D (ed): Fundamental Aspects of Biocompability: Crc Press Inc, Boca Raton, Florida 1981: Vol II, p 45—62.
24. Juilliere Y, Serruys PW, Beatt KJ, Sigwart U: Contribution of self expansion of stent and additional endoluminal dilatation within the stent on patency of human coronary arteries. Eur Heart J 9: 56, 1988.
25. Beatt KJ, Bertrand M, Puel J, Rickards T, Sekrruys PW, Sigwart U: Additional improvement in vessel lumen in the first 24 hours after stent implantation due to radial dilating force. JACC 1989: 13: 224 A (Abstract).
26. Schmitz HJ, Meyer J, van Essen R, Effert S: Restenosis following successful coronary angioplasty (PTCA): The result of inadequate dilatation? Relation between primary success and late results. Improvement of myocardial perfusion. Thrombosis, angioplasty, bypass surgery. 255—264, 1985.
27. Thubikar M, Baker J, Nolan S: Inhibition of atherosclerosis by reduction of arterial intramural stress in rabbits. Circulation 76 (IV): 314 A, 1987 (Abstract).
28. Williams JK, Armstrong ML, Heistad DD: Vasa vasorum in atherosclerotic coronary arteries: responses to vasoactive stimuli and regression of atherosclerosis. Circ Res 62: 515—523, 1988.
29. Schatz RA: A view of vascular stent. Circulation 79: 445—457, 1989.
30. Sigwart U, Urban P, Golf S, Kaufmann U, Imbert C, Fischer A, Kappenberger L: Emergency stenting for acute occlusion after coronary balloon angioplasty. Circulation 88: 1121—1127, 1988.
31. Roubin GS, Douglas JS, Lembo NJ, Black AJ, King SD III: Intracoronary stenting for acute closure following percutaneous transluminal coronary angioplasty (PTCA)(abs). Circulation 78: II-406A, 1988.
32. Bertrand ME, Rickards AF, Serruys PW: Coronary stenting implantation for primary and secondary prevention of restenosis after PTCA. Results of pilot multicenter trial (1986/1987) (CASIS Trial). Eur Heart J 9: 55, 1988.
33. King SB III: Vascular stents and atherosclerosis. Circulation 79: 460—469, 1989.
34. Kordenat RK, Kezdi P, Stanley EL: A new catheter technique for producing coronary thrombosis and selective coronary visualization. Am Heart J 83: 360—364, 1972.
35. Van der Werf F, Bergman SR, Flx KAA, de Geest H, Hoyng CF, Sobel BE, Collen D: Coronary thrombolysis with intravenously administered human tissue-type plasminogen activator by recombinant DNA Technology. Circulation 69: 605—610, 1984.
36. Moore S, Belbeck LW, Evans G, Pineau S: Effect of complete or partial occlusion of a coronary artery. Lab Invest 44: 151—157, 1981.
37. Van der Giessen WJ, Serruys PW, Visser WJ, Verdouw PD, van Schalkwijk WP, Jongking JF: Endothelialization of intravascular stents. J Inter Cardiol 1: 109—120, 1988.
38. Waller BF, McManus BM, Gorfinkel HJ, Kishel JC, Schmidt ECH, Kent KM, Roberts WC: Status of the major epicardial coronary arteries 80 to 150 days after percutaneous transluminal coronary angioplasty. Analysis of 3 necropsy patients. Am J Cardiol 51: 81—84, 1983.

39. Steele PM, Chesebro JH, Stanson AW, Holmes DR Jr, Dewanjee MK, Badimon L, Fuster V: Balloon angioplasty. Natural history of the pathophysiological response to injury in a pig model. Circ Res 57: 105—112, 1985.
40. Wilcox JN, Smith KM Williams SM, Gordon D: Platelet-derived growth factor mRNA detection in human atherosclerotic plaques by in situ hybridiztion J Clin Invest 82: 1134—1143, 1988.
41. Johnsson A, Heldin CH, Westermark NB, Wasteson A: Platelet-derived growth factor: Identification of constituent polypeptide chains. Biochem Biophys Res Commun 104: 66—74, 1982.
42. Hart CE, Forstrom JW, Kelly JD, Seifert RA, Smith RA, Ross R, Murray MJ, Bowenpope DF: Two classes of PDGF Receptor recognize different isoforms of PDGF. Science 240: 1529—1531, 1988.
43. Moore S: Thrombosis and atherogenesis. The chicken and the egg. Ann N Y Acad Sci 454: 146—153, 1985.
44. Heras M, Chesebro JH, Penny WJ, Balley KR, Badimon L, Fuster V: Effect of Thrombin inhibition on the development of acute platelet-thrombus deposition during angioplasty in pigs. Circulation 79: 657—665, 1989.
45. Clowes AW, Reidy MA: Mechanisms of aterial graft failure: the role of cellular proliferation. Ann NY Acad Sci 516: 673—678, 1987.
46. Koo EWY, Gottlieb AI: Endothelial stimulation of intimal cell proliferation in a procine aortic organ culture. Am J Pathol 134: 497—503, 1989.
47. Austin GE, Ratliff NB, Hollman J, Tabei S, Philips DF: Intimal proliferation of smooth muscle cells as an explanation for recurrent coronary artery after percutaneous transluminal coronary angioplasty. JACC 6: 369—375, 1985
48. Urban P, Sigwart U, Kaufman U, Kappenberger L: Restenosis within coronary stents: possible effect of previous angioplasty. JACC 13: 107 A, 1989.
49. Spears R, Reyes V, Sinclair N, Hopkins B, Schwartz L, Aldridge H, Plokker T: Percutaneous coronary laser balloon angioplasty: preliminary results of a multicenter trial. JACC 13: 16, 1989.
50. Robertson G, Hinohara T, Selmon M, Simpson J: Coronary atherectomy for the treatment of unfavorable PTCA lesion, JACC 1989: 13: 109 A (abstract).
51. Simpson J, Hinohara T, Selmon M, Robertson G, White N, Rorve M, Braden L: Comparison of early and recent experience in percutaneous coronary atherectomy. JACC 1989: 13: 108A (abstract).
52. Serruys PW, Luijten HE, Beatt KJ, Geuskens R, de Feyter PJ, van den Brand M, Reiber JHC, ten Katen HJ, van Es GA, and Hugenholtz PG: Incidence of restenosis after successful coronary angioplasty: A time-related phenomenon. A quantitative angiographic study in 342 patients at 1, 2, 3 and 4 months. Circulation 77: 361—371, 1988.
53. Serruys PW, Beatt KJ, Koning R, Bertrand M, Puel J, Rickards T, Sigwart U: Early and late assessment of morphological change after stent implantation. Circulation 1988: 78: II-408 A (abstract).
54. Litvack F: Intravascular stenting for prevention of restenosis: in search of the magic bullet. JACC 13: 1092—1093, 1989.

Appendix

Participating Centers and Collaborators: Catheterisation Laboratory, Thoraxcenter, Rotterdam, The Netherlands: KJ Beatt, MRCP, M. v.d. Brand, MD, P.J. de Feyter, MD, W. v.d. Giessen, MD, J.R.T.C. Roelandt, MD, P.W. Serruys MD, H. Suryapranata, MD; Department of Cardiology, Hôpital Cardiologique, Lille, France: M.E. Bertrand, MD, J.M. Lablanche, MD; Department of Clinical Measurement, National Heart Institute, London, United Kingdom: A.F. Rickards, MD, P. Urban, MD; Department of Clinical and Experimental Cardiology, CHRU Rangueil, Toulouse, France: J.P. Bounhoure, MD, A. Courtault,MD, F. Joffre, MD, J. Puel, MD, H. Rousseau, MD; Division of Cardiology, Department of Medicine, CHUV, Geneva, Switzerland: B. Meier, MD, W. Rutishauser MD; Division of Cardiology, Department of Medicine, CHUV, Lausanne, Switzerland: L. Kappenberger, MD, U. Sigwart, MD.

15. Coronary stenting, report of the initial clinical experience with the Palmaz-Schatz TM balloon expandable stent

RICHARD A. SCHATZ

Summary

In this chapter we report the short- and long-term clinical results of the elective use of a balloon expandable intracoronary stent in a large non-randomized multicenter trial. Two hundred patients were enrolled prospectively, 180 of whom had successful delivery of the stent. Of these 180 patients, 45 were treated with only aspirin and dipyridamole (Group A) and 235 with full anticoagulation in addition to antiplatelet agents (Group B). We found that acute closure did not occur in either group. Subacute closure did occur in 16% of patients in Group A and 3.7% of patients in Group B. Other complications in the entire series included death 1%, myocardial infarction 6%, urgent bypass surgery 2%, bleeding 7% and peripheral embolization of the stent 3%.

Four to six month angiographic follow-up is available in 88 patients (98 lesions) who received single stents (lesions less than 15 mm in length) and 38 patients (38 lesions) who received multiple tandem stents (lesions greater than 15 mm in length). Angiographic restenosis occurred in 18% of the former and 53% of the latter. Clinical restenosis occurred in only 5% of the former and 45% of the latter.

Despite a steep learning curve, these balloon expandable stents eliminate abrupt closure and reduce restenosis following angioplasty, especially in patients with lesions less than 15 mm in length. Anticoagulation is necessary for at least 1 month post-stenting. A large randomized trial is necessary to better define what role stents will play following PTCA in the future.

Introduction

Despite innovative technical advances in percutaneous transluminal coronary angioplasty (PTCA), restenosis and abrupt closure continue to occur at predictable rates following coronary angioplasty [1—7]. Vascular stents represent one of the many new approaches to these problems and have been

J. H. C. Reiber and P. W. Serruys (eds), Quantitative Coronary Arteriography, 313—325.

evaluated extensively by several investigators with mixed results [8—20]. In this chapter the worldwide clinical experience with a balloon expandable stent developed by Palmaz and colleagues will be reviewed.

Background

A variety of stent designs have been investigated since 1969 when Dotter first reported his results using wire coils [8]. Predominantly two basic designs were used: 1) self-expanding coils [9], or 2) heat sensitive coils (Nitinol) [10—11]. In 1985 Palmaz reported the first experimental work with a balloon expandable wire mesh [12], that was later replaced with a more streamlined but rigid slotted stainless steel tube that allowed for expansion by balloon inflation (Figure 1) [13—16]. This device worked well in relatively straight vessels, however inflexibility proved to be a problem in the approach to coronary arteries and thus was replaced with a more flexible design developed by Schatz et al. (Figure 2) [14]. The favorable biocompatibility profile of both of these devices was well documented in many preclinical experimental models. [15—18]

Following FDA approval 200 patients were enrolled prospectively into a multicenter study. Entry criteria were 1) symptomatic coronary artery disease (> 70% stenosis); 2) objective evidence of ischemia; 3) good left

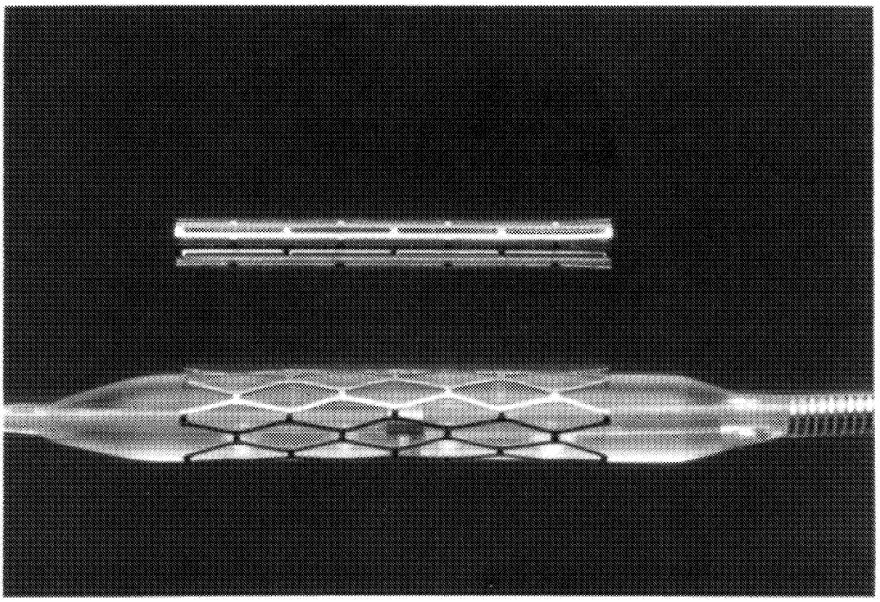

Fig. 1. Original "rigid" prototype of the Palmaz TM balloon expandable stent.

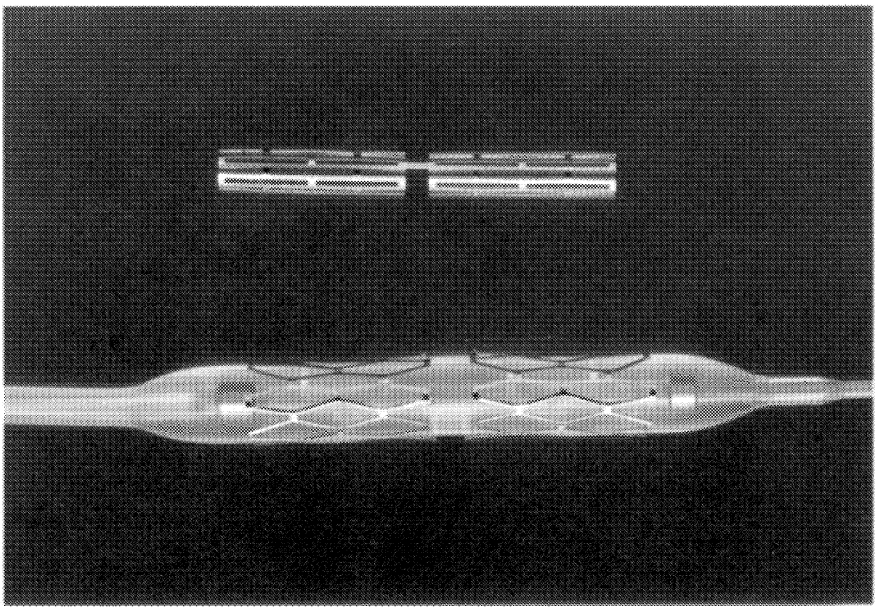

Fig. 2. Modified "articulated" Palmaz-Schatz TM tent for use in coronary arteries.

ventricular function; and 4) collateral flow to the target vessel. Exclusion criteria were 1) unprotected left main coronary artery disease; 2) extreme tortuosity of the target site; 3) acute myocardial infarction; 4) saphenous vein bypass graft lesions; 5) abrupt closure following PTCA; and 6) inability to give informed consent.

Based upon thrombogenicity testing in animals [17], the following anticoagulation regimen was used preoperatively; aspirin 5 grains orally, dipyridamole 75 mg orally three times a day, low molecular weight dextran 40—100 cc's per hour beginning two hours prior to stenting; intraoperative regimen: intravenous heparin to maintain an activated clotting time of 300 seconds, intracoronary nitroglycerin 200 mcg pre and post stenting, intravenous nitroglycerin to maintain the arterial blood pressure between 100 and 120 mmHg; postoperative regimen: calcium channel blockers, aspirin and dipyridamole for 3 months. The first 45 patients in the series received aspirin and dipyridamole alone, while the remaining 135 patients received either warfarin or home heparin in addition to aspirin and dipyridamole.

Results

The demographics of our patient population are listed in Table 1 and include 160 men and 40 women, mean age 56 years (range 24 to 84). Of the 188

Table 1. Demographics of the stent patient population.

Patient population (N = 200)	
Males	160
Females	40
Age, range (yr)	24—84
mean (yr)	56
CCS angina class	
0	12
1	12
2	57
3	65
4	54
Single vessel disease	184
Two vessel disease	13
Three vessel disease	3
Prior myocardial infarction	89
Stenosis ⩾ 70%	178
Total occlusion	22
Primary angioplasty	88
First restenosis	53
Second restenosis	38
Third restenosis	13
Fourth restenosis	4
Fifth restenosis	4
Vessel stented	
RCA	113
LAD	69
Circumflex/OMB	14
Diagonal	2
Left main	2

patients with angina 12 had Canadian Cardiovascular Society Class I angina, 57 Class II, 65 Class III, and 54 Class IV. Eighty-eight patients had no prior PTCA, 53 had one, 38 two, 13 three, 4 four, 4 five prior PTCA procedures. Twenty-two patients had total occlusions, the remainder had severe stenoses. Sixty-nine patients had stent delivery attempted in the LAD, 113 in the right coronary artery, 14 in the circumflex/obtuse marginal branch, 2 in a diagonal branch, and 2 in the left main coronary artery.

Of the 297 stents that were attempted in 200 patients, 276 were successfully delivered in 180 patients for a primary success rate of 93% by stent, 90% by patient. Thirty patients had delivery of the rigid stent attempted in whom 24 were successfully delivered. The remainder received the more flexible "articulated stent". Stent delivery failed for a variety of reasons, inflexibility with the rigid stent (N = 6) and snagging with the articulated stent (N = 14). Stent retrieval following failed delivery was successful in 10 of

20 patients, but was unsuccessful in 6 of 20 patients resulting in asymptomatic embolization of the device into the peripheral circulation during attempted withdrawal into the femoral sheath. In four other patients the stent was deployed proximal to the target lesion but a second stent could not be passed distally. One of these patients declined surgery despite ST elevation and pain following failed delivery and suffered a fatal myocardial infarction one week following discharge. Another underwent successful bypass surgery, one developed asymptomatic restenosis of the nonstented target lesion and the final stent in the fourth patient remains patient by angiography at 6 months.

Therefore, 180 patients had successful stent delivery. Their clinical outcome is shown in Table 2. Group A represents the first 45 patients in the series who received only aspirin and dipyridamole and Group B all remaining patients (N = 135) who received aspirin, dipyridamole and either full dose warfarin for 1—3 months (N = 132) or home heparin (N = 3).

Table 2. Clinical outcome following successful stent delivery.

Outcome following successful sent delivery (N = 180 pts)	Group A (N = 45)	Group B (N = 135)
Acute closure	0	0
Subacute closure (4—10 days)	7(16%)	5(3.7%)
Death	0	1(0.7%)
Urgent CABG	2	1(0.7%)
Follow-up range (months)	4—18	1—10
mean (months)	9 ± 2	4 ± 1

Abrupt closure defined as total thrombosis of the stent within 48 hours was absent in both groups, however 7 patients in Group A (16%) developed subacute closure (thrombosis 48 hours to 2 weeks following stenting). Four of these patients had discontinuation or interruption of their antiplatelet agent prior to thrombosis. Only 5 patients in Group B (3.7%) developed subacute closure, 4 of whom were successfully reperfused. No thrombosis occurred after two weeks or after discontinuation of anticoagulation.

Predictors of thrombosis despite anticoagulation included undersizing of the stent, failure to recognize and treat thrombus within the stent prior to discharge, outflow restriction, excessive stent overlap when placed in tandem, omission of dipyridamole and use of generic aspirin. Urgent bypass surgery was required in 2 patients in Group A for a guiding catheter induced dissection in one and a wire induced dissection in the other. One patient in Group B underwent successful urgent bypass surgery one week after stent placement which was complicated by thrombosis and myocardial infarction.

One patient died of an intracranial bleed 8 weeks after successful delivery of 2 tandem stents to a totally occluded circumflex artery.

Angiographic follow-up is available in 126 patients (136 lesions). Figures 3a and b compare the clinical outcome in these patients to angiographic

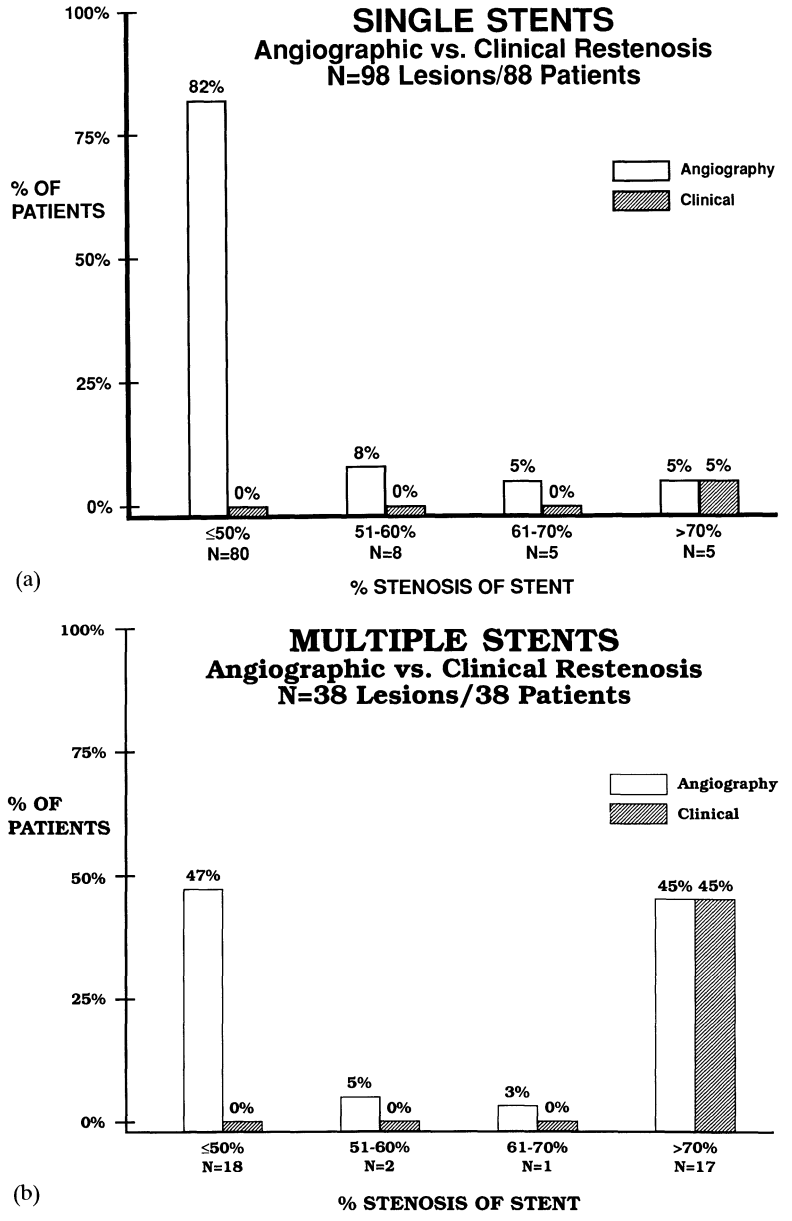

Fig. 3. Angiographic vs. clinical restenosis based upon angiographic follow-up of patients who received a single stents (a) and those who received multiple stents (b).

outcome. Restenosis (defined as > 50% luminal narrowing within the stent) occurred in 18% of those patients who received single stents (lesions $\leqslant 15$ mm in length) and 53% of those who received multiple stents, ($p < 0.001$) regardless of anticoagulation. Clinical restenosis (i.e. further intervention required) occurred in only 5% of the patients who received single stents. Figures 4 and 5 illustrate examples of successful long-term follow-up after stenting.

The overall complication rate is seen in Table 3. Major complications defined as death, myocardial infarction or urgent bypass surgery occurred in 9% of the patients. All other complications occurred in 12%, the majority of which were bleeding complications in Group B.

Table 3. Complications in all patients in whom stent delivery was attempted.

Total complication rate (N = 200 pts)	
Death	2/200 (1%)
Myocardial infarction	12/200 (6%)
Urgent bypass	4/200 (2%)
Bleeding	14/200 (7%)
Other	10/200 (5%)

The important findings of this initial series are that: 1) abrupt closure does not occur with this device; and 2) that compared to historic controls restenosis appears to be acceptably low, especially in patients who receive single stents for lesions $\leqslant 15$ mm in length. This may represent an improvement over routine PTCA alone.

The significance of our findings is enhanced further by the observation that a significant percentage of our patient population from the outset was at high risk for restenosis i.e. 53 (27%) patients had one prior PTCA, 59 (30%) more than one prior PTCA, 54 (27%) had unstable angina and 22 (11%) had total occlusions. Limitations of this device as with most other stent designs currently under investigation are: 1) radiolucency due to small mass; and 2) deliverability. The former problem can be addressed by different metals, such as tantalum [21] and the latter with a protective sheath to separate the leading edge of the stent from the vessel wall during delivery.

Conclusions

We conclude from this initial study of the Palmaz-Schatz TM coronary stent

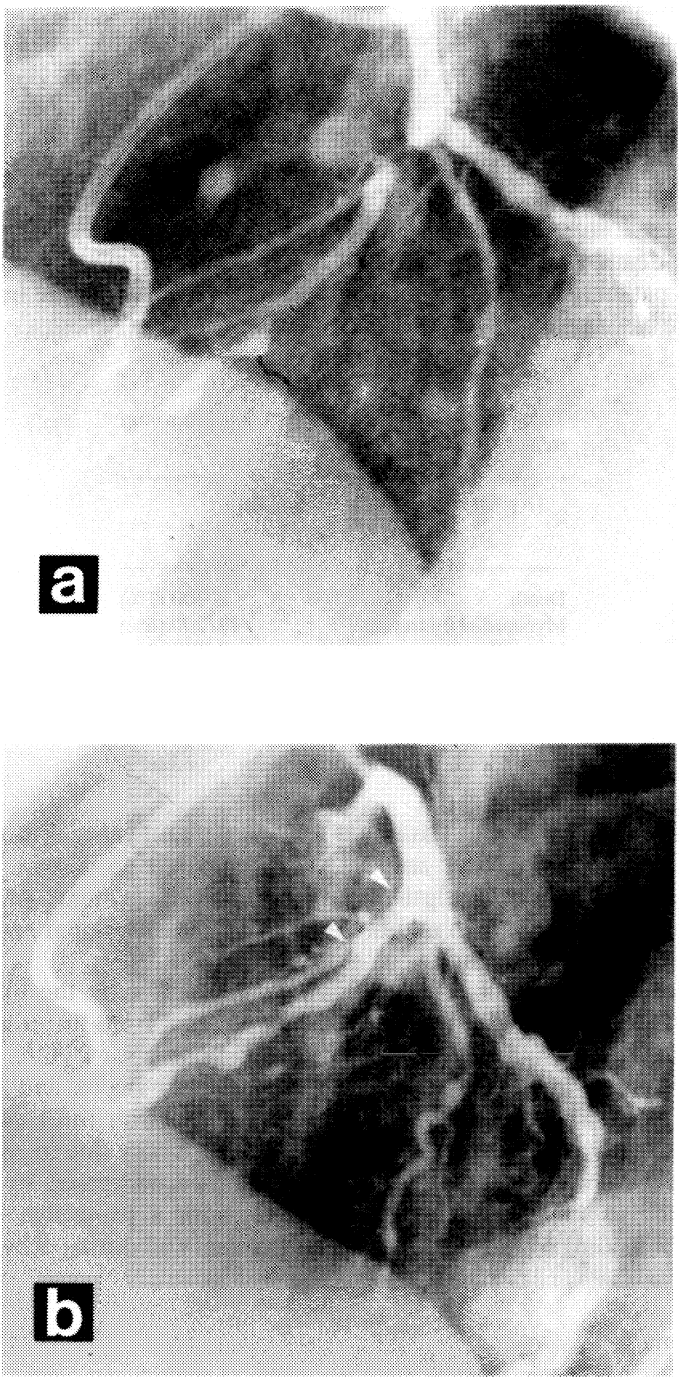
a
b

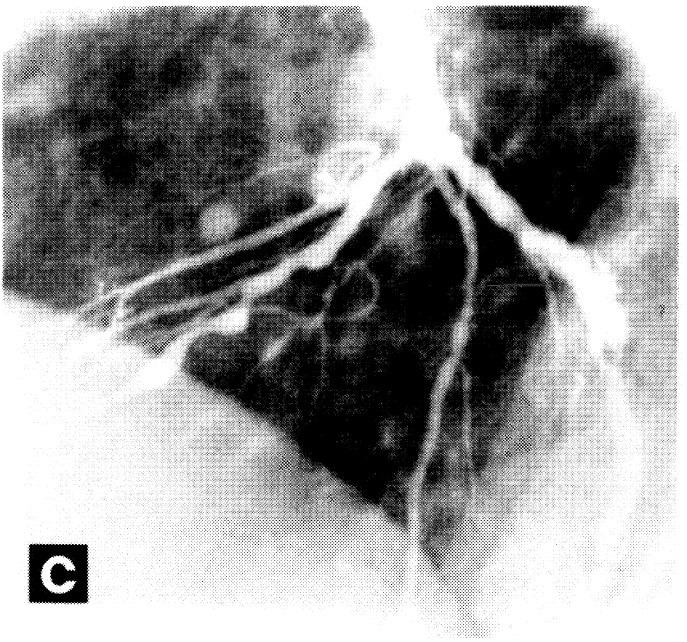

Fig. 4. (a) Angiogram of a 44 year old male with a high grade stenosis of the left anterior descending coronary (LAD), (b) post-stent, arrows and (c) six months later without anticoagulation.

that this particular stent design is: 1) relatively nonthrombogenic compared to published reports of other stents currently under investigation [19—20]; 2) abrupt closure does not occur with this stent design; 3) mortality and urgent bypass surgery rates are acceptably low: 4) subacute closure is common (16%) without anticoagulation but rare with anticoagulation (3.7%). This thrombosis rate may be improved by proper sizing of the stent and strict continuation of pharmocologic therapy during the first 2 weeks following stenting. At this time we recommend 1—3 months of anticoagulation for all patients who receive a stent; 5) initial angiographic follow-up suggests that restenosis following stenting may be significantly reduced when compared to historic controls especially for lesions $\leqslant 15$ mm (single stents); 6) restenosis is common following multiple stent delivery in tandem and may be due to variable degrees of overlap (increased concentration of metal).

Based on these data we are optimistic that a role exists for the elective use of coronary stents for prevention of restenosis in patients undergoing PTCA especially in those who receive single stents. A large randomized trial is necessary, though to better define this role.

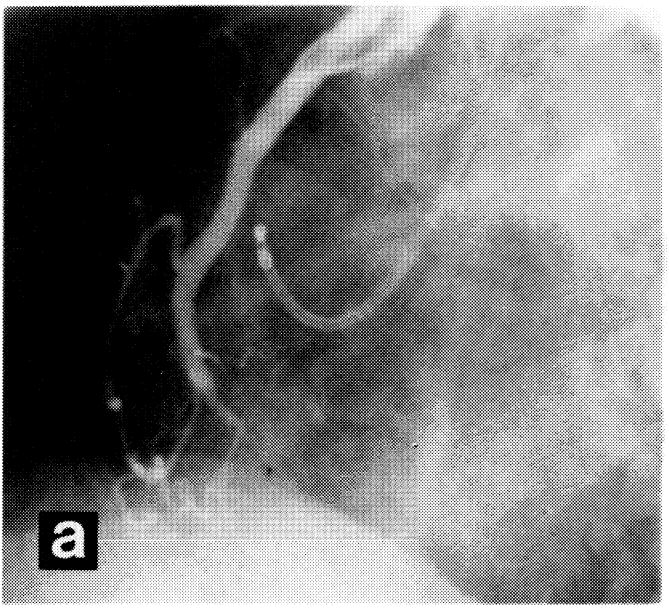
a

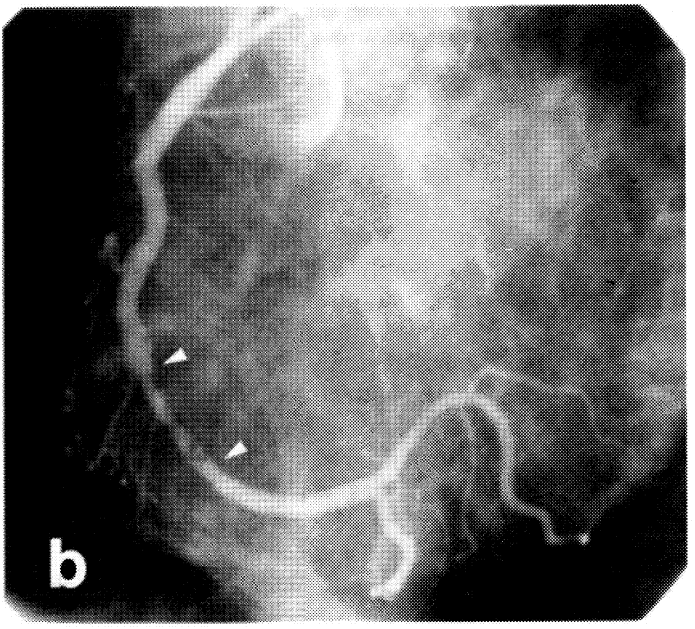
b

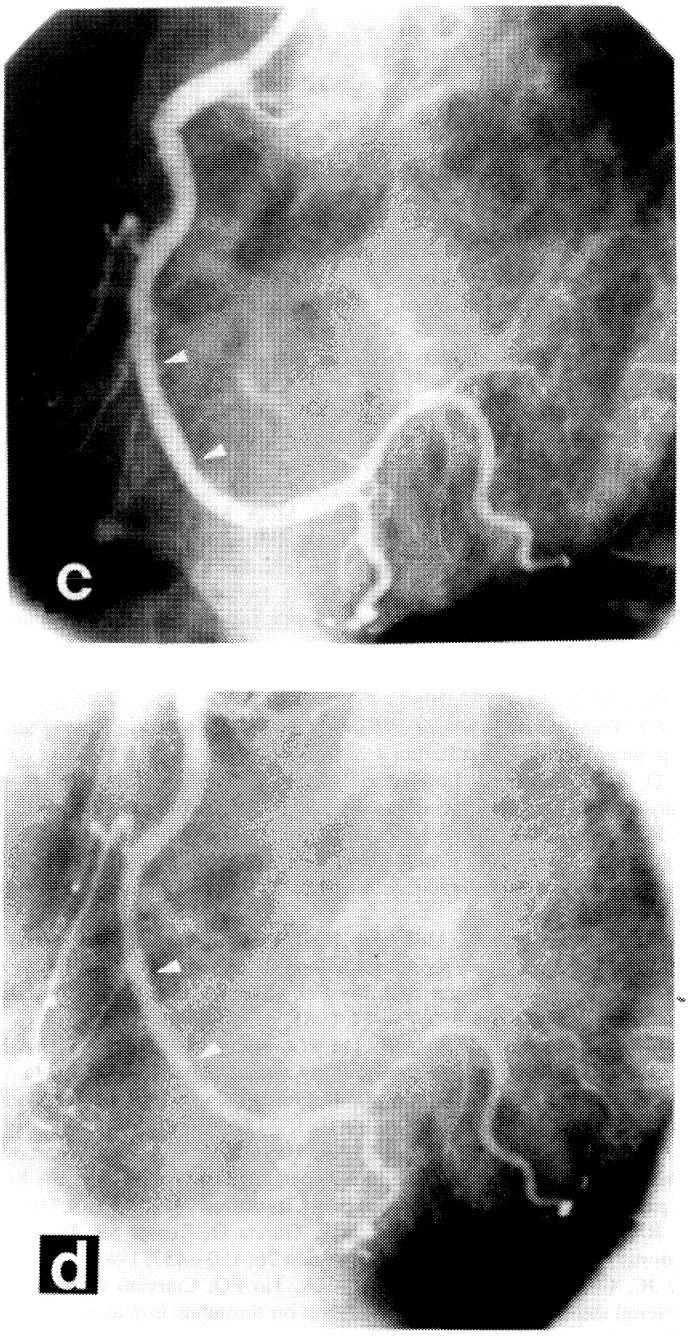

Fig. 5. (a) Angiogram of a 55 year old male with total occlusion of the right coronary artery, pre-stent, (b) post PTCA, (c) post-2 tandem stents, arrows, and, (d) six months later without anticoagulation.

References

1. Detre K, Holubkov R, Kelsey S, Cowley M, Kent K, Williams D, Myler R, Faxon D, Holmes D, Bourassa M, Block P, Gosselin A, Bentivoglio L, Leatherman L, Dorros G, King S, Galichia J, Al-Bassam M, Leon M, Robertson T, Passamani E: Coinvestigators of The National Heart, Lung, and Blood Institute's Percutaneous Transluminal Coronary Angioplasty Registry. Percutaneous Transluminal Coronary Angioplasty in 1985—1986 and 1977—1981. N Engl J Med 318: 265—270, 1988.
2. Ellis SG, Roubin GS, King SB III, Douglas JS JR, Shaw RE, Sterter SH, Myler RK: In-hospital cardiac mortality after acute closure after coronary angioplasty: Analysis of risk factors from 8207 procedures. J Am Coll Cardiol 11: 211, 1988.
3. Cowley MJ, Dorros A, Kelsey SF, Van Raden M, Detre KM: Acute coronary complications associated with percutaneous transluminal angioplasty. Am J Cardiol 53: 12C—16C, 1984.
4. Ellis SG, Roubin GS, King SB, Douglas JS, Weintraum WS, Thomas RG, Cox WR: Angiographic and clinical predictors of acute closure after native vessel coronary angioplasty. Circulation 77: 372—379, 1988.
5. Holmes DR Jr, Vliestra RE, Smith HC, Vetrovec GW, Cowley MJ, Faxon DP, Gruentzig Ar, Kelsey SF, Detre KM, Van Raden MJ, Mock MG: Restenosis after Percutaneous Transluminal Coronary Angioplasty (PTCA): A Report from the PTCA Registry of the National Heart, Lung and Blood Institute. Am J Cardiol 53 (suppl): 77C—81C, 1984.
6. Serruys PW, Luijten HE, Beatt KJ, Geuskews R, De Feyter PJ, Van den Brand M, Reiber JHC, Katen HJ ten, Vanes GA, Hugenholtz PG: Incidence of restenosis after successful coronary angioplasty: A time related phenomenon. Circ 77: 361—371, 1988.
7. McBride W, Lange RA, Hillis LD: Restenosis after successful coronary angioplasty. N Engl J Med 318: 1734—1737, 1988.
8. Dotter CT: Transluminally placed coil-spring endarterial tube grafts, long-term patency in canine popliteal artery. Invest Radiol 4: 329—332, 1969.
9. Maass D, Zollikofer ChL, Largiader F, Senning A: Radiological follow-up of transluminally inserted vascular endoprostheses: an experimental study using expanding spirals. Radiology 150: 659—663, 1984.
10. Cragg A, Lung G, Rysavy J, Castaneda F, Castaneda-Zuniga W, Amplatz K: Nonsurgical placement of arterial endoprosthesis: a new technique using nitinol wire. Radiology 147: 261—263, 1983.
11. Dotter CT, Buschmann RW, McKinney MK, Rosch J: Transluminal expandable nitinol coil stent grafting: preliminary report. Radiology 147: 259—260, 1983.
12. Palmaz JC, Sibbitt RR, Reuter SR, Tio FO, Rice WJ: Expandable intraluminal graft: prelininary study. Radiology 156: 73—77, 1985.
13. Palmaz JC, Windelar SA, Garcia F, Tio FO, Sibbitt RR, Reuter SR: Atherosclerotic rabbit aortas: Expandable intraluminal grafting. Radiol 160: 723—726, 1986.
14. Schatz RA, Palmaz JC, Tio F, Garcia: Report of new articulated balloon expandable intravascular stent (ABEIS) Circ 78 (Supp II): II—449, 1988.
15. Mullins CE, O,Laughlin MP, Vick III GW, Mayer DC, Myers TJ, Kearney DL, Schatz RA, Palmaz JC: Implantation of balloon expandable intravascular grafts by catheterization in pulmonary arteries and systemic veins. Circulation 77: 188—199, 1988.
16. Schatz RA, Palmaz JC, Tio FO, Garcia F, Garcia O, Reuter SR: Balloon expandable intracoronary stents in the adult dog. Circulation 76: 450—457, 1987.
17. Palmaz JC, Garcia O, Kopp DT, Schatz RA, Tio FO, Ciarvino O: Balloon expandable intra-arterial stents: Effects of anticoagulation on thrombus formation. Circ 76 (Supp IV): IV—45, 1987.
18. Palmaz JC, Kopp DT, Hayashi H, Schatz RA, Hunter G, Tio FO, Garcia O, Alvarado R, Rees C, Thomas SC: Normal and stenotic renal arteries: Experimental balloon-expandable intraluminal stenting. Radiol 164: 705—708, 1987.

19. Bertrand ME, Rickards AF, Serruys PW: Coronary stenting implantation for primary and secondary prevention of restenosis after PTCA. Results of a pilot multicenter trial (1986/1987) Eur Heart J, 9 (Supp A): 55, 1988 (Abstract).
20. Puel J, Rouseau, Joffre F, Hatem S, Fauvel JM, Bonhoure JP: Intravascular stents to prevent restenosis after transluminal angioplasty. Circulation 76: IV—27, 1987.
21. Schatz RA, Palmaz JC, Tio F, Garcia O: Report of a New Radiopaque Balloon Expandable Intravascular Stents (RBEIS) in Canine Coronary Arteries. Circulation 78 (Supp II): II—448, 1988.

Part VI

Recanalization techniques

16. Laser Balloon Angioplasty (LBA)

J. RICHARD SPEARS

Summary

A laser balloon catheter/delivery system has been developed to test the hypotheses that the combination of appropriate levels of heat and pressure during balloon inflation will improve luminal dimensions and morphology to a greater extent than the application of pressure alone as well as mitigate adverse biologic responses to mechanical injury. Experimentally, the conditions under which fusion of separated tissue layers of the atheromatous arterial wall can be achieved have been defined, and proposed beneficial effects on arterial recoil and intraluminal thrombus have been demonstrated. Recent clinical studies suggest that LBA improves coronary luminal dimensions over those achievable with initial PTCA by these mechanisms. Improved laser diffusing tip technology and continued laser dosimetry studies will be required to determine whether adverse biologic responses can be reduced by LBA.

Introduction

The occasional occurrence of acute closure and the unpredictable long term efficacy associated with percutaneous transluminal coronary angioplasty (PTCA) greatly limit the widespread applicability of the procedure. Mural disruption, arterial recoil, and presence of thrombus are probably the commonest causes for failure to achieve an adequate initial PTCA result. Although the mechanisms of restenosis after PTCA are currently conjectural, it is likely that suboptimal initial post PTCA luminal size and morphology [1, 2] and a reduced hemocompatibility of the new luminal surface, alone or in combination, contribute to many instances of restenosis. Separated flow patterns may predispose to chronic platelet and lipoprotein deposition, which could amplify any problem of reduced hemocompatibility. Exposure of collagen and other subendothelial proteins at the luminal surface and post PTCA persistence of thrombus, which is inherently thrombogenic, are likely

J. H. C. Reiber and P. W. Serruys (eds), Quantitative Coronary Arteriography, 329–339.

to be the principal causes of a reduced hemocompatibility. Cellular proliferation in response to growth factors released by platelets and leukocytes, present as a result of the reduced hemocompatibility, would be expected to occur, and organization of both old and new thrombus or microthrombi may also contribute to neointimal formation.

Laser balloon angioplasty (LBA) consists of the simultaneous application of laser-induced heat and pressure to all arterial tissues surrounding an inflated angioplasty balloon. The hypotheses are currently being tested that LBA is more effective than PTCA in improving luminal dimensions and morphology as well as in mitigating adverse biologic responses associated with mechanical injury.

Luminal dimensions and morphology

Tissue welding

Photothermal energy, delivered at a level below the threshold required for tissue vaporization, has been used for many years in a variety of medical and surgical specialities. Successful laser-induced repair of retinal tears and photocoagulation of ischemic diabetic retinal tissue are well characterized, commonly performed procedures, while laser/thermal anastomosis of a variety of soft tissues [3—10] has been applied clinically only recently [9]. Sigel et al. [11, 12], demonstrated experimentally that when vascular anastomoses are induced by an appropriate degree of electrocoagulation, continuity of connective tissue elements across the plane of juxtaposition appeared to account for tissue bonding. At the ultrastructural level, Schober et al. [13] showed that thermal cross-linking of fibrillary substructures of collagen was, at least in part, responsible for laser-induced welding at vascular anastomotic sites in a murine model.

In a series of *in-vitro* studies of separated layers of human postmortem atheromatous aortas, our group defined the conditions under which laser/thermal fusion of plaque-media pairs is expected to occur [14—19]. Continuous wave Nd: YAG (neodymium: yttrium aluminum garnet) laser radiation at 1.06 microns was found to be useful as a result of the relatively penetrating nature of the radiation, approximately 3—4 mm through most soft tissues. Alternative, less penetrating wavelengths, such as 488/515 nm from an argon-ion laser, 1.3 microns from a Nd: YAG laser, and solely indirect heating by contact with a hot surface have not been as useful, in our experience, in fusion of plaque-media pairs of human postmortem tissue when the depth of thermal penetration needed exceeds approximately 0.5 mm into the underlying arterial wall.

Given the fact that laser-induced tissue fusion is a pure thermal effect, ie., photochemical and other non-thermal effects of laser exposure do not appear to play a role, the temperature history of juxtaposed tissues is critical to the success of the fusion. We have found that a minimum temperature of 80° C is

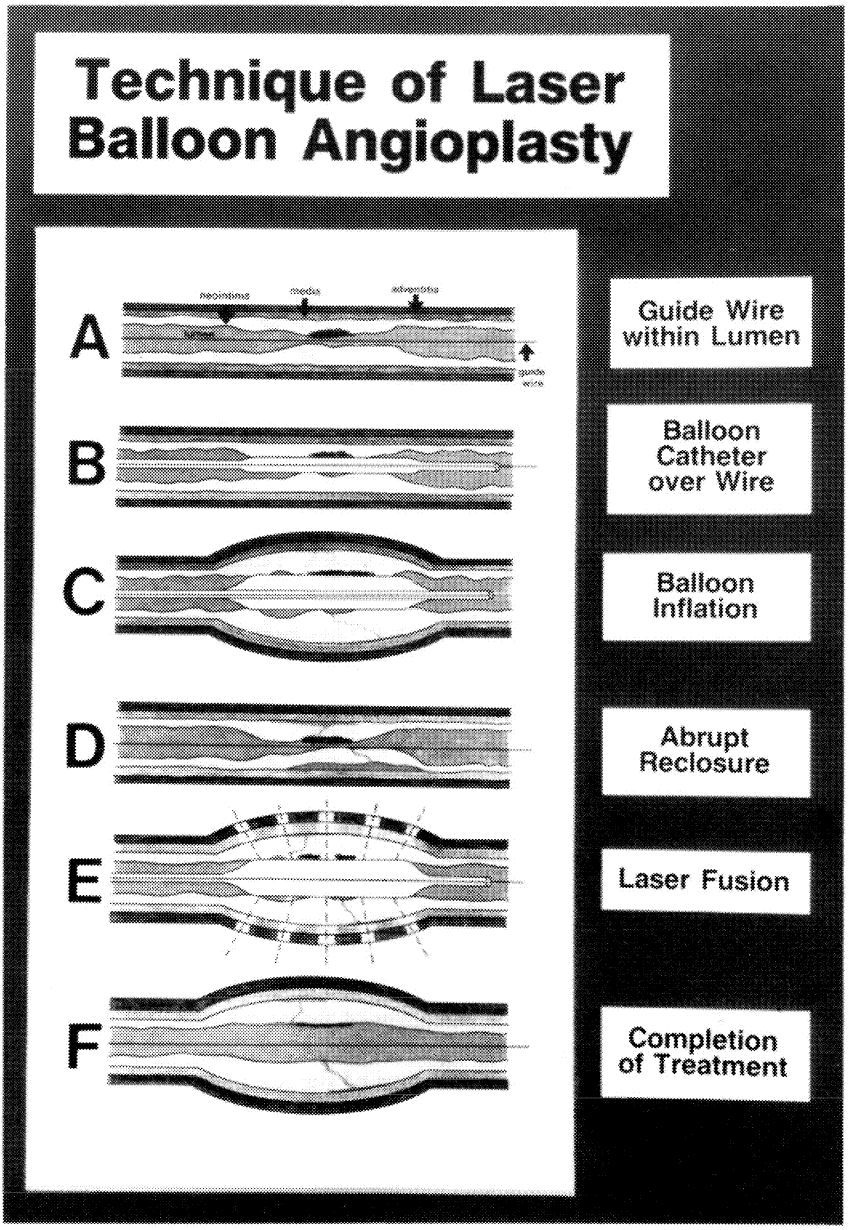

Fig. 1. Schematic diagram of LBA concept. Following conventional PTCA, mural dissection, arterial recoil, and thrombus contribute to acute closure. Appropriate application of cw Nd: YAG laser energy to heat tissues under pressure during balloon inflation may seal dissections, reduce arterial recoil, and desicate thrombus. Additional, more speculative, potentially beneficial effects may include reduction of luminal surface thrombogenicity and destruction of smooth muscle cell viability. Technical improvements in the ability to deliver a uniform cylindrical pattern of radiation from the LBA balloon and definition of optimal laser dosimetry for each proposed tissue effect are currently underway.

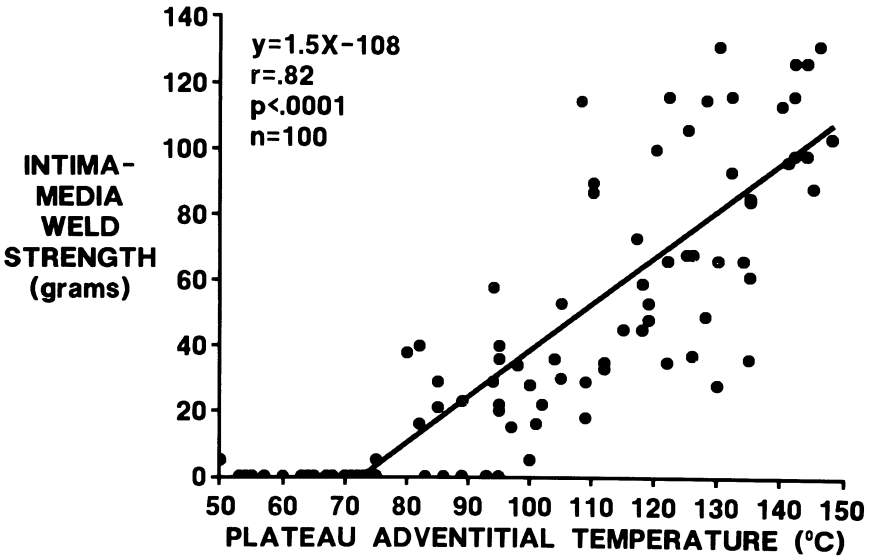

Fig. 2. Relationship between weld strength of Nd: YAG laser-exposed separated layers of human postmortem atherosclerotic aortic sections and plateau adventitial tissue temperature. (From Jenkins et al. Lasers Surg Med 8: 392—396, 1987. Reprinted with permission from Lasers Surg Med).

required, when cw Nd: YAG (1.06 microns) exposure durations of 20 sec or less are used, to initiate plaque-media fusion. A linear relationship has been found between peak plateau temperature and weld strength of juxtaposed tissues over a 80° C—150° C range. Ordinarily, vaporization of the water compartment of tissue would occur at 100° C, but a somewhat higher temperature (110° C—120° C) is required when tissue pressure is applied during laser exposure. Without application of tissue pressure on the order of > 0.5 atm, no tissue fusion occurs, probably because of inadequate contact between tissue layers. Actual vaporization of the solid components of tissue occurs at temperatures exceeding approximately 180° C. Thus, fusion of separated tissue layers can be achieved at temperatures well below the threshold for tissue vaporization.

According to the Arrhenius damage integral characterizing the degree of thermal injury to tissues in general [20], tissue damage is exponentially related to temperature and linearly related to the duration at a particular temperature. The peak temperature achieved is therefore more important than the duration at a given temperature. Nonetheless, the latter plays a role in tissue fusion studies, and a minimum exposure duration of approximately 10 sec is required for plaque-media bonding to occur, irrespective of the peak temperature achieved. Thereafter, a roughly linear relationship between

tissue weld strength and laser exposure duration obtains over a 10—30 sec range, with some plateauing of the effect between 20—30 sec.

For the above temperature history studies, a decremental power format was used to achieve a target tissue temperature relatively quickly, i.e., within 5 sec, with maintenance of a plateau temperature over the remainder of the exposure. Achieving a target tissue temperature quickly with this power to minimize the period of balloon occlusion, we have additionally found that tissue weld strength is improved, at a lesser energy cost, compared to that produced with constant power formats. Rapid tissue heating results in less energy required, very likely, because of a reduction in thermal diffusion; potentially increased and, therefore, more efficient absorption during heating; and possibly more effective denaturation associated with a more rapid rate of change in temperature.

Fortunately, except for temperature history and the need for some tissue pressure, no other variables studied to date have been found to greatly affect the weld strength of laser-exposed plaque-media pairs of tissue. Mean weld strength of bonds between heavily calcified plaque and media was somewhat lower than that for fibrous plaques, but the difference was not statistically significant. Likewise, weld strength was unaffected by the presence of blood vs. saline between tissue layers during laser exposure or by tissue pressure over a 0.5 to 4.0 atm range.

An important mechanism at the ultrastructured level responsible for laser/thermal fusion of tissue was described by Schober et al. [13] for a murine model of vascular anastomosis. Cross-linking of fibrillary substructures between adjacent collagen fibers within juxtaposed tissues effectively bonds the latter across the plane of tissue separation. We have shown that laser-induced fusion of plaque-media layers can be performed in a repetitive manner, and that transmission of laser radiation at 1.06 microns falls in a reversible manner during heating. Since a similar phenomenon of "hyperchromaticity" to UV radiation during heating of preparations of both DNA and collagen has been described [21, 22], it is attractive to postulate that the proposed mechanism for this latter phenomenon, reversible breakage of noncovalent bonds (e.g., hydrogen bonds), is also responsible for reversible transmission changes during tissue heating and for the ability to weld tissues in a repetitive manner.

For an in-vivo application of LBA in an atherosclerotic rabbit iliac artery model [23], a prototype balloon was used to deliver a 20 sec cw Nd: YAG laser dose which would achieve a peak plateau tissue temperature, 0.5 mm from the surface of the inflated balloon, of 100° C—110° C. Dissections produced by initial conventional balloon angioplasty with the same balloon were usually successfully sealed by subsequent treatment with LBA. Occasional failure to seal a dissection may have resulted from the fact that an axial length of only 5 mm along the middle portion of the balloon received an adequate laser power density; inherent azimuthal asymmetry in the circumferential distribution of radiation no doubt compounded the problem.

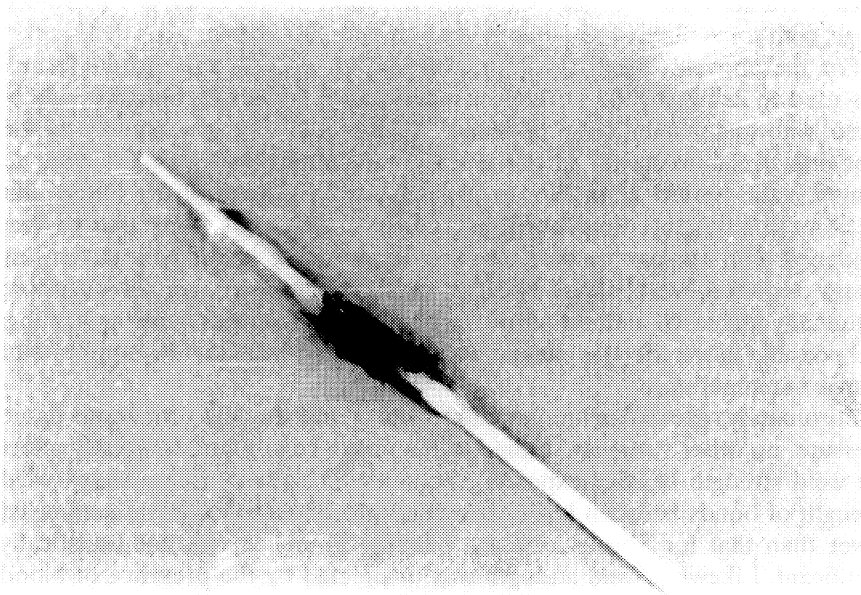

Fig. 3. 3.0 × 20 mm LBA balloon after treatment of a long (4 cm), total thrombotic occlusion experimentally in-vivo. A collar of desicated residue of thrombus is adherent to the balloon surface following multiple applications of a relatively high laser dose (450 watts). Lower laser doses result in dessication of thrombus with less adherence to the balloon.

Arterial recoil

Following successful PTCA, the mean luminal diameter is approximately 30% smaller than that of the inflated balloon diameter as a result, very likely, of passive viscoelastic recoil. Within 30 min after PTCA and at 1 day after PTCA, mean minimum luminal diameter decreases further but recovers to the same immediate post PTCA value at 1 month after the procedure, most likely as a result of temporary vasoconstriction [24, 25]. Thermal remodelling of elastic tissue and destruction of smooth muscle cell viability during LBA can be used to reduce both active and passive components of arterial recoil. Currently, the 1.06 micron laser doses required to achieve these effects are not well defined, but appear to be significantly lower than doses required for tissue fusion.

Prototype LBA balloons have been used experimentally on dog normal carotid and coronary arteries and on rabbit normal iliac arteries [26—28]. In each case, the peak tissue temperatures achieved near the 5 cm long mid-portion of the balloon approximated 90° C to 120° C, greatly exceeding that achieved near the proximal and distal ends of the 2 cm long balloon, estimated to be approximately 60° C—70° C. However, the reduction in

arterial recoil appeared uniform along the full length of the balloon in each model, and a marked reduction in the responses to vasoactive drugs was noted along the full length of laser-exposed arterial segments subacutely and at 1 month after treatment, unlike control segments treated with conventional angioplasty. Although loss of nuclei on H & E stained sections was demonstrable 1 day after LBA, compatible with loss of smooth muscle cell viability throughout the media, the latter was fully cellular 1 month after treatment, presumably as a result of fibroblast cell infiltration. The possibility exists that smooth muscle cells could also migrate into the laser-exposed segment and populate this region once again, but the random alignment of the cells seen at the 1 month follow-up period suggests that synchronized contraction would not be likely even if all cells had functional contractile proteins.

The in-vivo experimental studies provided additional important insights. Despite the relatively large number of animals treated with LBA, significant adverse effects on the arterial lumen were rare. LBA increased luminal diameter, as assessed by computerized analysis of digitized angiographic images, to a greater degree than conventional balloon angioplasty in each model. At a relatively high laser dose in the rabbit iliac model, however, the gain in diameter improvement was lost at 1 month after treatment. The predominant problem with the use of the high laser dose appeared to be the induction of excessive perivascular fibrosis with some resultant stricture formation, although neointimal thickening in response to the high dose might have increased slightly compared to that associated with a moderate laser dose. Interestingly, the degree of neointimal thickening appeared similar for arteries treated with conventional balloon angioplasty and moderate dose LBA, and no qualitative difference in the neointimal layer between the 2 groups was observable. The observation calls into question the hypothesis that smooth muscle cells in the media of the mechanically injured artery are responsible for neointimal thickening, in view of the loss of smooth cell viability throughout the media of LBA-treated segments.

Mitigation of adverse biologic responses

Presence of pre-existing thrombus, thrombogenicity of the murally disrupted luminal surface, increased vasomotor tone, and chronic neointimal thickening following PTCA might each be favorably affected by LBA at an appropriate laser dose.

Although thrombus is a well recognized problem in the clinical setting of myocardial infarction and unstable angina, particularly when an angiographic appearance of a cut-off or intra-luminal filling defect is noted, layered thrombus cannot be distinguished from atheromatous plaque angiographically yet may, nevertheless, be occasionally present in lesions of clinically stable patients. Remodelling of thrombus is unpredictable with conventional

balloon angioplasty, but we have found experimentally that LBA results in rapid desiccation of thrombus and is effective in remodelling the residue into a thin, smooth film which is adherent to the luminal surface. The absorption coefficient at 1.06 microns for thrombus is an order of magnitude higher than that for atheromatous plaque and the normal arterial wall. As a result, the temperature rise within thrombus adjacent to the LBA balloon is considerably greater than that for arterial tissues. When a laser dose is used which would ordinarily result in a peak temperature of 100° C within the arterial wall, a peak temperature of approximately 130° C to 150° C will be achieved within adjacent thrombus, which results in its rapid desication without vaporization of the solid component of the tissue. In addition to debulking and effective remodelling of the residue, the hypothesis that the heat-treated thrombus is rendered less thrombogenetic is currently being tested in our laboratory. Preliminary studies in our in-vivo dog model of thrombotic femoral artery occlusion suggest that both the laser dose given and the ability to distribute the laser energy in a uniform cylindrical pattern along the length and circumference of the balloon will be important factors in the long term success of LBA in the treatment of intraluminal thrombus.

Increased vasomotor tone, when demonstrable before and/or after PTCA, is felt by some investigators to be a risk factor for restenosis. As discussed earlier, thermal destruction of smooth muscle cells from LBA should abolish vasospasm. If vasospasm per se inhibits repair of the endothelial lining layer, LBA may be beneficial. However, the possibility exists that increased vasomotor tone after PTCA is simply a frequent marker of the presence of platelet aggregates or thrombus, and that elimination of vasospasm will have no effect on restenosis. In fact, the possibility should be considered that the increased velocity of flow associated with a vasoconstricted lumen may actually help to inhibit further propagation of any thrombus present.

Thrombogenicity of the murally disrupted luminal surface may play a role in both the short and long term success of PTCA. The hypothesis is currently being tested that an appropriate degree of laser/thermal denaturation of subendothelial proteins, such as collagen, basement membrane, fibronectin, etc., will reduce the thrombogenicity of the luminal surface of the mechanically injured arterial wall. It is well known that gluteraldehyde fixation of heterograft porcine valves with cross-linking of proteins such as collagen markedly reduces thrombogenicity of the valves. Since heat has been used in a manner similar to gluteraldehyde for ultrastructural fixation of tissues [29], and protein cross-linking is most likely an important mechanism of laser-induced fusion of tissues, it is possible that appropriate thermal fixation of subendothelial proteins during LBA may reduce surface thrombogenicity. Preliminary experimental studies by several groups suggest that platelet deposition may be reduced by LBA compared to conventional balloon angiopolasty, but a great deal of work is needed to define the temperature history range, if it exists, which will optimally produce such salutary effects.

The mechanisms for neointimal growth after PTCA are, of course,

currently poorly defined. If LBA proves useful in prevention of restenosis, the effective treatment of thrombus, reduction of thrombogenicity of the luminal surface, in addition to the creation of a larger, smoother surface, may be contributory. Loss of smooth muscle cell viability could likewise be helpful, but any potential benefit in this regard is highly speculative.

Clinical studies

It is beyond the scope of this chapter to describe the percutaneous coronary clinical LBA studies performed since the first patient was treated March 10, 1988. However, the acute and subacute results demonstrate that LBA is more effective than initial PTCA with a balloon of the same dimensions (3.0 × 20 mm) in increasing minimum luminal diameter as assessed by computerized image processing of digitized cineangiographic images [30—32]. Fusion of separated tissue layers, reduction of arterial recoil, and dessication of thrombus, as would be expected from experimental studies, appeared to account for the improvement in luminal dimensions and morphology. It therefore appears that LBA may be effective in the treatment of impending or overt acute closure associated with PTCA [31].

In order to test the potential utility of LBA acutely and for potentially reducing the incidence of restenosis associated with PTCA, the currently highly non-uniform pattern of radiation emitted by the LBA balloon will need to be corrected, and laser dosimetry studies, similar to those performed for defining the conditions under which tissue fusion can be expected, will be required for the variety of other, potentially beneficial effects of this new therapy.

References

1. Leimgruber PP, Roubin GS, Anderson V, Bredlau CB, Whitworth HB, Douglas JS Jr, King SB III, Gruentzig AR: Influence of intimal dissection on restenosis after successful coronary angioplasty. Circulation 72: 530—535, 1985.
2. Beatt KJ, Luijten HE, Suryapranata H, Feyter PJde, Serruys PW: Suboptimal post angioplasty result. The principle risk factor for "restenosis". Circulation 80 (Suppl II): II-257, 1989. (Abstract)
3. Gomes OM, Macruz R, Armelin E, Ribeiro MP, Brum JMG, Bittencourt D, Verginelli G, Zerbini EJ: Vascular anastomosis by argon laser beam. Texas Heart Inst J 10: 145—149, 1983.
4. Frazier OH, Painvin A, Morris JR, Thomsen S, Neblett CR: Laser-assisted microvascular anastomoses: Angiographic and anatomopathologic studies on growing microvascular anastomoses: Preliminary report. Surgery 97: 585—590, 1985.
5. Quigley MR, Bailes JE, Kwaan HC, Cerullo LJ, Brown JT, Lastre C, Monma D: Microvascular anastomosis using the milliwatt CO2 laser. Lasers Surg Med 5: 357—365, 1985.
6. Klink F, Grosspietzch R, von Klitzing L, Endell W, Wolfdietrich H., Obertheurer F:

Animal in-vivo studies and in-vitro experiments with human tubes for end-to-end anastomotic operation by a CO2 laser technique. Fertil Steril 30: 100—102, 1978.
7. Jain KK, Gorsich W : Repair of Small blood vessels with the Neodymium-YAG laser:A preliminary report. Surgery 85: 864—868, 1979.
8. White RA, Kopchok G, Donayre C, Abergel RP, Lyons R, Klein SR, Dwyer RM, Uitto J: Comparison of laser-welded and sutured arteriotomies. Arch Surg 121: 1133—1135, 1986.
9. White RA, White GH, Fujitani RM, Vlasak JW, Donayre CE, Kopchok GE, Peng SK: Initial human evaluation of argon laser-assisted vascular anastomoses. J Vasc Surg 9: 542—547, 1989.
10. Jain KK: Sutureless end-to-side microvascular anastomosis with a Nd-YAG laser. Lasers Surg Med 3: 311—316, 1984.
11. Sigel B, Dunn MR: The mechanism of blood vessel closure by high frequency electrocoagulation. Surg Gyn and Obst 121: 823—831, 1965.
12. Sigel B, Acevedo FJ: Electrocoaptive union of blood vessels: A preliminary experimental study. J Surg Res: III-90—96, 1963.
13. Schober R, Ulrich F, Sander T, Durselen H. Hessels S: Laser-induced alteration of collagen substructure allows microsurgical tissue welding. Science 232: 1421—1422, 1986.
14. Hiehle JF, Bourgelais DBC, Shapshay S, Schoen FJ, Kim DS, Spears JR: Nd:YAG laser fusion of human atheromatous plaque-arterial wall separations in vitro. Am J Cardiol 56: 953—957, 1985.
15. Jenkins RD, Sinclair IN, Anand R, Kalil AG, Frederick JS, Spears JR: Laser balloon angioplasty: Effect of tissue temperature on weld strength of human postmortem intima-media separations. Lasers Surg Med 8: 30—39, 1988.
16. Anand RK, Sinclair IN, Jenkins RD, JF Hiehle, Jr., James LM, Spears JR: Laser balloon angioplasty: Effect of constant temperature versus constant power on tissue weld strength. Laser Sur Med 8: 40—44, 1988.
17. Jenkins RD, Sinclair IN, Anand RK, James LM, Spears JR: Laser balloon angioplasty: Effect of exposure duration on shear strength of welded layers of postmortem human aorta. Lasers Surg Med 8: 392—396, 1988.
18. Spears JR, James LM, Leonard BM, Sinclair IN, Jenkins RD, Motamedi M, Sinofsky EL: Plaque-media rewelding with reversible tissue optical property changes during repetitive cw Nd: YAG laser exposure. Lasers Surg Med 8: 477—485, 1988.
19. Sinclair IN, Anand RK, Kalil AG, Jr., Schoen FJ, Bourgelais D, Spears JR: Laser balloon angioplasty: Factors affecting plaque-arterial wall thermal "weld" strength. Circulation 74: II-203, 1986. (Abstract)
20. Henriques FC, Moritz AR: Studies of thermal injury, I. the conduction of heat to and through skin and the temperature attained therein. A theoretical and experimental investigation. Am. J. Pathol., 23: 531, 1947.
21. Danielsen CC: Precision method to determine denaturation temperature of collagen using ultraviolet difference spectroscopy. Coll Relat Res 2: 143—150, 1982.
22. Hauschka PV, Harrington WF: Collagen structure in solution. III Effect of cross-links on thermal stability and refolding kinetics. Biochemistry: 3734—3745, 1970.
23. Jenkins RD, Sinclair IN, McCall PE, Schoen FJ, Spears JR: Thermal sealing of arterial dissections and perforations in atherosclerotic rabbits with laser balloon angioplasty. Lasers in Life Sciences 3: 1—18, 1989.
24. Fischell TA, Derby G, Tse TM, Stadius ML: Coronary artery vasoconstriction routinely occurs after percutaneous transluminal coronary angioplasty. A quantitative arterriographic analysis. Circulation 78: 1323—1334, 1989.
25. Nobuyoshi M, Kimura M, Nosaka H, Mioka S, Ueno K, Yokoi H, Hamasaki N, Horiuchi H, Ohishi H: Restenosis after successful percutaneous transluminal coronary angioplasty: Serial angiographic follow-up of 229 patients. J Am Coll Cardiol 12: 616—623, 1988.

26. Serur JR, Sinclair IN, Spokojny AM, Paulin S, Spears JR: Laser balloon angioplasty (LBA): Effect on the carotid lumen in the dog. Circulation 72: III-457, 1985 (Abstract).
27. Jenkins RD, Sinclair IN, Leonard BM, Sandor T, Schoen FJ, Spears JR: Laser balloon angioplasty versus balloon angioplasty in normal rabbit iliac arteries. Lasers Surg Med 9: 237—247, 1989.
28. Spears JR, Sinclair IN, Jenkins RD: Laser balloon angioplasty: Experimental in vivo and in vitro studies. Abela GS (ed), Kluwer Academic Publishers, Nowell, Mass, 1989: 167—188.
29. Login GR, Dvorak AM: Microwave energy fixation for electron microscopy. Am J Pathol 120: 230—243, 1985.
30. Spears JR, Dear WE, Safian RD, Sinclair IN, Pokker HWM, Aldridge H, Knudtson ML, Sigwart U, Rickards AF, and the LBA Study Group: Laser balloon angioplasty: angiographic results of a multicenter trial. Circulation 80 (Suppl II): II-476, 1989 (Abstract).
31. Sinclair IN, Dear WE, Safian RD, Pokker TM, Spears JR, and the LBA Study Group: Acute closure post PTCA successfully treated with laser balloon angioplasty. Circulation 80 (Suppl II): II-476, 1989 (Abstract).
32. Spears JR, Reyes VP, Wynne J, Fromm BS, Sinofsky EL, Andrus S, Sinclair IN, Hopkins BE, Schwartz L, Aldridge HE, Plokker HWT, Mast EG, Rickards A, Knudtson ML, Sigwart U, Dear WE, Ferguson JJ, Angelini P, Leatherman LL, Safian RD, Jenkins RD, Douglas J, King III SB: Percutaneous coronary laser balloon angioplasty: Initial results of a multicenter experience. J Am Coll Cardiol 16: 293—303, 1990.

17. Mechanical recanalization of coronary arteries

MICHEL E. BERTRAND, JEAN M. LABLANCHE and
CHRISTOPHE BAUTERS

The remarkable clinical success of percutaneous transluminal coronary angioplasty has stimulated innovative expression in research and clinical practice. Within the past 5 years, significant advances have been made in the original balloon catheter system described and used by A Gruentzig in 1977. Steerable balloon catheters with a truly low profile, excellent pushability and trackability are nowadays commonly used. New techniques (long guide wire technique, monorail system) have been proposed and are employed in many catheterization laboratories, at least in Europe.

More recently a different approach to the treatment of atherosclerotic disease was described. It consists of new tools based on the principle of mechanical recanalization: some of them are dedicated for the treatment of chronic coronary occlusions while others try to remove the atherosclerotic material. In this field, there are many possibilities: atheromatous removal can be obtained by resection of the plaque (Excisional atherectomy), while others tried to obtain a micropulverization of the atherosclerotic material with rotating abrasive tips (rotative atherectomy).

The goal of this chapter is to review the current systems performing mechanical recanalization of the coronary vessels with atherosclerotic obstruction.

Mechanical recanalization with a guide wire

For many years chronic total coronary occlusions were deemed unsuitable for coronary angioplasty until it was found that some of them could be crossed by guide wires and dilated with balloon angioplasty. All chronic total coronary occlusions are not associated with complete infarction of the respective myocardial area. According to the degree of collateralization, the myocardium may be completely necrotic, partially necrotic or almost normal. An occluded vessel with a good collateralization is hemodynamically similar to a 90% narrowing. This explains why certain occlusion with still viable myocardium can be considered for angioplasty.

The first step of the technique consists of trying to cross the obstruction

J. H. C. Reiber and P. W. Serruys (eds), Quantitative Coronary Arteriography, 341–350.

with a stiff guidewire: if this first attempt fails, a balloon with a very low profile is advanced until contact with the obstacle is almost established. With the guide wire sticking out of the balloon tip over a distance of 5 to 7 mm, both devices are pushed forward until the total obstruction has been crossed; next, the balloon is inflated.

Some authors proposed the Omniflex balloon system as an adequate tool for these lesions. More recently, Meier et al. developed a new guidewire (Magnum wire) for balloon recanalization of chronic total coronary occlusions [1]. This device overcomes some of the major shortcomings of conventional wires, such as insufficient pushability and a tendency to follow subintimal pathways. Magnum is characterized by a stiff solid-steel wire shaft ensuring excellent torque control combined with a distal portion made of a flexible and shapeable spring wire with an olive-shaped ball tip of 1 mm in diameter. This particular wire, retrogradely inserted in a balloon, protrudes from the balloon during the progression through the proximal part of the artery. The wire passes rarely the occlusion but when the balloon is advanced close to the olive, the wire is splinted and then thrust forward. Injection of contrast medium through the balloon or the guiding catheter provides information about a possible subintimal pathway or the successful passage.

Table 1 shows the rates of success and complications of these different attempts to mechanically recanalize complete coronary occlusions. At the average, the primary success is 56% with no deaths, no new Q wave infarctions, 8% of creatine kinase elevations and 1% of emergency bypass surgery. With the new version of the Magnum wire, Meier et al. obtained a 68% primary success rate.

Table 1. PTCA in complete chronic coronary occlusion

	NB	Range of duration (months)	Primary success	E.M. CABG	MI	Recurrence	
						Rest	Re-occl.
Dervan	13	1	54%	0%	0%	43	
Holmes	24	3	54%	4%	17%	20	
Serruys	49	2	57%	2%	18%	25	40%
Kereiakes	76	7	53%	1%	11%		75%
Holmes	67	2	66%			39	4
Kober	31	4	42%	0	0	46	8
Melchior	100	4	56%	0	2%	35	20

Nevertheless the chances to recanalize are mainly dependent on and decline with the age of occlusion. Moreover, the recurrence rate in the same population ranges from 20 to 75% (average 55%).

Directional atherectomy

The Simpson's atherocath is characterized by a cylindrical metal housing attached to the end of a braided double-lumen catheter [2]. The cylindrical housing has a "longitudinal window" which is positioned snuggly against the atheroma with the help of a small balloon opposite to the window. Inside the window, a rotating cutter-blade shaves off atherosclerotic material and deposits it in the distal part of the metal housing. A separate hand-held, battery-powered motor drive is attached to a cable connected to the cutter-blade.

The procedure is illustrated in Figure 1. The atherocath is advanced over the wire under fluoroscopic guidance. The window of the cylindrical housing is positioned across the stenosis. The positioning balloon is inflated, the

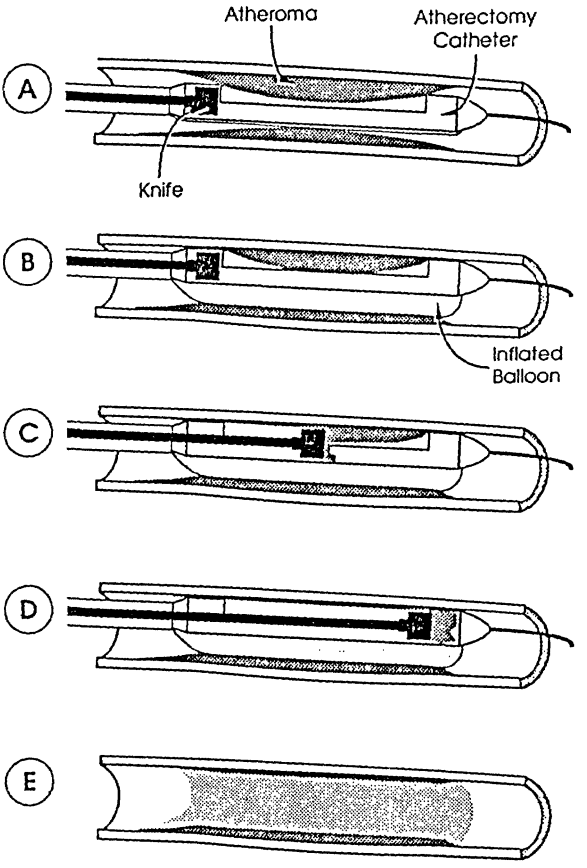

Fig. 1. Schematization of removal of plaque using the Simpson's device. (A) Catheter in position; (B) Balloon inflation to position the cutting blade; (C—D) Plaque removal; (E) Final result.

attached motor drive is activated and the cutter blade is slowly advanced through the metal housing, shaving off atheroma and depositing it distally. The positioning balloon is deflated, the catheter is torqued about 60 to 90° to reposition the window and to remove additional atheroma. When the collection chamber is full, the catheter is withdrawn from the patient and the cutter blade retracted into the proximal portion of the housing. Repeated passes are made until the desired result is achieved. A residual stenosis at the conclusion of the atherectomy procedure can lead to conclude with an appropriate-sized balloon catheter.

Atherectomy is more time consuming than PTCA because multiple passes must be made to achieve an optimal result. This technique permits studying material removed from each atherectomy site. This technique is relatively aggressive. In recent papers Safian et al. showed that on specimen removed during 53 atherectomy procedures, media was retrieved in 64% of cases and even adventitia was found in 23% of cases without acute clinical sequelae, but finally there was in these cases a perforation of the vessel wall [3].

The immediate results of a multicenter study are listed in Table 2: the primary success rate was 87.6%. 86 patients (18%) had a total of 109 in-hospital complications [4]. Major complications included death in 3 patients (0.6%), myocardial infarction in 23 (4.8%) (Q-wave MI in 3 and non-Q-wave in 20). Coronary bypass grafting was performed in 21 patients (4.4%) and balloon angioplasty "rescue" was performed in 10 patients (2%).

The long term results are available for only a small number of patients [5]. Among 73 patients with successful directional atherectomy 62 patients (85%) with 76 lesions underwent repeat catheterization between 3—9 months with mean of 5.3 months. Restenosis defined as $> 50\%$ reduction of luminal diameter was observed in 21 of 56 native vessels (38%) and in 11/20 grafts (59%). Restenosis rate was 27% in patients with none or only

Table 2. Directional atherectomy multicenter study

N. patients	480
N. lesions	534
Primary success	87.6%
Major vessel occlusion	15 (3.1%)
Branch vessel occlusion	19 (4%)
Coronary embolism	11 (2.3%)
Coronary spasm	8 (1.6%)
Coronary dissection	3 (0.6%)
Perforation	1 (0.2%)
Major arrhythmias	7 (1.5%)
Stroke	1 (0.2%)
Device complication	4 (0.2%)
Emery CABG	21 (4.4%)
MI	23 (4.8%)
Death	3 (0.6%)

one prior PTCA and in 47% of patients with 2 or more prior PTCA's. When atherectomy was performed in grafts the rates were 54 and 57%, respectively.

Thus, one can conclude from this small preliminary series that the restenosis rate after directional atherectomy is not very different from the one observed with conventional balloon angioplasty.

3-Rotational atherectomy

This method includes several devices:

High speed rotational atherectomy

The Rotablator TM, designed by D. Auth, consists of a rotative abrasive burr welded to a long flexible drive shaft tracking along a central flexible guide wire. The abrasive tip is an elliptically shaped burr of various size (1.0, 1.25, 1.5, 1.75, 2, 2.25, 2.5 mm diameter) (Figure 2). The burr is coated with diamond chips of 30 to 40 μm embedded in the metal. The drive shaft is housed in a 4F teflon sheath and connected to a turbine driven by compressed air. The shaft and the turbine spin in 150,000 rpm. The number of revolutions per minute is measured by a fiberoptic light probe and displayed on a control panel. The speed of rotation is controlled by the air pressure, which itself is controlled by a foot pedal. During rotation, a small volume of sterile saline solution irrigates the catheter sheath to lubricate and cool the rotating system. The burr and the drive shaft track along a central coaxial guide wire (0.009 inch) of which the last 2 cm is made of radio-opaque

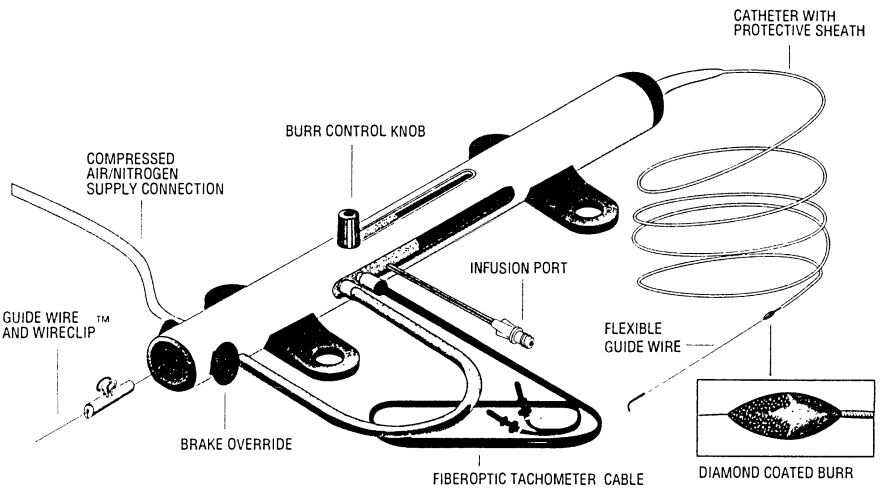

Fig. 2. Rotary atherectomy with Auth's system.

platinium. The central guide wire can be controlled and moved with a pin vise. The wire and abrasive tip can be advanced independently; thus, the wire could be placed in the selected arteries and serves to direct the burr safely through the diseased artery. The steerable guide wire does not rotate with the burr during atherectomy.

Several experimental studies, in vitro and in animals were performed within the last 3 years with the rotablator. Hansen and Auth et al. showed a significant reduction of stenosis with rotary atherectomy in 13 atherosclerotic iliac arteries [6]. Only two complications occurred: one perforation related to the guide wire and an acute occlusion due to an oversized olive burr. Ahn and Auth et al. demonstrated in human cadavers the capability of the device to transform calcified or fibrous plaques into a colloïdal suspension made of microparticles, generally smaller than five microns [7]. The authors did not find embolic or necrotic sequelae after peripheral injection of ablation particle fragments in dogs. We recently reported the histologic examination of human peripheral arterial segments treated with Rotablator TM during surgery [8]. The protocol included patients who had undergone bypass operation of iliac or femoral arteries. Through the arteriotomy, the device was introduced into the lumen and rotative abrasion was applied to this segment. The treated segment was then resected and the surgeon performed the bypass. This segment was studied with scanning electron microscopy. The abrased surface was smooth and polished. Obviously, the endothelium of the adjacent normal vessel had disappeared. There was however no damage to the media. If low speed rotation was applied, some irregularities due to debris and some disruption between the plaque and the media were observed.

In vivo, the first human rotational atherectomy was performed by Zacca et al. in 6 patients with femoro-popliteal stenosis [9]. All the stenotic segments were crossed and treated successfully without complications. In coronary arteries, Hansen and Auth et al. showed in 11 normal canine coronary arteries that this high speed rotating abrasive technique could be applied safely and resulted in minimal vessel damage [10]. Finally, we have reported in 1988 the first experience in human coronary arteries [11, 12].

The atherectomy device was introduced into the guiding catheter and positioned just before the distal tip of the 9F guiding catheter. Under fluoroscopy, the steerable guide wire was advanced through the narrowing and directed into the distal part of the coronary artery. The abrasive tip was then advanced along the guide wire and placed in contact with the stenosis and rotation was started. When the adequate speed of rotation was reached (175,000 rpm) the abrasive tip was gently advanced over the guidewire. If a resistance was encountered, the tip was successively pulled back and advanced to maintain a high speed rotation. Once the abrasive tip crossed the lesion, several passages were performed until the impression of mechanical resistance completely disappeared. On average, after 6 to 8 passages, the rotation was stopped and the abrasive tip pulled back into the guiding catheter, while the guidewire remained in the distal part of the vessel. Dye

injection verified the quality and the success of the procedure; finally, the rotational device and guidewire were completely withdrawn.

Primary success of rotational atherectomy is defined as a significant reduction (> 20%) in percentage stenosis without complications. When the residual stenosis after rotational atherectomy remained significant (> 50%), a percutaneous transluminal balloon angioplasty completed the procedure.

In Europe two groups performed rotative atherectomy with the Rotablator: Bertrand et al. presented a first series of 50 patients with 52 narrowings. In 3 patients the guide wire was unable to cross the narrowing. A primary success was obtained in 45 patients (90%). There were no deaths, Q-wave myocardial infarction or emergency bypass surgery. Two patients developed a non Q-wave MI.

Similar results were obtained by Erbel in Germany in a smaller series of 17 patients [13]. More recently, two American groups presented their initial experience with this device and obtained 78 and 97% of primary success [14, 15]. In terms of restenosis Bertrand et al. restudied angiographically 43 patients and observed a restenosis rate of 37% in patients treated by Rotablator alone, while in 17 patients in which the procedure was completed by balloon angioplasty the restenosis rate was 35%: W O'Neill observed a restenosis rate of 44% in 18 patients restudied with angiography [15].

Low speed rotational angioplasty

Kaltenbach and Valbracht [16] proposed a guide wire (Rotacs) with a ball tip connected to an electric motor rotating at 100—400 rpm. The main indication for this device is complete coronary occlusion: the ball tip of the guidewire is placed in contact with the atherosclerotic obstruction and then the motor is started to rotate at 200—300 rpm. The device was able to cross chronic occlusions in 60% of the cases in a series of 60 patients. Seventeen had an average angiographic follow-up of 3.7 months after the procedure. Three patients showed a good result, but 8 had restenosis which was successfully re-dilated, six others had re-occlusions.

Thus, in patients with chronic coronary occlusions not responding to conventional techniques the Rotacs was able to reopen 60% of the cases, however, the mid term results were favorable only in a few of them.

Transluminal extracting catheter (TEC)

The TEC is a percutaneously introduced flexible torque tube device that tracks over a flexible steerable guidewire under fluoroscopic control to the targeted coronary artery lesion [17]. When the radiopaque tip is properly positioned near the origin of the lesion, a two-stage trigger is activated on the hand-held control piece (Figure 3). Next, the conical cutter rotates at 750 rpm while suction is applied through the opening of the cutting window to extract the plaque fragments through the catheter and out of the patient's

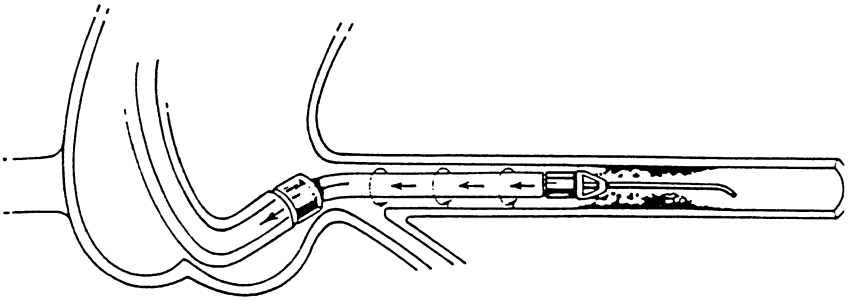

Fig. 3. Transluminal extracting catheter (TEC)- R. Stack.

body. Material extracted from the artery is collected in a glass reservoir attached to the rear panel of the control piece.

In experimental studies, normal vessels histology revealed focal intimal disruption; in atherosclerotic vessels the depth of excision was typically limited to the media but occasional disruption of the external elastic lamina was noted.

Preliminary studies were performed at Duke University: in 147 patients (155 lesions) a primary success was obtained in 93% of cases and emergency bypass surgery was performed in 5%. Forty nine patients were restudied with angiography and 21 (43%) had restenosis [18].

Kensey instrument

This device does not track over a guide wire. The tip rotates up to 100,000 rpm and simultaneously hurls high powered water jets laterally against the walls. This creates a vortex that sucks in the atheromatous debris for micro-pulverization.

In peripheral arteries, more than 100 patients have been treated with a success rate of 80%; in coronary arteries trials are underway.

Other devices

Every month, a number of new devices are introduced. Helical "corkscrew" blade (Leyser) etc., but most of them are still investigational and only used in experimental studies.

Comments

The unlimited imagination of interventional cardiologists and engineers

provide to the clinicians a lot of new tools: However the evaluation of these new devices should be focussed on the two following points:

1) Do these new tools fulfill their promises?
2) What are their respective indications?

It is clear that most of the new devices were invented to improve the results of PTCA which are globally satisfactory but need certain improvement in terms of prevention of acute complications and mainly restenosis. In general, these new means of mechanical recanalization have the same rate of primary success and acute complications as the conventional balloon angioplasty.

From the standpoint of restenosis it becomes clearly evident that the risk of restenosis is similar to those usually observed in patients treated with PTCA. This is not totally unexpected since most of these tools are clearly much more aggressive for the wall than the radial force exerted by a balloon. Thus, we may suspect that the healing process is very active and leads to an intensive myointimal proliferation.

Then the question of the superiority of these new tools over PTCA arises. First of all it should be noted that such a comparison is unfair since it is impossible to compare the small preliminary studies concerning the new tools of mechanical recanalization to the impressive cohort of many thousands of patients treated with balloon angioplasty throughout the world.

It is more interesting to remark that, finally all these devices, have certain specifications which could lead in the future to different indications. For example, one can propose that directional atherectomy of J. Simpson is certainly the best tool to remove the atherosclerotic material of large ($>4/5$ mm) coronary arteries, especially with eccentric lesions or in ostial obstructions. On the other hand, the flexibility and the small size of the Rotablator's burr is probably well adapted to distal diffuse narrowings.

Thus, in the future we could have particular indications reserved for these new devices, the conventional PTCA being the gold standard employed in most of the cases.

However, once the development phases have been completed, all these new tools must undergo controlled prospective randomized trials versus the current state-of-the-art of balloon angioplasty. However, they must also be compared to each other to determine the best use of these new technologies.

References

1. Meier B, Carlier M, Finci L, Nukta E, Urban Ph, Niederhauser W, Favre J: Magnum wire for balloon recanalization of chronic total coronary occlusions. Am J Cardiol 64: 148–154, 1989.
2. Simpson JB, Robertson GC, Selmon MR: Percutaneous coronary atherectomy. J Am Coll Card 11: 110, 1988 (Abstract).
3. Safian R, Gelbfish J, Erny R, Schnitt S, Baim D: Histologic findings of coronary atherectomy. Circulation 80: II-583, 1989 (Abstract).
4. Vlietstra R, Abbotsmith Ch, Douglas J, Hollman J, Muller D, Safian R, Selmon M:

Complications with directional coronary atherectomy. Experience at eight centers. Circulation 80: II-582, 1989 (Abstract).
5. Simpson J, Robertson G, Selmon M, Sipperly ME, Braden L, Hinohara T: Restenosis following successful directional coronary atherectomy. Circulation 80: II-582, 1989 (Abstract).
6. Hansen DD, Auth DC, Vrocko R, Ritchie JL: Rotational atherectomy in atherosclerotic rabbit iliac arteries. Am Heart J 115: 160—165, 1988.
7. Ahn SS, Auth DC, Marcus DR, Moore WS: Removal of focal atheromatous lesions by angioscopically guided high speed rotary atherectomy. J Vasc Surg 7: 292—299, 1988.
8. Fourrier JL, Stankowiak C, Lablanche JM, Prat A, Brunetaud JM, Bertrand ME: Histopathology after rotational angioplasty of peripheral arteries in human beings. J Am Coll Card 11: 109A, 1988 (Abstract).
9. Zacca NM, Raizner AE, Noon GP, Short HD, Weilbaecher DG, Gotto AM, Roberts R: Short term follow-up of patients treated with a recently developed rotational atherectomy device and in vivo assessment of the particles generated. J Am Coll Card 11: 109A, 1988 (Abstract).
10. Hansen DD, Auth DC, Hall M, Ritchie JL: Rotational endarterectomy in normal canine coronary arteries. Preliminary report. J Am Coll Card 11: 1073—1077, 1988.
11. Fourrier JL, Auth DC, Lablanche JM, Brunetaud JM, Gommeaux A, Bertrand ME: Human percutaneous coronary rotational atherectomy: preliminary results. Circulation 78: II-82, 1988 (Abstract).
12. Fourrier JL, Bertrand ME, Auth DC, Lablanche JM, Gommeaux A, Brunetaud JM: Percutaneous coronary rotational angioplasty in humans: Preliminary report. J Am Coll Card 14: 1278—1282, 1989.
13. Erbel R, Dietz U, Auth D, Haude M, Nixdorf U, Meyer J: Percutaneous transluminal coronary rotablation during heart catheterization. A Am Coll Card 13: 228A, 1989 (Abstract).
14. Ginsburg R, Teirstein P, Warth D, Haq N, Jenkins N, McCowan LC: Percutaneous transluminal coronary rotational atherobaltion: clinical experience in 40 patients. Circulation 80: II-584, 1989 (Abstract).
15. O'Neill WW, Friedman HZ, Cragg D, Strzelecki MR, Gangadharan V, Levine AB: Ramos RG: Initial clinical experience and early follow-up of patients undergoing mechanical rotary endarterectomy. Circulation 80: II-584, 1989 (Abstract).
16. Kaltenbach M, Vallbracht Ch, Kober G: Medium-term results after re-opening chronic coronary artery obstructions by low speed rotational angioplasty. Circulation 80: II-257, 1989 (Abstract).
17. Stack RS, Quigley PJ, Sketch MH, Stack RK, Walker C, Hoffmabn PU: Phillips HR Treatment of coronary artery disease with the transluminal extraction-endarterectomy catheter: initial results of a multicenter study. Circulation 80: II-583, 1989 (Abstract).
18. Sketch MH, Quigley PJ, Tcheng JE, Bauman RP, Phillips HR, Stack RS: Restenosis following coronary transluminal extraction-endarterectomy. Circulation 80: II-583, 1989 (Abstract).

18. Videometric, angiographic and angioscopic assessment of atherectomy; correlations and discrepancies

BERTHOLD HÖFLING, GERHARD BAURIEDEL and AUDREY VON PÖLNITZ

Summary

In this study we report on percutaneous atherectomy and the use of the adjunctive techniques of videometric and angioscopic assessment of results. The Simpson atherectomy catheter was used to treat 40 patients with a total of 72 lesions in the iliac ($n = 5$), superficial femoral ($n = 62$) and popliteal ($n = 5$) arteries; five patients had rest pain and two had gangrene. The primary success rate was over 90%. The percent of stenosis decreased from 87.2 ± 14% to 16.6 ± 15.5%; the walking distance improved from 80.5 ± 65.7 m to 152.8 ± 80.3 m; the Doppler index increased from 0.57 ± 0.17 to 0.81 ± 0.16. A geometric and densitometric analysis of the lesions was performed pre- and post-atherectomy in 10 patients with 13 lesions. A significantly higher densitometric and geometric residual stenosis was found as compared with the angiographic diameter stenosis. A higher 6-months restenosis rate, however, was not found in those cases with higher densitometric residual stenoses. Angioscopic inspection of the treated segment was found to be helpful in identifying residual stenotic material or flaps, as well as in evaluating total occlusions, but problematic for stenosis quantification. In the long-term, angiographic restenosis was found in 21% of lesions with a difference seen based on primary morphology: 27% for concentrics, 5% for eccentrics and 42% in total occlusions.

Introduction

Percutaneous balloon angioplasty is commonly used to treat obstructive vascular lesions in patients with peripheral vascular disease, but the treatment of occlusions and the long-term restenosis rate of 20 to 45% remain problematic [1—3]. Residual plaque material may contribute to this problem and therefore new techniques which remove plaque material are being developed. As new percutaneous interventional techniques are applied to the treatment of vascular disease, improvement in stenosis quantification and qualification may be useful, not only for the immediate assessment of the

J. H. C. Reiber and P. W. Serruys (eds), Quantitative Coronary Arteriography, 351—363.

intervention, but also for prognosis. We report on our results with the Simpson peripheral atherectomy catheter [4], which has been found to be safe and effective in peripheral vessels [5—7]. In addition, we report on the use of the adjunctive techniques of digital subtraction angiography with an on-line quantification method [8], as well as angioscopy [9—11] during the procedure.

Patients and methods

A total of 40 patients with symptomatic peripheral vascular disease were accepted for atherectomy after baseline angiography revealed a target lesion of $>70\%$ in diameter. Five patients had rest pain and 2 had gangrene. All patients underwent baseline Doppler ultrasound and standardized walking distance (3 km/hr with a 12.5% grade) evaluation, which were repeated at 1, 3, and 6 months. Control angiography was performed at 6 months. All patients were treated with aspirin before and for at least 6 months after the procedure.

The atherectomy procedure was performed under heparinization in the catheterization laboratory. After baseline angiography and angioscopy, the peripheral Simpson atherectomy catheter was advanced to the stenosis under fluoroscopic control. The essential feature of the catheter is a cylindrical housing with an opening encompassing one-third its circumference at its tip (Figure 1). The catheter was positioned such that the stenotic plaque protruded into the window of the housing; a low pressure balloon (10—40 p.s.i.) was then inflated, maintaining the housing securely in place within the vessel. The motor-driven cutter was then advanced, excising 1 mm slices of plaque (up to 15 mm in length), which were trapped in the distal housing cup. Captured material could then be submitted for histologic [12], biochemical and cell culture studies [13]. In the treatment of total occlusions a Dotter technique using either a guide wire, stylet of the introducer sheath, or PTA was first necessary to establish a channel into which the atherectomy catheter could be placed. The lumen was then enlarged by the removal of plaque material.

Angioscopic evaluation was performed before, during and after the intervention using a flexible fiberoptic endoscope (d = 1.5 or 1.0 mm, Miniflex Angioscope, American Edwards Lab.). The angioscope was coaxially guided by a cut X-ray dense catheter and inserted into the vessel through a 9F sheath. Constant saline irrigation ensured a sufficient field of view. A 250 W cold light source (American Edwards Lab.) provided intravascular illumination. The endoscope was coupled to a miniature video camera (Endovision 553, Storz Instr. FRG); images were relayed to a high resolution color video monitor. Permanent recordings were made using a video cassette recorder (U-matic VO-5800 PS, Sony).

Angioscopic inspection pre-atherectomy was performed for qualitative

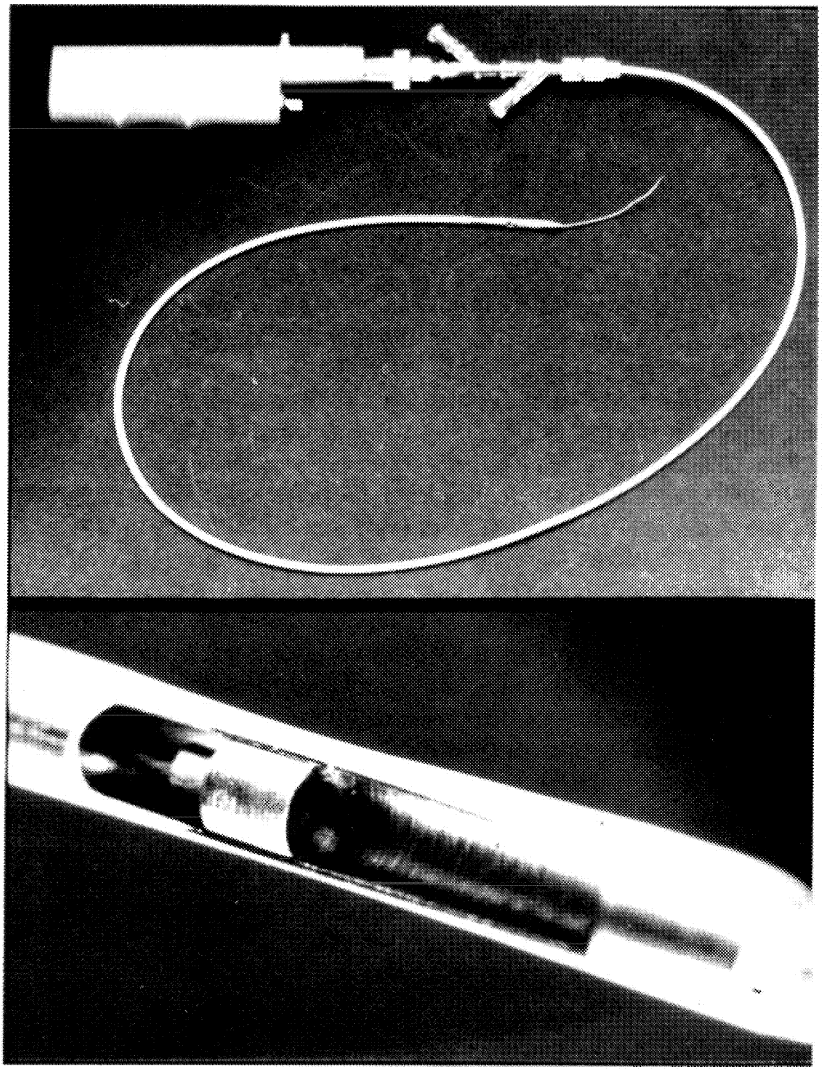

Fig. 1. The peripheral Simpson Atherectomy Catheter incorporates a guide wire at its tip, a cylindrical housing (enlargement), and a rotating cutting edge which is driven by a hand-controlled motor.

evaluation of stenosis morphology. The atherectomy procedure was then performed until good angiographic results were obtained (goal of $< 30\%$ residual stenosis); thereafter, the angioscope was again passed and the lesion inspected. If significant residual plaque material or flaps of the atherectomized segment were angioscopically detected and found to obstruct the recanalized lumen, they were exactly localized by fluoroscopic control of the guide catheter tip position, and additional passes of the atherectomy catheter

were performed before a final angioscopic inspection. In the case of total occlusions, angioscopic evaluation was initially performed in an effort to assess the characteristics of the occlusion. If an inner lumen could be detected, passage of a guide wire or catheter was attempted under visual control.

Digital image acquisition with on-line geometric and densitometric quantification was performed using a Digitron 3 (Siemens AG, Erlangen, FRG). This system allows digital image acquisition simultaneously with the usual angiographic imaging obtained during the procedure. On the video screen, an image was selected which was free of subtraction and motion artifacts, and which showed the stenosis with a minimum of geometric distortion or overlay. The operator had to define the reference segment of the "normal vessel", followed by the definition of a centerline through the stenosis. The remainer of all calculations proceeded with an automatic edge-detection algorithm. Results were immediately displayed on the video screen showing the stenotic diameter and calculated geometric area of stenosis. Simultaneously, the densitometric mearurement based on the densitometric evaluation of each pixel of the digitized image was displayed.

The videometric "geometric" and "densitometric" percent stenosis was defined as that value calculated by computer algorithm from the digitized image as described above. From the cinefilm, which was acquired simultaneously with the DSA, the so called angiographic percent stenosis was assessed. To this end, the contours of the vessel of interest were traced manally on a piece of paper held against the projection screen of the cineprojector. Using a mechanical caliper, the obstruction and reference diameters were measured from the paper, from which the angiographic percent diameter stenosis could be calculated.

Results are reported as mean $\pm$ s.d.. The paired Student's t-test (2-tailed) was used to calculate significance of differences pre-and post-atherectomy; the chi-square and Kruskal-Wallis tests were used to test differences between the methods. Significance was considered at the < 0.05 level.

Results

Angiographic results

Forty patients with 74 stenoses (iliac $n = 5$, superficial femoral $n = 64$, and popliteal $n = 5$) underwent atherectomy. Acute success (residual stenosis of $< 50\%$) could be achieved in 91% of occlusions (19/21) and in 93% of stenoses (50/53). The mean (angiographic) diameter stenosis was reduced from 87.2 $\pm$ 14% to 16.6 $\pm$ 15.5%.

A 6-month control angiography was performed in a total of 43 lesions. The mean 6-months stenosis was 35 $\pm$ 31%. Although not significant, there was a tendency for a higher mean 6-months stenosis in the concentric

(42.4%; $n = 11$) as compared to the eccentric lesions (25.7%; $n = 20$). Total occlusions showed the highest mean stenosis of 64.3%. An angiographic restenosis (defined as diameter stenosis $>70\%$) was found in 9/43 lesions (21%). When analyzing for primary morphology, a restenosis was found in 1/20 (5%) of eccentric lesions and in 3/11 (27%) of concentrics; total occlusions had a significantly higher restenosis rate of 42% (5/12).

Despite our efforts to optimize our results by angioscopic inspection of the treated site and the performance of additional passages of the atherectomy catheter should angioscopy detect residual stenoses or plaque material, there was no instance of vessel rupture or acute thrombosis. To date, there has been one incidence of clinically relevant distal embolization and two significant groin hematomas.

Videometric results

In 13 stenoses the routine angiographic %-diameter stenosis was compared with the videometric geometric and densitometric value, pre- and post atherectomy (Table 1, Figure 2). There was no significant difference in the pre-atherectomy values among the groups; post-procedure, however, both the densitometric and the geometric computer guided measurements were significantly higher ($p < 0.05$) than the angiographic measurement. However, the presence of a higher densitometric or geometric residual stenosis post-procedure did not correlate with the occurrence of a restenosis.

Table 1. Stenosis quantification before and after atherectomy; comparison between angiographic %-diameter stenosis and DSA-computer guided geometric and densitometric measurements.

	Angiographic $n = 13$	Geometric $n = 13$	Densitometric $n = 13$
Pre-atherectomy (%)	87.0 ± 11.8	91.3 ± 4.8	89.7 ± 6.2
Post-atherectomy (%)	18.5 ± 14.2	34.1 ± 23.0*	40.7 ± 21.7*

* $p < 0.05$ as compared to diameter residual stenosis.

Angiographic and videometric examples

Figure 3 shows an example of a subtotal concentric stenosis, pre- and post-atherectomy. There is good agreement between the geometric and densitometric calculations of the residual stenosis (43.8 and 44.8%), although the angiographic %-diameter stenosis was only 25%. This patient presented

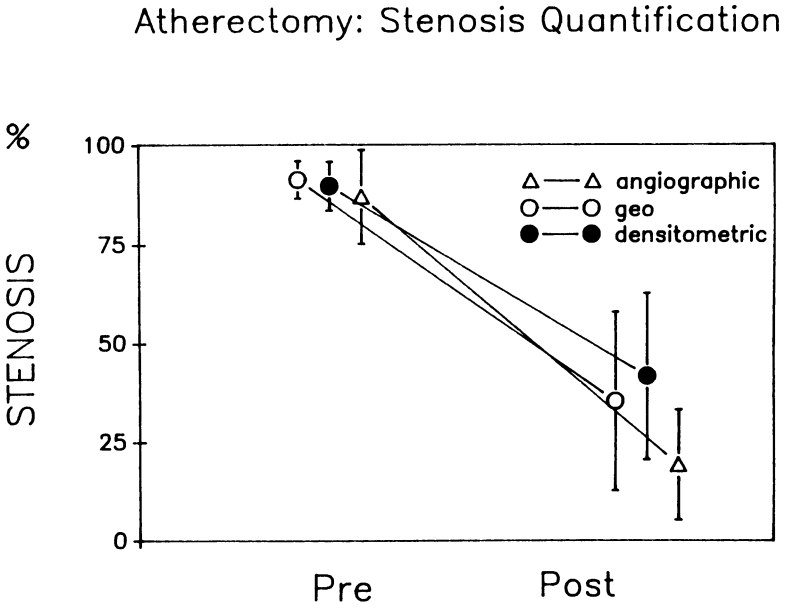

Fig. 2. In high grade stenoses (pre-atherectomy), there was no significant difference in stenosis quantification between routine angiographic %-diameter stenosis measurement and computer guided DSA-geometric (geo) and densitometric measurements. Post-atherectomy, however, both the geometric and densitometric residual stenoses were significantly higher than the angiographic %-diameter stenosis (see Table 1).

with a restenosis at 6-months post-atherectomy. In Figure 4 the high grade concentric stenosis could be effectively reduced, as measured both angiographically and with the geometric videometric analysis. However, the densitometric residual stenosis was significantly higher at 26.4%, most likely representing residual plaque or thrombus material, or both. This patient was also found to have a restenosis at 6 months angiographic follow-up. Figure 5 shows a total occlusion of the popliteal artery, which was initially recanalized with the mechanical Dotter technique, followed by atherectomy.

Angioscopic results

Angioscopic inspection was performed in 47 patients with a total of 62 lesions of the superficial femoral or popliteal arteries. Pre-atherectomy inspection usually revealed a red, pulsating vessel in the angiographically normal segments, while pale white or yellow plaque formation obstructing the lumen could be seen at the target lesion sites, qualitatively confirming the angiographic image. Occlusions could be clearly visualized with a total white out of the image. In some cases, the occlusion could be crossed with the angioscope. Somewhat surprising was the finding of an occasional angiogra-

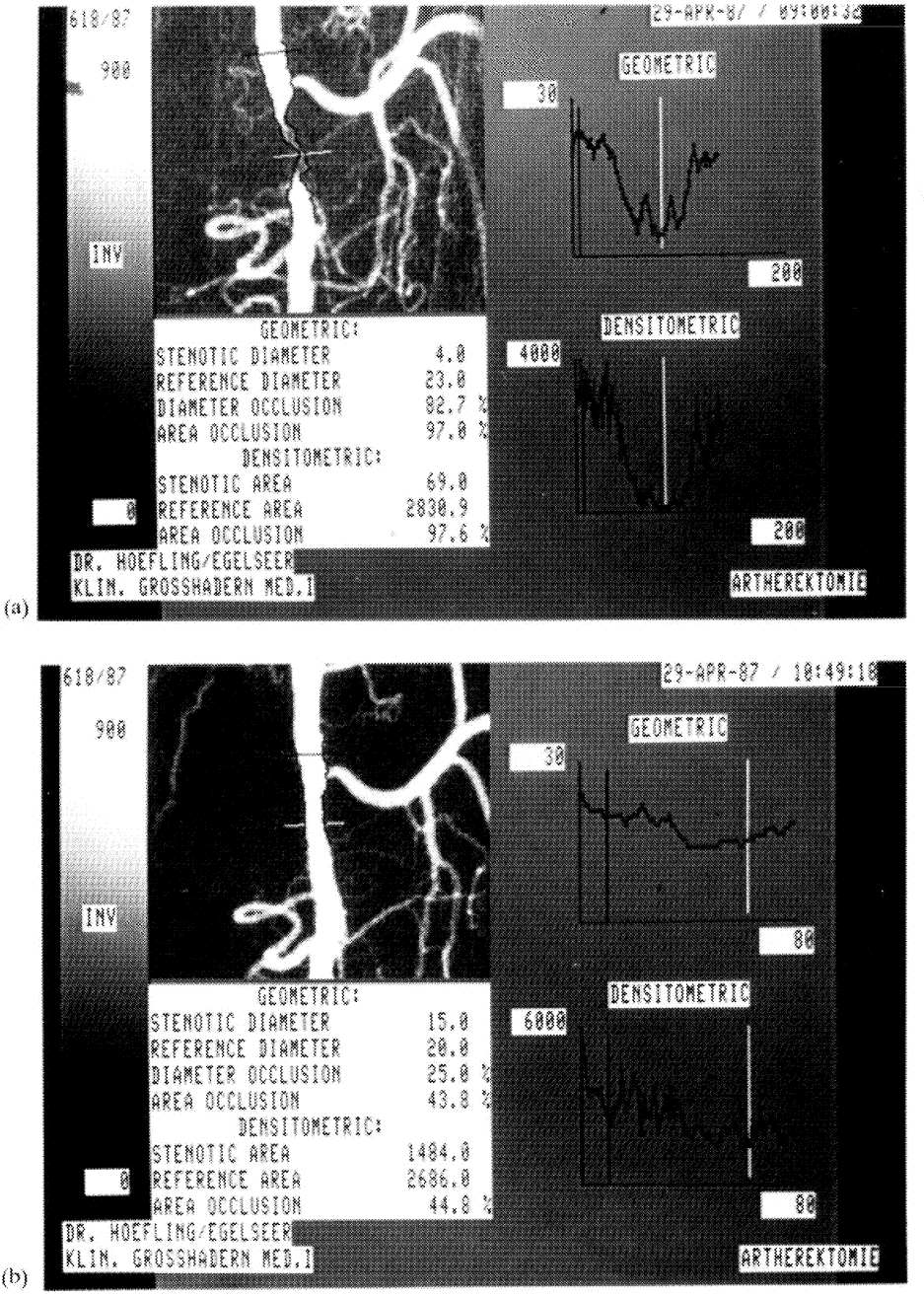

Fig. 3a and b. High grade concentric stenosis of the superficial femoral artery, before (a) and after (b) atherectomy. The residual diameter stenosis is 25%, while the geometric and densitometric % occlusions are over 49%. At 6-months a clinically significant angiographic restenosis was found.

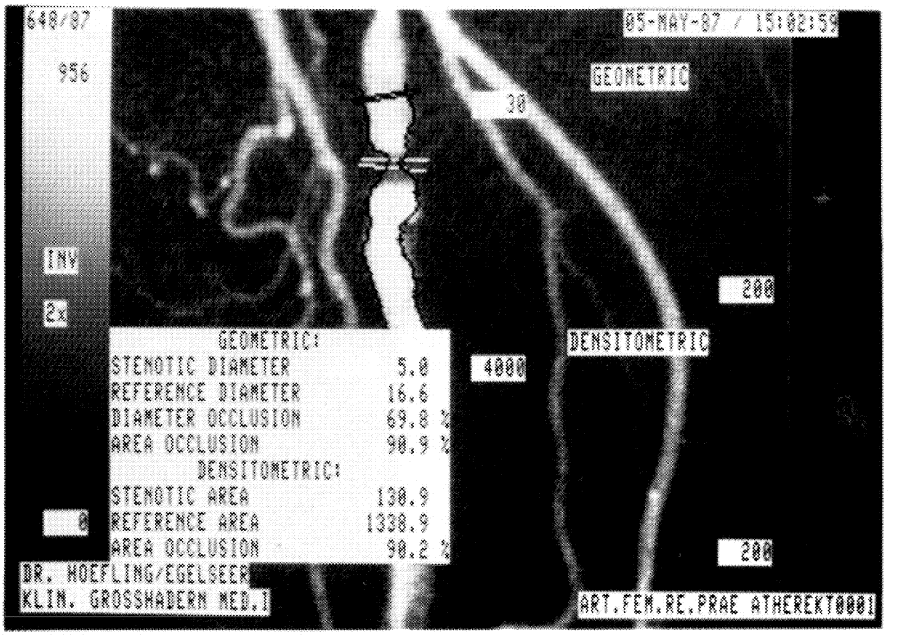

(a)

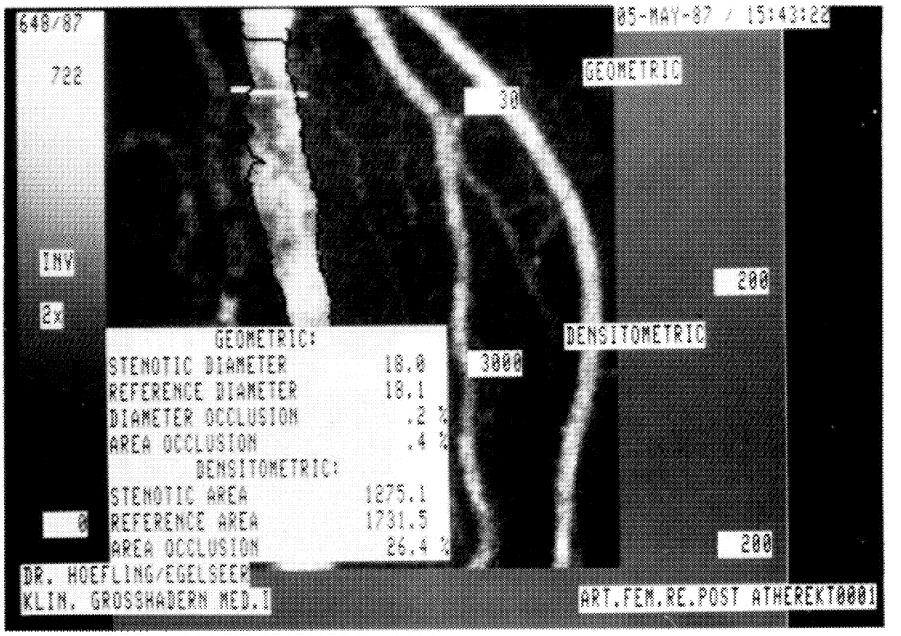

(b)

Fig. 4a and b. Short concentric stenosis pre- and post-atherectomy. Note the relative poor density of contrast medium post-procedure (post, a geometric occlusion of 0.4%; densitometric of 26.4%). At 6 months this vessel was thought to be clinically patent, but an angiographic restenosis was documented.

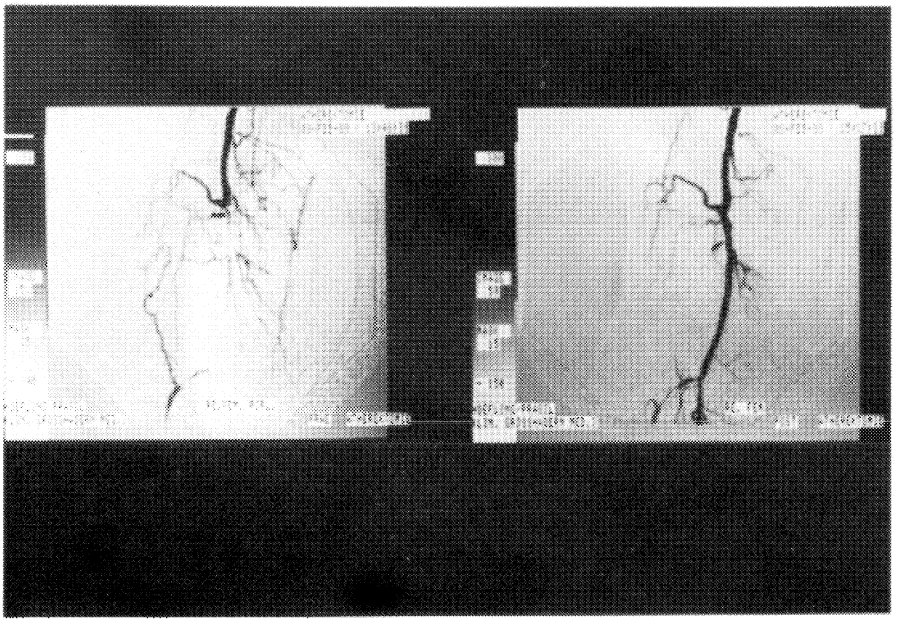

Fig. 5. Total occlusion of the popliteal artery before (6a) and after (6b) Dotter and atherectomy.

phic-long occlusion, which in reality consisted of one or more shorter occlusions, with intermediate non-collateralized segments with a relatively intact vascular relief.

Exact quantification of the degree of stenosis and circumferential morphologic categorization is difficult to perform, since a luminally centered alignment of the scope for a full cross-sectional view of the vessel is not always possible.

After achievement of an angiographically acceptable result, an angioscopic control of the treated areas revealed flaps or obstructing residual material in 26% of the inspected lesions. Based on this information and after fluoroscopic localization, additional passages of the atherectomy catheter were performed in an effort to optimize results. Figure 6 is an example of such an irregularly shaped residual flap detected with the angioscope, which could be removed by subsequent passes of the atherectomy catheter. Figure 7 shows the angioscopic view of the slit-like opening of a disrupted occlusion after passage of the angioscope and catheter used as a Dotter technique, but before treatment with the atherectomy catheter.

Clinical results

Rest pain was resolved in all successful cases, while gangrene healed in 1/2.

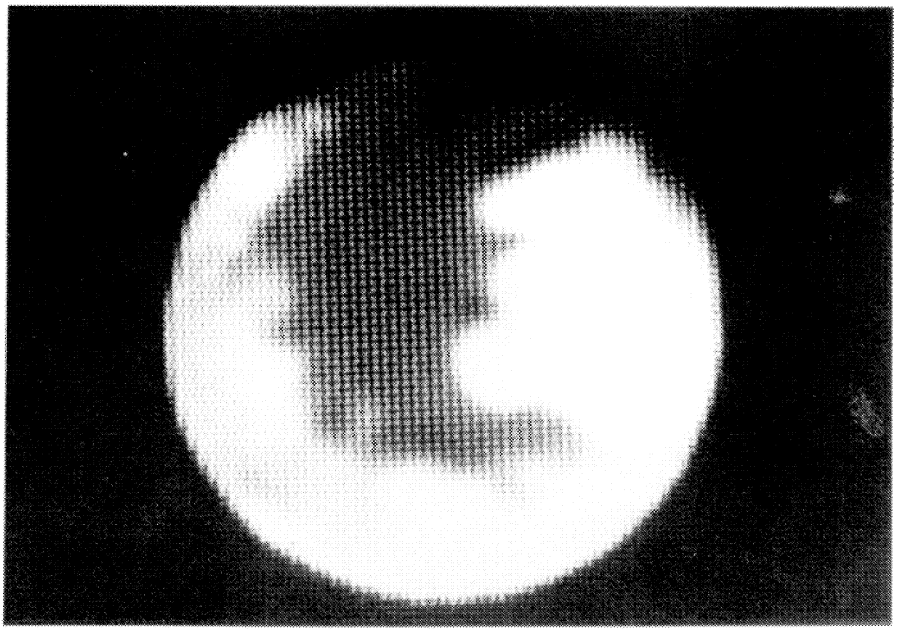

Fig. 6. Angioscopic view of a concentric lesion post-atherectomy. A large flap is seen protruding into the vessel lumen.

For the entire group, the baseline walking distance (WD) increased from 80.5 ± 65.7 m to 152.8 ± 80.3 m ($p < 0.001$; $n = 40$) and was maintained at 6 months follow-up (169.3 ± 80.6 m). The baseline ankle/brachial Doppler index of the treated leg was 0.57 ± 0.17 and rose significantly to 0.81 ± 0.16 ($p < 0.0001$); at 6 months: 0.78 ± 0.15.

Discussion

Percutaneous atherectomy is a new technique for removing obstructive plaque material in peripheral vessels, which is feasible, safe and effective. The presence of calcification does not preclude good results and total occlusions can also be treated, usually after an initial mechanical Dotter technique to establish vessel patency. Both eccentric and concentric lesions can be treated, although a better 6 months result was found in the eccentric lesions. Naturally, a longer term follow-up and a larger number of patients are needed to further validate the technique and to assess its role in the treatment of vascular disease.

The ability of the catheter to remove plaque material is important for the following reasons: a) perhaps lowering the long-term restenosis rate; b) the risk of distal embolization is largely eliminated; and c) the biopsy of plaque

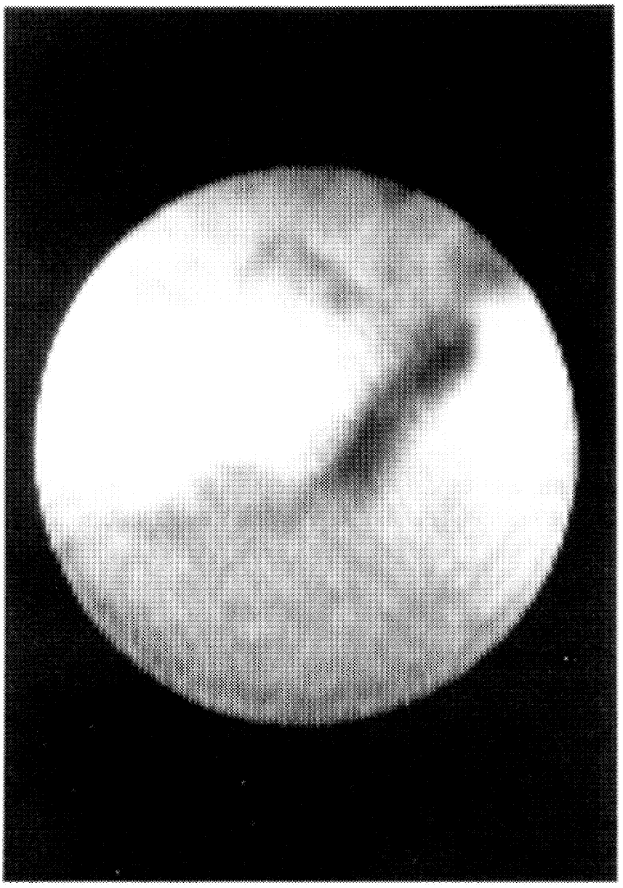

Fig. 7. Slit-like "lumen" of a total occlusion after Dotter (passage of the guide catheter) as seen through the angioscope.

material for histologic, biochemical and cell culture studies [13] may provide useful models for studying the process of restenosis and its pharmacological prevention.

Exact quantification of the degree of stenosis by angioscopy is indeed difficult due to vessel size and positioning of the angioscope within the lumen, as well as to errors based on depth perspective [10]. Qualitative inspection was found to be a useful adjunct to the procedure, since residual obstructing flaps or plaques after atherectomy were occasionally not seen angiographically. In addition, in cases of high grade stenosis (including 100% stenosis), initial passage of the angioscope or a guide wire under visual control may avoid guide wire or catheter induced complications. An interesting finding in total occlusions was the occasional collapsed "normal lumen" segment between short occlusions and the lack of thrombus material. The

latter could be due to the large flush volume used during angioscopy or a "true" finding related to the chronicity of the occlusion.

It should be mentioned, that the moving image obtained on the real-time video screen is to be preferred above still photographs which can be obtained from frozen images, to discern luminal irregularites. New improvements in angioscopic systems include more flexibility, steerability and miniaturization.

The speed of on-line quantification allows for the examination of the results directly and immediately during the procedure and thus may be helpful in decision making. It is, however, not yet clear, whether decisions regarding the need for an additional procedure should be made based on densitometric or geometric evaluation. Conceptually, poor density should reflect residual material in the vessel. In our small collective we could not show any significant increase in restenosis in those lesions with poorer density at the completion of the procedure, but a larger collective may be needed. In addition, a comparison of angioscopic findings with densitometric analysis may help to elucidate the nature of the "densitometric stenosis".

References

1. Zeitler E, Richter EL, Seyferth W: Femoropopliteal arteries. In: Percutaneous Transluminal Angioplasty. CT Dotter, AR Grüntzig, W Shoop (Eds). Springer Verlag, New York, 1983: 105—115
2. Schneider E, Gruntzig A, Bollinger A: Langzetergebnisse nach perkutaner transluminaler Angioplastie (PTA) bei 882 konsekutiven Patienten mit iliacalen und femore-poplitealen Obstruktionen. VASA 11: 322—326, 1982.
3. Krepel VM, van Andel GJ, van Erp WFM, Breslau PJ: Percutaneous transluminal angioplasty of the femoropopliteal artery: Initial and long-term results. Radiology 156: 325—328, 1985.
4. Simpson JB, Johnson DEW, Thapliyal HV, Marks DS, Braden LJ: Transluminal atherectomy: A new approach to the treatment of atherosclerotic vascular disease. Circulation 72, (Supp II): III-146, 1985 (Abstract)
5. Simpson JB, Selmon MR, Robertson GC, Ciprian PR, Hayden WG, Johnson DE, Fogarty TJ: Transluminal atherectomy for occlusive peripheral vascular disease. Am J Cardiol 61: 96G—101G, 1988.
6. Höfling B, von Pölnitz A, Backa D, v. Arnim Th, Lauterjung L, Jauch KW, Simpson JB: Percutaneous removal of atheromatous plaques in peripheral arteries. Lancet I: 384—387, 1988.
7. Höfling B, von Pölnitz A, Backa D, Meissner R, v. Arnim Th, Jauch G, Remberger K: Angiographische und funktionelle Ergebnisse sowie histologische Befunde nach perkutaner Atherektomie bei Patienten mit arterieller Verschlußkrankheit. Z Kardiol 75, 1989 (in press).
8. v. Arnim Th, Hengge M, Prasil J, Höfling B: Advances in X-ray equipment — digital subtraction angiography with on-line quantification. In: Interventional Cardiology and Angiology. B. Höfling, A.v. Pölnitz (Eds). Steinkopff Verlag, Darmstadt, 1989: 13—19.
9. Ferris EJ: Angioscopy: An extension of Angiography. Amer J Radiol. 143: 681—682, 1984.
10. Grundfest WS, Litvack F, Sherman T, Carroll R, Lee M, Chaux A, Kass R, Matloff J,

Berci G, Swan HJC, Morgenstern L, Forester JS: Delineation of peripheral and coronary detail by intraoperative angioscopy. Ann Surg 202: 394—400, 1985.

11. Höfling B, von Pölnitz A, Baurtiedel G, Backa D, Lauterjung L, Simpson JB: Use of angioscopy to assess the results of percutaneous atherectomy. Amer J Cardiac Imaging 3: 20—26, 1989.
12. von Pölnitz A, Backa D, Nerlich A, Höfling B: Histological evaluation of "vessel-biopsies" obtained with the Simpson atherectomy catheter. J Am Coll Cardiol 13: 149A, 1989.
13. Bauriedel G, Dartsch PC, Voisard R, Höfling B, Betz E. Selective percutaneous biopsy of atheromatous plaque tissue for cell culture. Basic Res Cardiol, 1989 (in press)

Part VII

Historic perspective

19. The history of coronary angiography

KURT AMPLATZ

Summary

The very early attempts to visualize the coronary arteries radiographically were made in South America and Europe. Contrast medium was injected either by direct needle puncture or surgically introduced catheters into the aortic root. Visualization was generally poor due to the rapid flow in the ascending aorta and the relatively slow delivery rate of contrast medium without power injectors. Other important limitations were the filming techniques due to the relatively weak generators which resulted in long exposure times and consequent blurring of the coronary arteries.

Both limitations, namely motion and poor concentration, were eliminated by the cardiac arrest technique introduced by Arnulf. Acetylcholin was injected intravenously or directed into the ascending aorta producing cardiac standstill of variable duration. During the cardiac arrest, the contrast medium was injected and radiographs of the motionless heart were obtained.

This procedure was considered heroic by most investigators who were looking for less invasive alternatives. The Swedish school, which had the advantage to be leading in the design of film changers and power injectors, carried out nonselective angiography on a large scale during decreased cardiac output accomplished by increased intrabronchial pressure. Another refinement which led to improved visualization of the coronary artery was the loop catheter which delivered the contrast medium directly behind the aortic valve into the sinus of Valsalva.

All indirect and semi-selective techniques were surpassed by selective coronary angiography introduced by Sones. A specially designed catheter is introduced into the surgically exposed brachial artery and manipulated selectively into the right and left coronary arteries. With the same end-hole catheter, left ventriculography is performed. The drawback of the original Sones technique is the necessity to expose the brachial artery surgically and the occasional semi-selective injection of the left coronary artery depending on its origin. Also, left ventriculography was of inferior quality because of the

J. H. C. Reiber and P. W. Serruys (eds), Quantitative Coronary Arteriography, 367–383.

end-hole catheter. Its major advantage is better control over bleeding which allows safe outpatient coronary angiography.

More recently, percutaneous transfermoral selective catheters have been developed (Judkins, Amplatz, Bourassa and others), which are gaining in popularity.

Prior to the advent of effective coronary surgery such as coronary bypass, there were few indications to visualize the coronary arterial tree. Consequently the early literature on coronary angiography is sparse. However, several pioneers attempted to angiographically demonstrate the coronary arteries with great difficulties due to technical and equipment limitations. Cineangiography was at its infancy yielding poor and blurred images at a tremendous radiation dose to the patient. Radiographic demonstration, therefore, was limited to a single radiograph and later on to film recording at 6—12 exposures per second using rapid film changers.

All early attempts to visualize the coronary arteries consisted of the injection of contrast media via direct needle puncture into the aorta which obviously resulted in marked dilution with poor visualization of the coronary arteries.

The procedure was carried out at a high risk due to its complex technique, and particularly the use of relatively toxic contrast media. Coronary angiography, therefore, was only performed at a few pioneer institutions, and the vast majority of the physicians attempted to establish the diagnosis by clinical means. In the early days the indications for coronary angiography were not well-established because of the high risk, which was usually not acceptable to the individual and his physician. Furthermore, in most institutions, a well-trained team of personnel and adequate X-ray facilities were not available.

One of the indications was the examination of patients who had atypical chest pain with a normal electrocardiogram. These patients were severely debilitated and may have profited by the angiographic demonstration of a normal coronary tree.

Later on with the advent of surgical techniques such as ligation of the mammary artery, wrapping omentum around the heart, the Vinberg procedure, etc., the indications for coronary angiography were markedly broadened.

The two major technical limitations which prevented adequate visualization of the coronary tree were weak radiographic generators and the slow injection of contrast medium into the ascending aorta. Under-powered generators required a long-exposure time which resulted inevitably in blurring of the beating heart. Even with relatively large-bore needles or later on catheters, contrast medium could not be delivered fast enough by hand injections. It is therefore not surprising that early pioneers of coronary angiography attempted to arrest the heart eliminating motion unsharpness and provided dense opacification of the aorta. Other investigators found some means of decreasing cardiac output, which in turn would increase the

relative concentration of contrast medium in the ascending aorta. Many ingenious more or less dangerous techniques have been described.

Castellanos [1], at the University of Havana, introduced in 1931 angiocardiography. This technique was presented in October, 1937 by him and co-workers before the Society of Clinical Studies in Havana [1, 2]. Prior to this date, Bleichroeder (1912) [3] and Forsmann, in Germany, realized in 1929 the first catheterization of his own right atrium by introducing a catheter into his antecubital vein [4]. Introduction of the catheter was carried out by one of his assistants. Forsmann shared the Nobel prize together with Cournand at the Mayo Clinic.

The Portuguese School of Lisbon under Moniz introduced the term angiopneumografia, which was the injection of contrast medium through a needle inserted directly into the right atrium in order to visualize the pulmonary artery [5, 6]. In 1936, Ameuille [7] and his co-workers repeated the same experiments injecting a solution of sodium iodine and coined the term pulmonary arteriography. In the opinion of Ameuille, the opacification of the pulmonary artery may be valuable for pulmonary disease, therefore, the term "angiopneumography" [7].

Castellanos [1] is taking credit for developing a simple and rapid opacification of the cardiac cavities and great vessels by direct needle puncture, published in 1937 [1].

The contrast medium is introduced into the cardiac cavities directly via a needle or by injection of a peripheral vein. Castellanos is therefore the father of intravenous angiography. This technique was adopted by Robb and Steinberg [8] of New York and became the most widely used angiographic technique in the United States.

Castellanos and co-workers were the first who demonstrated that it is possible to opacify the heart in humans using the same technique. Usually two exposures were made: One during the dextrocardiogram and one when the contrast medium had reached the left heart which was termed by Castellanos "levocardiogram". The time of the second exposure was determined by the preliminary injection of choline in order to determine the circulation time. With a stop watch in hand, the radiologist would then expose the second film at a predetermined time derived from the choline injection. Because of the weak generator, X-ray exposures were made without radiographic grid at one-tenth of a second, which obviously resulted in poor contrast and blurring.

Needless to say, all these early attempts to visualize the heart and great vessels did not provide satisfactory opacification of the coronary arteries. Meneses Hoyos, et al. [9] from Mexico recognized this drawback and introduced direct thoracic aortography in order to deliberately visualize the coronary arteries. He proved that this method is superior to indirect intravenous angiocardiography. Other investigators in fact had proven that out of 1200 intravenous angiocardiograms, only 10 showed visualization of the coronary arteries [10]. An 18-gauge needle was introduced directly into the

ascending aorta through the second left interior interspace (Figure 1) and 30 cc of 70% contrast medium were injected by hand (Figure 2).

One year earlier, Radner [11] attempted the same technique by puncture of the ascending aorta through the suprasternal notch. Meneses Hoyos showed his coronary arteriograms in October, 1946 at the Interamerican Congress of Cardiology held in Mexico City and takes priority of being the first to visualize the coronary arteries. Later on other investigators injected the contrast medium via catheter through brachial or femoral approach. These ureteral catheters had very thick walls and only relatively slow injec-

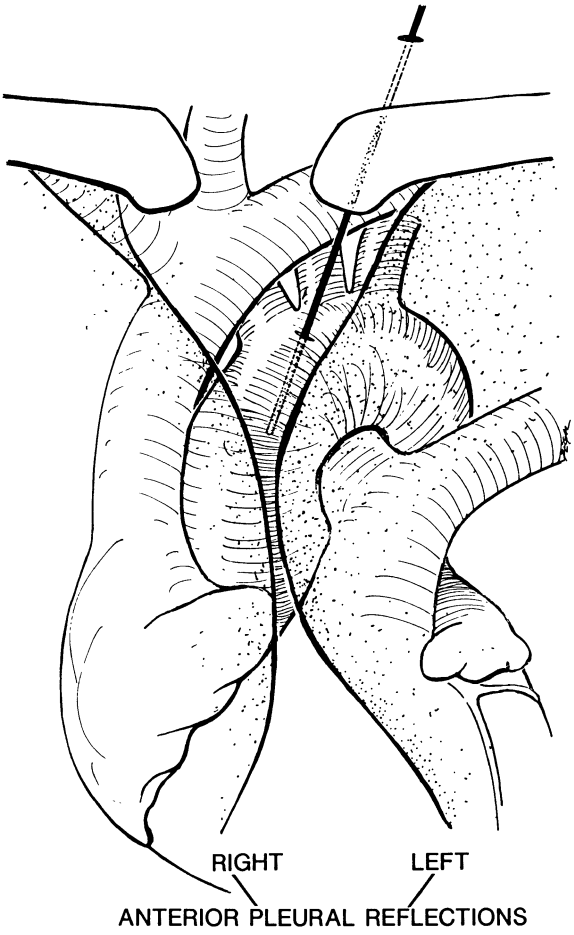

Fig. 1. Diagram demonstrating the direct needle technique by Meneses Hoyos introducing an 18-gauge needle from the second left anterior interspace into the ascending aorta. The sharp trocar was removed, and a blunt needle was advanced into the aortic root for opacification of the coronary arteries. A similar technique was described by Radner introducing the needle into the aortic arch via suprasternal puncture.

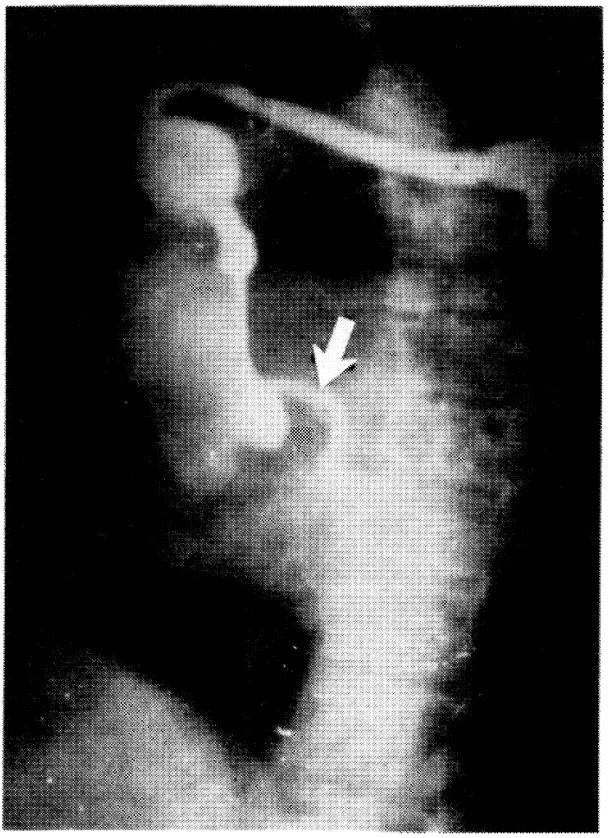

Fig. 2. Coronary arteriogram performed by Jorge Meneses Hoyos in 1953 via direct needle puncture of the ascending aorta through the left second anterior interspace. The angiogram was supposed to show the "right coronary artery" (arrow) in a patient with aneurysm of the descending aorta.

tions of contrast medium could be accomplished. This was also true for the direct needle techniques which had the advantage of providing higher flow rates because of shorter length. With either technique, the contrast concentration in the ascending aorta was poor and the radiographs were blurred because the heart was beating.

In 1959, Ponsdomenech [12] and Nunez introduced direct needle puncture of all cardiac chambers, which could also be used for visualization of the coronary arteries by opacifying the left ventricle (Figure 3).

In 1959, Mouquin [13] also suggested opacification of the coronary arteries by left ventriculography. By the injection of a large amount of contrast medium into the left ventricle via catheter, both coronary arteries could be visualized (Figure 4).

In 1956, Arnulf [14] from the University of Lyon, experimented with dogs

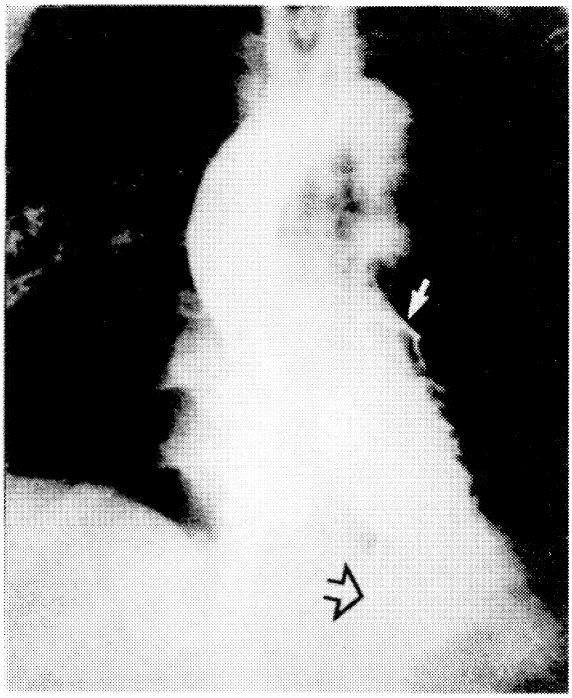

Fig. 3. Visualization of the coronary arteries by injection of contrast medium into the left ventricle via direct left ventricular puncture (open arrow).

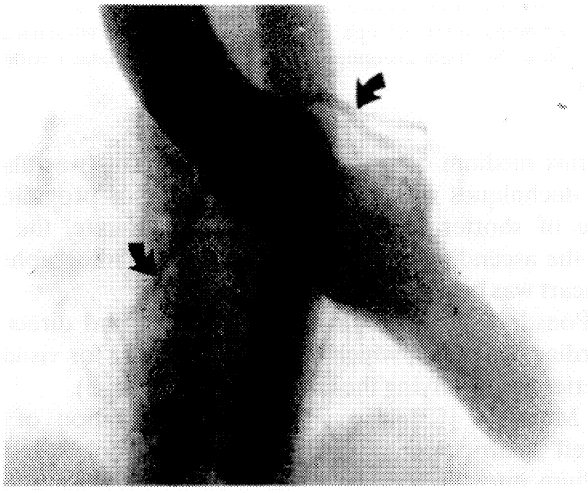

Fig. 4. Visualization of the coronary arteries by Mouquin via catheter left ventriculography.

in order to demonstrate the coronary arteries. By accident, one of the animals had an anesthesia-induced cardiac arrest at the same moment that the contrast medium was injected. X-rays were taken and the aorta and coronary arteries were well opacified without any motion (Figure 5). He concluded that only cardiac arrest can produce such superb visualization of the coronary arteries.

It so happened that he worked at the same time in the physiologic laboratory under Professor Hermann in order to study the effect of acetylcholine on the coronary circulation. By carrying out his experiments, he noticed that acetylcholine will arrest the heart, and he was able to prove that excellent coronary arteriograms could be obtained during acetylcholine arrest. He presented his data in 1957 at the International Society of Angiology in Atlantic City.

Prior to proceeding to human coronary angiography, the technique was worked out in detail in animals. A cardiac arrest of 6—8 seconds was obtained by the intravenous injection of 0.2—0.5 milligrams per kilo bodyweight. The tolerance of the human heart of acetylcholine is about 8—10 times greater than that of the dog. At that time psychiatrists used enormous dosages in order to perform shock therapy. Some of the side effects were attacks of cough, bronchospasm and nausea.

Cardiac arrest occurred only if the acetylcholine was delivered as a bolus into the antecubital vein (Figure 6). Not all animals responded the same way

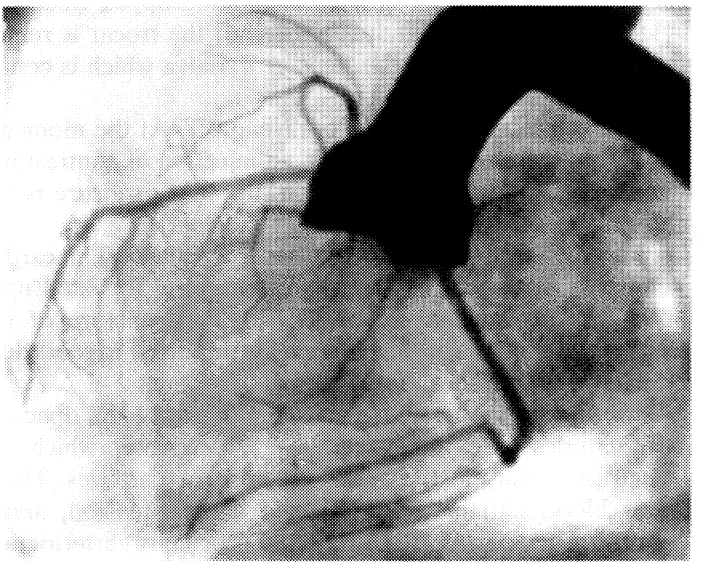

Fig. 5. Coronary arteriogram obtained by Arnulf in 1956. Just prior to the injection of contrast medium, the animal had a cardiac arrest. There is dense filling of the ascending aorta and coronary arteries and no motion artifact. Contrast medium delivered directly via needle into the ascending aorta.

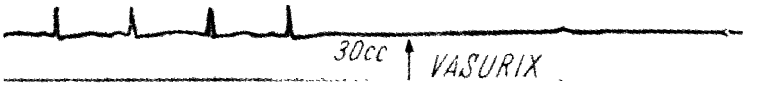

Fig. 6. Electrocardiogram made following intravenous injection of 0.4 mg/kilo body weight of acetylcholine. After cardiac arrest had occurred (arrow), the contrast medium was injected.

and there was a certain increasing tolerance after repeat injections. He carried out hundreds of injections of acetylcholine with increasing dosage until cardiac arrest for three minutes was obtained and well tolerated. Furthermore, the cardiac arrest could be terminated by the injection of atropine, which is the ideal antidote. He concluded that the technique is safe and proceeded to human coronary angiography.

The contrast medium was injected either by direct puncture of the aortic arch as described by Radner or by the injections through a catheter introduced through the carotid artery. One of the major advantages was that only one single radiograph was required because there was no cardiac motion. He carried out 24 coronary arteriograms during acetylcholine arrests in man via direct puncture of the aortic arch through the left second anterior intercostal space (Figure 7). The patients tolerated the procedure well and the visualization of the coronary arteries was excellent. The puncture of the aorta is without danger using a blunt needle with a diamond-tipped trocar according to Arnulf [15]. Once the aortic arch is punctured the trocar is removed and the blunt needle is advanced into the sinus of Valsalva which is confirmed by a radiograph.

Acetylcholine is injected as a bolus intravenously. At the moment cardiac arrest is evident on the electrocardiogram, an injection of contrast medium is started. Immediately following the injection, the first exposure is made and thereafter an additional five exposures one second apart.

Arnulf reported the safety of his method in 25 patients. The cardiac arrest was well tolerated by all patients, and injections were repeated up to three times. Not one single accident occurred with the puncture of the aorta, particularly there was no single hematoma. He reported a good demonstration of the coronary arteries in almost 100% of the patients.

Other means to alter the hemodynamics and improve the opacification of the coronary arteries were advocated: 1) *Hypotension* which results in improved contrast density in the aorta and coronary arteries. The simplest technique was blood letting, which resulted in hypotension, and in spite of the induced reflex tachycardia, superior coronary arteriograms were obtained; 2) *hypothermia* which is associated with bradycardia and hypotension; 3) increased intrabronchial pressure.

In addition to the previously proposed direct needle puncture of the aortic arch through the suprasternal notch or second left interior interspace, the

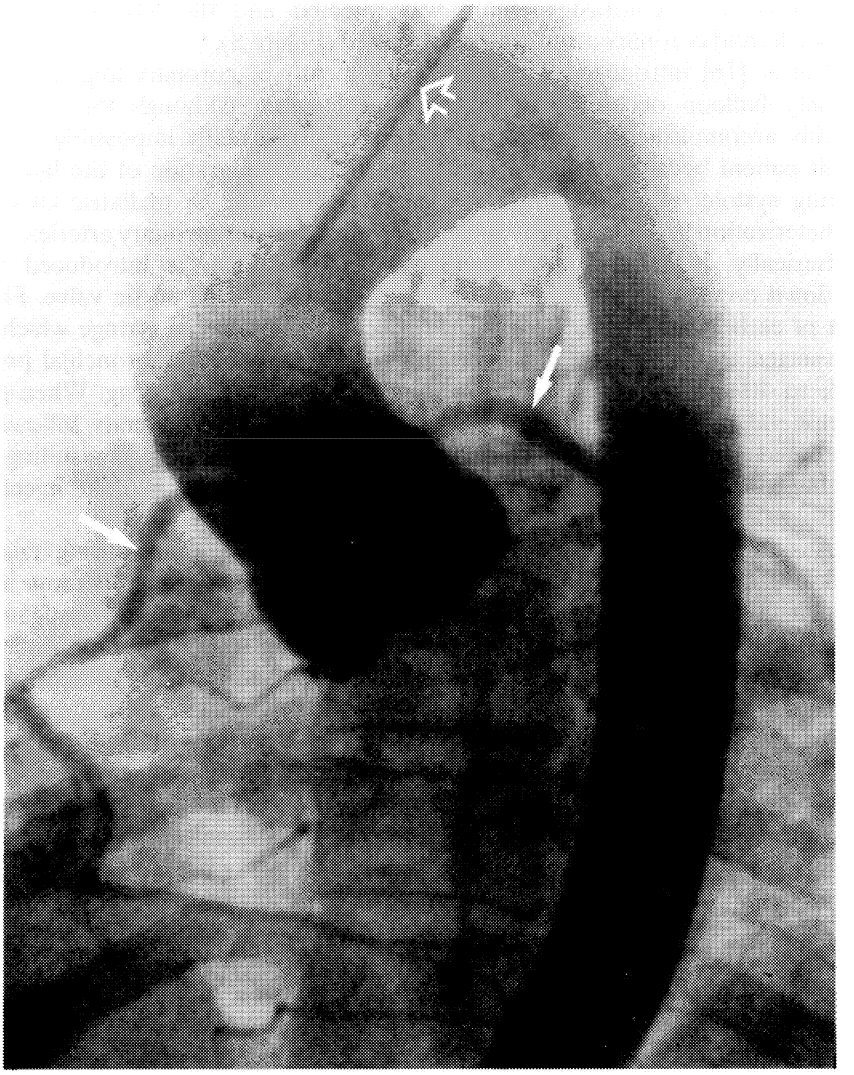

Fig. 7. Coronary arteriogram made by Arnulf during cardiac arrest. Opacification via needle (open arrow). Coronaries well opacified (solid arrows).

introduction of catheters through the carotid, brachial and femoral arteries were performed.

Taufic [15] proposed opacification via transbronchial needle puncture of the left atrium. This technique was already developed for pressure measurements particularly for the evaluation of mitral heart disease. A bronchoscope is inserted into the trachea until the carina is visualized, then a 15-gauge needle is passed through the scope into the left atrium. One cc/kilo body-

weight of 70% contrast medium was injected and the left atrium, left ventricle, and coronary arteries were opacified (Figure 8).

Dotter [16] introduced a very effective means of coronary angiography, namely balloon occlusion of the ascending aorta. Although this can be readily accomplished in babies and animals, it is virtually impossible in the adult patient because of the large balloon size and migration of the balloon during systole. However, this technique is still in use in pediatric cardiac catheterization for visualization of central shunts and the coronary arteries.

Basically, in Dotter's technique, a balloon catheter is introduced via cutdown on a peripheral artery and positioned above the aortic valve. Fifty cc's of carbon dioxide or nitrous oxide are drawn up into a syringe which is connected to the catheter. The anesthetist increases the intrabronchial pressure to 40—60 mm of mercury by squeezing the anesthesia bag. When the peripheral pulse disappears, which occurs usually 3—4 seconds following increased intrabronchial pressure, the balloon is rapidly inflated resulting in occlusion of the mid-ascending aorta. Contrast medium is then injected through the catheter and rapid films are obtained (Figure 9).

A safe and simple technique was coronary arteriography during raised endobronchial pressure. This technique was first suggested by Boerema and Blickman (1955) [17] and was also widely used by Swedish investigators (Jönsson et al. 1960) [18, 19]. Basically, during raised and obronchial pressure the venous return to the heart was decreased resulting in decreased cardiac output and a higher concentration of the injected contrast medium. Once a catheter was correctly positioned in the ascending aorta, the patient was anesthetized with sodium pentothal and the diaphragm was paralyzed with Sussinylcholine. The patient was hyperventilated for about one minute and the endobronchial pressure was raised to approximately 25 to 35mm of

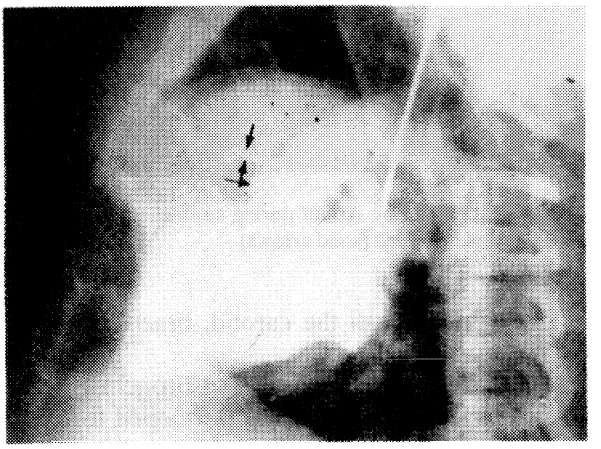

Fig. 8. Opacification of the left atrium left ventricle, and aorta via transbronchial left atrial needle puncture.

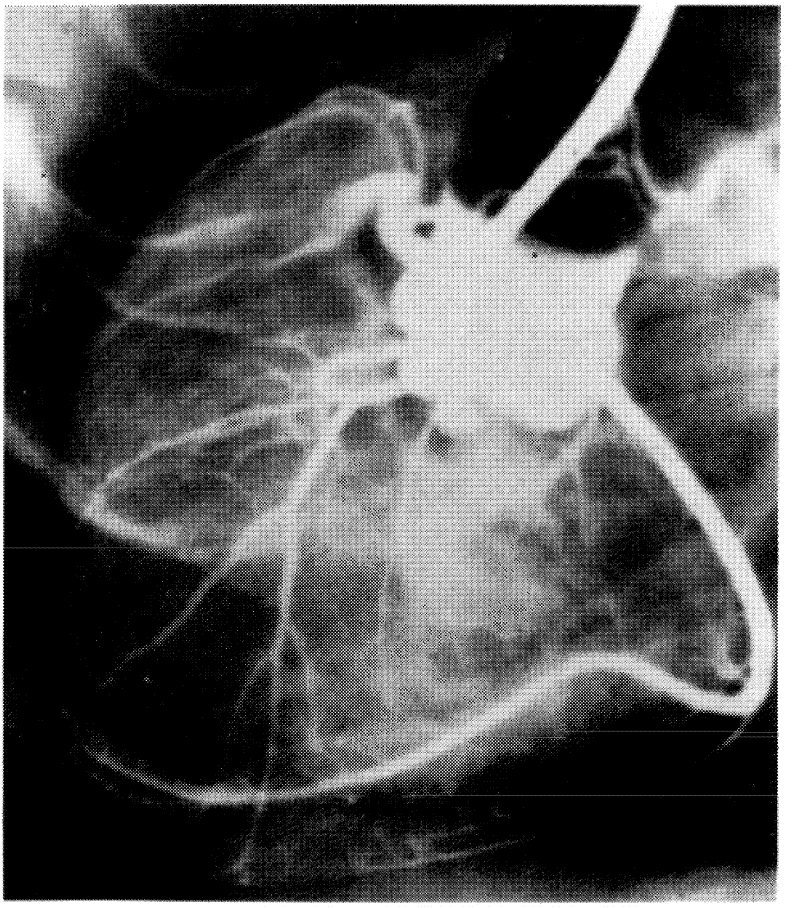

Fig. 9. Balloon occlusion coronary arteriogram according to Dotter demonstrating excellent opacification of the coronary arteries. This technique is still widely used in the evaluation of congenital heart disease.

mercury by manual compression of the breathing bag. At this moment, the contrast medium was injected by means of a Gidlund power injector. By doing so improved opacification of the coronary arteries was obtained (Figure 10).

A further improvement was achieved by the introduction of a loop-end catheter by Williams [20] and Littmann [21] (1960). The catheter loop has several holes on its inferior surface, delivering the contrast medium directly into the aortic sinuses behind the aortic valve, thus minimizing dilution (Figure 11).

This technique was carried out in a large group of patients by Paulin [22] with excellent results and virtually no complications. Bilgutay [23], at the University of Minnesota, improved the acetylcholine technique introduced by

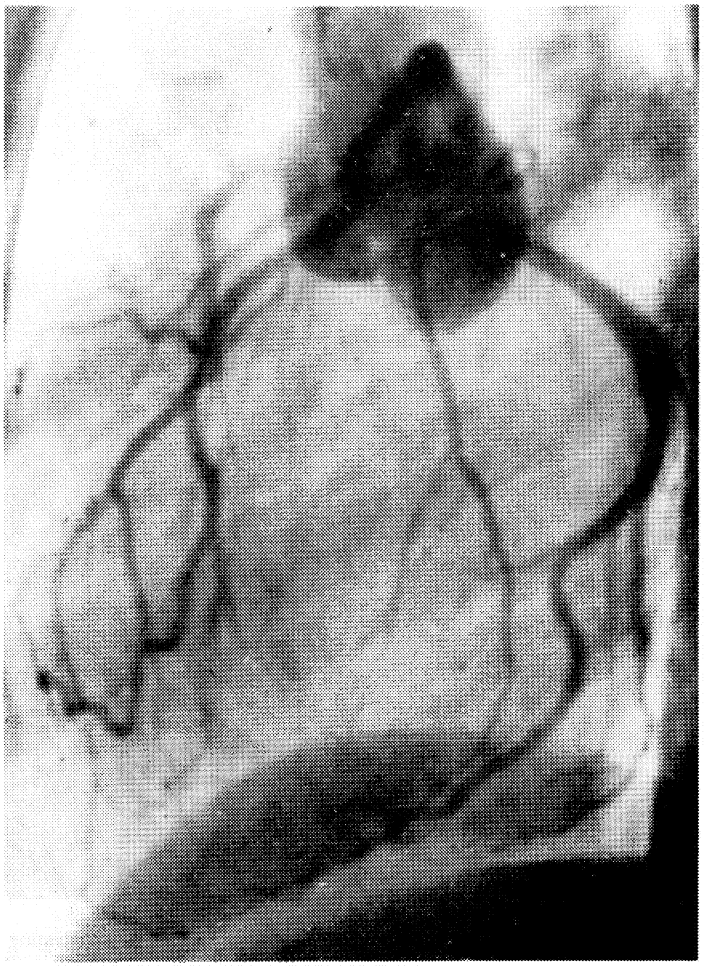

Fig. 10. Coronary arteriogram performed during increased intrabronchial pressure. The contrast medium is delivered behind the aortic valve leaflets through a catheter directly into the sinus of Valsalva, facilitating coronary artery filling.

Arnulf by injecting acetylcholine directly into the ascending aorta. A much smaller amount could be used, since with the intravenous injection, part of the acetylcholine is inactivated during its passage through the lung. Furthermore, the duration of systolic cardiac arrest could be terminated by a pacemaker which had been inserted into the right ventricle (Figure 12). In spite of cardiac arrest induced by acetylcholine, the ventricles remain responsive to direct mechanical or electrical stimulation. Later on, he described double-contrast coronary arteriography. As soon as the heart is arrested by the injection of acetylcholine, contrast medium is injected which is followed by the injection of 100cc of 100% carbon dioxide. Good double contrast

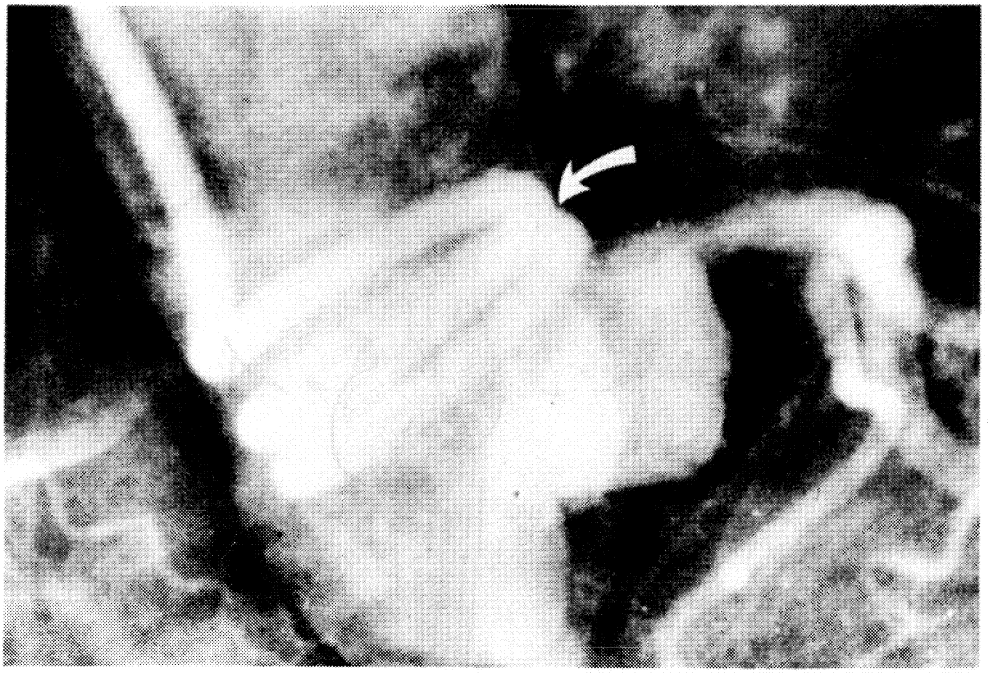

Fig. 11. Coronary arteriogram performed with the loop catheter. Contrast medium is injected into the sinus of Valsalva, resulting in excellent filling of the coronary arteries.

delineation of the aorta was achieved, but only the proximal portion of the coronary arteries were filled, which was quite different from the results obtained by Arnulf (Figure 13). Incomplete filling of the distal coronary arteries was very likely due to a too late injection at a time when systemic pressure was too low.

The major progress in opacification of the coronary arteries was described by Sones [24] advocating selective canalization of both coronary arteries and cine recording. With the classic Sones technique, the catheter is introduced via arterial cutdown into the right brachial artery. The catheter has a gentle curve and two sideholes similar to the bird's eye catheter. It is manipulated under fluoroscopic control selectively into the left and right coronary artery for selective opacification.

Ricketts and Abrams [25] described a percutaneous transfemoral technique for selective coronary angiography. However, their catheters did not come into commercial use. Judkins [26] and Amplatz [27] described at the same time percutaneous transfemoral catheterization techniques which have largely replaced the more cumbersome original Sones technique.

Several years thereafter Bourassa [28] from the Montreal Heart Institute described a new set of catheters which are somewhat similar to the Judkins

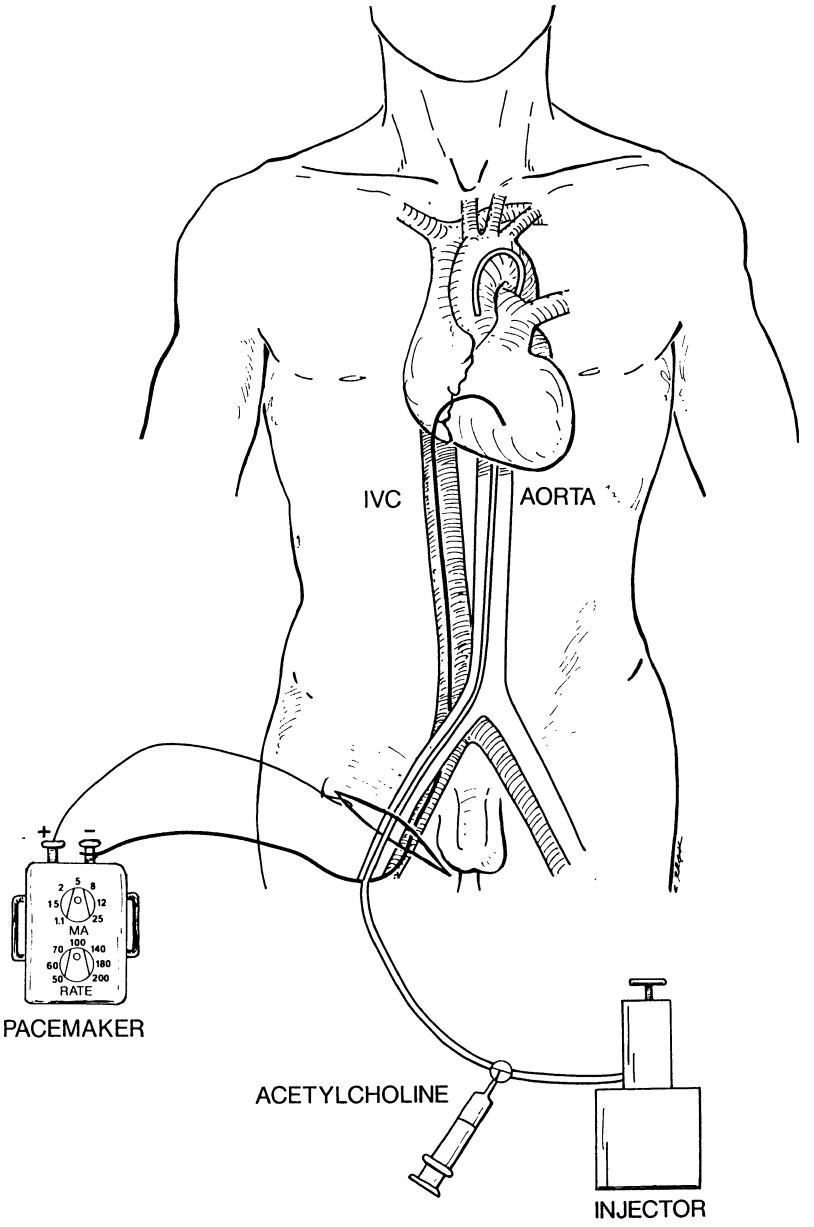

Fig. 12. Diagram demonstrating the improvement of Arnulf's technique by Bilgutay. Acetylcholine is injected directly into the sinus of Valsalva after a right-sided pacemaker had been introduced into the right ventricle. After cardiac arrest is achieved, the contrast medium is injected and the heart is re-started with the pacemaker.

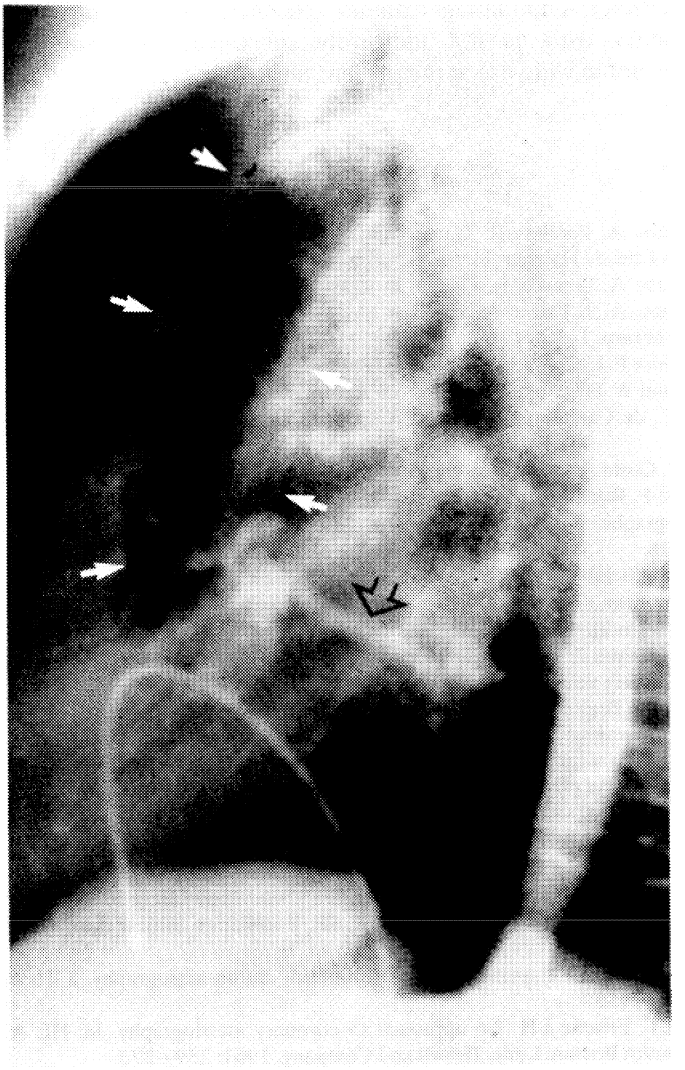

Fig. 13. Double contrast coronary arteriogram. Contrast medium and carbon dioxide were injected during cardiac arrest. The ascending and descending aorta are outlined by double contrast (arrows), but only the proximal portion of the coronary arteries is filled (open arrows).

catheter. At the present time, this technique is not widely used in the United States.

Another transfemoral catheterization technique was described by Schoonmaker and King. [29] The right and left coronary artery are catheterized with

a single catheter, eliminating catheter exchange. Successful cannulation of both coronary ostia is not uniformly successful, and consequently the technique is not in wide use at the present time.

References

1. Castellanos A, Pereiras R, Garcia A: La angio-cardiografia radio-opaca. Arch Soc de Estudios Clin. de Habaña. 31: 523—596, Sept—Oct, 1937.
2. Castellanos A, Pereiras R, Garcia A: La angio-cardiografia de la communicación interventricular. Arch Latino-Americanos de Cardiologia y Hematología, tomo VII, núm 1, Enero-Febrero, 1—19, 1938.
3. Bleichröder F: Intra-arterielle therapie. Berl Klin Wschr 49: 1503—1505, 1912.
4. Forssmann W: Die Sondierung des rechten Herzens. Klin Wschr 8: 2085—2087, 1929.
5. Moniz E, de Carvalho L, Lima A: Angiopneumographie. La Presse Med 39: 996—999, 1931.
6. Conte E, Costa A: Angiopneumography. Radiology 21: 461—465, 1933.
7. Ameuille P, Ronneaux G. Hinault V, Desgrez, Lemoine JM: Remarques sur quelques cas d'arteriographie pulmonaire chez l'homme vivant. Bull Soc Med Hop. Paris, 52: 729—739, 1936.
8. Robb GP, Steinberg I: A practical method of visualization of the chambers of the heart, the pulmonary circulation, and the great blood vessels in man. J Clin Invest. 17: 507, 1938 (Abstroct).
9. Meneses Hoyos J, Gomez del Campo C: Direct thoracic aortography and arteriography of the coronary vessels. Cardiologia 23: 251—254, 1953.
10. Gordon AJ, Brahms SA, Sussman ML: Visualization of the coronary circulation during angiocardiography. Am Heart J 39: 114—124, 1950.
11. Radner S: An attempt at the roentgenologic visualization of coronary blood vessels in man. Acta Radiol (Stockh.), 26: 497—502, 1945.
12. Ponsdomenech E, Núñez VB: Heart puncture in man for diodrast visualization of the ventricular chambers and great arteries. Am Heart J 41: 643—650, 1951.
13. Mouquin M, Brun Ph, Chartrain E, Bacquet G, Pierron J: Artériographie coronaire par voie artérielle rétrograde percutanée. Arch des Maladies du Coeur 52: 874—881, 1959.
14. Arnulf G, Buffard P: Die Arteriographie der Koronarien mittels Azetylcholin. Röntgen fortschritte 92: 115—129, 1960.
15. Taufic M, Asta JJ: Experimental transbronchial cardio-angiography. J Thorac Surg 29: 676—678, 1955.
16. Dotter CT, Frische LH: An approach to coronary arteriography. In: HL Abrams (ed), *Angiography*. Boston: Little, Brown and Company, 1961: 259—273.
17. Boerema I, Blickman JR: Reduced intrathoracic circulation as an aid in angiocardiography. J Thoracic Surg 30: 129—142, 1955.
18. Jönsson G. Visualization of the coronary arteries: preliminary report. Acta Radiol 29: 536—540, 1948.
19. Jönsson G, Brodén B, Karnell J: Thoracic aortography. Acta Radiol [Suppl.] (Stockh) 89: 1—176, 1951.
20. Bellman S, Frank HA, Lambert PB, Littman D, Williams JA: Coronary arteriography. I. Differential opacification of the aortic stream by catheters of special design — experimental development. New Engl J Med 262: 325—328, 1960.
21. Littman D, Dean DC, Crowley Jr FB, Gilson IT, Williams JA: Clinical coronary angiography. Am J Cardiol 7: 570—579, 1961.
22. Paulin S: Coronary angiography: A technical, anatomic, and clinical study. Acta Radiol [Suppl. 233] (Stockh.) 1—215, 1964.

23. Bilgutay AM, Gannon P, Sterns LP, Ferlic R, Lillehei CW: Coronary arteriography. New method under induced hypotension by pacing — experimental and clinical application. Arch Surg 89/5: 899—904, 1964.
24. Sones Jr FM, Shirey EK: Cine coronary arteriography. Mod Concepts Cardiovasc Dis 31: 735—738, 1962.
25. Ricketts HJ, Abrams HL: Percutaneous selective coronary cine arteriography. JAMA 181: 620—624, 1962.
26. Judkins MP: Selective coronary arteriography: I. A percutaneous transfemoral technic. Radiology 89: 815—824, 1967.
27. Amplatz K, Anderson R: Angiographic appearance of myocardial bridging of the coronary artery. Invest Radiol 3: 213—215, 1968.
28. Bourassa MG, Lesperance J, Campeau L: Selective coronary arteriography by the percutaneous femoral artery approach. Am J Roentgenol Radium Ther Nucl Med 1969; 107(2): 377—383.
29. Schoonmaker FW, King III SB: Coronary arteriography by the single catheter percutaneous femoral technique. Experience in 6800 cases. Circulation 50: 735—740, 1974.

Index

Developments in Cardiovascular Medicine

60. R.Th. van Dam and A. van Oosterom (eds.): *Electrocardiographic Body Surface Mapping*. Proceedings of the 3rd International Symposium on B.S.M., held in Nijmegen, The Netherlands (1985). 1986 ISBN 0-89838-834-1
61. M.P. Spencer (ed.): *Ultrasonic Diagnosis of Cerebrovascular Disease*. Doppler Techniques and Pulse Echo Imaging. 1987 ISBN 0-89838-836-8
62. M.J. Legato (ed.): *The Stressed Heart*. 1987 ISBN 0-89838-849-X
63. M.E. Safar (ed.): *Arterial and Venous Systems in Essential Hypertension*. With Assistance of G.M. London, A.Ch. Simon and Y.A. Weiss. 1987 ISBN 0-89838-857-0
64. J. Roelandt (ed.): *Digital Techniques in Echocardiography*. 1987 ISBN 0-89838-861-9
65. N.S. Dhalla, P.K. Singal and R.E. Beamish (eds.): *Pathology of Heart Disease*. Proceedings of the 8th Annual Meeting of the American Section of the I.S.H.R., held in Winnipeg, Canada, 1986 (Vol. 1). 1987 ISBN 0-89838-864-3
66. N.S. Dhalla, G.N. Pierce and R.E. Beamish (eds.): *Heart Function and Metabolism*. Proceedings of the 8th Annual Meeting of the American Section of the I.S.H.R., held in Winnipeg, Canada, 1986 (Vol. 2). 1987 ISBN 0-89838-865-1
67. N.S. Dhalla, I.R. Innes and R.E. Beamish (eds.): *Myocardial Ischemia*. Proceedings of a Satellite Symposium of the 30th International Physiological Congress, held in Winnipeg, Canada (1986). 1987 ISBN 0-89838-866-X
68. R.E. Beamish, V. Panagia and N.S. Dhalla (eds.): *Pharmacological Aspects of Heart Disease*. Proceedings of an International Symposium, held in Winnipeg, Canada (1986). 1987 ISBN 0-89838-867-8
69. H.E.D.J. ter Keurs and J.V. Tyberg (eds.): *Mechanics of the Circulation*. Proceedings of a Satellite Symposium of the 30th International Physiological Congress, held in Banff, Alberta, Canada (1986). 1987 ISBN 0-89838-870-8
70. S. Sideman and R. Beyar (eds.): *Activation, Metabolism and Perfusion of the Heart*. Simulation and Experimental Models. Proceedings of the 3rd Henry Goldberg Workshop, held in Piscataway, N.J., U.S.A. (1986). 1987 ISBN 0-89838-871-6
71. E. Aliot and R. Lazzara (eds.): *Ventricular Tachycardias*. From Mechanism to Therapy. 1987 ISBN 0-89838-881-3
72. A. Schneeweiss and G. Schettler: *Cardiovascular Drug Therapoy in the Elderly*. 1988 ISBN 0-89838-883-X
73. J.V. Chapman and A. Sgalambro (eds.): *Basic Concepts in Doppler Echocardiography*. Methods of Clinical Applications based on a Multi-modality Doppler Approach. 1987 ISBN 0-89838-888-0
74. S. Chien, J. Dormandy, E. Ernst and A. Matrai (eds.): *Clinical Hemorheology*. Applications in Cardiovascular and Hematological Disease, Diabetes, Surgery and Gynecology. 1987 ISBN 0-89838-807-4
75. J. Morganroth and E.N. Moore (eds.): *Congestive Heart Failure*. Proceedings of the 7th Annual Symposium on New Drugs and Devices, held in Philadelphia, Pa., U.S.A. (1986). 1987 ISBN 0-89838-955-0
76. F.H. Messerli (ed.): *Cardiovascular Disease in the Elderly*. 2nd ed. 1988 ISBN 0-89838-962-3
77. P.H. Heintzen and J.H. Bürsch (eds.): *Progress in Digital Angiocardiography*. 1988 ISBN 0-89838-965-8

Developments in Cardiovascular Medicine

78. M.M. Scheinman (ed.): *Catheter Ablation of Cardiac Arrhythmias.* Basic Bioelectrical Effects and Clinical Indications. 1988 ISBN 0-89838-967-4
79. J.A.E. Spaan, A.V.G. Bruschke and A.C. Gittenberger-De Groot (eds.): *Coronary Circulation.* From Basic Mechanisms to Clinical Implications. 1987 ISBN 0-89838-978-X
80. C. Visser, G. Kan and R.S. Meltzer (eds.): *Echocardiography in Coronary Artery Disease.* 1988 ISBN 0-89838-979-8
81. A. Bayés de Luna, A. Betriu and G. Permanyer (eds.): *Therapeutics in Cardiology.* 1988 ISBN 0-89838-981-X
82. D.M. Mirvis (ed.): *Body Surface Electrocardiographic Mapping.* 1988 ISBN 0-89838-983-6
83. M.A. Konstam and J.M. Isner (eds.): *The Right Ventricle.* 1988 ISBN 0-89838-987-9
84. C.T. Kappagoda and P.V. Greenwood (eds.): *Long-term Management of Patients after Myocardial Infarction.* 1988 ISBN 0-89838-352-8
85. W.H. Gaasch and H.J. Levine (eds.): *Chronic Aortic Regurgitation.* 1988 ISBN 0-89838-364-1
86. P.K. Singal (ed.): *Oxygen Radicals in the Pathophysiology of Heart Disease.* 1988 ISBN 0-89838-375-7
87. J.H.C. Reiber and P.W. Serruys (eds.): *New Developments in Quantitative Coronary Arteriography.* 1988 ISBN 0-89838-377-3
88. J. Morganroth and E.N. Moore (eds.): *Silent Myocardial Ischemia.* Proceedings of the 8th Annual Symposium on New Drugs and Devices (1987). 1988 ISBN 0-89838-380-3
89. H.E.D.J. ter Keurs and M.I.M. Noble (eds.): *Starling's Law of the Heart Revisted.* 1988 ISBN 0-89838-382-X
90. N. Sperelakis (ed.): *Physiology and Pathophysiology of the Heart.* (Rev. ed.) 1988 ISBN 0-89838-388-9
91. J.W. de Jong (ed.): *Myocardial Energy Metabolism.* 1988 ISBN 0-89838-394-3
92. V. Hombach, H.H. Hilger and H.L. Kennedy (eds.): *Electrocardiography and Cardiac Drug Therapy.* Proceedings of an International Symposium, held in Cologne, F.R.G. (1987). 1988 ISBN 0-89838-395-1
93. H. Iwata, J.B. Lombardini and T. Segawa (eds.): *Taurine and the Heart.* 1988 ISBN 0-89838-396-X
94. M.R. Rosen and Y. Palti (eds.): *Lethal Arrhythmias Resulting from Myocardial Ischemia and Infarction.* Proceedings of the 2nd Rappaport Symposium, held in Haifa, Israel (1988). 1988 ISBN 0-89838-401-X
95. M. Iwase and I. Sotobata: *Clinical Echocardiography.* With a Foreword by M.P. Spencer. 1989 ISBN 0-7923-0004-1
96. I. Cikes (ed.): *Echocardiography in Cardiac Interventions.* 1989 ISBN 0-7923-0088-2
97. E. Rapaport (ed.): *Early Interventions in Acute Myocardial Infarction.* 1989 ISBN 0-7923-0175-7
98. M.E. Safar and F. Fouad-Tarazi (eds.): *The Heart in Hypertension.* A Tribute to Robert C. Tarazi (1925-1986). 1989 ISBN 0-7923-0197-8
99. S. Meerbaum and R. Meltzer (eds.): *Myocardial Contrast Two-dimensional Echocardiography.* 1989 ISBN 0-7923-0205-2

Developments in Cardiovascular Medicine

100. J. Morganroth and E.N. Moore (eds.): *Risk/Benefit Analysis for the Use and Approval of Thrombolytic, Antiarrhythmic, and Hypolipidemic Agents.* Proceedings of the 9th Annual Symposium on New Drugs and Devices (1988). 1989 ISBN 0-7923-0294-X
101. P.W. Serruys, R. Simon and K.J. Beatt (eds.): *PTCA - An Investigational Tool and a Non-operative Treatment of Acute Ischemia.* 1990 ISBN 0-7923-0346-6
102. I.S. Anand, P.I. Wahi and N.S. Dhalla (eds.): *Pathophysiology and Pharmacology of Heart Disease.* 1989 ISBN 0-7923-0367-9
103. G.S. Abela (ed.): *Lasers in Cardiovascular Medicine and Surgery.* Fundamentals and Technique. 1990 ISBN 0-7923-0440-3
104. H.M. Piper (ed.): *Pathophysiology of Severe Ischemic Myocardial Injury.* 1990 ISBN 0-7923-0459-4
105. S.M. Teague (ed.): *Stress Doppler Echocardiography.* 1990 ISBN 0-7923-0499-3
106. P.R. Saxena, D.I. Wallis, W. Wouters and P. Bevan (eds.): *Cardiovascular Pharmacology of 5-Hydroxytryptamine.* Prospective Therapeutic Applications. 1990 ISBN 0-7923-0502-7
107. A.P. Shepherd and P.A. Öberg (eds.): *Laser-Doppler Blood Flowmetry.* 1990 ISBN 0-7923-0508-6
108. J. Soler-Soler, G. Permanyer-Miralda and J. Sagristà-Sauleda (eds.): *Pericardial Disease.* New Insights and Old Dilemmas. Preface by Ralph Shabetai. 1990 ISBN 0-7923-0510-8
109. J.P.M. Hamer: *Practical Echocardiography in the Adult.* With Doppler and Color-Doppler Flow Imaging. 1990 ISBN 0-7923-0670-8
110. A. Bayés de Luna, P. Brugada, J. Cosin Aguilar and F. Navarro Lopez (eds.): *Sudden Cardiac Death.* 1991 ISBN 0-7923-0716-X
111. E. Andries and R. Stroobandt (eds.): *Hemodynamics in Daily Practice.* 1991 ISBN 0-7923-0725-9
112. J. Morganroth and E.N. Moore (eds.): *Use and Approval of Antihypertensive Agents and Surrogate Endpoints for the Approval of Drugs affecting Antiarrhythmic Heart Failure and Hypolipidemia.* Proceedings of the 10th Annual Symposium on New Drugs and Devices (1989). 1990 ISBN 0-7923-0756-9
113. S. Iliceto, P. Rizzon and J.R.T.C. Roelandt (eds.): *Ultrasound in Coronary Artery Disease.* Present Role and Future Perspectives. 1990 ISBN 0-7923-0784-4
114. J.V. Chapman and G.R. Sutherland (eds.): *The Noninvasive Evaluation of Hemodynamics in Congenital Heart Disease.* Doppler Ultrasound Applications in the Adult and Pediatric Patient with Congenital Heart Disease. 1990 ISBN 0-7923-0836-0
115. G.T. Meester and F. Pinciroli (eds.): *Databases for Cardiology.* 1991 ISBN 0-7923-0886-7
116. B. Korecky and N.S. Dhalla (eds.): *Subcellular Basis of Contractile Failure.* 1990 ISBN 0-7923-0890-5
117. J.H.C. Reiber and P.W. Serruys (eds.): *Quantitative Coronary Arteriography.* 1991 ISBN 0-7923-0913-8
118. E. van der Wall and A. de Roos (eds.): *Magnetic Resonance Imaging in Coronary Artery Disease.* 1991 ISBN 0-7923-0940-5

Developments in Cardiovascular Medicine

119. V. Hombach, M. Kochs and A.J. Camm (eds.): *Interventional Techniques in Cardiovascular Medicine.* 1991 ISBN 0-7923-0956-1
120. R. Vos: *Drugs Looking for Diseases.* Innovative Drug Research and the Development of the Beta Blockers and the Calcium Antagonists. 1991 ISBN 0-7923-0968-5
121. S. Sideman, R. Beyar and A. G. Kleber (eds.): *Cardiac Electrophysiology, Circulation, and Transport.* 1991 ISBN 0-7923-1145-0
122. D.M. Bers: *Excitation-Contraction Coupling and Cardiac Contractile Force.* 1991 ISBN 0-7923-1186-8

Previous volumes are still available

KLUWER ACADEMIC PUBLISHERS – DORDRECHT / BOSTON / LONDON